

INFORMATION TO USERS

This manuscript has been reproduced from the microfilm master. UMI films the text directly from the original or copy submitted. Thus, some thesis and dissertation copies are in typewriter face, while others may be from any type of computer printer.

The quality of this reproduction is dependent upon the quality of the copy submitted. Broken or indistinct print, colored or poor quality illustrations and photographs, print bleedthrough, substandard margins, and improper alignment can adversely affect reproduction.

In the unlikely event that the author did not send UMI a complete manuscript and there are missing pages, these will be noted. Also, if unauthorized copyright material had to be removed, a note will indicate the deletion.

Oversize materials (e.g., maps, drawings, charts) are reproduced by sectioning the original, beginning at the upper left-hand corner and continuing from left to right in equal sections with small overlaps.

Photographs included in the original manuscript have been reproduced xerographically in this copy. Higher quality 6" x 9" black and white photographic prints are available for any photographs or illustrations appearing in this copy for an additional charge. Contact UMI directly to order.

Bell & Howell Information and Learning
300 North Zeeb Road, Ann Arbor, MI 48106-1346 USA

UMI[®]
800-521-0600

NOTE TO USERS

Page(s) not included in the original manuscript are unavailable from the author or university. The manuscript was microfilmed as received.

352

This reproduction is the best copy available.

UMI

University of Alberta

**Plane Turbulent Jets in Shallow Tailwater
and
Their Application to Energy Dissipation**

by

Samir Ali Ead



A thesis submitted to the
Faculty of Graduate Studies and Research
in partial fulfillment of the requirements for the degree of
Doctor of Philosophy

in

Water Resources Engineering
Department of Civil and Environmental Engineering
Edmonton, Alberta
Spring 1999



National Library
of Canada

Acquisitions and
Bibliographic Services

395 Wellington Street
Ottawa ON K1A 0N4
Canada

Bibliothèque nationale
du Canada

Acquisitions et
services bibliographiques

395, rue Wellington
Ottawa ON K1A 0N4
Canada

Your file Votre référence

Our file Notre référence

The author has granted a non-exclusive licence allowing the National Library of Canada to reproduce, loan, distribute or sell copies of this thesis in microform, paper or electronic formats.

The author retains ownership of the copyright in this thesis. Neither the thesis nor substantial extracts from it may be printed or otherwise reproduced without the author's permission.

L'auteur a accordé une licence non exclusive permettant à la Bibliothèque nationale du Canada de reproduire, prêter, distribuer ou vendre des copies de cette thèse sous la forme de microfiche/film, de reproduction sur papier ou sur format électronique.

L'auteur conserve la propriété du droit d'auteur qui protège cette thèse. Ni la thèse ni des extraits substantiels de celle-ci ne doivent être imprimés ou autrement reproduits sans son autorisation.

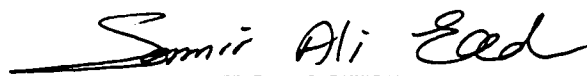
0-612-39523-5

**University of Alberta
Library Release Form**

Name of Author: Samir Ali Ead
Title of Thesis: Plane Turbulent Jets in Shallow
Tailwater and Their Application to
Energy Dissipation
Degree: Doctor of Philosophy
Year this Degree Granted: 1999

Permission is hereby granted to the University of Alberta library to reproduce single copies of this thesis and to lend or sell such copies for private, scholarly, or scientific research purposes only.

The author reserves all other publication and other rights in association with the copyright in the thesis, and except as herein before provided, neither the thesis nor any substantial portion thereof may be printed or otherwise reproduced in any material form whatever without the author's prior written permission.

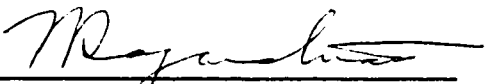


110 RH, Michener Park
Edmonton, Alberta
Canada, T6H 4M4

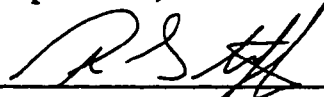
Date: 18 Dec. 98

University of Alberta
Faculty of Graduate Studies and Research

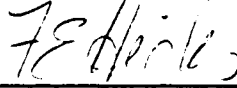
The undersigned certify that they have read, and recommend to the Faculty of Graduate Studies and Research for acceptance, a thesis entitled "**Plane Turbulent Jets in Shallow Tailwater and Their Application to Energy Dissipation**" submitted by **Samir Ali Ead** in partial fulfillment of the requirements for the degree of **Doctor of Philosophy in Water Resources Engineering**.



Dr. N. Rajaratnam
(Supervisor)



Dr. P. M. Steffler



Dr. F. E. Hicks



Dr. J. Leonard



Dr. S. J. Stanley



Dr. W. H. Hager
(External Examiner)

Date: 10th Dec 1998

بِسْمِ اللَّهِ الرَّحْمَنِ الرَّحِيمِ

أَوَلَمْ يَرَ الَّذِينَ كَفَرُوا أَنَّ السَّمَاوَاتِ
وَالْأَرْضَ كَانَتَا رَتْقًا فَفَتَقْنَاهُمَا وَجَعَلْنَا مِنَ الْمَاءِ
كُلَّ شَيْءٍ حَيٍّ أَفَلَا يُؤْمِنُونَ .

(سورة الأَنْعَام - آية ٣٠)

In the Name of Allah, the Most Gracious, the Most Merciful

*"Do not those who disbelieve see that the
heavens and the earth were joined together;
then We (God Almighty) tore them asunder?
And We made of water every living thing
Will they not then believe?"*

The Quran, 21: 30

Abstract

This thesis is written in the paper format. It includes three contributions and this abstract presents a brief summary of these three contributions.

The first contribution introduces a new design concept for energy dissipation below flow regulators. Instead of using a single-leaf sluice gate, a double-leaf gate design has been suggested. The two leaves were arranged in such a way that a plane turbulent jet issued at an angle towards the water surface through the opening between the two leaves. The bottom leaf remains fixed while the top leaf (control leaf) is moved up and down to regulate the flow. By using this arrangement, the high velocity supercritical stream was deflected away from the bed to the water surface. Besides minimizing erosion, a lifting device of smaller capacity is adequate for operating the control leaf. Existing regulators can be modified by adding an upward sloping sill just below the gate. Twenty one experiments were conducted for different offset ratios, submergence ratios, width ratios, angles of inclination and Froude numbers. The flow patterns, velocity decay, momentum decay and bed shear stress were studied experimentally. The main characteristics of the deflected jet and the surface jet were also investigated and compared with those of free and submerged jumps, and surface jets. The new dissipator performs well in comparison with free and submerged jumps.

The second contribution presents a theoretical and experimental study of plane turbulent surface jets with finite tailwater depth. The momentum flux and the rise in the water surface elevation at the section where the surface jet attaches to the bed were evaluated theoretically. Nine experiments with different Froude numbers and offset ratios, were conducted to observe and quantify the growth of the surface jet, the decay of the velocity scale and the momentum flux and the variation of the volume flux. The

momentum flux of the forward flow in the surface jet was found to decay appreciably with the distance from the nozzle. This decay is shown to be due to the entrainment of the return flow which has negative momentum and also due to the increase in the tailwater depth, further away from the nozzle, which produces this return flow. This study has contributed to an understanding of the behavior of turbulent surface jets when the ambient fluid has a limited extent.

The third contribution presents a theoretical and laboratory study of plane turbulent wall jets in shallow tailwater. The momentum flux, in terms of that at the nozzle, was evaluated theoretically. A theoretical expression for the depression in the water surface elevation at the gate (housing the nozzle) was also obtained. An extensive set of experiments, with different Froude numbers and tailwater depth ratios, was conducted to observe and quantify the growth of the wall jet, the decay of the velocity scale and the momentum flux and the variation of the volume flux. Also, experiments were conducted to measure the bed shear stress and the length of the re-circulating flow region and to evaluate the drop in the water surface elevation at the wall. The depression in the water surface elevation in the vicinity of the wall produced return flow with negative momentum which resulted in a considerable decay of the momentum flux of the forward flow in the wall jet. Expressions describing the different flow characteristics of the wall jet, based on the experimental observations, were developed. The experimental and the corresponding theoretical results agreed quite well. This study has contributed to an understanding of the behavior of turbulent wall jets when the receiving water body has a limited extent.

ACKNOWLEDGMENTS

First and foremost I am thankful to Allah the Almighty (God) for his grace and Mercy.

I would like to express my sincere gratitude to my supervisor Dr. N. Rajaratnam for his patience, support and continuous encouragement throughout the course of this study. Dr. Rajaratnam devoted his time and effort to make this study a success. I consider it a matter of great privilege and a rare opportunity to work under his supervision.

I wish to extend my thanks to Dr. W. H. Hager, my external examiner, for his time and effort in reading this thesis thoroughly and making many helpful comments and suggestions.

Thanks are due to Mr. Sheldon Lovell for his help in the construction and maintenance of the experimental arrangement.

I would like to acknowledge the financial support provided by the Natural Sciences and Engineering Research Council of Canada through an operating grant to my supervisor.

Special thanks are to my wife, Shazy, and to my children, Ahmed, Maha and Rana, for their patience, encouragement and support during this study.

My thanks also go to my mother, brother and sisters for always being there.

Table of Contents

Chapter 1

Introduction.....	1
1.1 General.....	1
1.2 Organization of the Thesis.....	2
1.3 References.....	4

Chapter 2

Literature Review.....	5
2.1 Introduction.....	5
2.2 Energy Dissipators.....	5
2.3 Hydraulic Jump Stilling Basins.....	7
2.3.1 Classical hydraulic jump.....	8
2.3.2 Forced hydraulic jump.....	9
2.4 Plane Turbulent Jets in Deep Tailwater.....	11
2.4.1 Plane turbulent free jets.....	11
2.4.2 Plane turbulent surface jets.....	14
2.4.3 Plane turbulent wall jets.....	16
2.5 Turbulent Jets in Close Proximity of Boundaries.....	21
2.6 References.....	32

Chapter 3

Experimental Arrangement and Instrumentation Techniques.....	39
3.1 Introduction.....	39
3.2 Experimental Arrangement.....	39
3.2.1 The flume.....	39
3.2.2 Pressure transducers.....	40
3.2.3 Data acquisition system.....	41
3.3 Velocity Measurements.....	42
3.3.1 Prandtl tube.....	42
3.3.2 Pitch probe.....	43
3.4 Bed Shear Stress Measurements.....	46
3.4.1 Introduction.....	46
3.4.2 Preston tube technique.....	48
3.5 The Experiments.....	49

3.6	Experimental Errors and Uncertainties.....	49
3.6.1	Introduction and basic concepts.....	49
3.6.2	Estimate of uncertainty	53
3.7	References.....	58

Chapter 4

A Double-Leaf Gate for Energy Dissipation Below Regulators.....		66
4.1	Introduction.....	66
4.2	Dimensional Analysis.....	67
4.3	Experimental Study	69
4.3.1	Experimental arrangement.....	69
4.3.2	Experiments.....	70
4.4	Experimental Results and Analysis.....	71
4.4.1	Flow patterns.....	71
4.4.1.1	Width ratio $w/W = 1.00$ and $\theta = 30$ degrees.....	72
4.4.1.2	Width ratio $w/W = 1.00$ and $\theta = 10$ degrees.....	74
4.4.1.3	Width ratio $(w/W) < 1.00$ and $\theta = 10$ degrees.....	75
4.4.1.4	Hysteresis effects	76
4.4.2	Velocity profiles.....	77
4.4.3	Reverse flow.....	79
4.4.4	Velocity decay.....	80
4.4.5	Inclined jet	83
4.4.6	Surface jet.....	85
4.4.7	Surface-jet discharge.....	86
4.4.8	Surface-jet momentum flux	87
4.4.9	Bed shear stress	88
4.4.9.1	Pattern A	89
4.4.9.2	Pattern B.....	90
4.4.9.3	Pattern C.....	91
4.5	Conclusions and Recommendations.....	92
4.6	References	94

Chapter 5

Plane Turbulent Surface Jets in Shallow Tailwater.....	161
5.1 Introduction	161
5.2 Theoretical Considerations.....	162
5.3 Dimensional Analysis.....	168
5.4 Experimental Study.....	169
5.4.1 Experimental arrangement	169
5.4.2 Experiments.....	170
5.5 Experimental Results and Analysis.....	170
5.5.1 Eddy length.....	170
5.5.2 Velocity profiles.....	172
5.5.3 Reverse flow.....	172
5.5.4 Surface jet.....	173
5.5.5 Velocity and length scales.....	174
5.5.6 Surface-jet discharge.....	176
5.5.7 Surface-jet momentum flux.....	178
5.6 Engineering Significance.....	179
5.7 Conclusions.....	181
5.8 References.....	182

Chapter 6

Plane Turbulent Wall Jets in Shallow Tailwater.....	229
6.1 Introduction	229
6.2 Theoretical Considerations.....	231
6.2.1 Neglecting the bed shear stress.....	232
6.2.2 Considering the bed shear stress.....	234
6.3 Dimensional Analysis	238
6.4 Experimental Study.....	239
6.4.1 Experimental arrangement.....	239
6.4.2 Experiments.....	240
6.5 Experimental Results and Analysis.....	241
6.5.1 Eddy length.....	241
6.5.2 Velocity profiles.....	242
6.5.3 Wall jet.....	243
6.5.4 Velocity and length scales.....	244
6.5.5 Wall-jet discharge.....	246

6.5.6	Bed shear stress.....	248
6.5.7	Wall-jet momentum flux.....	249
6.6	Conclusions.....	251
6.7	References.....	251

Chapter 7

Conclusions and Recommendations.....	293
---	------------

Appendix

1.	A Double Leaf Gate for Energy Dissipation Below Regulators	298
1.1	Velocity Measurements along Vertical Sections at x-stations.....	298
1.2	Velocity Measurements for the Inclined Jet.....	310
1.3	Bed Shear Stress Measurements.....	315
1.4	Variation of Velocity Scale, Length Scale, Jet Discharge and Momentum Flux with Distance.....	318
2.	Plane Turbulent Surface Jets in Shallow Tailwater.....	334
2.1	Velocity Measurements along Vertical Sections at x-stations.....	334
2.2	Variation of Velocity Scale, Length Scale, Jet Discharge and Momentum Flux with Distance.....	343
3.	Plane Turbulent wall Jets in Shallow Tailwater.....	353
3.1	Velocity Measurements along Vertical Sections at x-stations.....	353
3.2	Bed Shear Stress Measurements.....	359
3.3	Variation of Velocity Scale, Length Scale, Jet Discharge and Momentum Flux with Distance.....	360

List of Tables

<u>Table</u>	<u>Title</u>	<u>Page</u>
3.1	Explicit equations for Patel's calibration curves for Preston tube.....	63
3.2	Primary details of experiments of a double-leaf gate (series A).....	64
3.3	Primary details of experiments of the plane turbulent surface jets.....	65
3.4	Primary details of experiments of the plane turbulent wall jets (series A)..	65
4.1	Primary details of experiments (series A).....	97
5.1	Primary details of experiments	184
6.1	Primary details of experiments (series A).....	254

List of Figures

Figure	Title	Page
2.1	Definition sketch of plane turbulent free jets.....	38
2.2	Definition sketch of plane turbulent surface jets.....	38
2.3	Definition sketch of plane turbulent wall jets.....	38
3.1	Experimental flume.....	59
3.2	Typical calibration of pressure transducers.....	60
3.3	Prandtl tube.....	60
3.4	Pitch probe.....	61
3.5	Calibration curves for the pitch probe.....	62
4.1	Definition sketch of double-leaf gate dissipator.....	98
4.2	Modification to existing regulators.....	98
4.3	Experimental flume.....	99
4.4	Pitch probe.....	100
4.5	Prandtl tube.....	101
4.6(a-c)	(a) Pattern A.....	102
	(b) Pattern B.....	103
	(c) Pattern C.....	104
4.7(a-c)	Flow patterns A, B & C for double-leaf gate dissipator.....	105
4.8(a-d)	Boundaries of the flow patterns	
	(a) $\theta=30^\circ$, $Z_0/b_0=30.00$	106
	(b) $\theta=30^\circ$, $Z_0/b_0=13.50$	106
	(c) $\theta=30^\circ$, $Z_0/b_0=6.75$	107
	(d) $\theta=10^\circ$, $Z_0/b_0=13.50$	107
4.9	Jet trajectories.....	108
4.10	Oscillating zones.....	109
4.11	Width ratio $w/W=0.50$	110
4.12(a-n)	(a) Typical velocity profiles for pattern C	111
	(b) Typical velocity profiles for pattern B	111
	(c-d) Typical velocity profiles for pattern A	112
	(e) Typical velocity profiles for pattern AB.....	113
	(f) Typical velocity profiles for pattern A.....	113
	(g-h) Typical velocity profiles for pattern A.....	114

	(i-j) Typical velocity profiles for pattern A.....	115
	(k-l) Typical velocity profiles for pattern A.....	116
	(m-n) Typical velocity profiles for pattern A.....	117
4.13	Reverse flow near the bed ($x=2m$).....	118
4.14(a-d)	(a-b) Variation of the depth-averaged reverse velocity with distance.....	119
	(c-d) Variation of the depth-averaged reverse velocity with distance.....	120
4.15(a-n)	(a-b) Maximum velocity decay in flow pattern A.....	121
	(c-d) Maximum velocity decay in flow pattern A.....	122
	(e-f) Maximum velocity decay in flow pattern A.....	123
	(g-h) Maximum velocity decay in flow pattern A.....	124
	(i-j) Maximum velocity decay in flow pattern A.....	125
	(k-l) Maximum velocity decay in flow patterns A, B & C.....	126
	(m-n) Maximum velocity decay in flow patterns A & AB.....	127
4.16	Consolidated plot for all the maximum-velocity decay profiles in flow pattern A.....	128
4.17	Comparison between the double-leaf gate and the baffle wall dissipators.....	129
4.18(a-b)	Comparison between the double-leaf gate, the free and the submerged jumps.....	130
4.19(a-b)	Comparison between the double-leaf gate, the free and the submerged jumps.....	131
4.20	Locus of the maximum velocity.....	132
4.21(a-j)	(a-b) Velocity distributions for the inclined jet (Expt. 3)	
	(a) Typical velocity profiles.....	133
	(b) Similarity profile.....	133
	(c-d) Velocity distributions for the inclined jet (Expt. 9)	
	(c) Typical velocity profiles.....	134
	(d) Similarity profile.....	134
	(e-f) Velocity distributions for the inclined jet (Expt. 12)	
	(e) Typical velocity profiles.....	135
	(f) Similarity profile.....	135
	(g-h) Velocity distributions for the inclined jet (Expt. 14)	
	(g) Typical velocity profiles.....	136
	(h) Similarity profile.....	136

	(i-j) Velocity distributions for the inclined jet (Expt. 16)	
	(i) Typical velocity profiles.....	137
	(j) Similarity profile.....	137
4.22	Consolidated non-dimensional plot for the velocity distribution in the inclined jet.....	138
4.23	Maximum-velocity decay with distance along the inclined jet.....	139
4.24(a-ab)	(a-b) Velocity distribution in surface jet (Expt. 2)	
	(a) Velocity profiles.....	140
	(b) Similarity profile... ..	140
	(c-d) Velocity distribution in surface jet (Expt. 3)	
	(c) Velocity profiles.....	141
	(d) Similarity profile.....	141
	(e-f) Velocity distribution in surface jet (Expt. 4)	
	(e) Velocity profiles.....	142
	(f) Similarity profile.....	142
	(g-h) Velocity distribution in surface jet (Expt. 8)	
	(g) Velocity profiles.....	143
	(h) Similarity profile.....	143
	(i-j) Velocity distribution in surface jet (Expt. 9)	
	(i) Velocity profiles.....	144
	(j) Similarity profile.....	144
	(k-l) Velocity distribution in surface jet (Expt. 12)	
	(k) Velocity profiles.....	145
	(l) Similarity profile.....	145
	(m-n) Velocity distribution in surface jet (Expt. 14)	
	(m) Velocity profiles.....	146
	(n) Similarity profile.....	146
	(o-p) Velocity distribution in surface jet (Expt. 15)	
	(o) Velocity profiles.....	147
	(p) Similarity profile.....	147
	(q-r) Velocity distribution in surface jet (Expt. 16)	
	(q) Velocity profiles.....	148
	(r) Similarity profile.....	148
	(s-t) Velocity distribution in surface jet (Expt. 17)	
	(s) Velocity profiles.....	149
	(t) Similarity profile.....	149

	(u-v) Velocity distribution in surface jet (Expt. 18)	
	(u) Velocity profiles.....	150
	(v) Similarity profile.....	150
	(w-x) Velocity distribution in surface jet (Expt. 19)	
	(w) Velocity profiles.....	151
	(x) Similarity profile.....	151
	(y-z) Velocity distribution in surface jet (Expt. 20)	
	(y) Velocity profiles.....	152
	(z) Similarity profile.....	152
	(aa-ab) Velocity distribution in surface jet (Expt. 21)	
	(aa) Velocity profiles.....	153
	(ab) Similarity profile.....	153
4.25	Consolidated non-dimensional plot for the velocity distribution in the surface jet.....	154
4.26(a-b)	Growth rate of the surface-jet half-width	
	(a) b_o is the length scale.....	155
	(b) b_{io} is the length scale.....	155
4.27(a-b)	Variation of the surface-jet discharge, Q/Q_o , with distance, x/b_o	
	(a) Effect of the offset ratio Z_o/b_o	156
	(b) Effect of the inclination angle θ and the width ratio w/W	156
4.28(a-b)	Variation of the surface-jet momentum flux, M_x/M_o , with distance, x/b_o	
	(a) Effect of the offset ratio Z_o/b_o	157
	(b) Effect of the inclination angle θ and the width ratio w/W	157
4.29(a-c)	Shear stress distribution for pattern A	
	(a) Variation of shear stress with distance.....	158
	(b) Similarity profile.....	158
	(c) Study of shear stress and length scales.....	158
4.30(a-b)	Shear stress distribution for pattern B.....	159
4.31(a-d)	(a-b) Shear stress distributions for pattern C.....	160
	(c-d) Study of shear stress and length scales for pattern C.....	160
5.1(a-b)	(a) Definition sketch.....	185
	(b) Flow pattern.....	185
5.2	Water surface elevation ($F_o = 4.0$, $Z_o/b_o = 10$).....	186
5.3	Variation of (ϕ) with the offset ratio (η)	187

5.4	Variation of (θ) with the offset ratio (η) for different Froude numbers.....	184
5.5	Variation of (M_L/M_o) with the offset ratio (η) for different Froude numbers.....	189
5.6	Variation of (F_p/M_o) with the offset ratio (η) for different Froude numbers.....	190
5.7	Experimental flume.....	191
5.8	Streamlined entrance to produce an uniform jet of thickness b_o	192
5.9	False floor to produce an offset distance of Z_o	193
5.10	Prandtl tube.....	194
5.11(a-d)	(a) Surface jet ($F_o = 7.20$, $Z_o/b_o = 100$).....	195
	(b) Surface jet ($F_o = 4.80$, $Z_o/b_o = 50$).....	195
	(c) Surface jet ($F_o = 4.80$, $Z_o/b_o = 25$).....	196
	(d) Surface jet ($F_o = 4.00$, $Z_o/b_o = 10$).....	196
5.12(a-i)	(a) Typical velocity profiles (Expt. 1).....	197
	(b) Typical velocity profiles (Expt. 2).....	198
	(c) Typical velocity profiles (Expt. 3).....	199
	(d) Typical velocity profiles (Expt. 4).....	200
	(e) Typical velocity profiles (Expt. 5).....	201
	(f) Typical velocity profiles (Expt. 6).....	202
	(g) Typical velocity profiles (Expt. 7).....	203
	(h) Typical velocity profiles (Expt. 8).....	204
	(i) Typical velocity profiles (Expt. 9).....	205
5.13	Variation of the eddy length with the offset ratio.....	206
5.14(a-b)	(a) Variation of the depth-averaged reverse velocity with distance.	207
	(b) Effect of the offset ratio on the magnitude and the location of the maximum reverse velocity.....	208
5.15(a-b)	Velocity distribution in partially-developed flow ($x/b_o = 6$)	
	(a) Velocity profiles.....	209
	(b) Similarity profile.....	209
5.16(a-r)	(a-b) Velocity distribution in fully-developed flow (Expt. 1)	
	(a) Velocity profiles.....	210
	(b) Similarity profile.....	210
	(c-d) Velocity distribution in fully-developed flow (Expt. 2)	

	(c) Velocity profiles.....	211
	(d) Similarity profile.....	211
	(e-f) Velocity distribution in fully-developed flow (Expt. 3)	
	(e) Velocity profiles.....	212
	(f) Similarity profile.....	212
	(g-h) Velocity distribution in fully-developed flow (Expt. 4)	
	(g) Velocity profiles.....	213
	(h) Similarity profile.....	213
	(i-j) Velocity distribution in fully-developed flow (Expt. 5)	
	(i) Velocity profiles.....	214
	(j) Similarity profile.....	214
	(k-l) Velocity distribution in fully-developed flow (Expt. 6)	
	(k) Velocity profiles.....	215
	(l) Similarity profile.....	215
	(m-n) Velocity distribution in fully-developed flow (Expt. 7)	
	(m) Velocity profiles.....	216
	(n) Similarity profile.....	216
	(o-p) Velocity distribution in fully-developed flow (Expt. 8)	
	(o) Velocity profiles.....	217
	(p) Similarity profile.....	217
	(q-r) Velocity distribution in fully-developed flow (Expt. 9)	
	(q) Velocity profiles.....	218
	(r) Similarity profile.....	218
5.17	Consolidated non-dimensional plot for the velocity distribution in the surface jet.....	219
5.18(a-d)	(a) Variation of the maximum jet velocity, u_m , with distance.....	220
	(b) Variation of u_m/U_o with x/b_o	221
	(c) Variation of $(U_o/U_m)^2$ with x/b_o	222
	(d) Effect of the offset ratio on the breakdown distance.....	223
5.19	Variation of the jet half-width with distance.....	224
5.20(a-c)	(a) Variation of the surface jet discharge with distance.....	225
	(b-c) Effect of Z_o/b_o on the magnitude and the location of the maximum discharge.....	226
5.21	Variation of the surface jet momentum flux with distance.....	227
5.22	Modified regulators.....	228
5.23	Modified spillways.....	228

6.1(a-c)	(a) Definition sketch.....	255
	(b) Flow pattern.....	255
	(c) Typical velocity distribution.....	255
6.2	Water surface elevation ($F_o = 8$, $y/b_o = 25$).....	256
6.3(a-b)	(a) Variation of θ with η for various Froude numbers F_o , with and without shear stress.....	257
	(b) Variation of θ with η for various shear coefficients ϵ	258
6.4 (a-b)	(a) Variation of η_r with F_o for various values of ϵ	259
	(b) Variation of η_r with ϵ for various values of F_o	260
6.5	Variation of (M_∞/M_o) and (F_{gw}/M_o) with (η)	261
6.6	Experimental flume.....	262
6.7	Streamlined entrance to produce an uniform jet of thickness b_o	263
6.8	Prandtl tube.....	264
6.9(a-d)	(a) Wall jet ($F_o = 8$, $y/b_o = 25$).....	265
	(b) Wall jet ($F_o = 8$, $y/b_o = 35$).....	265
	(c) Wall jet ($F_o = 8$, $y/b_o = 40$).....	266
	(d) Wall jet ($F_o = 8$, $y/b_o = 50$).....	266
6.10	Variation of the eddy length, L_e/b_o , with $(\eta-\eta_r)$	267
6.11(a-f)	(a) Typical velocity fields of wall jets in shallow tail waters (Expt. 1).....	268
	(b) Typical velocity fields of wall jets in shallow tail waters (Expt. 2).....	269
	(c) Typical velocity fields of wall jets in shallow tail waters (Expt. 3).....	270
	(d) Typical velocity fields of wall jets in shallow tail waters (Expt. 4).....	271
	(e) Typical velocity fields of wall jets in shallow tail waters (Expt. 5).....	272
	(f) Typical velocity fields of wall jets in shallow tail waters (Expt. 6).....	273
6.12(a-b)	Velocity distribution in partially-developed flow ($x/b_o = 6$)	
	(a) Velocity profiles.....	274
	(b) Similarity profile.....	274

6.13(a-l)	(a-b) Velocity distribution in fully-developed flow (Expt. 1)	
	(a) Velocity profiles.....	275
	(b) Similarity profile.....	275
	(c-d) Velocity distribution in fully-developed flow (Expt. 2)	
	(c) Velocity profiles.....	276
	(d) Similarity profile.....	276
	(e-f) Velocity distribution in fully--developed flow (Expt. 3)	
	(e) Velocity profiles.....	277
	(f) Similarity profile.....	277
	(g-h) Velocity distribution in fully-developed flow (Expt. 4)	
	(g) Velocity profiles.....	278
	(h) Similarity profile.....	278
	(i-j) Velocity distribution in fully-developed flow (Expt. 5)	
	(i) Velocity profiles.....	279
	(j) Similarity profile.....	279
	(k-l) Velocity distribution in fully-developed flow (Expt. 6)	
	(k) Velocity profiles.....	280
	(l) Similarity profile.....	280
6.14	Consolidated non-dimensional plot for the velocity distribution in the wall jet.....	281
6.15(a-d)	(a) Variation of the maximum jet velocity, u_m , with distance.....	282
	(b) Variation of u_m/U_o with x/b_o	283
	(c) Variation of $(U_o/U_m)^2$ with x/b_o	284
	(d) Effect of the tailwater depth ratio on the breakdown distance.....	285
6.16	Variation of the jet half-width with distance.....	286
6.17(a-c)	(a) Variation of the wall jet discharge with distance.....	287
	(b-c) Effect of y/b_o on the magnitude and the location of the maximum discharge.....	288
6.18(a-d)	(a-b) Variation of the bed shear stress with distance.....	289
	(c-d) Variation of the bed shear stress with distance.....	290
6.19	Determination of the shear force coefficient ϵ	291
6.20	Variation of the wall jet momentum flux with distance.....	292

Notations*

Symbol	Description
A	flow pattern [4], function of the offset ratio [5], function of the tailwater depth ratio [6];
A', B', C'	functions of the offset ratio [5], functions of the tailwater depth ratio [6];
AB	flow pattern [4];
B	flow pattern [4], function of the offset ratio [5], constant equal to 0.82 [6];
b	length scale [2,4,5,6];
b _A , b _B , b _C	shear stress length scales [4];
b _o	slot width [2,3,4,5,6];
b _s	length scale for surface jet [4];
b _τ	shear stress length scale [6];
b _u , b _l	length scales for inclined jet [4];
C	flow pattern [4], function of the offset ratio [5];
C ₁ , C ₂ , C ₃	constants [2];
C _f	skin friction coefficient = $\tau_o/(\rho U_o^2/2)$ [2];
C _{fm}	skin friction coefficient = $\tau_m/(\rho U_o^2/2)$ [4];
C _{fo}	skin friction coefficient = $\tau/(\rho U_o^2/2)$ [6];
d	external diameter of the Preston tube [3];
Δp	dynamic pressure [3];
E	kinetic energy of the flow at any section [2];

* The number in square brackets [] denote relevant chapter number

E_o	the value of E at the slot [2];
F_1	supercritical Froude number in hydraulic jump [2];
$F_{\delta w}$	loss in the hydrostatic pressure force at the wall [6];
F_o	supercritical Froude number at the slot [3,4,5,6];
$F_{p\sim}$	maximum increase of the hydrostatic pressure force [5];
F_τ	integrated bed shear stress, per unit width, from the slot till the jet surfaces [6];
$F_{\tau x}$	integrated bed shear stress, per unit width, over a distance x from the slot [6];
g	acceleration due to gravity [2,3,4,5,6];
h_1, h_2, h_3	piezometric pressure heads sensed by the pitch probe tubes [3];
h_{c1}	lower critical baffle height [2];
h_{c2}	upper critical baffle height [2];
h_o	static piezometric pressure head [3];
h_s	strip height [5];
k_1, k_2, k_3, k_4, k_5	calibration coefficients that are functions of the pitch or yaw angle θ [3];
L	the horizontal distance from the gate to the point where the velocity is $0.5U_o$ [4];
L_e	length of recirculating flow region (eddy length) [5,6];
l	distance measured across the inclined jet from the point of u_m [4];
M	momentum flux at a distance x from the wall [2], surface jet momentum flux at a distance x from the wall [4,5], wall jet momentum flux at a distance x from the gate [6];
M_{\sim}	momentum flux at the section where the jet occupies the whole depth [5,6];

M_o	jet momentum flux at the slot [2,4,5,6];
M_r	momentum flux through a single strip of the forward flow [5];
m	constant equals to $\cot(\theta_w/2)$ [2];
p	mean pressure at any point [2];
Q	jet discharge at a distance x measured from the slot [2], discharge [3], surface jet discharge per unit width [5], wall jet discharge per unit width [6];
Q_m	maximum value of Q [5,6];
Q_o	value of Q at the slot [2,5,6];
Q_r	volume flux through a single strip of the forward flow [5];
q	jet discharge per unit width [2,4];
q_o	value of q at the slot [4];
R	Reynolds number [2,4,5,6], hydraulic radius [3], Result [3];
S	channel slope [3], submergence ratio = $\{(y_1 - Z_o)/b_o\}$ [4], submergence factor = $\{(y_1 - y_2)/y_1\}$ [6];
U	mean velocity [3];
U_1, U_2	mean velocities at depths of y_1 and y_2 [3];
U_o	velocity issuing from the slot [2,3,4,5,6];
$-\overline{uv}(y)$	Reynolds stress [3];
u	time-averaged velocity at any point [2,3,4,5,6];
u_*	shear velocity [2,3];
u_1, u_2	upper and lower velocities of a single strip in the forward flow [5];
u_m	maximum value of u [2,4,5,6];
u_r	depth-averaged reverse velocity [4,5];
u_{rm}	maximum value of u_r [5];

V	velocity vector [3], uniform velocity of the flow when the jet occupies the whole depth [5,6];
V_1	the average velocity at the toe of the hydraulic jump [2];
v	time-averaged velocity in y-direction [2];
v_e	entrainment velocity [2];
W	flume width [3,4,5,6];
W_R	uncertainty interval [3];
w	opening width [4];
\bar{x}	longitudinal distance measured from the slot [2];
\bar{x}_o	length of the potential core [2];
x	longitudinal distance measured from the virtual origin [2], longitudinal distance measured from the gate [4,5,6];
x_{M1}	the distance after which the momentum flux starts to decay [6];
x_{M2}	the distance at which the momentum flux approaches zero [6];
x_o	distance from the baffle front to the gate [2], longitudinal distance to the point of maximum surface velocity [4], the distance at which the velocity and length scales breakdown [5,6];
x_{oA}, x_{oB}, x_{oC}	characteristic lengths for shear stress [4];
x_{Qm}	longitudinal distance at which the surface-jet discharge is maximum [5], distance at which the wall jet discharge is maximum [6];
x_{rm}	the distance at which the maximum reverse velocity occurs [5];
y	coordinates [2], height above the bed [3,4,5,6];
y_1	initial depth of the hydraulic jump [2], vertical distance above the bed [3];
y_2	subcritical sequent depth of the hydraulic jump [2,6], vertical distance above the bed [3];

y_o	depth of flow [3,4,5], depth of flow (equal to $Z_o + b_o + \delta_x$) [5];
y_t	tailwater depth [2,3,4,5,6];
Z_o	height of the lower edge of the slot above the bed [2,3,4,5];
α_e	entrainment coefficient [2];
δ	boundary layer thickness [2,6];
δ_{\max}	maximum value of δ_x [5];
δ_w	drop in the water surface elevation at the wall [6];
δ_x	increase of water surface elevation at a distance x from the gate [5];
ε	function of the offset ratio [5], shear force coefficient at a longitudinal distance L_e from the slot = F_x/M_o [6];
ε_x	shear force coefficient at a longitudinal distance x from the slot = F_x/M_o [6];
ϕ	function of the offset ratio and the Froude number [5], function of the shear force coefficient and the Froude number [6];
γ	specific weight of water [5,6];
η	y/b [2], offset ratio = Z_o/b_o [5], tailwater depth ratio = y_t/b_o [6];
η_r	the value of η in the free hydraulic jump [6];
κ	Von Karman constant [3];
μ	dynamic viscosity [4,5,6];
ν	kinematic viscosity = μ/ρ [2,3,5,6];

θ	pitch or yaw angle [3], deflection angle [4], δ_{\perp}/b_o [5], δ_w/b_o [6];
θ_r	the value of θ in the free hydraulic jump = $(\eta_r - 1)$ [6];
θ_w	the angle the wall makes with the jet axis [2];
ρ	density of water [2,3,4,5,6];
τ	shear stress at depth y above the bed [3], bed shear stress [4,6];
τ_l	laminar shear stress [2];
τ_m	maximum value of τ [4,6];
τ_{md} & τ_{mu}	maximum value of t for pattern C [4];
τ_o	wall shear stress [2,3];
τ_t	turbulent shear stress [2];

Chapter 1

Introduction

1.1 General

Retaining structures (like dams and regulators) are hydraulic structures built on water ways to control large volumes of water under high pressures. The release of the retained water (over spillways, through outlet conduits or gates) is associated with tremendous amount of energy at the base or downstream of these structures. The resulting flow usually takes the form of a turbulent jet. This turbulent jet can be plane or axisymmetric depending on the shape of the outlet. Also, the jet can be a free jet, surface jet or wall jet depending on the relative locations of the rigid boundaries and the free surface with respect to the jet. The tremendous amount of kinetic energy carried by turbulent jets can cause erosion in tailwater channels, partial or complete failure of hydraulic structures, generation of tailwater waves and scour. Energy dissipators are devices used to protect the tailwater channel by dissipating the excess hydraulic energy in the turbulent jets. A comprehensive understanding of the behavior of a turbulent jet in a particular problem enables the engineer to design a suitable energy dissipator for such problem.

Tollmien (1926) and Görtler (1942) performed the first theoretical studies on turbulent jets while Förthmann (1936) performed the first experimental work (Abramovich, 1963). Since then, a tremendous amount of work on turbulent jets has been published. The two books written by Abramovich (1963) and Rajaratnam (1976) present an extensive treatment of turbulent jets.

Although the available knowledge on turbulent jets is claimed to be comprehensive, there are many practical problems in hydraulic engineering in which the

behavior of turbulent jets is still not well understood. This thesis presents three contributions on the behavior of plane turbulent jets in shallow tailwater.

1.2 Organization of the Thesis

In this thesis, the results of theoretical and experimental studies on three practical problems dealing with the behavior of plane turbulent jets in shallow tailwater are presented. Each piece of work is introduced in a separate chapter. Following is a brief introduction to each chapter.

Chapter 2 presents a review of previous theoretical and experimental investigations related to the present study. This chapter starts with an introduction followed by a brief description of the different types of energy dissipators including the classical and the forced hydraulic jump stilling basins. It also introduces previous studies on plane turbulent jets in tailwaters of unlimited extent. Also, the available studies on turbulent jets issuing in the close proximity of boundaries are reviewed.

Chapter 3 describes the experimental arrangement, instrumentation and techniques used in the present study. Primary details of experiments are given. A brief review of experimental errors and uncertainties is also presented.

Chapter 4 presents the results of an experimental study on a double-leaf gate as an energy dissipator. The main objective of this study was to introduce a simple and efficient energy dissipator downstream of flow regulators. Section 4.1 is an introduction for this chapter. In the introduction, the disadvantages of the hydraulic jump stilling basins are mentioned. Also, a brief description of the new model is explained. In section 4.2, the main non-dimensional parameters affecting the flow characteristics in the double-leaf gate model are figured out using dimensional analysis.

The details of the experiments are given in section 4.3. The main characteristics of the inclined jet, the surface jet and the reverse flow are presented in section 4.4. Conclusions and recommendations for future research work are given in section 4.5.

Chapter 5 presents a theoretical and an experimental study of plane turbulent surface jets in shallow tailwater. The main objective of this study was to show that the behavior of plane turbulent surface jets in shallow tailwater is significantly different than that in deep tailwater. The reverse pressure gradient associated with the surface jet causes more than 90% of the momentum flux to decay. Section 5.1 is an introduction with a brief review of previous studies. Section 5.2 shows a theoretical approach where the momentum loss and piezometric-pressure increase are evaluated. Dimensional considerations and experimental arrangement are presented in sections 5.3 and 5.4 respectively. In section 5.5, the eddy length, similarity of the velocity profiles, breakdown in the velocity and length scales, the surface jet discharge variation and decay of momentum flux, are evaluated experimentally. The conclusions of this study are formulated in section 5.6.

Chapter 6 presents a theoretical and an experimental analysis of the effects of the tailwater shallowness on the different characteristics of the plane turbulent wall jet. Section 6.1 introduces, in brief, some of the previous studies in which the momentum flux was assumed preserved. Experimental studies showing momentum decay in turbulent jets out of a wall and in turbulent jets in channels of limited depth, are also presented in the same section. Section 6.2, theoretical approach, started with an explanation of the difference between the surface and plane turbulent jets regarding the formation of the tailwater depth in each of the two problems. The tailwater depth in the surface jet is dependent on the jet characteristics. In plane jets, the tailwater depth is an independent variable. Formulations for the momentum decay and the water surface

depression at the gate, with and without the inclusion of bed shear stress, are shown in the same section. Dimensional analysis, experimental arrangement, experimental results and analysis and conclusions are shown in sections 6.3 to 6.6 respectively.

Chapter 7 presents a general discussion on the three contributions presented in Chapters 4 to 6. For each of these contributions, a brief summary and suggestions for future research are made.

1.3 References

- Abramovich, G. N. (1963). "The theory of turbulent jets." English translation published by M.I.T. Press, Massachusetts, 671p.
- Förthmann, E. (1936). "Turbulent jet expansion." English translation NACA TM-789. (Original Paper in German, 1934. Ing. Archiv., 5).
- Görtler, H. (1942). "Berechnung von Aufgaben der freien Turbulenz auf Grund eines neuen Näherungsansatzes. ZAMM, 22, pp. 244-254.
- Rajaratnam, N. (1976). Turbulent Jets. Elsevier Publishing Co., The Netherlands, 304p.
- Tollmien, W. (1926). "Berechnung turbulenter Ausbreitungsvorgänge." Z. angew. Math. Mech. 6, pp. 468-478; [English Transl. NACA TM 1085 (1945)].

Chapter 2

Literature Review

2.1 Introduction

This chapter contains four sections. In section 2.2, energy dissipators are defined and classified and the way the kinetic energy is dissipated, in each of them, is introduced in brief. Advantages and disadvantages of the hydraulic jump stilling basins are discussed in section 2.3. Sections 2.2 and 2.3 help in the understanding and evaluation of the double-leaf gate energy dissipator introduced in chapter 4. In section 2.4, plane turbulent jets in deep tailwater are presented. Equations of motion and empirical relationships, based on experimental observations, are described. Section 2.5 shows experimental observations and results for turbulent jets issuing in the close proximity of boundaries. Sections 2.4 and 2.5 are prerequisite for the understanding and evaluation of the present study (mainly chapters 5 & 6).

2.2 Energy Dissipators

Energy dissipators are devices used to dissipate kinetic energy and are used in places where excess kinetic energy could cause serious damage such as erosion, partial or complete failure of hydraulic structures and generation of tailwater waves. Vischer and Hager (1995) mentioned that the process of energy dissipation in hydraulic engineering can be usefully classified into two cases. Firstly, a particle of water within a water current where energy dissipation occurs because of the energy dissipating eddies which are generated in zones of large velocity gradients. They added that, to achieve a considerable loss of energy, it is important to create high turbulence zones. Secondly, a particle of water moving in a stream of air where energy dissipation occurs due to the air resistance exerted on the drop of water. The energy loss is large if the water drop is small and the relative velocity between the

drop and the ambient air is large. Following is a brief description of the different types of energy dissipators as classified by Vischer and Hager (1995).

Energy dissipation by expansion and deflection: In sudden expansions an impact loss occurs when a faster current impacts with a slower one, inducing separation zone/s of large velocity gradients. Sudden expansions are used in most of the energy dissipators as the outflow velocity, in such structures, is much less than the inflow velocity. Classical hydraulic jumps and forced hydraulic jumps are good examples of this type of dissipators.

Energy dissipation by counterflow: Counterflow is the principal of directing two or more jets against each other to dissipate their energy. For the impact losses to be maximum, the different jets should be more or less of the same size. Koch (1968) studied two jets of similar size and velocity. They impacted at a small angle and then united to form a single jet. He noticed that the impact yielded poor results as the generated velocity gradients were small. Uymaz (1988) studied scour below a vertical gate in the case of simultaneous flow over and under the gate. He found that the final depth of scour is smaller as compared to the cases of flow only under or over the gate, although more water can be discharged in the former case. He concluded that the overtopping of a sluice gate is not critical from the downstream scour point of view.

Energy dissipation by rough channels and cascades: Hydraulic energy can be effectively dissipated in a short distance in channels with considerable roughness. A short baffled apron can form an effective roughness in a canal or spillway drop. Peterka (1963) recommended baffle heights equal to 0.8 of the critical depth of the design discharge for a baffle apron slope of 50%. A good example of energy cascades is the stepped spillway. A study of stepped spillways as energy dissipators was conducted by Chamani (1997).

Energy dissipation with vortex devices: Although vortex devices have been known for a long time (Thoma, 1930), they have been recently applied in hydraulic

engineering. A vortex chamber is a cylindrical tank with a tangential inlet and an axial outlet. In the vortex chamber, the inflow creates a strong vortex and the outflow is a rotating and hollow water jet with an air core. Therefore, a considerable part of its energy is dissipated. The same principle is applied in vortex tubes where the flow is guided tangentially into the tube and then proceeds axially in a helical path along the wall where the energy is mainly dissipated by wall friction.

Energy dissipation by air entrainment: In most of energy dissipators, the loss of kinetic energy occurs due to a mixing process between fast and slow currents. It has been found that when a fast current entrains air, the mixing process does not consume as much energy if compared with the mixing of two water currents. As water is 800 to 900 times denser than air, it is logical to have an insignificant loss of kinetic energy when water jets entrain ambient air.

Energy dissipation by jet diffusion: It is mentioned above that air entrainment is not efficient in dissipating the excess energy of water jets. This is in the case of normal air entrainment which results in air bubbles flowing in a stream of water. However, if much air entrainment occurs in such a way that the water stream is transformed into a spray, a significant amount of kinetic energy can be dissipated. The drops of water in such a spray are strongly affected by air drag. More dissipation is anticipated with smaller water drops especially when their speed is high relative to the surrounding air. The classic example of the energy dissipation by spray action, or jet diffusion, is the flip bucket spillway. For the flip buckets to be successful as spray generators, they might need additional splitting devices to be installed on their crests or on the buckets to increase diffusion especially when the supercritical stream is relatively thick.

2.3 Hydraulic Jump Stilling Basins

In chapter 4, a double-leaf gate energy dissipator downstream of regulators, will be introduced. As the classical and forced hydraulic jump stilling basins have

been widely used downstream of regulators, it has been essential to discuss them in some details.

2.3.1 Classical hydraulic jump

Hydraulic jumps have been widely used as energy dissipators on different types of hydraulic structures. The hydraulic jump is a rapid transition from supercritical to subcritical flow. A jump is called a classical jump when it is formed in a smooth, wide and horizontal rectangular channel. In the classical hydraulic jump, the water depth increases abruptly from an initial depth of y_1 to a sequent depth of y_2 at which the water surface becomes level. The supercritical Froude number is $F_1 = V_1/(gy_1)^{0.5}$ where V_1 is the average velocity at the toe of the jump where the water depth is y_1 . A relation between the sequent and the initial depths of the classical hydraulic jump could be obtained by applying the momentum equation between the beginning and end sections of the hydraulic jump. At these two sections, velocity distributions were assumed uniform, the pressure distributions were assumed hydrostatic and the turbulent velocity fluctuations were neglected. The integrated boundary shear stress, between the beginning and end sections, was also neglected. The ratio of the sequent to initial depths, y_2/y_1 , considering the above assumptions, is given by the equation

$$\frac{y_2}{y_1} = \frac{1}{2} \left[\sqrt{1 + 8F_1^2} - 1 \right] \quad (2.1)$$

The above equation is the well-known Belanger equation.

The flow in the hydraulic jump, two-phase flow due to air entrainment, is highly turbulent with pressure and velocity fluctuations. A substantial amount of the kinetic energy is dissipated in the hydraulic jump mainly due to turbulence production

and dissipation in the surface roller which extends from the toe of the jump to a section very close to the end of the jump. The efficiency of the hydraulic jump as an energy dissipator depends on the type of the jump, which is mainly dependent on the supercritical Froude number, the tailwater depth and the bed slope. The advantage of using the hydraulic jump as an energy dissipator is that dissipation occurs in the distance between the beginning and end sections of the jump which is relatively short (almost 6 times the sequent depth, y_2). Disadvantages in using the hydraulic jump as an energy dissipator is that the hydraulic jump is always associated with wave formation in the downstream tailwater. Also, the formation of the hydraulic jump is sensitive to the tailwater depth. In other words, for a classical jump to occur downstream of a gate, the tailwater depth in the channel should be equal to the sequent depth y_2 that corresponds with y_1 and F_1 . If the tailwater depth is less than the sequent depth, the jump is called a “repelled jump” and usually occurs downstream of the stilling basin (on the unprotected stream bed) causing serious erosion problems and a considerable amount of damage could happen. If the tailwater depth is greater than the sequent depth, the jump becomes submerged. The “submerged jump” is not as efficient as the classical jump regarding its ability to dissipate the excess energy. Therefore, using the hydraulic jump as an energy dissipator has been always critical especially when the downstream conditions are not fixed. For regulators built on irrigation canals, the tailwater depth always varies according to the irrigation demands and using the hydraulic jump as the energy dissipation element in such situations is unacceptable.

2.3.2 Forced hydraulic jump

In order to keep the hydraulic jump within the stilling basin, for a range of tailwater levels, an external force is required. This force could be in the form of baffle blocks, baffle walls (see for example Rajaratnam, 1967 and Peterka, 1963), or a

favorable slope to the basin floor. According to the momentum balance equation, the external force allows the jump to occur for lower values of tailwater depth. Rajaratnam (1968) found that for a given classical jump and a roughness height of about $0.5 y_1$, the required tailwater depth is about $0.8 y_2$. But, the existence of such blocks might create a cavitation problem (as mentioned by Rajaratnam (1995) and Hager (1992)). Baffle walls may also be used with deeply submerged sluice gates to deflect the high velocity stream to the free surface. Wu and Rajaratnam (1995) mentioned that using baffles in deeply submerged flows for the aforementioned reason is not always successful. For some flow conditions, a reattached high velocity wall jet might form. This will be discussed in some detail later in this chapter.

More details about the evaluation of hydraulic jumps as energy dissipators are available in Elevatorski (1959), Peterka (1963), Rajaratnam (1967) and Hager (1992).

It seems from the above brief description of the different types of energy dissipators that they could be reclassified according to the types of jets used in them. All inflows to the different types of energy dissipators take the form of a turbulent jet whose momentum is partially dissipated in a mixing process. This turbulent jet might be a free jet, a surface jet, a wall jet, a radial jet, an oscillating jet, a counter-current jet, a split jet or a rotating jet. Plane free, surface and wall jets, are the most common types used in hydraulic engineering. In the following section, plane turbulent jets in deep tailwater will be presented. In Section 2.5, the behavior of turbulent jets in the close proximity of boundaries (either rigid boundaries or the free surface) will be discussed.

2.4 Plane Turbulent Jets in Deep Tailwater

2.4.1 Plane turbulent free jets

A plane turbulent free jet, as defined by Rajaratnam (1976), is a jet of water coming out of a plane slot into a large body of water. The height of the jet is $2b_0$ and its uniform velocity at the slot is U_0 . The free jet mixes violently with the surrounding fluid creating turbulence and the jet itself grows thicker (see Fig. 2.1). In the axial direction, the jet flow can be divided into two regions, the developing flow region and the developed flow region. The developing flow region is a wedge-like region with a constant velocity equal to U_0 . This wedge is known as the potential core and is surrounded by mixing layers on top and bottom. The length of the potential core is about $12b_0$. In the developed flow region, turbulence penetrates to the axis and as a result the maximum jet velocity, which is the centerline velocity, starts to decay. If $u = u(x,y)$ is the mean velocity in the axial direction, Förthmann (1936) found that the distributions of the axial velocity $u(y)$ with y , at different x -stations, were similar with u_m and b , at each station, chosen as the velocity and length scales respectively. The maximum velocity u_m is equal to the value of u at the centerline and b is the value of y where u is equal to half the maximum velocity u_m . In order to benefit from this property of similarity and to use it for predicting the mean velocity field in any particular problem, the velocity and length scales should be predictable. The equations of motion of the plane turbulent free jet in the axial direction were given by Rajaratnam (1976) as

$$u \frac{\partial u}{\partial x} + v \frac{\partial u}{\partial y} = \frac{-1}{\rho} \frac{\partial p}{\partial x} + \frac{1}{\rho} \frac{\partial \tau_x}{\partial y} \quad (2.2)$$

$$\frac{\partial u}{\partial x} + \frac{\partial v}{\partial y} = 0 \quad (2.3)$$

where u and v are the mean velocities in x and y directions respectively, p is the mean pressure at any point and τ_t is the turbulent shear stress. Rajaratnam (1976) integrated the above equations for a plane turbulent jet issuing into a large body of water and expanding under zero pressure gradient (i.e. $\partial p / \partial x = 0$). The integration results showed that the axial momentum of the jet is preserved. Rajaratnam (1976) also found that the maximum velocity u_m is inversely proportional to the square root of x ($u_m \propto x^{-1/2}$) and the jet half width b is directly proportional to x ($b \propto x$).

Förthmann (1936) conducted the first experimental study on plane turbulent free jets. The thickness of the jet $2b_0$ was equal to 30mm with a length equal to 650mm. These dimensions could assure two dimensional flow, especially in the central region of the flume. It was mentioned before that Förthmann's (1936) results showed similar distributions of the velocity profiles when u_m and b were chosen as the velocity and length scales respectively. Further measurements on plane free jets were made by Albertson et al. (1950), Zijnen (1958) and Heskestad (1965). Zijnen (1958) found that the similarity profile of the velocity distribution at any x -station could be represented by a Gaussian distribution as

$$u/u_m = \exp\left(-0.693\eta^2\right) \quad (2.4)$$

where η is equal to y/b . Dimensional analysis shows that the decay of the maximum velocity u_m in terms of that at the nozzle U_0 can be given as

$$\frac{u_m}{U_o} = \frac{C_1}{\sqrt{x/b_o}} \quad (2.5)$$

To evaluate C_1 , Abramovich (1963), using the experimental results of Förlthmann (1934) and others, found this constant to be 3.78 and Görtler (1942) found it to be 3.39. Also, this constant was given a value of 3.52 and 3.24 in the experiments conducted by Zijnen (1958) and Albertson et al. (1950). Rajaratnam (1976) concluded, based on the aforementioned values, that this constant could be given an average value of 3.50 for all practical purposes. For the evaluation of the length scale b , it was found that $b = C_2 \cdot x$ and the constant C_2 was given values of 0.097 and 0.114 by Abramovich (1963) and Görtler (1942), respectively. Rajaratnam (1976) commented that the value of 0.097 was found to be better than the value of 0.114 for the constant C_2 . He added that C_2 could be given a value of 0.10 for convenience.

If Q_o is the jet discharge at the nozzle and Q is the jet discharge at a distance x measured from the nozzle, experiments showed that Q/Q_o is greater than unity and assumes very large values for large values of x . The jet discharge increases because of the considerable amount of the surrounding fluid that the jet entrains as it travels forward. The discharge variation with distance could be described by the following equation

$$\frac{dQ}{dx} = 2v_e = 2\alpha_e u_m \quad (2.6)$$

where v_e is the entrainment velocity and α_e is the entrainment coefficient. The above equation shows that the entrainment velocity, at any x -station, is directly proportional

to the maximum velocity at this station. Using the value of $C_2 = 0.10$, Rajaratnam (1976) found that the entrainment coefficient α_e was equal to 0.053.

The discharge at any section Q , in terms of the discharge at the nozzle Q_0 , may be written as

$$\frac{Q}{Q_0} = C_3 \sqrt{x/b_0} \quad (2.7)$$

The coefficient C_3 was evaluated by Albertson et al. (1950) and was found to be equal to 0.44. If E is the kinetic energy of the flow at any section and E_0 is the value of E at the slot, Albertson et al. (1950) and Rajaratnam (1976), using $C_1 = 3.50$ and $C_2 = 0.10$, evaluated E/E_0 as

$$\frac{E}{E_0} = \frac{2.64}{\sqrt{x/b_0}} \quad (2.8)$$

2.4.2 Plane turbulent surface jets

Fig. 2.2 shows a plane turbulent surface jet of thickness b_0 and uniform velocity U_0 . The jet length and the ambient depth are assumed to be much larger than the slot width. As soon as the jet leaves the slot, a shear layer develops. The section at which the shear layer meets the water surface is the end of the potential core and downstream of this section the flow is developed. The length of the potential core is approximately $12b_0$.

The equations of motion for the plane turbulent surface jets could be written as

$$u \frac{\partial u}{\partial x} + v \frac{\partial u}{\partial y} = \frac{-1}{\rho} \frac{\partial p}{\partial x} + \frac{1}{\rho} \frac{\partial \tau_t}{\partial y} \quad (2.9)$$

$$\frac{\partial u}{\partial x} + \frac{\partial v}{\partial y} = 0 \quad (2.10)$$

where u and v are the velocities in the x and y directions, respectively, and τ_t is the turbulent shear stress.

The experimental observations of Rajaratnam (1969) and Vanvari and Chu (1974) showed that the velocity profiles $u(y)$ at different x -stations are similar. The maximum velocity u_m , at, or very close to, the free surface was chosen as the velocity scale and b , which is the vertical distance between the point of u_m and that of $0.5u_m$, was chosen as the length scale. Rajaratnam and Humphries (1984) mentioned that the similarity profile of the velocity distributions could be satisfactorily described by the exponential equation

$$u/u_m = \exp(-0.693\eta^2) \quad (2.11)$$

where η is equal to y/b . Integrating Eq. 2.9, with respect to y , for a plane turbulent surface jet with zero pressure gradient (i.e. $\partial p/\partial x = 0$), Eq. 2.9 could be reduced to

$$\frac{d}{dx} \int_0^{\infty} \rho u^2 dy = 0 \quad (2.12)$$

According to Eq. 2.12, the momentum flux of the surface jet in the longitudinal direction would be preserved.

Using simple dimensional considerations with the equations of motion in the integral form, it could be shown that $u_m \propto x^{-1/2}$ and $b \propto x$.

Experimental results of Vanvari and Chu (1974) and Rajaratnam and Humphries (1984) showed that the maximum velocity u_m , in terms of the uniform velocity at the nozzle U_o , could be described as

$$\frac{u_m}{U_o} = \frac{3.1}{\sqrt{x/b_o}} \quad (2.13)$$

They also showed that the length scale b grows linearly with the longitudinal distance measured from the virtual origin which is located roughly $10b_o$ behind the nozzle. The rate of growth was about 0.07 which is about 0.7 times that of the plane free jets. The length scale b , in terms of the slot width b_o , could be written as

$$\frac{b}{b_o} = 0.07 \frac{x}{b_o} = 0.07 \frac{\bar{x}}{b_o} + 0.7 \quad (2.14)$$

where \bar{x} and x are the longitudinal distances measured from the nozzle and the virtual origin, respectively. Also, based on the above results, the coefficient of entrainment α_e was estimated to be 0.037.

2.4.3 Plane turbulent wall jets

A plane turbulent wall jet, as defined by Rajaratnam (1976), is a jet of thickness b_o and uniform velocity U_o issuing from a rectangular slot tangentially to a flat plate submerged in a semi-finite expanse of the fluid (see Fig. 2.3). As soon as the jet leaves the slot, a shear layer develops on the fluid side while a boundary layer develops on the wall side. The section at which the two layers meet is the end of the

potential core and downstream of this section the flow is developed. Experimental observations of the variation of the axial velocity $u(y)$ with y , at different x -stations, showed that the velocity profiles have the same shape at the different stations. Förlthmann's (1936) data showed that, at any x -station, the axial velocity u increases from zero at the wall to reach its maximum value u_m at a distance of $y = \delta$ and then decreases to reach zero at large y . The boundary layer is the region between $y = 0$ and $y = \delta$. The region above the boundary layer is known as the free mixing region. To check for the similarity of the velocity profiles, the maximum velocity u_m was chosen as the velocity scale and the length scale b was taken as the distance, above the flume bed, at which the axial velocity $u = 0.5u_m$ and $\partial u/\partial y$ is negative. Using the experimental observations of Förlthmann (1936), Rajaratnam (1976) found that the velocity profiles were similar. Rajaratnam (1976) also wrote the equations of motion for the plane turbulent wall jets in the form

$$u \frac{\partial u}{\partial x} + v \frac{\partial u}{\partial y} = \frac{-1}{\rho} \frac{\partial p}{\partial x} + \frac{1}{\rho} \frac{\partial \tau}{\partial y} \quad (2.15)$$

$$\frac{\partial u}{\partial x} + \frac{\partial v}{\partial y} = 0 \quad (2.16)$$

In Eq. 2.15, $\tau = \tau_l + \tau_t$, where τ_l and τ_t are, respectively, the laminar and the turbulent shear stresses.

Rajaratnam (1976) integrated Eq. 2.15, with respect to y , for a plane turbulent wall jet with zero pressure gradient (i.e. $\partial p/\partial x = 0$). Hence, Eq. 2.15 could be reduced to the form

$$\frac{d}{dx} \int_0^{\infty} \rho u^2 dy = -\tau_o \quad (2.17)$$

where $\tau_o = \tau_o(x)$ is the wall shear stress at a distance x measured from the virtual origin. Eq. 2.17 shows a momentum decay in the longitudinal direction. The rate of momentum decay at any x -station is equal to the wall shear stress at that station. According to Eq. 2.17, if the bed shear stress is to be neglected in a particular problem, the momentum flux in the longitudinal direction would be preserved. Using dimensional considerations along with the equations of motion in the integral form, Rajaratnam (1976) found that $u_m \propto x^{-1/2}$, $b \propto x$ and $\tau_o \propto 1/x$.

Concerning the experimental results, Förthmann (1936) was the first to conduct experiments on plane turbulent wall jets. The slot width and length were 30 mm and 650 mm, respectively. He found that the velocity distributions are similar for x greater $20b_o$. Other experiments on turbulent plane jets have been conducted by Zerbe and Selna (1946), Sigalla (1958), Myers et al. (1961), Schwarz and Cosart (1961). Myers et al. (1961) and Schwarz and Cosart (1961) which showed that the velocity distribution in the boundary layer could be described by a power law with an exponent of $1/14$. Moreover, Myers et al. (1961) found that the velocity distribution in the boundary layer could be represented by the logarithmic law in the form

$$u/u_* = 5.6 \log(yu_*/\nu) + 4.9 \quad (2.18)$$

where $u_* = (\tau_o/\rho)^{0.5}$ is the shear velocity. Other values of the coefficients in Eq. 2.18 were reported by Mathieu and Tailland (1963). Rajaratnam (1976) mentioned that the velocity distributions of the entire wall jet, at different x -stations, were found to be

similar in the experimental studies performed by Förthmann (1936), Sigalla (1958), Myers et al. (1961) and Schwarz and Cosart (1961). An empirical equation was given by Verhoff (1963) to describe the similarity profile as

$$u / u_m = 1.48\eta^{1/7} [1 - \text{erf}(0.68\eta)] \quad (2.19)$$

Rajaratnam and Subramanya (1968), using most of the available observations on the decay of the maximum velocity along with those of Rajaratnam (1965), found that the maximum velocity u_m in terms of that at the nozzle U_o could be described by the following equation

$$\frac{u_m}{U_o} = \frac{3.5}{\sqrt{x/b_o}} \quad (2.20)$$

Rajaratnam (1976), using the observations of Sigalla (1958), Schwarz and Cosart (1961), Myers et al. (1961), found that the length scale b_o grows linearly with the longitudinal distance measured from the virtual origin, which is located roughly $10b_o$ behind the nozzle, as

$$\frac{b}{b_o} = 0.068 \frac{x}{b_o} = 0.068 \frac{\bar{x}}{b_o} + 0.68 \quad (2.21)$$

where \bar{x} and x are the longitudinal distances measured from the nozzle and the virtual origin, respectively. The rate of growth of the length scale was found to be about 0.068 which is very close to that of the surface jet but only 0.7 times that of the free jet.

Shear stress observations of Myers et al. (1961) showed that the variation of the skin friction coefficient $C_f = \tau_o/\rho U_o^2/2$ could be expressed by the equation

$$C_f = \frac{\tau_o}{\rho U_o^2/2} \approx \frac{0.20}{(x/b_o).R^{1/12}} \quad (2.22)$$

where τ_o is the wall shear stress and $R = U_o b_o/\nu$ is the Reynolds number.

Based on the above relations of the velocity and length scales and the similarity profile of the velocity distribution, Rajaratnam (1976) found that the forward flow discharge Q at any section, in terms of that at the nozzle Q_o , may be written as

$$Q/Q_o = 0.248\sqrt{\bar{x}/b_o} \quad (2.23)$$

Using Eq. 2.20 with Eq. 2.23, it could be shown that the entrainment coefficient α_e is equal to 0.035, which is very close to that of the surface jet but only about 0.7 that of the free jet.

Regarding the developing region, Rajaratnam (1976) mentioned that the growth of the boundary layer δ could be described by the equation

$$\delta/\bar{x} = 0.37/(U_o \bar{x}/\nu)^{1/5} \quad (2.24)$$

Assuming that the mixing region spreads inwards at an angle of 5° , Rajaratnam (1976) found that the length of the potential core could be described by the equation

$$0.0875\left(\frac{\bar{x}_o}{b_o}\right) + 0.37\left(\frac{\bar{x}_o}{b_o}\right)^{4/5} \cdot \frac{1}{R^{1/5}} = 1.0 \quad (2.25)$$

Rajaratnam (1965) showed also that, in the developing region, the flow rate Q in terms of the flow rate at the slot Q_o could be written as

$$\frac{Q}{Q_o} = \left[1 + 0.04 \frac{\bar{x}}{b_o} + 0.0046 \left(\frac{\bar{x}}{b_o} \right)^{0.8} \right] \quad (2.26)$$

Also, the entrainment velocity v_e could be expressed as

$$v_e = \frac{dQ}{d\bar{x}} = 0.04U_o + 0.0037 \frac{U_o}{\left(\bar{x}/b_o\right)^{0.2}} \quad (2.27)$$

Neglecting the second term on the R.H.S of Eq. 2.27, the entrainment coefficient α_e is equal to 0.04.

2.5 Turbulent Jets in Close Proximity of Boundaries

In this section, the differences between the classical turbulent jets in deep tailwater and those that issue in the close proximity of boundaries are revealed. For example, it might be reasonable to assume a constant momentum flux in turbulent jets in deep receiving water bodies (Schlichting (1960), Rajaratnam (1976)). But, it would be unrealistic, as will be explained in the next chapters, to assume that the momentum flux is preserved in a turbulent jet in shallow tailwater. Following are some applications where turbulent jets issue close to rigid boundaries or to the free surface.

Johnson (1990) mentioned that recent shallow-water discharge observations indicated that the classical integral method of analysis, which has been successfully applied to a range of unconfined and partially confined receiving water situations (see for example Rajaratnam (1976)), has to be treated with caution. This caution results from the fact that in shallow tailwaters there is a possibility of reattachment of the jet to different boundaries (Coanda effect) and the presence of internal jumps in some outfall flow patterns.

Johnson (1990) added that the general near-field characteristics of jets entering relatively deep tailwater are reasonably understood and could be represented by using the integral method of analysis where Reynolds stress closure was provided by some suitable entrainment assumptions. The close proximity of both the bed and the free surface has a great influence on the near field flow patterns in cases of buoyant (density of the jet is different from density of the receiving water) and nonbuoyant jets (jet and receiving water have the same density) entering shallow tailwater. To varying degrees, the presence of induced eddies, internal jumps, and significant pressure variations related to water surface oscillations all serve to complicate the fundamental entrainment processes that are commonly associated with turbulent jets entering unconfined environments. These additional processes are usually unsteady, unstable, and produced by nonlinear effects, which indicate that their mathematical models pose a considerable challenge. Recent research has shown that within certain parameter ranges in shallow tailwater conditions, existing theory and analysis for fully and partially unconfined conditions can be used. In other ranges, however, such analysis is uncertain and meaningful predictions can only be clarified through the analysis of data from experimental studies that quantitatively describe the aforementioned additional mixing processes.

Johnson (1990) studied experimentally a plane jet emerging from a slot of width b_0 with velocity U_0 . The centerline of the slot was a distance Z_0 above the flume

bed. The tailwater depth y_t in the channel was such that the free surface was $(y_t - Z_o)$ above the slot centerline. Johnson (1990) mentioned that when the jet emerges from a horizontal slot into a shallow tailwater it would, in general, curve either towards the channel bed or towards the free surface. It has been necessary in some engineering conditions to define the conditions under which the jet would deflect to the surface rather than the channel bed and vice versa. Dimensional analysis showed that this feature of the flow is dependent on three non-dimensional parameters which are the Froude number $U_o/(gh_o)^{0.5}$, the offset ratio Z_o/b_o and the submergence ratio $(y_t - Z_o)/b_o$.

The experimental observations of Coates (1976) showed, as mentioned by Johnson (1990), that for a given Froude number and offset ratio, if the submergence depth is gradually increased, the jet would change from a surface jet to a bed jet at a particular value of the submergence ratio. For the same offset ratio but at a different Froude number, the change from surface-type jet to bed-type jet would occur at a different submergence ratio.

Johnson and Halliwell (1986) argued that the above simple description is not complete. They noticed that at large values of the submergence ratio, the Coanda effect was apparent and the jet attached to the channel bed. Decreasing the submergence ratio, the jet remained as a bed jet until the submergence ratio reached a particular value where a distinct changeover occurred and the jet attached to the free surface rather than the bed. The jet remained attached to the free surface with further reduction of the submergence ratio. On the other hand, when they repeated their observation while increasing the submergence ratio gradually, they found that the changeover condition from surface jet to bed jet occurred at larger values of the submergence ratio. Further study showed that there was indeed a region where the jet could attach either to the bed or to the free surface for the same non-dimensional flow-defining parameters. This phenomenon was anticipated by Bourque and Newman (1960). They worked on a two-dimensional jet emerging from a slot and

reattaching to an adjacent flat plate. Bourque and Newman (1960) commented that the flow exhibited a hysteresis phenomenon.

Bakhmeteff and Feodoroff (1957), as mentioned by Johnson (1990), investigated the plane turbulent jet problem experimentally. They described the various flow patterns that were observed as the tailwater depth increases. They worked on the whole range of submergence starting from the free flow conditions till the jet was totally submerged. Five discharge regimes were observed: free nappe flow, plunging repelled jump, direct repelled undular jump, springing vein, and tranquil flow. They explained that these regimes were dependent on the kineticity ($\lambda = q^2 g^{-1} b_o^{-3}$), which is a form of the Froude number. For plunging repelled jump ($\lambda = 3-4$), undular jump ($\lambda = 1-3$), and tranquil flow ($\lambda < 1$).

Rajaratnam and Subramanya (1968) studied, experimentally, the diffusion characteristics of a submerged plane turbulent jet issuing from a nozzle located over an abrupt drop in the bed. They studied in detail the growth of the wall jet beyond the impingement region. They concluded that, after a certain distance downstream of the reattachment line, the velocity profiles were similar and the similarity profile was the same as that of the classical wall jet. They found that beyond a certain point the maximum-velocity decay profiles were similar to the classical wall jet decay. They also found that when the jet issued tangential to the bed, it behaved in the same way as the classical wall jet regarding the velocity profiles and the decay of the maximum velocity. The only difference was the length scale which grew at a faster rate than that of the classical wall jet. Also, Rajaratnam and Subramanya (1968) measured the bed shear stress and found that the shear stress distributions were similar when represented in a dimensionless form.

Dodds (1960), as mentioned by Sawyer (1962), introduced a simple model of the cavity flows of a curved two-dimensional reattaching turbulent jet using plausible assumptions regarding the bifurcation of the jet at reattachment. He had expressions relating the cavity pressure and cavity length to the jet momentum per unit jet width and the geometry of the boundaries. A spread parameter, which is a measure of the rate of spread, was involved in these expressions and was connected with the entrainment properties of the inner edge of the jet.

Sawyer (1962) conducted an experiment to determine the flow pattern, the cavity pressure and cavity length for a flow under a curved two-dimensional turbulent jet discharging parallel to a flat plate at some height above the bed. This work, as mentioned by Sawyer, was performed to give some experimental backing to the simple model proposed by Dodds (1960) and Bourque (1959) and to find the value of the spread parameter involved in their expressions. Sawyer (1962) mentioned that a stable flow pattern was achieved and the mechanism of that stable flow pattern was that the entrainment of fluid, by the turbulent jet, near the bed caused a pressure difference across the jet, curving the jet towards the bed. On striking the bed, the jet bifurcated. The reverse flow, or the volume gained by the cavity, balanced the volume entrained, or the volume lost from the cavity. Sawyer (1962) commented that this balance, between the quantity of air entrained by the jet from the cavity and the quantity of reversed flow at reattachment, was not exact. The experiments showed that there was a secondary flow that fed air from outside into the cavity. However, near the center of the slot length, it was estimated that this lack of balance was negligible and the flow approached very closely to two-dimensional conditions.

Also, Sawyer (1962) expressed the curvature of the jet as the ratio of the pressure difference across the jet to the jet momentum. By determining the geometry of the jet centerline, assumptions regarding the jet velocity profile and rate of spread

(as measured by the spread parameter) led to an expression for the amount of air entrained by the jet along its inner edge, which was taken to be the volume flow fed back into the cavity at reattachment. Hence, the division of the volume flow of the jet at reattachment was determined. Assumptions regarding the velocity profile shapes of the initial reversed flow and the initial attached downstream flow, with the aid of a momentum balance equation at reattachment point, were used to determine the division of momentum flow at reattachment. Concerning the velocity profile, Sawyer assumed that the velocity profile of the jet was similar to that of a two-dimensional plane jet. Sawyer also used Dodd's (1960) assumption that the initial reversed flow and initial downstream flow had velocity profiles similar to that of a half Görtler (1942) jet profile. It was assumed also that the pressure inside the cavity was constant so that there was a constant pressure difference acting across the jet.

Sawyer (1962) concluded that the variations of the pressure difference across the jet and the length of the cavity with the height of slot from the bed agreed quite well with those predicted by Dodds (1960) analysis in that they were consistent with a choice of spread parameter which was constant at the value of 15. Sawyer also commented that the value of the spread parameter for which the analysis was in best agreement with the results was not, in fact, the true value of the spread parameter for the curved jet. The discrepancy between the two values was a measure of the collective errors in the various assumptions made in the analysis. Thus, the choice of the spread parameter to be 15 was considered, by Sawyer, to be the fixing of a convenient empirical constant in order that the results could be applied to give reasonably accurate predictions of the cavity length and cavity pressure. Sawyer (1962) also mentioned that the difference in the rate of entrainment between the inner and outer edges of the jet due to curvature effects did not affect the growth rate of the jet as a whole. The difference in the entrainment rates was responsible only for the locus of the maximum velocity not to be a streamline.

Reichardt (1942) found experimentally, as mentioned by Sawyer (1962), that the value of the spread parameter for the two-dimensional plane jet was 7.67. Sawyer (1962) expected that the value of this parameter relevant to entrainment along the inner edge of the curved jet would be higher than 7.67 due to suppression of turbulent mixing, as a consequence of curvature.

Townsend (1956) mentioned that the mechanism of entrainment was intimately connected with the growth of turbulent shear flow, and it was possible to use entrainment properties in the setting up of mean flow equations for such flows. It was mentioned also by Sawyer (1962) that the entrainment properties of a curved two-dimensional turbulent jet were expected to differ from those of the corresponding plane jet. Momentum transport arguments indicated that the entrainment along the inner edge was reduced whereas entrainment along the outer edge was enhanced. Sawyer (1962) also argued that the curvature of the jet enhanced the mixing properties of the jet. He described a small parcel of fluid that is transported from a higher velocity region to a lower velocity region nearer to the outside edge of the jet. Sawyer argued that if this parcel of fluid arrived with some excess velocity over its surroundings, it would be subjected to a greater centrifugal force than its surroundings. But its surroundings were subjected to centrifugal forces and pressure forces which just balanced in the mean. Hence it was expected that the parcel of fluid would experience a total force tending to move it further outwards, which implied a more vigorous mixing than that which occurred with no curvature. A reverse argument holds for the mixing at the inner edge where mixing is expected to be relatively weak.

If a turbulent wall jet is obstructed by a baffle wall, it could either be deflected to the free surface or, for some flow conditions, it might reattach to the flume bed.

Wu and Rajaratnam (1995) studied the effect of two dimensional baffles on submerged hydraulic jumps. They classified the flow into two different stable flow states, the deflected surface jet state and the reattaching wall jet state. They also stated that, in the deflected surface jet state, the main flow is deflected to the water surface to form a surface jet downstream of the baffle, thereby deflecting the high velocity supercritical stream away from the bed to the surface to protect the channel bed. On the other hand, the deflected jet might induce a wave attack on the banks of the downstream channel. In the reattaching wall jet state, the main flow passes over the baffle to impinge and reattach to the bed immediately downstream the baffle.

Wu and Rajaratnam (1995) also added that, for a given tailwater depth and baffle position, two critical baffle heights exist (h_{c1} and h_{c2}) which are independent of the gate opening or gate Froude number. If the baffle height is smaller than h_{c1} , the flow will be in the stable reattaching wall jet state. If the baffle height is larger than h_{c2} , the flow will be in the stable deflected surface jet state. If the baffle height is between h_{c1} and h_{c2} , the flow can be stable in either state, depending on the initial flow state, and the flow can change from one state to the other by external interference. For the relation between the two critical depths h_{c1} and h_{c2} Wu and Rajaratnam (1995) stated that h_{c1} was about 0.02 of the tailwater depth y_t and the regression equation for h_{c2} could be written as

$$\frac{h_{c2}}{y_t} = 0.0382 - 0.0078 \left(\frac{x_o}{y_t} \right) + 0.0261 \sin^2 \left(\frac{x_o}{y_t} \right) \quad (2.28)$$

where x_o is the distance from the baffle front to the gate and y_t is the tailwater depth.

Based on the results of detailed measurements, Wu and Rajaratnam (1995) concluded that, in the region upstream of the baffle, the forward velocity profiles were found to be similar in their lower part and could be described by the

corresponding plane turbulent wall jet curve. These velocity profiles were not similar in the upper part due to the effect of the strong surface eddy formed upstream of the baffle. In the deflected surface jet state, the maximum velocity decayed continuously to reach its minimum value somewhere below the water surface and then speeded up, due to the existence of a surface hump, till it hit the water surface. After this, the maximum velocity in the surface jet decayed continuously. In the reattaching wall jet state, the maximum velocity decayed all the way from the gate. For the same boundary conditions, the decay of the maximum velocity was faster in the deflected surface jet state than that of the reattaching wall jet state. The scales for the surface jet (the maximum surface velocity, the surface hump height, the location of the maximum surface velocity and the location of the top of the surface hump) were generally affected by the following four variables: tailwater depth, gate Froude number, baffle location and baffle height.

For turbulent jets discharged from slots or orifices in walls into large ambients at rest, it has been generally assumed (Albertson et al. (1950), Schlichting (1960), Rajaratnam (1976)) that the momentum flux would be preserved. In some experimental investigations (Miller and Comings (1957); Goldschmidt and Eskinazi (1966); Heskestad (1965) and Kotsovinos (1975)), it has been noticed that the momentum flux decayed to some extent at large distances from the origin of the jets.

Based on an approximate integral analysis, Kotsovinos (1978) developed an equation to describe the variation of the momentum flux with the longitudinal distance from the nozzle producing the jet. He estimated the various terms in the momentum balance equation and concluded that the induced outer flow was the main reason of the momentum decay in plane jets out of a wall. Discussing Kotsovinos's results, Schneider (1985) commented that Kotsovinos's (1978) approximation breaks down with infinite distances from the orifice. He added that this breakdown was due

to the fact that Kotsovinos (1978) did not consider the reactive effect of the decrease of the momentum flux on the induced flow. Kotsovinos's (1978) momentum decay equation was given as

$$\frac{M(x)}{M_o} = 0.983 - 0.06931 \ln\left(\frac{x}{6b_o}\right) \quad (2.29)$$

Schneider (1985) noticed that in turbulent jets the assumption of constant momentum flux is in apparent agreement with the experimental results of Bradbury (1965). However, other researches showed that the theory and the experimental results were not in agreement. Miller and Comings (1957) showed that the maximum velocity decay was slightly larger than that predicted by the classical boundary layer theory whereas the jet width was in agreement with theory. Schneider (1985) commented that the above observations suggest that the momentum decays slowly with distance from the orifice. It should be noted, as mentioned in Schneider (1985), that Miller and Comings (1957) performed their experiments with a nozzle located in a wall perpendicular to the jet axis, while such wall did not exist in Bradbury's (1965) experiments which indicated that the existence of the wall might be the reason for such momentum decay. The problem became even more controversial when Hussain and Clark (1977) concluded that the total momentum flux (including the mean momentum flux due to velocity fluctuations) increased with increasing distance and was not completely balanced by the mean static pressure integral.

Schneider (1985) studied laminar and turbulent plane and axisymmetric jets emerging from orifices in plane or conical walls to determined the entrainment of the momentum and the discharge into a jet. In that study the problem of the jet flows at large distances from an orifice in a wall was studied by coupling the jet flow with the

induced outer flow. The momentum flux in the jet boundary layer was considered to be a slowly-varying function of the distance, and the coupling is established by accounting for the momentum flux from the induced outer flow into the jet (entrainment of momentum). Schneider (1985) benefited from the observations of Taylor (1958), Wygnanski (1964), Rubin and Falco (1968) and Kraemer (1971) who studied the induced outer flows with and without walls. It could be concluded that the streamlines of the outer flow enter the turbulent jet at an angle of $0.5\theta_w$ where θ_w is the angle the wall makes with the jet axis (θ_w would be $\pi/2$ in case of an infinite plane wall perpendicular to the jet axis). For turbulent (plane or axisymmetric) flow, the analysis provided answers to the questions concerning the invariance of the momentum flux, and unveiled the source of previous discrepancies. Schneider (1985) found that in turbulent jets out of a wall, the axial velocity decayed more rapidly than that predicted by the classical boundary layer solutions. Also, the momentum flux vanished with infinite distance from the orifice. Schneider's analysis explained the reason of the discrepancies found in the previous experimental data on turbulent jets. For a plane turbulent jet out of a wall, Schneider's analysis predicted that the momentum M would slowly vary as

$$\frac{M(x)}{M_o} = \left(\frac{x_o}{x} \right)^{\frac{\alpha_e}{2} \cdot m} \quad (2.30)$$

where α_e is the entrainment coefficient. Schneider (1985) mentioned that the entrainment coefficient is equal to 0.085 in plane turbulent jets as found by Tollmien (1926) and Reichardt (1942), m is a constant equal to $\cot(\theta_w/2)$ for plane turbulent

jets and x_0 is a constant of integration. For the particular case of a plane turbulent jet issuing from a vertical upstream wall, $m = 1$ and Eq. 2.30 becomes

$$\frac{M(x)}{M_0} = \left(\frac{x_0}{x} \right)^{\frac{\alpha_e}{2}} \quad (2.31)$$

Swan Jr. et al.(1989) studied the variation of momentum and mass fluxes as well as the growth for plane turbulent surface jets with limited depth of tailwater. They conducted 10 experiments to study the effect of the finite depth of tailwater on the characteristics of the surface jet and to observe the variation of the momentum and volume fluxes and the breakdown of the surface jet due to the limited depth of the ambient. They also used the experimental results of Vanvari and Chu (1974) and Rajaratnam and Humphries (1984). Their results showed a momentum decay and a breakdown (or variation from that of jets in infinite ambient) in the velocity and length scales due to the jet confinement. The study of Swan Jr. et al. (1989) provided a general understanding of the problem of surface jets with a finite depth of tailwater. However, their analysis did not consider the adverse pressure gradient in the momentum balance.

2.6 References

- Abramovich, G. N. (1963). "The theory of turbulent jets." English translation published by M.I.T. Press, Massachusetts, 671p.
- Albertson, M. L., Dai. Y. B., Jensen, R. A. & Rouse, H. (1950). "Diffusion of submerged jets." Trans. ASCE. 115, 639-664.
- Bakhmeteff, B. A., and Feodoroff, N. V. (1957). "Patterns of flow through horizontal slits." 19th Int. Congress Appl. Mech., 1: 1 (1957).

- Bourque, C. (1959). M.Sc. Thesis, University of Laval. Also Aero. Quart. 11, p. 201.
- Bourque, C., and Newman, B. G. (1960). "Reattachment of a two-dimensional, incompressible jet to an adjacent flat plate." Aero. Quart. 11, 201.
- Bradbury, L. J. S. (1965). "The structure of a self-preserving turbulent plane jet." J. Fluid Mech. 23, pp. 31-64.
- Chamani, M. (1997). "Skimming flow in a model of a stepped spillway." Ph.D. Thesis, University of Alberta.
- Coates, A. D. (1976). "The numerical and experimental studies on the dynamics of fluids." Ph.D. Thesis, Heriot-Watt University, Edinburgh.
- Dodds, J. I. (1960). Ph.D. Thesis, Cambridge University.
- Elevatorski, E. A. (1959) "Hydraulic energy dissipators." McGraw-Hill, New York.
- Förthmann, E. (1936). "Turbulent jet expansion." English translation NACA. TM-789. (Original Paper in German, 1934. Ing. Archiv., 5).
- Görtler, H. (1942). "Berechnung von Aufgaben der freien Turbulenz auf Grund eines neuen Näherungsansatzes. ZAMM, 22, pp. 244-254.
- Goldschmidt, V., and Eskinazi, S. (1966). "Two phase turbulent flow in a plane jet." Trans. ASME, Series E, J. Appl. Mech., 33(4), 735-747.
- Hager, W. H. (1992). "Energy dissipators and hydraulic jump." Kluwer Academic Publishers, Dordrecht, 288p.
- Heskestad, G. (1965). "Hot wire measurements in a plane turbulent jet." Trans. ASME, Series E, J. Appl. Mech., 32(4), 721-734.
- Hussain, A. K. M. F. and Clark, A. R. (1977). "Upstream influence on the near field of a plane turbulent jet." Phys. Fluids 20, 1416-1426.
- Johnson, A. J., and Halliwell, A. R. (1986). "Jet behavior in shallow receiving water." Proc. Instn. Civ. Engrs., Part 2, 81:549.

- Johnson, J. A. (1990). "Jet outfalls entering shallow tailwaters." Encyclopedia of Fluid Mechanics (1986-1993), Vol. 10 (Surface and ground water flow phenomena), Chapter 7, pp. 267-294.
- Koch, K. (1968). "Die gegenseitige Strahlablenkung auf horizontaler Sohle." Bericht 18, Versuchsanstalt für Wasserbau, Technische Universität München: München.
- Kotsovinos, N. E. (1975). "A study of the entrainment and turbulence in a plane turbulent jet." W. M. Keck Lab. Hydr. Water Resources, Calif. Inst. Tech. Rept. KH R-32.
- Kotsovinos, N. E. (1978). "A note on the conservation of the axial momentum of a turbulent jet." J. Fluid Mech., 87(7), pp. 55-63.
- Kraemer, K. (1971). "Die Potentialströmung in der Umgebung von Freistrahlen." Z. Flugwiss. 19, pp. 93-104.
- Mathieu, J. and Tailland, A. (1963). "Etude d'un jet plan dirigé tangentiellement à une paroi" C. R., Acad. Sci., Paris, 257, pp. 44-47.
- Miller, D. R., and Comings, E. W. (1957). "Static pressure distribution in the free turbulent jet." J. Fluid Mech., 3(10), pp. 1-16.
- Myers, G. E., Schauer, J. J and Eustis, R. H. (1961). "The plane turbulent wall jet." I, Jet development and friction factor, Tech. Rep., 1, Department of Mechanical Engineering, Stanford University. (Also published in Trans. ASME., J. Basic Eng., 1963).
- Peterka, A. J. (1963). "Hydraulic design of stilling basins and energy dissipators." Engrg. Monograph 25, U.S.D.I. Bureau of Reclamation: Denver, Col.
- Rajaratnam, N. (1965). "Flow below a submerged sluice gate as a wall jet problem." Proc. 2nd Aus. Conf. on Hydraulics and Fluid Mechanics, Auckland, New Zealand, pp. 131-146.

- Rajaratnam, N. (1967). "Hydraulic jumps.", *Advances in Hydrosience*, Vol. 4, pp. 198-276.
- Rajaratnam, N. (1968). "Hydraulic jumps on rough beds." *Trans. Engineering Institution of Canada* 11(A-2), pp. 1-8.
- Rajaratnam, N. (1969). "Diffusion of a supercritical stream on a stagnant pool." *Trans. Engng. Inst. Of Canada*, Vol. 12, No. A-1, pp. 1-5.
- Rajaratnam, N. (1976). *Turbulent Jets*. Elsevier Publishing Co, The Netherlands, 304p.
- Rajaratnam, N. (1995). "Almanac of energy dissipation mechanisms." *IAHR, Hydraulic Structures Design Manual*, 9, Energy Dissipators, Chapter 3, pp. 23-42.
- Rajaratnam, N. and Subramanya, K. (1968). "Plane turbulent reattached wall jets." *J. Hydraulics Div., ASCE*, Vol. 94, No. HY1, pp. 95-112.
- Rajaratnam, N., and Humphries, J. A. (1984). "Turbulent non-buoyant surface jet." *J. Hydr. Res.*, 22(2), pp. 103-115.
- Reichardt, H. (1942). "Gesetzmässigkeiten der freien Turbulenz." *VDI-Forschungsheft*, p. 414.
- Rubin, S. G. and Falco, R. (1968). "Plane laminar jet. *AIAA J.* 6, pp. 186-187.
- Sawyer, R. A. (1962). "The flow due to a two-dimensional jet issuing parallel to a flat plate." *J. Fluid Mech.* 9(4), pp. 543-560.
- Schlichting, H. (1960). "Boundary layer theory." 4th Edn. McGraw-Hill: New York.
- Schneider, W. (1985). "Decay of momentum flux in submerged jets." *J. Fluid Mech.*, 154(5), pp. 91-110.
- Schwarz, W. H. and Cosart, W. P. (1961). "The two-dimensional turbulent wall jet." *J. Fluid Mech.*, 10, pp. 481-495.
- Sigalla, A. (1958). "Measurements of skin friction in a plane turbulent wall jet." *J. R. Aeronaut., Soc.* 62, pp. 873-877.

- Swean Jr, T. F., Ramberg, S. E., Plesniak, M. W. Stewart., M. B. (1989). "Turbulent surface jet in channel of limited depth." J. Hydr. Engrg., ASCE, 115(12), pp. 1587-1606.
- Taylor, G. I. (1958). "Flow induced by jets." J. Aero. Sci. 25, pp. 464-465.
- Thoma, D. (1930). "Die Rückstromdrossel." VDI-Zeitschrift 74:1098.
- Tollmien, W. (1926). "Berechnung turbulenter Ausbreitungsvorgänge." Z. angew. Math. Mech. 6, pp. 468-478; [English Transl. NACA TM 1085 (1945)].
- Townsend, A. A. (1956). "The structure of turbulent shear flow." Cambridge University Press, 315 pp.
- Uyumaz, A. (1988). "Scour downstream of vertical gate." J. Hydr. Engrg., Vol. 114, No. 7, pp. 811-816.
- Vanvari, M. R., and Chu, V. H. (1974). "Two-dimensional turbulent surface jets of low Richardson number." Tech. Report No. 74-2 [FML], Fluid Mech. Lab., Dept. of Civ. Engrg. and Appl. Mech., McGill Univ., Montreal, Canada.
- Verhoff, A. (1963). "The two-dimensional turbulent wall jet with and without an external stream." Rep. 626, Princeton Univ.
- Vischer, D. L., and Hager, W. H. (1995). "Energy dissipators." IAHR, Hydraulic Structures Design Manual, 9, Chapter 2, pp. 9-22.
- Wu, S. and Rajaratnam, N. (1995). "Effect of baffles on submerged flows" J. Hydr. Engrg., ASCE, 121(9), pp. 644-652.
- Wyganski, I. (1964). "The flow induced by two-dimensional and axisymmetric turbulent jets issuing normally from an infinite plane surface." Aeron. Q. 15, pp. 373-380.
- Zerbe, J. and Selna, J. (1946). "An empirical equation for the coefficient of heat transfer to a flat surface from a plane heated air jet directed tangentially to the surface." NACA, TN, 1070.

Zijnen, B. G. Van der Hegge (1958). "Measurements of the velocity distribution in a plane turbulent jet of air." Appl. Sci. Res., Sect. A, 7, pp. 256-276.

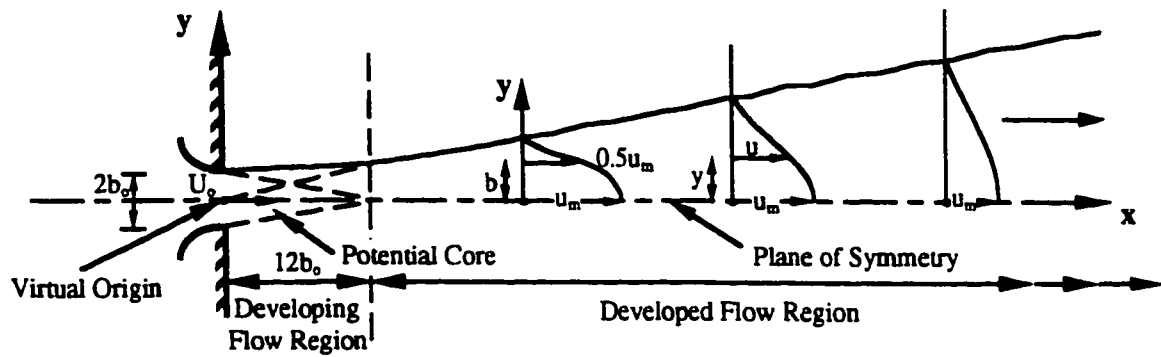


Fig. 2.1 Definition sketch of plane turbulent free jets

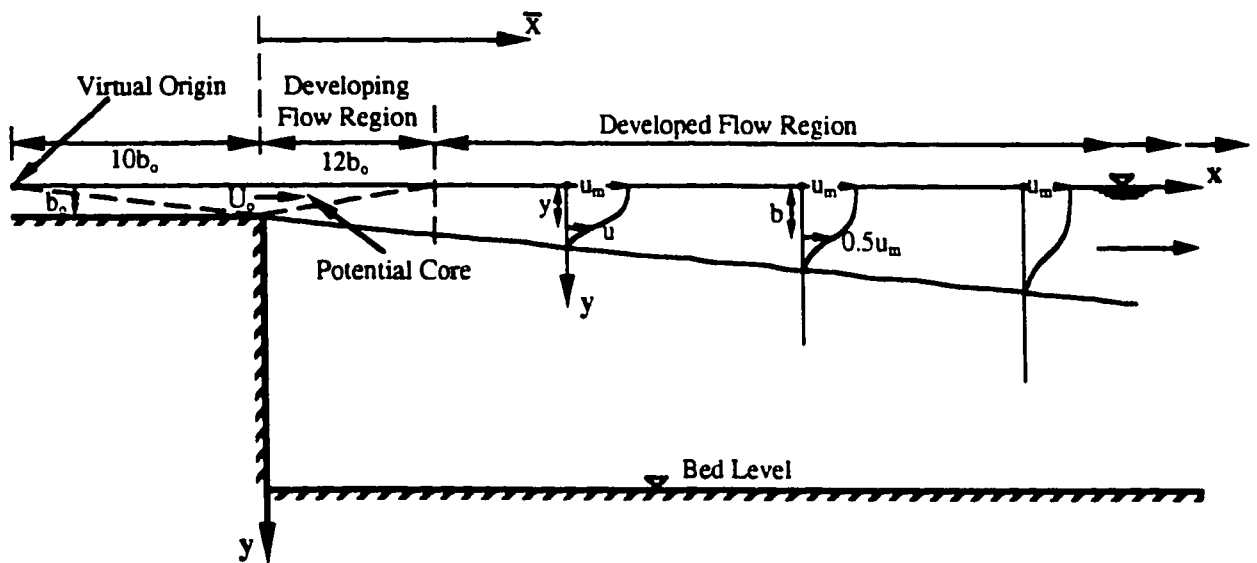


Fig. 2.2 Definition sketch of plane turbulent surface jets

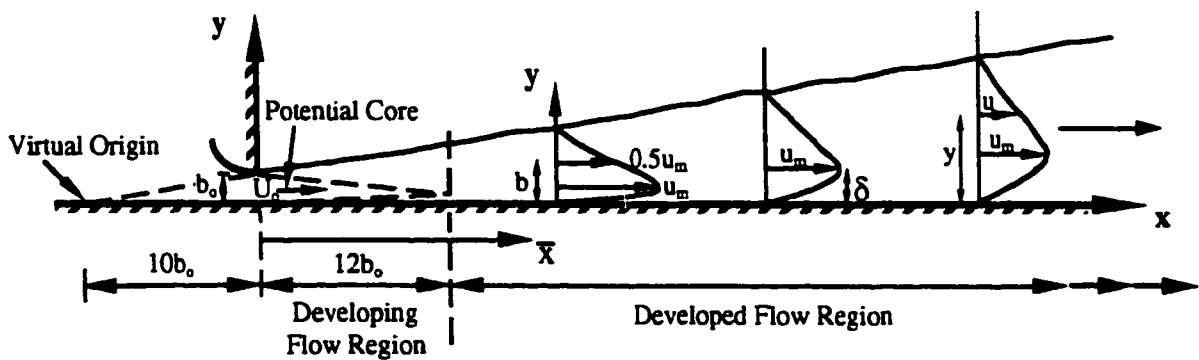


Fig. 2.3 Definition sketch of plane turbulent wall jets

Chapter 3

Experimental Arrangement and Instrumentation Techniques

3.1 Introduction

This chapter describes the laboratory equipment and the experimental procedure used with the double-leaf gate dissipator, the plane turbulent surface jets and the plane turbulent wall jets. The experimental study was carried out at the T. Blench Hydraulics Laboratory, University of Alberta.

3.2 Experimental Arrangement

3.2.1 The flume

All of the experiments were conducted in a straight rectangular flume, 0.446 m wide, 0.60 m deep and 7.6 m long, with a smooth aluminum bottom and plexiglas sides (see Fig. 3.1). The flume was supported on a pivot and a scissors jack which was operated manually to adjust the slope of the flume in the longitudinal direction. A head gate installed at the flume entrance was used to create the required flow. In the double leaf gate dissipator, the head gate was split into two leaves. The upper leaf was located upstream of the lower one to create an opening which produced an inclined jet. A single-leaf head gate was used to create the plane surface and wall jets. Streamlined lip(s) were fixed on the gate to produce a supercritical stream with a thickness equal to the gate opening, b_0 . A tail gate, installed at the downstream end of the flume, was used to control the tailwater depth in the flume. False floors, with the same width as the flume, were used in the surface jet experiments to change the offset distance and to create the required offset ratio. A traverse system was mounted on the flume to hold the different probes and the point gauge. It could be moved manually in

the longitudinal, as well as in the transverse, direction. A manometer board was fixed on one of the flume side walls and was connected to the probe(s) in use.

Water was supplied to the head tank of the flume from an underground sump. The head tank was 3.40 m long and the width of the head tank decreased gradually from 1.20 m, at the upstream end, to 0.446 m (the flume width) as shown in Fig. 3.1. Two pumps were used to supply the head tank with the required discharge. The discharge was measured by a magnetic flow meter located in the supply line.

3.2.2 Pressure transducers

Variable reluctance differential pressure transducers (Validyne model DP45-16 Northridge, Calif) were used in the experiments to measure the pressure difference. The range of these transducers was ± 1.4 inch (35.56 mm) of water. Thus, the maximum velocity that these transducers could measure was 0.83 m/s. The accuracy of these transducers, as given by the manufacture, was 0.25% of the full scale (2.8 inches) which is ± 0.1778 mm of water or 0.059 m/s. Validyne CD379 portable digital transducer demodulators were used to display the readings of the pressure transducers. The signals from the demodulators were then fed into a computer equipped with a data acquisition system for further analysis.

The transducers were calibrated by applying known heads of water of up to ± 1 inch (± 25.4 mm) with 0.1 inch increments of the pressure head. The adjustment of the demodulators was dependent on the type of the probe connected to the transducer. In case of a Prandtl tube, the positive side of the transducer was connected to the total head tube and the negative side was connected to the static head tube. With this connection the demodulator would show positive readings all the time. Hence, the demodulator was adjusted, using the zero and the span screws on the demodulator, to give zero volt for zero pressure head and +1 volt for +1 inch pressure head. With the Pitch probe (three holes probe) the situation was different as the pressure difference

between any two holes could be either positive or negative. Therefore, the demodulators had to be adjusted for both the positive as well as the negative sides. In this case, the demodulators were adjusted to give zero volts for zero pressure head and ± 1 volt for ± 1 inch pressure head.

After adjusting the demodulators, the transducers had to be calibrated between the upper and the lower limits (from -1 inch pressure head to +1 inch pressure head). An incremental pressure head of 0.1 inch was applied. Fig. 3.2 shows the results of three calibration tests conducted at the beginning of the main experiments (Double-leaf gate, Surface jets and Wall jets). Also, the transducers were tested and re-calibrated, if necessary, at the beginning of each run within the main experiments. Fig. 3.2 shows that the transducers had a linear response to the applied pressure difference.

3.2.3 Data acquisition system

A data acquisition system consisting of a Macintosh IIfx computer equipped with a data acquisition board and several programs written in the LabView language, was used. Different programs were available for use with different probes. The input to these programs was the calibration equations of the probes and the pressure transducers, and the output was the magnitude and the direction of the velocity vector, the piezometric pressure and the shear stress. The arithmetic means and the standard deviations of all quantities measured were displayed on strip charts on the screen in real time and then saved in an open file. These programs allowed the user to set the total number of samples required at each point and the sampling rate or frequency. For the experiments conducted in this study, a total of 5000 samples were recorded, at each point in the flow, at a frequency of 40 Hz. It should be mentioned that when the pressure difference was outside the transducers' range (± 25.4 mm), the pressure connections were switched to a manometer board and the differential

pressure head results were obtained manually from the manometer and entered into the computer.

3.3 Velocity Measurements

Two probes were used for the measurement of the velocity in this study. A Prandtl tube (or Pitot-static tube) was used, when the direction of flow was known, to measure one-dimensional velocity. A pitch probe was used in two-dimensional flows. The sizes of these probes, their equations and experimental connections are presented in this section.

3.3.1 Prandtl tube

A Prandtl tube with an external diameter of 3.0 mm was used to measure one dimensional velocity in the longitudinal direction. It was used in the double-leaf gate experiment only after the jet surfaced and moved parallel to the flume bed. It was also used in the surface jet and wall jet experiments. The Prandtl tube was also used as a Preston tube for measuring the bed shear stress (Preston (1954); Patel (1965)).

Fig. 3.3 shows a Prandtl tube with an external diameter of 3 mm connected to one transducer. Also included in the same connection was a manometer for use in cases where the pressure difference was outside the transducer range (± 25.4 mm). The positive side of the transducer was connected to the total pressure hole of the Prandtl tube and the negative side was connected to the static pressure hole of the Prandtl tube. When the pressure difference was outside the transducer range, the clamps on the transducer-probe tubes were closed and the clamps on the manometer-probe tubes were opened and the pressure difference was obtained from the manometer (see Fig. 3.3).

3.3.2 Pitch probe

A pitch probe was used in the double-leaf gate experiment to measure the velocity in the inclined jet from the slot till the jet surfaced. It was used because of the two dimensional nature of the flow within this region. The flow is considered two-dimensional when the magnitude and direction of the velocity are unknown but the plane containing the velocity vector is determinable (either exactly or approximately). The velocity vector was measured in the centerline plane parallel to the flume side walls. The lateral component of the velocity was neglected as it was very small compared to the longitudinal and the vertical components especially in the middle third of the flume. The pitch probe used in this study was made of three tubes of external diameters of 1.0 mm and was made and calibrated at the T. Blench Hydraulics Laboratory, University of Alberta.

Fig. 3.4 shows the pitch probe used in this study. It consisted of three stainless steel tubes rigidly soldered together. The nose of the probe was machined so that the face of the central tube is perfectly flat and the side tubes were chamfered at an angle of 45°. Three transducers were used in the pitch probe connection. The positive side of each transducer was connected to one of the pitch probe holes and the negative side was connected to a reference level. Hence, each traducer was used to measure the pressure difference between one of the pitch probe holes and the corresponding reference level. If the pressure difference sensed by a transducer, as displayed in the corresponding demodulator, was outside the transducer range (± 25.4 mm), the corresponding reference level was adjusted (either raised or lowered) to bring the pressure difference within the transducer range. The three reference tubes were directly connected to three glass tubes on the manometer board. After adjusting the reference levels, the levels were read in the corresponding glass tubes on the manometer board and then typed into the computer.

Rajaratnam and Muralidhar (1967) discussed the theory of pitch probes based on simple pressure head equations. Assume a pitch probe is placed in a two dimensional flow in the plane containing the velocity vector V , see Fig. (3.5), at an angle θ with the velocity vector . Therefore, the piezometric pressure heads sensed by the three tubes of the pitch probe could be written as

$$h_1 = h_o + K_1 \frac{V^2}{2g} \quad (3.1)$$

$$h_2 = h_o + K_2 \frac{V^2}{2g} \quad (3.2)$$

$$h_3 = h_o + K_3 \frac{V^2}{2g} \quad (3.3)$$

where h_o is the static piezometric pressure head at the point under consideration and K_1 , K_2 , and K_3 are calibration coefficients and are functions of the pitch angle θ .

Combining the above equations, it could be shown that

$$\frac{h_2 - h_3}{h_2 - h_1} = \frac{K_2 - K_3}{K_2 - K_1} = K_4 \quad (3.4)$$

and

$$V = \frac{\sqrt{2g(h_2 - h_1)}}{\sqrt{K_2 - K_1}} = K_5 \sqrt{2g(h_2 - h_1)} \quad (3.5)$$

where new coefficients, K_4 and K_5 were introduced. Rotating the pitch probes through known angles (in the range of zero to 60 degrees) in the potential core of a plane turbulent jet produced by a deeply submerged sluice gate, Rajaratnam and Muralidhar (1967) determined the calibration curves for the coefficients K_1 to K_5 as functions of the pitch angle θ . Rajaratnam and Muralidhar's (1967) measurements showed that the calibration curves were symmetrical about the zero pitch angle (i.e. any calibration coefficient had the same value at the corresponding positive and negative angles). Fig. 3.5 shows the calibration results.

The data acquisition system used the above equations and those describing the relations shown in Fig. 3.5 to solve for the velocity vector (the magnitude and direction of the velocity). Following are the steps followed in the calculation of the velocity vector.

1. The pressure differences between each tube, of the pitch probe, and the corresponding reference level were measured by the differential pressure transducers;
2. Knowing the reference levels, the pressure heads (h_1 , h_2 and h_3) at the nose of the three tubes, were calculated;
3. The differential pressure heads, (h_2-h_3) and (h_2-h_1) were calculated;
4. Eq. 3.4 was used to obtain K_4 ;
5. Having K_4 , θ (the direction of the velocity vector) could be evaluated from Fig. 3.5;
6. Having θ , K_5 could be evaluated from Fig. 3.5;
7. Having K_5 , the magnitude of the velocity vector, V , could be obtained from Eq. 3.5;

8. One of the equations (Eq. 3.1, Eq. 3.2 or Eq. 3.3) could be used along with the corresponding pressure head h_1 , h_2 or h_3 to obtain the static piezometric pressure head, h_o .

3.4 Bed Shear Stress Measurements

3.4.1 Introduction

The main factor in the evaluation of an energy dissipator is its ability to minimize erosion of the downstream bed. Therefore, measuring the bed shear stress in the first experiment (double-leaf gate energy dissipator) was essential. In the plane turbulent surface jet experiment, the bed shear stress was neglected as it was caused by the reverse flow which was relatively weak. In the plane turbulent wall jet experiment, the bed shear stress was measured and included in the momentum balance equation. Several methods have been used to measure shear stress, τ_o , or friction velocity, $u_* = (\tau_o/\rho)^{0.5}$, as stated by Nezu and Nakagawa (1993)

1. In normal and uniform flow, u_* may be evaluated as follows

$$u_* = \sqrt{gRS} \quad (3.6)$$

where R is the hydraulic radius and S is the channel slope.

2. u_* can be determined using a measured mean velocity profile with the consideration of the logarithmic law as

$$u_* = \frac{U_2 - U_1}{5.75 \log\left(\frac{y_2}{y_1}\right)} \quad (3.7)$$

where U_1 and U_2 are, respectively, the mean velocities at depths of y_1 and y_2 above the bed. In Eq. 3.7 the value of the Von Karman constant, κ , was assumed to be 0.4.

3. Measuring the Reynolds stress distribution, $-\overline{uv}(y)$, u_* can be determined as

$$\frac{\tau}{\rho} \equiv -\overline{uv} + \nu \frac{\partial U}{\partial y} = u_*^2 \left(1 - \frac{y}{y_0} \right) \quad (3.8)$$

where U is the mean velocity, y is the height, above the channel bed, of the point under consideration, y_0 is the flow depth and ν is the kinematic viscosity of water.

4. The velocity distribution measured in the viscous sublayer, if it exists, can be used to determine u_* as follows

$$\frac{U}{u_*} = \frac{yu_*}{\nu} \quad (3.9)$$

5. Bed shear stress can be measured directly using a Preston tube.

Nezu and Nakagawa (1993) mentioned that the accuracy of the first method depends directly on small deflections of the channel bed and of the water surface. Also, the friction velocity determined from Eq. 3.6 is not a local but an overall value. They added that the difficulty of obtaining measurements within the viscous sublayer, makes method 4 extremely difficult to use. The third method is mostly used for turbulent studies and needs accurate turbulence measurements. Method 2 has been used in open channel flows but Nezu and Nakagawa (1993) commented that u_* must be evaluated from method 3 to check the validity of assuming $\kappa = 0.4$ in method 2.

We were left with the Preston tube technique, mentioned in method 5, for measuring the local bed shear stress for the type of flows studied in this research.

3.4.2 Preston tube technique

Preston (1954), based on the existence of the law of the wall, found a relation between the dynamic pressure (the difference between the total pressure head sensed by a total head tube, or the so-called Preston tube, resting on the bed and the static pressure head). If τ_o is the wall shear stress, Δp is the dynamic pressure, d is the external diameter of the Preston tube and ρ and ν are, respectively, the fluid density and kinematic viscosity. Simple dimensional analysis showed that

$$\frac{\tau_o d^2}{4\rho\nu^2} = F\left(\frac{\Delta p d^2}{4\rho\nu^2}\right) \quad (3.10)$$

Many researches have been performed to determine the function F and the calibration of Patel (1965) is considered to be the most definitive one. In the present study, the shear stress on a smooth bed was evaluated based on Patel's (1965) results. It should be noted that Patel's original equations were not always explicit and this needed a trial and error procedure which was not convenient. Hence, explicit equations were derived from the original equations as shown in Table. 3.1, where the trial and error procedure was eliminated and the bed shear stress could be calculated easily. In the present study, a Prandtl tube (Pitot-static tube) was used as a Preston tube to measure the dynamic pressure Δp which was sensed by a transducer and sent as a signal to the data acquisition system for the calculation of the shear stress using the modified equations shown in Table. 3.1.

3.5 The Experiments

In the present study, three research topics have been examined which are the study of a double-leaf gate as an energy dissipator, plane turbulent surface jets in shallow tailwater and plane turbulent wall jets in shallow tailwater. A number of experiments were conducted for each study. Tables 3.2, 3.3 and 3.4 show the details of the experiments conducted in each of the three research topics respectively. In the double-leaf gate energy dissipator, twenty one experiments were conducted as shown in Table 3.2. The effect of the offset ratio Z_o/b_o , submergence ratio $(y_t - Z_o)/b_o$, width ratio w/W , the Reynolds number R and the Froude number F_o , on the different characteristics of the flow were studied. Other experiments (series B) were conducted to classify the different flow patterns and to check for the existence of hysteresis effects. In the plane turbulent surface jets in shallow tailwater, nine experiments were conducted as shown in Table 3.3. The flow characteristics were investigated for different values of the offset ratio Z_o/b_o , the Reynolds number R and the Froude number F_o . Data from six experiments was included in the analysis of the plane turbulent wall jets in shallow tailwater and the details of these experiments are shown in Table 3.4. The first two experiments were conducted in the present study while experiments 3 to 6 were conducted (in the same flume) by Wu and Rajaratnam (1995). A further series of experiments (series B) were conducted to measure the drop in the water surface elevation at the gate, from that of the tailwater as well as the length of the surface eddy. Specific details about the experiments are provided in chapters 4, 5 and 6.

3.6 Experimental Errors and Uncertainties

3.6.1 Introduction and basic concepts

Concerning the reliability estimates of experimental results, two categories of experiments exist: single-sample and multiple-sample experiments. A given

experiment is of the multiple-sample type if a sufficiently large number of measurements are taken (replications), by different observers, using various methods, instruments and sometimes more than one laboratory, such that statistical evaluation of the results can be made. On the other hand, a single-sample experiment is the one in which uncertainties are not found from such repetition.

The majority of engineering experiments, including the present work, are of the single-sample type. Even multiple-sample experiments are, in part, single-sample, due to the presence of several factors reducing the effect of repetition. Generally, measurements taken by a single observer do not provide consistent results and even measurements taken by different observers might not be completely independent. The same equipment can give different results when used by different observers and equipment of different designs, used by the same observer, usually give different results.

Kline and McClintock (1953) and Kline (1985) introduced a useful and practical way of describing uncertainties in basic variables for engineering single-sample experiments. Also included in their analysis is how uncertainties propagate into other dependent variables. Following is a brief description of their analysis.

The difference between the true and the measured values of a certain variable is called an *error*. The *uncertainty* of such measurement is defined as what the observer thinks, with a certain degree of confidence, the expected error might be. Although the error is a fixed quantity, the associated uncertainty can vary substantially. A *variable* is a basic quantity measured directly and the *result* is obtained from the basic variables after calculations and/or corrections. *Propagation of uncertainty* is the way in which uncertainties in the basic variables affect the uncertainties of the results.

Errors are usually classified into three groups which are accidental (or random) errors, fixed errors, and mistakes. *Accidental errors* are those varying errors

which occur without a known reason. Their sources are unrecoverable such as instrumental friction and time lag, personal observation power and many others. *Fixed errors* are those which cause repeated readings to be in error by the same amount with no apparent reason. If the reason is known, as a dent on the probe, it can be fixed and hence the error is removed. With undetected reasons, fixed errors remain in the measurements. *Mistakes* are completely faulty readings of scales, watches, and other measuring devices. These errors are usually detectable on inspection as "way-out" and are rejected. In error analysis, it is usually assumed that all the fixed errors and mistakes have been detected and removed and hence, only the random errors are considered.

The accidental (or random) errors were found, in most of the cases, to have a normal (Gaussian) distribution. In single-sample experiments, because measurements are not repeated, no measure of errors is obtained and hence the distribution function can not be established. Consequently, the experimenter has to rely on his/her past experience and judgment. He/she can think of what would happen if the experiment was repeated a very large number of times. Kline and McClintock (1953) proposed that a good and concise way to describe the uncertainty in a variable is to specify the most likely value (usually the arithmetic mean of several readings) and an uncertainty interval with a specified confidence level. If the arithmetic mean of an observed variable is m and the uncertainty interval is W , the observed variable can be described as

$$\text{Variable} = m \pm W \text{ (confidence or probability level)} \quad (3.11)$$

the following is an example of Eq. 3.11

$$\text{Velocity} = 1.5 \pm 0.05 \text{ m/s (95\%)}$$

Based on this statement, the experimenter believes that the true value of the velocity is probably 1.5 m/s and if a large number of observations are taken, 95% of them will fall within ± 0.05 m/s of the mean value. The uncertainty interval, W , is not a variable but a fixed value selected so that the experimenter could estimate that, with assumed confidence level (here 95%), the error is less than $\pm W$.

In most experiments, it is essential to calculate the uncertainty in the results from the estimates of uncertainty in the measurements. Kline and McClintock (1953) described a method to compute the propagation of uncertainty into a result R . Assume that the result R is a function of n independent variables X_1, X_2, \dots, X_n and the corresponding uncertainty intervals for these variables are $W_{X1}, W_{X2}, \dots, W_{Xn}$, with the same confidence levels. the result R can be expressed in a functional form as

$$R = R(X_1, X_2, \dots, X_n) \quad (3.12)$$

The uncertainty interval of the result, W_R , is described as

$$W_R = \sqrt{\left(\frac{\partial R}{\partial X_1} W_{X1}\right)^2 + \left(\frac{\partial R}{\partial X_2} W_{X2}\right)^2 + \dots + \left(\frac{\partial R}{\partial X_n} W_{Xn}\right)^2} \quad (3.13)$$

Eq. 3.13 has been successfully used for uncertainty analysis in fluid mechanics. Sometimes Eq. 3.12 takes the form

$$R = X_1^{m_1} X_2^{m_2} \dots X_n^{m_n} \quad (3.14)$$

Then by using Eq. 3.14 in Eq. 3.13, a more useful form of Eq. 3.13 is obtained as follows

$$\frac{W_R}{R} = \sqrt{\left(m_1 \frac{W_{x1}}{X_1}\right)^2 + \left(m_2 \frac{W_{x2}}{X_2}\right)^2 + \dots \dots \dots \left(m_n \frac{W_{xn}}{X_n}\right)^2} \quad (3.15)$$

From this equation, the share of uncertainty for each variable in the total uncertainty of the result can be detected. If improvement in accuracy is necessary, the most effective instruments or measurements can be chosen. Uncertainty measurements can provide necessary information to accurately find which instrument has to be improved.

3.6.2 Estimate of uncertainty

The possible sources of errors for the measured variables in the experiments conducted in the present study are presented in this section. Also, the uncertainties of the results are calculated based on Eq. 3.15. The confidence level for all uncertainty estimates was taken as 95% (or 19 to 1 odds or 1 in 20 chance).

The main dimensions of the flume were measured by a scale to the nearest 1 mm and hence the estimated uncertainty was ± 0.5 mm. The depth of flow was calculated from the water surface and bed elevations using a scale to the nearest 1 mm. The uncertainty in measuring the bed level was ± 0.5 mm whereas that of the water surface was ± 2 mm (due to the existence of surface waves). If the water depth is y_o and the water surface and bed levels are respectively L_s and L_b then

$$y_o = L_s - L_b \quad (3.16)$$

Differentiating Eq. 3.16 w.r.t L_s and L_b and substituting the results along with the uncertainty estimates of the surface and bed levels in Eq. 3.13, the uncertainty of the water depth can be estimated as follows

$$W_{y_o} = \pm \sqrt{(1 \times 2)^2 + (-1 \times 0.5)^2} = \pm 2.06 \text{ mm} \quad (3.17)$$

A vernier was used to measure the slot width b_o to the nearest 0.1 mm. So, the estimated uncertainty in this measurement was ± 0.1 mm. The uncertainty in the discharge measurement was estimated to be ± 0.1 l/s. Using the above uncertainty estimates, the uncertainty in the jet velocity at the slot U_o and the average velocity V , after the jet occupied the whole depth, can be calculated, as an example, in experiment 1 in the plane turbulent wall jet study (see Table 3.4) as follows

$$\begin{aligned} W &= 446 \pm 0.5 \text{ mm;} \\ b_o &= 10 \pm 0.1 \text{ mm;} \\ y_o &= 500 \pm 2.06 \text{ mm;} \\ Q &= 11.15 \pm 0.1 \text{ l/s;} \\ U_o &= Q/(W.b_o) = 2.50 \text{ m/s;} \\ V &= Q/(W.y_o) = 0.05 \text{ m/s.} \end{aligned}$$

Then using Eq. 3.15 we get

$$\frac{W_{U_o}}{U_o} = \sqrt{\left(1 \times \frac{0.1}{11.15}\right)^2 + \left(-1 \times \frac{0.5}{446}\right)^2 + \left(-1 \times \frac{0.1}{10}\right)^2} \quad (3.18)$$

or

$$\frac{W_{U_o}}{U_o} = \sqrt{(8.044 + 0.126 + 10.000).10^{-5}} = 1.35\% \quad (3.19)$$

and

$$\frac{W_V}{V} = \sqrt{\left(1 \times \frac{0.1}{11.15}\right)^2 + \left(-1 \times \frac{0.5}{446}\right)^2 + \left(-1 \times \frac{2.06}{500}\right)^2} \quad (3.20)$$

or

$$\frac{W_v}{V} = \sqrt{(8.044 + 0.126 + 1.697) \cdot 10^{-5}} = 1\% \quad (3.21)$$

With $U_o = 2.50$ m/s and $V = 0.05$ m/s, Eq. 3.19 and Eq. 3.21 show that the uncertainties in U_o and V are respectively 0.03375 m/s and 0.0005 m/s. The above example shows that the accuracy of U_o can be enhanced by improving the discharge and the slot width measurements. It shows also that the accuracy of U_o is not much affected by the accuracy in measuring the flume width. To make V more accurate, focus should be given mainly to the discharge measurements. The accuracy of V is less affected by the water depth measurement and the effect of the flume width accuracy is almost negligible.

The accuracy of the pressure transducers used in this study, based on the manufacturer's specifications, was $\pm 0.25\%$ of the full scale and this included the effects of linearity, hysteresis and repeatability. The range of the pressure head that these transducers could measure was ± 1.4 inches. However, the calibration of the transducers in the lab showed higher accuracy. For the unidirectional flows, the transducers were calibrated between zero and 1 inch (full scale = 1 inch = 25.4 mm). For the two-dimensional flows, the transducers were calibrated between -1 inch and +1 inch (full scale = 2 inches = 50.8 mm). Therefore, the uncertainty in the differential pressure head measurements in the one dimensional and two dimensional flows were respectively ± 0.0635 mm and ± 0.127 mm.

As was mentioned before, the velocity in the uni-directional flows was measured with a Prandtl tube (Pitot-static tube). In the two-dimensional flows, a pitch probe was used. Accuracy of the velocities measured with a Prandtl tube depended mainly on the accuracy of measuring the differential pressure head, the probe alignment, turbulence and wall effects. The Prandtl tubes are sensitive to an error in

alignment of more than ± 5 degrees. The accuracy in alignment of the probe could be estimated to be within ± 2 degrees. No correction was made for turbulence and wall effects. Therefore, in estimating uncertainties in the velocity measurements using a Prandtl tube, only errors from pressure transducers (or manometer) were considered. Eq. 3.15 can be used to predict uncertainties in the velocity measurements as follows.

$$\text{Differential pressure head (transducer)} = h \pm 0.0635 \text{ mm}$$

$$\text{Differential pressure head (manometer)} = h \pm 2 \text{ mm}$$

where h is the differential pressure head in mm sensed by the transducer or measured by a manometer. Assuming the velocity measurement, u , depends only on the differential pressure head accuracy, Eq. 3.15 can be written as

$$\frac{W_u}{u} = \frac{1}{2} \cdot \frac{W_h}{h} = \frac{g \cdot W_h}{u^2} \quad (3.22)$$

where g is the acceleration due to gravity. Using transducers, it was mentioned before that $W_h = \pm 0.0635$ mm in one dimensional flow velocity measurements. Assuming velocity u of 0.1, 0.2, 0.3 and 1.0 m/s, Eq. 3.22 shows uncertainties, W_u/u of 6.2%, 1.6%, 0.7% and 0.06% respectively. Eq. 3.22 shows that the uncertainty in the velocity measurements is inversely proportional to the magnitude of the velocity. In other words, the larger uncertainties in the velocity measurements should exist in the reverse flow zone where the velocities were relatively low. However, the overall uncertainty could be less than the calculated one due to the large number of samples (5000 samples) taken at each point. The corresponding estimates in case of using manometers could be easily obtained by repeating the above calculations for $W_h = \pm 2$ mm.

In two dimensional flows, velocity was measured with a pitch probe. In the present study, the pitch probe was only used in the double-leaf gate experiment to measure the velocity in the inclined jet from the slot till the jet surfaced. Different types of errors made it difficult to estimate uncertainties in the velocities measured with the pitch probe. Sources of errors in these measurements may include the presence of velocity and/or pressure gradients across the three holes of the probe, calibration curve fitting, probe misalignment, blockage error and existence of a third component of the velocity normal to the plane containing the probe. Errors because of using pitch probes were less, in this study, as the velocity measurements were taken in the plane of symmetry. Also, the pitch probe was not used near the boundaries where strong velocity gradients exist. Calculating the combined effects of the above-mentioned errors on the resultant accuracy of the velocity measurements would be a study by itself. However, rough estimates could be made to give an idea about the size of these errors based on flow visualization, inspection of velocity measurements and past experience. For small pitch angles (less than 15 degrees), pitch probes are considered to be as accurate as Prandtl tubes (Pitot-static tubes). With larger pitch angles, more uncertainty in the velocity measurements is expected. The uncertainty in the measurement of the probe angle was ± 0.5 degrees. The uncertainty in the measurement of the attack angle or pitch angle (see Fig. 3.5) could be estimated to be within ± 2 degrees. The effect of the pressure and velocity gradients on the velocity measurements could not be roughly estimated.

It was mentioned before that the bed shear stress was measured with a Prandtl tube sitting on the smooth bed of the flume. The uncertainty in the probe alignment was ± 2 degrees. Neglecting the turbulence and the wall effects, only the errors in measuring differential pressure heads, using pressure transducers, may be considered. If the uncertainty in measuring the differential pressure head, using pressure

transducers, is $W_h = \pm 0.0635$ mm, Eq. 3.13 can be used, along with the relations shown in Table 3.1, to predict uncertainties in measuring the bed shear stress.

3.7 References

- Kline, S. J. (1985). "The purposes of uncertainty analysis." ASME Journal of Fluids Engineering, Vol. 107, pp. 153-160.
- Kline, S. J. and McClintock, F. A. (1953). "Describing uncertainties in single-sample experiments." Mechanical Engineering, Vol. 75, pp. 3-8.
- Nezu, I., and Nakagawa, H. (1993). "Turbulence open-channel flows." IAHR Monograph Series, A.A Balkema Publishers.
- Patel, V. C. (1965). "Calibration of the Preston tube and limitations on its use in pressure gradients." J. Fluid Mech., Vol. 23, pp. 185-208.
- Preston, J. H. (1954). "The determination of turbulent skin friction by means of Pitot tubes." J. Royal Aero. Soc., Vol. 54, pp. 109-121.
- Rajaratnam, N., and Muralidhar, D. (1967). "Yaw and pitch probes." Hydraulic Instrumentation Series, Dept. of Civil Engrg., University of Alberta.
- Wu, S. and Rajaratnam, N. (1995). "Free jumps, submerged jumps and wall jets." J. Hydr. Res., 33(2), pp. 197-212.

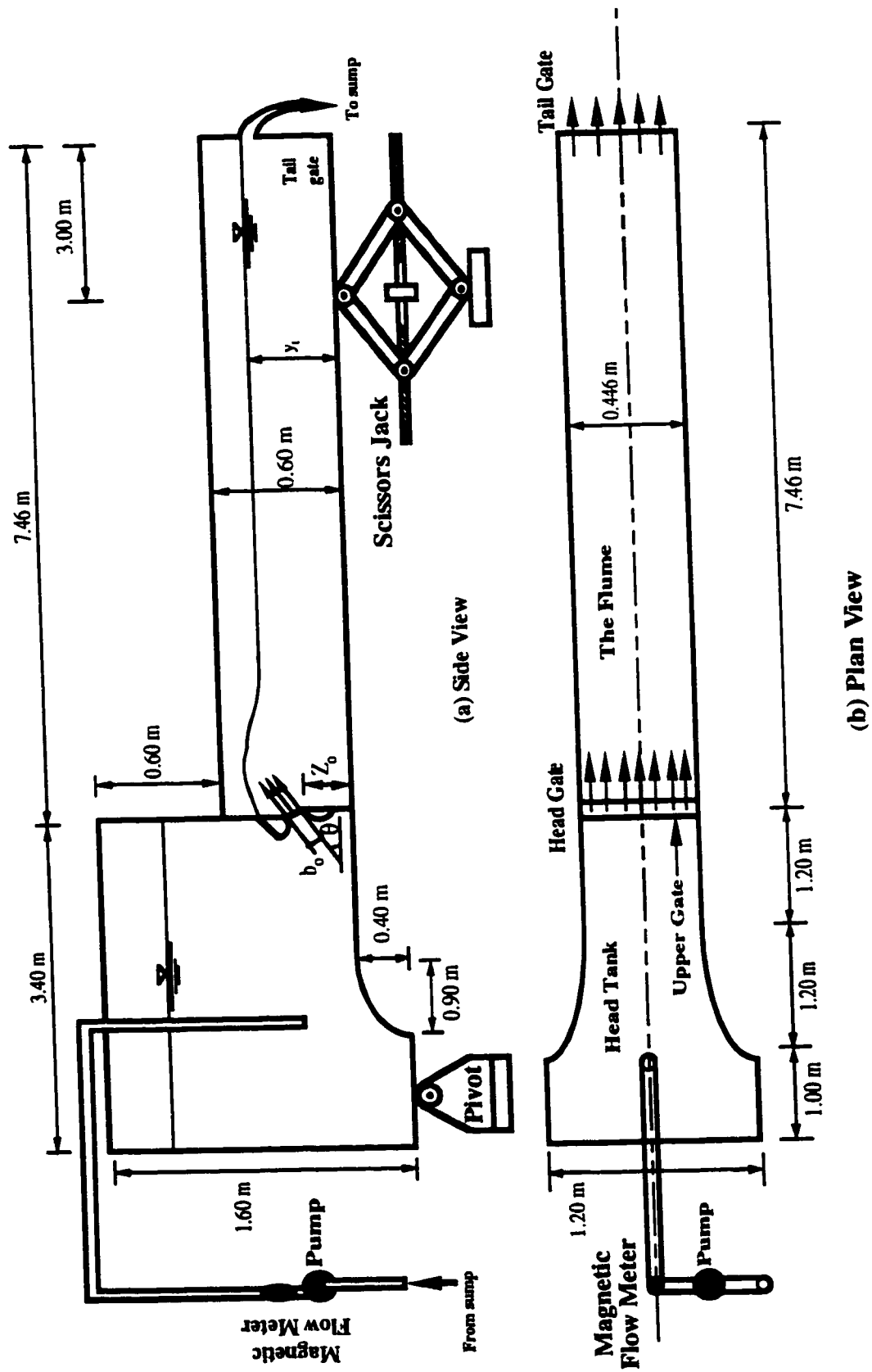


Fig. 3.1 Experimental flume

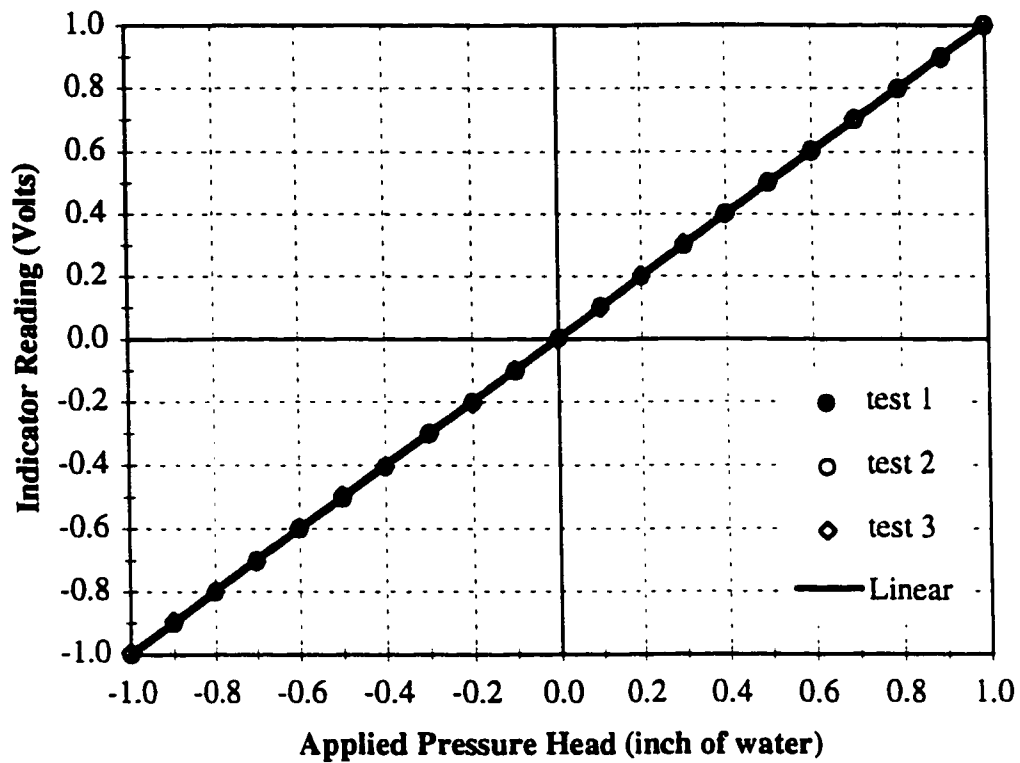


Fig. 3.2 Typical calibration of pressure transducers

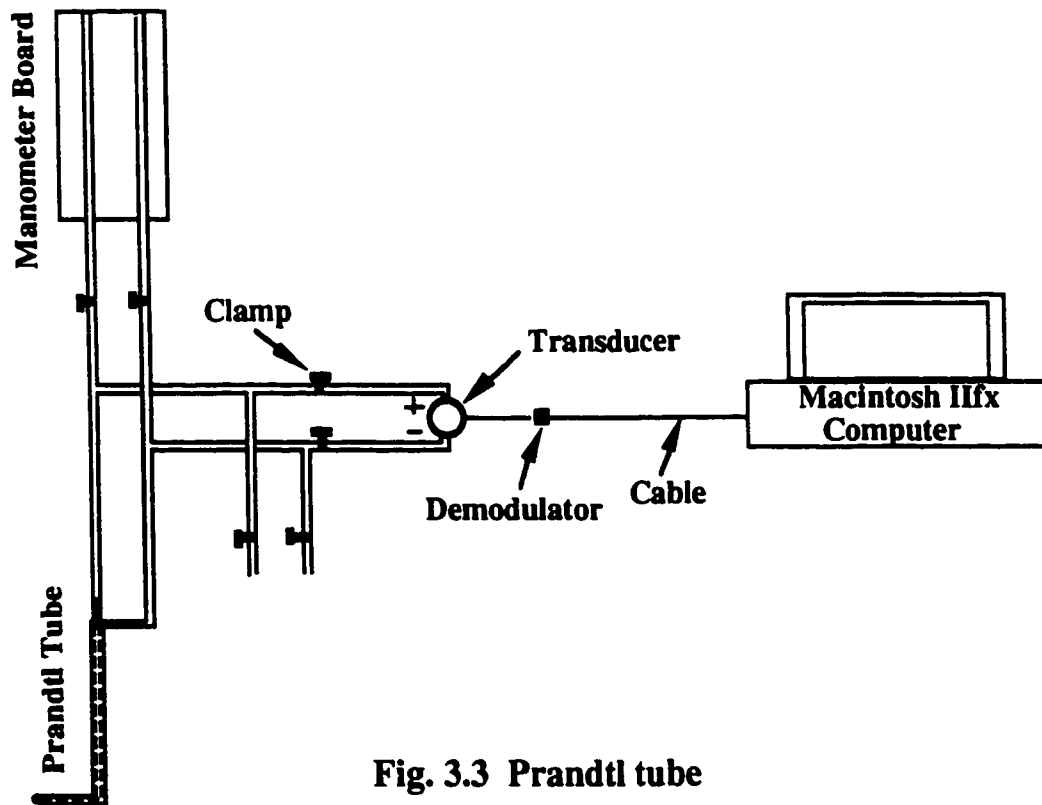


Fig. 3.3 Prandtl tube

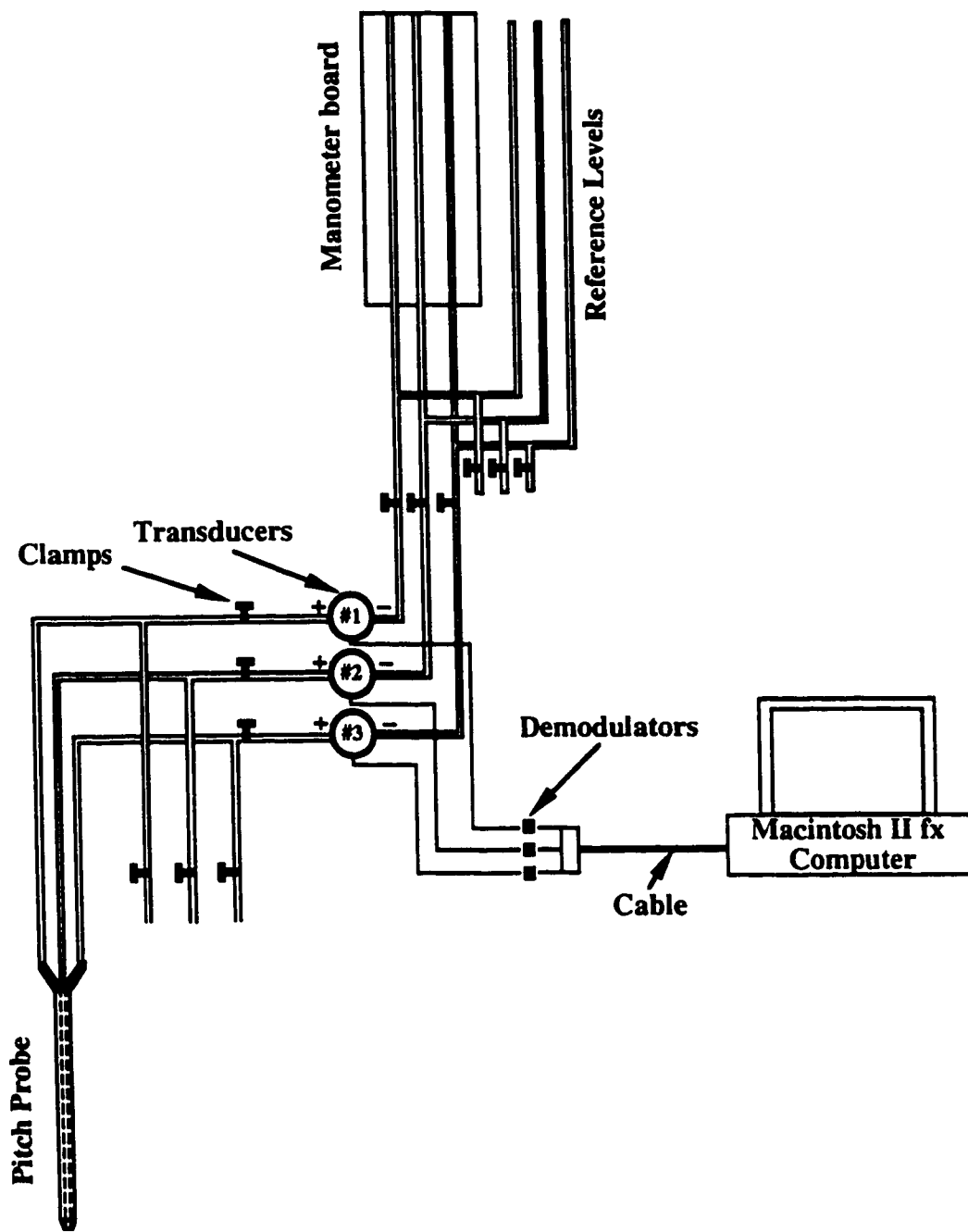


Fig. 3.4 Pitch probe

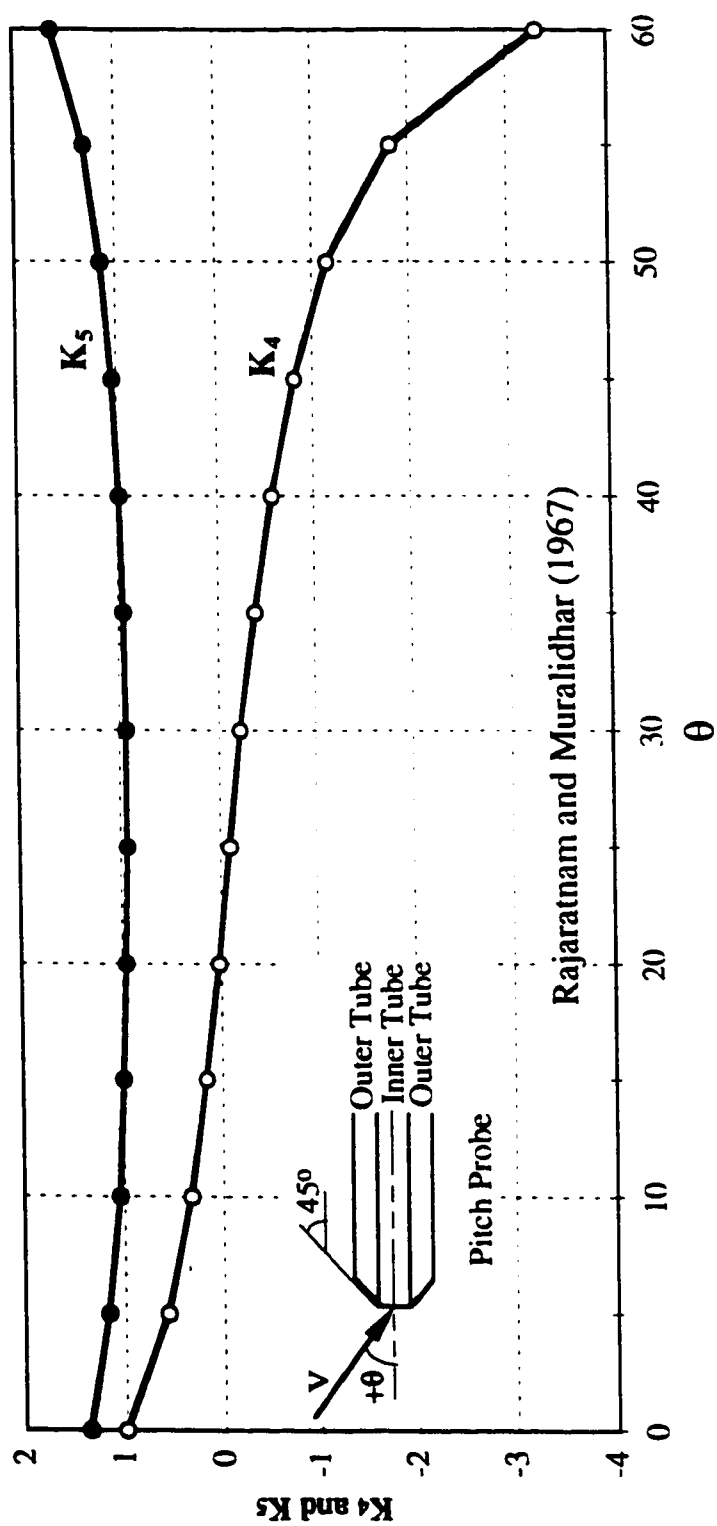


Fig. 3.5 Calibration curves for the pitch probe

Table 3.1 Explicit equations for Patel's calibration curves for Preston tube

	Region 1	Region 2	Region 3
Original equations (Patel, 1965)	$y_* = 0.5x_* + 0.037$	$y_* = 0.8287 - 0.1381x_* + 0.1437x_*^2 - 0.006x_*^3$	$x_* = y_* + 2\log(1.95y_* + 4.1)$
Range of validity (Patel, 1965)	$y_* < 1.5$	$1.5 < y_* < 3.5$	$3.5 < y_* < 5.3$
Range in terms of τ_{o*}	$\tau_{o*} < 32$	$32 < \tau_{o*} < 3,162$	$3,162 < \tau_{o*} < 199,526$
y_* in terms of x_*	$y_* = 0.5x_* + 0.037$	$y_* = 0.8287 - 0.1381x_* + 0.1437x_*^2 - 0.006x_*^3$	$y_* = -0.96562 + 0.71911x_* + 0.017594x_*^2 - 0.00053x_*^3$
x_* in terms of y_*	$x_* = -0.074 + 2y_*$	$x_* = -0.61306 + 3.0882y_* - 0.57057y_*^2 + 0.055727y_*^3$	$x_* = 1.3272 + 1.2866y_* - 0.024433y_*^2 + 0.00106y_*^3$
Range in terms of x_*	$x_* < 2.926$	$2.926 < x_* < 5.59$	$5.59 < x_* < 7.619$
Range in terms of Δp_*	$\Delta p_* < 843$	$843 < \Delta p_* < 389,045$	$389,045 < \Delta p_* < 41,591,061$
$\Delta p/\tau_{o*}$ in terms of x_*	$\Delta p/\tau_{o*} = 0.918 + 3.482x_* - 2.996x_*^2 + 1.6358x_*^3$	$\Delta p/\tau_{o*} = 114.58 - 111.19x_* + 35.967x_*^2 - 2.826x_*^3$	$\Delta p/\tau_{o*} = 10.706 + 2.748x_* + 2.881x_*^2 + 0.0215x_*^3$

Note: $x_* = \log\left(\frac{\Delta p d^2}{4\rho v^2}\right) = \log(\Delta p_*)$ and $y_* = \log\left(\frac{\tau_{o*} d^2}{4\rho v^2}\right) = \log(\tau_{o*})$

Table 3.2 Primary details of experiments of the double-leaf gate (series A)

Expt. (1)	θ (2)	b_o (mm) (3)	Z_o (mm) (4)	y_i (mm) (5)	W (mm) (6)	w (mm) (7)	U_o (m/s) (8)	F_o (9)	Z_g/b_o (10)	$(y_i-Z_o)/b_o$ (11)	w/W (12)	R (13)	Pattern (14)
1	30	9	270	270	446	446	1.43	4.80	30.00	0.00	1.00	12836	C
2	30	9	270	279	446	446	1.43	4.80	30.00	1.00	1.00	12836	B
3	30	9	270	473	446	446	1.43	4.80	30.00	22.50	1.00	12836	A
4	30	9	270	540	446	446	1.43	4.80	30.00	30.00	1.00	12836	A
5	30	9	270	270	446	446	2.14	7.20	30.00	0.00	1.00	19254	C
6	30	9	270	279	446	446	2.14	7.20	30.00	1.00	1.00	19254	B
7	30	9	270	338	446	446	2.14	7.20	30.00	7.50	1.00	19254	B
8	30	9	270	405	446	446	2.14	7.20	30.00	15.00	1.00	19254	AB
9	30	9	270	540	446	446	2.14	7.20	30.00	30.00	1.00	19254	A
10	30	9	270	279	446	446	3.09	10.40	30.00	1.00	1.00	27812	B
11	30	9	270	338	446	446	3.09	10.40	30.00	7.50	1.00	27812	B
12	30	9	270	540	446	446	3.09	10.40	30.00	30.00	1.00	27812	A
13	30	20	270	270	446	446	1.06	2.40	13.50	0.00	1.00	21261	C
14	30	20	270	540	446	446	1.06	2.40	13.50	13.50	1.00	21261	A
15	30	20	135	405	446	446	1.06	2.40	6.75	13.50	1.00	21261	A
16	30	20	0	270	446	446	1.06	2.40	0.00	13.50	1.00	21261	A
17	30	20	0	270	446	446	1.59	3.60	0.00	13.50	1.00	31892	A
18	30	20	270	540	446	446	2.13	4.80	13.50	13.50	1.00	42523	A
19	10	20	270	540	446	446	2.13	4.80	13.50	13.50	1.00	42523	A
20	10	20	270	540	446	357	2.13	4.80	13.50	13.50	0.80	42523	A
21	10	20	270	540	446	223	2.13	4.80	13.50	13.50	0.50	42523	A

Table 3.3 Primary details of experiments of the plane turbulent surface jets

Expt. (1)	b_o (mm) (2)	Z_o (mm) (3)	y_t (mm) (4)	W (mm) (5)	U_o (m/s) (6)	F_o (7)	Z_o/b_o (8)	$(y_t - Z_o)/b_o$ (9)	R (10)
1	5	500	505	446	1.60	7.2	100	1.00	8000
2	10	500	510	446	0.75	2.4	50	1.00	7500
3	10	500	510	446	1.50	4.8	50	1.00	15000
4	10	500	510	446	2.25	7.2	50	1.00	22500
5	10	300	310	446	1.88	6.0	30	1.00	18800
6	20	500	520	446	2.13	4.8	25	1.00	42600
7	10	200	210	446	0.90	2.9	20	1.00	9000
8	10	100	110	446	1.25	4.0	10	1.00	12500
9	10	50	60	446	0.50	1.6	5	1.00	5000

Table 3.4 Primary details of experiments of the plane turbulent wall jets (series A)*

Expt. (1)	b_o (mm) (2)	W (mm) (3)	U_o (m/s) (4)	F_o (5)	y_t (mm) (6)	y_2 (mm) (7)	$\eta = y_t/b_o$ (8)	$S = \eta/\eta_t - 1$ (9)	R (10)
1	10	446	2.50	8.0	500	108	50	3.63	25000
2	10	446	1.25	4.0	500	52	50	8.68	12500
3	10	446	1.72	5.5	440	73	45	5.04	17200
4	15	446	2.86	7.5	530	151	35	2.51	42900
5	15	446	2.86	7.5	460	151	30	2.05	42900
6	15	446	2.86	7.5	390	151	25	1.59	42900

* Experiments 3, 4, 5 and 6 were conducted by Wu and Rajaratnam (1995)

Chapter 4

A Double-Leaf Gate for Energy Dissipation Below Regulators¹

4.1 Introduction

Hydraulic jumps have been widely used for energy dissipation below hydraulic structures. The formation of a hydraulic jump is very sensitive to the tailwater condition and as a result a specific tailwater level has to be maintained for a jump to form at a required location for any given flow rate. If the tailwater is raised above this specific level, the jump becomes submerged and if it is lowered below that level, the jump becomes repelled. Different types of hydraulic jumps have been evaluated as energy dissipators as summarized by Elevatorski (1959), Peterka (1963), Rajaratnam (1967) and Hager (1992). For regulators that are constructed in irrigation systems, the downstream water levels generally vary according to the irrigation demands and the hydraulic jump solution is generally unsuitable. Baffle walls and baffle blocks have been used in hydraulic jump stilling basins either to force the jump to form just downstream of the gate, if the tailwater depth is less than the sequent depth, or to deflect the high velocity stream to the free surface, if the tailwater depth is greater than the sequent depth. But baffles might be exposed to cavitation damage for relatively high velocity jets and further, they are not suitable for some flow conditions under which a reattached high velocity wall jet might form, as mentioned by Wu and Rajaratnam (1995).

This study introduces a new concept of a double-leaf gate as an energy dissipator which has the same advantage as the baffles of directing the high velocity

¹ The main content of this chapter has been published in the Journal of Hydraulic Engineering of the American Society of Civil Engineers, Vol. 124, No. 11, pp.1134-1145, 1998.

stream to the free surface, without the risk of cavitation damage (see Fig. 4.1). Further, the performance of this scheme is independent of the tailwater fluctuations and as a result it can be used with variable tailwater conditions. In the double-leaf gate, the two leaves are arranged in such a way that a jet issues at an angle towards the water surface through the opening between the two leaves. The bottom leaf remains fixed while the top leaf (control leaf) is moved up and down to regulate the flow. Although only the upper gate is used for regulation, the lower one can also be lifted, when necessary, to flush out accumulated sediment deposits. In addition to being simple and efficient as an energy dissipator, splitting the vertical gate into two portions will be of benefit in decreasing the capacity, weight and size of the overhead gate control structure. (In the double-leaf gate dissipator a concrete apron is still required to satisfy the percolation length and to prevent erosion whenever the bottom gate is raised).

Fig. 4.1 shows a double-leaf gate where b_o is the opening width, Z_o is the height of the lower edge of the slot above the bed; U_o is the velocity of the jet issuing from the opening; y_t is the tailwater depth and θ is the angle of inclination of the jet. In this design, the upper gate is located upstream of the lower one to create the opening which produces the inclined jet. The Froude number of the jet is $F_o = U_o / (gb_o)^{0.5}$; S equal to $(y_t - Z_o) / b_o$ is the submergence ratio of the jet, defined as the ratio of the depth of water above the lower edge of the opening to the opening width; and Z_o / b_o is the offset ratio. Existing regulators can be modified using this idea by adding an upward sloping sill just under the gate as shown in Fig. 4.2.

4.2 Dimensional Analysis

Considering the problem illustrated in Fig. 4.1, any property (m) of the flow can be expressed as a function of various parameters of the flow, fluid properties and channel dimensions as

$$m = f(U_o, g, b_o, Z_o, w, W, y_t, \theta, \rho, \mu) \quad (4.1)$$

where w and W are the opening and the flume widths, respectively. The above relation can be represented in a dimensionless form as

$$M = f' \left[\frac{U_o}{\sqrt{gb_o}}, \frac{\rho U_o b_o}{\mu}, \frac{w}{W}, \frac{w}{b_o} \frac{y_t - Z_o}{b_o}, \frac{Z_o}{b_o}, \theta \right] \quad (4.2)$$

Eq. 4.2 shows that any property of the flow can be expressed as a function of the Froude number, the Reynolds number, the width ratio, the aspect ratio, the submergence ratio, the offset ratio and the deflection angle of the jet. For large values of the Reynolds number, $R = \rho U_o b_o / \mu$, where ρ and μ are, respectively, the mass density and dynamic viscosity of the fluid, viscosity is known to have negligible effects. Also, the aspect ratio of the jet w/b_o ranged between 11.15-22.30 which is large enough for the jet flow to be considered two-dimensional especially in the middle third of the flume where the measurements were taken. Hence, Eq. 4.2 becomes

$$M = f'' \left[\frac{U_o}{\sqrt{gb_o}}, \frac{w}{W}, \frac{y_t - Z_o}{b_o}, \frac{Z_o}{b_o}, \theta \right] \quad (4.3)$$

Experiments were conducted for different Froude numbers, width ratios, submergence ratios, offset ratios and two deflection angles of θ (30° and 10°).

4.3 Experimental Study

4.3.1 Experimental arrangement

This concept of double-leaf gate energy dissipator was studied in the laboratory in a flume, 0.446 m wide, 0.60 m deep and 7.6 m long, with aluminum bottom and plexiglas sides (see Fig. 4.3). Two pumps were used to supply the flume with the required discharge. The discharge was measured by a magnetic flow meter located in the supply line. Water entered the flume through an opening between two aluminum gates. The upper gate was located upstream of the lower one in such a way that the jet issued from the opening towards the water surface at a certain angle. Two streamlined lips were fixed on the upper and lower gates to produce a supercritical stream with a thickness equal to the gate opening b_0 . A tail gate was used to control the tailwater depth in the flume.

Two systems were used for measuring the time-averaged velocity and bed shear stress. In one system a pitch probe was used whereas in the other, a Prandtl tube was used (see Fig. 4.4 and Fig. 4.5). The pitch probe was made of three tubes of external diameters of 1.0 mm and was made and calibrated in the Hydraulics laboratory. The pitch probe was used in measuring the velocity distribution in the jet directed towards the water surface. This probe was always placed normal to the jet and was used in measuring the velocity profiles across the jet. The Prandtl tube with an external diameter of 3.0 mm, was used in measuring the velocity distribution along vertical sections in the jet after it surfaced. The Prandtl tube was also used as a Preston tube for measuring the bed shear stress (Preston (1954); Patel (1965)).

Three transducers (Validyne model DP45-16 Northridge, Calif) were used in the experiments to measure the pressure differences. The output ends of the transducers were connected to a flat cable that was connected to a Macintosh IIfx computer. In cases where the pressure differences were within the range of the transducers (± 1 inch), two transducers were used. The first one was connected between the middle and

the upper tubes of the pitch probe while the other was connected between the middle and the lower tubes. In cases where the pressure differences were outside the transducers range, each transducer had to be connected between one of the tubes and a reference level and the reference was adjusted at each point to make the pressure difference, between the two sides of the transducer, within its range. The Prandtl tube was used in measuring the velocities downstream of the point of collision, with the free surface or the bed, and used also to measure the bed shear stress. Usually, one transducer was required to connect the static and the total head tubes of the Prandtl tube. In cases where the pressure difference at a point was outside the transducer range, the two tubes were switched to a manometer board to measure the pressure difference and then calculate the velocity at that point.

The computer took samples from the transducers at a certain sampling rate, couples every sequence of two signals to obtain the magnitude of the velocity, attack angle and the pressure in case of the pitch probe or the magnitude of the velocity in case of the Prandtl tube. The computer displayed the results on a strip chart on the screen in real time. When the required number of samples were taken (usually 5000 samples were recorded at each point with a sampling rate of 40 samples/second) the computer processed all the samples to obtain the mean value and the standard deviation for each variable and saved the results in an open file. The computer programs used in the experiments were written in LabView language.

4.3.2 Experiments

A total of 21 experiments (series A) were conducted and the primary details of these experiments are shown in Table 4.1. Eighteen of these experiments (Expt.1-Expt.18) were conducted for a deflection angle of θ equal to 30 degrees and a width ratio of 1.00. Three experiments (Expt.19-Expt.21) were conducted for a deflection

angle of θ equal to 10 degrees and width ratios of 1.00, 0.80 and 0.50 respectively. The values of the various parameters (b_o , Z_o , y_t , w , U_o) were selected to achieve a wide and a practical range of the offset ratio, the submergence ratio, the width ratio and the Froude number. Four offset ratios of 0.00, 6.75, 13.50 and 30.00 were used. The submergence ratio S was varied from zero to about 30. Three width ratios of 1.00, 0.80 and 0.50 were studied. Experiments were conducted for Froude numbers equal to 2.40, 3.60, 4.80, 7.20 and 10.40. The Reynolds number of the jet was in the range of 12000 to 43000. Two conditions had to be satisfied in the selection of the deflection angle θ . The first was to avoid the jet reattachment to the rigid boundaries (the flume bed or the gate). The second was to have a reasonable horizontal component of the jet velocity. A deflection angle of θ equal to 30 degrees satisfied these two conditions. Other experiments (series B) were conducted to classify the different flow patterns and to check for the existence of any hysteresis effects.

4.4 Experimental Results and Analysis

4.4.1 Flow patterns

Preliminary experiments (series B) were conducted to determine the different flow patterns for a range of the Froude number and the submergence ratio. The different flow patterns are shown in Fig. 4.6(a-c) and Fig. 4.7(a-c). Two deflection angles of 30 and 10 degrees were used. For the 30 degrees' angle, experiments were performed with one width ratio of 1.00 and four offset ratios of 30.00, 13.50, 6.75 and 0.00. For the 10 degrees angle, experiments were performed with three width ratios of 1.00, 0.80, 0.50 and one offset ratio of 13.50. For each angle, offset ratio and width ratio, the critical submergence ratios at which the flow changed from one pattern to another were determined through the following steps. (1) Open the tail gate completely and start the pump to obtain the desired discharge. (2) Slowly raise the tail

gate in small increments and wait for the flow to become stable. (3) Determine the tailwater elevations at which the flow changes from one pattern to another. (4) Lower the tail gate slowly in small increments and wait for the flow to become stable. (5) Repeat step (3) to see as to whether hysteresis effects existed.

4.4.1.1 Width ratio $w/W = 1.00$ and $\theta = 30$ degrees

For experiments conducted with $w/W = 1.00$ and $\theta = 30$ degrees, three stable flow patterns were observed as shown in Fig. 4.6(a-c) and Fig. 4.7(a-c). Fig. 4.8(a-c) show the classification of these flow patterns according to the submergence ratio $S = (y_t - Z_o)/b_o$, Froude number $F_o = U_o/(gb_o)^{0.5}$ for three values of the offset ratio Z_o/b_o of 30.00, 13.50 and 6.75 respectively. Starting with the tailwater at or below the lower edge of the opening (i.e. $S \leq 0$), the jet issued as a free jet and plunged into the tailwater where it impinged on the bed at a certain section (see Fig. 4.6(c) & Fig. 4.7(c)). At the line of impingement, the jet bifurcated into one jet traveling downstream and another jet traveling upstream. The forward flowing jet proceeded as a wall jet whereas the backward flow diffused in the confined pool under the jet. This flow was referred to as pattern C. When the tailwater was raised above the lower edge of the slot, the air cavity under the jet started to fill, inducing an upward pressure on the jet. This pressure raised the jet trajectory and consequently the line of impingement started to move downstream (see Fig. 4.9). With further increase in the tailwater depth, the plunging jet changed into a surface jet as shown in Fig. 4.6(b) & Fig. 4.7(b) and was referred to as pattern B. The upward pressure on the jet increased with increasing tailwater depth until the jet started to oscillate and this flow was referred to as pattern AB. In the oscillating zone, the jet oscillated between the angle of the slot and an enhanced angle. At the angle of the slot, the upward pressure became maximum and pushed the jet towards the gate while at the steeper angle, the pressure under the jet was

relieved allowing the jet to return back to its original direction and so on. The oscillating pattern AB produced strong surface waves and should be excluded from design unless a suitable wave suppresser is used. These oscillations were totally suppressed with a piece of wood placed on the water surface where the jet surfaced. With a further increase of the tailwater, water started to accumulate above the jet producing a downward force that balanced the upward pressure and finally the jet stopped oscillating and pattern A started to form (see Fig. 4.6(a) & Fig. 4.7(a)). In flow pattern A, the jet issued with the slot angle, kept its initial direction until it reached a certain point after which the jet path became steeper with the angle of the jet increasing to about 45 degrees. Finally, the jet hit the water surface at a certain line and then proceeded as a surface jet. In the stable flow pattern A, two eddies formed, one above and another below the jet, as shown in Fig. 4.7(a). The upper eddy was confined by the jet, the water surface and the gate whereas the lower eddy was bounded by the jet on the top and the channel bed. Pattern B also showed a surface jet but the jet from the slot was not submerged near the gate.

This design of the double-leaf gate dissipator would be used mainly in rivers and main canals where the sluices are submerged enough for pattern A to exist during operation. The other flow patterns were covered only to account for operations during canal filling, emptying or other special operations. In these streams, the tailwater variations, due to the different water requirements, should be within zone A. It can be noticed from Fig. 4.8(a-c) that the oscillating zones are relatively wide which may require the sluices to be deeply submerged so that pattern A can form. Hence, it was of great importance to modify² the model in such a way that the oscillating zones are eliminated, or at least minimized, and hence pattern A can form with less submergence.

² Modification of the model has been tentatively accepted at the 1st Minia Conference for Advanced Trends in Engineering, MICATE'99, Minia, Egypt.

Two methods were tried, first by decreasing the deflection angle (i.e. using $\theta < 30$ degrees) and the other by having the jet ventilated (i.e. $w/W < 1$).

4.4.1.2 Width ratio $w/W = 1.00$ and $\theta = 10$ degrees

One experiment (Expt. 19) was conducted with $w/W = 1.00$, $Z_o/b_o = 13.50$ and $\theta = 10$ degrees. Some observations were also taken for an offset ratio equal to zero. For $Z_o/b_o = 13.50$, the same behavior of the jet was repeated as it issued with the original angle (i.e. 10 degrees) until it assumed a larger angle at a later stage as with the case of the 30 degrees jet. With $\theta = 10$ degrees, the upper cavity was larger and this helped in minimizing the oscillating zone. Other than this benefit, the different flow characteristics for the two angles were quite similar. For $Z_o/b_o = 0.00$, the 10 degrees jet tended to reattach to the bed by the Coanda effect. Therefore, the 10 degrees angle can only be used in the prototypes of relatively large offset ratios. As the 30 degrees angle is suitable for both the small and the large offset ratios, it is recommended for double-leaf gate dissipators. However, more experiments are needed to determine the minimum angle that can be used in the double-leaf gate dissipators. It is important to note that at a certain angle and offset ratio the jet reattaches to the bed only when the submergence exceeds a certain limit. In the recommended study, each angle should be studied with different offset ratios. For each combination of an angle and an offset ratio, the minimum submergence at which the jet reattaches to the bed should be determined. This study will help the designers to select the suitable angle when the ranges of the offset ratio and the submergence ratio are known in the prototype. (Note that the offset ratio and the submergence ratio change not only with Z_o and y_t but also with the change of the opening according to the irrigation demands).

4.4.1.3 Width ratio (w/W) < 1.00 and $\theta = 10$ degrees

It was mentioned earlier that raising the tailwater above the slot level was associated with an increase in the upward pressure induced on the jet, resulting in jet oscillation. As the jet occupied the whole width of the flume, the downstream water could not accumulate above the jet until the water surface elevation reached the crest of the jet trajectory. Raising the tailwater above the crest level resulted in the accumulation of water above the jet and hence an increase in the downward pressure. The jet stopped oscillating when a balance in the upward and downward pressures was reached. To overcome this pressure unbalance in the oscillating zone, two experiments (Expt. 20 and Expt. 21) were conducted with width ratios equal to 0.8 and 0.5 (see Fig. 4.11 for $w/W=0.50$) and an offset ratio of 13.50. In these experiments, the jet occupied part of the flume width leaving two gaps, or ventilation zones, between the jet and the side walls (see Fig. 4.11). As soon as the tailwater elevation exceeded the slot level, the water under the jet moved up through the side gaps and accumulated above the jet. No oscillations (pattern AB) were observed in these two experiments. In this design, i.e. $w/W < 1.00$, only flow patterns A, B and C existed (see Fig. 4.8(d)). The tailwater had to be above the lower edge of the slot for patterns B and A to form. If the only concern is to eliminate the oscillating zone, a width ratio of 0.8 (or even 0.9) is adequate. Other advantages of having a width ratio less than unity will be discussed later. The modified double-leaf gate dissipator, with $w/W < 1.00$, can be used in shallow tailwater streams as well as deep ones. It should be noted that in shallow-tailwater streams the formation of the classical hydraulic jump is difficult and to form just downstream of the gate, the jump should be forced by baffle blocks or baffle walls or by any other means. Therefore, double-leaf gate basins are strongly recommended to be used, instead of common basins, in such streams.

4.4.1.4 Hysteresis effects

Preliminary experiments (series B) were conducted to classify the different flow patterns and the results of these experiments are shown in Fig. 4.7(a-c) and Fig. 4.8(a-d). In these experiments, the tailwater depth was varied in such a manner as to observe the different flow patterns. The critical submergence ratios, at which the flow changed from one pattern to another, were found with the tailwater depth increased in small steps. Experiments were also performed with decreasing tailwater depth to see as to whether hysteresis effects were present. For the experiments with the 9 mm slot width, switching of the flow pattern from C to B and from B to C occurred when the tailwater level was at the upper and lower edges of the slot respectively as shown in Fig. 4.8(a) thus showing minor hysteresis effects. However, appreciable hysteresis effects were present for the 20 mm slot as shown in Fig. 4.8(b-c). With raising the tailwater, the jet switches from pattern C to pattern A with the oscillatory regime AB existing in between and flow pattern B did not exist. When the tailwater was lowered, the situation became different as pattern B set in at the lower limit of the oscillating zone. The jet switched to the plunging pattern (C) when the water level fell to the lower edge of the slot. The difference in behavior between the 9 mm and the 20 mm jets was perhaps due to the relatively larger momentum flux in the 20 mm jets. In weak jets, if the minor hysteresis through the opening is overlooked, a specific flow pattern is formed for each combination of the Froude number and the submergence ratio, whether the tailwater was raised or lowered. In large momentum jets, the original state of the jet is the third factor in determining the flow pattern. While raising the tailwater and assuming the jet is originally of the plunging type, it prefers to stay as a plunging jet for as maximum submergence as possible. The same occurs while lowering the tailwater and assuming the jet is originally of pattern B as it also tries to keep its state for as minimum submergence as possible. The ventilated jets did not show any hysteresis effects as shown in Fig. 4.8(d). For the oscillating jet regime, the maximum height reached by

the jet increased with the Froude number. To delineate the range of the oscillating jet, the variation of the tailwater depth normalized with $(U_o^2 \sin^2 \theta / 2g)$ was plotted against the Froude number as shown in Fig. 4.10 where the range of the tailwater through which the oscillation occurs decreased as the offset ratio decreased. No oscillations were observed for Z_o/b_o equal to zero. The ventilated jets suffered neither oscillations nor hysteresis effects because the upward and the downward pressures acting on the jet were in balance at any tailwater level. In conclusion, the unbalance between the upward and the downward pressures acting on the jet is assumed to be the main reason causing the jet oscillations as well as the hysteresis effects.

4.4.2 Velocity profiles

Time-averaged velocity profiles were obtained for the whole flow field including the inclined jet from the slot, the surface jet for flow patterns A, B and AB and the wall jet on the bed for pattern C and also in the recirculating flow regions for several experiments. A total of 14 experiments were conducted and the details of these experiments are shown in Fig. 4.12(a-n) and are included in table 4.1. These observations were taken for the different Froude numbers ($F_o = 2.40, 3.60, 4.80, 7.20$ and 10.40), six submergence ratios ($S = 0.00, 1.00, 13.50, 15.00, 22.50$ and 30.00) and four offset ratios ($Z_o/b_o = 0.00, 6.75, 13.50$ and 30.00). The velocity profiles in the inclined jet from the slot are discussed later. Velocity measurements could not be obtained in the strong shear layer separating the forward and the backward flows because the flow within this layer was very turbulent. In this layer the velocity fluctuations were larger than the local mean velocity. Hence, velocities within this layer were predicted by linear interpolation.

Fig. 4.12(a) shows the velocity profiles for pattern C where the jet plunged into the tailwater till it hit the bed at a certain line and then moved as a wall jet. Fig. 4.12(b)

shows the velocity profiles for pattern B where the jet issued from the slot as a curved surface jet and then proceeded as a horizontal surface jet. For flow patterns C and B which are shown in Figs. 4.12(a and b), respectively, the Froude number is the same but the tailwater in pattern C was at the lower edge of the slot whereas in pattern B, the tailwater was at the upper edge. Fig. 4.12(c-n) show flow pattern A except for Fig. 4.12(e) which shows flow pattern AB. In flow pattern A, the jet issued from the opening with a certain angle and then assumed a larger angle at a later stage. After the jet surfaced it proceeded as a surface jet. These figures show the velocity profiles for the surface jet as well as the reverse flow. In the surface jet the maximum velocity is located at, or very close, to the free surface and the velocity distribution seems to be linear. The velocity distribution of the return flow is almost uniform except near the bed and at the jet edges. The velocity profiles of pattern AB, shown in Fig. 4.12(e), are very similar to those of pattern A. In pattern AB, the velocity measurements were affected by the jet oscillation especially in the far field where the mean velocities were relatively small and could easily be affected by the flow unsteadiness. Fig. 4.12(k-n) show pattern A for the Froude number, the submergence ratio and the offset ratio are equal to 4.80, 13.50 and 13.50 respectively. Fig. 4.12(k) and Fig. 4.12(l) are for the same width ratio of $w/W = 1.00$ but the deflection angles, in the two experiments, were 30 and 10 degrees respectively. The velocity profiles shown in Fig. 4.12(k and l) are almost identical indicating that the deflection angle has almost no effect on the velocity characteristics of the surface jet if the Froude number, the submergence ratio, the offset ratio and the width ratio are kept constant. Fig. 4.12 (l-n) show the effect of the width ratio on the velocity distributions. In these three figures the width ratios w/W are 1.00, 0.80 and 0.50 respectively while the other variables are the same. These figures show that the decrease in the width ratio is associated with a faster decay of the maximum velocity.

4.4.3 Reverse flow

The reverse flow underneath the surface jet is driven by an adverse pressure gradient. This flow is the source of the entrained fluid required for the expansion of the surface jet (see Fig. 4.13 for the reverse flow near the bed). The velocity profiles shown in Fig. 4.12(c-n) indicate that the velocity in the reverse flow below the surface jet is almost uniform except near the bed and at the jet edges. Fig. 4.14(a-d) show the variation of the depth-averaged reverse velocity u_r for different Froude numbers, submergence ratios, offset ratios, inclination angle and width ratios. Fig. 4.14(a) shows that the depth-averaged reverse velocity increases as the Froude number increases, and as the offset ratio decreases but is only slightly affected by the submergence factor as long as the flow pattern remains the same. For the oscillating jet flow pattern AB, u_r was found to have significantly smaller values, especially in the far field. Fig. 4.14(b) shows the longitudinal variation of (u_r/U_o) for patterns A and AB. The maximum value of the normalized reverse velocity is affected by the offset ratio. For $Z_o/b_o = 30.00$, this maximum value is about 10% U_o whereas it is 14% and 18% for $Z_o/b_o = 13.50$ and 6.75 respectively. Fig. 4.14(c-d) show the effect of the jet angle θ and the width ratio w/W on the depth-averaged reverse velocity distributions. It can be shown that the deflection angle θ does not have a significant effect on the depth-averaged reverse velocity distributions. Decreasing the width ratio from 0.80 to 0.50 was associated with a little decrease in the depth-averaged reverse velocity downstream of the peak of the profile. In conclusion, the normalized depth-averaged reverse-velocity distributions are mainly affected by the offset ratio, Z_o/b_o . For $Z_o/b_o = 30.00$, the normalized depth-averaged velocity distributions can be represented by the following equation

$$\frac{u_r}{U_o} = 3.0951 * 10^{-6} \left(\frac{x}{b_o} \right)^2 - 0.0007 \left(\frac{x}{b_o} \right) - 0.0557 \quad (4.4)$$

with a value of the correlation coefficient r^2 of 0.89

The corresponding equation for $Z_o/b_o = 13.50$ is

$$\frac{u_r}{U_o} = 1.466 * 10^{-5} \left(\frac{x}{b_o} \right)^2 - 0.0014 \left(\frac{x}{b_o} \right) - 0.0955 \quad (4.5)$$

with a value of the correlation coefficient r^2 of 0.93

4.4.4 Velocity decay

For each velocity profile, the maximum velocity u_m may be considered as an important characteristic and as a scale. Fig. 4.15(a-n) show the decay of the maximum velocity u_m at any section with the longitudinal distance measured from the slot for flow patterns A, B, C and AB. Half of these plots are presented in a dimensionless form to show the decay of the maximum velocity u_m in terms of the velocity of the jet at the slot U_o with the normalized distance from the gate x/b_o along with the corresponding curves for plane turbulent wall jets and surface jets (Rajaratnam 1976; Rajaratnam and Humphries 1984). As flow pattern A has been recommended for operation in the prototype, more focus was given to pattern A compared to the other flow patterns. A study of the above mentioned figures shows that, in flow pattern A, the decay of the maximum velocity occurs in three stages. The first stage is the decay in the inclined jet, from the slot to the surfacing of the jet. The maximum velocity in this stage decays very rapidly. This zone may be considered the most efficient zone in dissipating the energy of the jet and up to 80% of the issuing velocity can decay within this zone. The fast decay in this region is due to the high entrainment rate of curved turbulent jets. The second stage starts at the section of minimum velocity and indicates an increase due to the fall from the surface hump, which forms at the location where the inclined jet

surfaces, and ends at the section of the next maximum. The velocity decays again in the third stage due to the turbulent mixing in the surface jet. This stage shows a very slow decay in comparison with the first stage. It may also be noticed that the decay of the maximum velocity in the last stage is very similar to that of the plane surface and wall jets. The overall decay was found to be more than that of the surface and wall jets in the range of x/b_0 of 220. It was mentioned earlier that the factors that affect the flow characteristics are the Froude number, the offset ratio, the submergence ratio, the inclination angle, the width ratio and, of course, the flow pattern.

Figs. 4.15(a-n) were designed in such a way that only one parameter is changing while the other parameters are kept constant. Figs. 4.15(a-b) show experiments 4, 9 and 12 where the flow is of pattern A. The changing parameter in the three experiments was the Froude number which was equal to 4.8, 7.2 and 10.4 in the three experiments respectively. Fig. 4.15(b) shows that the Froude number has no effect on the decay of the maximum velocity if U_0 and b_0 are used as the velocity and length scales respectively. Figs. 4.15(c-d) show experiments 3 and 4 where the flow is also of pattern A. The changing parameter was the submergence ratio equal to 22.5 and 30.0 respectively. Figs. 4.15(c-d) show that the submergence ratio has no effect on the velocity decay (as long as the change in the submergence does not change the pattern of flow). Figs. 4.15(e-f) shows experiments 14, 15 and 16 (pattern A) where the changing parameter was the offset ratio which had the values of 13.50, 6.75 and 0.00 in the three experiments respectively. Figs. 4.15(e-f) show that the change in the offset ratio can affect the velocity decay significantly. The smaller the offset ratio, the faster is the velocity decay. This might be explained that decreasing the offset ratio is associated with an increase in the velocity of the return flow which in turn causes the main flow velocity to decay faster. The changing parameter in Figs. 4.15(g-h) was the inclination angle of the jet. This figure shows experiments 18 and 19 (pattern A) where the inclination angle of the jet θ was equal to 30 and 10 degrees respectively. It can be seen

from Figs. 4.15(g-h) that changing the inclination angle does not have any significant effect on the velocity decay. The last parameter to be considered was the width ratio w/W . Figs. 4.15(i-j) show experiments 19, 20 and 21 where the width ratio was equal to 1.0, 0.8 and 0.5 respectively. Figs. 4.15(i-j) show that the smaller the width ratio the faster is the maximum velocity decay. This seems logical as decreasing the width ratio enhances the mixing of the jet with its surroundings which results in a faster decay of its maximum velocity.

The maximum velocity decay in the flow patterns A, B and C are shown in Figs. 4.15(k-l) where all the other parameters, except for the submergence ratio, were kept constant. At $x/b_o = 220$, u_m/U_o was almost identical in flow patterns A and B. Flow pattern C showed a faster decay. At $x/b_o = 120$, u_m/U_o was nearly one third that of flow patterns A and B. Figs. 4.15(m-n) show experiments 9 and 8 for flow patterns A and AB respectively. It is clear that the maximum velocity decay in both flow patterns is almost the same. A consolidated plot for all the maximum velocity decay profiles in flow pattern A is shown in Fig. 4.16.

To evaluate the double-leaf gate as an energy dissipator, comparisons with well-known dissipators were essential. Fig. 4.17 shows a comparison between the decay of the maximum velocity in the double-leaf gate dissipator for flow pattern A with the results of Wu and Rajaratnam (1995) for a surface jet produced with a baffle wall for submerged flow. For a Froude number equal to 7.20, Fig. 4.17 shows that in the first stage, the decay of the maximum velocity in the present study is much faster. The overall decay for greater distances is almost the same in both the experiments.

Comparisons of the maximum velocity decay in the double-leaf gate dissipator with those of the free and the submerged hydraulic jumps are shown in Figs. 4.18(a-b) and 4.19(a-b). In Figs. 4.18(a-b), U_o was taken as the velocity scale and b_o as the length scale whereas in Figs. 4.19(a-b), the length scale was taken as L , where L is the

horizontal distance from the gate to the point where the velocity is $0.5U_0$. Fig. 4.18(a) shows that the maximum velocity decay in the first stage of the double-leaf gate dissipator is similar to that of the free jump whereas in the far field, the free jump basin appears to be more efficient. However, the overall decay in the two cases is comparable. The double-gated jet is much more efficient than the submerged jump, especially in the first stage of decay as shown in Fig. 4.18(b). With L as a length scale, Figs. 4.19(a-b) show a better similarity between the double-leaf gate dissipator, the free and the submerged jump stilling basins. As b_0 is relatively small, L is considered to be more reliable and hence the maximum velocity decay for the present study is considered, in general, to be very similar to that of free and submerged jumps.

4.4.5 Inclined jet

Fig. 4.20 shows the locus of the maximum velocity along with the water surface profiles for pattern A in experiments 4, 9 and 12 respectively. The jet issues from the slot with an initial angle θ of 30 degrees. The jet keeps its initial direction until it reaches a certain point after which the jet path becomes steeper with the angle of the jet increasing to about 45 degrees. It was noticed that the point at which the jet changes its direction is very close to the end of the first stage of the maximum velocity decay. This bending of the jet is similar to the Coanda effect of jets located near boundaries. This aspect of the curved jet has been attributed to the pressure difference across the jet. Changing the direction was also explained by Sawyer (1962).

Some observations were also taken for a deflection angle of $\theta = 10$ degrees. For the large offset ratios, the same behavior of the jet was observed as it issued with the original angle until it assumed a larger angle at a later stage as with the case of the 30 degrees jet. With $\theta = 10$ degrees, the upper cavity was larger and this minimized the oscillating zone. Other than this, the different flow characteristics for the two angles

were quite similar. For the small offset ratios, the 10 degrees jet tended to reattach to the bed by the Coanda effect. Therefore, the 10 degrees angle can only be used with prototypes having large offset ratios. As the 30 degrees angle is suitable for both small and large offset ratios, it is recommended for use in double-leaf gate dissipators.

Fig. 4.21(a-j) show the velocity distributions and the similarity profiles for the inclined jet for experiments 3, 9, 12, 14 and 16 respectively. In these plots, each group of data points are for a certain Froude number, submergence ratio, offset ratio, width ratio and distance from the slot. The velocity distributions in the five experiments mentioned above, along with the Gaussian distribution for the simple submerged plane jet, are represented in Fig. 4.22. The maximum velocity within each section was chosen to be the velocity scale. The jet half width b was taken as the length scale which is the inclined distance across the jet between the point of u_m and the point of $0.5u_m$. As the velocity distribution was not symmetrical about the jet centerline, two length scales were used, one for the upper half b_u of the velocity distribution and the other length scale b_l for the lower half. It was found that b_l is approximately $0.90 b_u$. The maximum velocity decay with distance in the inclined jet zone is shown in Fig. 4.23 along with the relevant plots for the plane wall and surface jets. Fig. 4.23 shows that the maximum velocity starts to decay earlier and the rate of decay is faster in the inclined jet than those of the plane wall and surface jets. The best fit to the data showed an exponential decay for the maximum velocity and can be described by the equation

$$\frac{u_m}{U_o} = 1.0642 * e^{-0.0467\left(\frac{x}{b_o}\right)} \quad (4.6)$$

Rajaratnam and Humphries (1984) described the decay of the maximum velocity in the plane surface jets using the following equation

$$\frac{u_m}{U_o} = \frac{3.1}{\sqrt{x/b_o}} \quad (4.7)$$

The corresponding equation for the plane wall jet is

$$\frac{u_m}{U_o} = \frac{3.5}{\sqrt{x/b_o}} \quad (4.8)$$

4.4.6 Surface jet

Fig. 4.24(a-ab) show the velocity distributions and the similarity profiles for the surface jet for flow patterns A, B and AB. These figures represent experiments 2, 3, 4, 8, 9, 12, 14, 15, 16, 17, 18, 19, 20 and 21 respectively. Each figure shows the surface jet velocity distributions for a specific Froude number, offset ratio, submergence ratio, width ratio and inclination angle. The plots shown in each figure are for different longitudinal distances from the slot. In these figures, the maximum velocity, u_m , which occurs at, or very close to, the free surface is the velocity scale and b_s is the length scale which is equal to the distance where the normalized velocity is equal to 0.5. Fig. 4.25 shows a consolidated non-dimensional plot of all the experiments along with the Gaussian distribution. The forward velocity profiles are approximately similar. This similarity profile seems to be almost linear and a similar observation has been made by Wu and Rajaratnam (1995). The deviation of the similarity profile from the Gaussian distribution that describes the velocity profiles in the simple surface jet might be due to the shallow tailwater conditions. Some scatter in the results can be observed in the lower portion of Fig. 4.25. Swaan Jr. et al. (1989) mentioned that the distortion in the lower portion of the forward flow occurs in the region of the jet where the reverse flow velocity is approaching the magnitude of the jet velocity and the breaking down of the jet behavior is expected.

Fig. 4.26(a-b) show the growth of the surface jet half-width b_s . In Fig. 4.26(a), the jet half-width was normalized by the slot width b_o and x_o is the value of x where the maximum surface velocity occurred. It can be noticed from Fig. 4.26(a) that, at the beginning of the surface jet, the jet half-width ranged between 2.5 to 10 times the slot width. It can be shown also that the jet half-width increases with the Froude number increase, with the width ratio decrease and is slightly affected by the submergence and offset ratios. In the analysis of Schneider (1985), It was concluded that the jet half-width is not highly affected by the degree of the downstream constraint. In Fig. 4.26(b), the jet half-width at the first station, b_{so} , was used as the length scale. It can be shown that the growth rate is nearly the same as that of the classical surface jet (Rajaratnam and Humphries, 1984) over some distance after which the growth of the jet becomes very weak. The reason of this break down is perhaps due to the weak entrainment ability of the jet due to the jet confinement by the downstream shallow tailwater conditions. The characteristics of this breakdown will be studied in details in the next two chapters.

4.4.7 Surface-jet discharge

Fig. 4.27(a-b) show the variation of the surface jet discharge intensity Q for flow pattern A, in terms of the discharge intensity at the slot Q_o , with the dimensionless distance measured from the gate. As the entrainment rate is relatively high in the inclined-jet region, the dimensionless discharge reaches its maximum value at the point of impingement with the free surface. Downstream of this point, the degree of the jet confinement becomes larger as the jet grows. Hence, the entrainment rate becomes weaker in the surface jet resulting in a decrease in the jet discharge. The underlying recirculation region ends where the ratio $Q/Q_o = 1$. Fig. 4.27(a) shows the effect of the offset ratio Z_o/b_o on the discharge variation. For Z_o/b_o was equal to 30.0, the maximum value for Q/Q_o was about 4.5. This value was about 3.5 and 1.5 for Z_o/b_o was equal to

13.5 and 0.0 respectively. This indicates the significant effect of the offset ratio on the variation of the jet discharge with distance. Wu and Rajaratnam (1995), in studying the effect of baffles on submerged flows, found that the maximum discharge ratio is as high as 2.50 while the same ratio was found to be about 4.00 in the study done by Swean Jr. et al. (1989). It can be concluded that the decrease in the offset ratio, or the degree of the jet confinement, is associated with a significant decrease in the jet-discharge ratio. This seems reasonable as the reverse flow, that is required to supply the entrained fluid, is affected by the jet confinement.

The effect of the inclination angle θ and the width ratio w/W on the discharge variation is shown in Fig. 4.27(b). In experiments 18 and 19, the width ratio was 1.0 and the inclination angle was 30 and 10 degrees, respectively. In experiments 19, 20 and 21, the inclination angle was 10 degrees and the width ratio was 1.0, 0.8 and 0.5 respectively. Fig. 4.27(b) shows that the inclination angle does not have any significant effect on the discharge variation. The inclination angle only affected the longitudinal distance to the peak where this distance was found to be inversely proportional to the inclination angle. The surface-jet discharge was affected significantly by the changes in the width ratio. The maximum value of Q/Q_0 was about 5.0, 4.0 and 3.0 for the width ratio was equal to 0.5, 0.8 and 1.0 respectively.

4.4.8 Surface-jet momentum flux

The presence of a strong reverse flow approximately parallel to the surface jet would reduce the momentum flux in the surface jet. Assuming a linear velocity distribution for the surface jet, it can be shown that:

$$\frac{M}{M_0} = \left(\frac{2}{3}\right) \left(\frac{U_m}{U_0}\right) \left(\frac{Q}{Q_0}\right) = \left(\frac{2}{3}\right) \left(\frac{U_m}{U_0}\right)^2 \left(\frac{b_s}{b_0}\right) \quad (4.9)$$

where M is the momentum flux in the surface jet at any station and M_0 is the momentum flux at the slot. The above relation confirms the decay of the momentum flux as the growth rate of the length scale b_z is very weak and the velocity decays rapidly (as mentioned earlier). Fig. 4.28(a-b) show the variation of the dimensionless momentum flux M/M_0 versus the dimensionless distance x/b_0 and a significant reduction in the momentum flux can be seen. Considerable momentum losses in free jets were also found in the data obtained by Goldschmidt and Eskinazi (1966), Heskestad (1965), Miller and Comings (1957) and Kotsovinos (1975) as presented in Kotsovinos (1978). This phenomenon was found also in surface jets as analyzed by Swear Jr. et al. (1989). Kotsovinos (1978) mentioned that the main reason for the momentum losses is the jet interaction with the reverse flow. Fig. 4.28(a) shows the effect of the offset ratio on the momentum decay. This figure shows three offset ratios of 30.0, 13.5 and 0.00 where it is easy to see that the surface-jet momentum flux decays faster for smaller offset ratios. Fig. 4.28(b) shows the effect of the inclination angle and the width ratio on the momentum decay. Neither the angle nor the width ratio had a significant effect on the momentum decay. As decreasing the width ratio resulted in an increase in the discharge ratio and a faster decay in the maximum velocity (see sections 4.4.7 and 4.4.4), it was logical that the momentum flux would not be affected by the width ratio changes (see Eq. 4.9).

4.4.9 Bed shear stress

One main consideration in this study was to prevent erosion of the downstream bed. It was therefore important to consider the bed shear stress in the downstream channel for the different flow patterns. A Prandtl tube was used as a Preston tube to measure the bed shear stress.

4.4.9.1 Pattern A

Fig. 4.29(a-c) show the variation of the bed shear stress for pattern A for four Froude numbers, three submergence ratios, three offset ratios, three width ratios and two inclination angles. In this flow pattern, it was found that the bed shear stress τ reached a maximum value of τ_m at a distance of x_{oA} from the gate and was symmetrical on either side of the maximum (see Fig. 4.29(a-b)). Fig. 4.29(a) shows the variation of the bed shear stress with the distance from the gate. Fig. 4.29(b) shows the variation of the dimensionless shear stress τ/τ_m with the dimensionless distance $(x-x_{oA})/b_A$ where b_A is the longitudinal distance between the point of τ_m and that of $0.5\tau_m$. The effect of the offset ratio on the coefficient of skin friction $C_{fo} = \tau_m / (\rho U_o^2 / 2)$ and the normalized longitudinal distance to the peak x_{oA}/b_o is shown in Fig. 4.29(c). The coefficient of skin friction was found to vary mainly with the offset ratio. It was found to decrease from about 0.0003 for $Z_o/b_o = 0.0$ to 0.00007 for $Z_o/b_o = 30.0$. Also, the normalized longitudinal distance to the peak x_{oA}/b_o was found to depend mainly on the offset ratio. The variation of the coefficient of skin friction C_{fo} and the longitudinal distance to the peak x_{oA}/b_o with the offset ratio are described by Eq. 4.10 and Eq. 4.11 respectively

$$C_{fo} = 0.289 * 10^{-3} * e^{-0.0468 \left(\frac{Z_o}{b_o} \right)} \quad (r^2 = 0.88) \quad (4.10)$$

$$\frac{x_{oA}}{b_o} = 19.63 + 3.60 \frac{Z_o}{b_o} \quad (r^2 = 0.95) \quad (4.11)$$

4.4.9.2 Pattern B

Fig. 4.30(a-b) show the bed shear stress distribution for pattern B for three different Froude numbers and two different submergence ratios. Similar to flow pattern A, the bed shear stress τ reached a maximum value of τ_m at a distance of x_{oB} from the gate but was asymmetrical about its maximum value. For the Froude number $F_o = 10.40$, the bed shear stress was found to decrease dramatically with the submergence ratio increasing from 1.0 to 7.5 (see Expt. 10 & 11). Hence, it is recommended, in the case of the large Froude numbers, to keep the slot slightly submerged to suppress the bed shear stress. In Fig. 4.30(b), the bed shear stress is normalized by its maximum value τ_m and the longitudinal distance from the location of the maximum shear stress is normalized by b_B which is the distance, to the left of the peak, between the point of the zero shear and that of the maximum shear. Fig. 4.30(b) shows that the bed shear stress distributions are almost similar. The similarity profile can be represented by the following equation:

$$\frac{\tau}{\tau_m} = 0.90 - 0.18 \left(\frac{x - x_{oB}}{b_B} \right) - 0.63 \left(\frac{x - x_{oB}}{b_B} \right)^2 + 0.49 \left(\frac{x - x_{oB}}{b_B} \right)^3 - 0.10 \left(\frac{x - x_{oB}}{b_B} \right)^4 \quad (4.12)$$

It should be mentioned that, in flow pattern B the strong turbulent layer separating the forward and the backward flows was very close to the bed. Hence, the bed shear stress could not be measured for $Z_o/b_o < 30$ and consequently the variation of the bed shear and the length scales with the offset ratio could not be evaluated in this flow pattern.

4.4.9.3 Pattern C

Fig. 4.31(a-d) show the bed shear stress distribution for pattern C for three different Froude numbers, two different offset ratios and the same submergence. Fig. 4.31(a) shows that the bed shear stress increased from zero at the line of impingement located at a distance of x_{oc} from the gate to a maximum value of τ_{md} downstream with another maximum value τ_{mu} on the upstream side of the impingement line with a distance of b_c between these two maximums. A normalized distribution of the shear stress variation is shown in Fig. 4.31(b) by choosing the maximum positive shear stress as the shear scale. The length scale, b_c , was taken as the longitudinal distance between the maximum negative and positive shear and x_{oc} is the distance, measured from the gate, to the point of impingement with the bed or the point of zero shear. The skin friction coefficient corresponding to τ_{md} varied mainly with the offset ratio Z_o/b_o , decreasing from about 0.004 for $Z_o/b_o = 14.0$ to about 0.0008 for $Z_o/b_o = 30.0$. Further, τ_{mu} was equal to $0.75 \tau_{md}$. The variation of the skin friction $C_{fo} = \tau_{md} / (\rho U_o^2 / 2)$ with the offset ratio is shown in Fig. 4.31(c). Eq. 4.13 describe this relation.

$$C_{fo} = 15.64 * 10^{-3} * e^{-0.1 \left(\frac{Z_o}{b_o} \right)} \quad (r^2 = 0.78) \quad (4.13)$$

It was found that b_c/Z_o and x_{oc}/Z_o varied mainly with the Froude number. These relations are shown in Fig. 4.31(c-d) and are described by Eq. 4.14 and Eq. 4.15 respectively.

$$\frac{x_{sc}}{Z_o} = 0.385 F_o \quad (r^2 = 0.95) \quad (4.14)$$

and the variation of b_c/Z_o with the Froude number is given as

$$\frac{b_c}{Z_o} = 0.43 F_o - 0.053 F_o^2 \quad (r^2 = 0.92) \quad (4.15)$$

4.5 Conclusions and Recommendations

This study introduces a new design concept for energy dissipation below regulators. In the new design, a high velocity jet is deflected to the free surface by means of a double-leaf gate with the upper gate located upstream of the lower to create the opening which produces the inclined jet.

Dimensional analysis showed that the dimensionless variables involved in this problem are the Froude number, the width ratio, the submergence ratio, the offset ratio and the inclination angle of the jet.

Based on a laboratory study, four flow regimes were defined. Pattern A occurs with a relatively large submergence. The jet moves towards the water surface and after impinging on it, proceeds as a surface jet. Pattern B occurs with relatively small submergence. The jet penetrates the free surface and returns back to proceed also as a surface jet. In this flow pattern, the jet is not submerged at the gate. In pattern C, the jet plunges into the tailwater and after impingement on the bed, travels as a wall jet. In between zones A and B, the jet oscillates due to unbalanced pressure across the jet. The jet oscillation, i.e. pattern AB, does not exist in the models with the width ratio less than 1.0. Flow pattern A is recommended for design and can easily be achieved in flow regulators.

Velocity distributions and bed shear stresses were measured. The velocity distributions for the inclined jet are similar and the similarity profile is the same as that of the plane turbulent jet. The velocity profiles of the surface jet are also similar but the distribution is almost linear due to the confinement of the spreading jet by the shallow tailwater. The decay of the maximum velocity was studied and compared with that for free and submerged jumps. The decay process was divided into three stages of the deflected jet in which the decay was rapid; the convergence stage in which the falling jet speeds up; and the surface jet stage in which the maximum velocity decays rather slowly. It was found that the decay of the maximum velocity in the double-leaf gate design is as effective as that in free and submerged jumps.

The shallow tailwater condition affects the main characteristics of the surface jet. It decreases the entrainment rate and as a result the growth rate of the length scale becomes very weak. Further, this confinement enhances the rate of the velocity decay. The momentum flux in the jet is not preserved due to the entrainment of the fluid traveling towards the gate with appreciable horizontal velocity.

Bed shear stress in the downstream channel were found to have certain characteristic distributions. In flow pattern A, the shear stress increases until it reaches a peak value and then decreases. The distribution is symmetrical about the peak. In pattern B, the distribution looks like that of pattern A but is not symmetrical. In pattern C, the shear stress increases from zero at the line of impingement to two maximum values, one on either side. The shear stress in pattern A was very small compared with that for pattern C.

Considering the lifting of the gates in a flow regulator, the weight of the gate in kg/m^2 varies widely depending on the head and the gate size. However, a single gate can weigh up to several tons. There are some flow regulators on rivers that have more than 100 vents. If a double-leaf gate design is used instead of single-leaf gates, up to 50% of the power and height of the lifting device can be saved. These savings can be

added to the advantage of having minimum scour downstream of this type of regulators. Also, in this type of regulators, a short apron can be used if adequate sheet piles are installed. The apron for hydraulic jump dissipators tends to be longer. For modifying existing regulators an upward sloping sill may be installed under the gate.

The ventilation of the jet (i.e. using jets with $w/W < 1.00$) is very important and is highly recommended in the prototype. It eliminates the oscillating zone and leads to a faster decay of the maximum velocity. With the jet ventilated, the double-leaf gate regulator can be used in deep as well as in shallow tailwater streams.

Experiments with $Z_g/b_o = 0.0$ indicated that the jet issued as in pattern A and was stable in this flow pattern unless it was forced towards the bed. In the later case, the jet changed into a wall jet and remained stable in this pattern. However, the design with the gate opening at the bed needs further study, especially for the effect of the angle on the jet stability.

Gate vibration is a serious problem that can cause structural damage and all precautions have to be taken to prevent vibration of the leaves in the prototype. Although the 30 degrees jet was found to be suitable for the large as well as the small offset ratios, more angles have to be checked especially the 45 degrees angle.

4.6 References

- Bakhmeteff, B. A. and Feodoroff, N. V. (1941). "Discussion of energy loss at the base of a free overfall." Trans. ASCE, Vol. 108, pp. 1364-1373.
- Elevatorski, E. A. (1959) "Hydraulic energy dissipators." McGraw-Hill, New York.
- Goldschmidt, V., and Eskinazi, S. (1966). "Two phase turbulent flow in a plane jet." Trans. ASME, Series E, J. Appl. Mech., 33(4), 735-747.
- Hager, W. H. (1992). "Energy dissipators and hydraulic jump." Kluwer Academic Publishers, 288p.

- Heskestad, G. (1965). "Hot wire measurements in a plane turbulent jet." Trans. ASME, Series E, J. Appl. Mech., 32(4), 721-734.
- Kotsovinos, N. E. (1975). "A study of the entrainment and turbulence in a plane turbulent jet." W. M. Keck Lab. Hydr. Water Resources, Calif. Inst. Tech. Rept. KH R-32
- Kotsovinos, N. E. (1978). "A note on the conservation of the axial momentum of a turbulent jet." J. Fluid Mech., 87(7), pp. 55-63.
- Liu, H. K. (1949). "Diffusion of flow from submerged sluice gate." Thesis presented to the State Univ. of Iowa, Iowa, in partial fulfillment of the requirements for the degree of M. Sc., 32p.
- Long, D, Rajaratnam, N. and Steffler, P. M. (1990). "LDA study of flow structure in submerged hydraulic jump" J. Hydr. Res., 28(4), pp. 437-460.
- Miller, D. R., and Comings, E. W. (1957). "Static pressure distribution in the free turbulent jet." J. Fluid Mech., 3(10), pp. 1-16.
- Narasimhan, S. and Bhargava, V. P. (1976). "Pressure fluctuations in submerged jump." J. Hydr. Div., ASCE, 102(3), pp. 339-350.
- Ohtsu, I., Yasuda, Y. and Awazu, S. (1990). "Free and submerged hydraulic jumps in rectangular channels." Report of the Research Institute of Science and Technology, Nihon University, No. 35, Feb. 1990, 50 p.
- Patel, V. C. (1965). "Calibration of the Preston tube and limitations on its use in pressure gradients." J. Fluid Mech., Vol. 23, pp. 185-208.
- Peterka, A. J. (1963). "Hydraulic design of stilling basins and energy dissipators." Engrg. Monograph 25, U.S.D.I. Bureau of Reclamation: Denver, Col.
- Peterka, A. J. (1963). "Hydraulic design of stilling basins and energy dissipators." Engrg. Monograph 25, U.S.D.I. Bureau of Reclamation: Denver, Col.
- Rajaratnam, N. (1965). "The hydraulic jump as a wall jet." J. Hydr. Div., ASCE, 91(5), pp. 107-132.

- Rajaratnam, N. (1967). "Hydraulic jumps.", *Advances in Hydrosience*, Vol. 4, pp. 198-276.
- Rajaratnam, N. (1976). Discussion of "pressure fluctuations in submerged jump." *J. Hydr. Div., ASCE*, 102(12), pp. 1785-1787.
- Rajaratnam, N. and Subramanya, K (1967). "Diffusion of rectangular wall jets in wider channels.", *Contributions to Turbulent Wall Jets in Hydraulic Engineering and Other Related Problems*, Dept. of Civil Engineering, Univ. of Alberta, Edmonton, Canada.
- Rajaratnam, N., and Humphries, J. A. (1984). "Turbulent non-buoyant surface jet." *J. Hydr. Res.*, 22(2), pp. 103-115.
- Rouse, H. Siao, T. T. and Nagaratnam, S. (1959). "Turbulence characteristics of the hydraulic jump." *Trans. ASCE*, Vol. 124, pp. 926-966.
- Sawyer, R. A. (1962). "The flow due to a two-dimensional jet issuing parallel to a flat plate." *J. Fluid Mech.* 9(4), pp. 543-560.
- Schneider, W. (1985). "Decay of momentum flux in submerged jets." *J. Fluid Mech.*, 154(5), pp. 91-110.
- Schröder, R. (1963). "Die turbulente Strömung im freien Wechselsprung." *Habilitationsschrift, Mitteilung 59, Institut für Wasserbau und Wasserwirtschaft, TU Berlin, Berlin.*
- Sweat Jr, T. F., Ramberg, S. E., Plesniak, M. W. Stewart., M. B. (1989). "Turbulent surface jet in channel of limited depth." *J. Hydr. Engr., ASCE*, 115(12), pp. 1587-1606.
- Wu, S. (1994). "Four contributions to the application of turbulent jet theory in hydraulic engineering." PhD thesis, University of Alberta, Edmonton, Alberta, Canada.
- Wu, S. and Rajaratnam, N. (1995). "Effect of baffles on submerged flows" *J. Hydr. Div., ASCE*, 121(9), pp. 644-652.

Table 4.1 Primary details of experiments (series A)

Expt. (1)	θ (2)	b_o (mm) (3)	Z_o (mm) (4)	y_i (mm) (5)	W (mm) (6)	w (mm) (7)	U_o (m/s) (8)	F_o (9)	Z_d/b_o (10)	$(y_i-Z_o)/b_o$ (11)	w/W (12)	R (13)	Pattern (14)
1	30	9	270	270	446	446	1.43	4.80	30.00	0.00	1.00	12836	C
2	30	9	270	279	446	446	1.43	4.80	30.00	1.00	1.00	12836	B
3	30	9	270	473	446	446	1.43	4.80	30.00	22.50	1.00	12836	A
4	30	9	270	540	446	446	1.43	4.80	30.00	30.00	1.00	12836	A
5	30	9	270	270	446	446	2.14	7.20	30.00	0.00	1.00	19254	C
6	30	9	270	279	446	446	2.14	7.20	30.00	1.00	1.00	19254	B
7	30	9	270	338	446	446	2.14	7.20	30.00	7.50	1.00	19254	B
8	30	9	270	405	446	446	2.14	7.20	30.00	15.00	1.00	19254	AB
9	30	9	270	540	446	446	2.14	7.20	30.00	30.00	1.00	19254	A
10	30	9	270	279	446	446	3.09	10.40	30.00	1.00	1.00	27812	B
11	30	9	270	338	446	446	3.09	10.40	30.00	7.50	1.00	27812	B
12	30	9	270	540	446	446	3.09	10.40	30.00	30.00	1.00	27812	A
13	30	20	270	270	446	446	1.06	2.40	13.50	0.00	1.00	21261	C
14	30	20	270	540	446	446	1.06	2.40	13.50	13.50	1.00	21261	A
15	30	20	135	405	446	446	1.06	2.40	6.75	13.50	1.00	21261	A
16	30	20	0	270	446	446	1.06	2.40	0.00	13.50	1.00	21261	A
17	30	20	0	270	446	446	1.59	3.60	0.00	13.50	1.00	31892	A
18	30	20	270	540	446	446	2.13	4.80	13.50	13.50	1.00	42523	A
19	10	20	270	540	446	446	2.13	4.80	13.50	13.50	1.00	42523	A
20	10	20	270	540	446	446	2.13	4.80	13.50	13.50	0.80	42523	A
21	10	20	270	540	446	446	2.13	4.80	13.50	13.50	0.50	42523	A

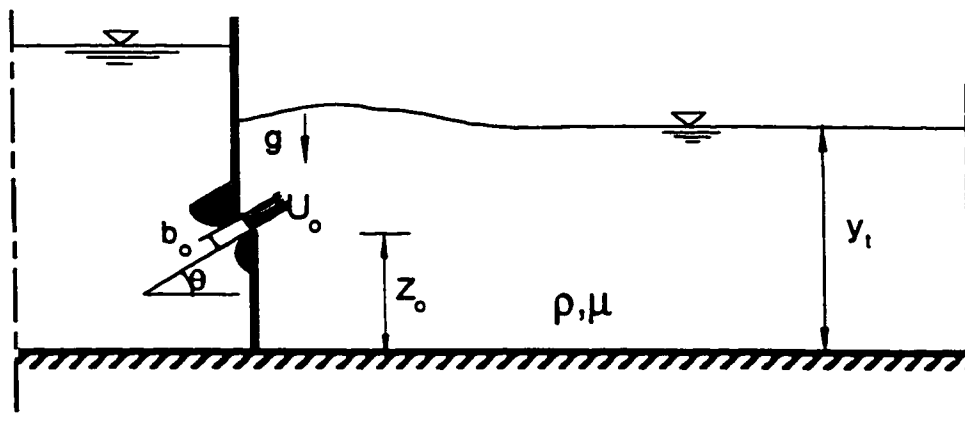


Fig. 4.1 Definition sketch of double-leaf gate dissipator

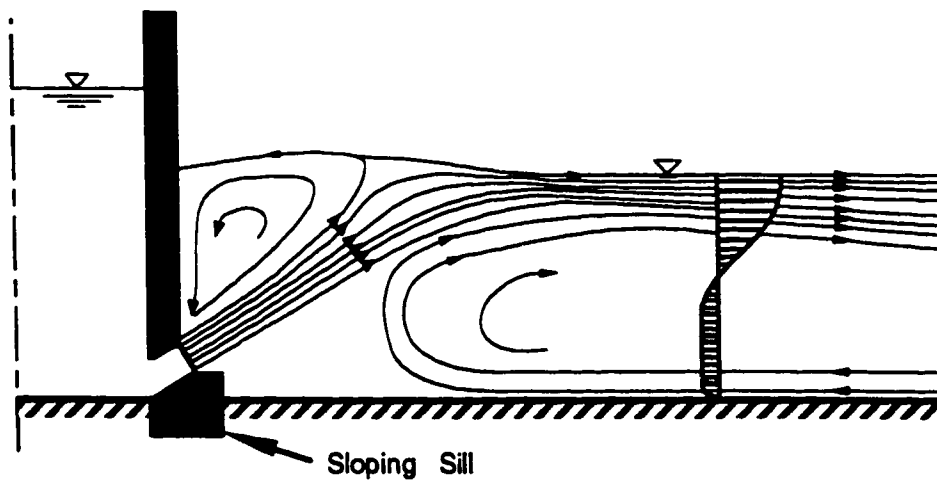


Fig. 4.2 Modification to existing regulators

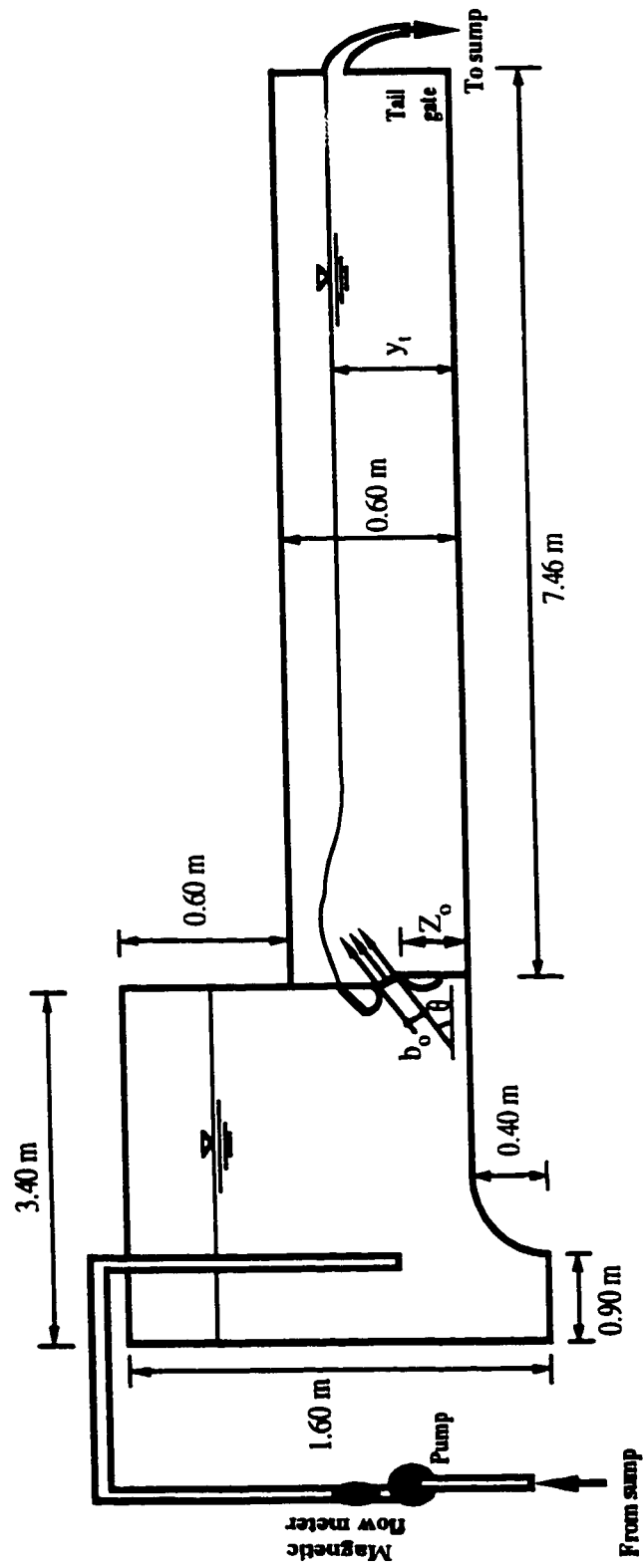


Fig. 4.3 Experimental flume

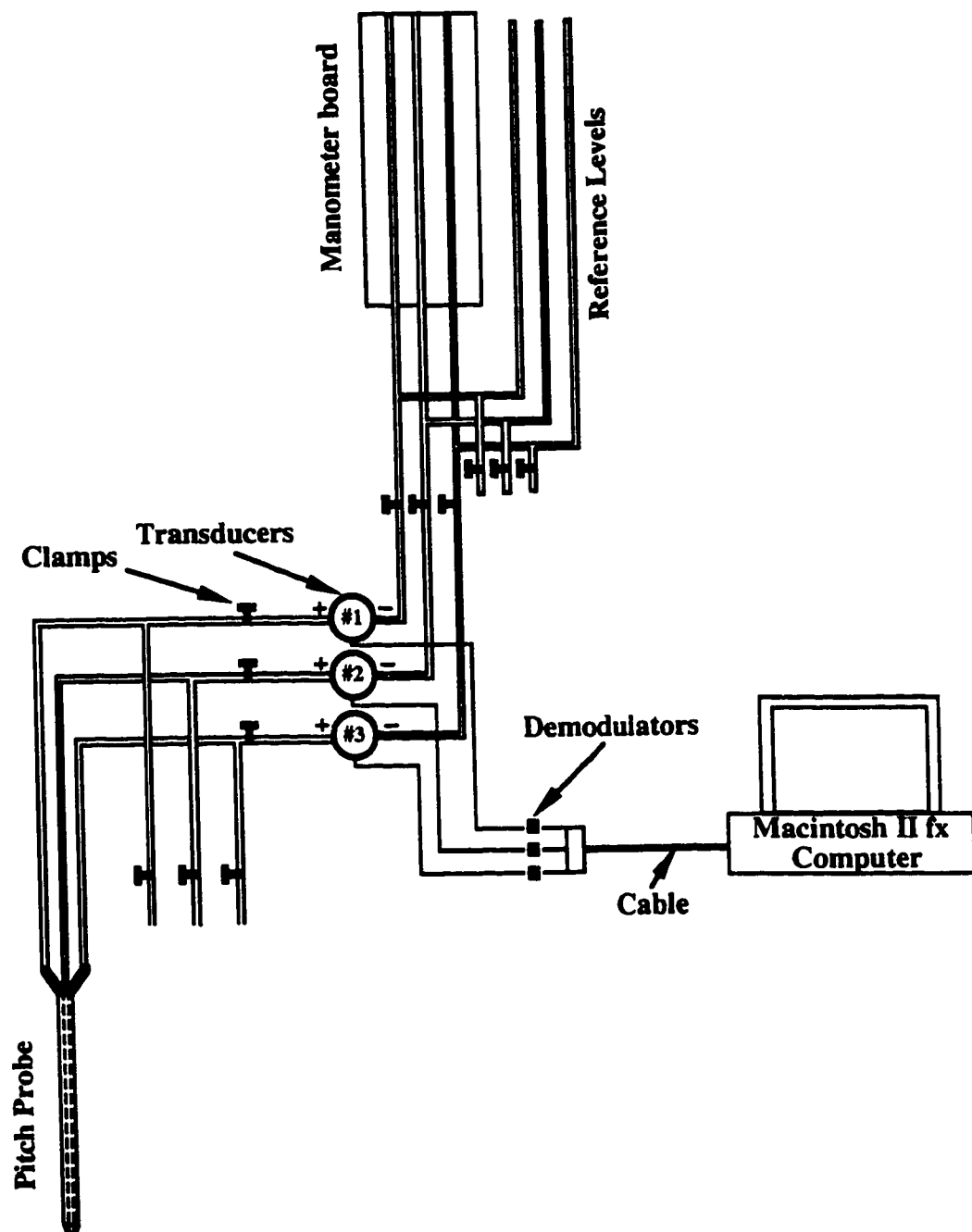


Fig. 4.4 Pitch probe

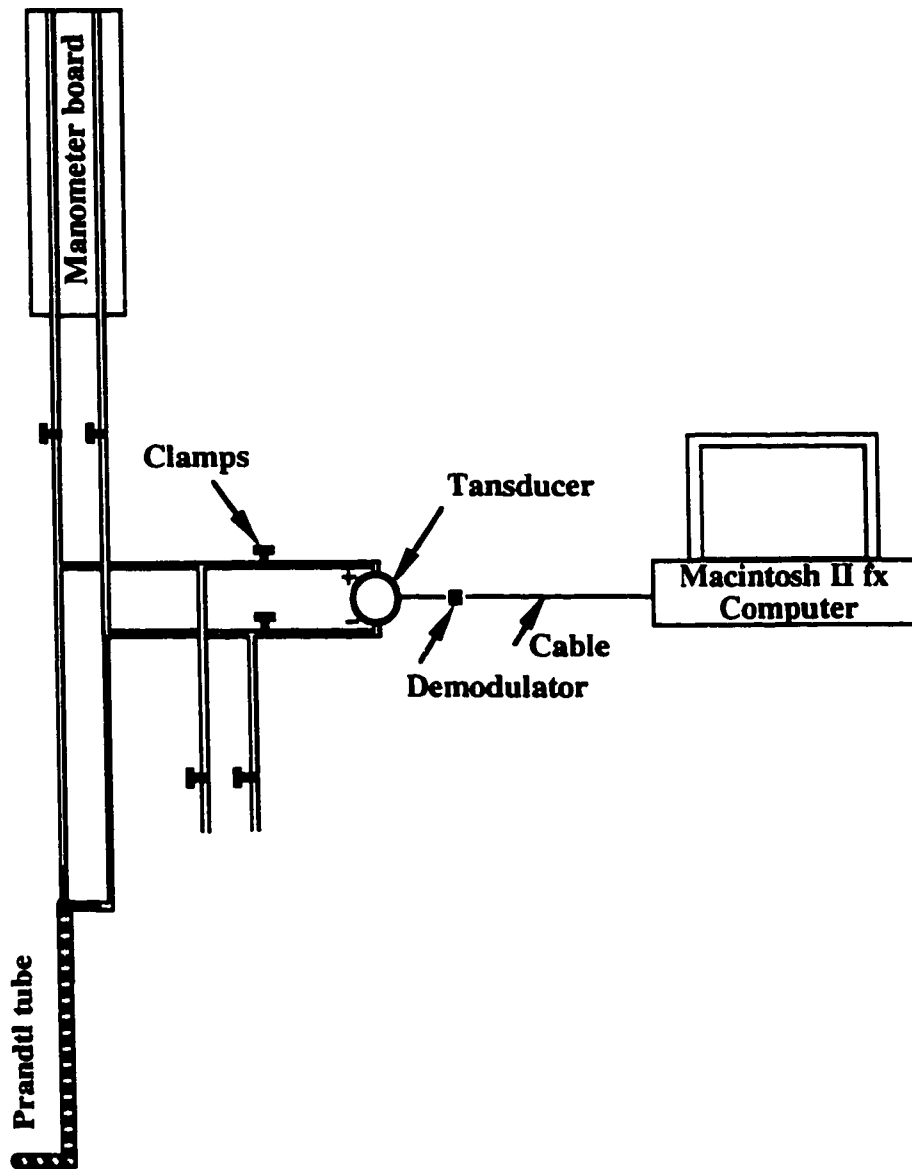


Fig. 4.5 Prandtl tube

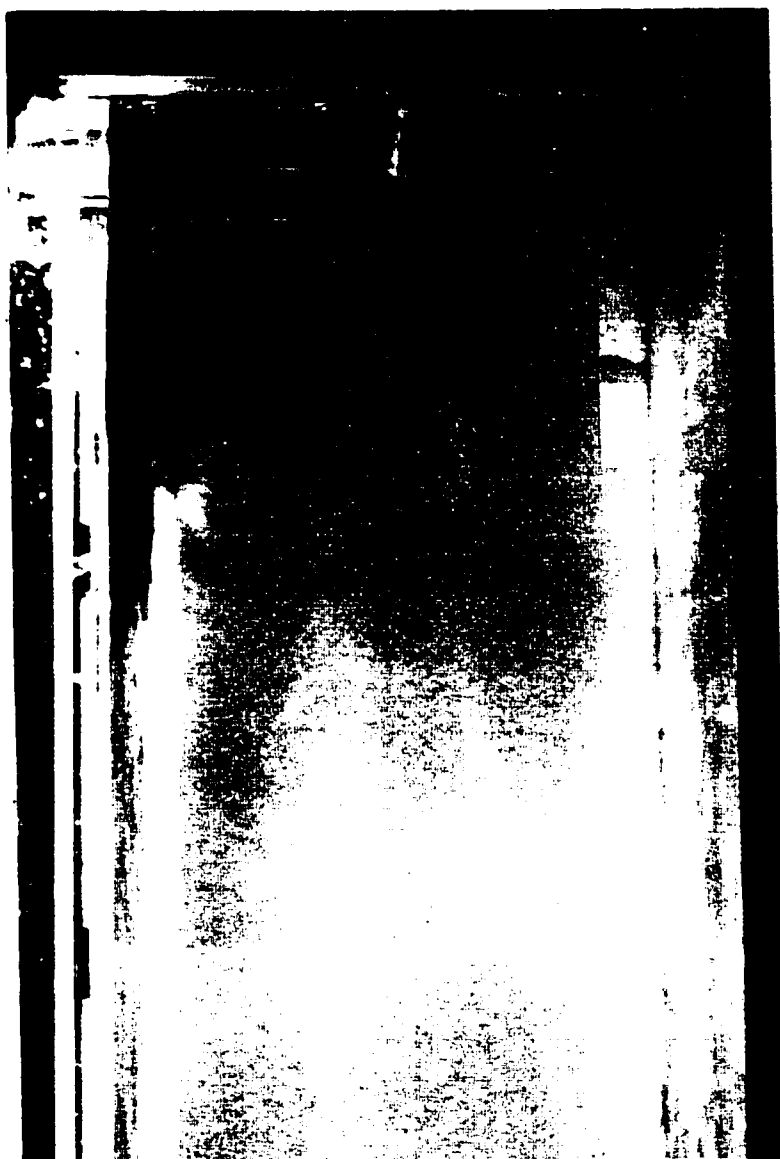


Fig. 4.6(a) Pattern A

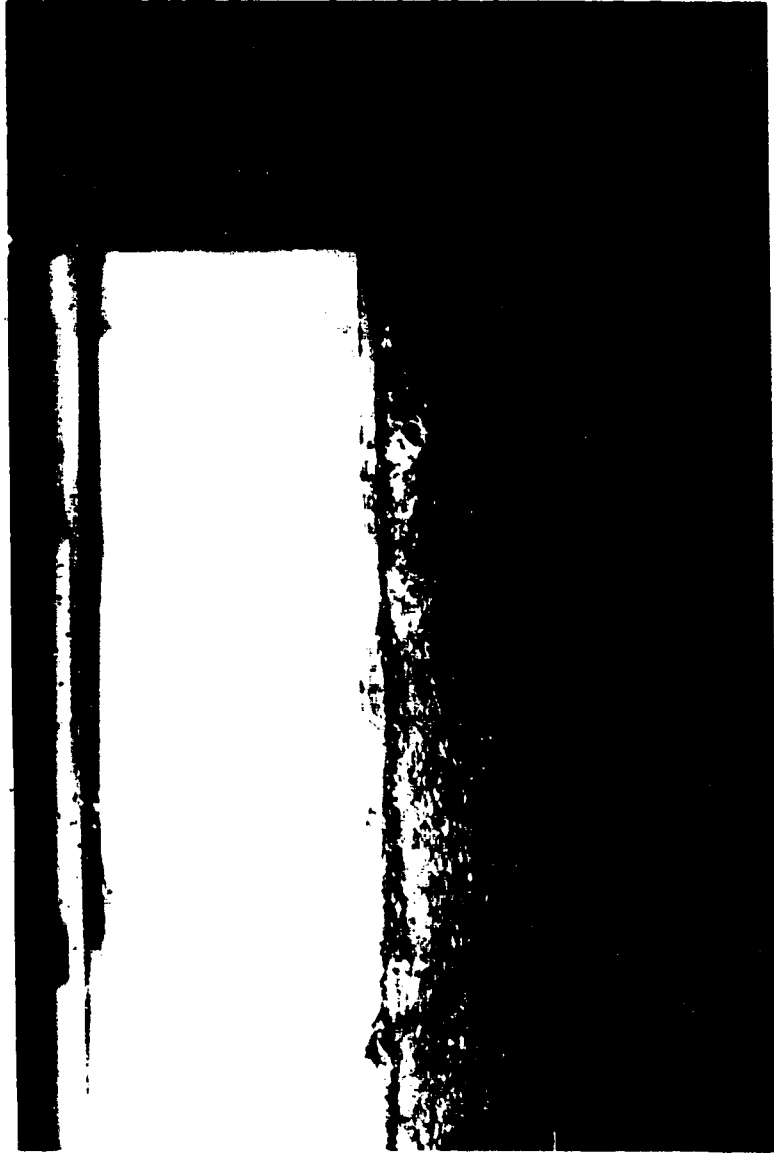
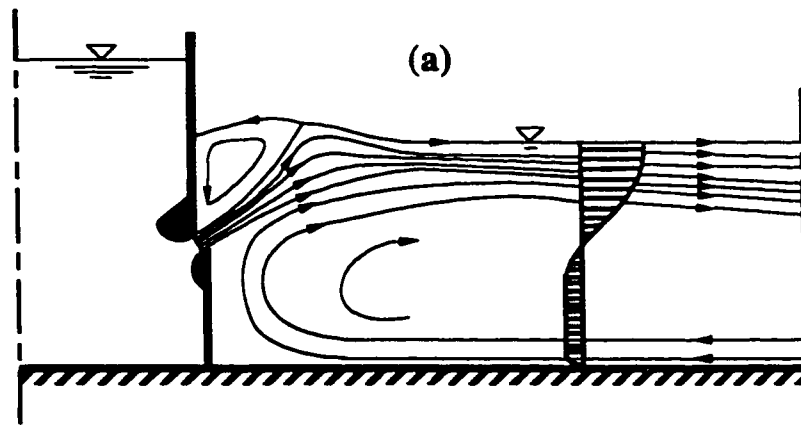


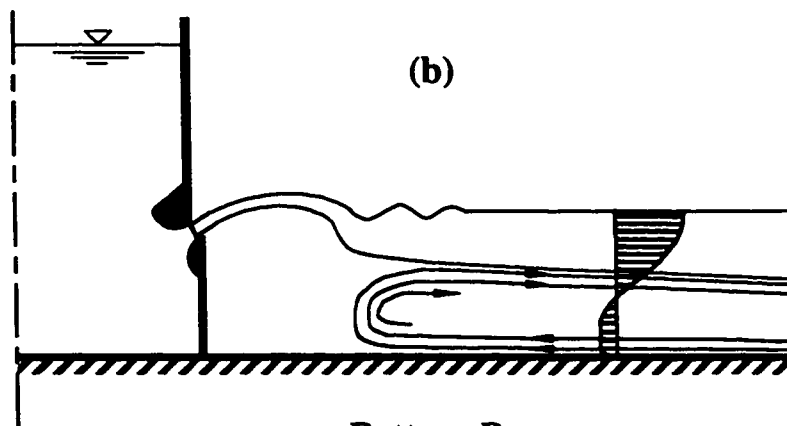
Fig. 4.6(b) Pattern B



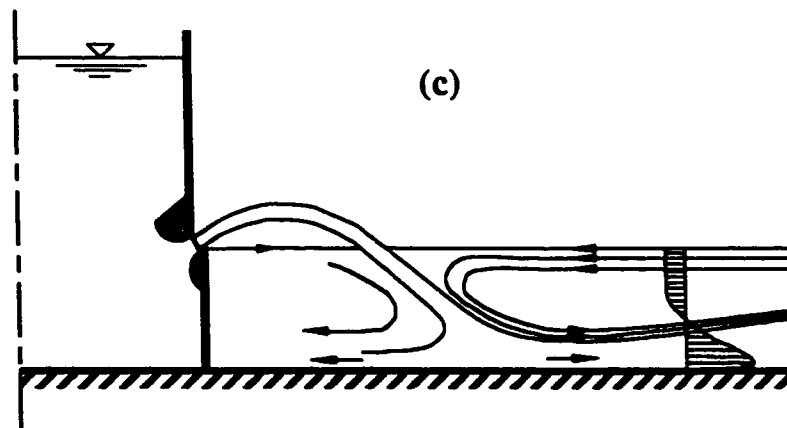
Fig. 4.6(c) Pattern C



Pattern A



Pattern B



Pattern C

Fig. 4.7(a-c) Flow patterns A, B & C for double-leaf gate dissipator

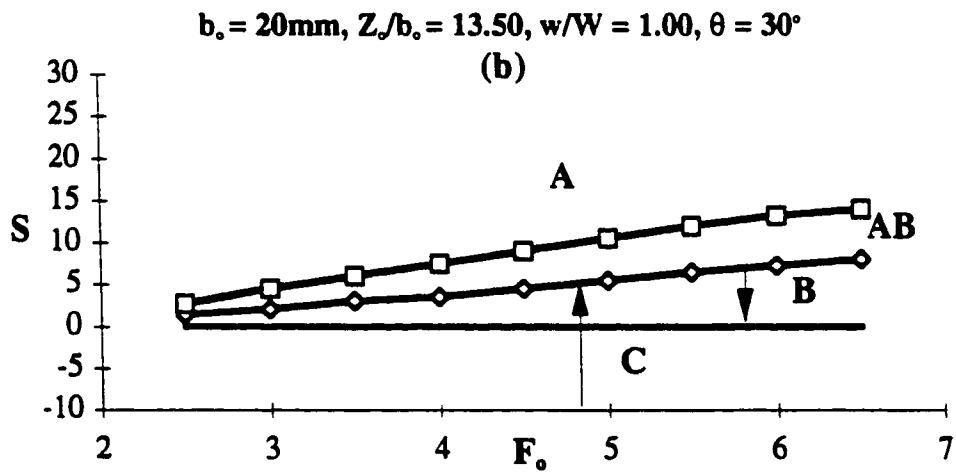
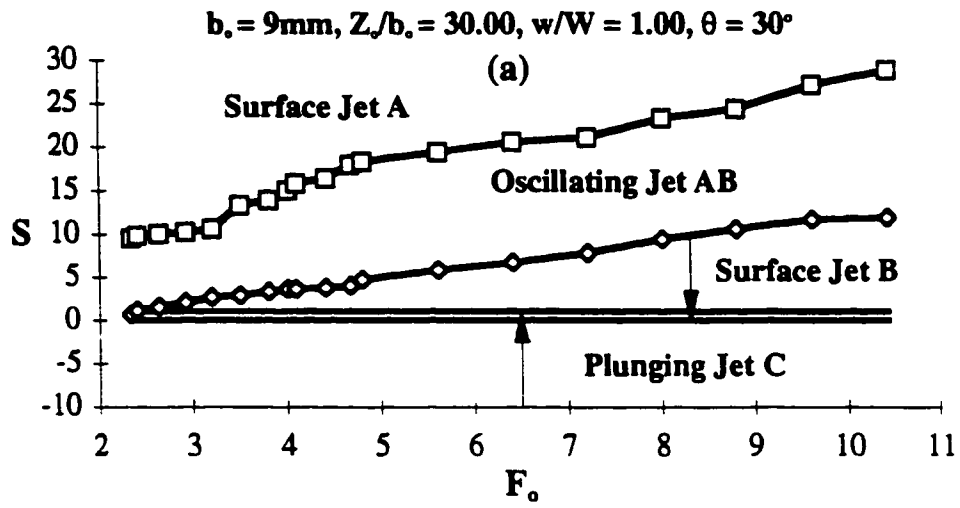


Fig. 4.8(a-b) Boundaries of the flow patterns
 (a) $\theta=30^\circ$, $Z_o/b_o=30.00$; and (b) $\theta=30^\circ$, $Z_o/b_o=13.50$

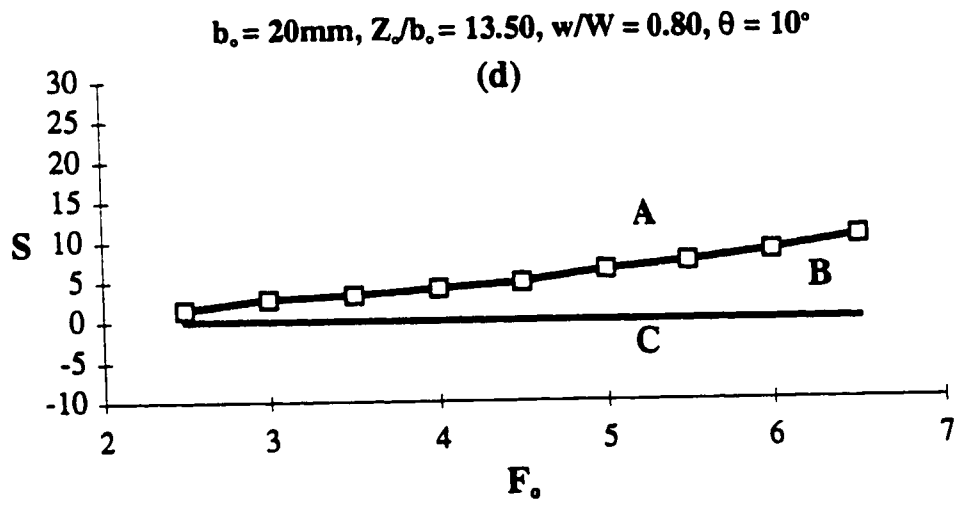
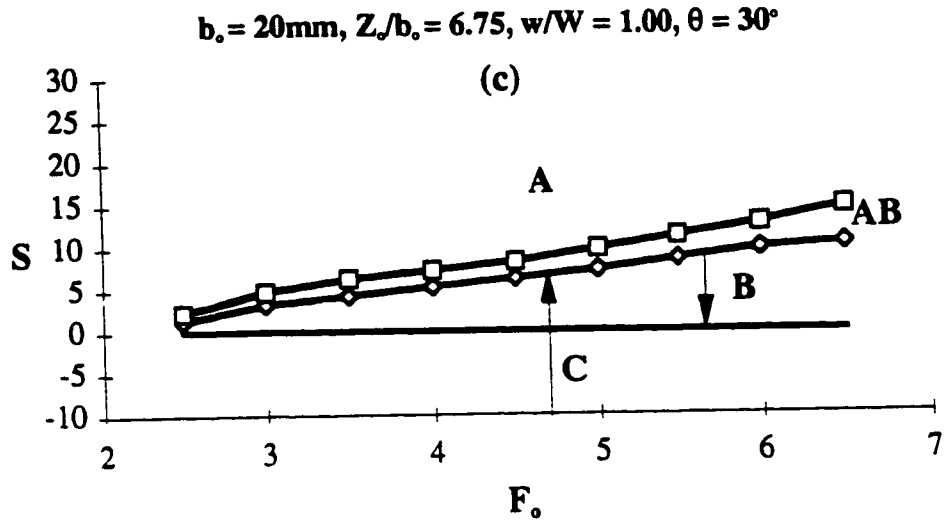


Fig. 4.8(c-d) Boundaries of the flow patterns
 (c) $\theta=30^\circ, Z_o/b_o=6.75$; and (d) $\theta=10^\circ, Z_o/b_o=13.50$

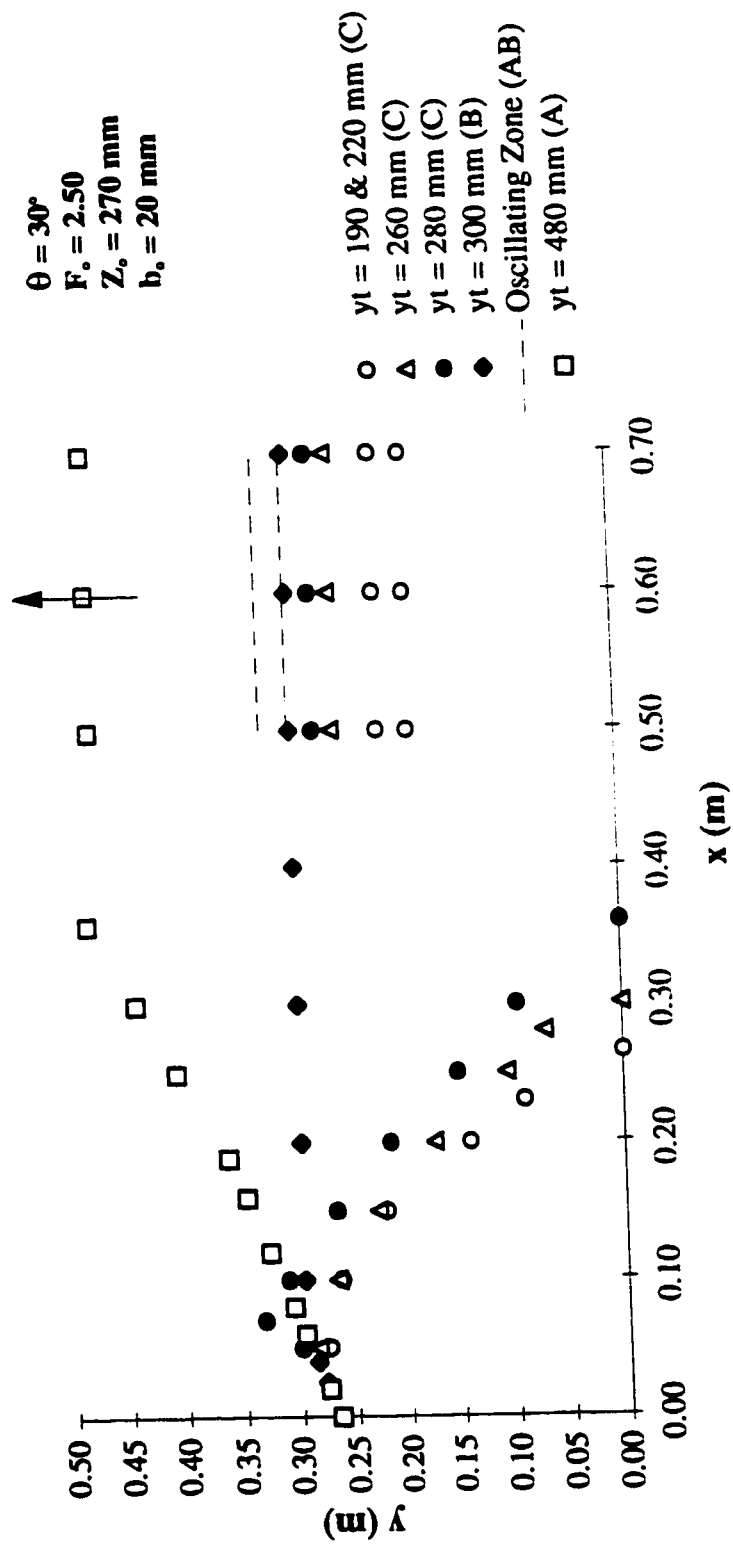


Fig. 4.9 Jet trajectories

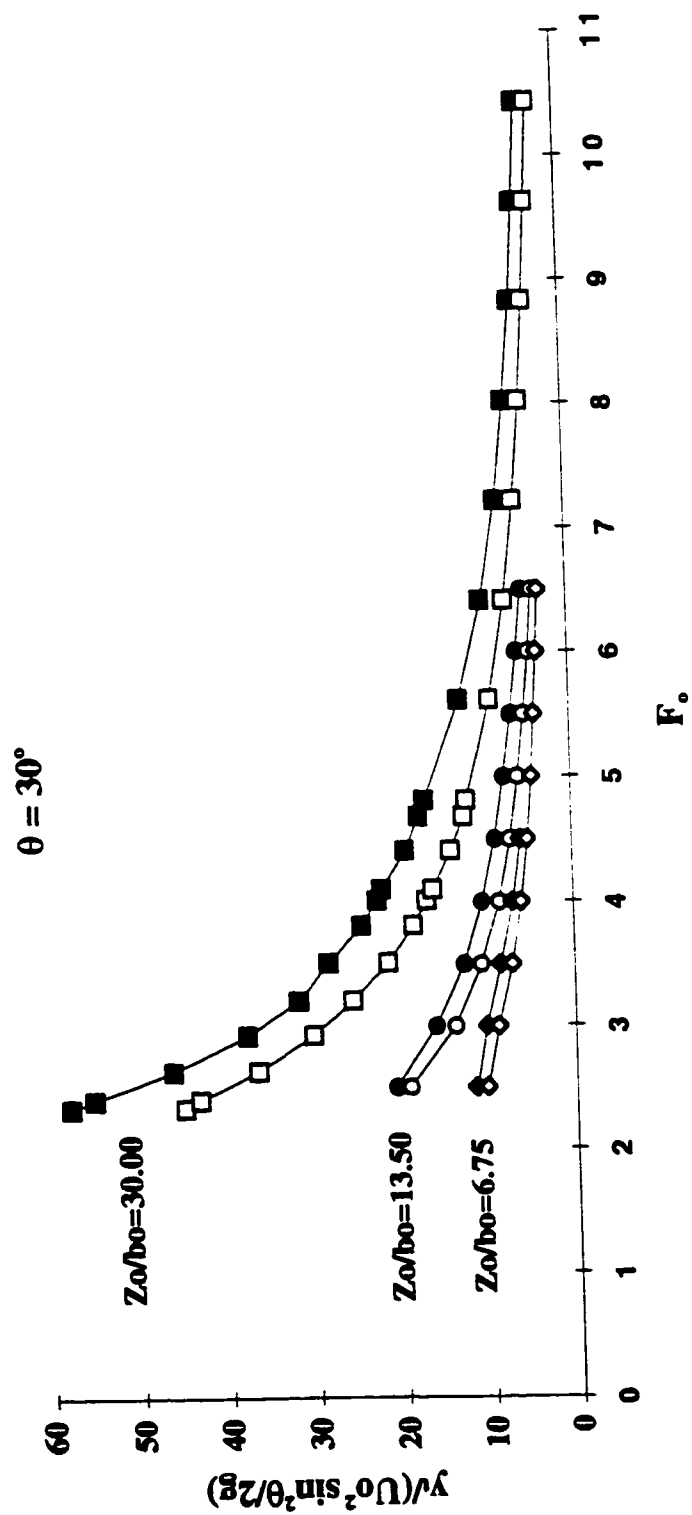


Fig. 4.10 Oscillating zones



Fig. 4.11 Width ratio $w/W = 0.50$

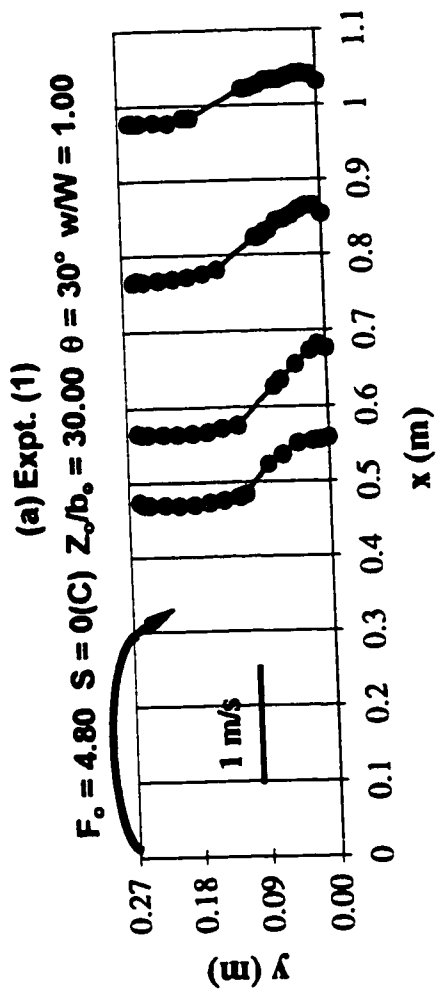


Fig. 4.12(a) Typical Velocity Profiles for Pattern C

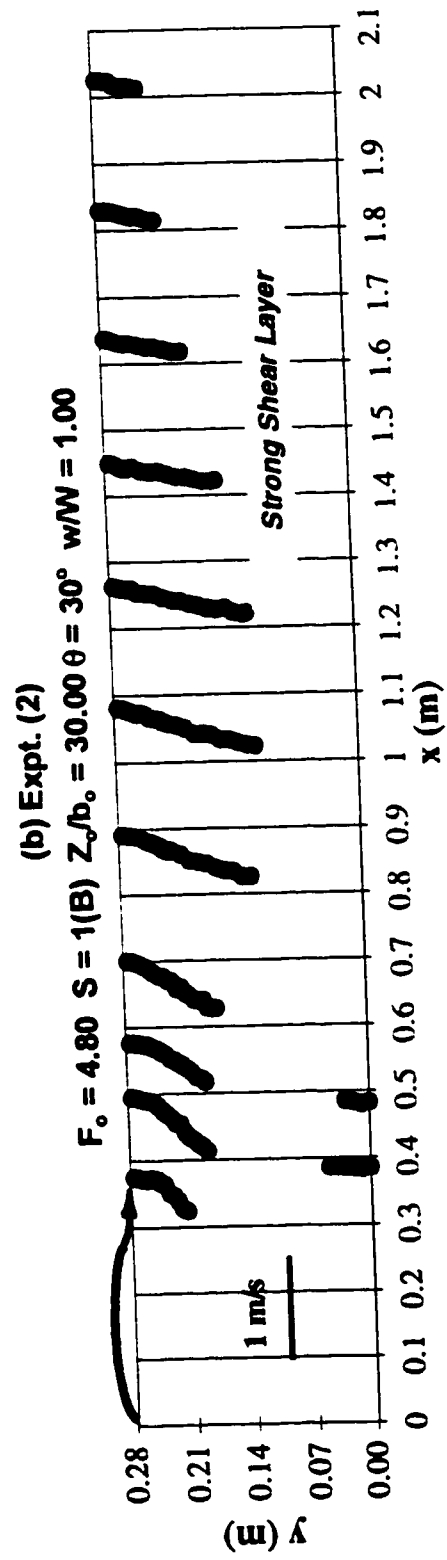


Fig. 4.12(b) Typical Velocity Profiles for Pattern B

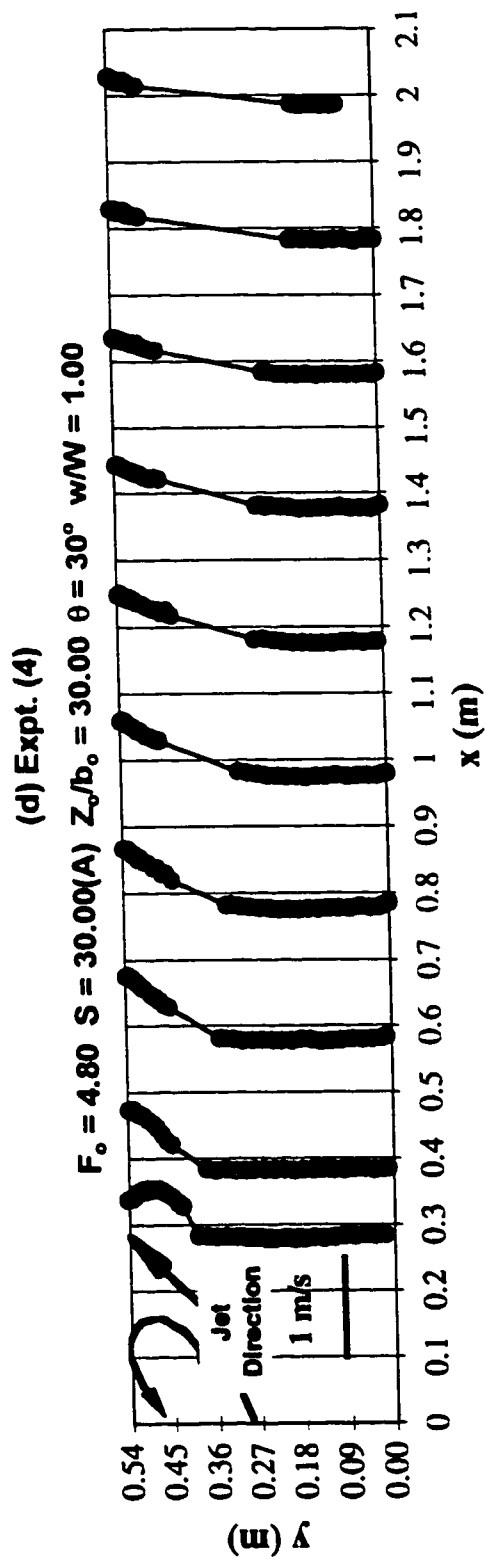
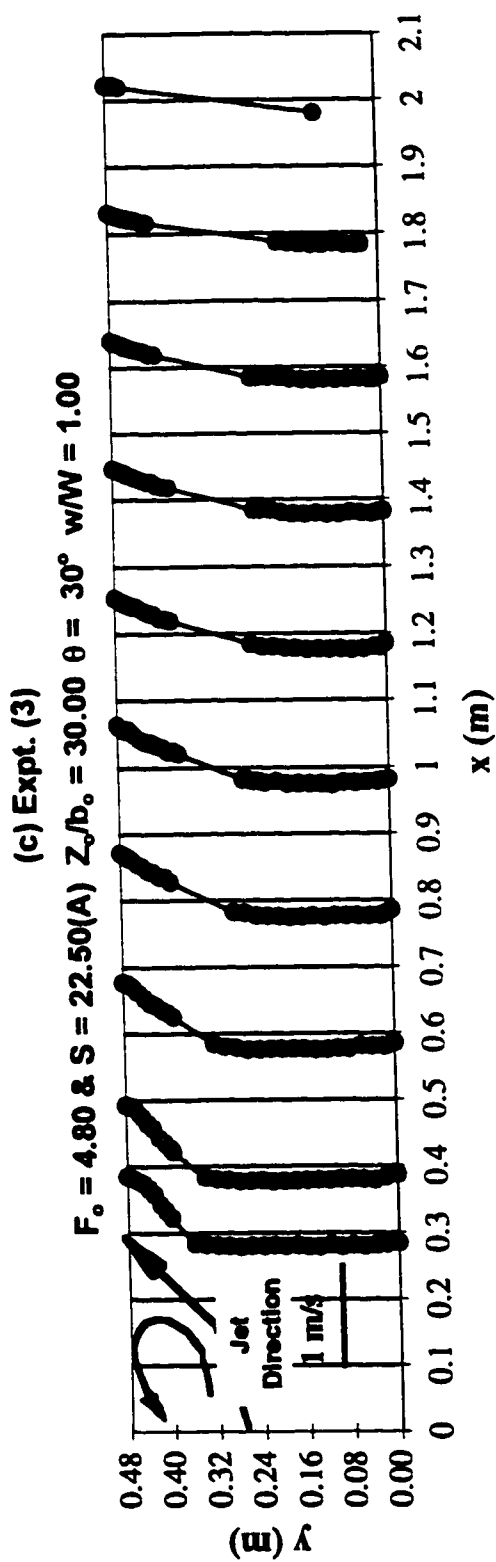


Fig. 4.12(c-d) Typical Velocity Profiles for Pattern A

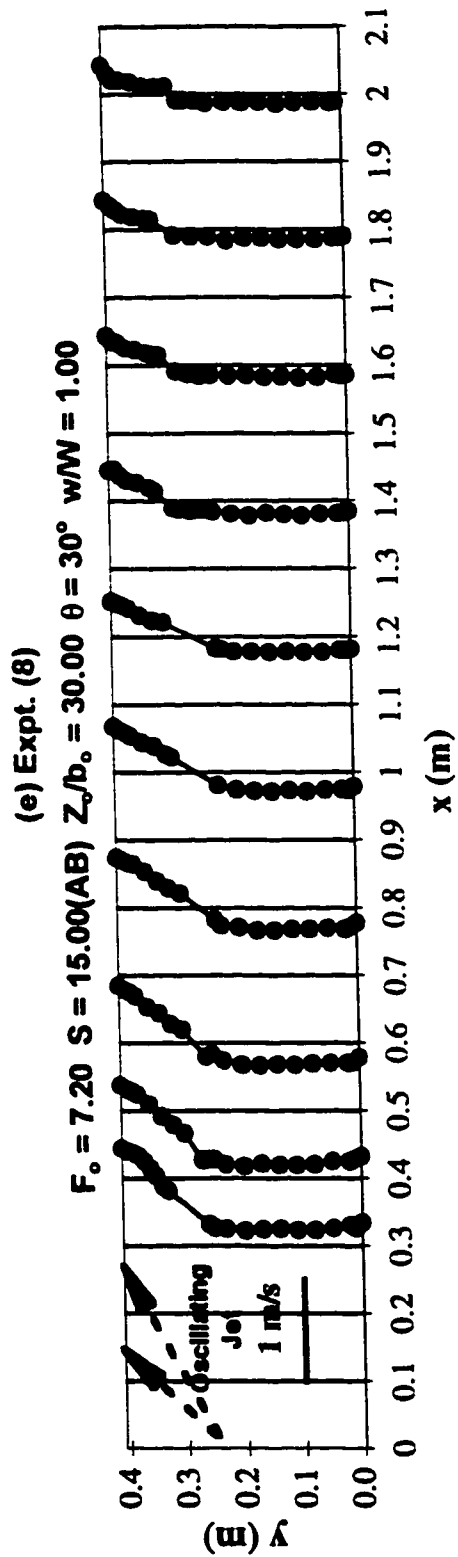


Fig. 4.12(e) Typical Velocity Profiles for Pattern AB

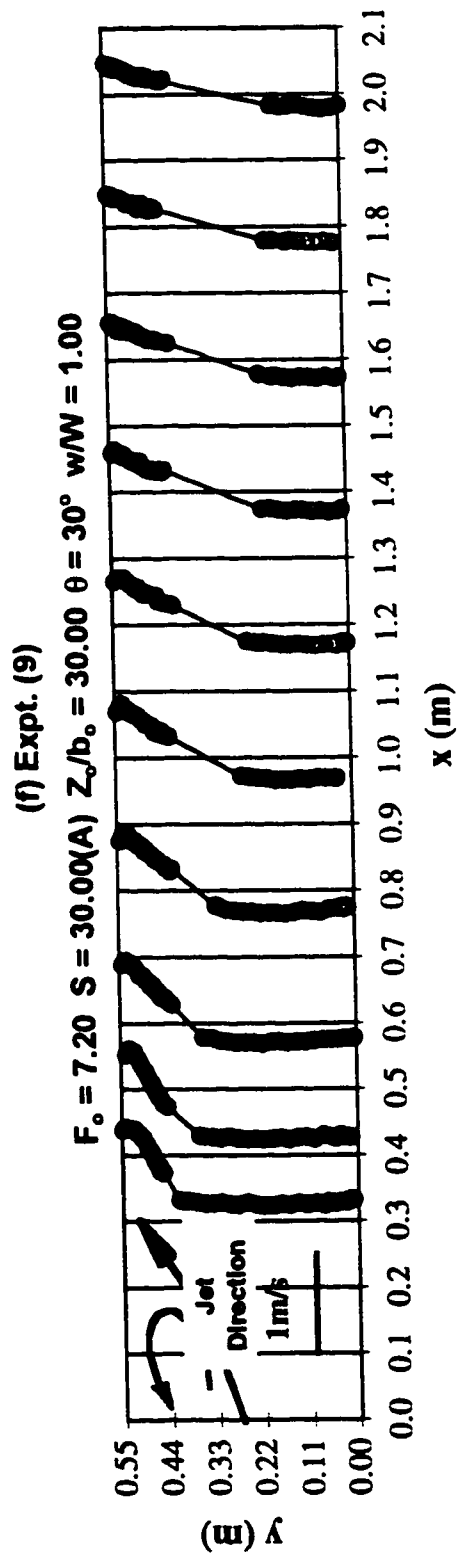


Fig. 4.12(f) Typical Velocity Profiles for Pattern A

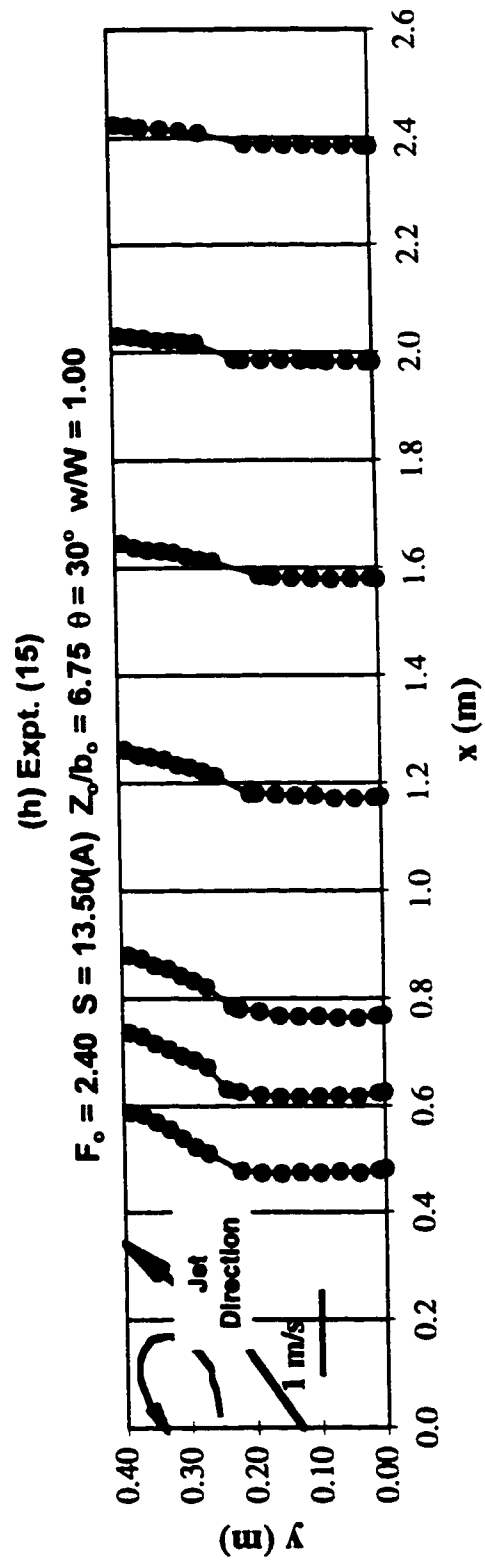
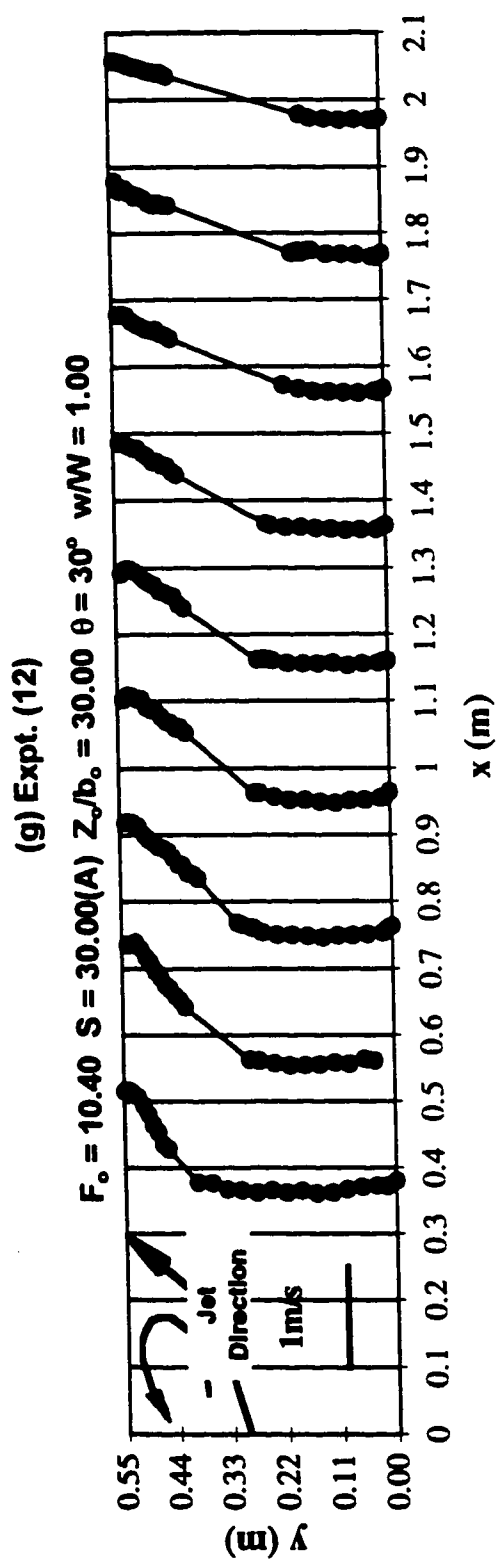


Fig. 4.12(g-h) Typical Velocity Profiles for Pattern A

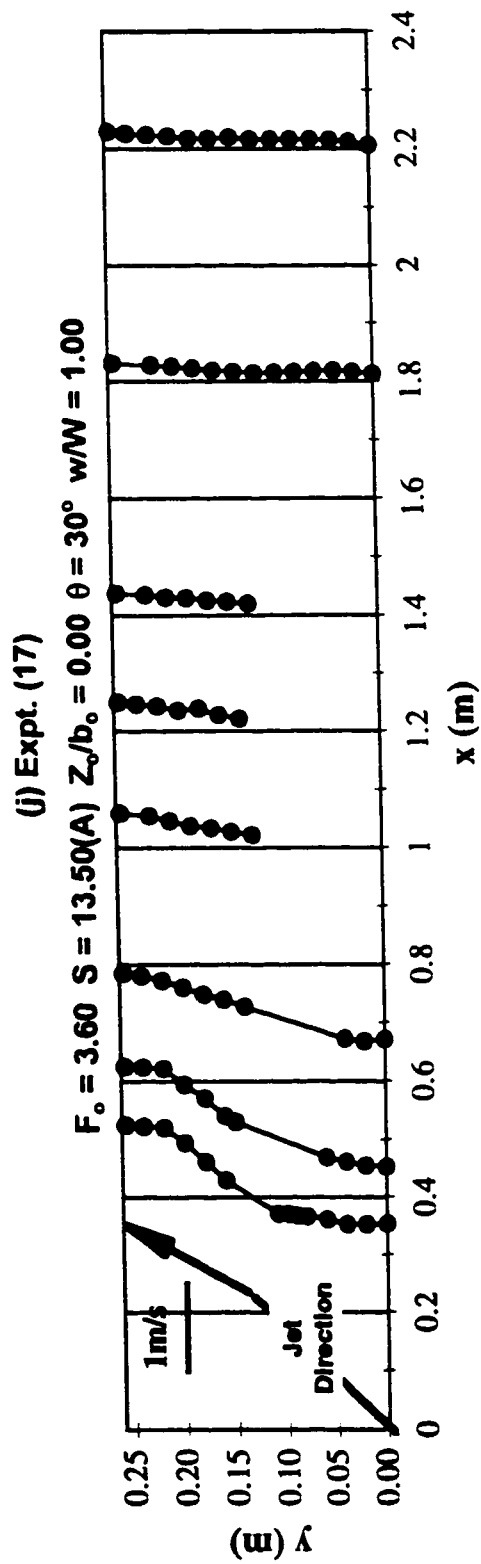
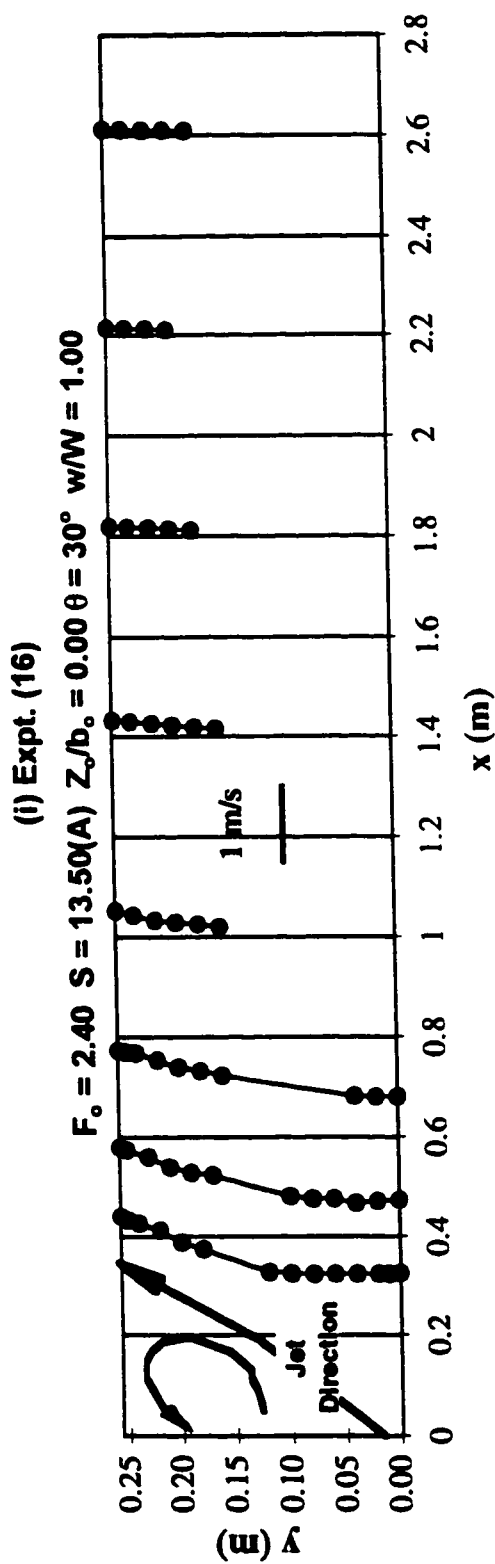


Fig. 4.12(i-j) Typical Velocity Profiles for Pattern A

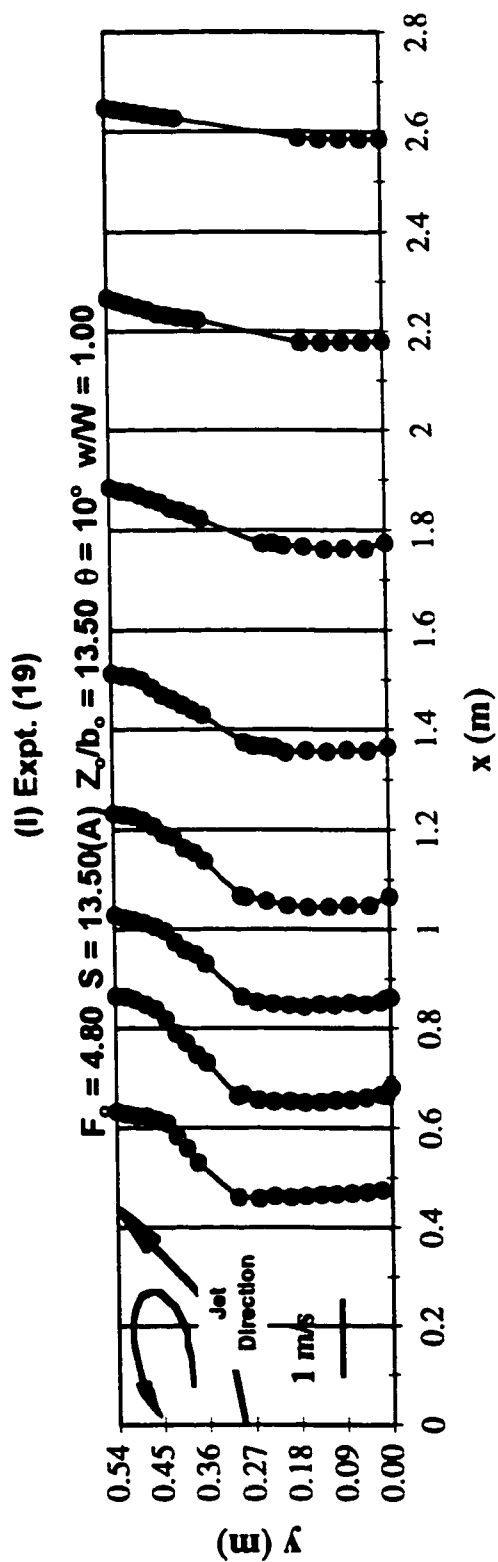
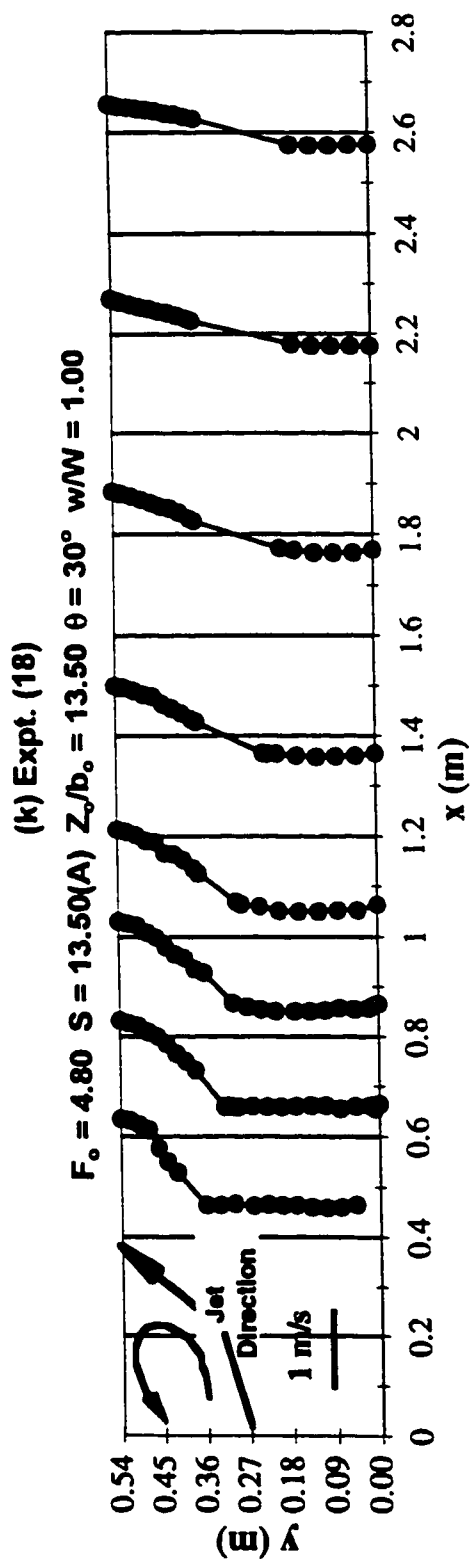


Fig. 4.12(k-l) Typical Velocity Profiles for Pattern A

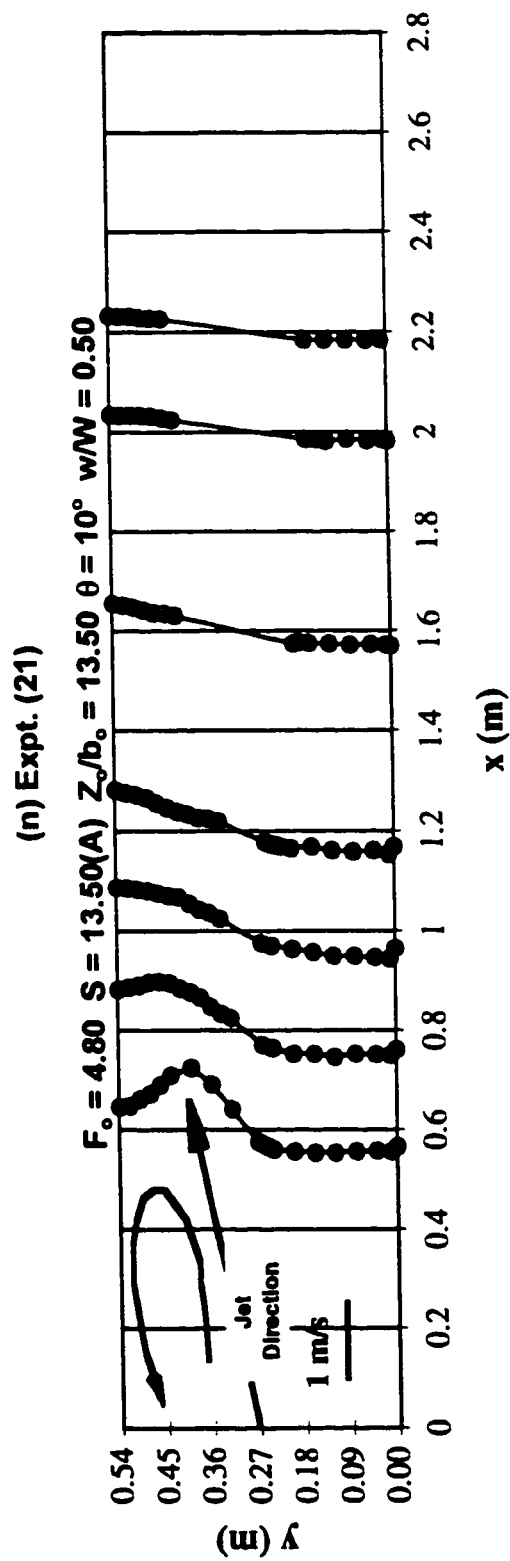
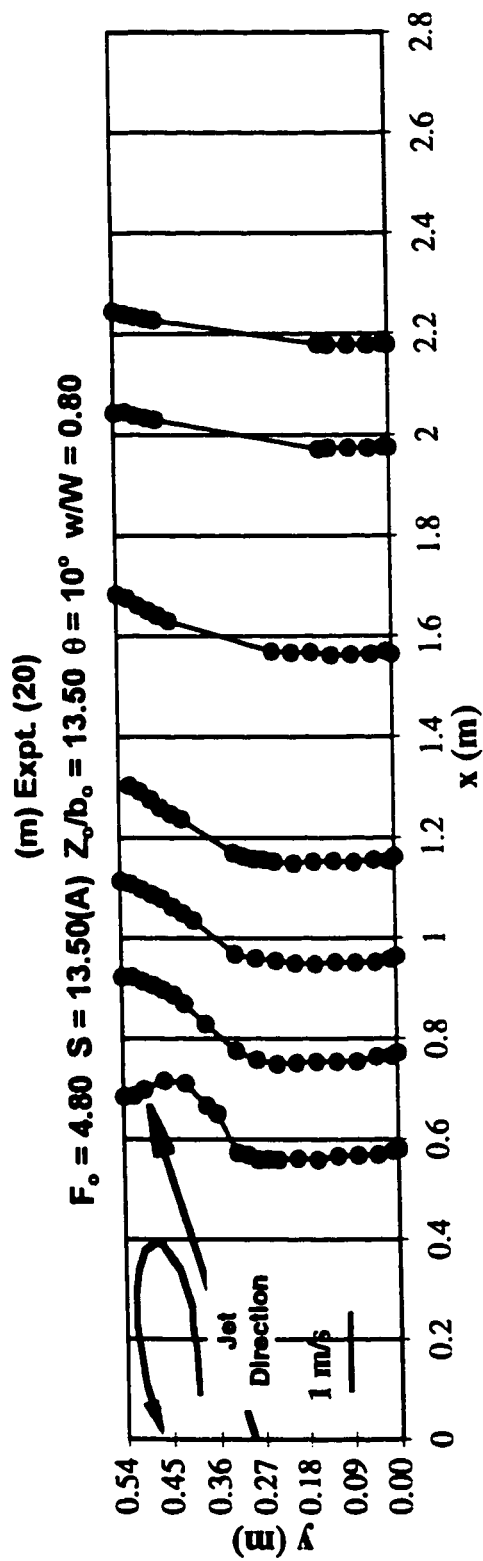


Fig. 4.12(m-n) Typical Velocity Profiles for Pattern A

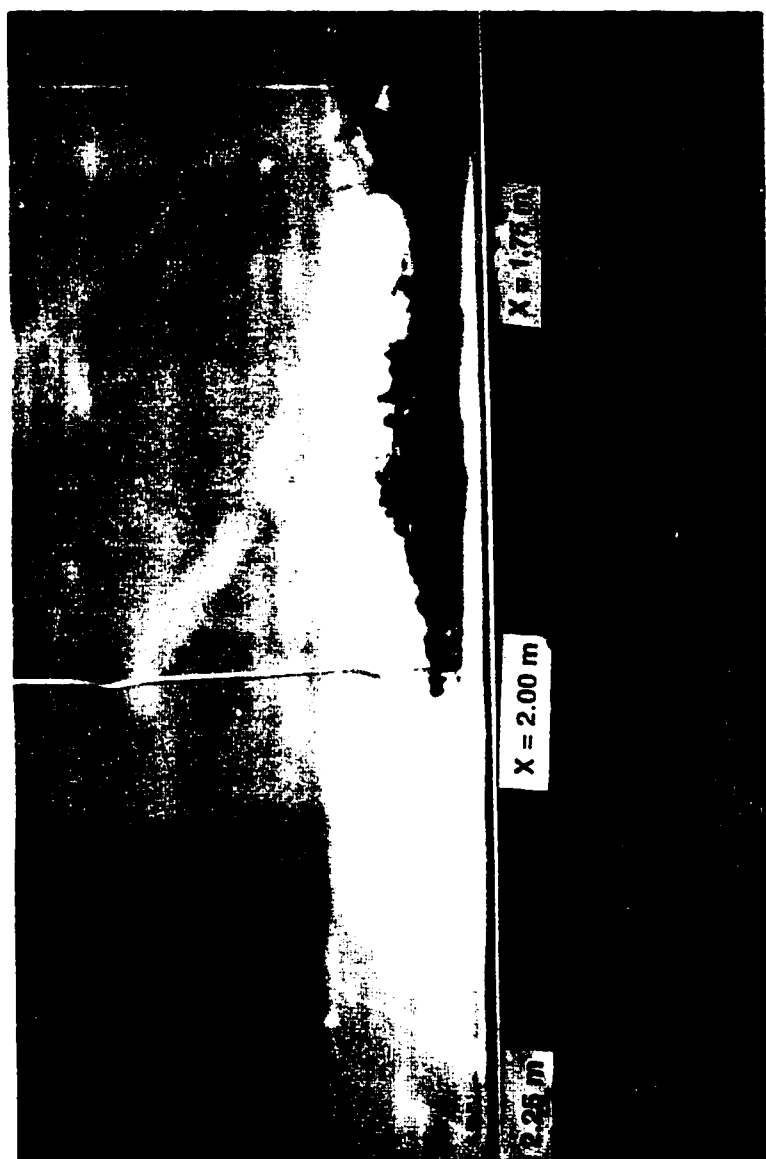


Fig. 4.13 Reverse flow near the bed ($x = 2$ m)

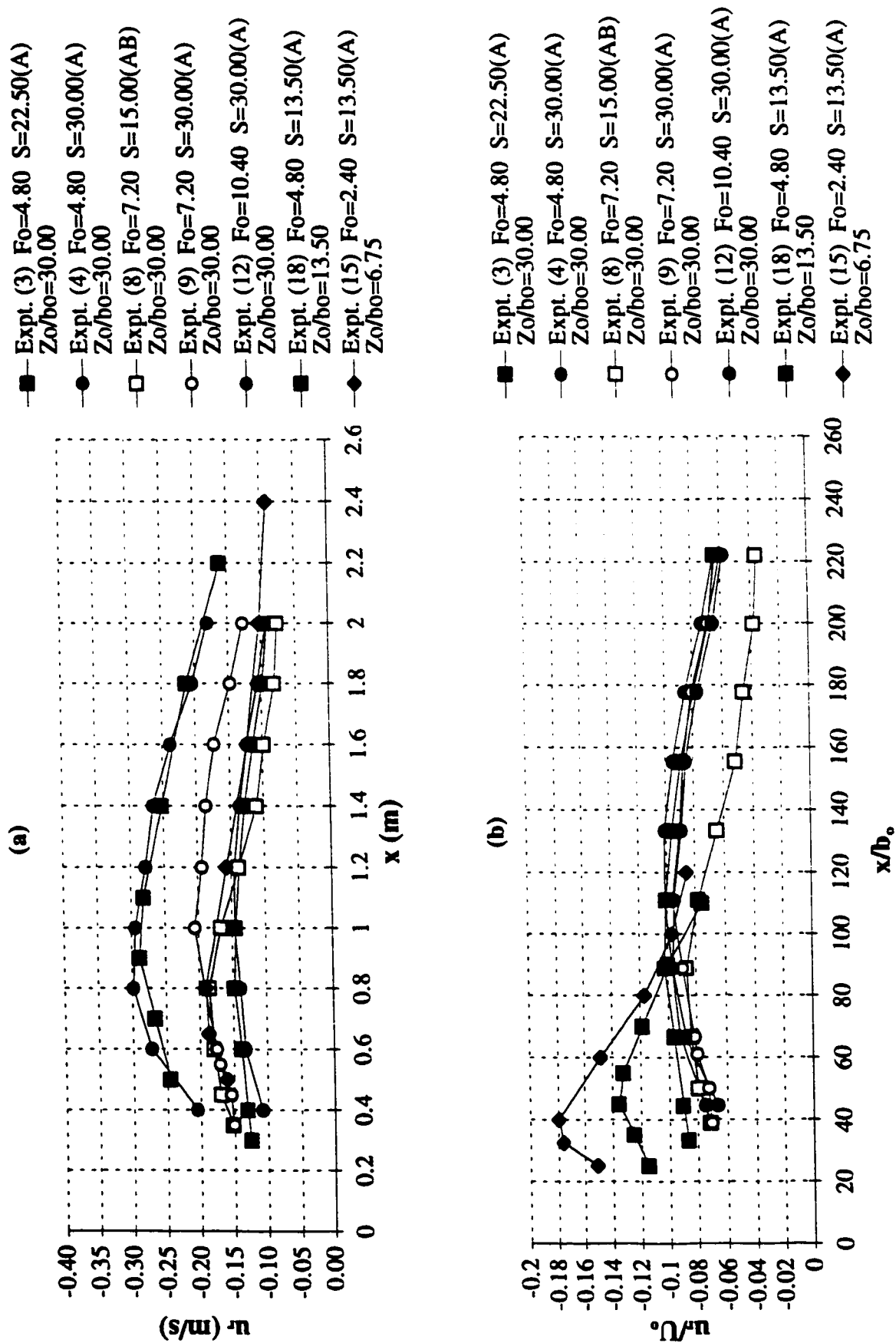


Fig. 4.14(a-b) Variation of the depth-averaged reverse velocity with distance

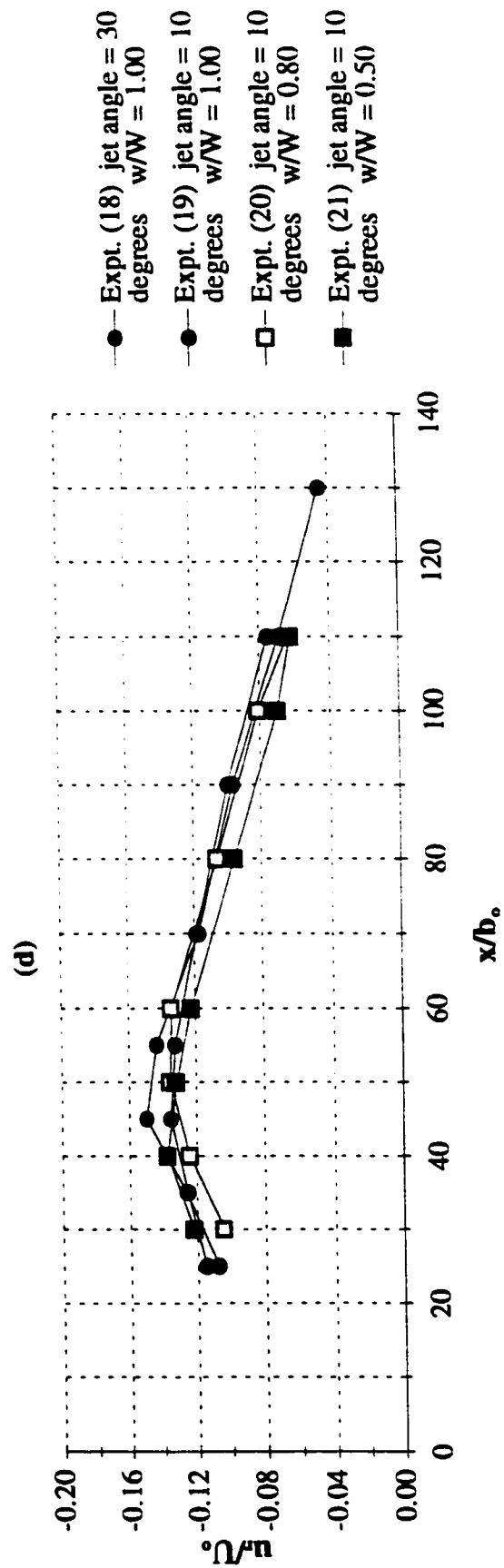
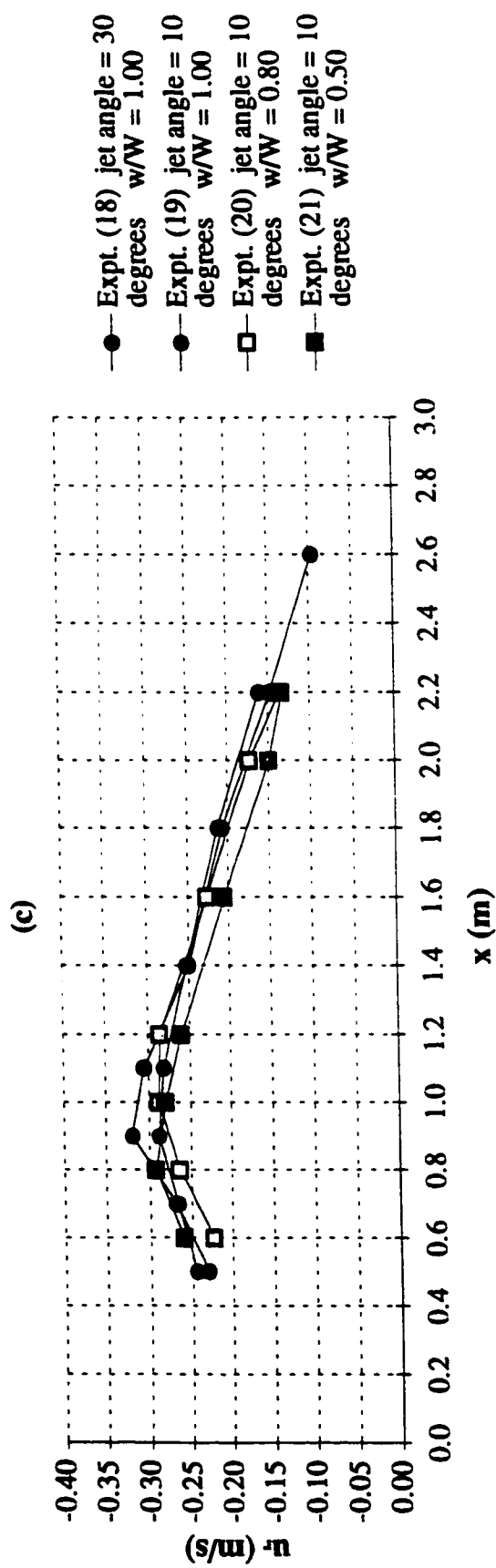


Fig. 4.14(c-d) Variation of the depth-averaged reverse velocity with distance

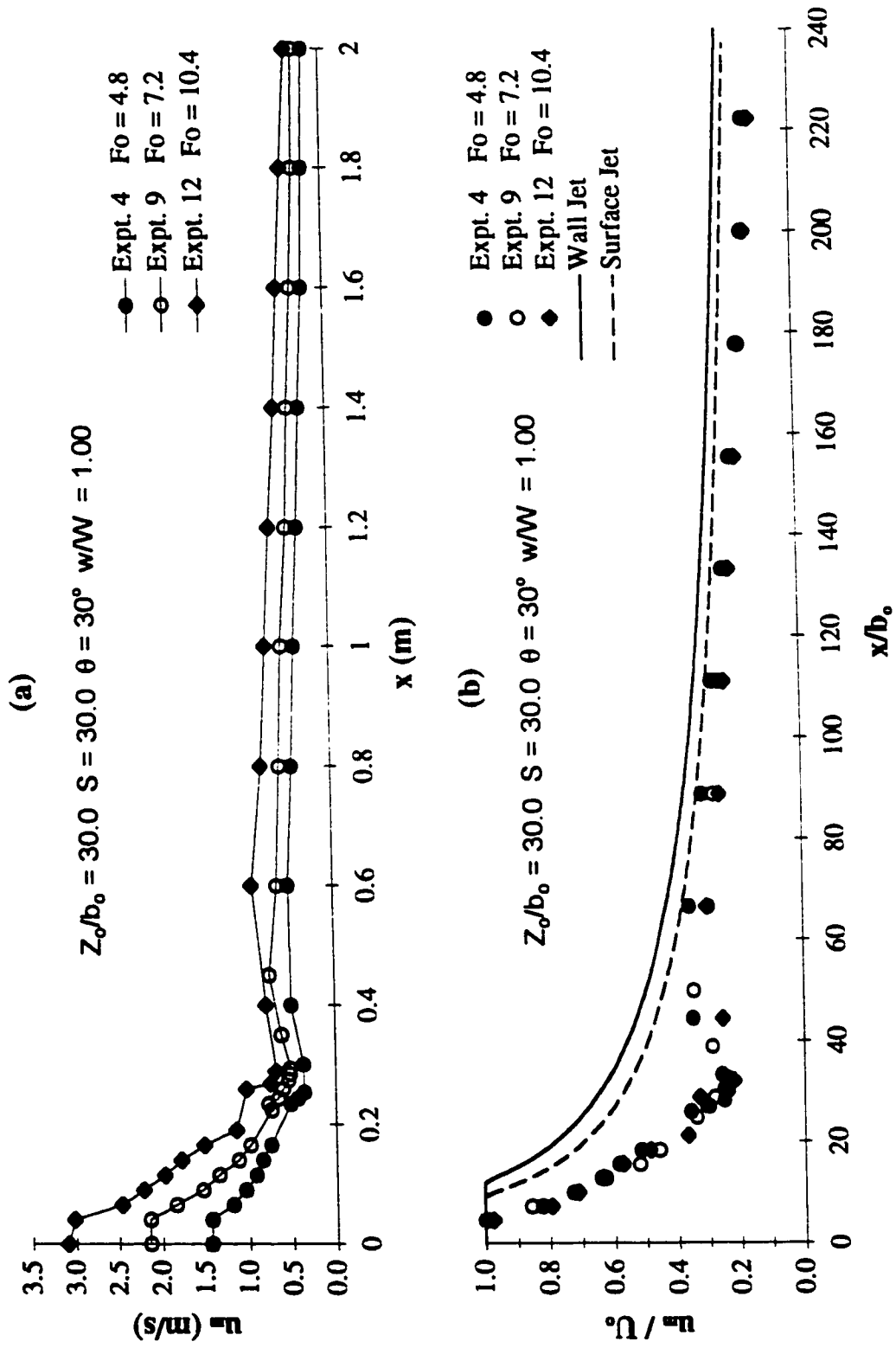


Fig. 4.15(a-b) Maximum-velocity decay in flow pattern A

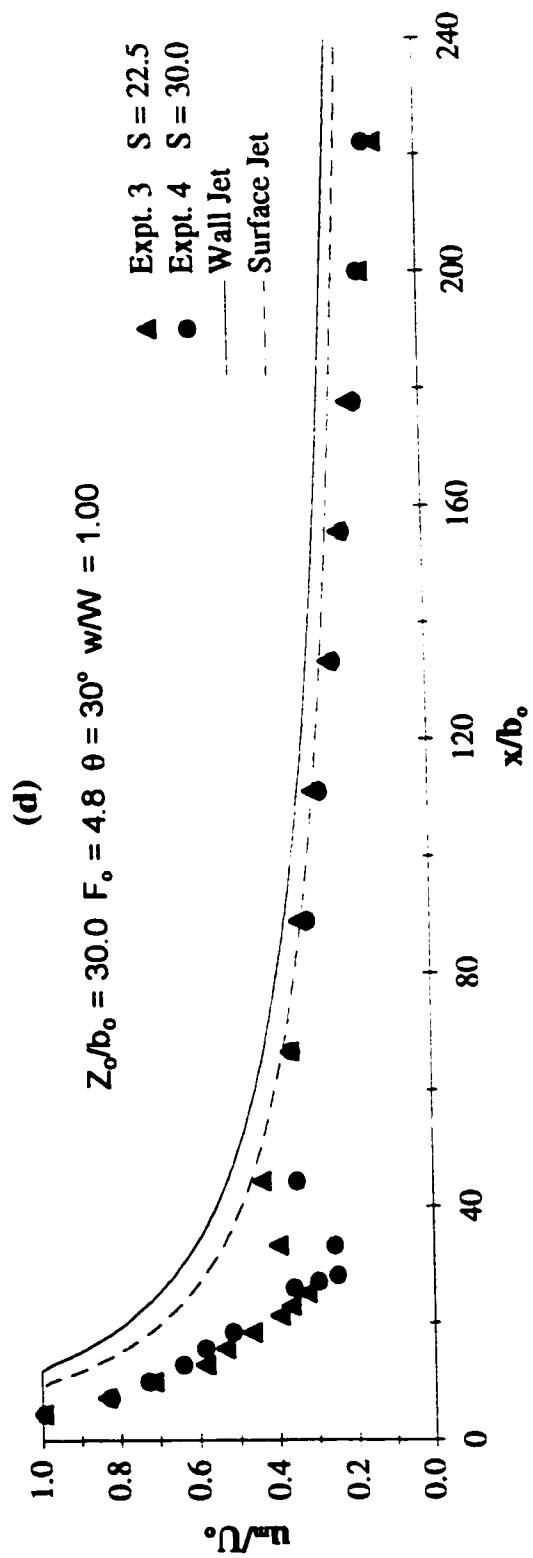
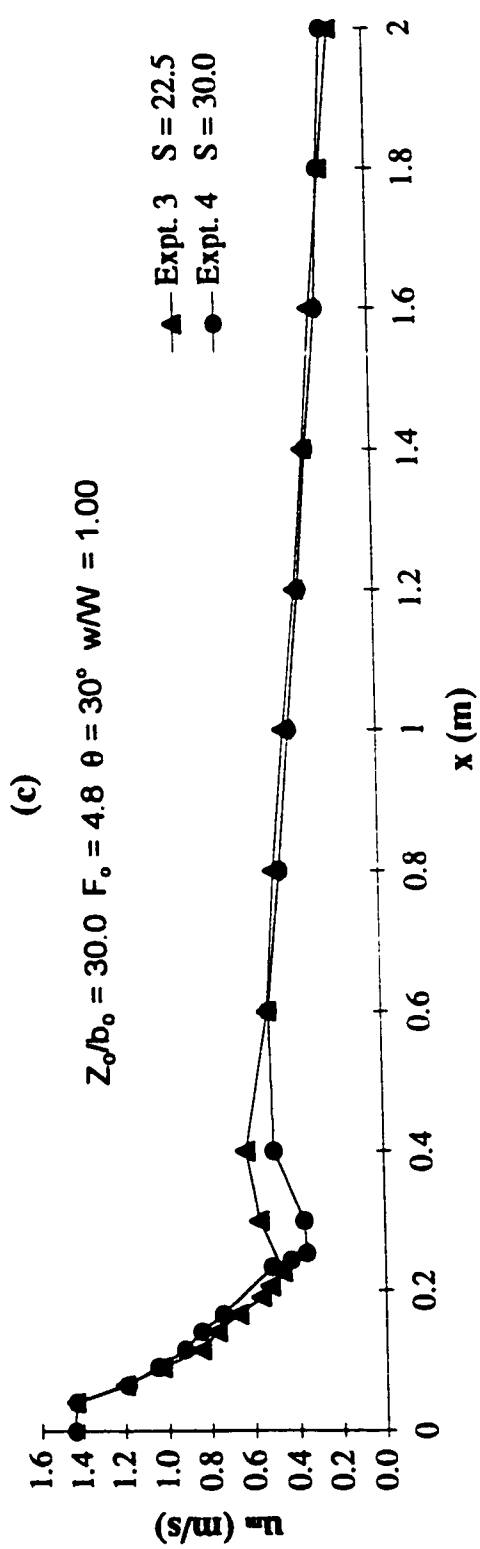


Fig. 4.15(c-d) Maximum-velocity decay in flow pattern A

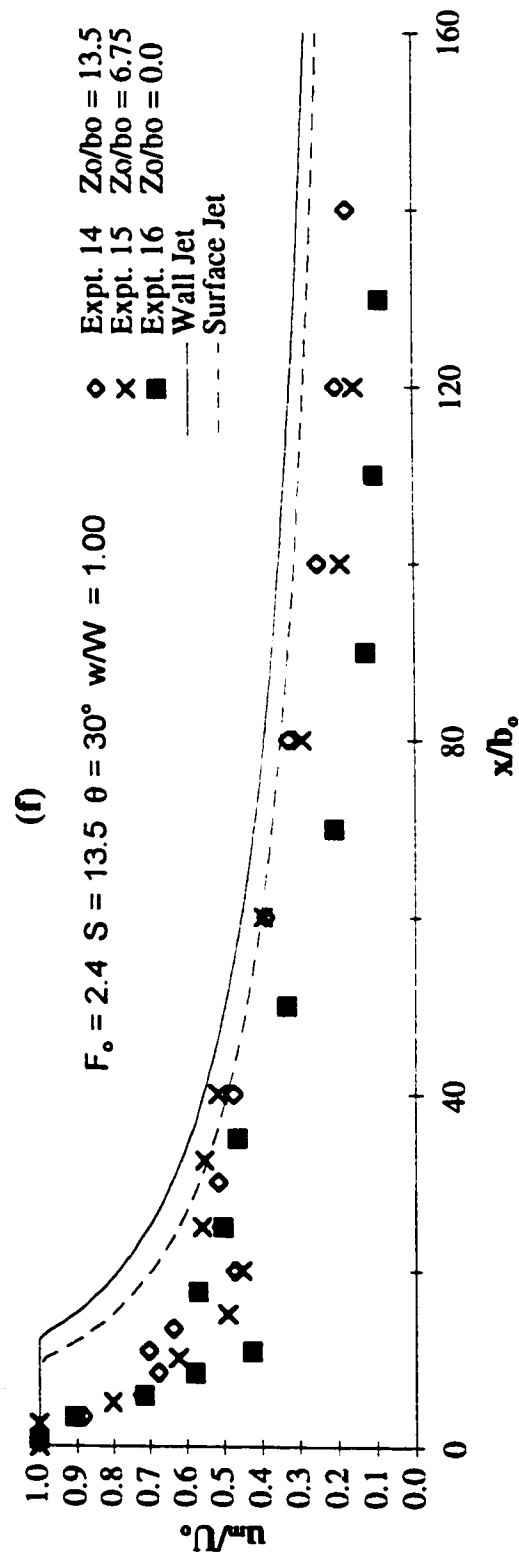
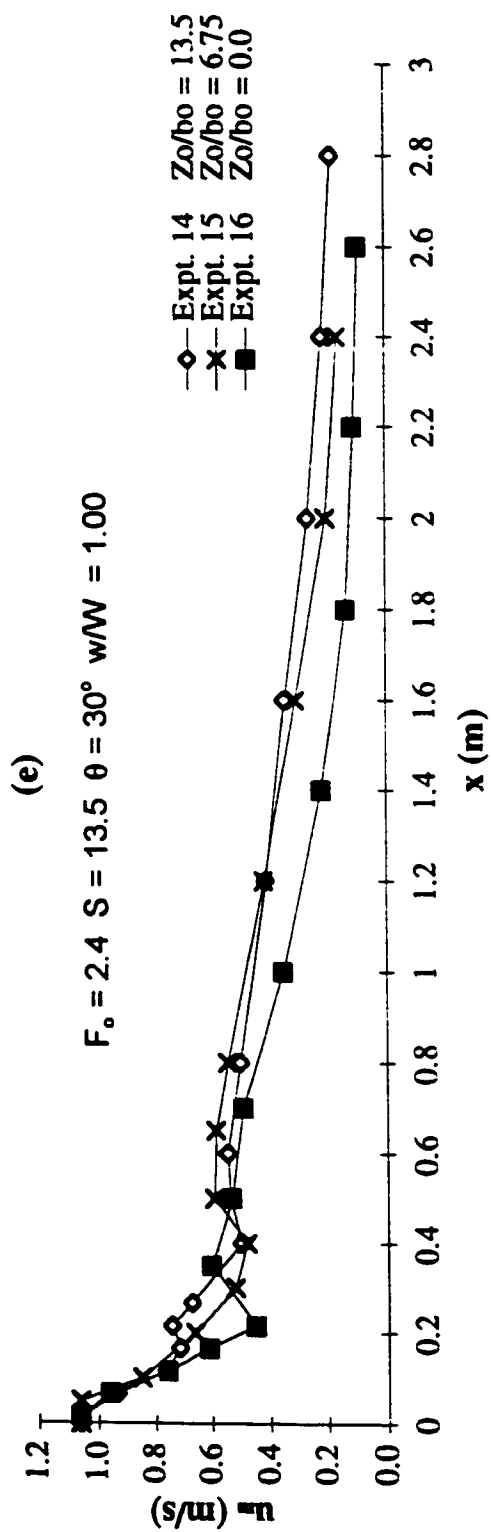


Fig. 4.15(e-f) Maximum-velocity decay in flow pattern A

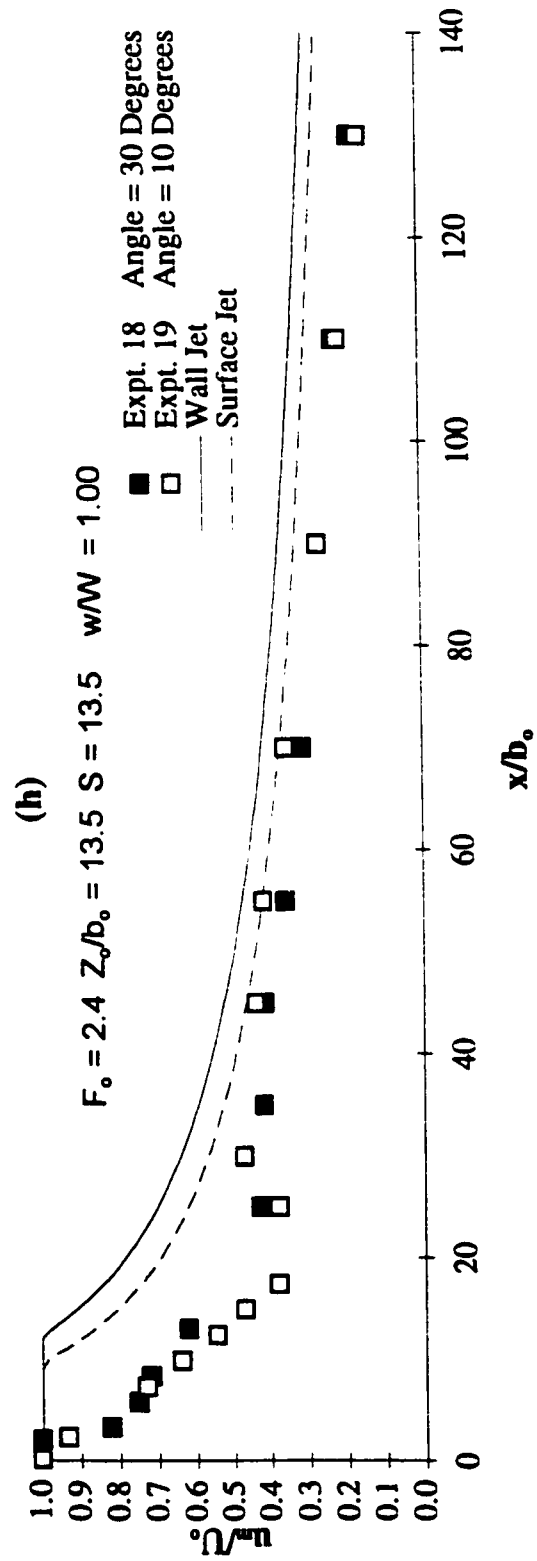
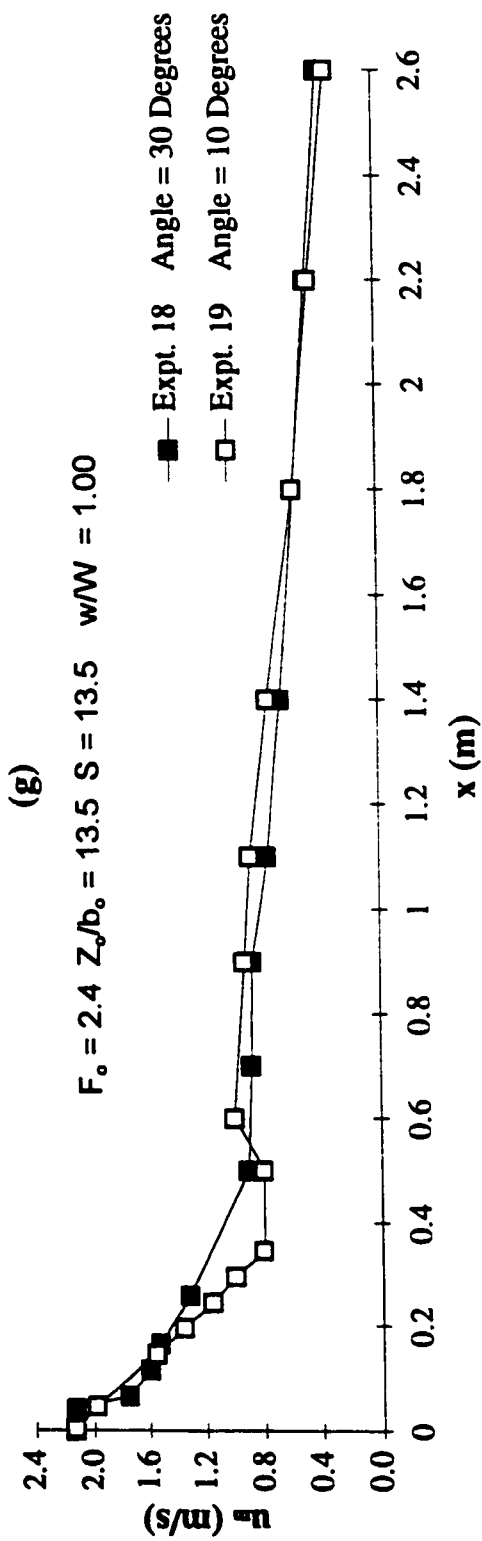


Fig. 4.15(g-h) Maximum-velocity decay in flow pattern A

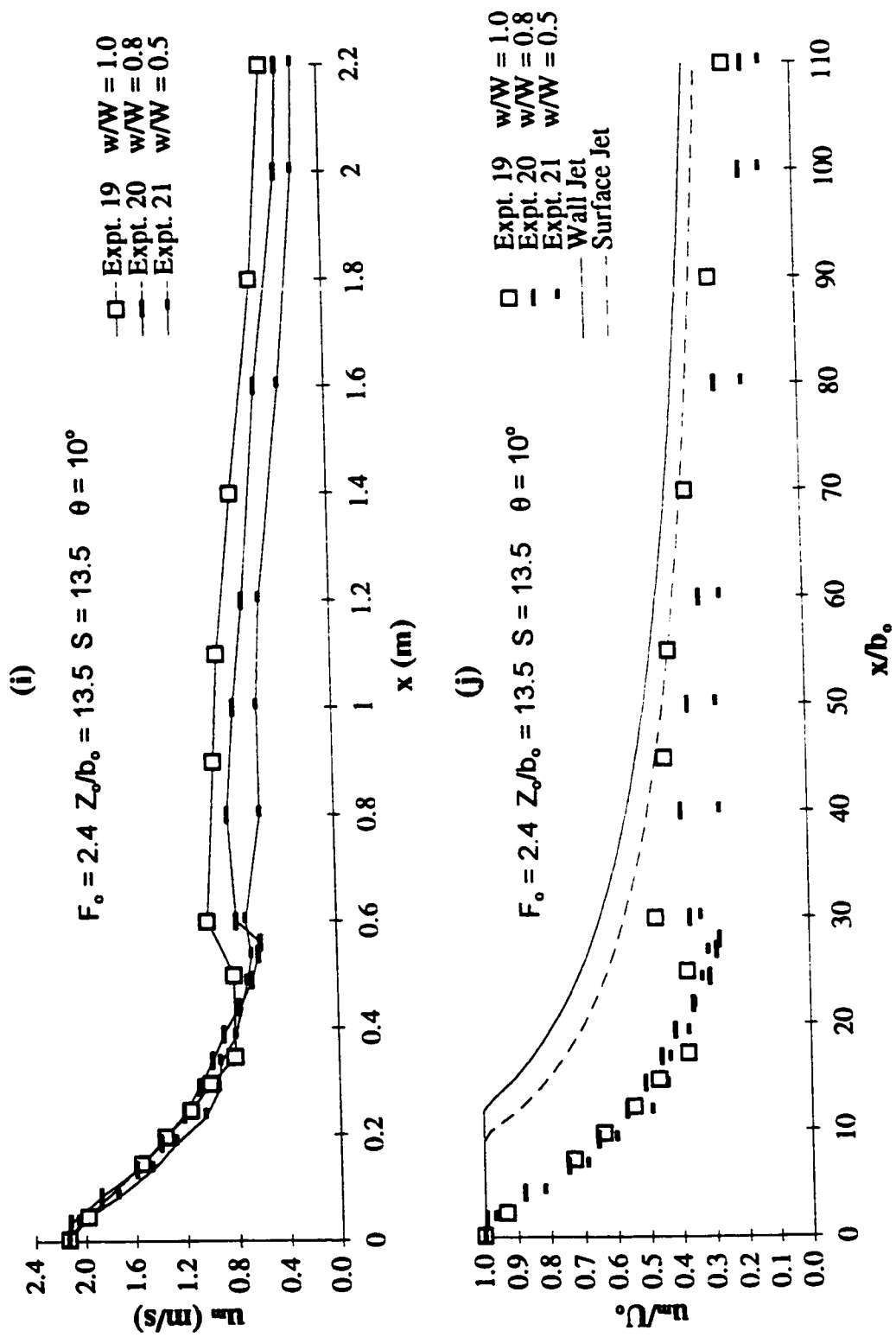


Fig. 4.15(i-j) Maximum-velocity decay in flow pattern A

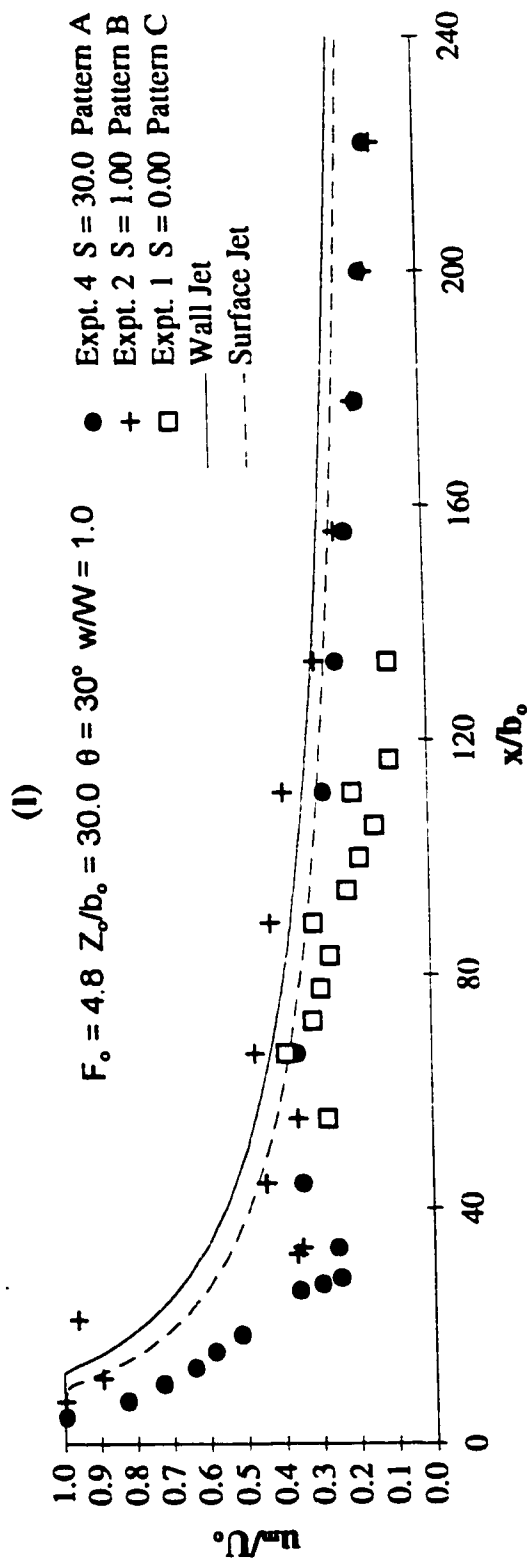
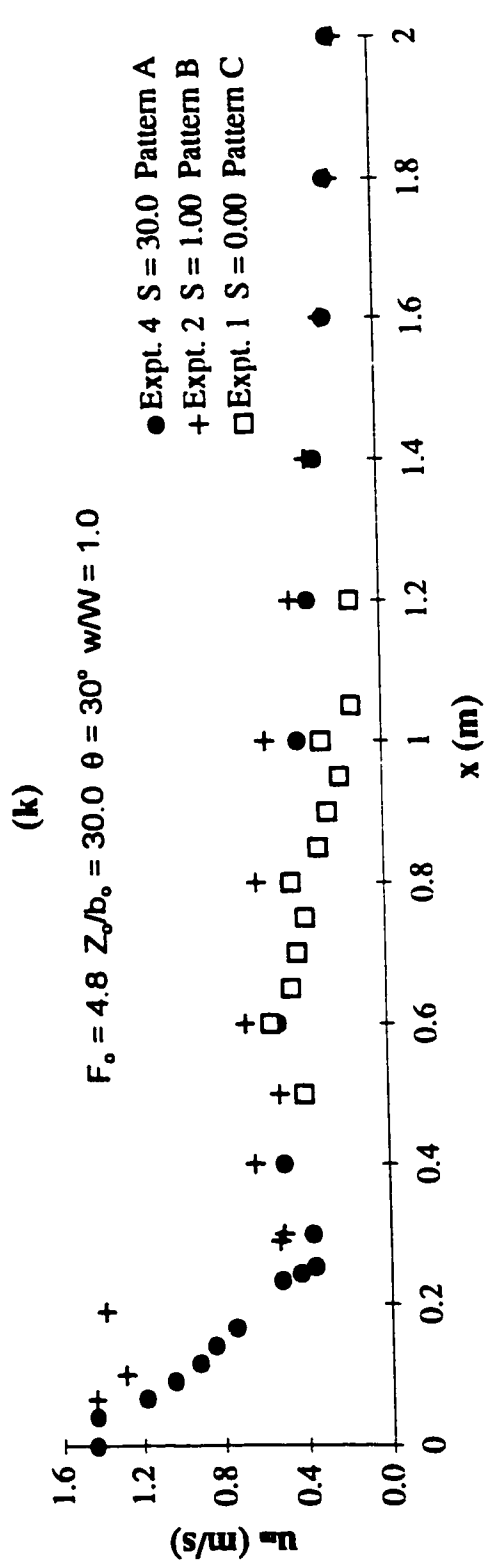


Fig. 4.15(k-l) Maximum-velocity decay in flow pattern A, B & C

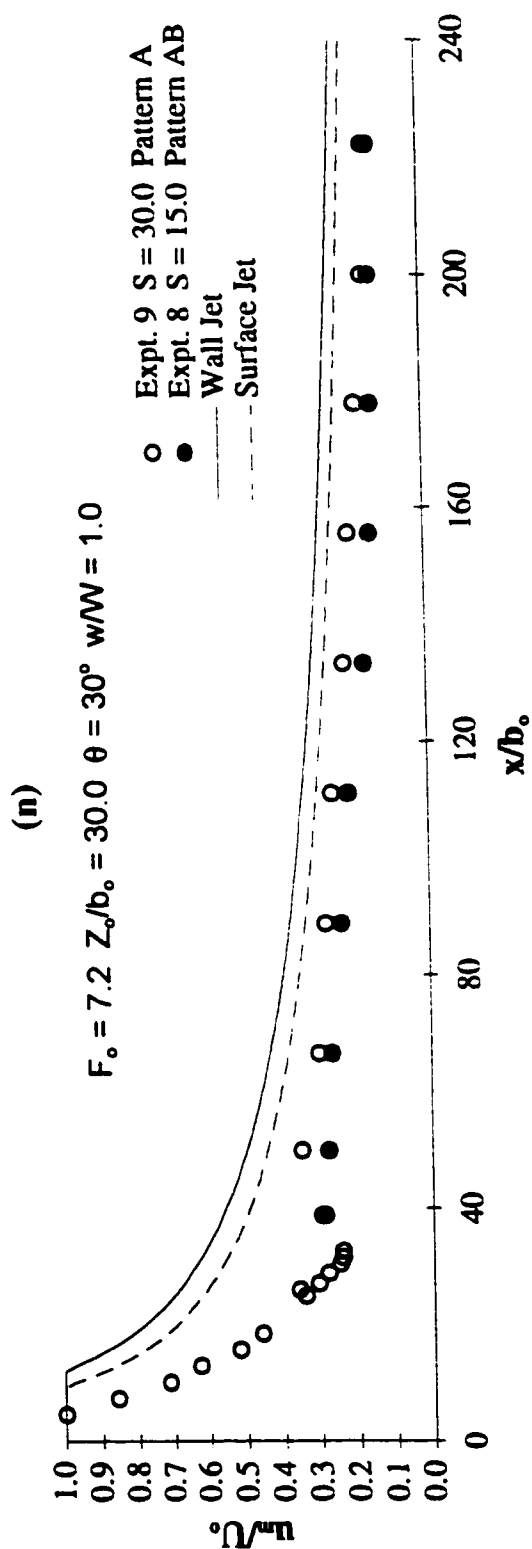
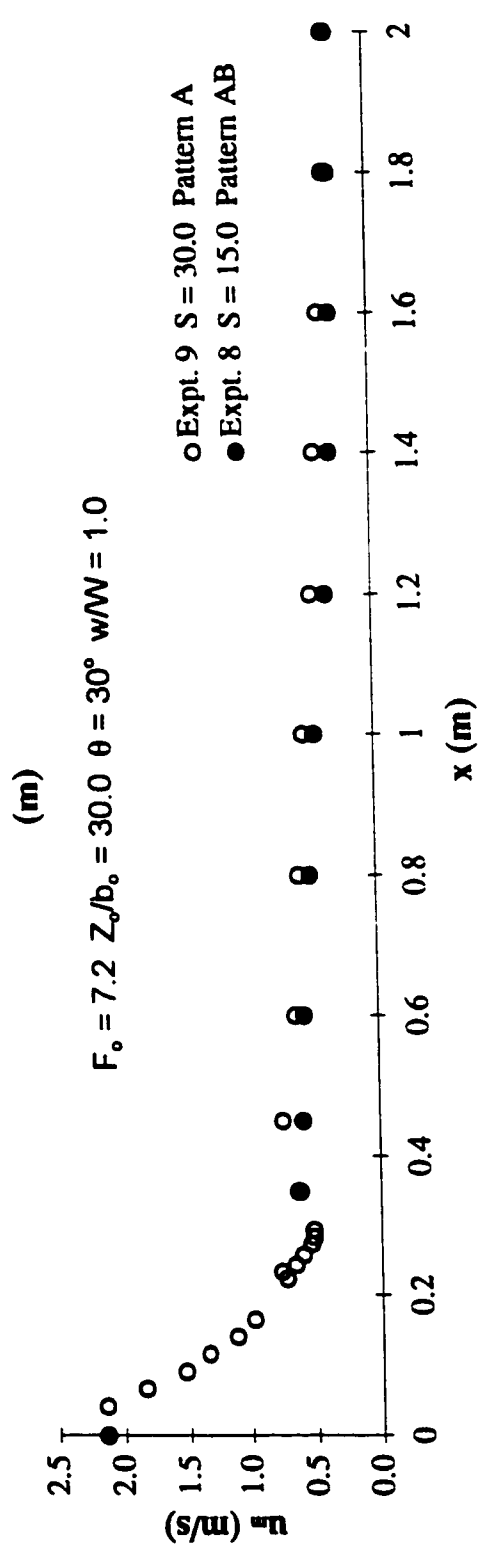


Fig. 4.15(m-n) Maximum-velocity decay in flow pattern A & AB

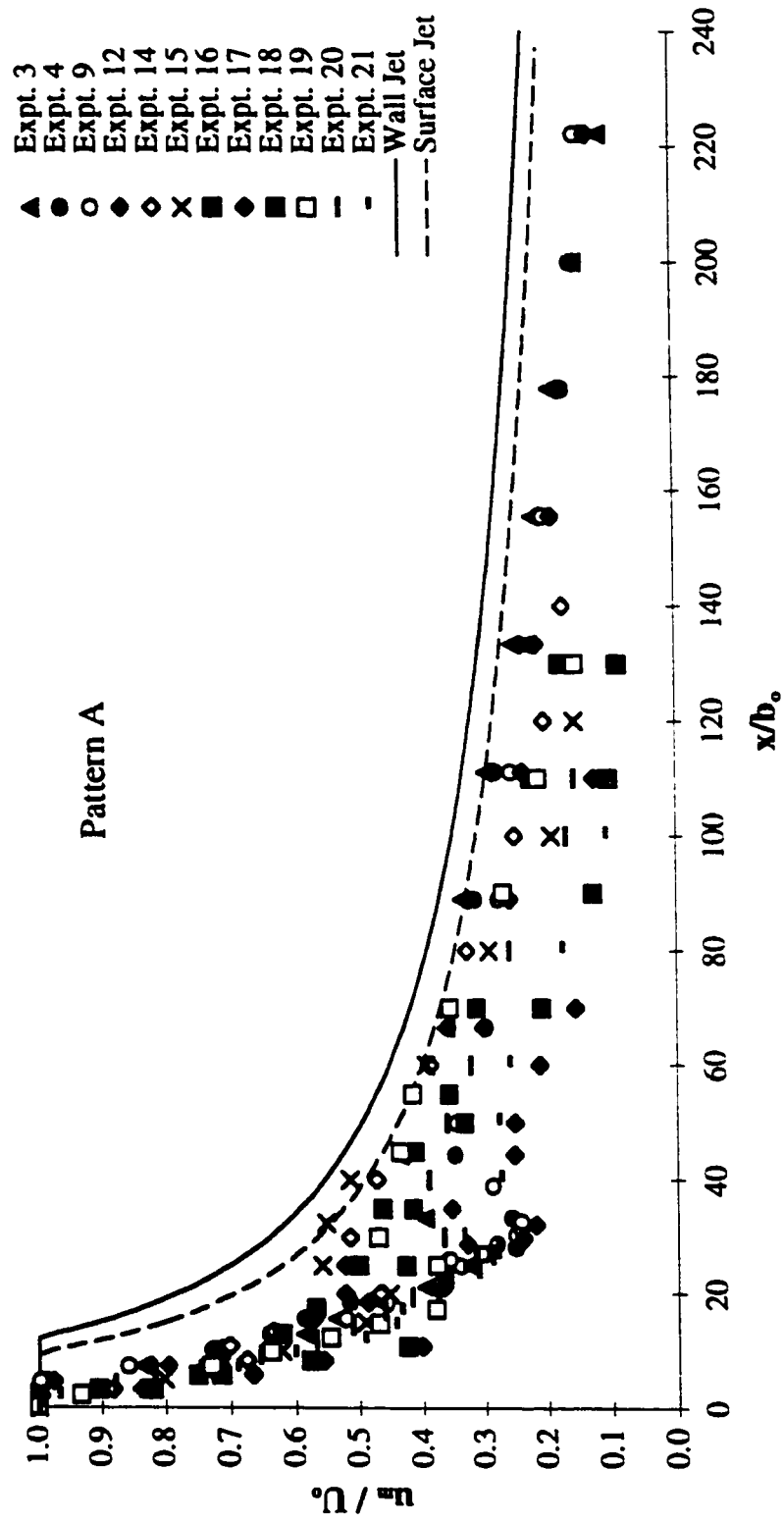


Fig. 4.16 Consolidated plot for all the maximum-velocity decay profiles in flow pattern A

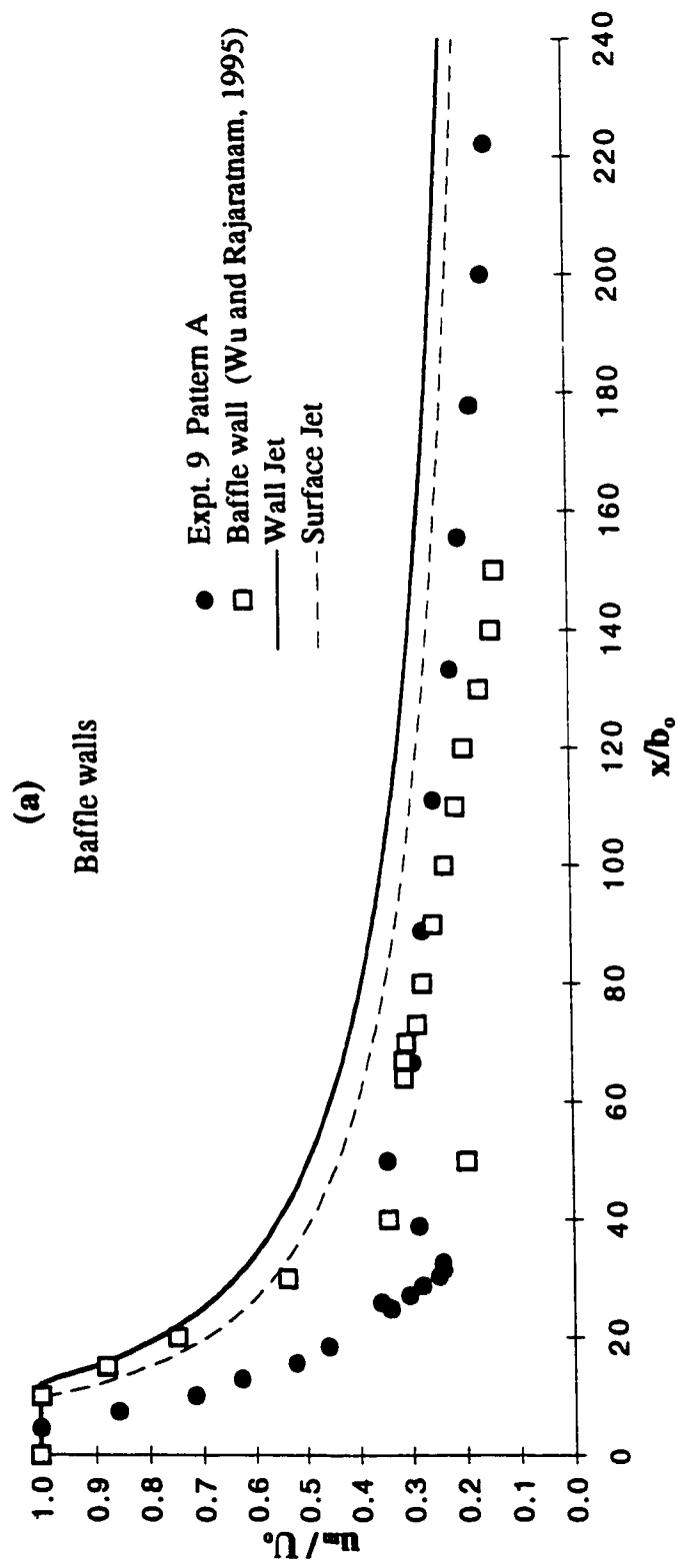


Fig. 4.17 Comparison between the double-leaf gate and the baffle wall dissipators

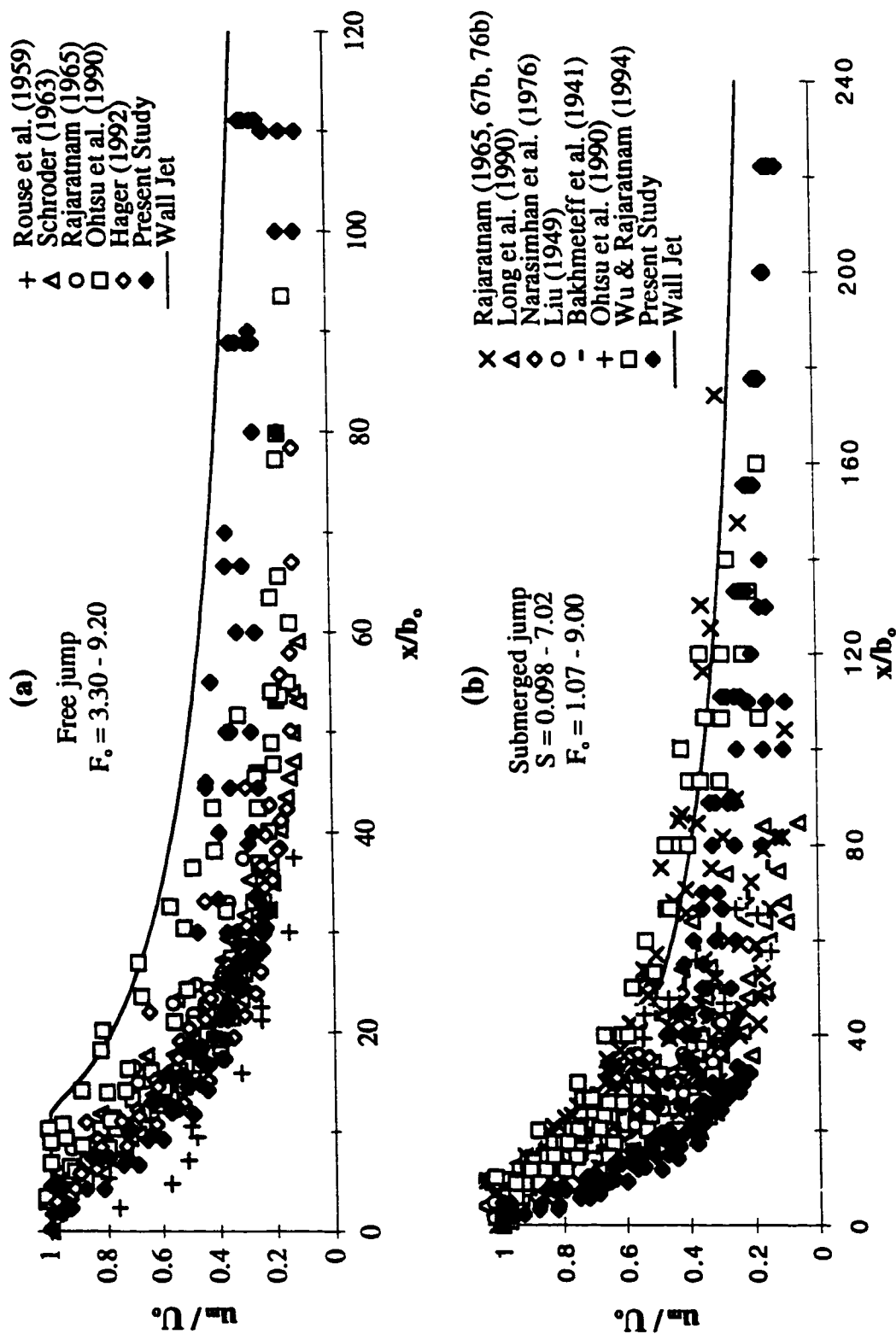


Fig. 4.18(a-b) Comparison between the double-leaf gate, the free and the submerged jumps

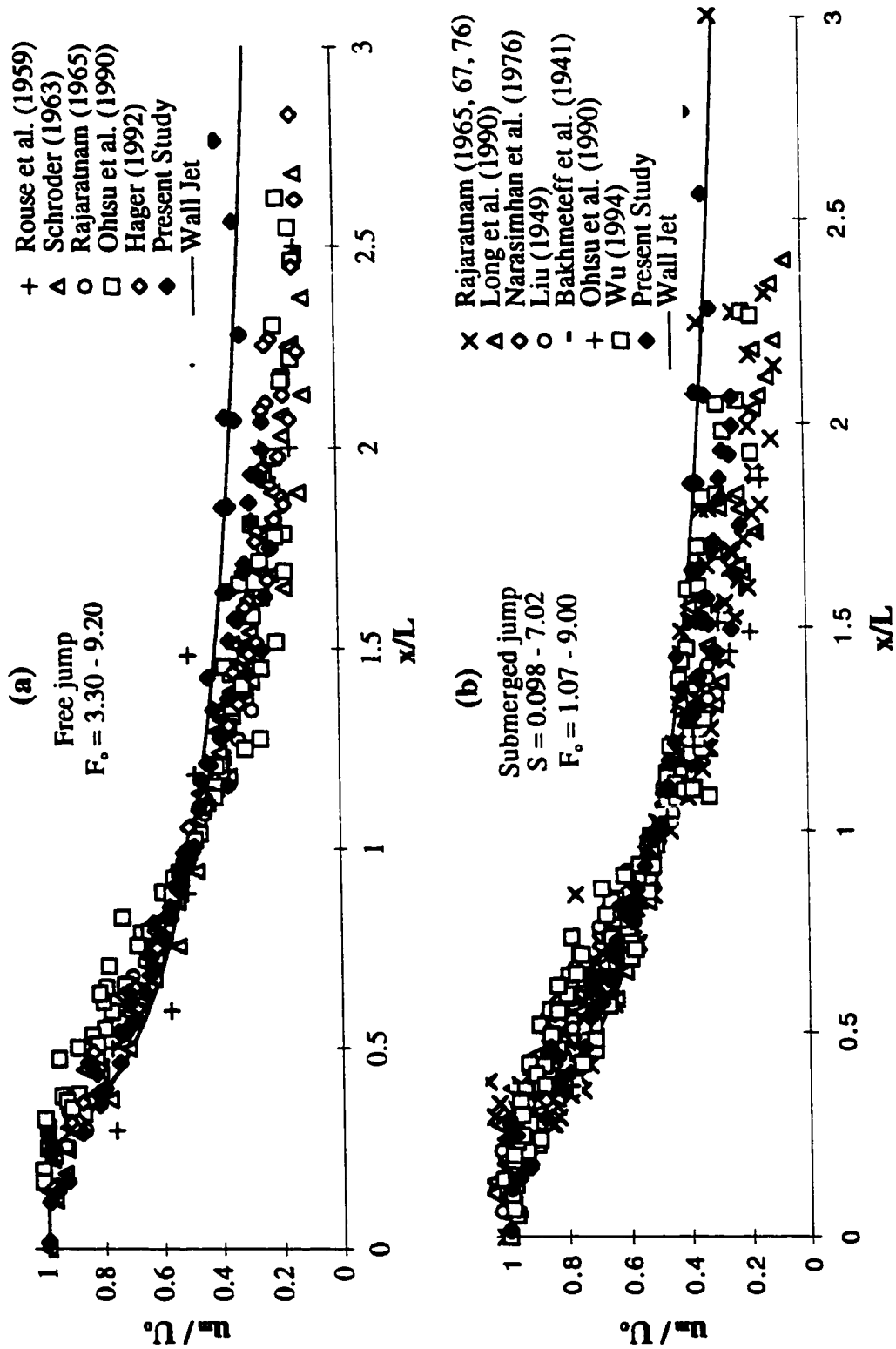


Fig. 4.19(a-b) Comparison between the double-leaf gate, the free and the submerged jumps

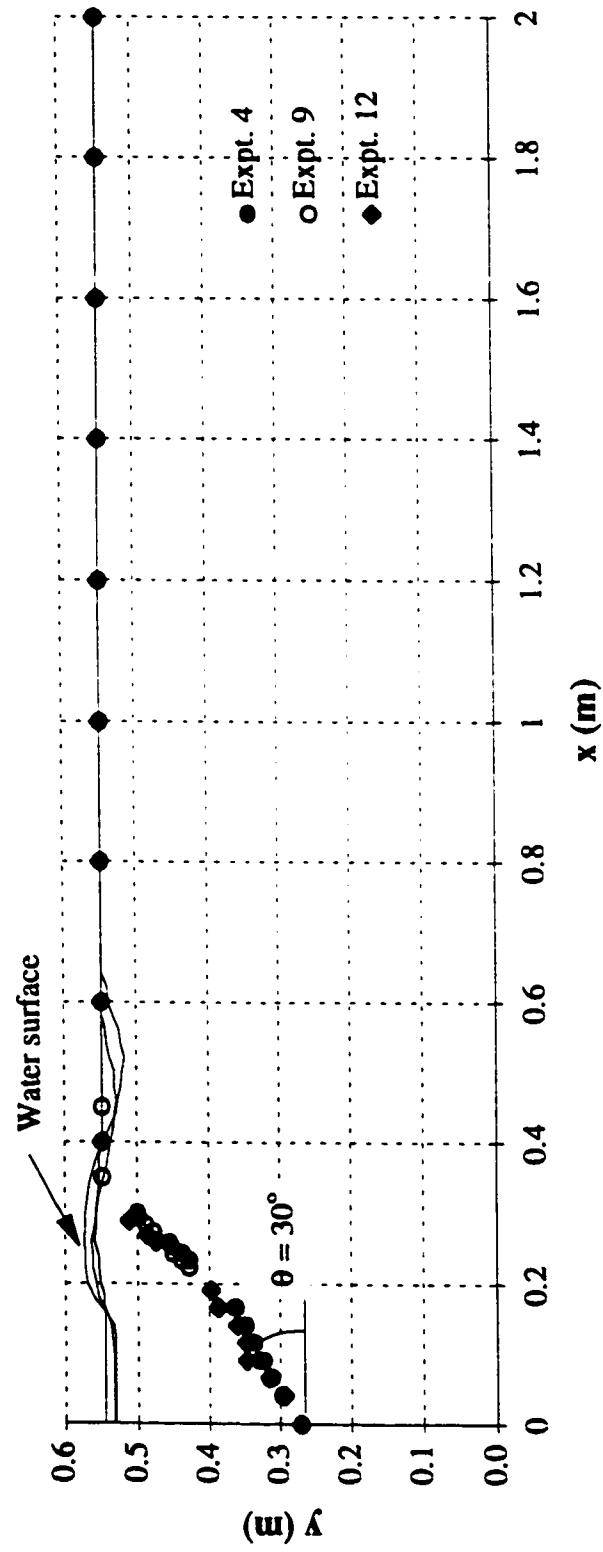


Fig. 4.20 Locus of the maximum velocity

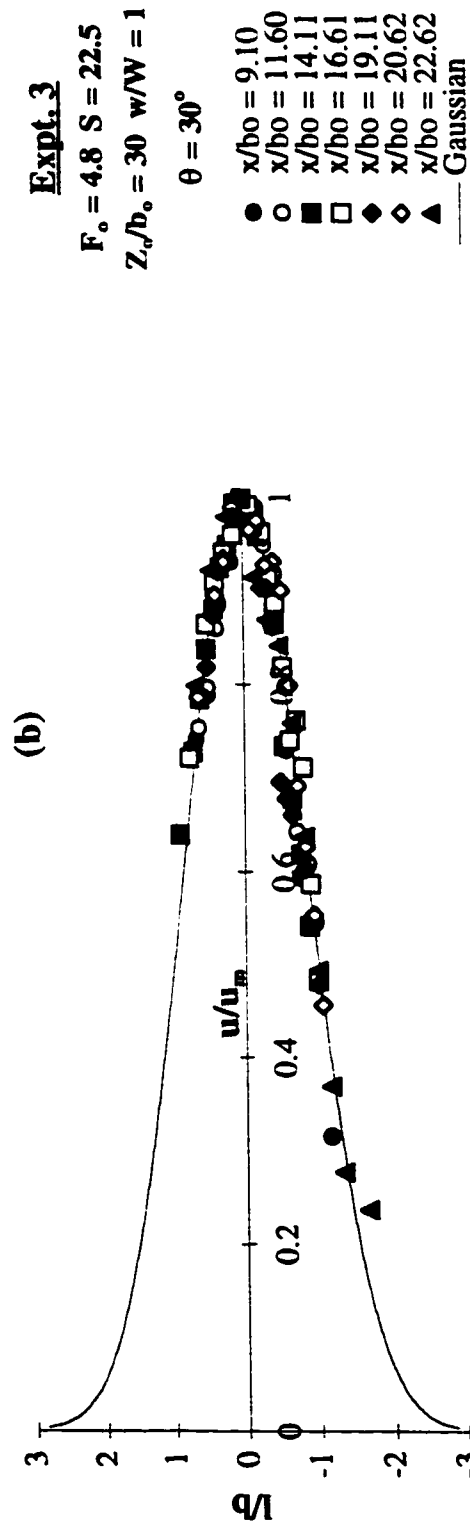
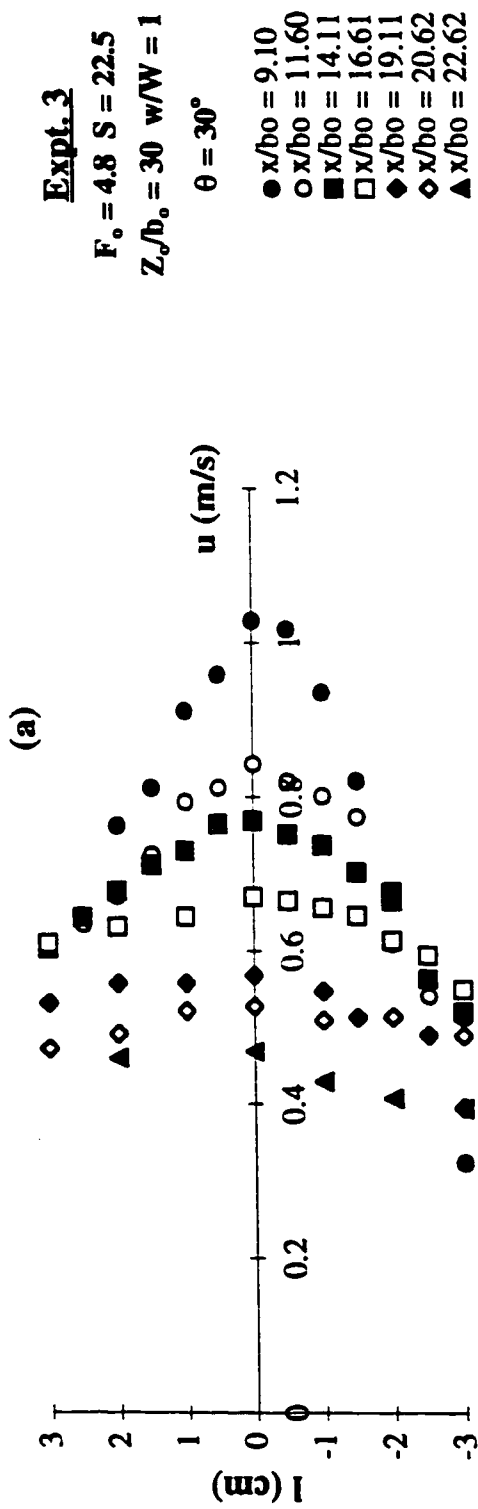


Fig. 4.21(a-b) Velocity distributions for the inclined jet (Expt. 3)
 (a) Typical velocity profiles; (b) Similarity profile

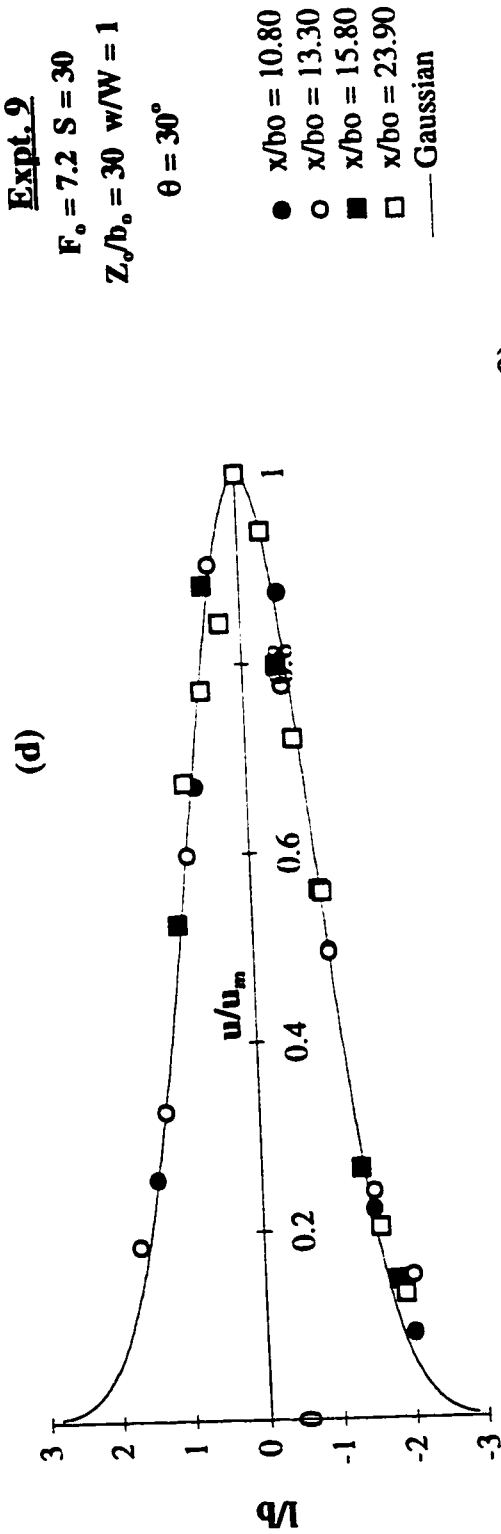
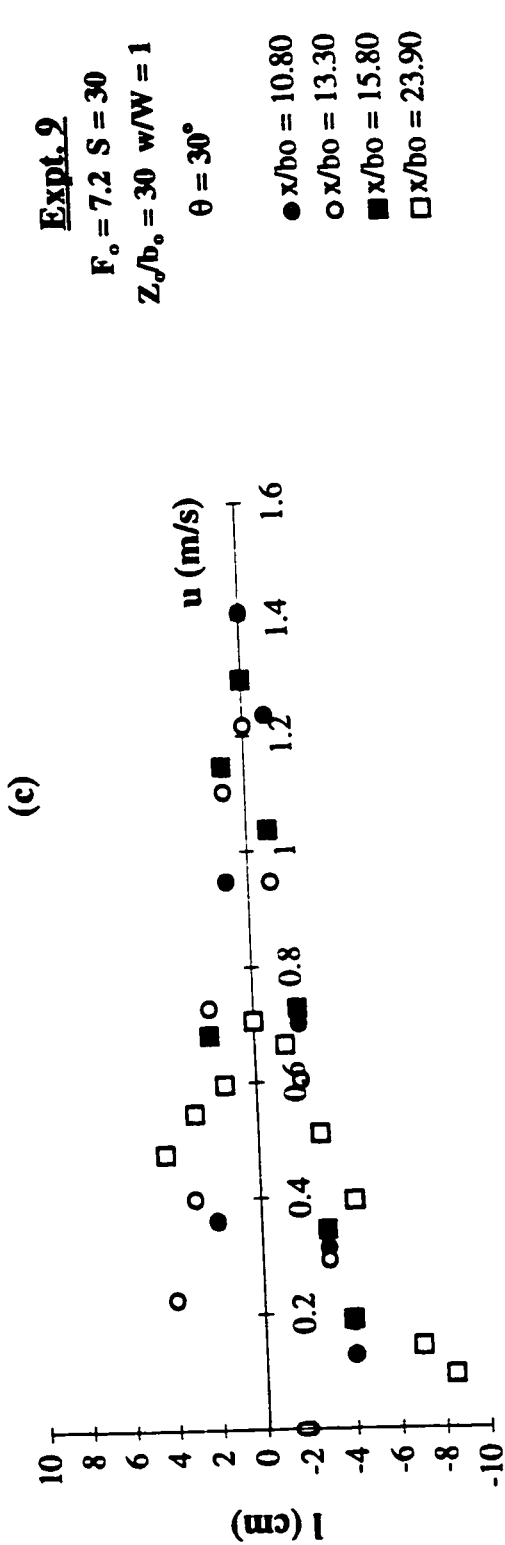


Fig. 4.21(c-d) Velocity distributions for the inclined jet (Expt. 9)
 (c) Typical velocity profiles; (d) Similarity profile

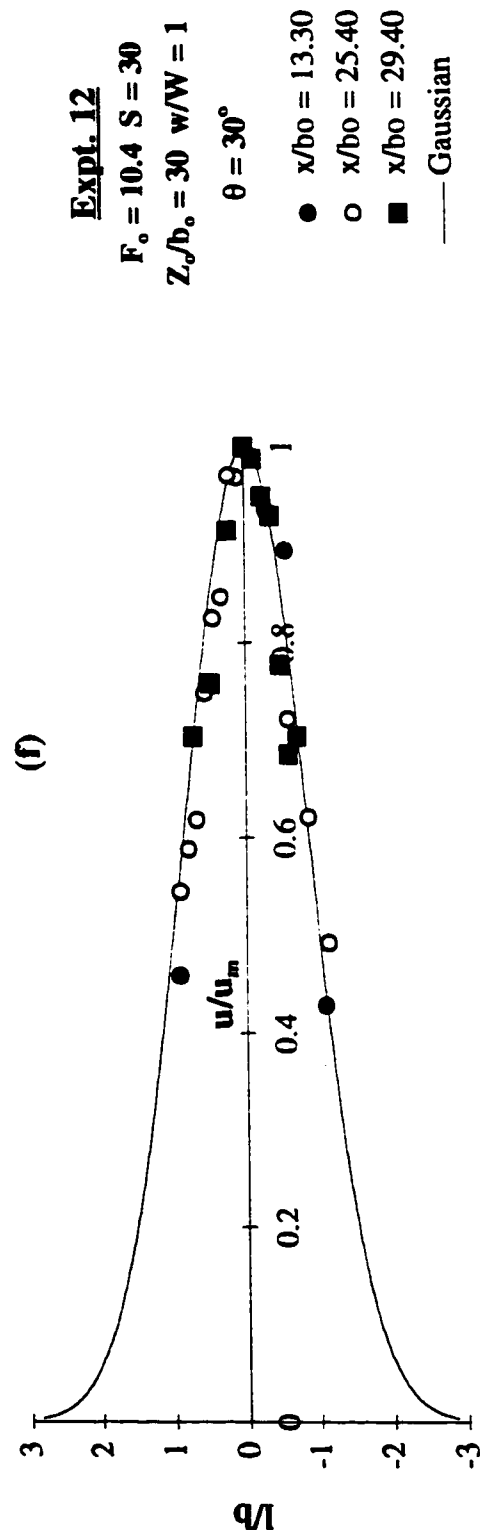
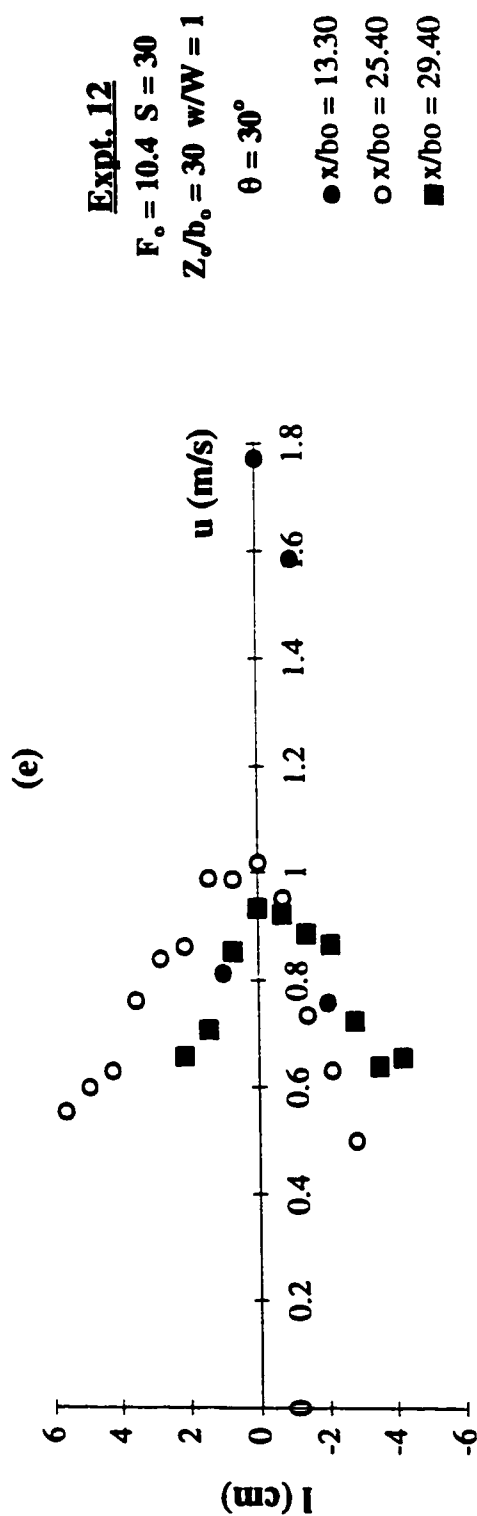


Fig. 4.21(e-f) Velocity distributions for the inclined jet (Expt. 12)
(e) Typical velocity profiles; (f) Similarity profile

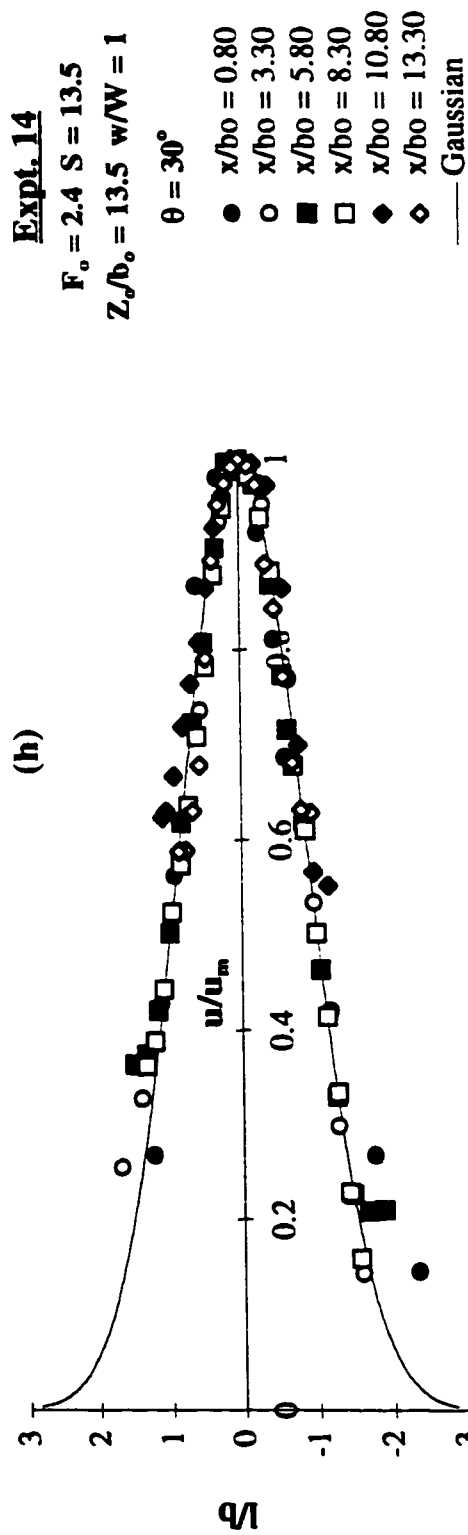
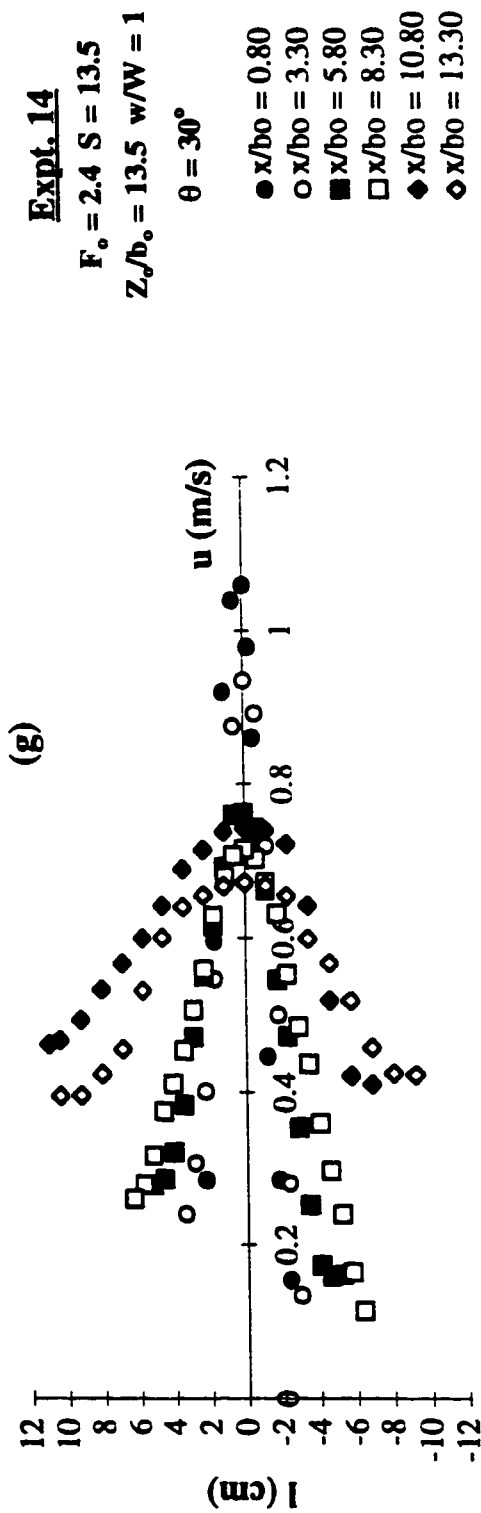
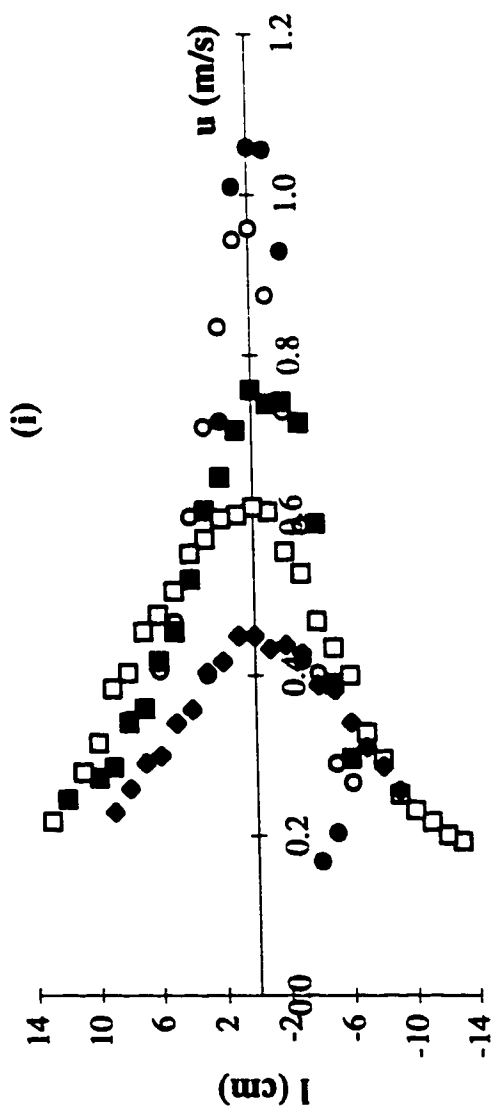


Fig. 4.21(g-h) Velocity distributions for the inclined jet (Expt. 14)
 (g) Typical velocity profiles; (h) Similarity profile



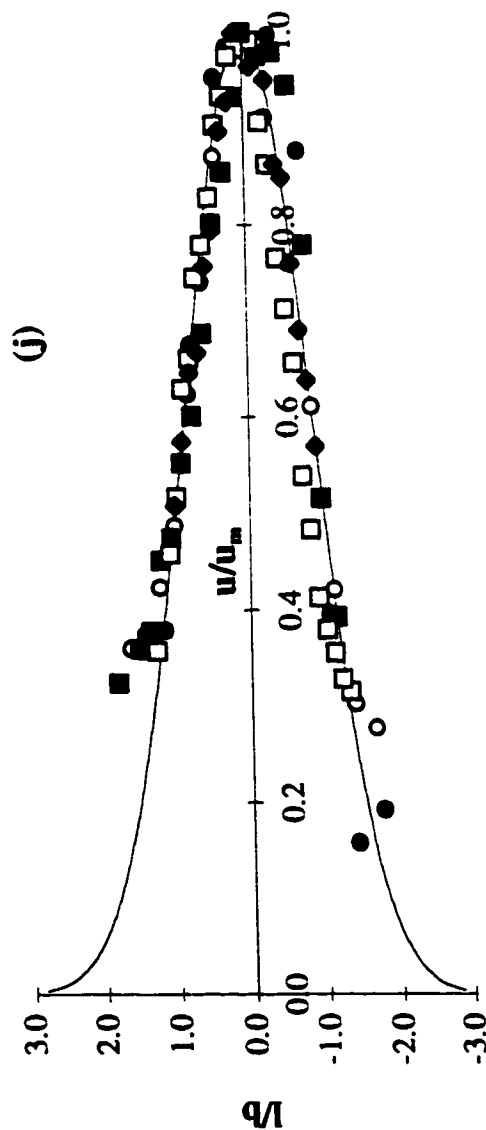
Expt. 16

$F_o = 2.4$ $S = 13.5$

$Z_o/b_o = 0$ $w/W = 1$

$\theta = 30^\circ$

- $x/b_o = 0.89$
- $x/b_o = 3.30$
- $x/b_o = 5.80$
- $x/b_o = 8.30$
- ◆ $x/b_o = 10.80$



Expt. 16

$F_o = 2.4$ $S = 13.5$

$Z_o/b_o = 0$ $w/W = 1$

$\theta = 30^\circ$

- $x/b_o = 0.89$
- $x/b_o = 3.30$
- $x/b_o = 5.80$
- $x/b_o = 8.30$
- ◆ $x/b_o = 10.80$
- Gaussian

Fig. 4.21(i-j) Velocity distributions for the inclined jet (Expt. 16)
 (i) Typical velocity profiles; (j) Similarity profile

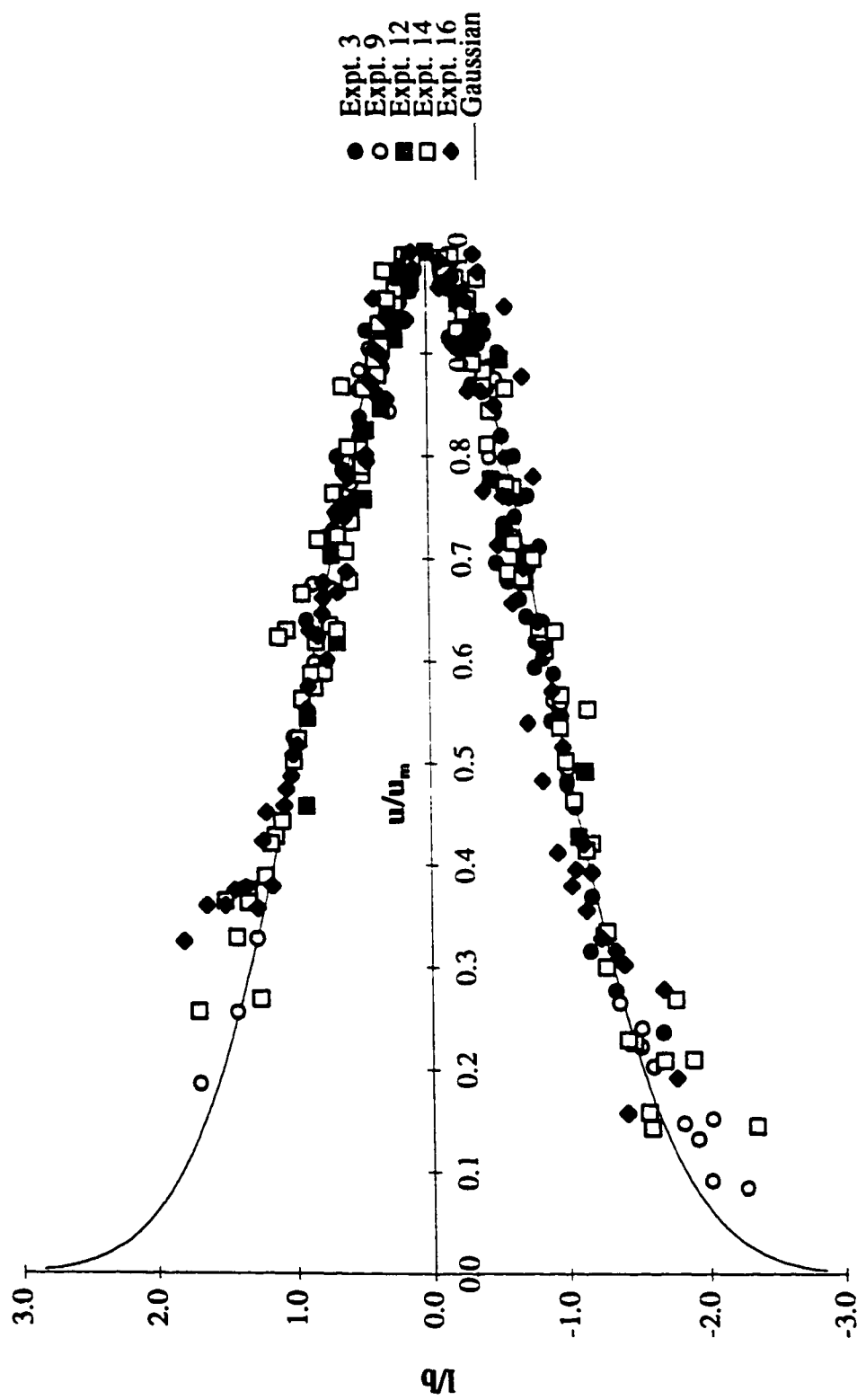


Fig. 4.22 Consolidated non-dimensional plot for the velocity distribution in the inclined jet

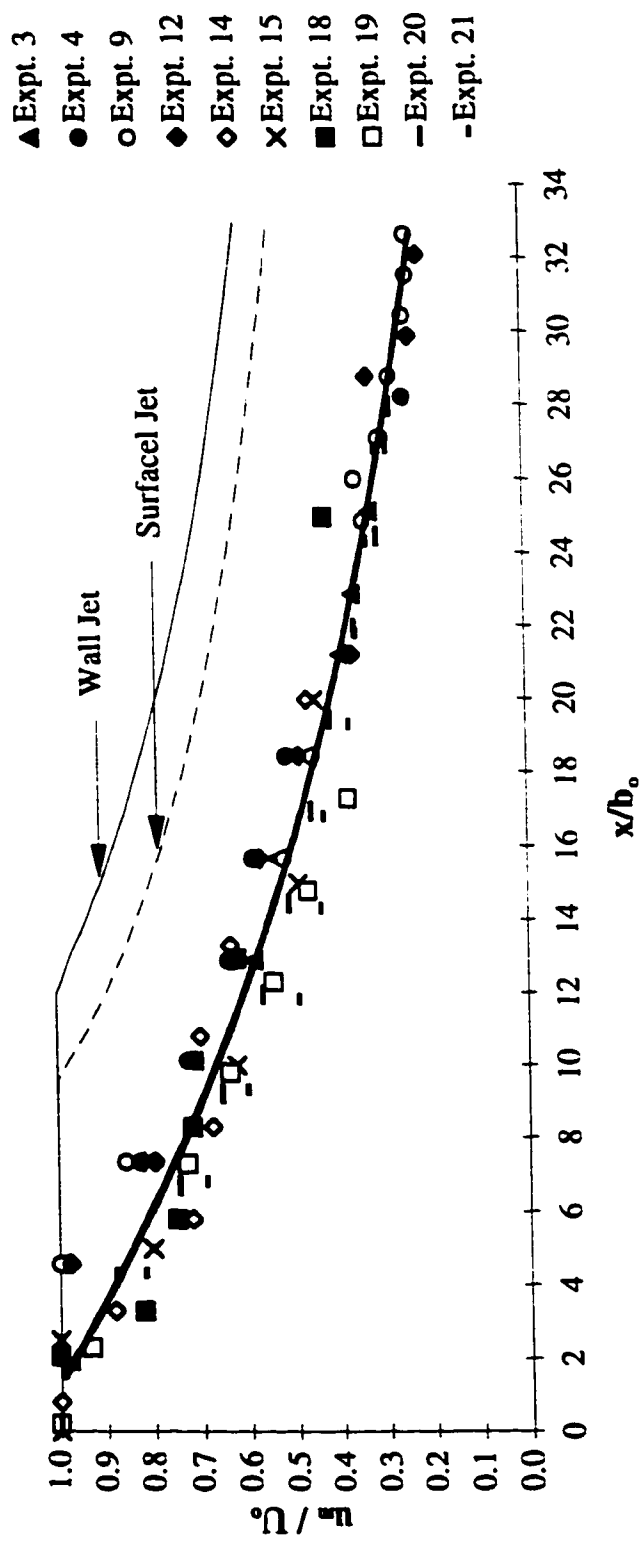


Fig. 4.23 Maximum-velocity decay with distance along the inclined jet

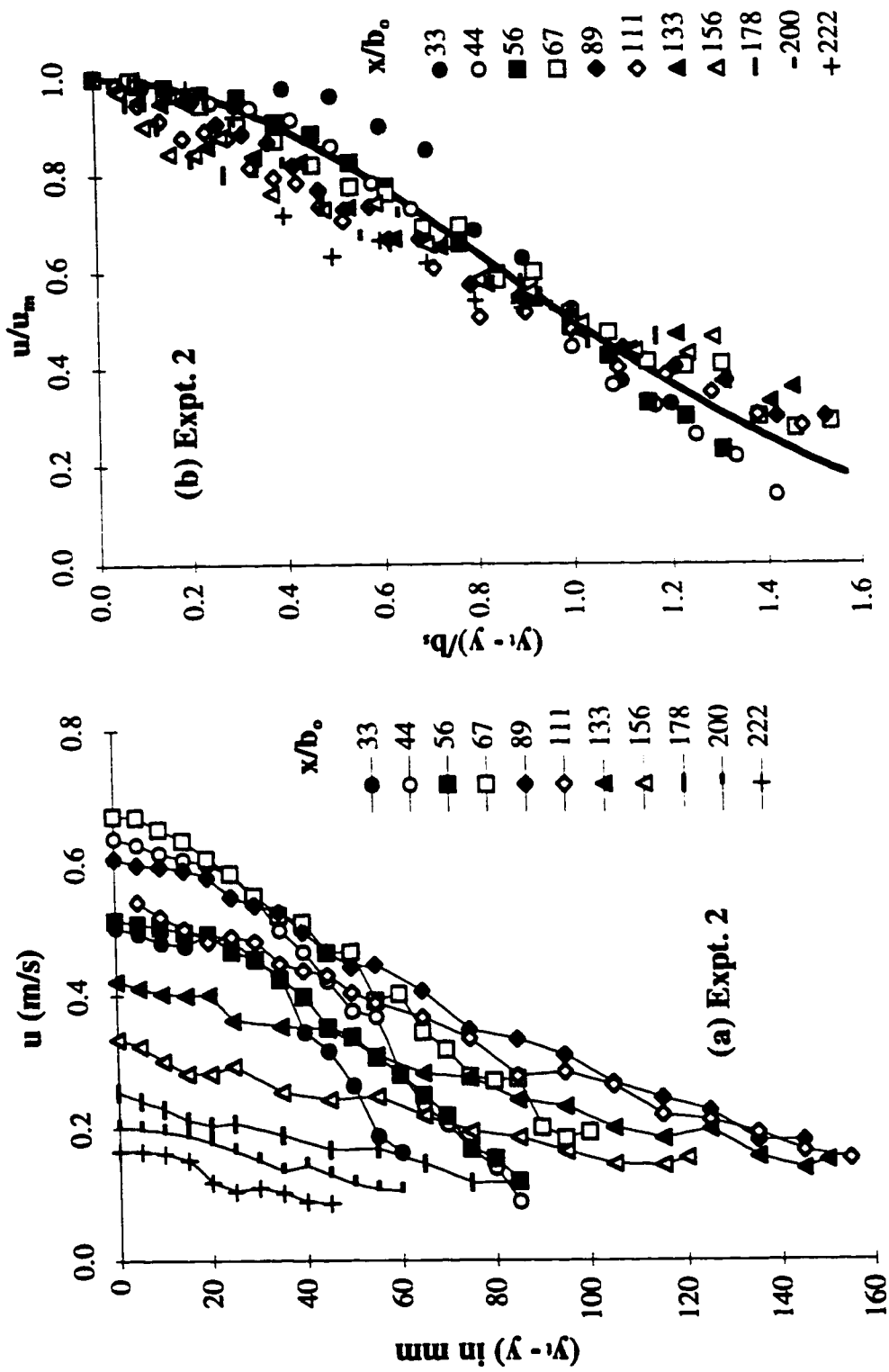


Fig. 4.24(a-b) Velocity distribution in surface jet (Expt. 2)
(a) Velocity profiles; and (b) Similarity profile

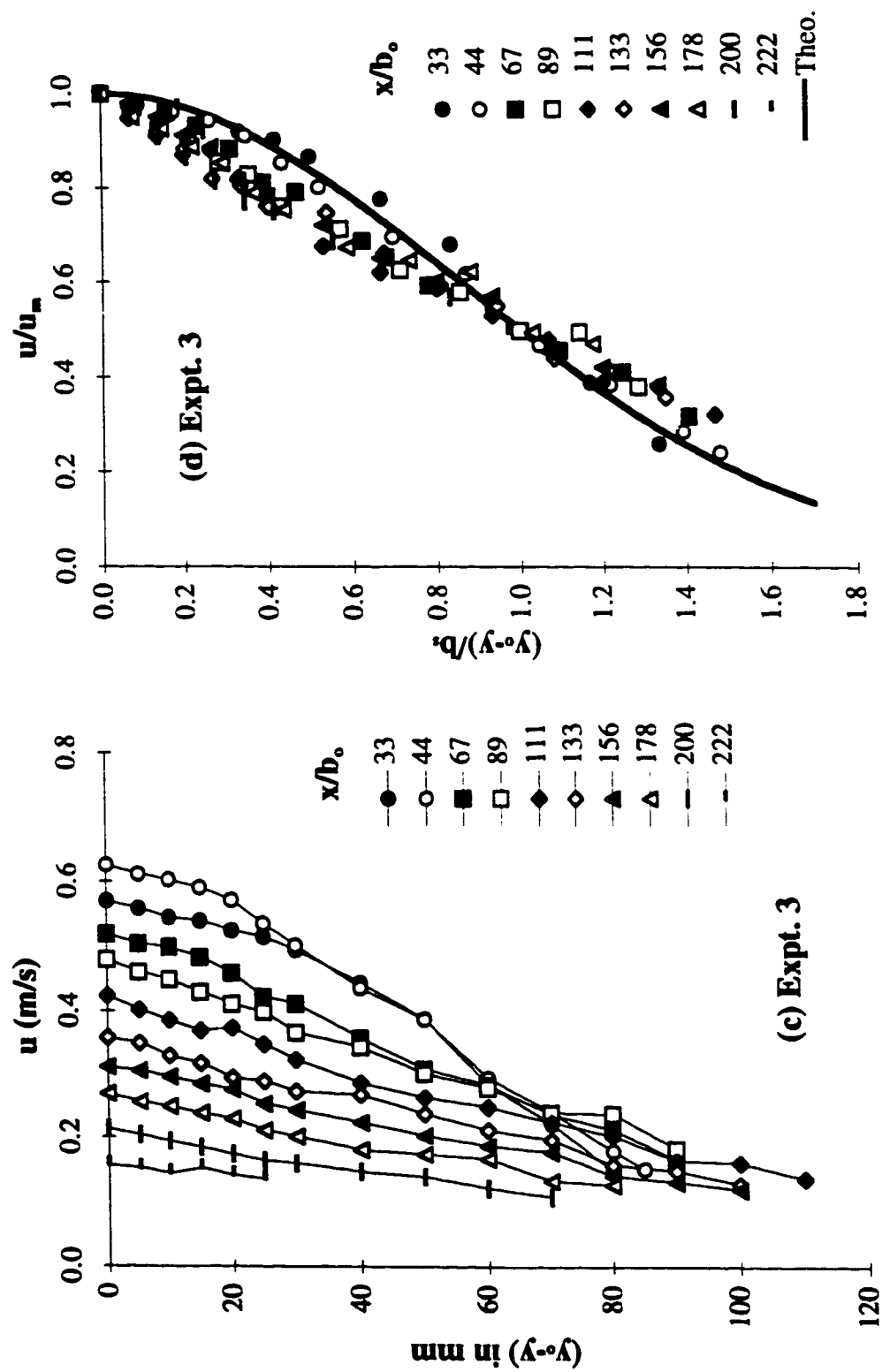


Fig. 4.24(c-d) Velocity distribution in surface jet (Expt. 3)
(c) Velocity profiles; and (d) Similarity profile

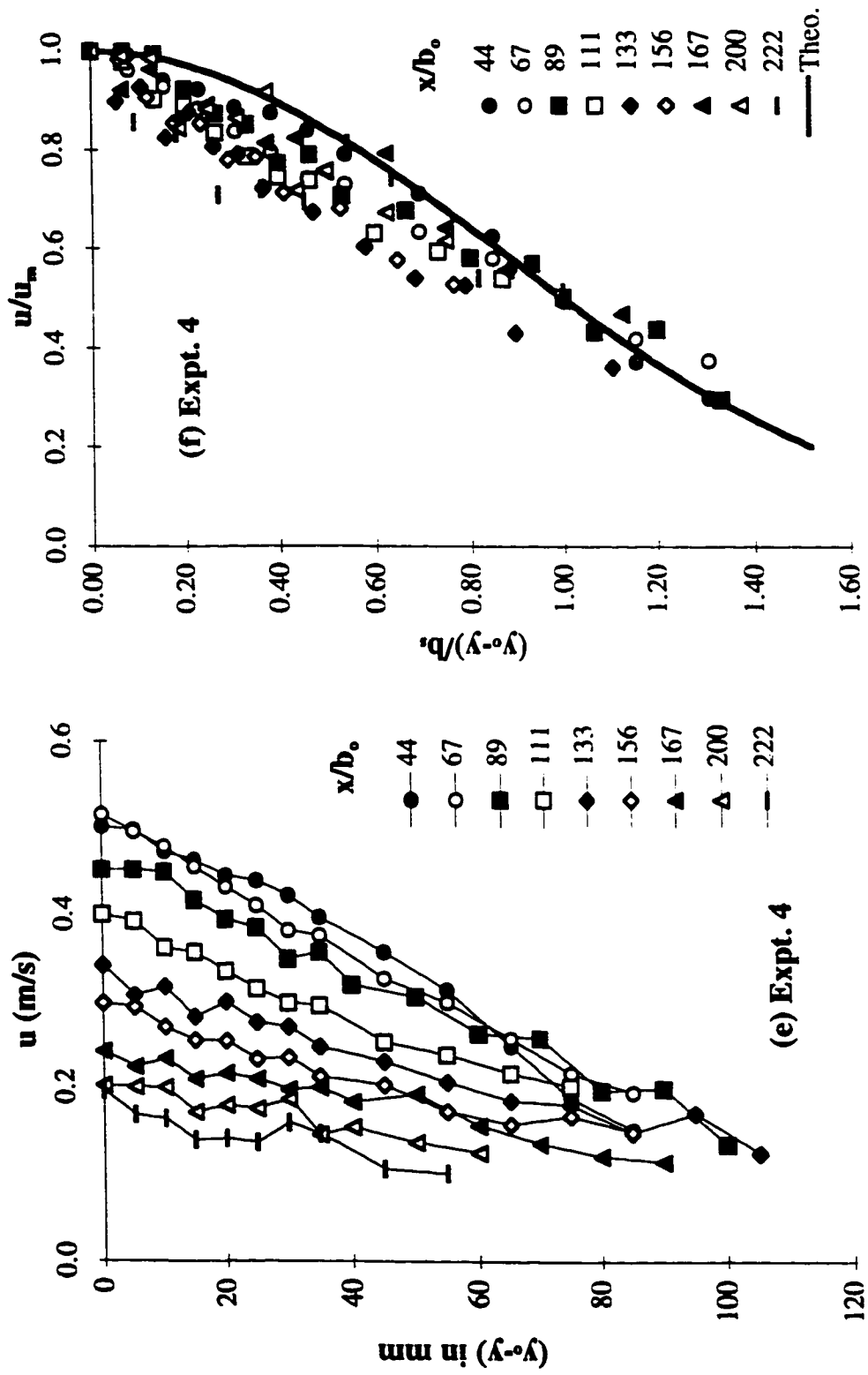


Fig. 4.24(e-f) Velocity distribution in surface jet (Expt. 4)
(e) Velocity profiles; and (f) Similarity profile

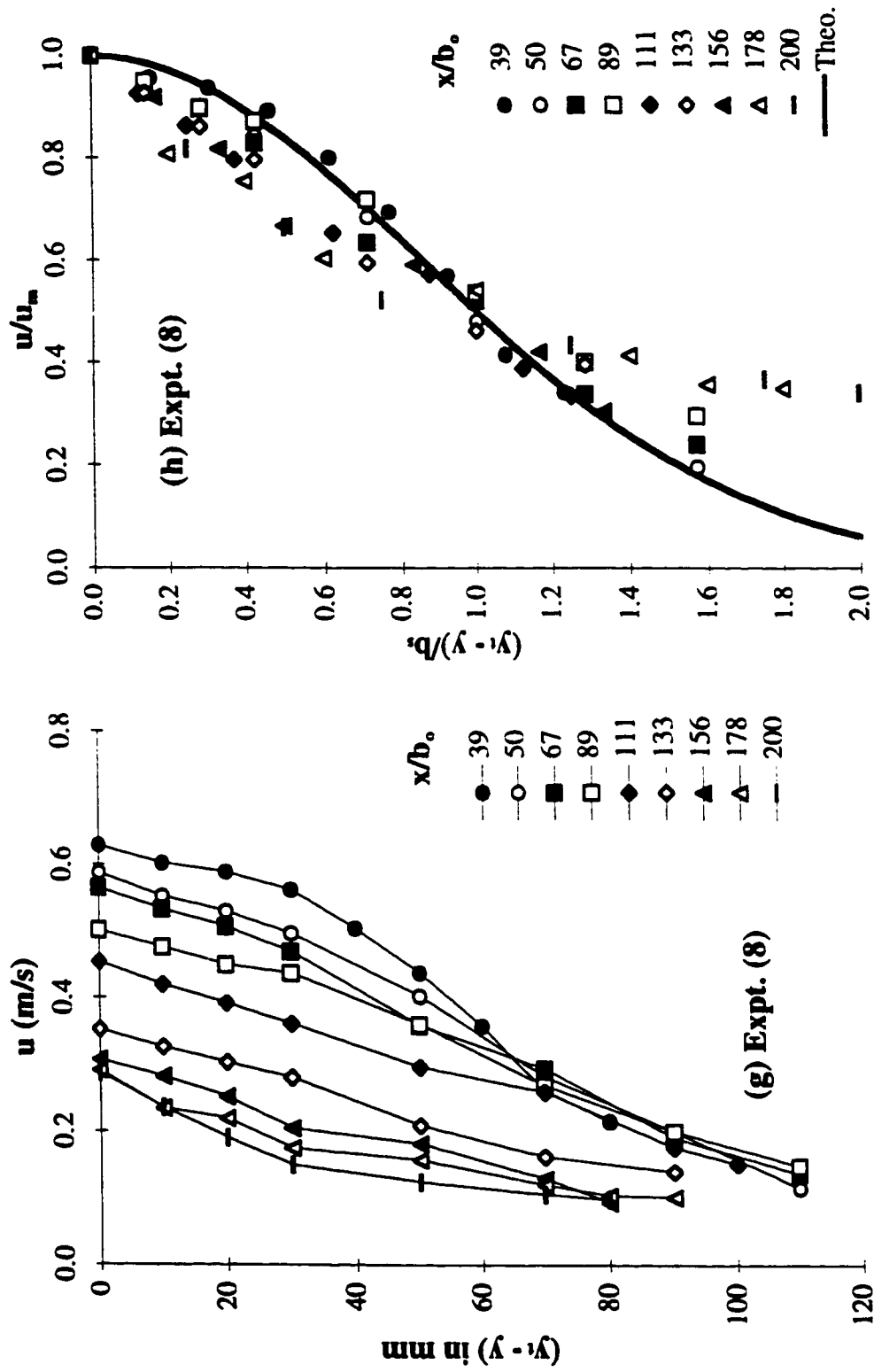


Fig. 4.24(g-h) Velocity distribution in surface jet (Expt. 8)
(g) Velocity profiles; and (h) Similarity profile

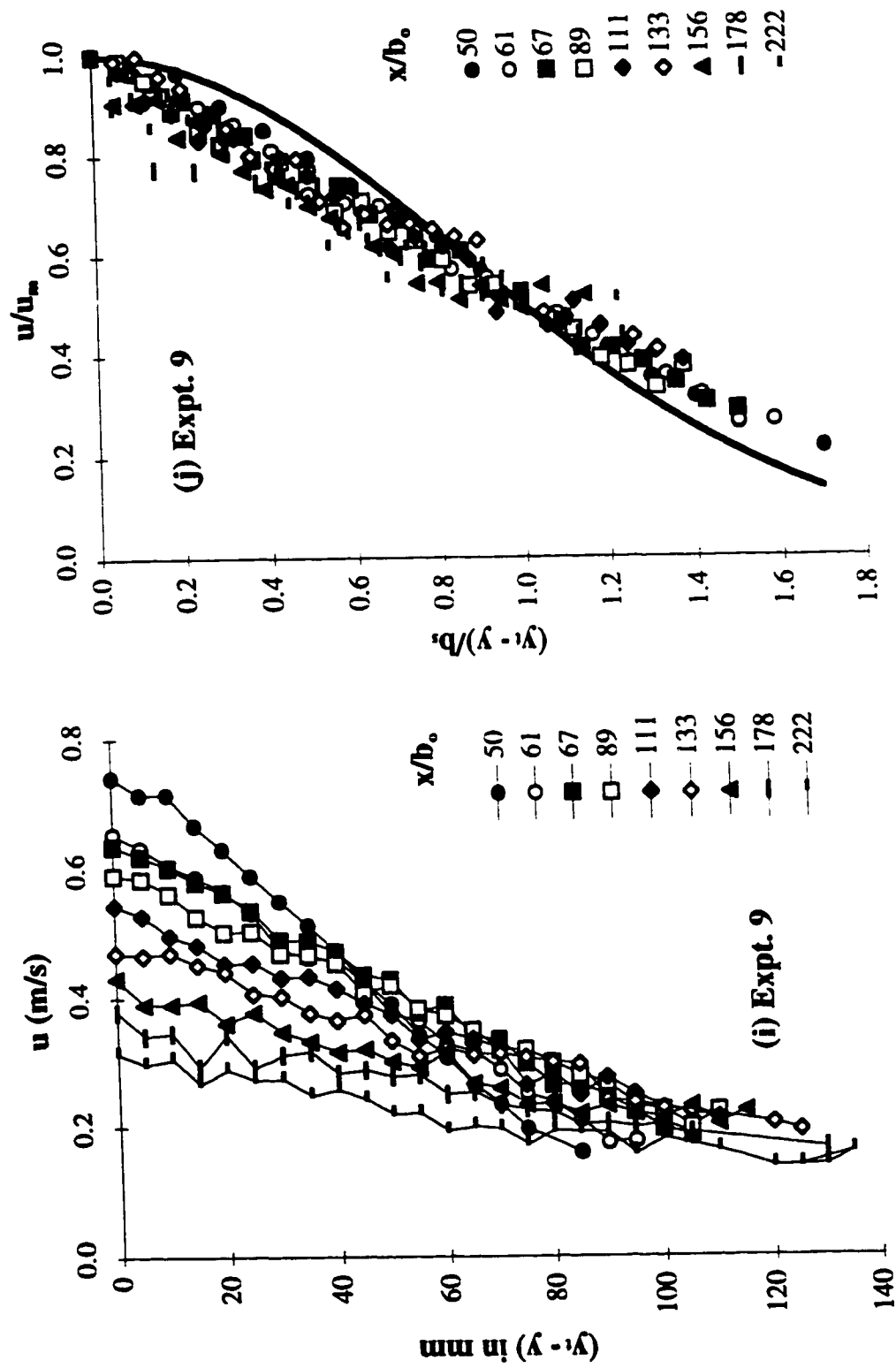


Fig. 4.24(i-j) Velocity distribution in surface jet (Expt. 9)
(i) Velocity profiles; and (j) Similarity profile

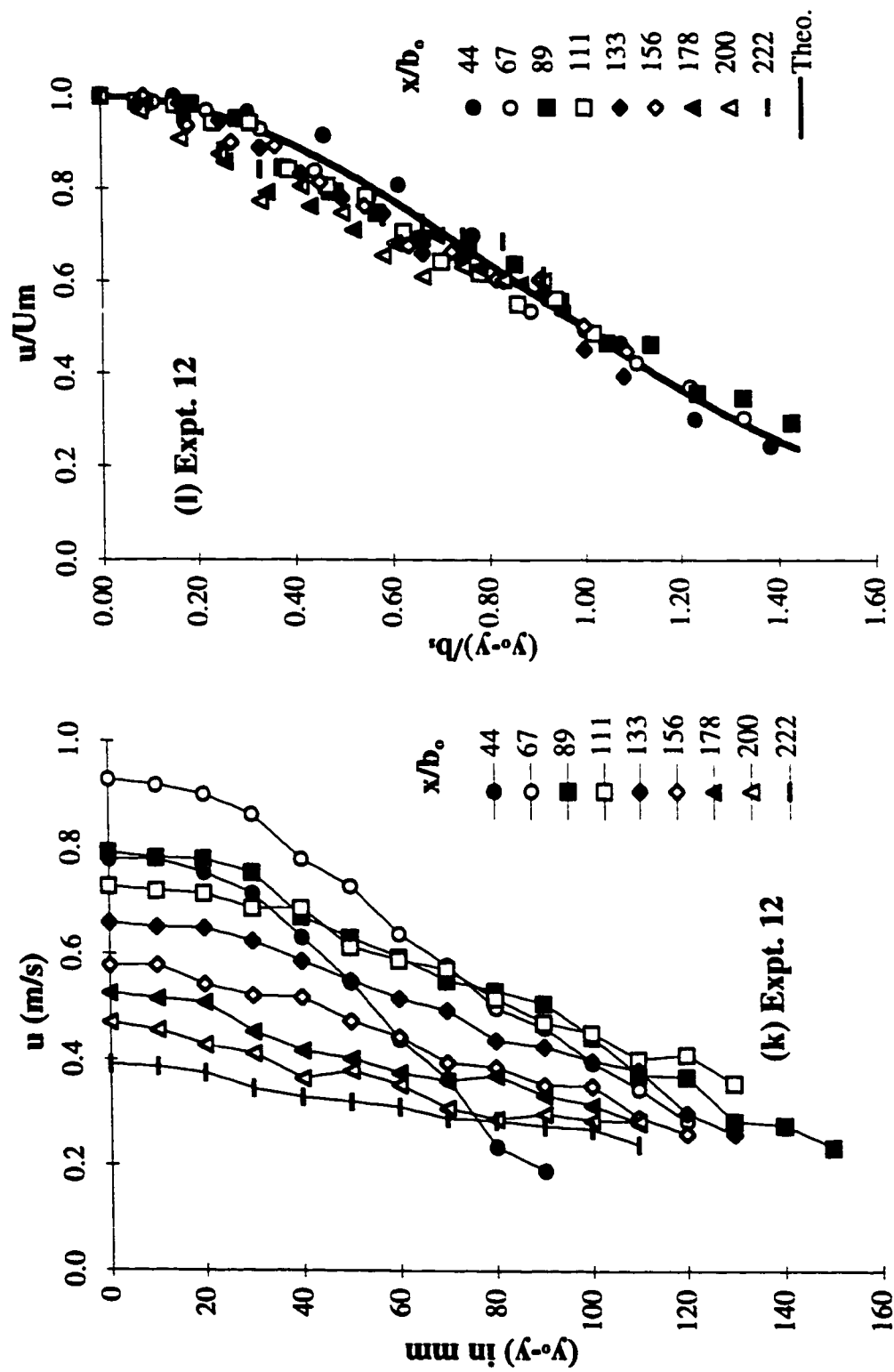


Fig. 4.24(k-l) Velocity distribution in surface jet (Expt. 12)
(k) Velocity profiles; and (l) Similarity profile

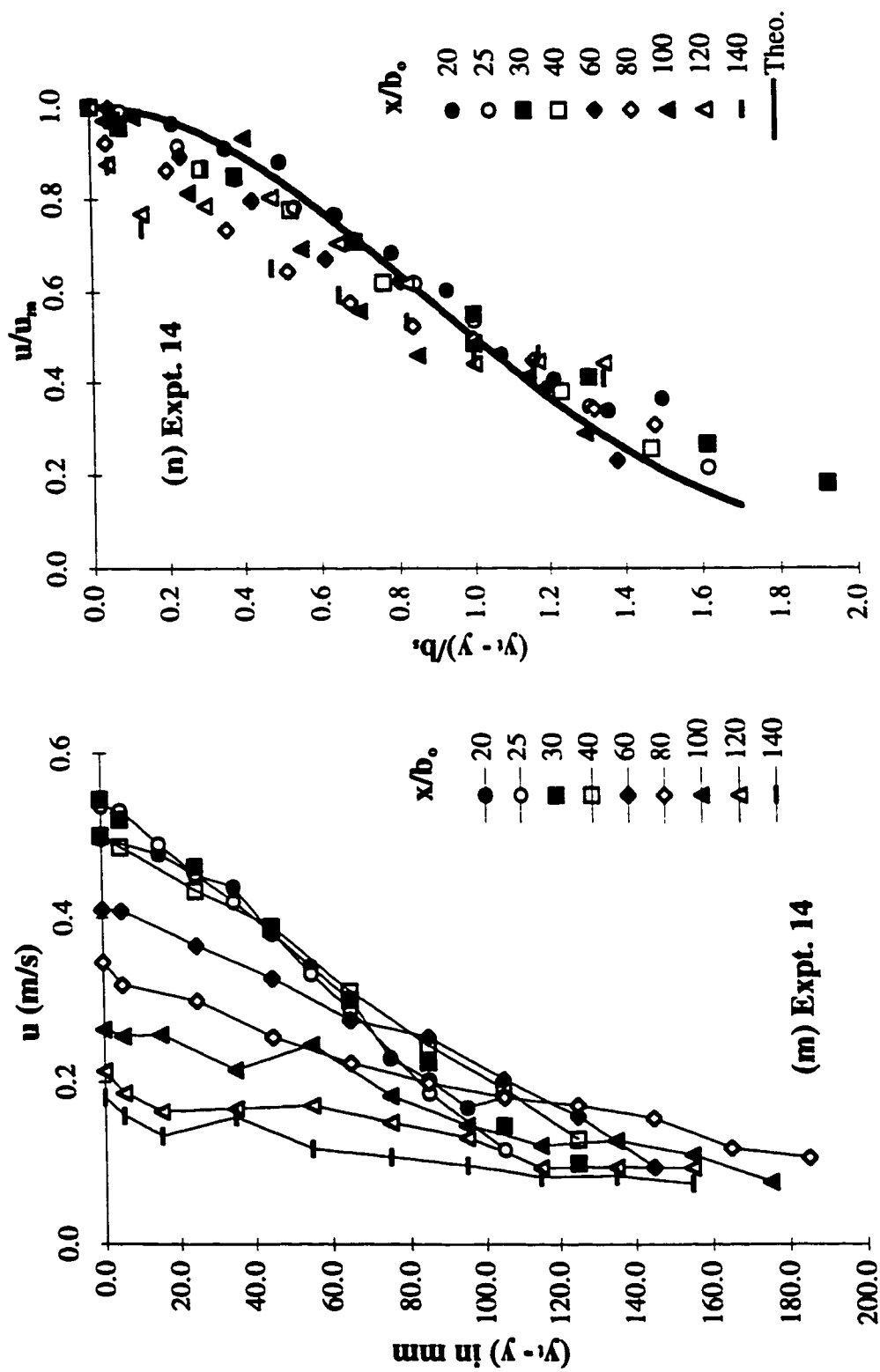


Fig. 4.24(m-n) Velocity distribution in surface jet (Expt. 14)
(m) Velocity profiles; and (n) Similarity profile

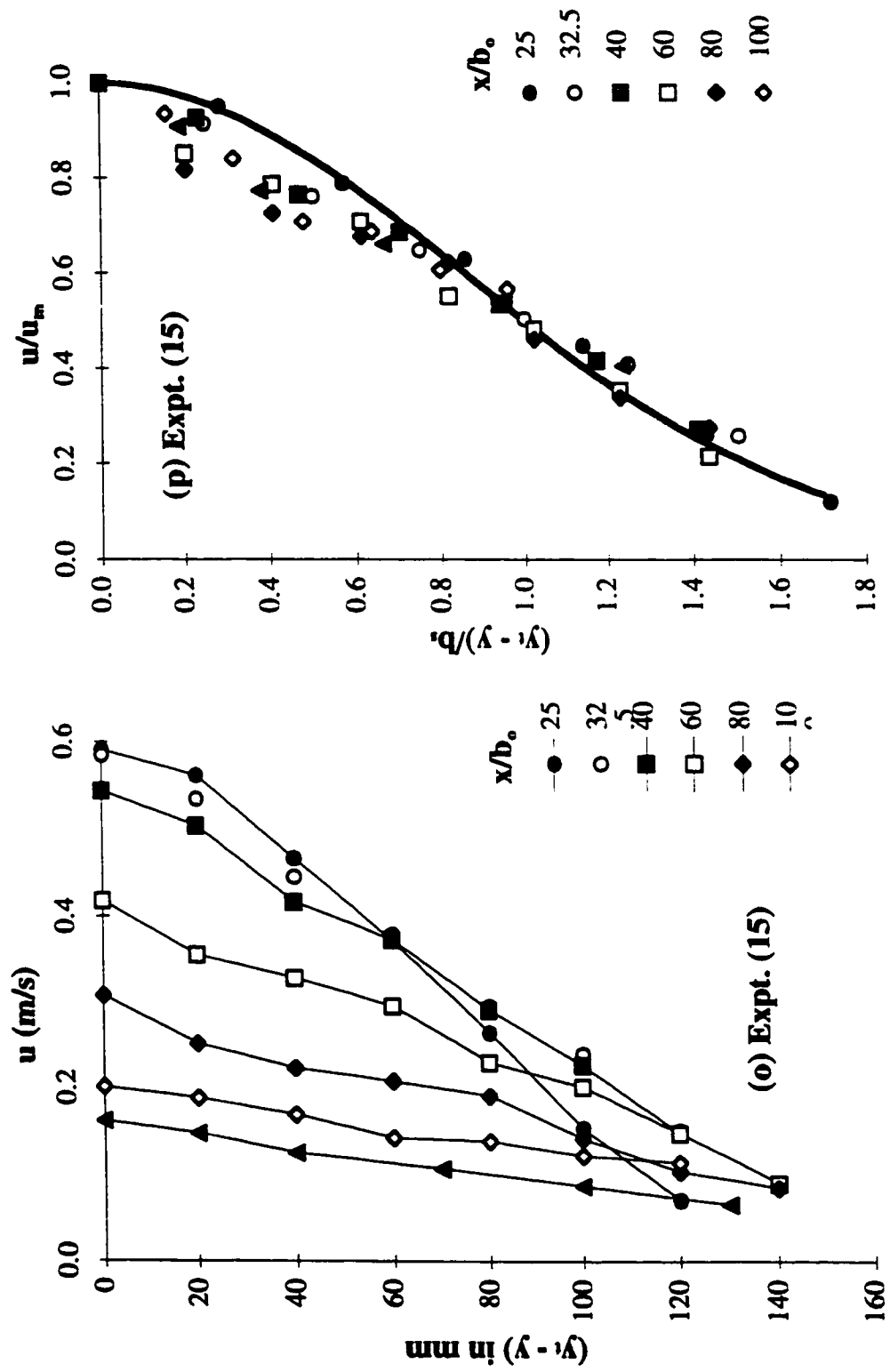


Fig. 4.24(o-p) Velocity distribution in surface jet (Expt. 15)
(o) Velocity profiles; and (p) Similarity profile

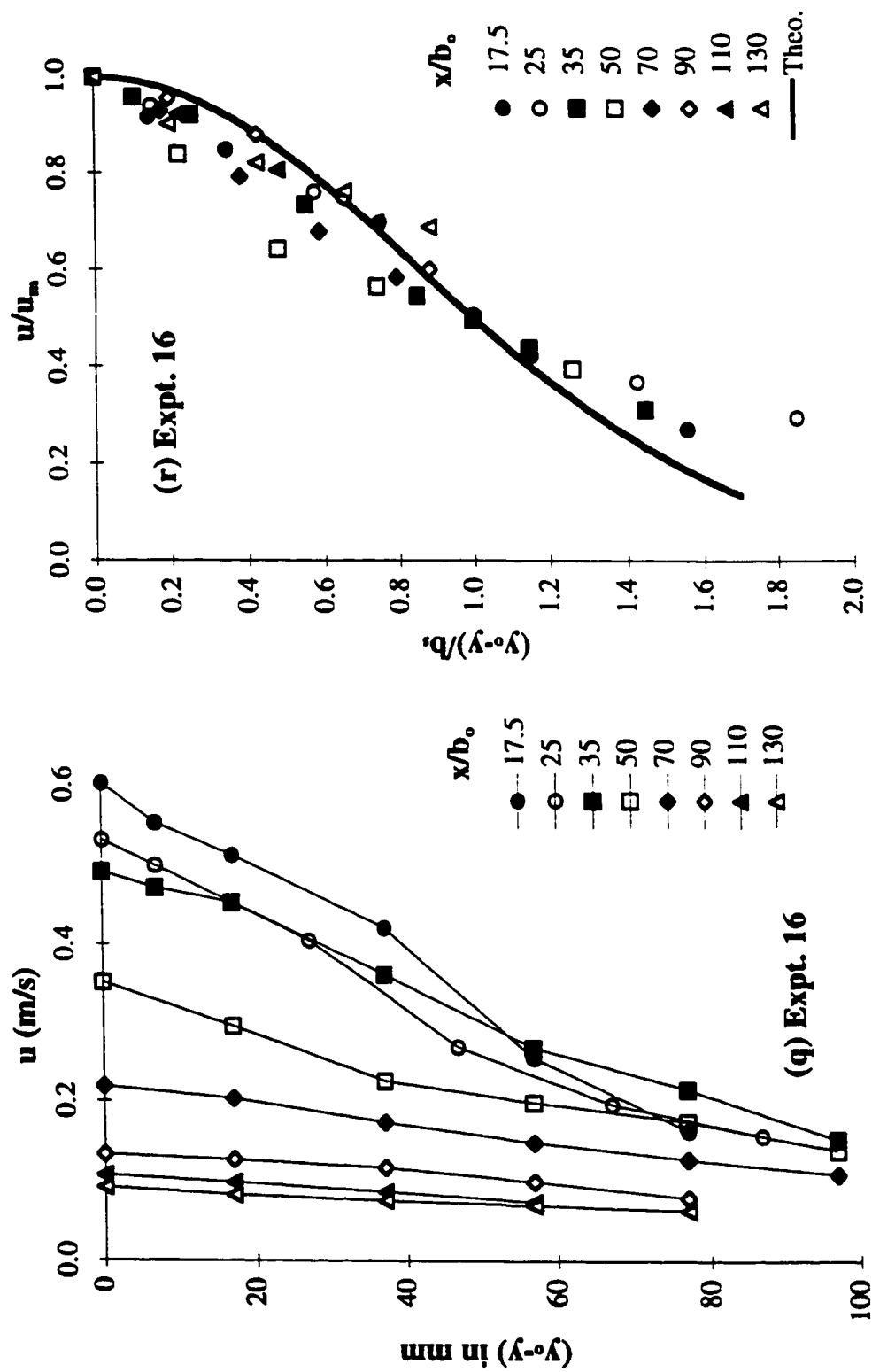


Fig. 4.24(q-r) Velocity distribution in surface jet (Expt. 16)
(q) Velocity profiles; and (r) Similarity profile

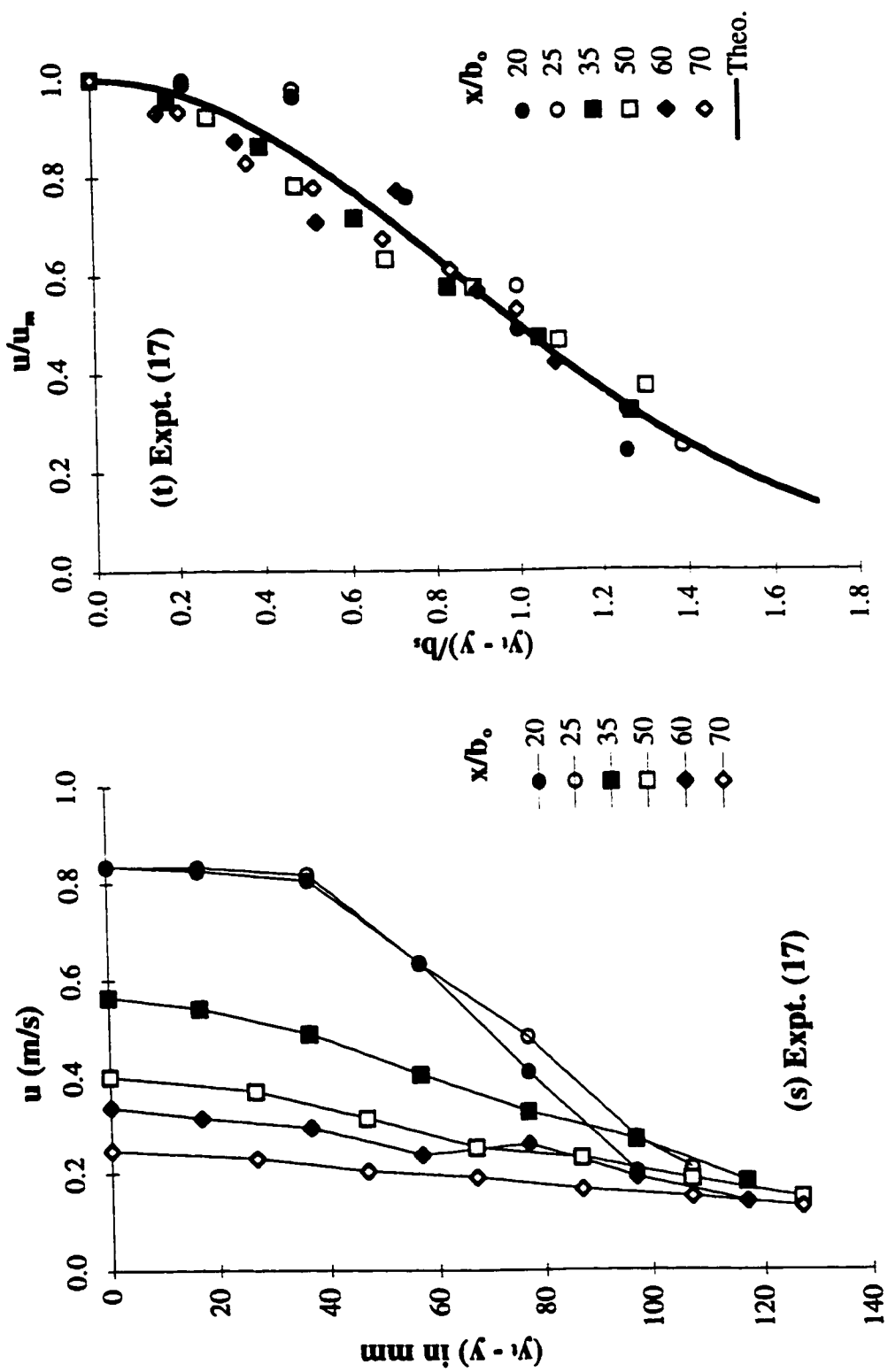


Fig. 4.24(s-t) Velocity distribution in surface jet (Expt. 17)
(s) Velocity profiles; and (t) Similarity profile

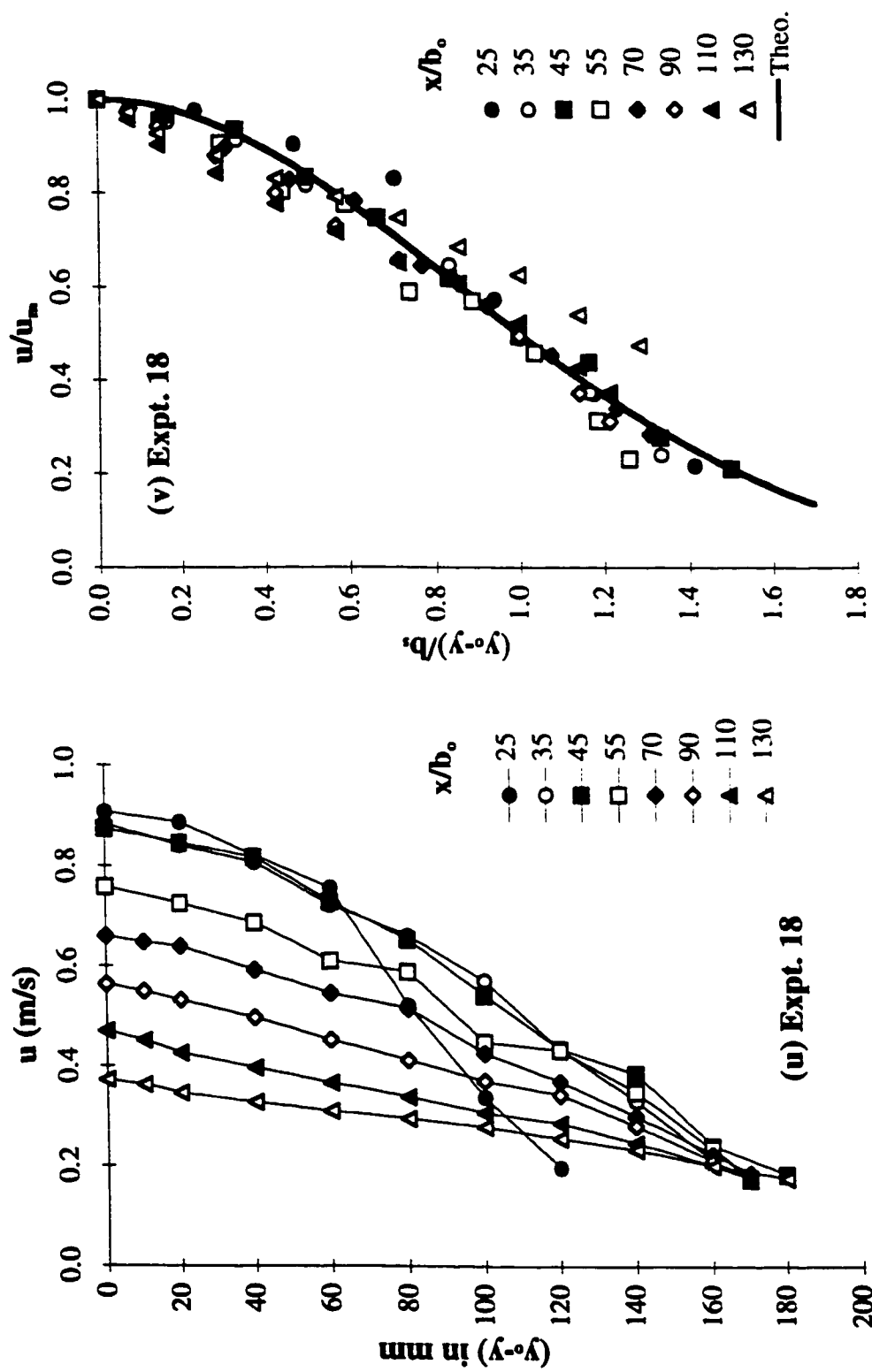


Fig. 4.24(u-v) Velocity distribution in surface jet (Expt. 18)
(u) Velocity profiles; and (v) Similarity profile

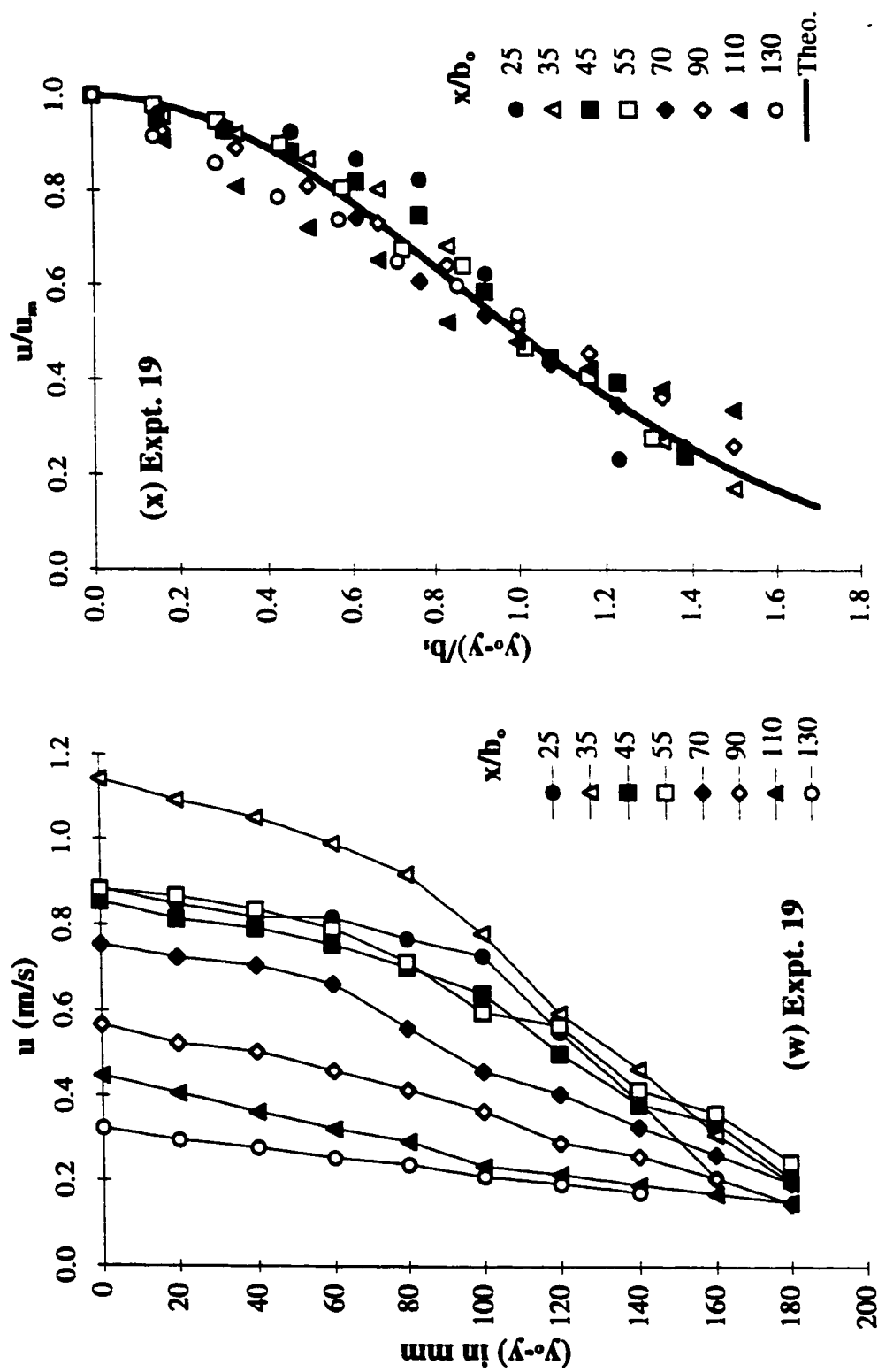


Fig. 4.24(w-x) Velocity distribution in surface jet (Expt. 19)
(w) Velocity profiles; and (x) Similarity profile

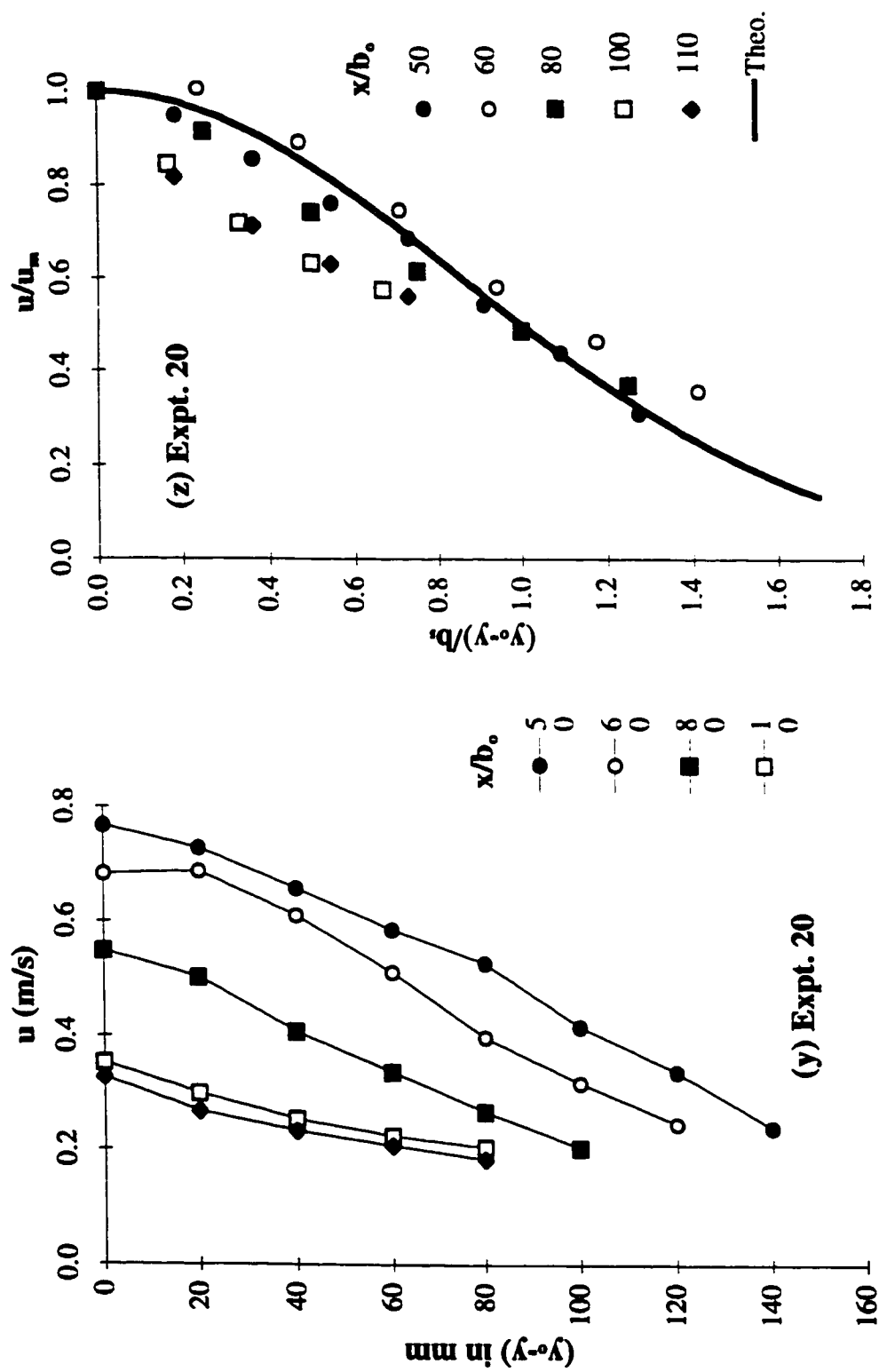


Fig. 4.24(y-z) Velocity distribution in surface jet (Expt. 20)
(y) Velocity profiles; and (z) Similarity profile

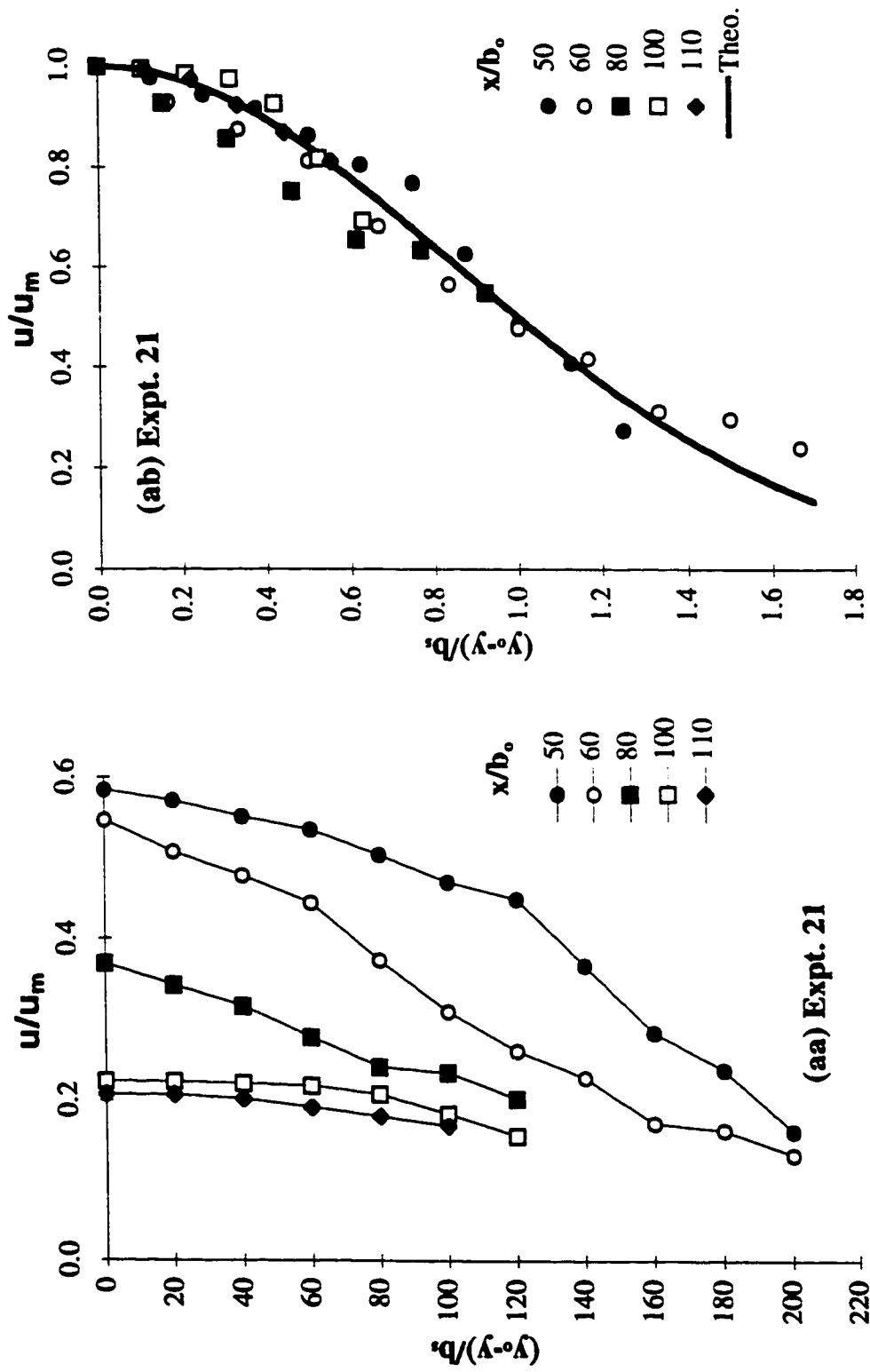


Fig. 4.24(aa-ab) Velocity distribution in surface jet (Expt. 21)
(aa) Velocity profiles; and (ab) Similarity profile

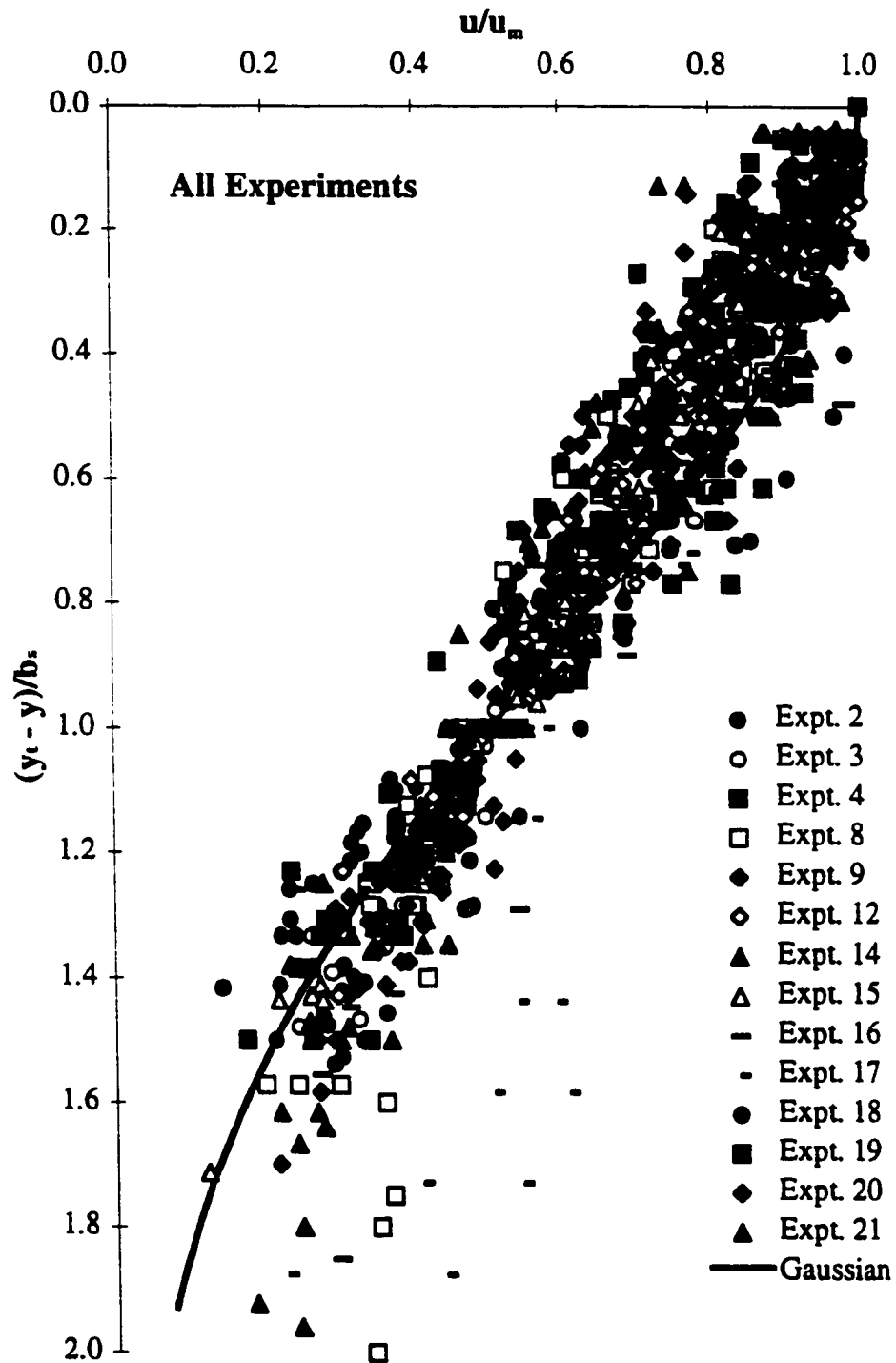


Fig. 4.25 Consolidated non-dimensional plot for the velocity distribution in the surface jet

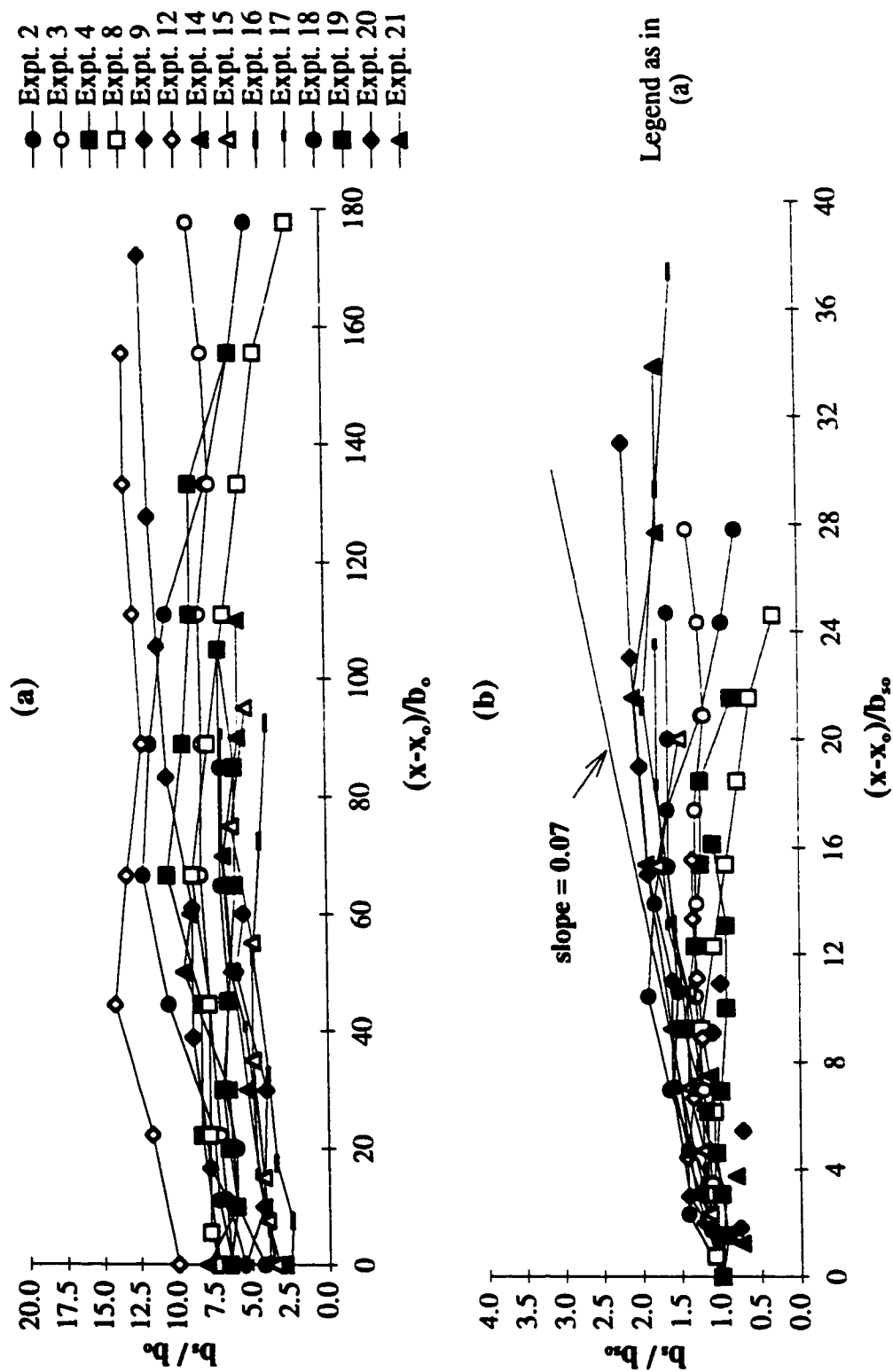


Fig. 4.26(a-b) Growth rate of the surface jet half-width: (a) b_o is the length scale; and (b) b_{so} is the length scale

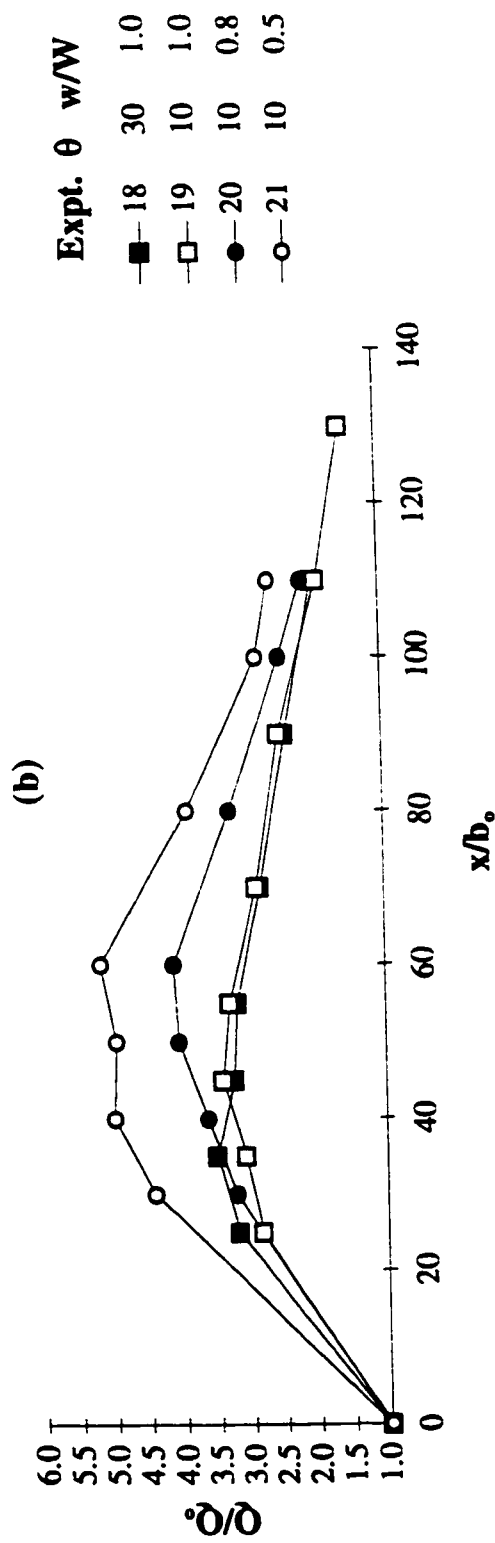
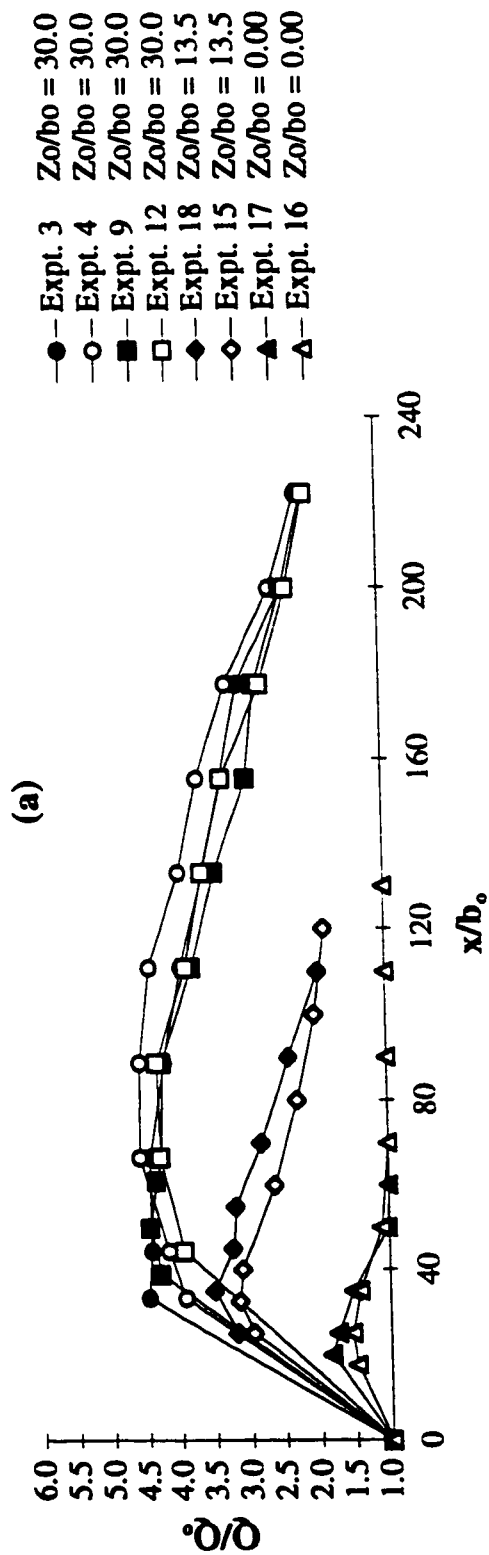


Fig. 4.27(a-b) Variation of the surface-jet discharge, Q/Q_0 , with distance, x/b_0 .
 (a) Effect of the offset ratio Z_0/b_0 ; & (b) Effect of the inclination angle θ and the width ratio w/W

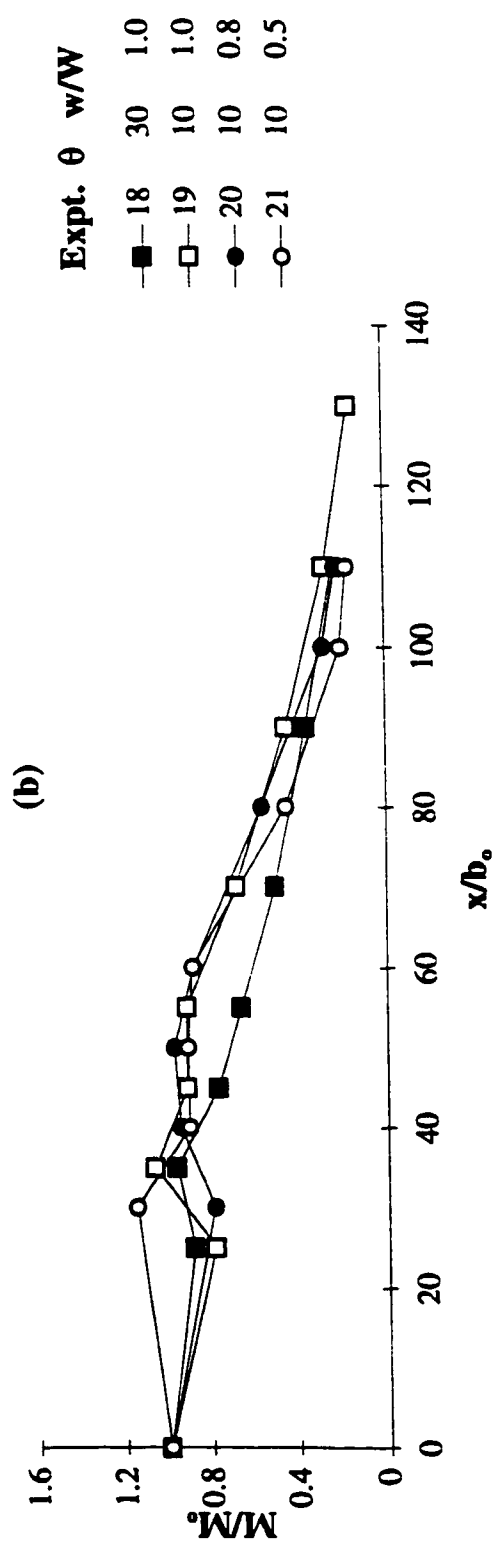
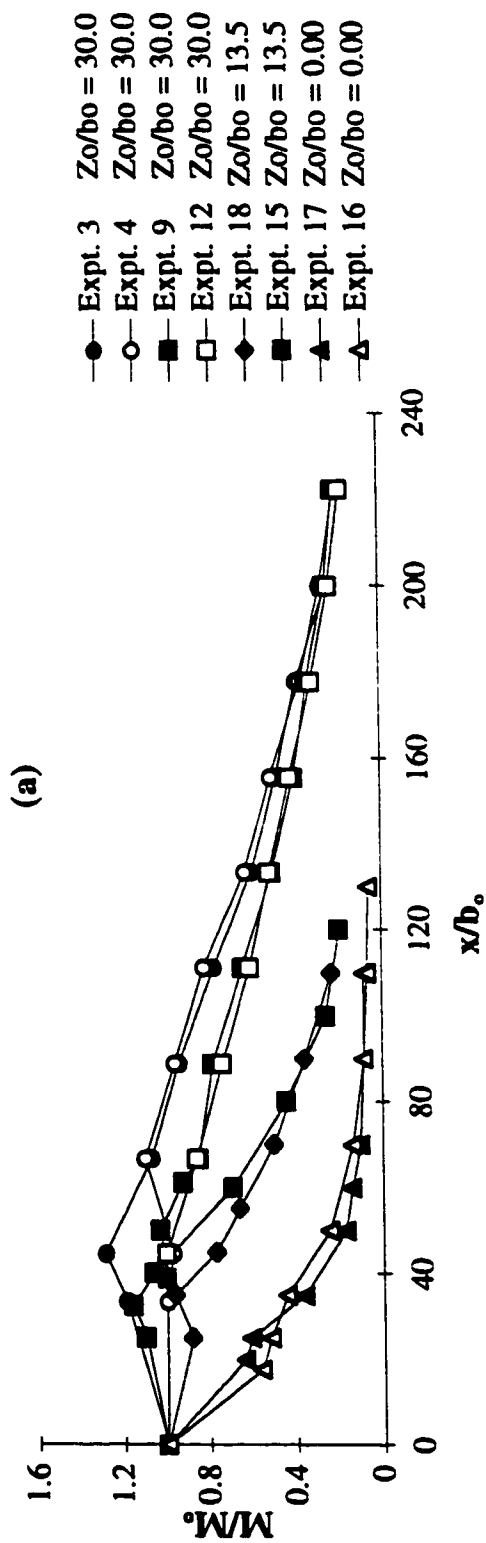


Fig. 4.28(a-b) Variation of the surface-jet momentum flux, M/M_o , with distance, x/b_o .
 (a) Effect of the offset ratio Z_o/b_o ; & (b) Effect of the inclination angle θ and the width ratio w/W

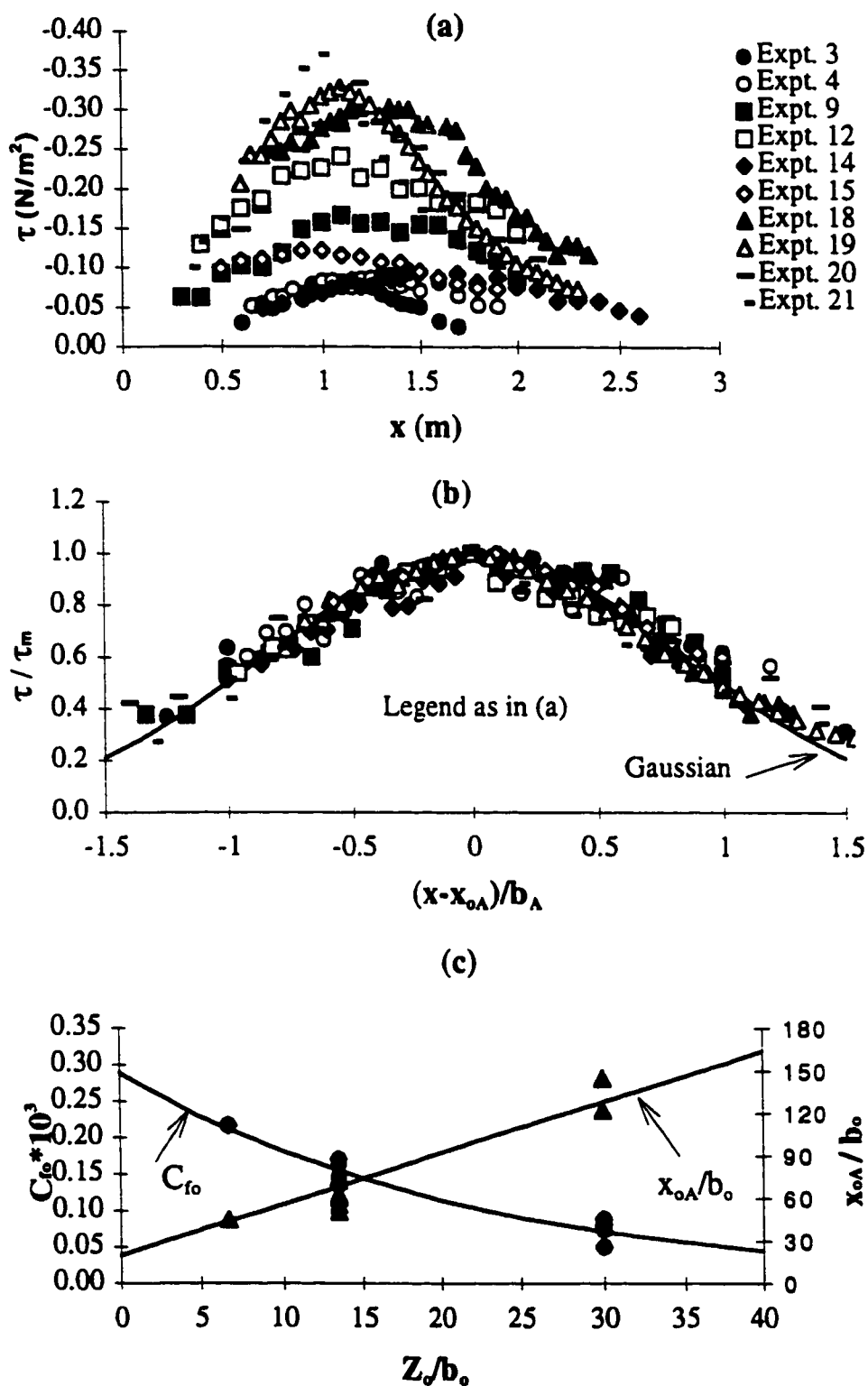


Fig. 4.29(a-c) Shear stress distribution for pattern A
(a) Variation of shear stress with distance; (b) Similarity profile; and (c) study of shear stress and length scales

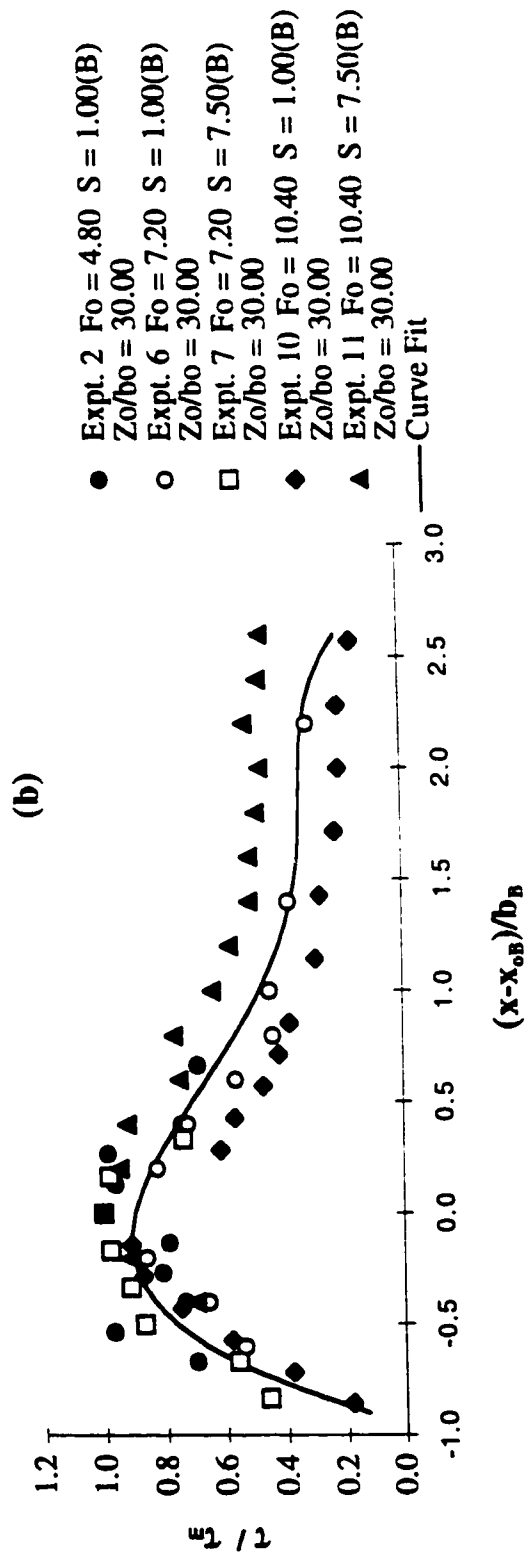
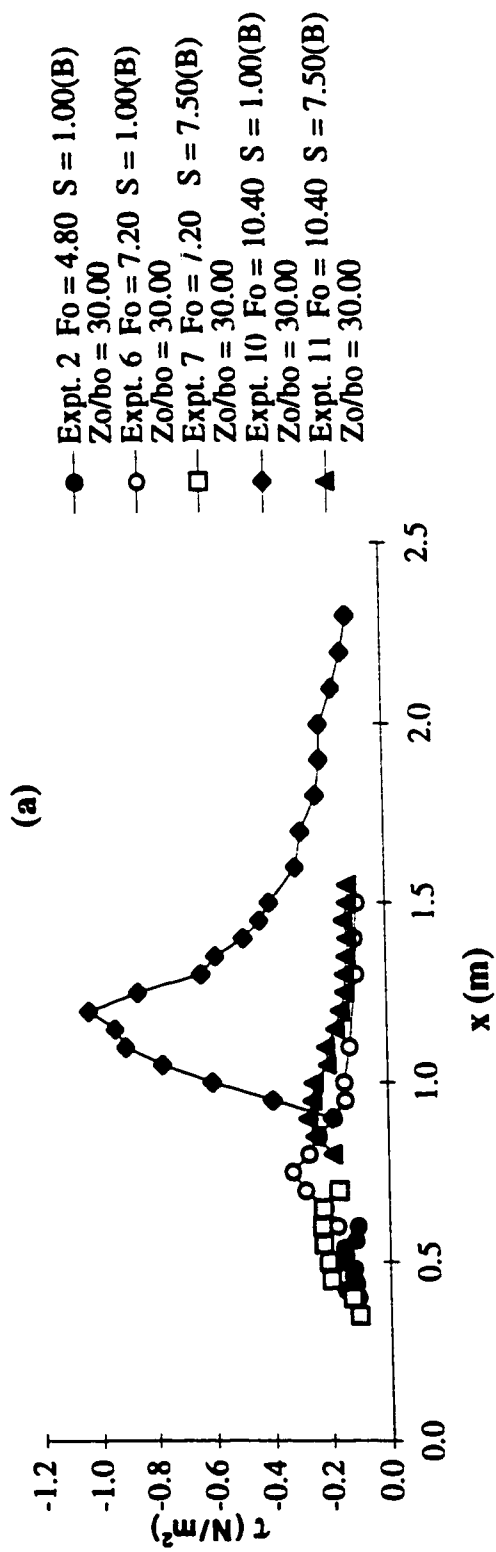
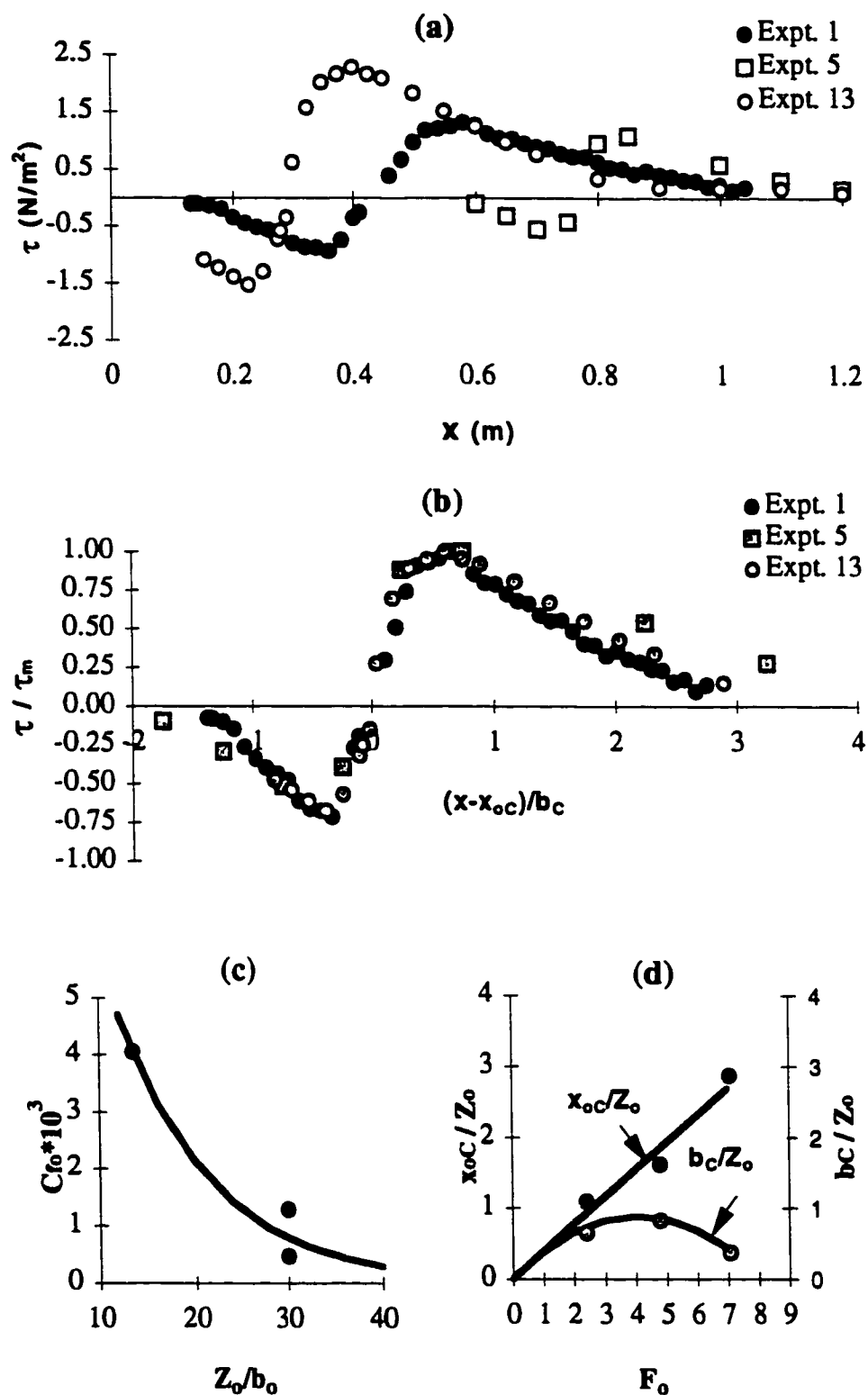


Fig. 4.30(a-b) Shear stress distribution for pattern B



**Fig. 4.31 (a-b) Shear stress distributions for Pattern C
(c-d) Study of shear stress and length scales for pattern C**

Chapter 5

Plane Turbulent Surface Jets in Shallow Tailwater*

5.1 Introduction

For turbulent jets discharged from slots or orifices in walls into large ambients at rest, it has been generally assumed (Albertson et al. (1950), Schlichting (1960), Rajaratnam (1976)) that the momentum flux would be preserved. In some experimental investigations (Miller and Comings (1957); Goldschmidt and Eskinazi (1966); Heskestad (1965) and Kotsovinos (1975)), it has been noticed that the momentum flux decayed to some extent at large distances from the origin of the jets. Kotsovinos (1978) mentioned that the momentum flux could decay to about 80% of that at the source at a longitudinal distance equal to $100 b_0$ for plane turbulent jets where b_0 is the slot width. Kotsovinos (1978) attributed this loss of momentum flux to the negative momentum carried by the entrained fluid which approached the jet at an angle of about $\pi/4$ radians from the forward direction of the jet. Based on an approximate integral analysis, Kotsovinos (1978) developed an equation to describe the variation of the momentum flux with the longitudinal distance from the nozzle producing the jet. Schneider (1985) attempted to explain this decay of momentum flux by combining the analysis of the jet with the flow in the region surrounding the jet. He coupled the jet and the induced outer flow through momentum and volume balances.

Swean Jr. et al. (1989) studied the variation of momentum and mass fluxes as well as the growth for plane turbulent surface jets with limited depth of tailwater. They conducted 10 experiments to study the effect of the finite depth of tailwater on the characteristics of the surface jet and to observe the variation of the momentum and

* The main content of this chapter has been submitted to the Journal of Hydraulic Engineering of the American Society of Civil Engineers for possible publication.

volume fluxes and the breakdown of the surface jet due to the limited depth of the ambient. They also used the experimental results of Vanvari and Chu (1974) and Rajaratnam and Humphries (1984). Their results showed a momentum decay and a break down (or variation from that of jets in infinite ambient) in the velocity and length scales due to the jet confinement. The study of Swean Jr. et al. (1989) provides a general understanding of the problem of surface jets with a finite depth of tailwater. However, their analysis did not consider the adverse pressure gradient in the momentum balance. As the depth of flow increases gradually in the longitudinal direction, it is important to include the excess pressure due to this increasing depth.

This chapter presents the results of a theoretical and an experimental study of turbulent surface jets with finite depth of tailwater. It was conducted to investigate the nature of the jet growth, the decay of the maximum velocity, the variation of the momentum and volume fluxes in the forward flow region of the surface jet, and the effect of the depth of tailwater on these properties. With the double-leaf gate energy dissipator introduced in chapter 4, the jet velocity and the momentum flux were found to decay dramatically. To understand the reasons behind this decay, it was important to study the behavior of turbulent jets of simpler geometry in shallow tailwater. In this chapter, the plane turbulent surface jet was chosen for this purpose. The plane turbulent surface jet issued from the opening with the inclination angle and the submergence ratio equal to zero. Hence, the plane turbulent surface jet, presented in this chapter, is considered to be a special case of the inclined turbulent jet presented in chapter 4.

5.2 Theoretical Considerations

Assume a plane turbulent surface jet of thickness b_0 with a flow rate per unit width of Q_0 and momentum flux per unit width of M_0 entering a rectangular channel horizontally at a height of Z_0 above the bed of the channel as shown in Fig. 5.1(a). Let U_0 be the velocity of the jet at the nozzle. The downstream control gate is adjusted so

that the depth of flow at the nozzle is equal to $(Z_o + b_o)$ and so that the surface jet enters the channel horizontally. My experimental observations (presented later) have shown that the water surface rises gradually as the distance x from the gate or nozzle increases, and that this increase is important for flows with finite depth of tailwater. Assume that δ_- is the maximum rise in the water surface elevation (see Fig. 5.1(a) and Fig. 5.2) and let δ_x be the corresponding rise at a section located at a longitudinal distance of x from the gate. The maximum value of δ_x would be δ_- which would occur at the section where the jet attaches to the bed. It appears that the longitudinal adverse pressure gradient is created to produce the return flow underneath the surface jet, for the jet entrainment.

Assuming hydrostatic pressure distributions on the wall containing the nozzle and at the downstream section where the expanding surface attaches to the bed, and that the velocity distribution at the nozzle and the downstream section is uniform (see Fig. 5.1(b)) and neglecting the integrated bed shear stress caused by the reverse flow, the continuity and the momentum equations could be written as

$$U_o b_o = V. (Z_o + b_o + \delta_-) \quad (5.1)$$

$$M_o - M_- = \gamma \delta_- (Z_o + b_o) + 0.5 \gamma \delta_-^2 \quad (5.2)$$

where V and M_- are respectively the uniform velocity and the momentum flux at the downstream section, and M_o is the momentum flux at the nozzle.

Multiplying Eq. 5.1 by $\rho U_o V$ and rearranging, Eq. 5.1 is rewritten as

$$\frac{M_-}{M_o} = \frac{1}{(1 + Z_o/b_o + \delta_-/b_o)} = \frac{1}{(1 + \eta) + \theta} \quad (5.3)$$

where η is the offset ratio equal to Z_o/b_o and $\theta = \delta_-/b_o$.

Dividing Eq. 5.2 by M_o and rearranging, Eq. 5.2 becomes

$$1 - \frac{M_-}{M_o} = \frac{2\theta(1+\eta) + \theta^2}{2F_o^2} \quad (5.4)$$

Solving equations 5.3 and 5.4, we obtain a cubic equation in θ as

$$\theta^3 + 3(1+\eta)\theta^2 + 2[(1+\eta)^2 - F_o^2]\theta - 2\eta F_o^2 = 0 \quad (5.5)$$

Eq. 5.5 has three real roots, one is positive and the other two are negative. Since the experiments showed positive values for δ_- (see Fig. 5.2), the positive root of Eq. 5.5 was only considered as the relevant physical solution. However, the negative roots (that represent a depression in the water elevation) may be relevant for other problems. The positive root of Eq. 5.5 can be written as

$$\theta = \frac{2}{\sqrt{3}} \sqrt{(1+\eta)^2 + 2F_o^2} \cos(\phi/3) - (1+\eta) \quad (5.6)$$

The negative roots of Eq. 5.5 are

$$\theta = \frac{-1}{\sqrt{3}} \sqrt{(1+\eta)^2 + 2F_o^2} \left[\cos(\phi/3) + \sqrt{3} \sin(\phi/3) \right] - (1+\eta) \quad (5.7)$$

and,

$$\theta = \frac{-1}{\sqrt{3}} \sqrt{(1+\eta)^2 + 2F_o^2} \left[\cos(\phi/3) - \sqrt{3} \sin(\phi/3) \right] - (1+\eta) \quad (5.8)$$

where ϕ is a function of η and the Froude number F_o at the nozzle equal to $[U_o/(gb_o)^{0.5}]$ and is described by the equation

$$\phi = \tan^{-1} \left(\sqrt{\frac{[(1+\eta)^2 + 2F_o^2]^3}{27F_o^4}} - 1 \right) \quad (5.9)$$

With the exception of relatively small values of η ($\eta < 10$ as shown in Fig. 5.3), ϕ is equal to $\pi/2$. Using this value of ϕ , Eq. 5.6 reduces to

$$\theta = \sqrt{(1+\eta)^2 + 2F_o^2} - (1+\eta) \quad (5.10)$$

Eq. 5.7 and Eq. 5.8 respectively reduce to

$$\theta = -\sqrt{(1+\eta)^2 + 2F_o^2} - (1+\eta) \quad (5.11)$$

$$\theta = -(1+\eta) \quad (5.12)$$

It was mentioned before that the positive root would only be considered as the relevant solution. Hence, to estimate θ for the different values of η and F_o , Eq. 5.10 was considered as the solution of Eq. 5.5.

Further, M_{∞} can be evaluated by combining Eq. 5.3 and 5.10 as

$$\frac{M_{\infty}}{M_o} = \left((1 + \eta)^2 + 2F_o^2 \right)^{-1/2} \quad (5.13)$$

It is interesting to note that substituting in Eq. 5.5 with $\eta = 0$, (the supercritical jet is on the bed), results in a quadratic equation. Solving this quadratic equation

$$\theta = 0.5 \left(\sqrt{1 + 8F_o^2} - 3 \right) \quad (5.14)$$

which is closely related to the well-known Belanger equation. Eq. 5.5 could be simplified if the second term on the right hand side of Eq. 5.2 is neglected. For this assumption to be valid, δ_{∞} should be small compared to $(Z_o + b_o)$. With this simplification, Eq. 5.5 reduces to

$$(1 + \eta)\theta^2 + \left[(1 + \eta)^2 - F_o^2 \right] \theta - \eta F_o^2 = 0 \quad (5.15)$$

The positive root for this equation is

$$\theta = \frac{+\sqrt{\left[(1 + \eta)^2 - F_o^2 \right]^2 + 4\eta(1 + \eta)F_o^2} - \left[(1 + \eta)^2 - F_o^2 \right]}{2(1 + \eta)} \quad (5.16)$$

Using Eq. 5.3 with Eq. 5.16, the momentum flux M_{∞} becomes

$$\frac{M_{\infty}}{M_o} = \frac{1}{(1+\eta)+\theta} = \frac{-\sqrt{[(1+\eta)^2 - F_o^2]^2 + 4\eta(1+\eta)F_o^2} + [(1+\eta)^2 + F_o^2]}{2F_o^2} \quad (5.17)$$

Let $F_{p\infty}$ be the maximum excess in the hydrostatic pressure force at the downstream section caused by the maximum increase of the depth of δ_{∞} in the water surface elevation. Assuming that the decrease in the momentum flux is only due to $F_{p\infty}$, it can be shown that

$$\frac{F_{p\infty}}{M_o} = 1 - \frac{M_{\infty}}{M_o} = \frac{0.5\theta^2 + \theta(1+\eta)}{F_o^2} \quad (5.18)$$

Equation (5.10) was solved along with equation (5.18) to evaluate $F_{p\infty}$. Again, by neglecting the term $(0.5\gamma\delta_{\infty}^2)$ in equation (5.2), a simpler relation for $F_{p\infty}$ could be obtained as follows

$$\frac{F_{p\infty}}{M_o} = 1 - \frac{M_{\infty}}{M_o} = \frac{\theta(1+\eta)}{F_o^2} = \frac{\sqrt{[(1+\eta)^2 - F_o^2]^2 + 4\eta(1+\eta)F_o^2} - [(1+\eta)^2 - F_o^2]}{2F_o^2} \quad (5.19)$$

Based on these theoretical formulations, the variation of θ , which is equal to the maximum rise in the water surface elevation in terms of the slot width, with the offset ratio η , is shown in Fig. 5.4 as solutions of Eq. 5.10 and 5.16, with and without considering the term $(0.5\gamma\delta_{\infty}^2)$, respectively. Fig. 5.4 shows the variation for the jet Froude number F_o from 1.6 to 7.2 and it may be observed that both equations give almost the same value for θ if the offset ratio exceeds a certain value. This value of η

was found to increase with the Froude number and is equal to 20 for $F_o = 7.2$ and falls to about 5 for $F_o = 1.6$. For any given Froude number, θ decreases as the offset ratio increases. For the offset ratio equal to 100, θ decreases from about 0.5 for $F_o = 7.2$ to almost zero for $F_o = 1.6$.

Eq. 5.13 and Eq. 5.17 were plotted in Fig. 5.5 to show the variation of the dimensionless momentum flux with the offset ratio η for the different Froude numbers. Fig. 5.5 shows that both equations exhibit the same momentum decay for offset ratios equal to or greater than 25. Further, F_o appears to have no effect on the momentum decay for η greater than about 25. Fig 5.4 also shows that the momentum flux in terms of that at the nozzle, is equal to 0.040, 0.020, 0.013 and 0.010 respectively for η equal to 25, 50, 75 and 100. Eq. 5.18 is plotted in Fig. 5.6 to show the variation of $F_{p\infty}/M_o$ with η . For the offset ratio equal to 25, 50, 75 and 100, $F_{p\infty}/M_o$ is equal to 0.960, 0.980, 0.987 and 0.990 respectively.

5.3 Dimensional Analysis

Considering the problem illustrated in Fig. 5.1(a), any property (m) of the flow can be expressed as a function of various parameters of the flow, fluid and channel dimensions as

$$m = f(U_o, g, b_o, Z_o, \rho, \mu) \quad (5.20)$$

The above relation can be represented in a dimensionless form as follows

$$M = f\left[\frac{U_o}{\sqrt{gb_o}}, \frac{\rho U_o b_o}{\mu}, \frac{Z_o}{b_o}\right] \quad (5.21)$$

The above relation shows that any property of the flow can be expressed as a function of the Froude number, the Reynolds number and the offset ratio. For large values of the Reynolds number, $R = \rho U_o b_o / \mu$, where ρ and μ are, respectively, the mass density and viscosity of the fluid, viscosity is known to have negligible effects. Hence, Eq. 5.21 becomes

$$M = f'' [F_o, \eta] \quad (5.22)$$

Eq. 5.22 shows that the main variables affecting the different characteristics of the flow are the Froude number and the offset ratio.

5.4 Experimental Study

5.4.1 Experimental arrangement

Surface jets were produced in a flume, 0.446 m wide, 0.60 m deep and 7.6 m long, with aluminum bottom and Plexiglas sides (see Fig. 5.7). Two pumps were used to supply the head-tank feeding the flume. The discharge was measured by a magnetic flow-meter located in the supply line. Water entered the flume through an opening between two aluminum gates, provided with streamlined entrances thereby producing an uniform jet with a thickness of b_o (see Fig. 5.8). A tailgate was used to control the tailwater depth in the flume. In all the experiments the tailgate was adjusted so that the jet issued from the slot horizontally. False floors of different heights were used to produce the required offset distance Z_o (see Fig. 5.9).

A Prandtl tube with an external diameter of 3.0 mm was used to measure the time-averaged longitudinal velocity u (see Fig. 5.8 & Fig. 5.10). Velocity distributions of the forward and backward flows were measured along vertical sections at different longitudinal distances from the nozzle producing the jet. Velocity measurements were

also made, when needed, downstream of the line of the jet attachment to the bed. All the measurements were taken in the middle third of the flume.

One transducer (Validyne model DP45-16 Northridge, Calif) was used in the experiments to measure the pressure difference indicated by the Prandtl tube. The output of the transducer was connected to a Macintosh IIfx computer. When the pressure difference was outside the transducer range (± 25.4 mm), the pressure connections were switched to a manometer board (see Fig. 5.10). The computer displayed the results on a strip chart on the screen in real time. When the required number of samples (usually 5000) were recorded at each point with a sampling rate of 40 samples/s, the computer processed all the samples to obtain the mean value and the standard deviation for each variable and saved the results in an open file. The computer programs used in the experiments were written in LabView Language.

5.4.2 Experiments

A total of 9 experiments were conducted and the primary details of these experiments are shown in Table 5.1. The values of the various parameters (b_o , Z_o , U_o) were selected to achieve a wide range of the offset ratio and the Froude number. Seven offset ratios of 5, 10, 20, 25, 30, 50 and 100 were used. Experiments were conducted for Froude numbers equal to 1.60, 2.40, 2.90, 4.00, 4.80, 6.00 and 7.20. The Reynolds number of the jet was in the range of 5000 to 43000. Fig. 5.11(a-d) show the surface jets produced with the offset ratio equal to 100, 50, 25 and 10 respectively.

5.5 Experimental Results and Analysis

5.5.1 Eddy length

As soon as the jet issues from the slot, a recirculating flow region starts to develop between the jet and the flume bed (see Fig. 1(b)). The normalized eddy length L_e/b_o was equal to 50, 80, 140, 160, 200, 320 and 640 for offset ratios Z_o/b_o equal to

5, 10, 20, 25, 30, 50, 100 respectively. The eddy lengths were predicted either from the typical velocity profiles shown in Fig. 5.12 or by using dye injection. Dye injection was used where velocity measurements could not be taken near the bed as in experiments 2, 4 and 6.

If L_e is the length of the recirculating region (or the eddy length), it could be written that

$$L_e = f[U_o, b_o, \rho, \mu, Z_o] \quad (5.23)$$

Using the π theorem, it can be shown that

$$\frac{L_e}{b_o} = f\left[\frac{Z_o}{b_o}, \frac{\rho U_o b_o}{\mu}\right] \quad (5.24)$$

For large values of the Reynolds number, viscous effects may be neglected and Eq. 5.24 reduces to

$$\frac{L_e}{b_o} = f''\left[\frac{Z_o}{b_o}\right] \quad (5.25)$$

The experimental results are shown plotted in Fig. 5.13 with L_e/b_o versus Z_o/b_o . Fig. 5.13 shows a linear relationship between the eddy length L_e and the offset distance Z_o . The best-fit linear equation shows that L_e is 6.50 times Z_o . Rajaratnam (1969) found this constant to be about 7.50.

5.5.2 Velocity profiles

Time-averaged velocity profiles were obtained for the whole flow field including the surface jet and the recirculating flow regions for several experiments. Fig. 5.12(a-i) show velocity profiles for Expt. 1 to Expt. 9 respectively and the details of these experiments are included in table 5.1. These observations were taken for seven Froude numbers ($F_o = 1.60, 2.40, 2.90, 4.00, 4.80, 6.00$ and 7.20 and seven offset ratios ($Z_o/b_o = 5, 10, 20, 25, 30, 50$ and 100). These figures show the velocity profiles for the surface jet as well as the reverse flow. Intensive velocity measurements were taken especially in the surface jet zone for the precise calculation of the volume and the momentum fluxes. In the surface jet, the maximum velocity is located at, or very close to the free surface and the velocity distribution seems to be linear. The velocity distribution of the return flow is almost uniform except near the bed and at the jet edges. Velocity measurements could not be obtained in the strong shear layer separating the forward and the backward flows because the flow within this layer was very turbulent. In this layer the velocity fluctuations were larger than the local mean velocity. Hence, mean velocities within this layer were predicted by linear interpolation.

5.5.3 Reverse flow

It is believed that the reverse flow underneath the surface jet is driven by the adverse pressure gradient (see Fig. 5.2). This reverse flow is the source of the entrained fluid required for the expansion of the surface jet. It may be observed from Fig. 5.12(a-i) that the mean velocity in the reverse flow below the surface jet is almost uniform except near the bed and at the jet edges. Fig. 5.14(a) shows the variation of the depth-averaged reverse-velocity in terms of the velocity at the opening u_r/U_o with the dimensionless longitudinal distance from the opening x/b_o for the different Froude numbers and offset ratios. Experiments 2, 3 and 4 were conducted for the same offset ratio and for three different Froude numbers ($2.40, 4.80$ and 7.20 respectively). The

variation of the reverse-velocity was almost identical in the three experiments indicating that the dimensionless reverse velocity does not depend on the Froude number. The observations shown in Fig. 5.14(a) indicate that this variation depends only on the offset ratio. The maximum value of the reverse-velocity, u_{rm} , decreases as the offset ratio increases as shown in Fig. 5.14(b) and is described by the equation

$$\left(\frac{u_{rm}}{U_o}\right) = 11 * 10^{-4} \left[\left(\frac{Z_o}{b_o}\right) - 175 \right] \quad (r^2 = 0.95) \quad (5.26)$$

If x_{rm} is the value of x where u_{rm} occurs, x_{rm}/b_o was found to increase with the offset ratio as shown in Fig. 5.14(c) and this variation is described by the equation

$$\left(\frac{x_{rm}}{b_o}\right) = 2.65 \left[\left(\frac{Z_o}{b_o}\right) + 7.65 \right] \quad (r^2 = 0.99) \quad (5.27)$$

These equations show that for offset ratios equal to 5 and 100, the normalized maximum reverse velocity is 0.19 and 0.08, respectively, and the normalized locations of these values are about 33.50 and 285.25, respectively.

5.5.4 Surface jet

The velocity measurements in the surface-jet zone shows that the maximum velocity u_m occurs at or very near the free surface. To test for the similarity of the forward-flow velocity distributions, the maximum velocity, u_m , at any station was chosen as the velocity scale. The length scale, b , is the distance between the point of u_m and that of $0.5u_m$. Fig. 5.15(a-b) show the velocity distributions and the similarity profiles in the partially-developed flow region. In this figure, u/u_m was plotted against

$(y_o - y)/b$ where y_o is the depth of flow at any station and y is the height, above the flume bed, of the point under consideration. This plot represents a station located approximately in the middle of the developing region (at $x/b_o = 6$). Within the potential core, the flow is uniform whereas outside the potential core the distribution of the velocity is almost linear.

The velocity distributions and the similarity profiles in the fully-developed flow region ($x/b_o \geq 12$) are shown in Fig. 5.16(a-r). These figures represent Expt. 1 to Expt. 9 respectively. The plots shown in each figure are for different longitudinal distances from the slot. Fig. 5.17 shows a consolidated non-dimensional plot of all the experiments. A study of these profiles established that the velocity distributions are similar. The similarity profile is almost linear. This linear velocity distribution has been observed earlier by Wu and Rajaratnam (1995) and can also be observed in the results of Swean Jr et al. (1989). There is some scatter in the data near the bottom of the forward flow region and this could be due to the interaction with the backward flow and the resulting turbulence.

5.5.5 Velocity and length scales

Having found that the velocity profiles in the forward flow are similar, it is necessary to study the variation of the velocity scale, u_m , and the length scale, b , with the distance x . Fig. 5.18(a) shows the decay of the maximum velocity with the longitudinal distance from the nozzle. The maximum velocity at the nozzle was varied from 0.5 to 2.25 m/s and u_m was measured for x up to about 3.20 m. At the last section, the maximum velocity was in the range of 0.04-0.35 m/s. Fig. 5.18(b) shows the decay of the maximum velocity u_m at any section in terms of the velocity of the jet at the nozzle U_o with the normalized distance from the gate x/b_o . The decay of the maximum velocity shows the existence of two stages. The first stage represents the plane surface jet with large depth of tailwater and starts at the end of the development

region. The decay of the normalized velocity scale in this region can be described by the following equation

$$\frac{u_m}{U_o} = \frac{4.20}{\sqrt{x/b_o}} \quad (5.28)$$

The second stage of the velocity decay starts at a distance x_o from the gate, where the observations begin to deviate from the curve describing Eq. 5.28 and the maximum velocity decays more rapidly. This behavior can be noticed more easily in Fig. 5.18(c) which shows the variation of $(U_o/u_m)^2$ with x/b_o where Eq. 5.28 would plot as a straight line. The decay of the maximum velocity in this stage can be described by the following quadratic equation

$$\frac{u_m}{U_o} = A \left(\frac{x}{b_o} \right)^2 + B \left(\frac{x}{b_o} \right) + C \quad (5.29)$$

where the coefficients A, B are C are functions of the offset ratio, Z_o/b_o as

$$A = 0.006 \left(\frac{Z_o}{b_o} \right)^{-1.94} \quad (r^2 = 0.95) \quad (5.30)$$

$$B = -0.258 \left(\frac{Z_o}{b_o} \right)^{-1.14} \quad (r^2 = 0.95) \quad (5.31)$$

$$C = 2.964 \left(\frac{Z_o}{b_o} \right)^{-0.37} \quad (r^2 = 0.86) \quad (5.32)$$

The value of x_o , was also found to be a function of the offset ratio (see Fig. 5.18(d)) and is described by the equation

$$\left(\frac{x_o}{b_o}\right) = -0.02\left(\frac{Z_o}{b_o}\right)^2 + 4.00\left(\frac{Z_o}{b_o}\right) + 6.25 \quad (r^2 = 0.99) \quad (5.33)$$

These considerations show that as the tailwater depth decreases, the length of the first stage of decay decreases and the maximum-velocity decay will be more rapid. It was also found that the Froude number does not have any significant effect on the velocity decay.

A breakdown in the growth of the length scale, b , occurred in all the 9 experiments, as shown in Fig. 5.19. The location of this breakdown, where the rate of growth begins to deviate from the linear growth rate of surface jets on deep tailwater, was very close to the location where the corresponding breakdown occurred in the velocity scale variation and can also be described by Eq. 5.33. The original growth rate of the jet half-width was 0.065 which is somewhat smaller than the value of 0.070 found by Rajaratnam and Humphries (1984). After the breakdown, the jet half-width grew at a rate which varied from 0.007 to 0.033.

5.5.6 Surface-jet discharge

For every experiment, at each section where velocity observations were made, the forward flow rate Q and the momentum flux M per unit width were calculated as the sum of the fluxes through thin strips (whose thickness varied from 2.5 to 20 mm). If the upper and the lower ordinates of a single strip are u_1 and u_2 respectively, the discharge and the momentum fluxes per unit width through this strip were calculated using the following relations

$$Q_s = \frac{1}{2}(u_1 + u_2).h_s \quad (5.34)$$

$$M_s = \left[\frac{1}{3}(u_1 - u_2)^2 + u_1 u_2 \right].h_s \quad (5.35)$$

where Q_s , M_s and h_s are the discharge, the momentum and the height of the strip respectively.

Fig. 5.20(a) shows the variation of the relative discharge Q/Q_o in the surface jet with distance x/b_o and a number of interesting observations could be made from a study of Fig. 5.20(a). Firstly, the relative discharge increases with the relative distance at the same rate as that of the surface jet with large tailwater up to a certain section and then deviates from it, to reach eventually the value of one. Secondly, the maximum value of the relative discharge decreases from about 4 for $Z_o/b_o = 100$ to 1.5 for $Z_o/b_o = 5$. If x_{Qm} , is the longitudinal distance where the relative discharge reaches the maximum value, x_{Qm}/b_o decreases from about 200 for $Z_o/b_o = 100$ to about 20 for $Z_o/b_o = 5$. The variation of Q/Q_o with x/b_o is not dependent on the Froude number and could be represented by a cubic equation of the form

$$\frac{Q}{Q_o} = A' \left(\frac{x}{b_o} \right)^3 + B' \left(\frac{x}{b_o} \right)^2 + C' \left(\frac{x}{b_o} \right) + 1 \quad (5.36)$$

where the coefficients A' , B' and C' are functions of the offset ratio, Z_o/b_o as follows

$$A' = 0.0003 \left(\frac{Z_o}{b_o} \right)^{-1.85} \quad (r^2 = 0.98) \quad (5.37)$$

$$B' = -0.009 \left(\frac{Z_o}{b_o} \right)^{-1.00} \quad (r^2 = 0.99) \quad (5.38)$$

$$C' = 0.07 \left(\frac{Z_o}{b_o} \right)^{-0.18} \quad (r^2 = 0.95) \quad (5.39)$$

For a surface jet with very large value of Z_o/b_o , the variation of Q/Q_o with x/b_o should be independent of the offset ratio and for such a jet, $Q/Q_o = \text{constant} \cdot (x/b_o)^{0.50}$. This equation is shown plotted in Fig. 5.20(a) with the value of the constant chosen as 0.35.

Fig. 5.20(b-c) show the variation of the maximum value of the relative flow Q_m/Q_o and the distance where this occurs x_{Q_m}/b_o with the offset ratio Z_o/b_o and these variations could be described by the equations

$$\frac{Q_m}{Q_o} = -3.4 * 10^{-4} \left(\frac{Z_o}{b_o} \right)^2 + 0.064 \left(\frac{Z_o}{b_o} \right) + 1.00 \quad (r^2 = 0.97) \quad (5.40)$$

$$\frac{x_{Q_m}}{b_o} = -9.2 * 10^{-3} \left(\frac{Z_o}{b_o} \right)^2 + 2.914 \left(\frac{Z_o}{b_o} \right) \quad (r^2 = 0.99) \quad (5.41)$$

5.5.7 Surface-jet momentum flux

It was mentioned earlier that the surface jet loses a substantial portion of the momentum flux as it travels downstream when the depth of tailwater is relatively shallow. Fig. 5.21 shows the variation of the normalized momentum flux of the surface jet with the normalized distance from the nozzle for different offset ratios. A relatively simple function was found to describe this variation and is written as

$$\frac{M}{M_o} = \cos \left[\left(\frac{\pi}{\epsilon} \right) \cdot \left(\frac{x}{b_o} \right) \right] \quad (5.42)$$

where ϵ is a function of the offset ratio and is given by the equation

$$\epsilon = 8.80 \left(\frac{Z_o}{b_o} + 13.40 \right) \quad (r^2 = 0.98) \quad (5.43)$$

It can be seen also from Fig. 5.21 that the Froude number has no effect on the momentum-distribution profiles. It should be remembered that the great percentage of the momentum that is lost is converted into pressure in the form of a water depth increase. Fig. 5.21 shows that the losses in the normalized momentum flux are 0.95, 0.94, 0.97, 0.95 and 0.92 for the offset ratios equal to 100, 50, 30, 20 and 10 respectively. As these measurements were taken at or downstream of the point of the jet reattachment to the bed, these values of the normalized momentum flux should be comparable to the corresponding theoretical values shown in Fig. 5.5 which are 0.99, 0.98, 0.97, 0.95 and 0.92 respectively. It is interesting to see the agreement between the predicted and the measured values.

5.6 Engineering Significance

Based on the results presented in this chapter, plane turbulent surface jets in shallow tailwater may be recommended to be used, in practice, as energy dissipators. One application of the new dissipators is to be used in flow regulators. In a flow regulator, a sluice gate is usually used where a supercritical jet issues under the gate, tangential to the channel bed. To minimize downstream scour, a long concrete apron is required. Also, baffle blocks (or walls) may be needed for a higher efficiency of the basin. In deeply submerged flow regulators, the flow discharge is mainly dependent on

the head difference between the upstream water level and the downstream tailwater. The location of the opening does not have any significant effect on the flow discharge. In this case, a double-leaf gate can be used with the supercritical jet issuing in-between the two gates, as a surface jet (see Fig. 5.22). The lower gate is adjusted to Z_0 above the downstream bed level while the upper gate is moved up or down till the required opening/discharge is reached. In the new arrangement, the turbulent jet is lifted away from the stream bed to the water surface. According to the theoretical and experimental analyses discussed earlier, when the jet attaches to the channel bed, a great portion of the momentum flux is already lost and a uniform velocity is attained. Between the gate and the attachment section, the channel bed is only affected by the reverse flow which is relatively weak and lining the channel bed, in this recirculating zone, with relatively coarse material might be enough to prevent any sediment motion. If a suitable sheet pile wall is installed below the gate for percolation requirements, only a very short concrete seat is required. Also, splitting the vertical gate into two portions will be of benefit in decreasing the capacity, weight and size of the overhead gate control structure as it is required to control either the upper or the lower gate at a time instead of controlling a complete sluice gate. In conclusion, the new basin is simple, short, efficient and economic and is recommended for deeply submerged flow regulators to replace existing basins.

This model may also be used in spillways with relatively shallow tailwater (see Fig. 5.23). The concrete apron of the spillway will be Z_0 above the channel bed. This model may be applied on a small scale first and the results should be compared with those of a similar basin (like the submerged bucket basin) before being generally used.

In the above applications, given the thickness of the opening in the flow regulator (or the anticipated thickness of the supercritical stream at the toe of the spillway), the supercritical Froude number and the tailwater depth in the downstream

channel, Z_o and δ_o can be easily calculated for design purposes (using Eq. 5.6 or Eq. 5.16 with the relation $y_t = Z_o + b_o + \delta_o$).

5.7 Conclusions

For turbulent surface jets in shallow tailwater, it has been shown theoretically and experimentally that the momentum flux is not preserved. In the theoretical study, the momentum loss and the piezometric-pressure increase were evaluated at a section just downstream of the line of the jet attachment to the bed. The experimental results showed that the length of the return-flow region is about 6.50 times the offset distance. The velocity profiles in the surface jet were found to be similar, in the developing as well as in the developed regions. Two stages were seen to exist in the decay of the maximum velocity. The rate of the velocity decay in the first stage was independent of the relative depth of the tailwater whereas the faster rate in the second stage depended on it. The length of the first stage of velocity decay was directly proportional to the offset ratio. The length scale of the jet grew at a rate of 0.065 in the early stage and the rate of growth was much smaller in the second stage. The volume flux in the surface jet with limited tailwater was affected significantly. The decay of the momentum flux in the surface jet with the distance from the nozzle was observed and correlated with the offset ratio and the relative longitudinal distance. On the whole, the results from this study highlight the effect of limited tailwater depth on the behavior of plane turbulent surface jets. Based on the momentum and velocity decay results, surface jets in shallow tailwater may be recommended to be used as energy dissipators. Two applications were discussed, flow regulators and spillways.

5.8 References

- Albertson, M. L., Dai. Y. B., Jensen, R. A. & Rouse, H. (1950). "Diffusion of submerged jets." Trans. ASCE. 115, 639-664.
- Goldschmidt, V., and Eskinazi, S. (1966). "Two phase turbulent flow in a plane jet." Trans. ASME, Series E, J. Appl. Mech., 33(4), 735-747.
- Heskestad, G. (1965). "Hot wire measurements in a plane turbulent jet." Trans. ASME, Series E, J. Appl. Mech., 32(4), 721-734.
- Kotsovinos, N. E. (1975). "A study of the entrainment and turbulence in a plane turbulent jet." W. M. Keck Lab. Hydr. Water Resources, Calif. Inst. Tech. Rept. KH R-32.
- Kotsovinos, N. E. (1978). "A note on the conservation of the axial momentum of a turbulent jet." J. Fluid Mech., 87(7), pp. 55-63.
- Miller, D. R., and Comings, E. W. (1957). "Static pressure distribution in the free turbulent jet." J. Fluid Mech., 3(10), pp. 1-16.
- Rajaratnam, N. (1969). "Diffusion of a supercritical stream on a stagnant pool." Trans. Engr. Inst. of Canada, 12(A-1), 1-5.
- Rajaratnam, N. (1976). "Turbulent Jets." Elsevier Publishing Co, The Netherlands, 304p.
- Rajaratnam, N., and Humphries, J. A. (1984). "Turbulent non-buoyant surface jet." J. Hydr. Res., 22(2), pp. 103-115.
- Schlichting, H. (1960). "Boundary layer theory." 4th Edn. McGraw-Hill: New York.
- Schneider, W. (1985). "Decay of momentum flux in submerged jets." J. Fluid Mech., 154(5), pp. 91-110.
- Swean Jr, T. F., Ramberg, S. E., Plesniak, M. W. Stewart., M. B. (1989). "Turbulent surface jet in channel of limited depth." J. Hydr. Engrg., ASCE, 115(12), pp. 1587-1606.

- Vanvari, M. R., and Chu, V. H. (1974). "Two-dimensional turbulent surface jets of low Richardson number." Tech. Report No. 74-2 [FML], Fluid Mech. Lab., Dept. of Civ. Engrg. and Appl. Mech., McGill Univ., Montreal, Canada.
- Wu, S. and Rajaratnam, N. (1995). "Effect of baffles on submerged flows" J. Hydr. Engrg., ASCE, 121(9), pp. 644-652.

Table 5.1 Primary details of experiments

Exp.	b_o (mm)	Z_o (mm)	y_z (mm)	W (mm)	U_o (m/s)	F_o	Z_o/b_o	$(y_z-Z_o)/b_o$	R
(1)	(2)	(3)	(4)	(5)	(6)	(7)	(8)	(9)	(10)
1	5	500	505	446	1.60	7.2	100	1.00	8000
2	10	500	510	446	0.75	2.4	50	1.00	7500
3	10	500	510	446	1.50	4.8	50	1.00	15000
4	10	500	510	446	2.25	7.2	50	1.00	22500
5	10	300	310	446	1.88	6.0	30	1.00	18800
6	20	500	520	446	2.13	4.8	25	1.00	42600
7	10	200	210	446	0.90	2.9	20	1.00	9000
8	10	100	110	446	1.25	4.0	10	1.00	12500
9	10	50	60	446	0.50	1.6	5	1.00	5000

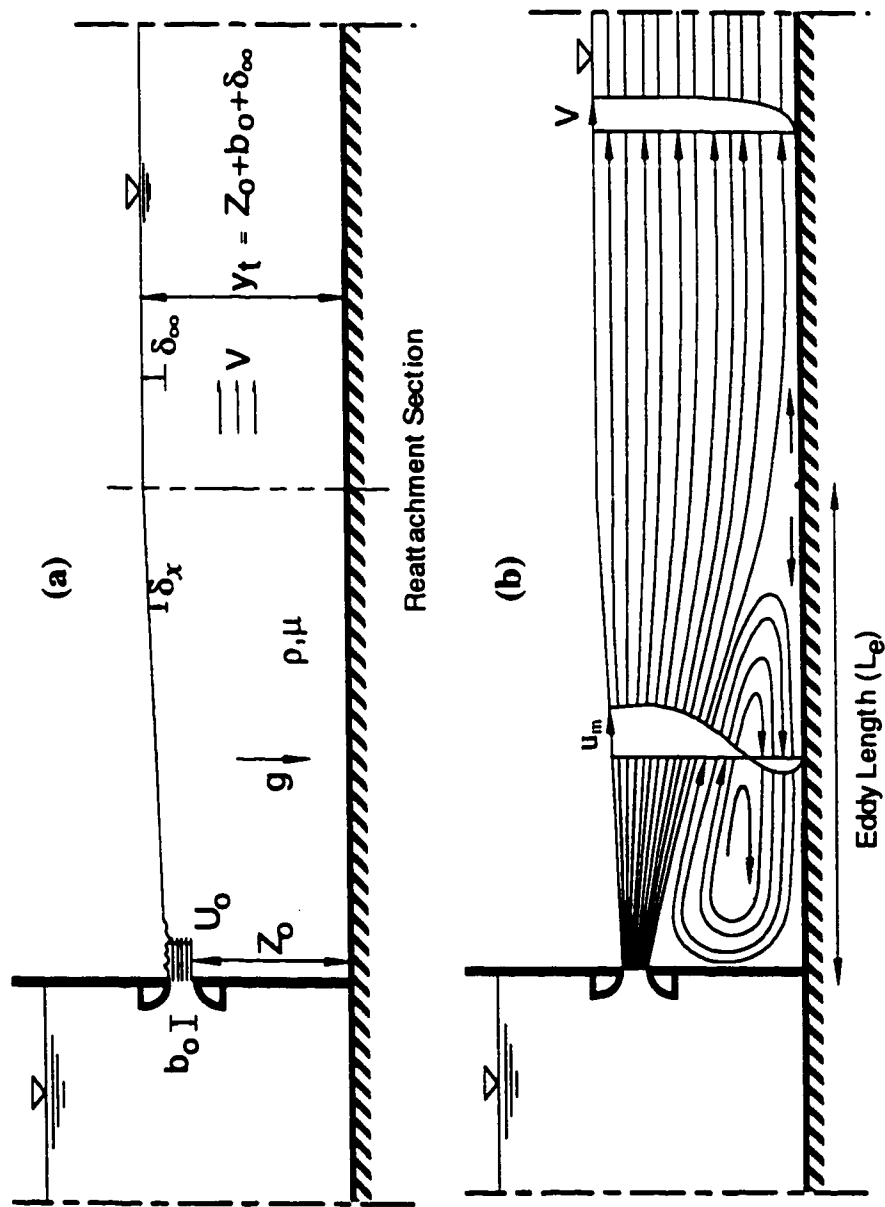


Fig. 5.1 (a) Definition sketch; (b) Flow pattern

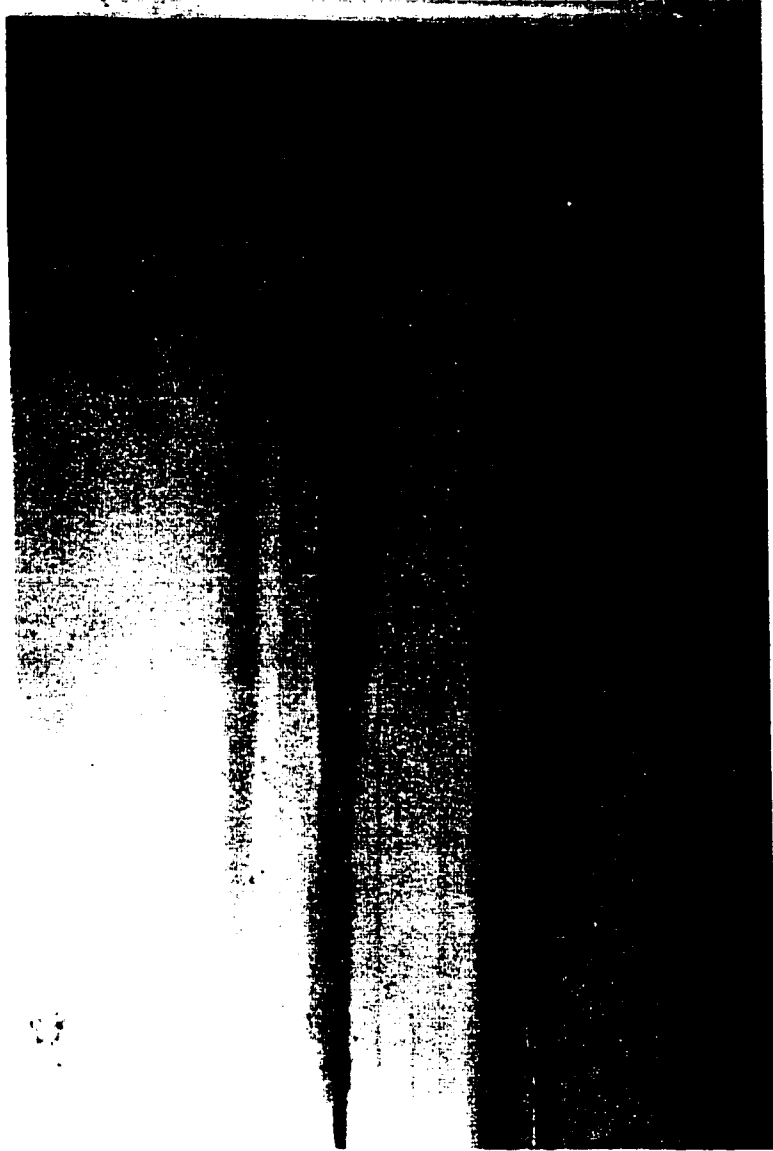


Fig. 5.2 Water surface elevation ($F_o = 4.0$, $Z_o/b_o = 10$)

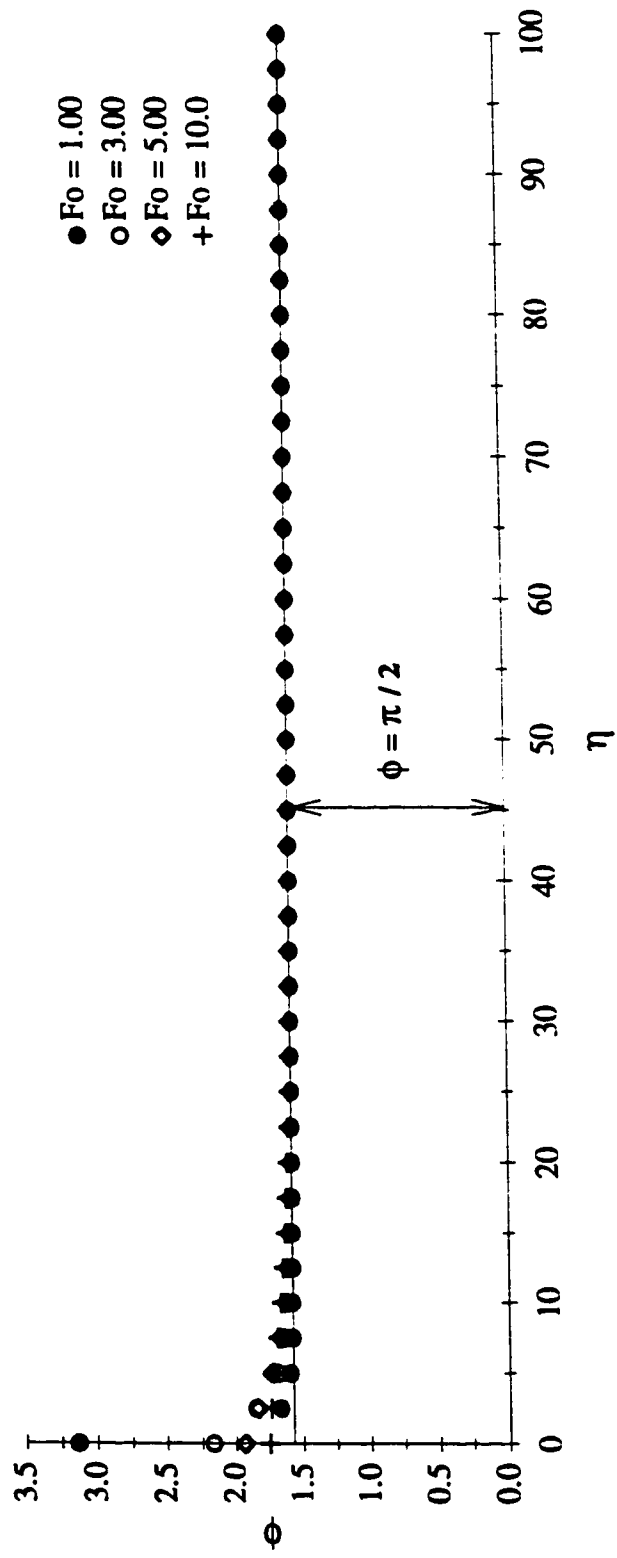


Fig. 5.3 Variation of (ϕ) with the offset ratio (η)

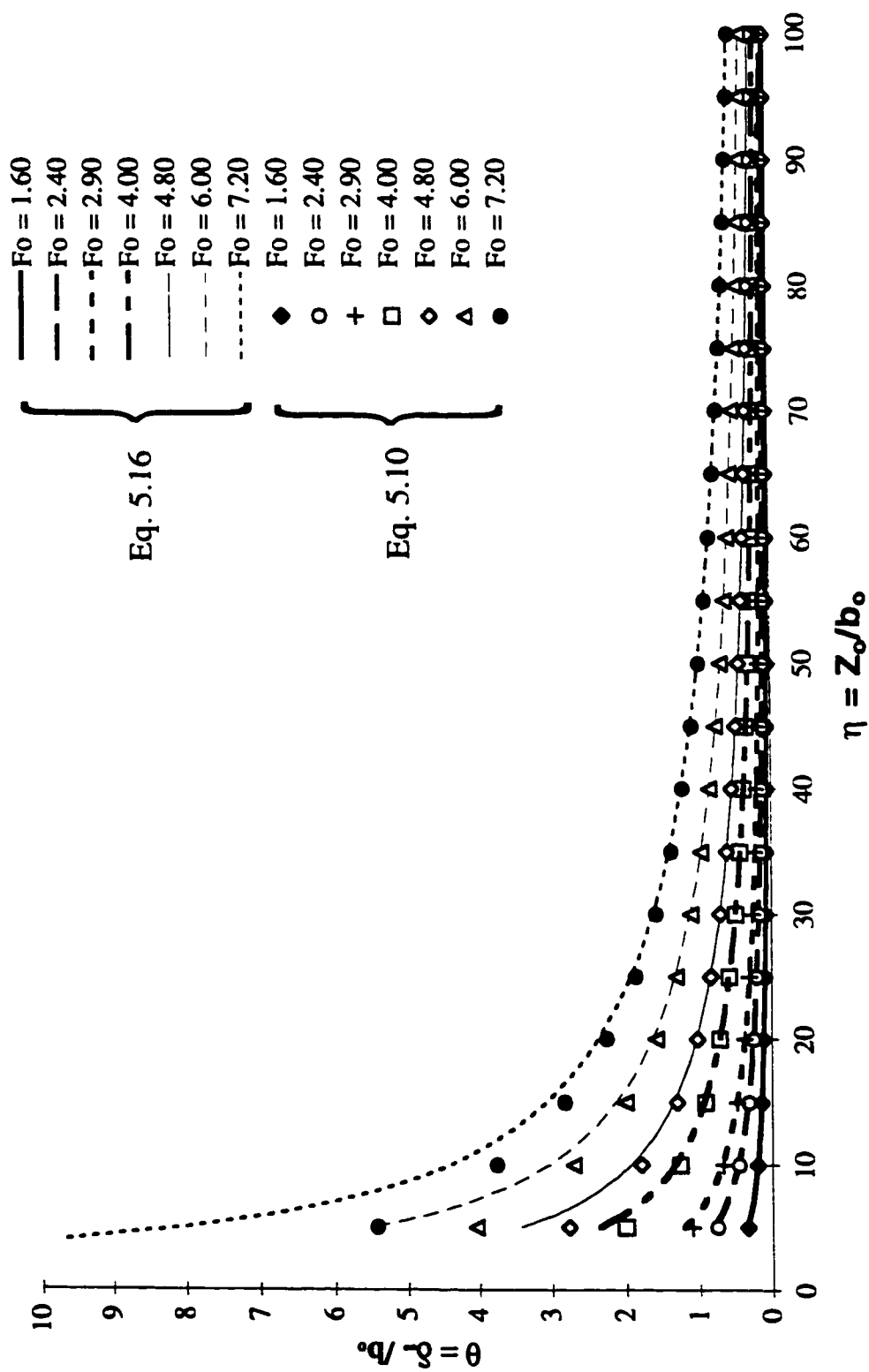


Fig. 5.4 Variation of (θ) with the offset ratio (η) for different Froude numbers

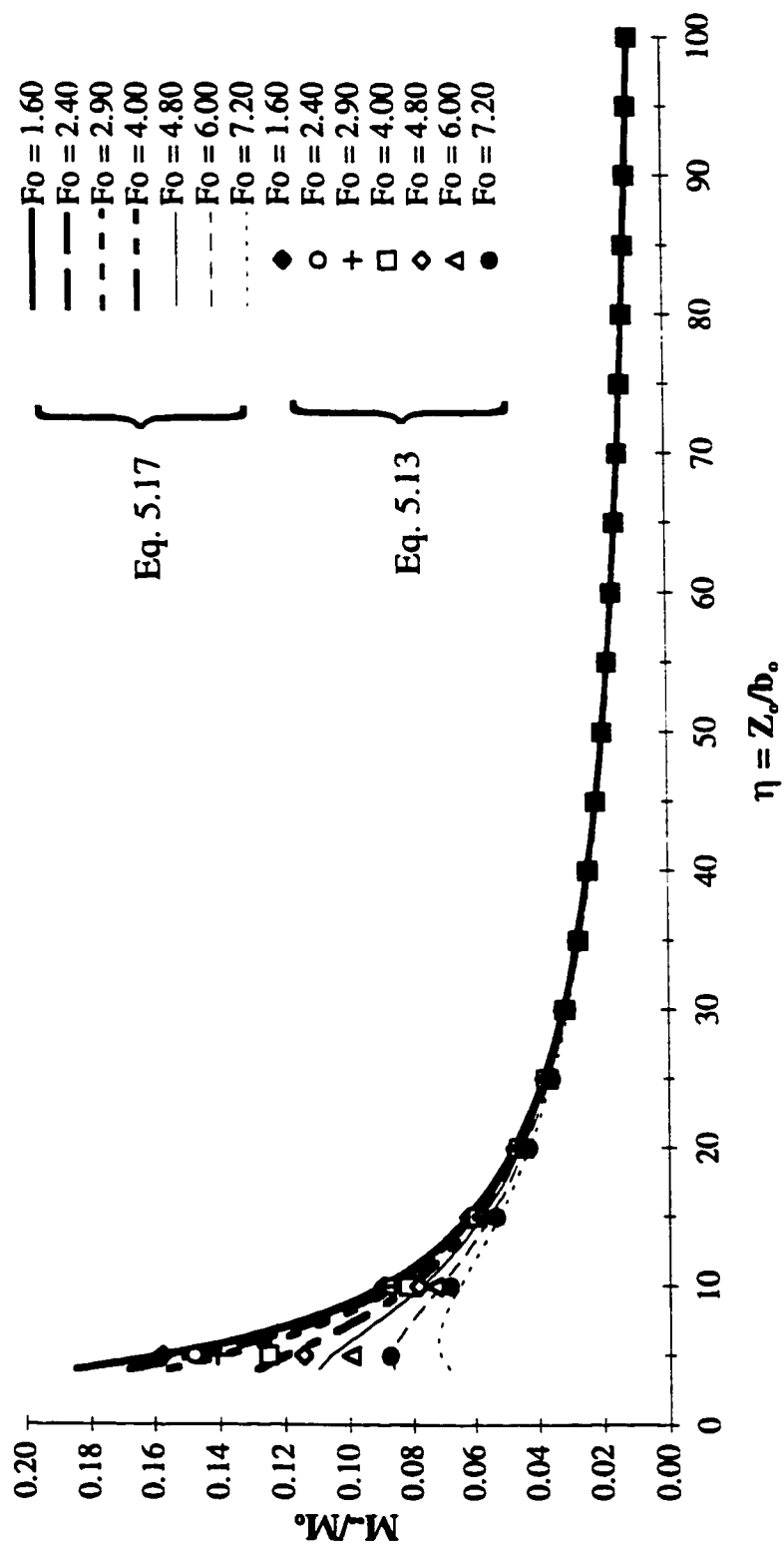


Fig. 5.5 Variation of (M_1/M_0) with the offset ratio (η) for different Froude numbers

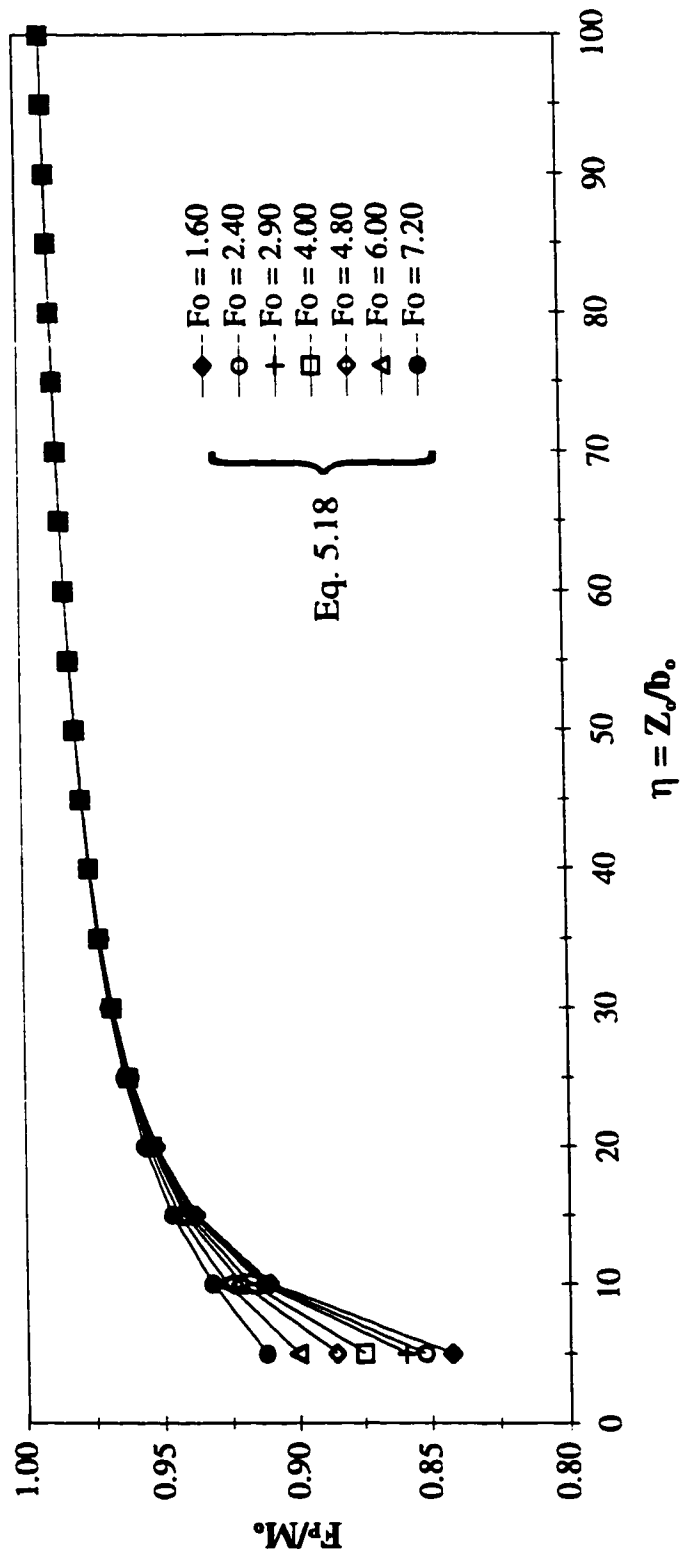


Fig. 5.6 Variation of (F_P/M_o) with the offset ratio (η) for different Froude numbers

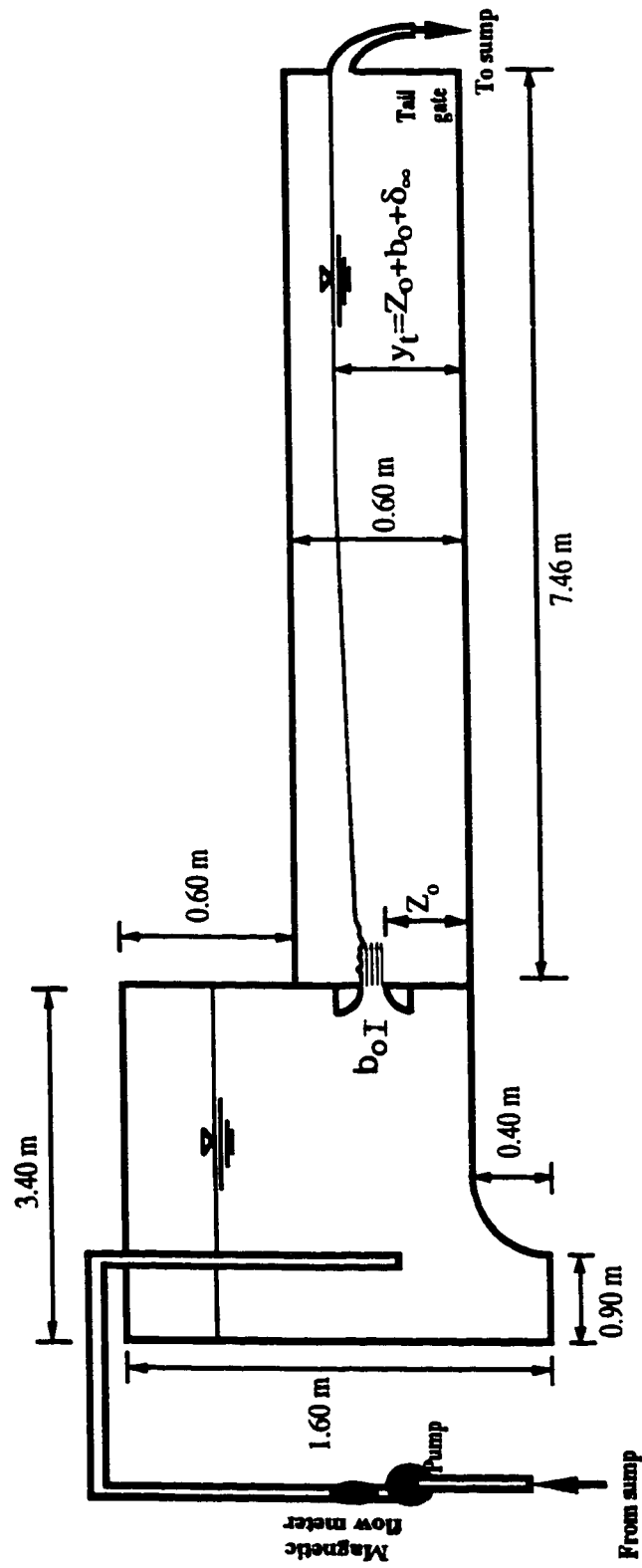


Fig. 5.7 Experimental flume



Fig. 5.8 Streamlined entrance to produce an uniform jet of thickness b .



Fig. 5.9 False floor to produce an offset distance of Z_0 .

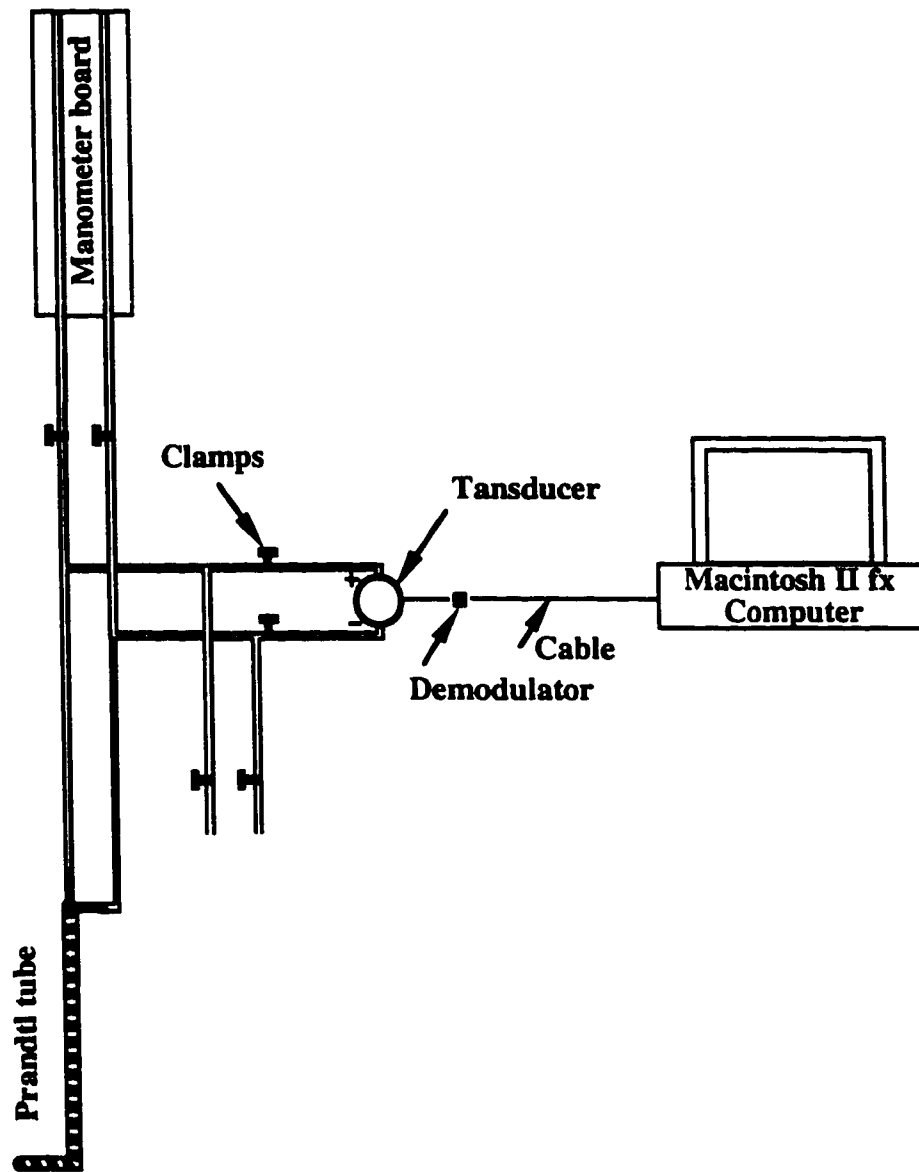


Fig. 5.10 Prandtl tube

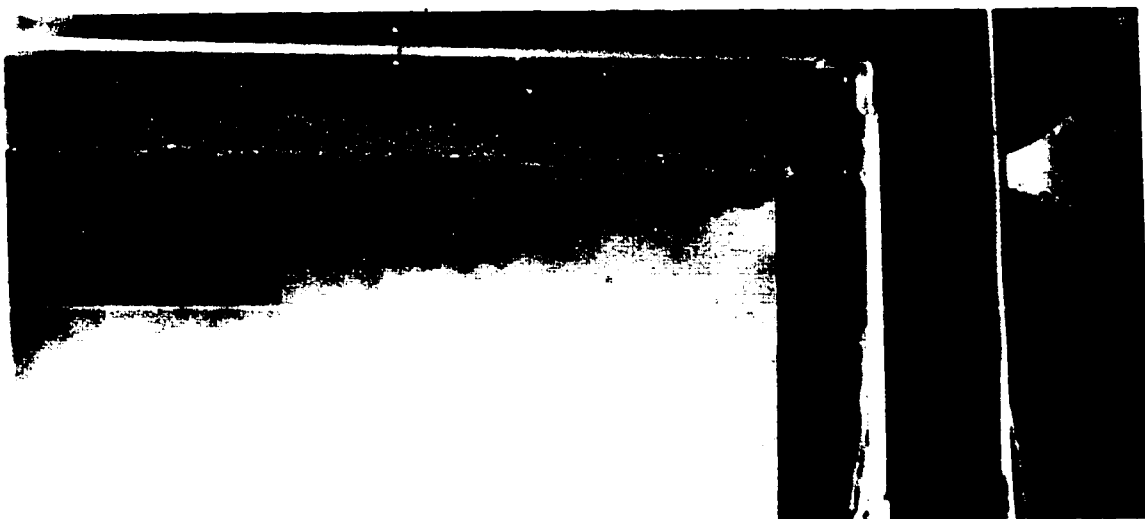


Fig. 5.11(a) Surface jet ($F_* = 7.20$, $Z_*/b_* = 100$)



Fig. 5.11(b) Surface jet ($F_* = 4.80$, $Z_*/b_* = 50$)

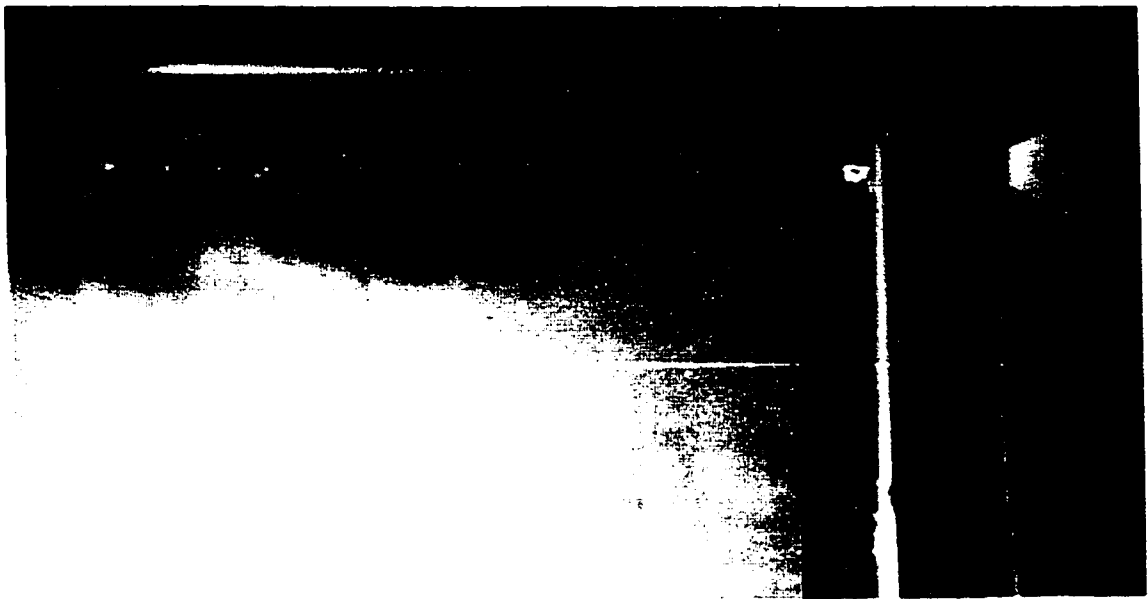


Fig. 5.11(c) Surface jet ($F_o = 4.80$, $Z_o/b_o = 25$)

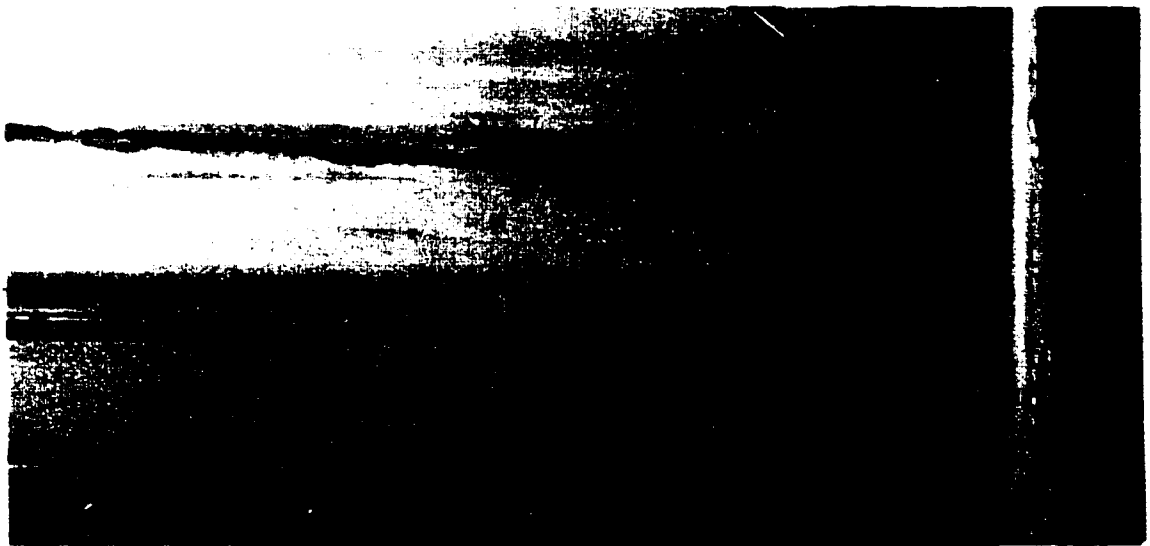


Fig. 5.11(d) Surface jet ($F_o = 4.00$, $Z_o/b_o = 10$)

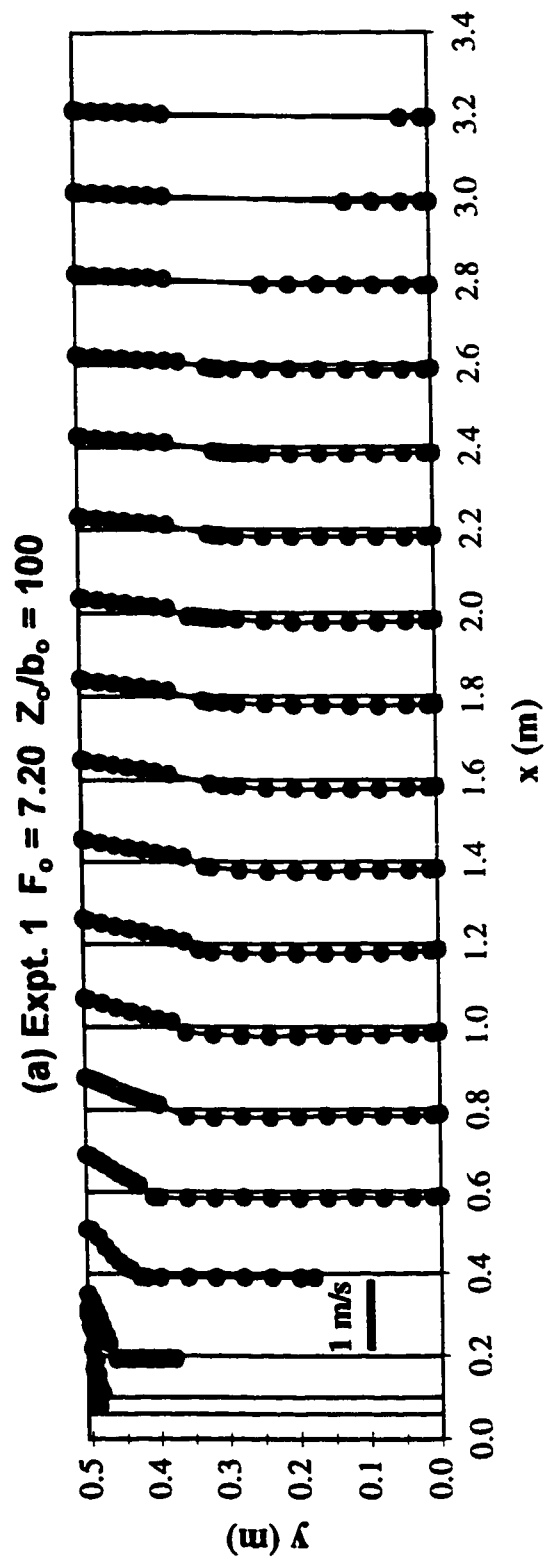


Fig. 5.12(a) Typical velocity profiles (Expt. 1)

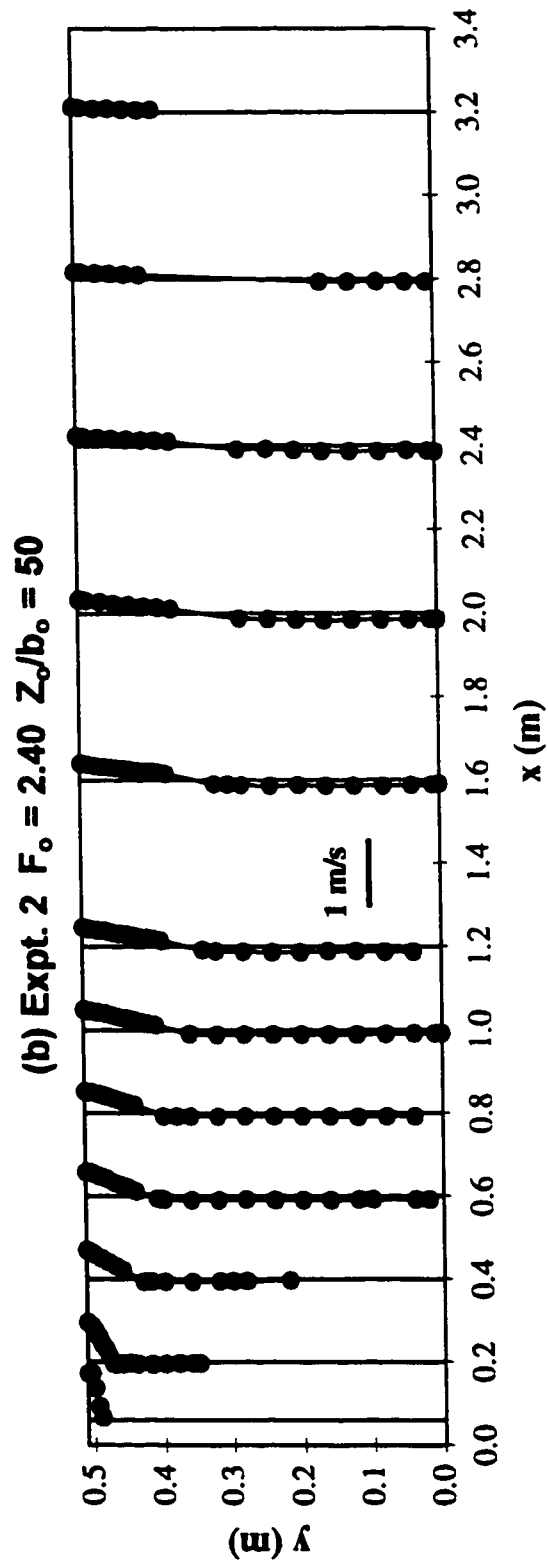


Fig. 5.12(b) Typical velocity profiles (Expt. 2)

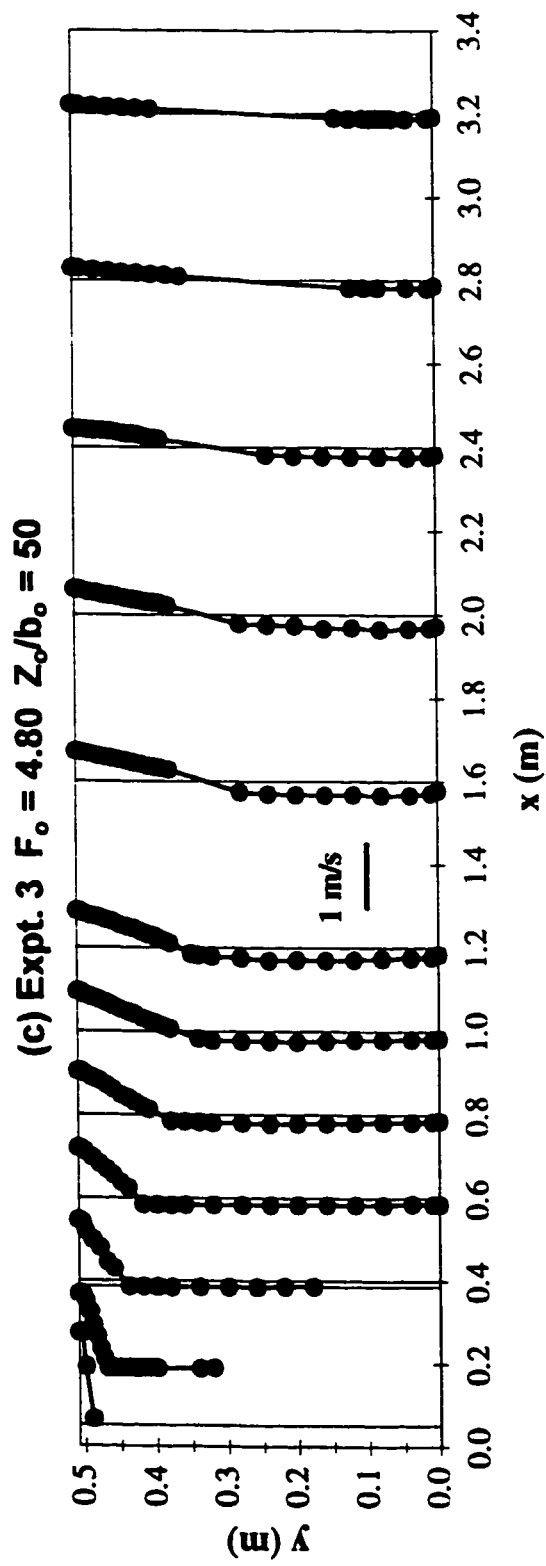


Fig. 5.12(c) Typical velocity profiles (Expt. 3)

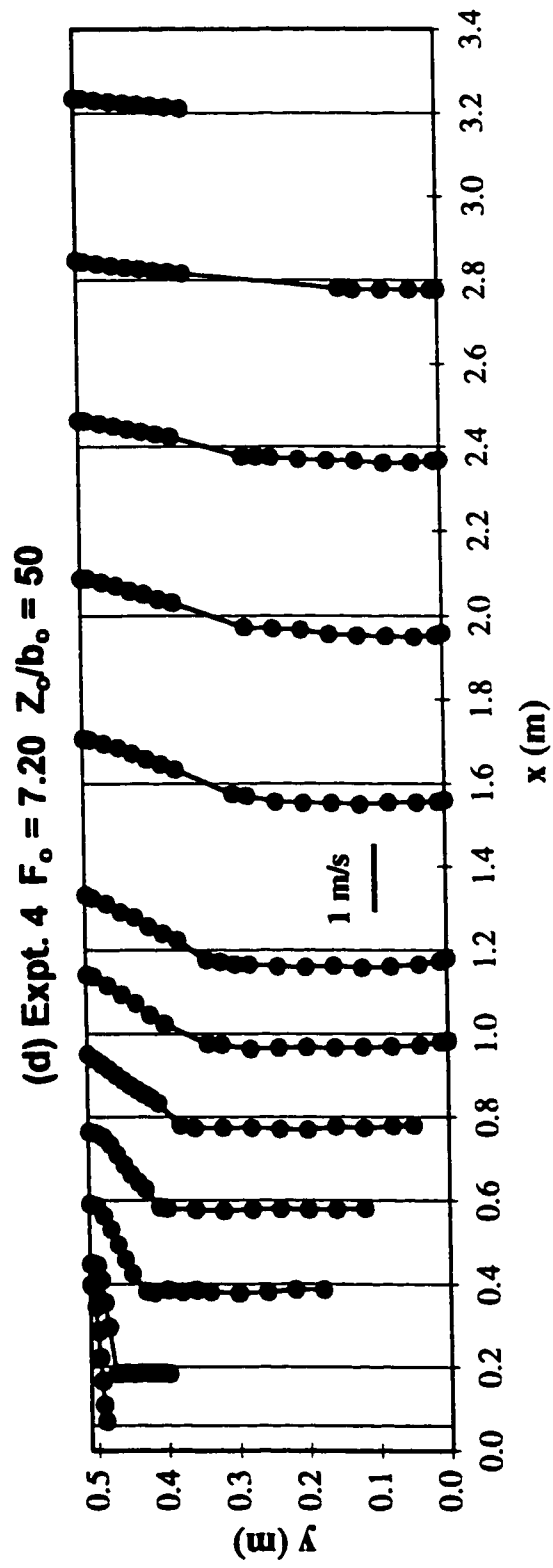


Fig. 5.12(d) Typical velocity profiles (Expt. 4)

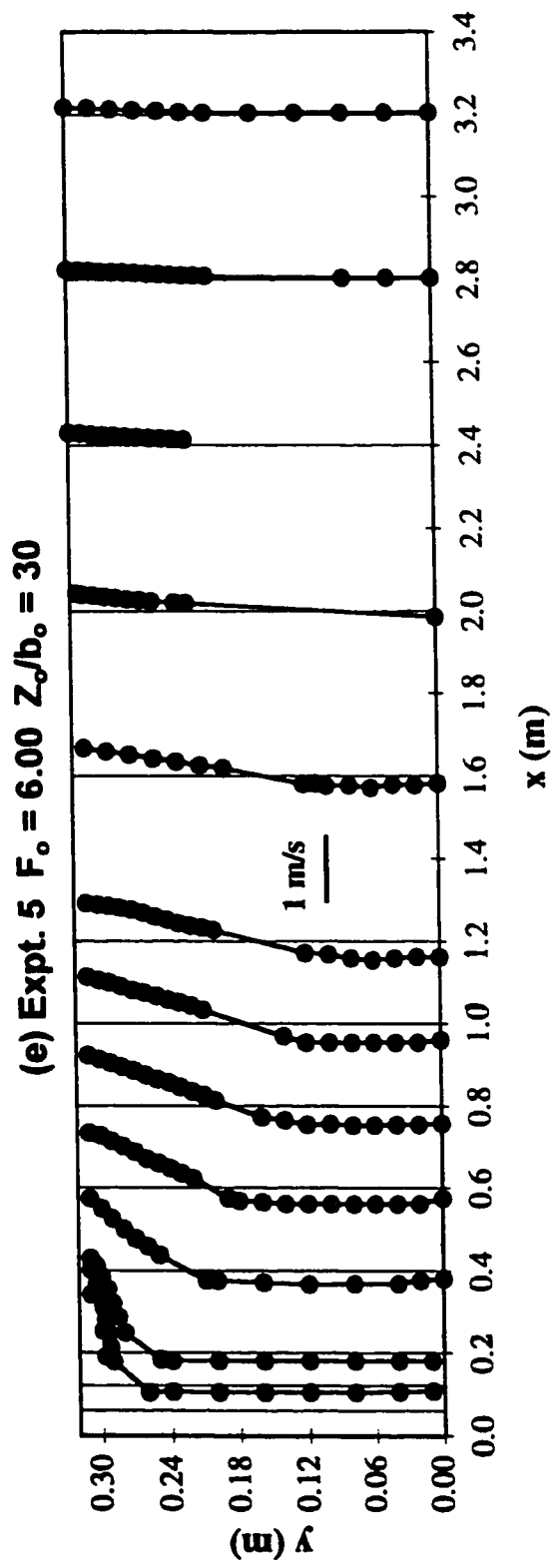


Fig. 5.12(e) Typical velocity profiles (Expt. 5)

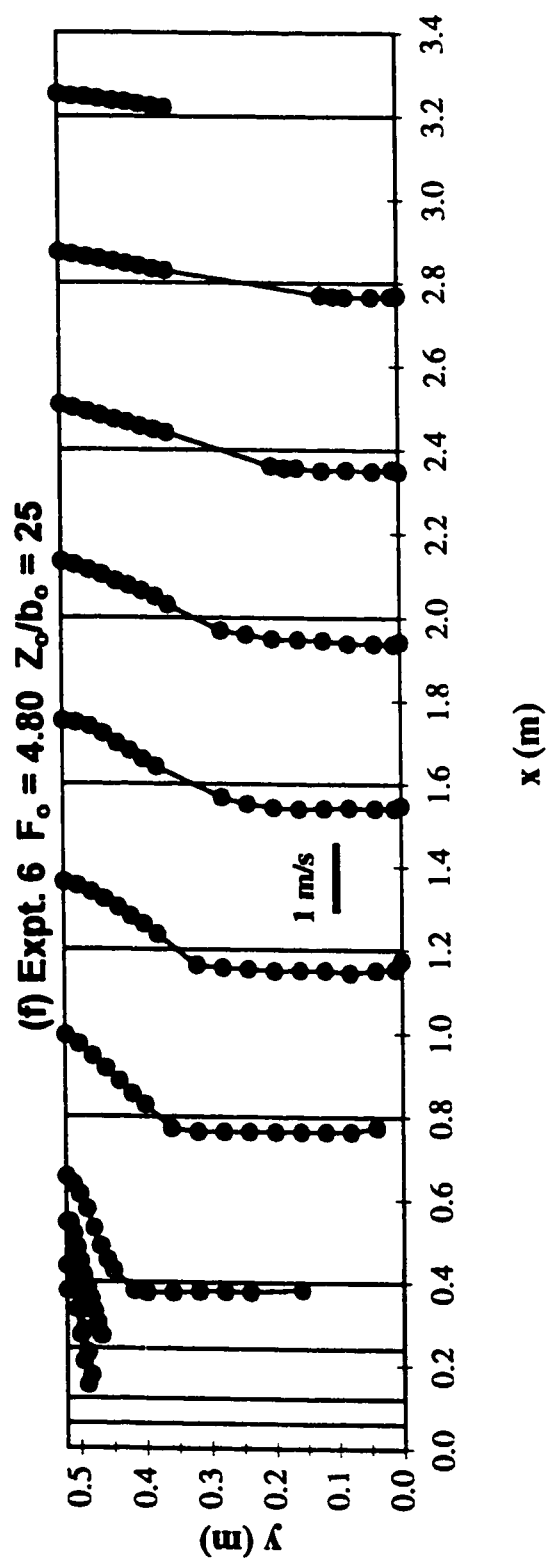


Fig. 5.12(f) Typical velocity profiles (Expt. 6)

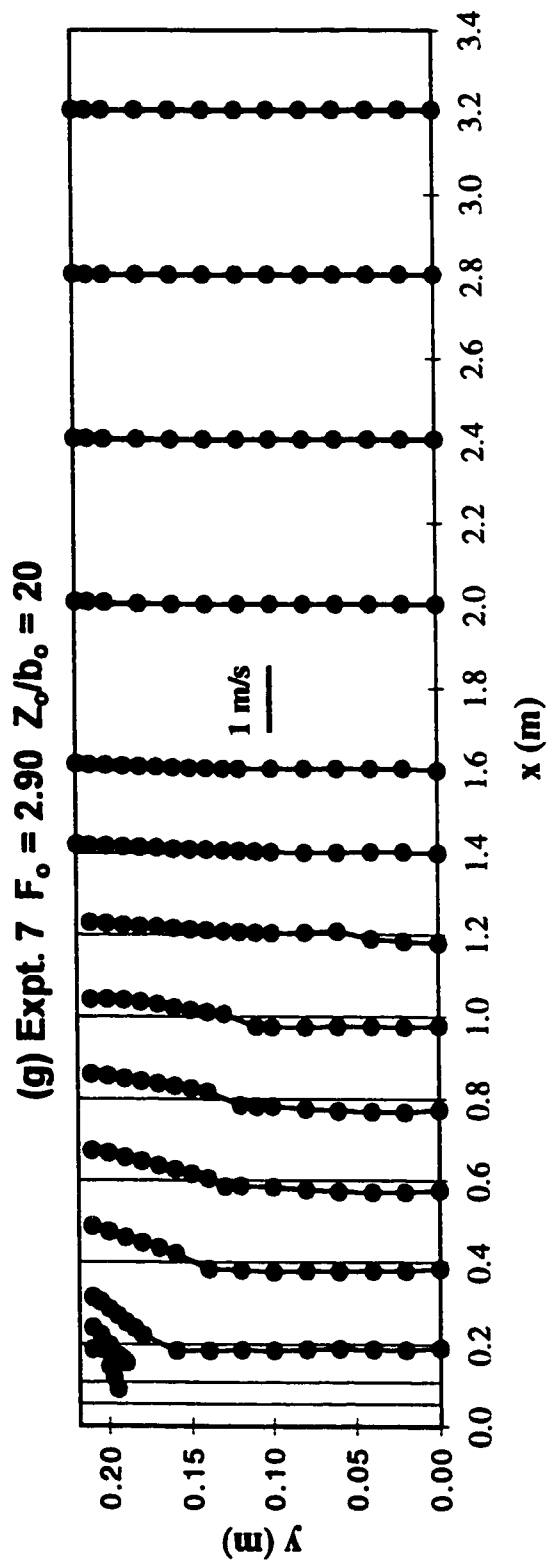


Fig. 5.12(g) Typical velocity profiles (Expt. 7)

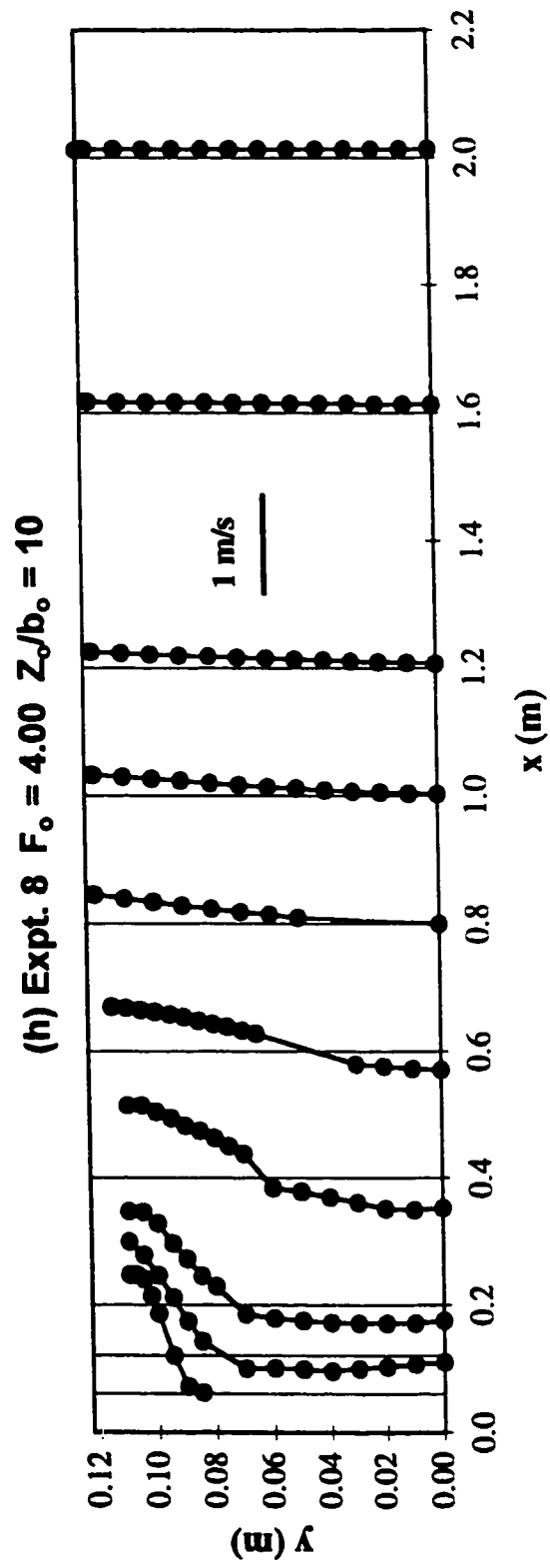


Fig. 5.12(h) Typical velocity profiles (Expt. 8)

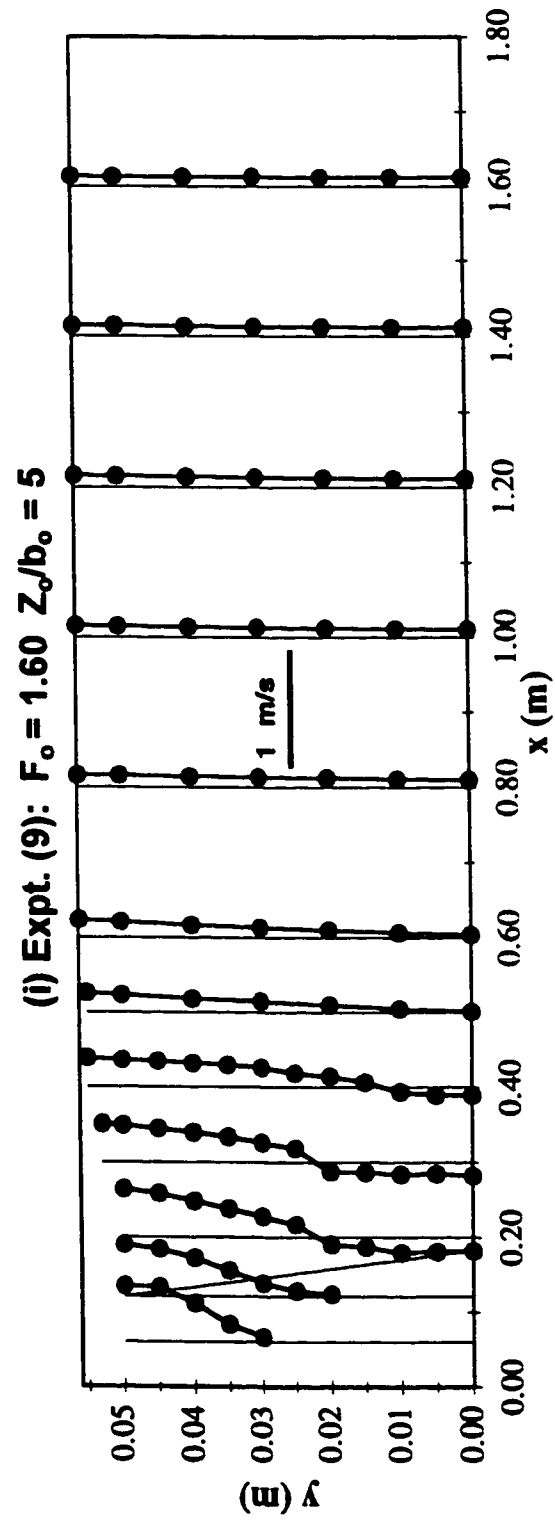


Fig. 5.12(i) Typical velocity profiles (Expt. 9)

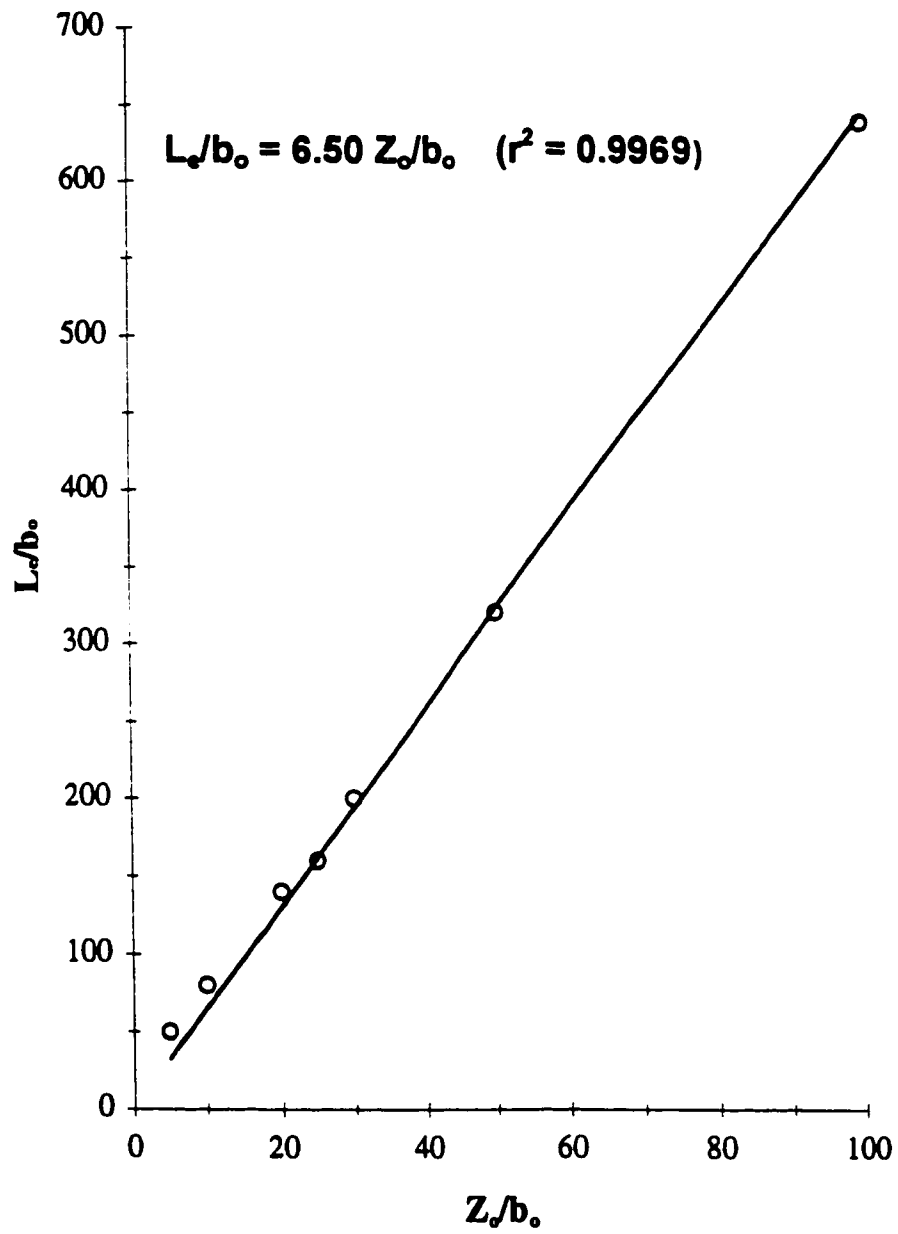


Fig. 5.13 Variation of the eddy length with the offset ratio

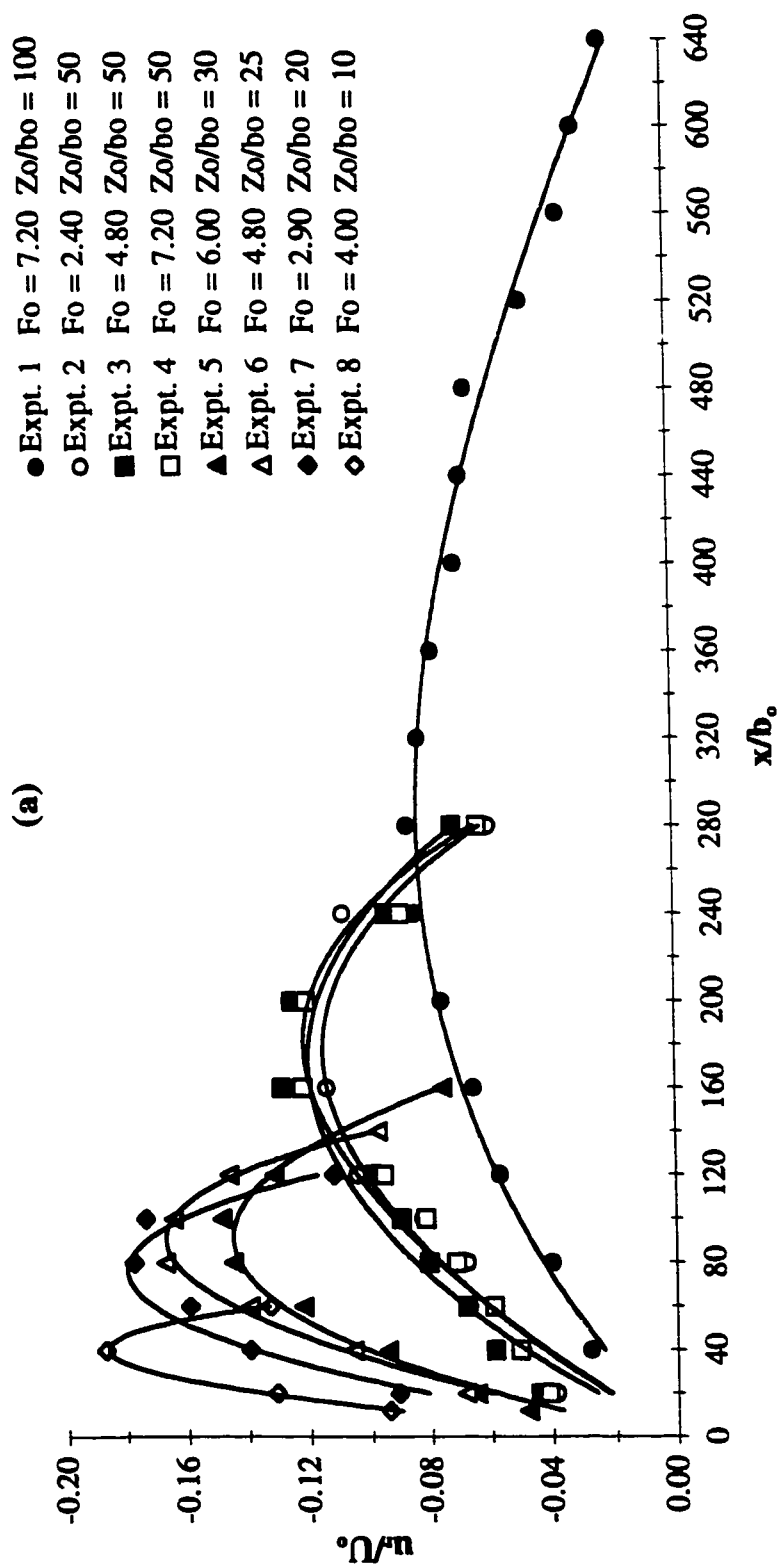


Fig. 5.14(a) Variation of the depth-averaged reverse velocity with distance

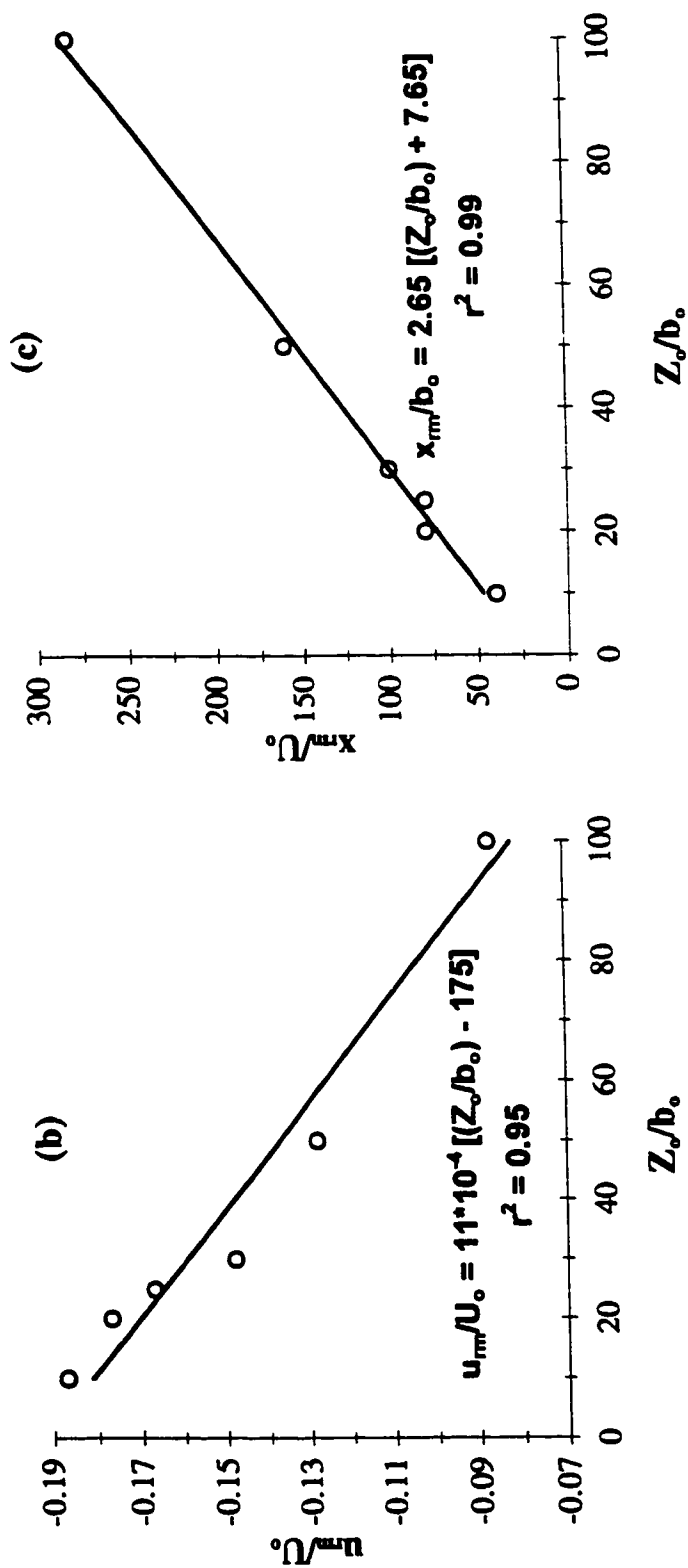


Fig. 5.14(b-c) Effect of the offset ratio on the magnitude and the location of the maximum reverse velocity

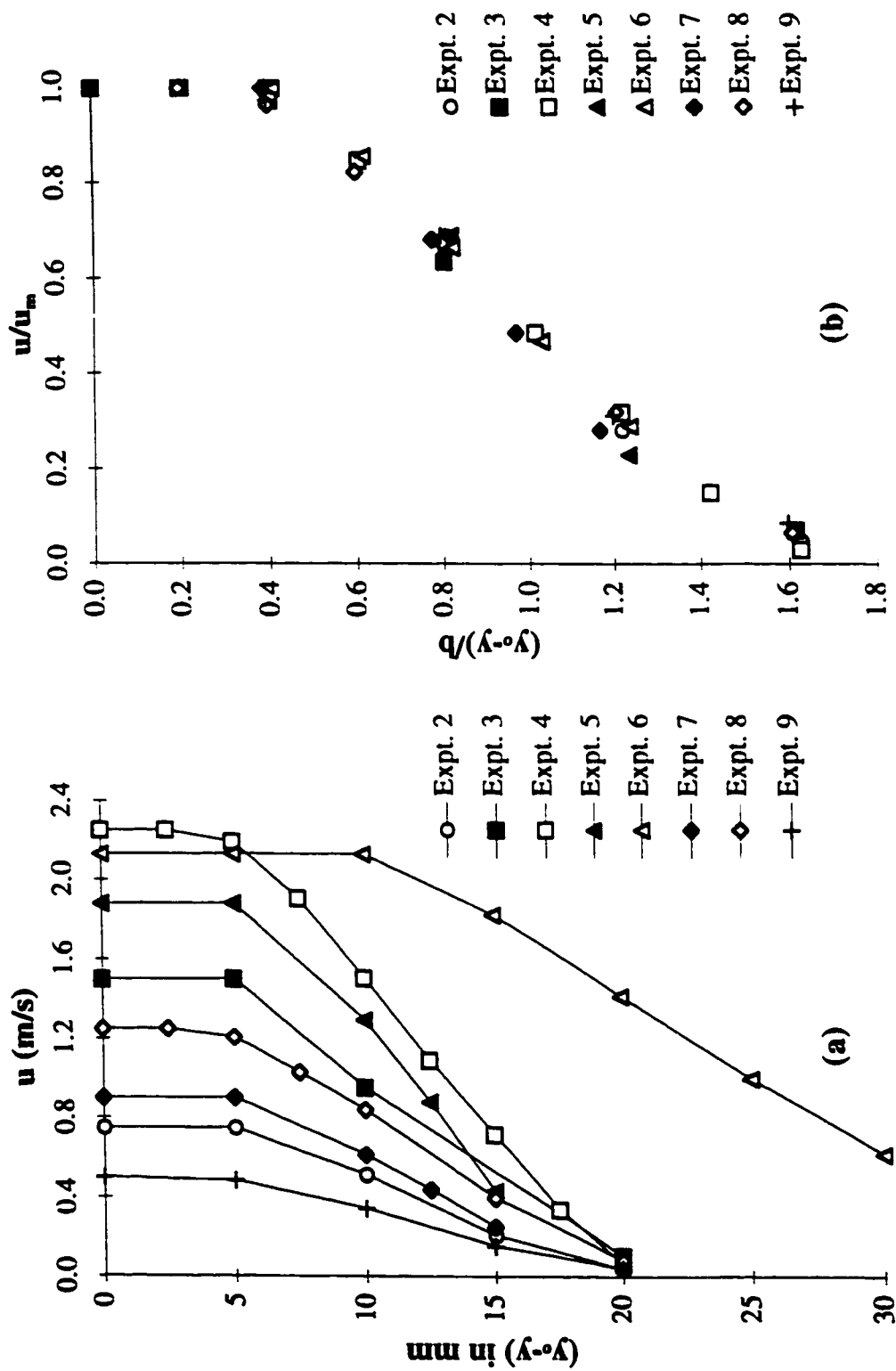


Fig. 5.15(a-b) Velocity distribution in partially-developed flow ($x/b_0 = 6$)
(a) Velocity profiles; and (b) Similarity profiles

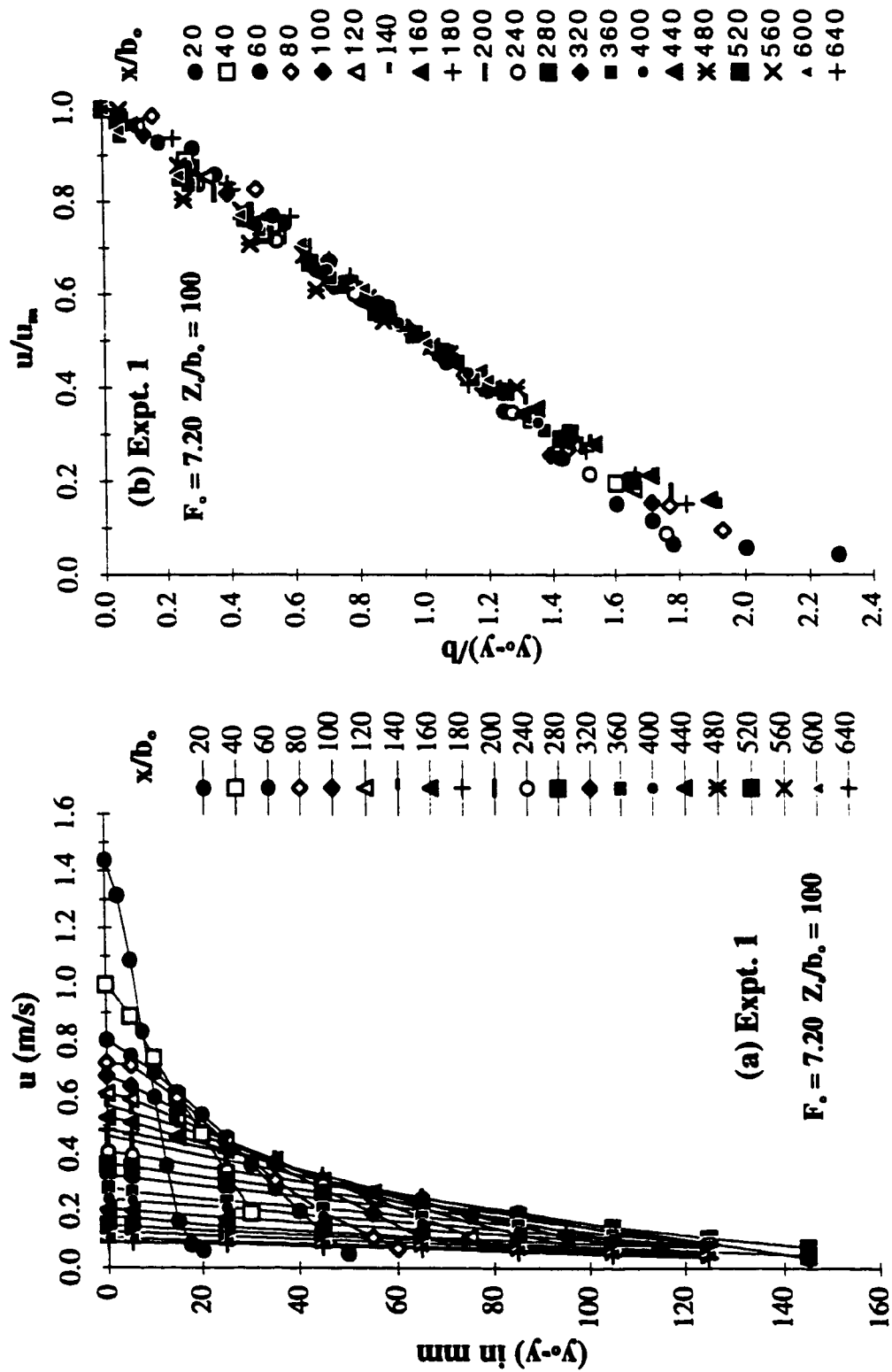


Fig. 5.16(a-b) Velocity distribution in fully-developed flow (Expt. 1)
(a) Velocity profiles; and (b) Similarity profile

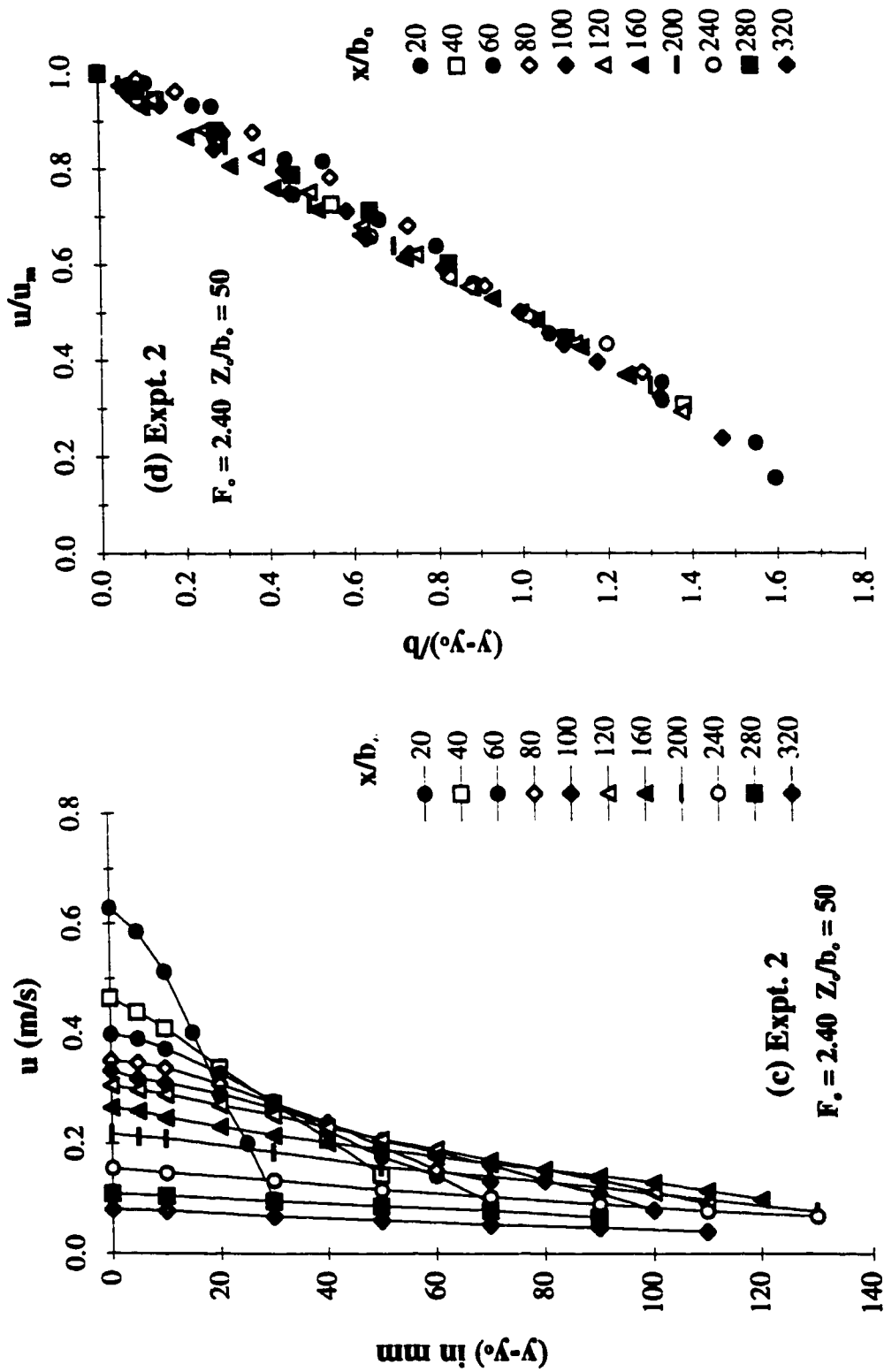


Fig. 5.16(c-d) Velocity distribution in fully-developed flow (Expt. 2)
 (c) Velocity profiles; and (d) Similarity profile

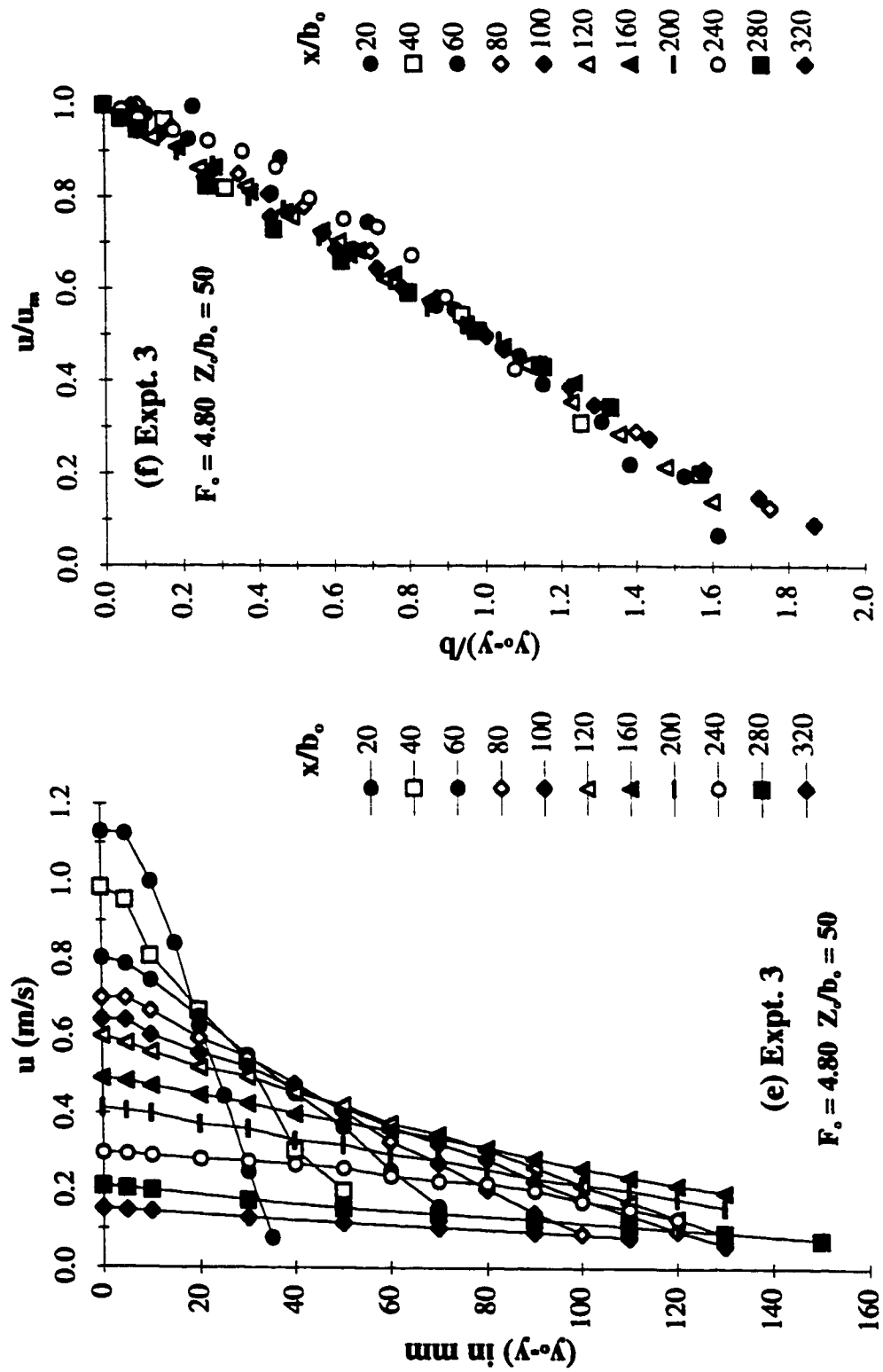


Fig. 5.16(e-f) Velocity distribution in fully-developed flow (Expt. 3)
(e) Velocity profiles; and (f) Similarity profile

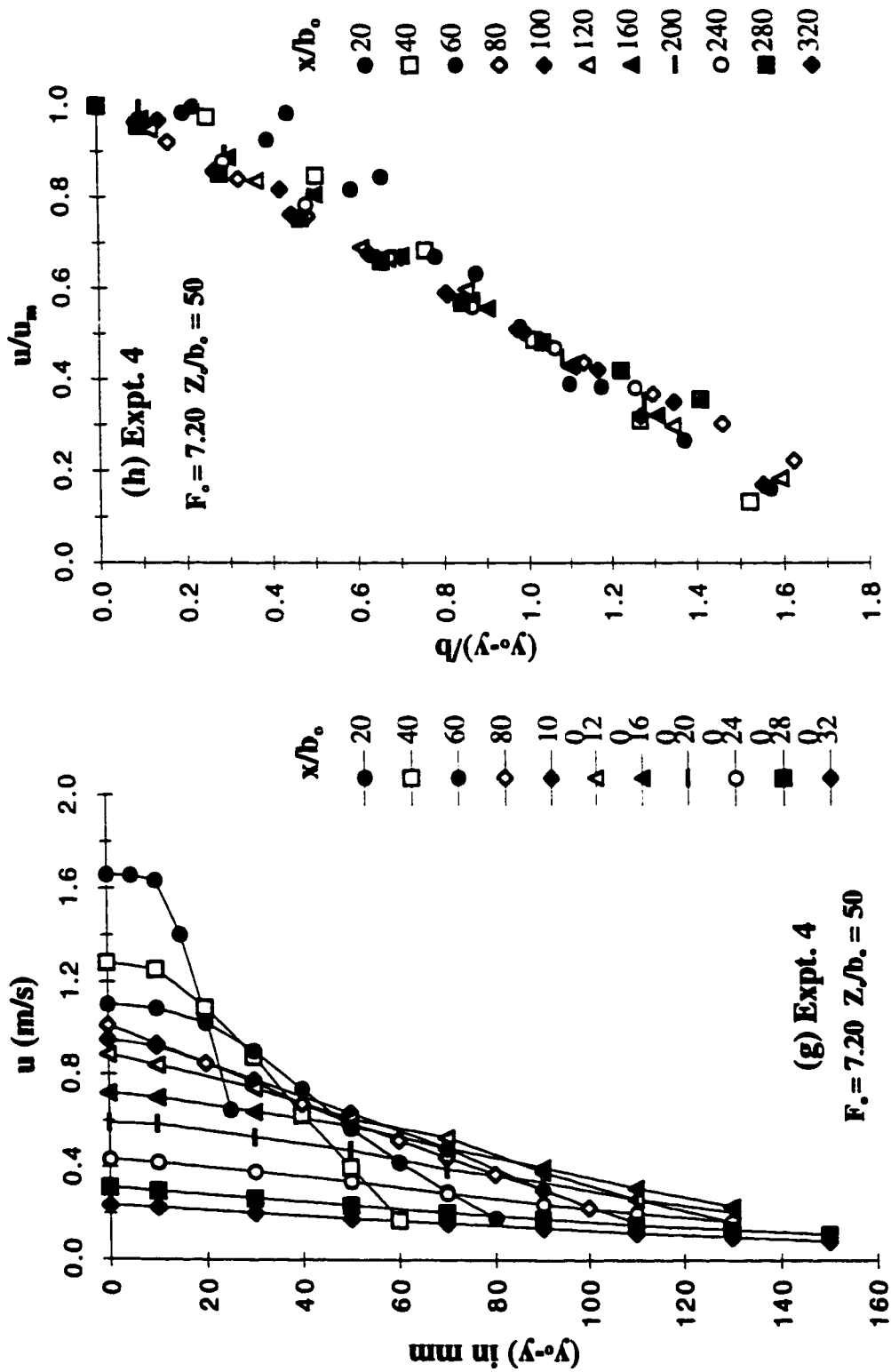


Fig. 5.16(g-h) Velocity distribution in fully-developed flow (Expt. 4)
(g) Velocity profiles; and (h) Similarity profile

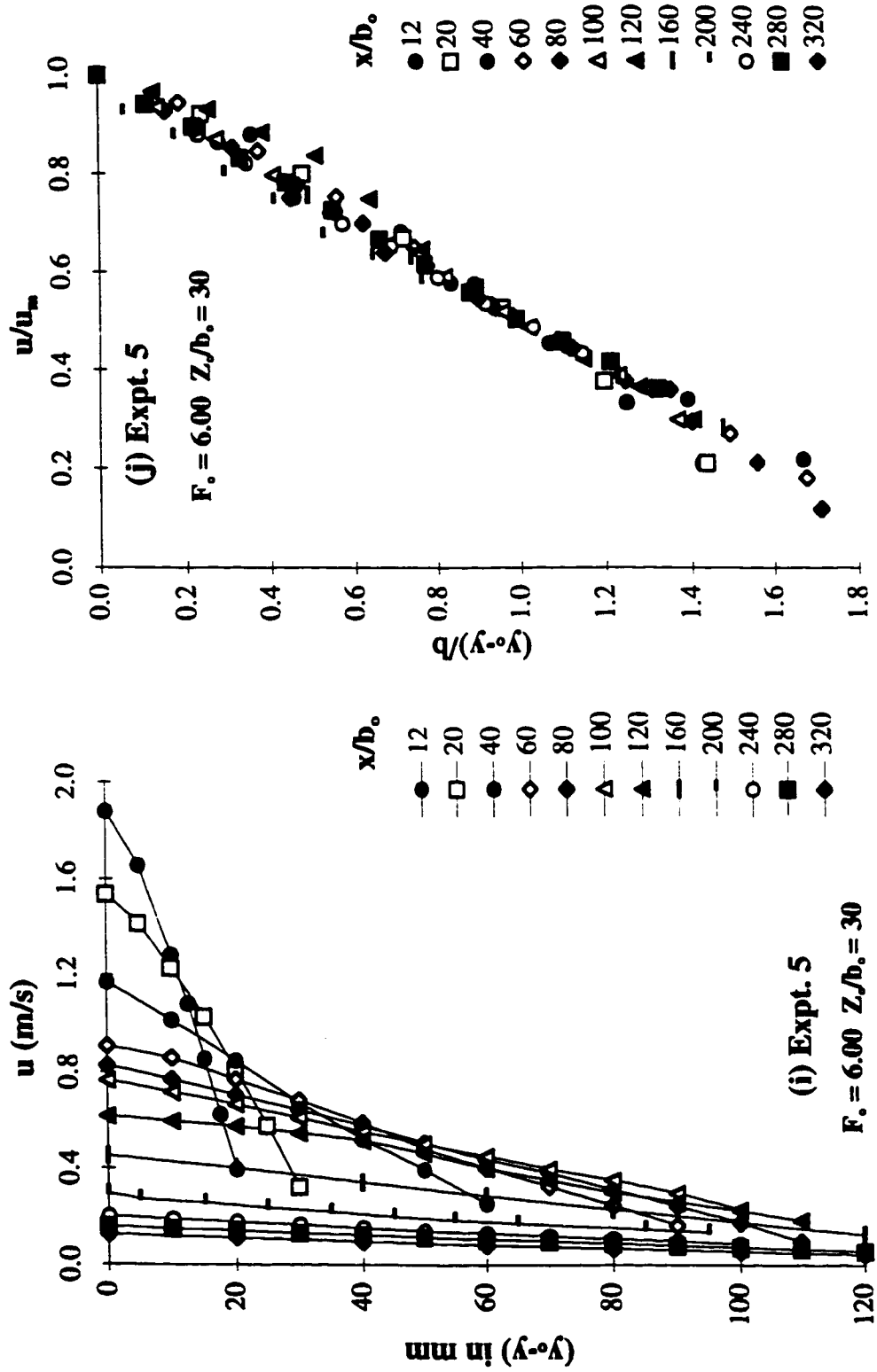


Fig. 5.16(i-j) Velocity distribution in fully-developed flow (Expt. 5)
 (i) Velocity profiles; and (j) Similarity profile

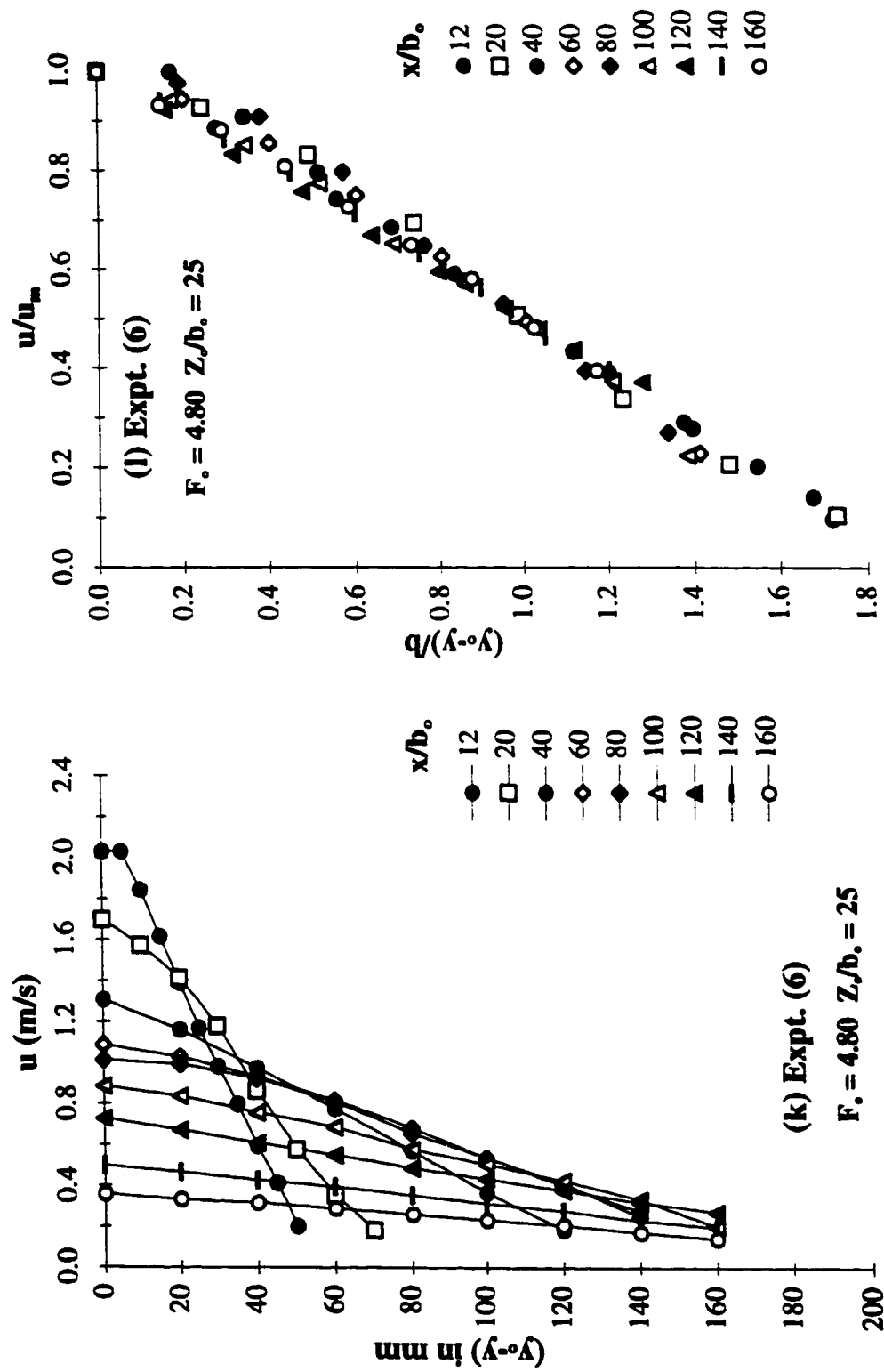


Fig. 5.16(k-l) Velocity distribution in fully-developed flow (Expt. 6)
(k) Velocity profiles; and (l) Similarity profile

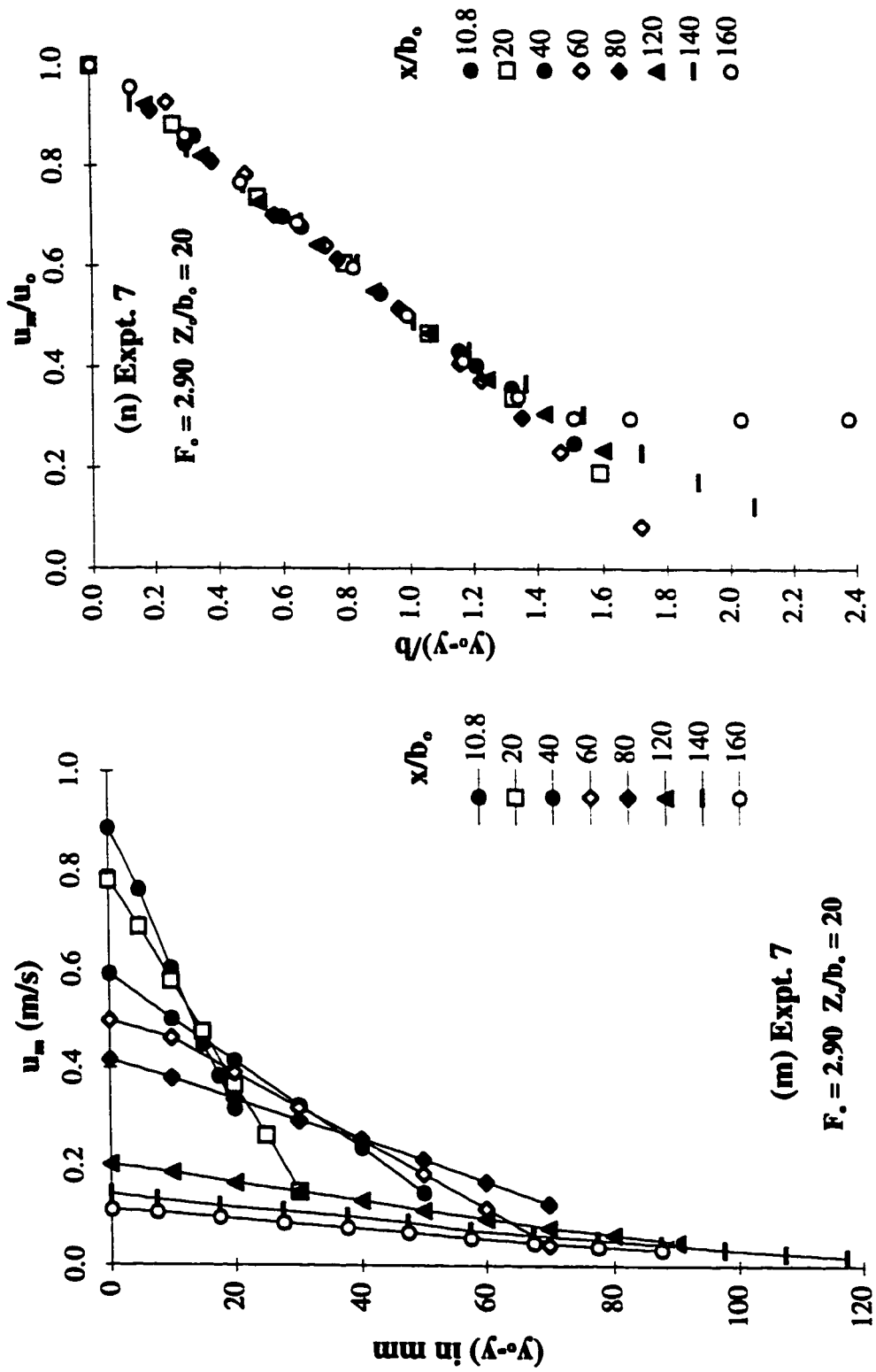


Fig. 5.16(m-n) Velocity distribution in fully-developed flow (Expt. 7)
 (m) Velocity profiles; and (n) Similarity profile

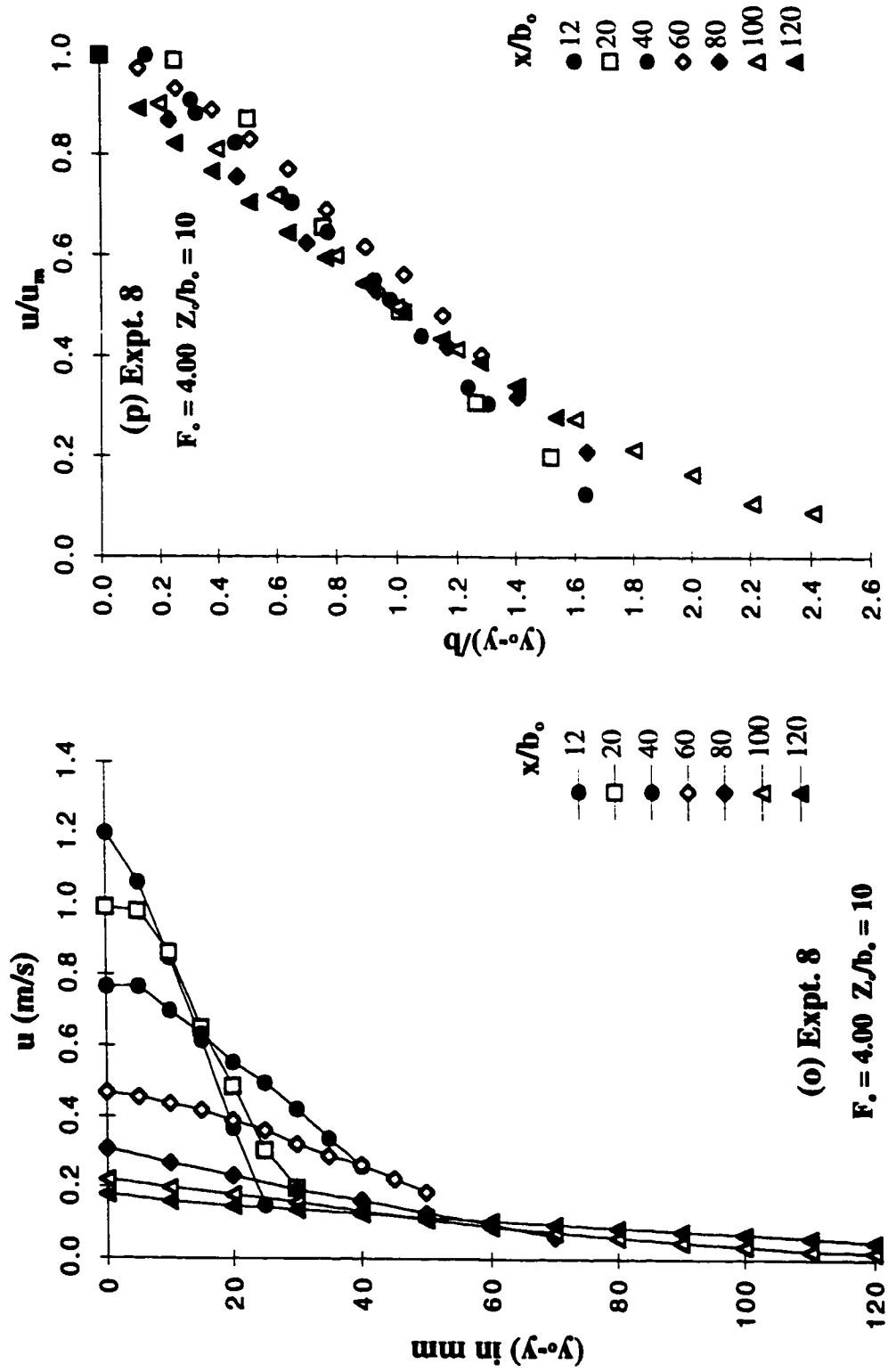


Fig. 5.16(o-p) Velocity distribution in fully-developed flow (Expt. 8)
 (o) Velocity profiles; and (p) Similarity profile

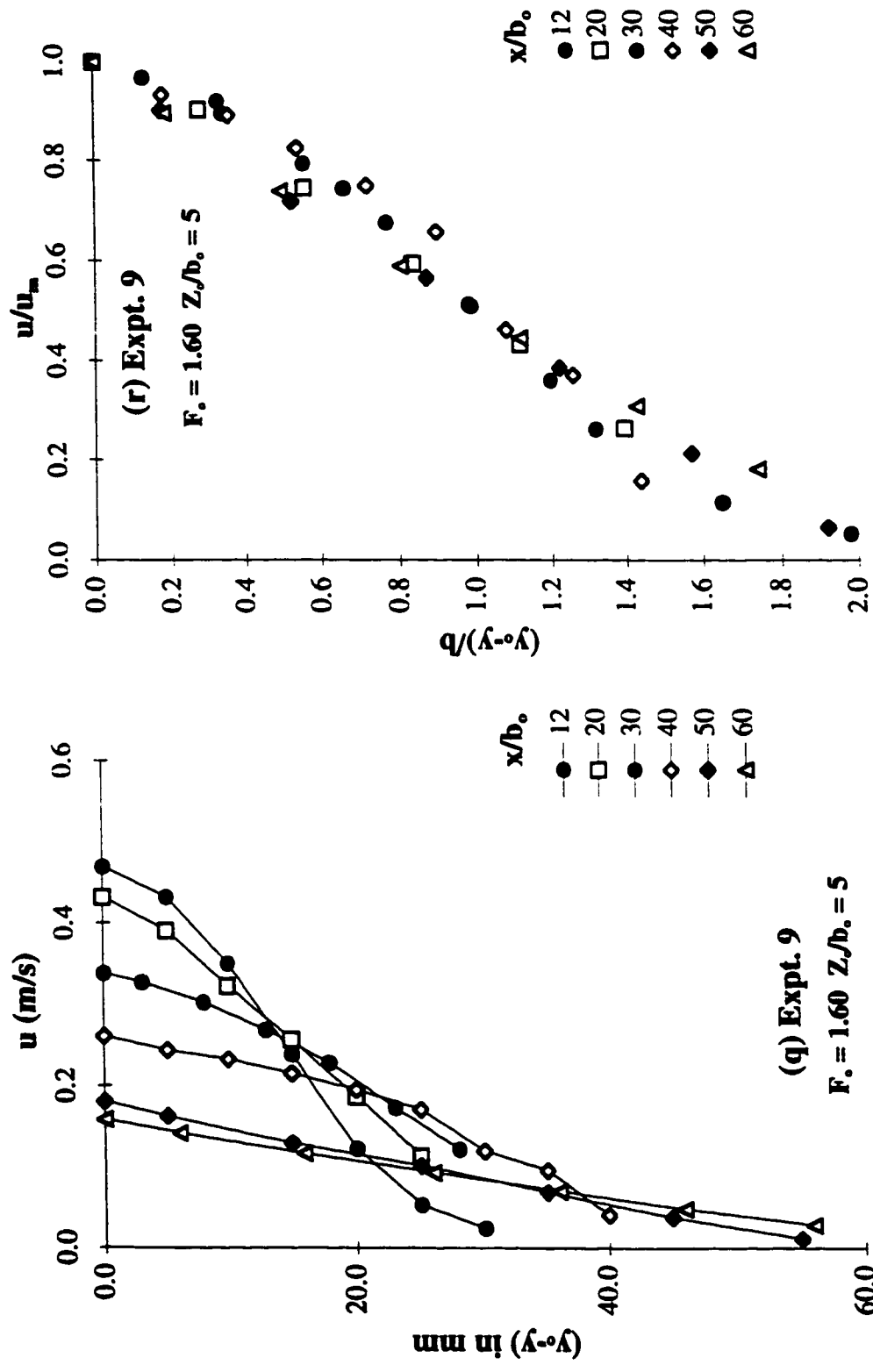


Fig. 5.16(q-r) Velocity distribution in fully-developed flow (Expt. 9)
 (q) Velocity profiles; and (r) Similarity profile

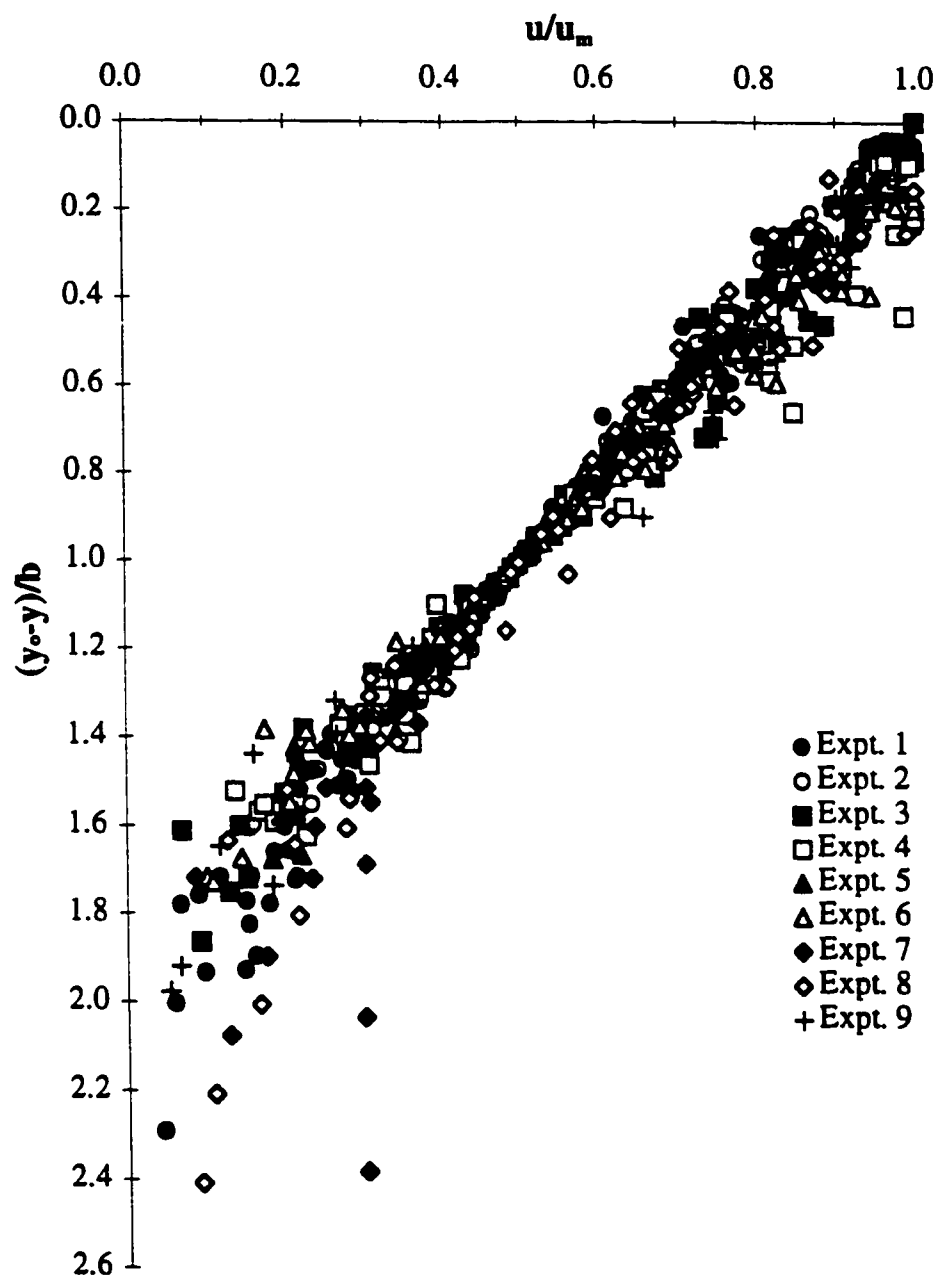


Fig. 5.17 Consolidated non-dimensional plot for the velocity distribution in the surface jet

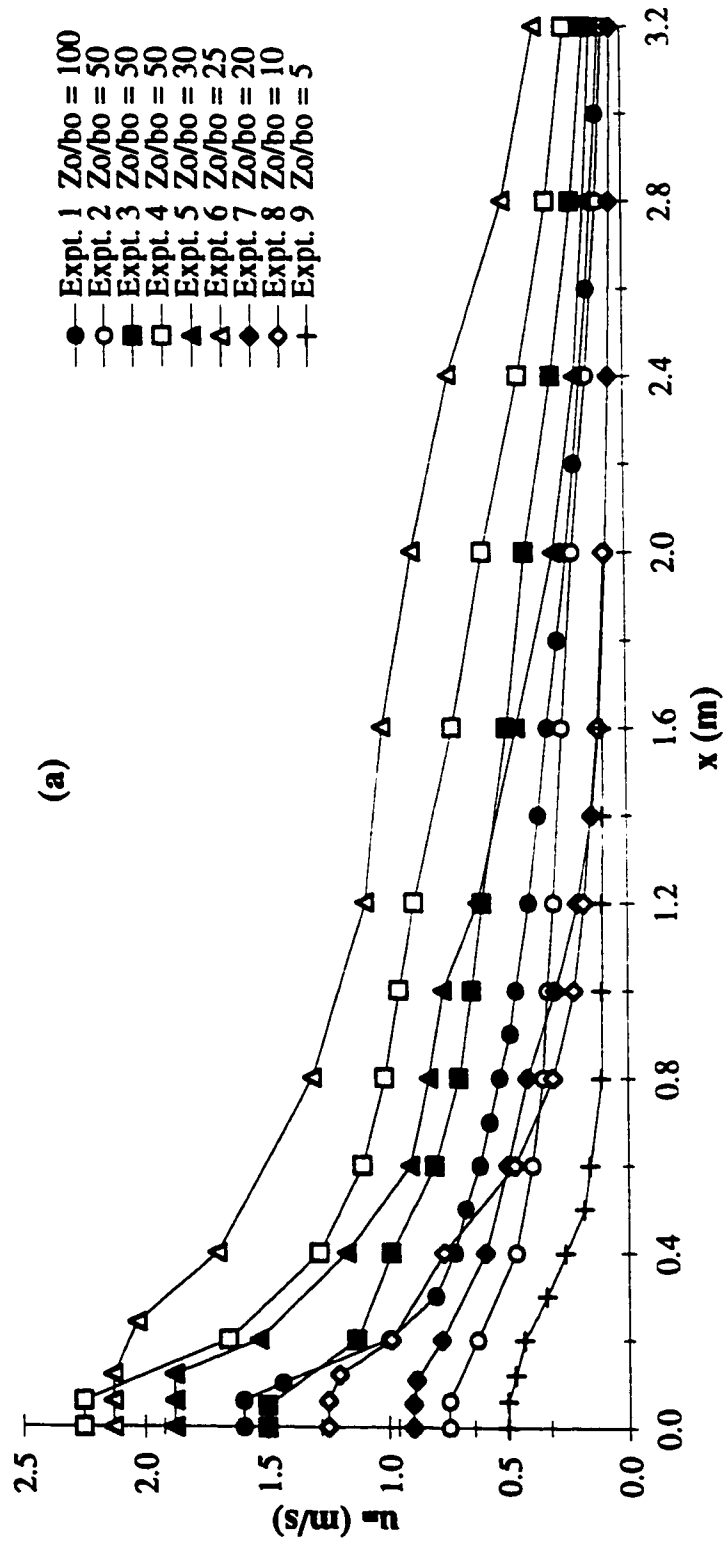


Fig. 5.18(a) Variation of the maximum jet velocity, u_m , with distance

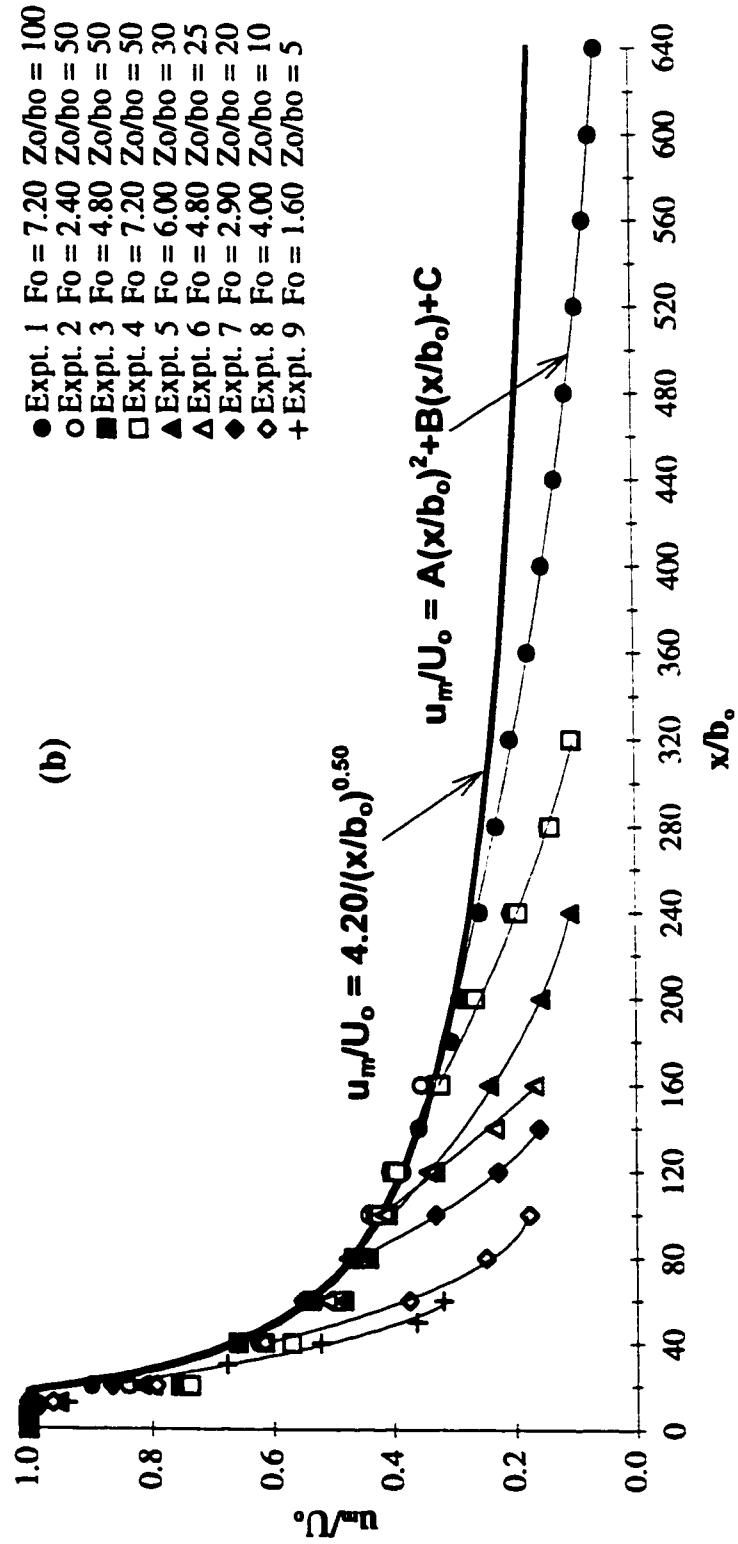


Fig. 5.18(b) Variation of u_m/U_o with x/b_o .

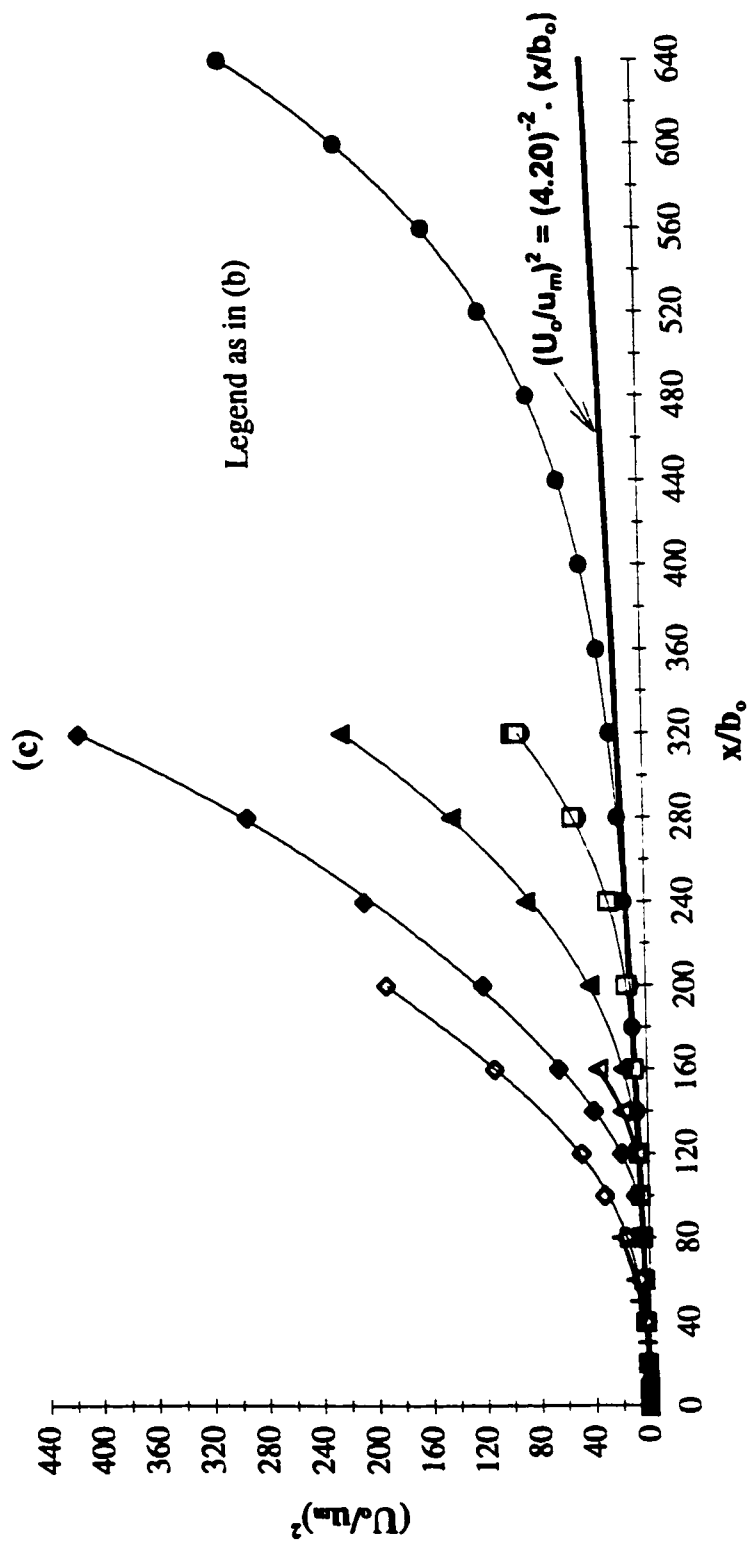


Fig. 5.18(c) Variation of $(U_o/U_m)^2$ with x/b_o .

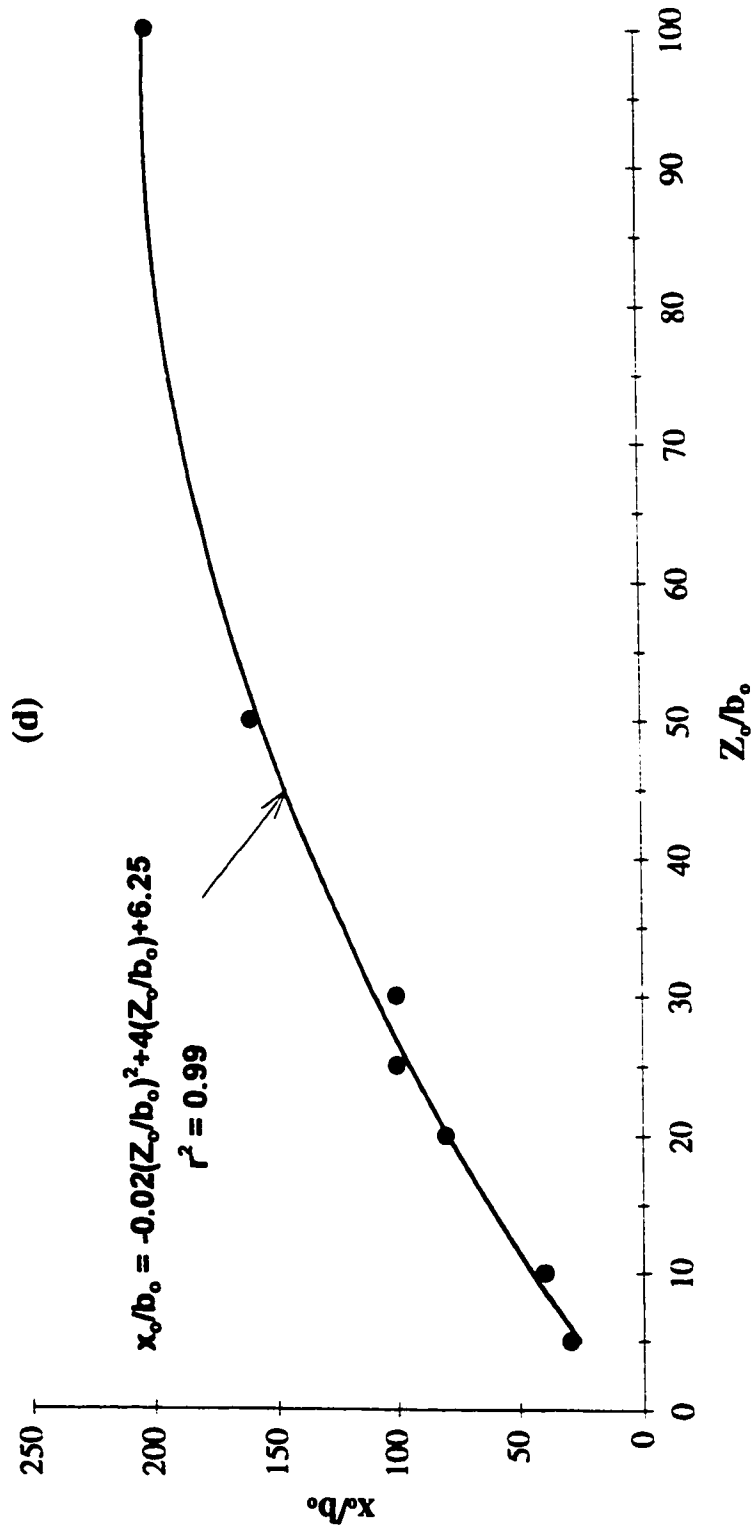


Fig. 5.18(d) Effect of the offset ratio on the breakdown distance

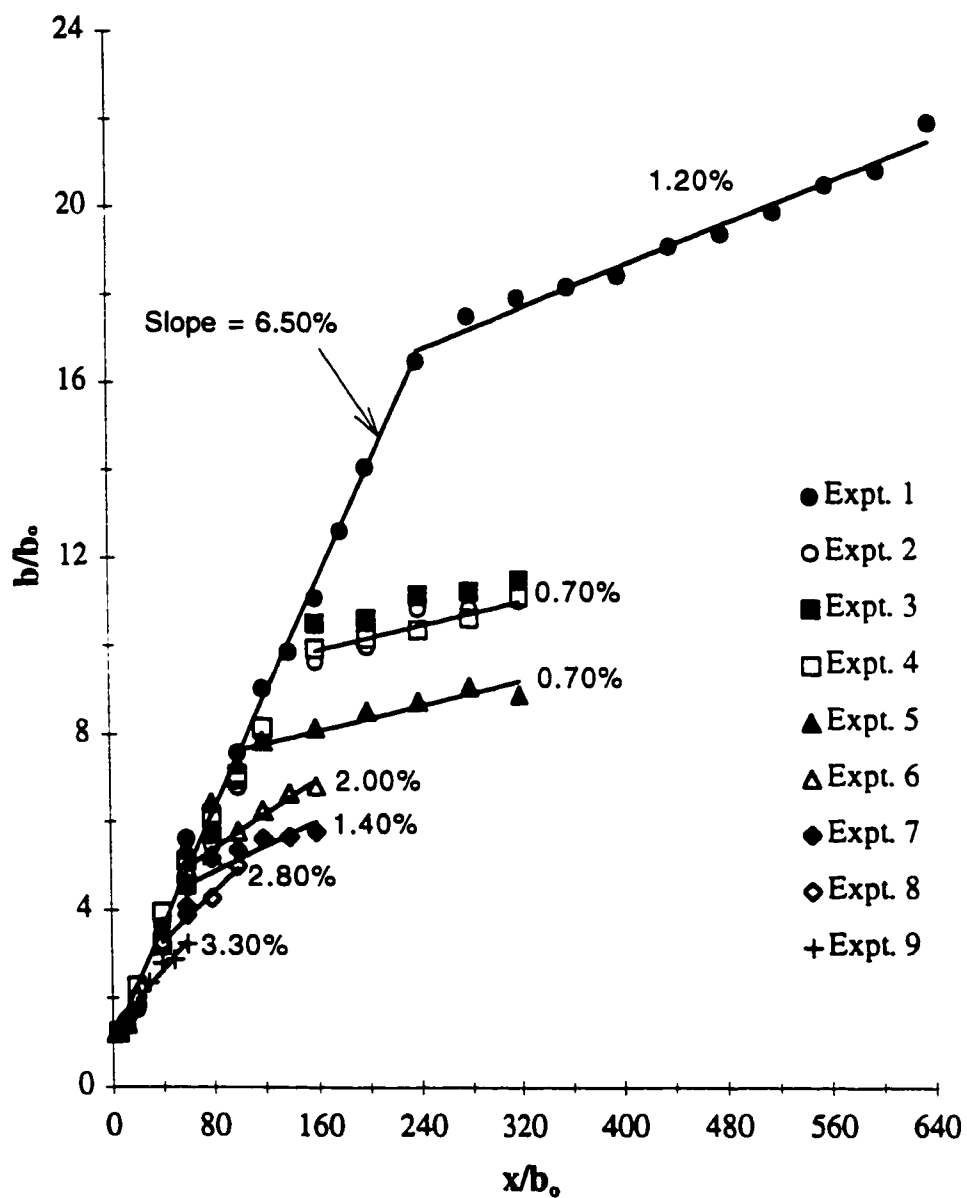


Fig. 5.19 Variation of the jet half-width with distance

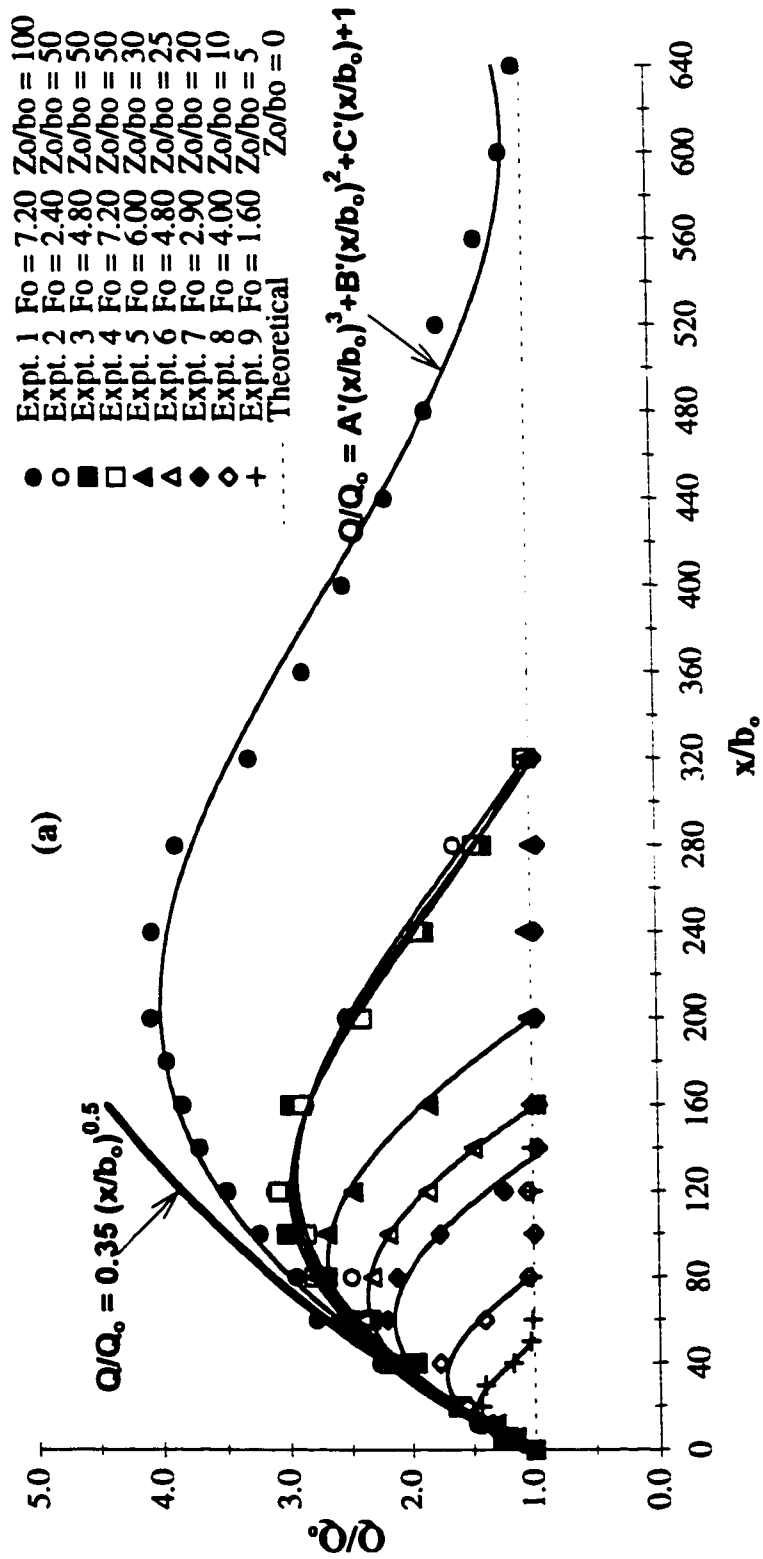


Fig. 5.20(a) Variation of the surface jet discharge with distance

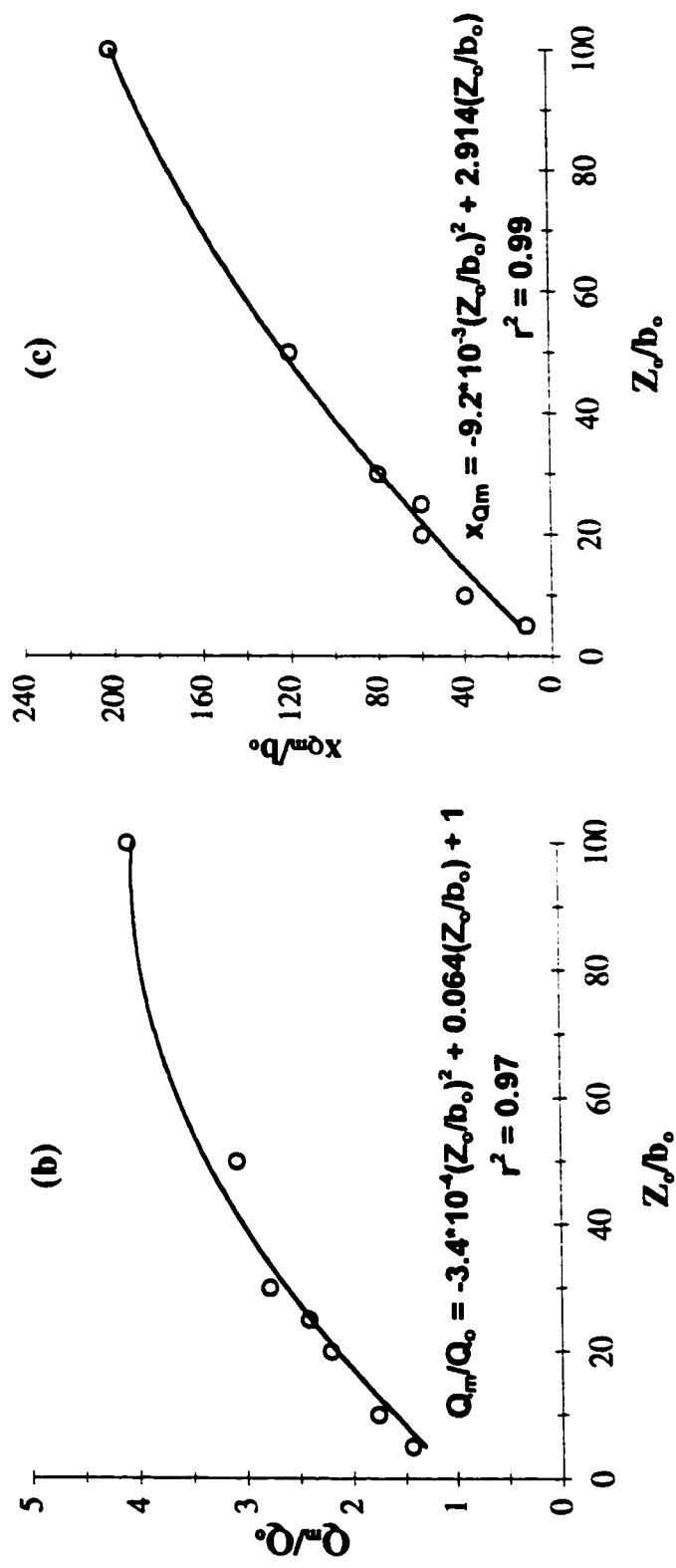


Fig. 5.20(b-c) Effect of Z_o/b_o on the magnitude and location of the maximum discharge

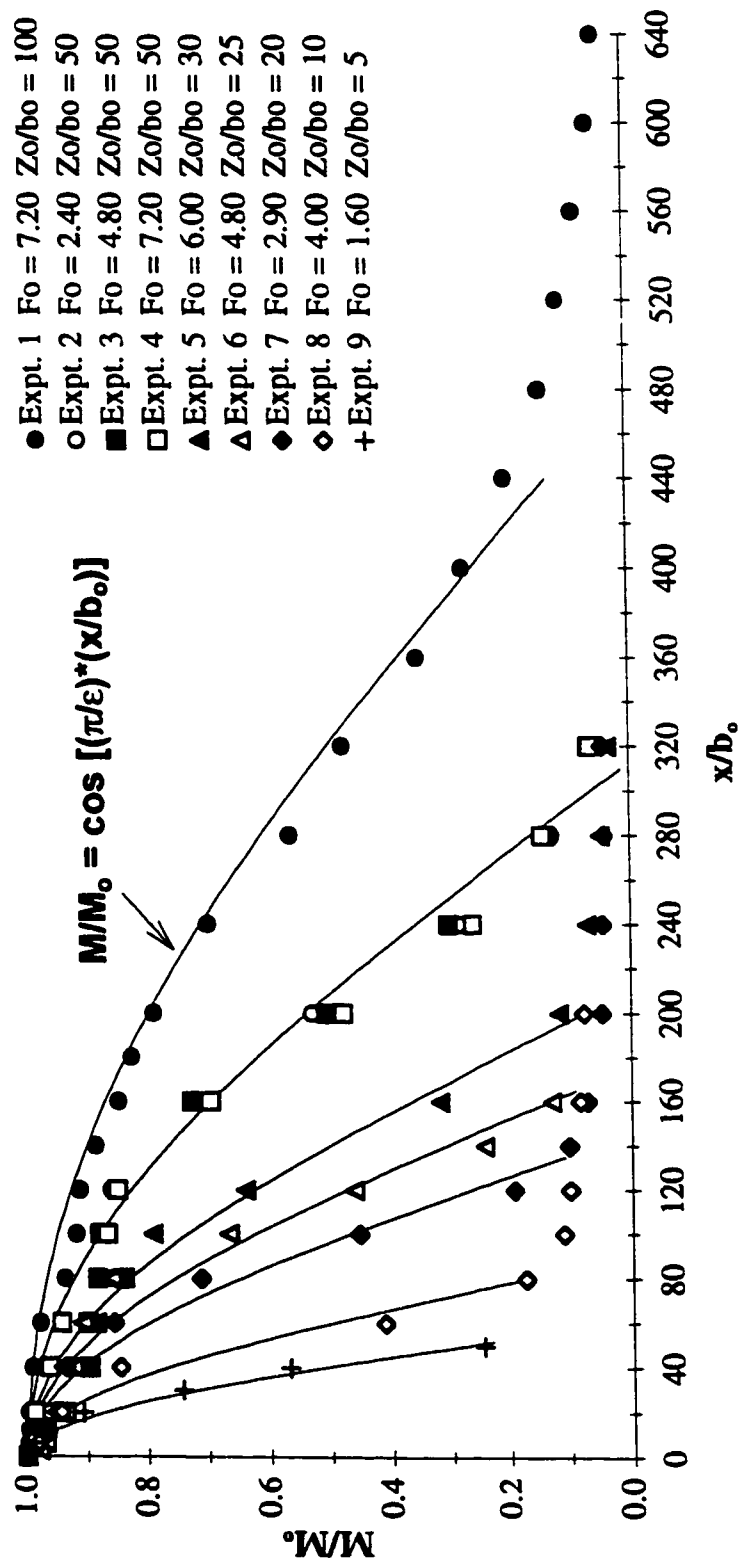


Fig. 5.21 Variation of the surface jet momentum flux with distance

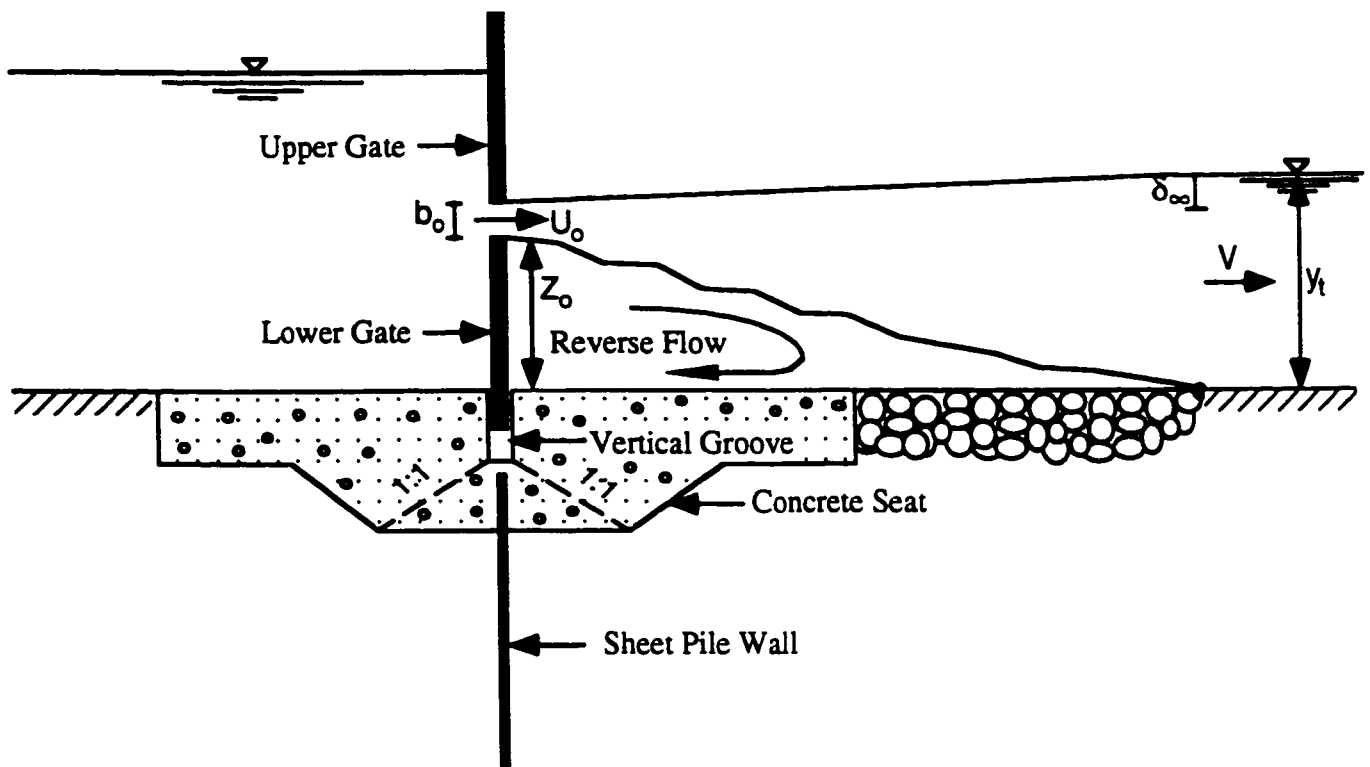


Fig. 5.22 Modified regulators

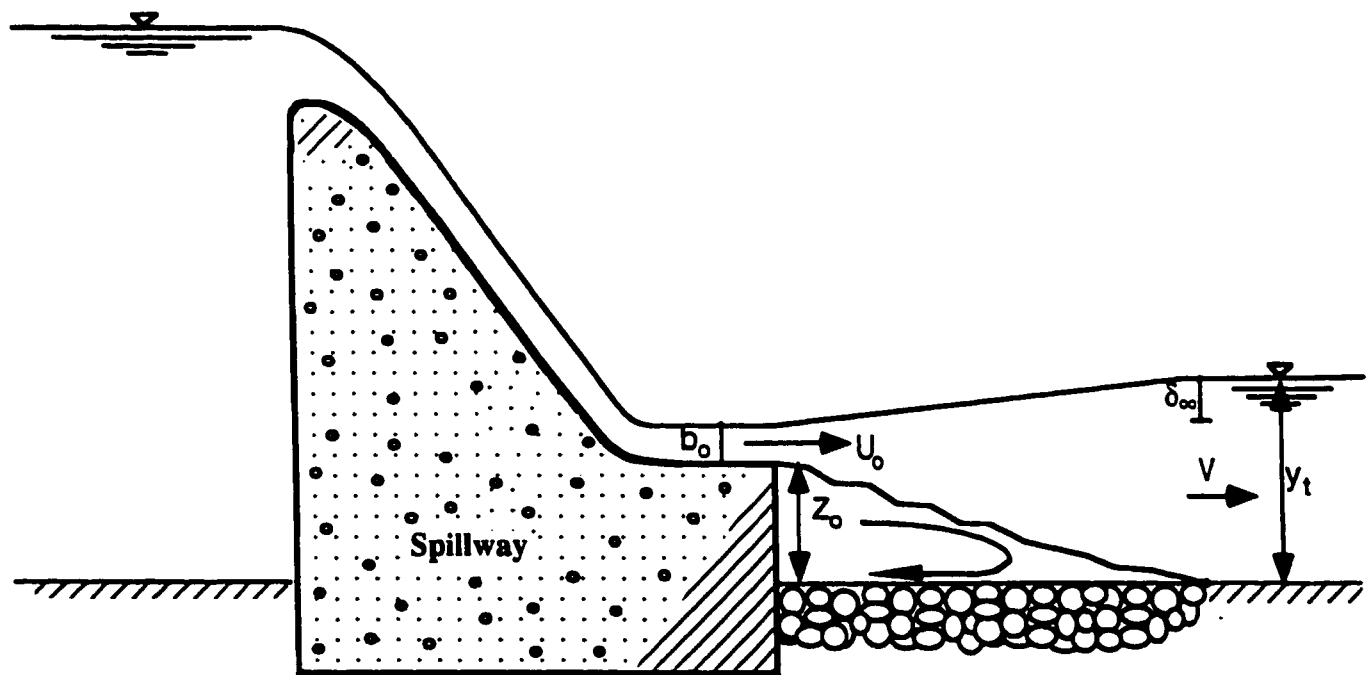


Fig. 5.23 Modified spillway

Chapter 6

Plane Turbulent Wall Jets in Shallow Tailwater*

6.1 Introduction

For turbulent jets discharged from slots or orifices in walls into large ambients at rest, it has been generally assumed (Albertson et al. (1950), Schlichting (1960), Rajaratnam (1976)) that the momentum flux would be preserved. In some experimental investigations (Miller and Comings (1957); Goldschmidt and Eskinazi (1966); Heskestad (1965) and Kotsovinos (1975)), it has been noticed that the momentum flux decayed to some extent at large distances from the origin of the jets. Kotsovinos (1978) noticed that the momentum flux could decay to about 80% of that at the source at a longitudinal distance equal to $100 b_0$ for plane turbulent jets where b_0 is the slot width. Kotsovinos (1978) attributed this loss of momentum flux to the negative momentum carried by the entrained fluid which approached the jet at a angle of about $\pi/4$ radians from the forward direction of the jet. Based on an approximate integral analysis, Kotsovinos (1978) developed an equation to describe the variation of the momentum flux with the longitudinal distance from the nozzle producing the jet. Schneider (1985) attempted to explain this decay of momentum flux by combining the analysis of the jet with the flow in the region surrounding the jet. Schneider coupled the jet and the induced outer flow through momentum and volume balances.

Swean Jr. et al. (1989) studied the variation of momentum and mass fluxes as well as the growth for plane turbulent surface jets with limited depth of tailwater. They conducted 10 experiments to study the effect of the finite depth of tailwater on the characteristics of the surface jet and to observe the variation of the momentum and

*The main content of this chapter has been submitted to the Journal of Hydraulic Research of the International Association of Hydraulic Research for possible publication.

volume fluxes and the breakdown of the surface jet due to the limited depth of the ambient. They also used the experimental results of Vanvari and Chu (1974) and Rajaratnam and Humphries (1984). Their results showed a momentum decay and a break down (or variation from that of jets in infinite ambient) in the velocity and length scales due to the jet confinement. The study of Swean Jr. et al. (1989) provides a general understanding of the problem of turbulent jets with a finite depth of tailwater. However, their analysis did not consider the adverse pressure gradient in the momentum balance. As the depth of flow decreases in the vicinity of the gate, it is important to include the depression in the pressure force due to this decreasing depth.

For plane turbulent wall (or bed) jets discharged into relatively deep tailwater, if the shear stress on the bed is neglected, it has been generally assumed (see for example: Rajaratnam 1976) that, as in the case of plane free jets, the momentum flux would be preserved. Since the plane wall jet model has been used to analyze a number of flows in hydraulic structures, wherein the tailwater depth may not even be very large, it was thought that it would be interesting and useful to study the variation of the momentum flux in a plane wall jet with a range of tailwater levels, including the effects of the bed friction.

The double-leaf gate energy dissipator was introduced in chapter 4 where the jet velocity and the momentum flux were found to decay rapidly. To understand the reasons behind this decay, it was important to study the behavior of plane turbulent jets, of simpler geometry, in shallow tailwater. In chapter 5, plane turbulent surface jet in shallow tailwater were presented. In this chapter, plane turbulent wall jets in shallow tailwater are presented.

This chapter presents the results of a theoretical and experimental investigation of plane turbulent wall jets with finite depth of tailwater, dealing with the growth of the jet, decay of the maximum velocity, the variation of the momentum and volume fluxes

in the forward flow region of the wall jet, the variation of the shear stress on the bed and the effect of the depth of tailwater on these properties.

6.2 Theoretical Considerations

From the first glance, it might appear that the theoretical formulation of the plane wall jets is very similar to that of the plane surface jets with the only difference in the location of the nozzle. But there is a subtle difference related to the tailwater depth in the two problems which makes surface jets and wall jets distinguishable. In surface jets, the tailwater depth is divided into three parts which are, from bottom to top, the offset distance, the slot width and the rise of the water surface elevation above the upper edge of the slot (see Fig. 5.1(a)). The third factor, or the rise of the water surface elevation, is dependent on the jet thickness, the Froude number and the offset distance (see Eq. 5.5). The surface jet (by definition) issues from a slot with the water surface elevation exactly at the upper edge of the slot. Hence, any surface jet with a specific thickness, offset distance and Froude number can only form with a specific value of the tailwater depth. In other words, in the surface jet problem, the tailwater depth is dependent on the different characteristics of the jet. In the wall jet, the tailwater depth is an independent variable. In other words, a wall jet with a specific thickness and Froude number can form with an infinite number of tailwater depths. This subtle difference makes the theoretical formulation totally different in the two problems. In the surface jet problem, the tailwater depth was manipulated through its three components while in the wall jet it is treated as an independent variable.

Consider a plane turbulent wall jet of thickness b_0 with a flow rate per unit width of Q_0 and momentum flux per unit width of M_0 entering a rectangular channel, tangentially on its bed as shown in Fig. 6.1(a). Let U_0 be the velocity of the jet at the nozzle. The downstream control gate is adjusted so that the tailwater depth y_t is large

enough to make the water level immediately downstream of the gate (housing the slot) horizontal. Taking the tailwater surface elevation as a reference, our experimental observations (presented later) show a depression, δ_w , in the water surface elevation at the gate (see Fig. 6.1(a-b) and Fig. 6.2). It appears that the depression in the water surface elevation at the vicinity of the wall is created to produce an adverse pressure gradient to drive the return flow above the wall jet, for the jet entrainment.

Assuming hydrostatic pressure distributions on the gate containing the slot and at the downstream section where the expanding wall jet attaches to the water surface and occupies the whole depth, and that the velocity distribution at the nozzle and the downstream section is uniform (see Fig. 6.1(b)), a theoretical analysis was performed and is presented herein.

6.2.1 Neglecting the bed shear stress

The continuity and the momentum equations could be written as

$$U_o b_o = V y_t \quad (6.1)$$

$$M_o - M_{\infty} = \gamma \delta_w (y_t - \delta_w) + 0.5 \gamma \delta_w^2 \quad (6.2)$$

where V is the uniform velocity at the downstream section, M_{∞} and M_o are, respectively, the momentum fluxes, per unit width, at the downstream section and at the nozzle, and γ is the weight per unit volume of water.

Multiplying Eq. 6.1 by $\rho U_o V$ where ρ is the mass density of water and rearranging, Eq. 6.1 is rewritten as

$$\frac{M_{\infty}}{M_o} = \frac{V}{U_o} = \frac{1}{y_1/b_o} = \frac{1}{\eta} \quad (6.3)$$

where η is the tailwater depth ratio equal to y_1/b_o .

Dividing Eq. 6.2 by M_o and rearranging, Eq. 6.2 becomes

$$1 - \frac{M_{\infty}}{M_o} = \frac{2\theta(\eta - \theta) + \theta^2}{2F_o^2} \quad (6.4)$$

where θ is the depression ratio at the gate, equal to δ_w/b_o and F_o is the Froude number at the slot equal to $[U_o/(gb_o)^{0.5}]$ and g is the acceleration due to gravity.

Solving equations 6.3 and 6.4, we obtain a quadratic equation in θ

$$\eta\theta^2 - 2\eta^2\theta + 2(\eta - 1)F_o^2 = 0 \quad (6.5)$$

The negative root of Eq. 6.5 was considered as the relevant solution which can be written as

$$\theta = \eta - \sqrt{\eta^2 - 2\left(\frac{\eta - 1}{\eta}\right)F_o^2} \quad (6.6)$$

Eq. 6.6 indicates that in submerged flows below the gate (either submerged jumps or wall jets), if the Froude number and the tailwater depth ratio are known, the drop in the water surface elevation at the gate can be predicted. According to Eq. 6.6, an increase in the Froude number F_o results in a larger drop in the water surface elevation at the

gate and its vicinity which in turn creates a steeper water surface slope for driving a larger return flow.

If θ_r and η_r are the values of θ and η for the corresponding free hydraulic jump at the gate, it can be shown that

$$\theta_r = (\eta_r - 1) \quad (6.7)$$

Combining Eqs. 6.6 and 6.7 results in a quadratic equation, the solution of which can be written as

$$\eta_r = 0.5 \left(\sqrt{1 + 8F_o^2} - 1 \right) \quad (6.8)$$

This is the well-known Belanger equation.

If $F_{\delta w}$ is the reduction in the hydrostatic pressure force at the gate corresponding to a depression of δ_w in the water surface elevation, it can be shown that

$$\frac{F_{\delta w}}{M_o} = 1 - \frac{M_w}{M_o} = \frac{\eta - 1}{\eta} \quad (6.9)$$

6.2.2 Considering the bed shear stress

The integrated bed shear stress from the gate up to the section at which the wall jet surfaces can be expressed in terms of the inlet momentum flux as

$$F_\tau = \int_{x=0}^{x=L_e} \tau dx = \epsilon M_o \quad (6.10)$$

where F_t is the integrated bed shear stress per unit width, τ is the bed shear stress at a distance x from the gate, ϵ is the shear force coefficient equal to F_t/M_o and L_e is the distance from the gate to the section where the wall jet surfaces which may be referred to as the length of the recirculation region or surface eddy. The momentum balance equation can be written as

$$M_o - M_e - \epsilon M_o = \gamma \delta_w (y_t - \delta_w) + 0.5 \gamma \delta_w^2 \quad (6.11)$$

Eq. 6.1 & Eq. 6.11 can be rearranged and solved together to finally give a quadratic equation in θ

$$\eta \theta^2 - 2\eta^2 \theta + 2[(1 - \epsilon)\eta - 1]F_o^2 = 0 \quad (6.12)$$

The negative root of Eq. 6.12 was considered as the relevant solution and can be written as

$$\theta = \eta - \sqrt{\eta^2 - 2\left(\frac{\eta(1 - \epsilon) - 1}{\eta}\right)F_o^2} \quad (6.13)$$

Eq. 6.13 is the general form of Eq. 6.6 with the bed shear stress taken into consideration. Substituting Eq. 6.7 in Eq. 6.13 results in a cubic equation

$$\eta_r^3 - (1 + 2F_o^2 - 2\epsilon F_o^2)\eta_r + 2F_o^2 = 0 \quad (6.14)$$

The above equation has three real roots. The following root is considered as the relevant solution

$$\eta_r = \frac{2}{\sqrt{3}} \sqrt{1 + 2F_o^2} \cos(\phi/3) \quad (6.15)$$

where ϕ is given by the equation

$$\phi = \tan^{-1} \left(\frac{\sqrt{\frac{4(1 + 2F_o^2 - 2\epsilon F_o^2)^3}{27} - (2F_o^2)^2}}{-(2F_o^2)^2} \right) \quad (6.16)$$

Eq. 6.15 is the general equation of the free hydraulic jump and Eq. 6.8 (known as Belanger Equation) is a special case that is only valid when the bed shear stress is neglected. These equations, although of different forms, give the same results when the shear force coefficient ϵ is equal to zero.

It should be mentioned that the evaluation of M_-/M_o is not affected by the consideration of the bed shear stress and is still represented by Eq. 6.3. With the inclusion of the bed shear stress, Eq. 6.9 becomes

$$\frac{F_{bw}}{M_o} = 1 - \frac{M_-}{M_o} - \frac{F_t}{M_o} = \frac{\eta(1 - \epsilon) - 1}{\eta} = \frac{\eta - 1}{\eta} - \epsilon \quad (6.17)$$

Based on these theoretical formulations, the variation of θ , which is equal to the depression in the water surface elevation at the wall in terms of the slot width, with $\eta =$

y_t/b_o , is shown in Fig. 6.3(a) as solutions of Eq. 6.13 and Eq. 6.6, with and without considering the bed shear stress, respectively (ϵ equal to 0.15 and 0), for values of the Froude number varying from 2 to 10. Fig. 6.3(a) also shows the θ - η relationship for the free jump represented by Eq. 6.7. Fig. 6.3(a) shows that for any Froude number, the maximum value of θ occurs in the free jump when there is no submergence and that θ decreases after the jump gets submerged and η increases. The values of η at the intersections of Eq. 6.6 and Eq. 6.13 with the free jump line, for the different Froude numbers, are given by Eq. 6.8 and Eq. 6.15 respectively. In Fig. 6.3(a), for a given Froude number, the continuous line shows the variation of θ for $\epsilon = 0.15$ whereas a string of symbols shows the corresponding variation for ϵ equal to zero. Fig. 6.3(a) shows that the inclusion of the bed shear stress reduces the water surface depression at the gate. This difference increased with the Froude number for a constant η and decreased as η increased for a constant Froude number.

In Fig. 6.3(b) three sets of curves are shown for Froude numbers equal to 10.0, 6.00 and 3.00 for several values of ϵ from 0 to 0.25. For a given η , the height of the spread between the set of curves including the string of points, increased with the Froude number, indicating the importance of considering the bed shear stress for relatively large Froude numbers. For a given Froude number, the corresponding height decreased as η increased, reaching almost zero for very large values of η , indicating the importance of the bed shear stress for relatively shallow tailwater.

Fig. 6.4(a-b) show the variation of the sequent depth ratio η_f , in a free hydraulic jump, with the Froude number F_o and the shear force coefficient ϵ ,

respectively. The curves in Fig. 6.4(a) were drawn for the shear force coefficient ϵ varying from 0.00 to 0.25, whereas the curves in Fig. 6.4(b) were drawn for three values of the Froude number of 10.0, 5.0 and 2.0. In Fig. 6.4(a), the bold line represents Eq. 6.8 (Belanger equation) and the white circles represent Eq. 6.15 (for $\epsilon = 0.00$). Clearly, both equations gave identical results though they have different forms. All the other curves, in Fig. 6.4(a), represent Eq. 6.15 for different values of ϵ . While Fig. 6.4(a) shows that the deviation between Eq. 6.8 and Eq. 6.15 increases with the Froude number, Fig. 6.4(b) indicates the same for the increase in ϵ .

Eq. 6.3 is plotted in Fig. 6.5 to show the variation of the normalized momentum flux (M_w/M_o) with the tailwater depth ratio η . Fig. 6.5 shows that the momentum flux decays rapidly with η up to 30 after which the decrease is rather negligible. It was found that the minimum momentum flux, in terms of that at the nozzle, is equal to 0.04, 0.02, 0.013 and 0.01, respectively, for η equal to 25, 50, 75 and 100. Fig. 6.5 also shows the variation of the loss of hydrostatic pressure force at the gate due to the depression in the water surface in terms of the momentum flux at the slot with the tailwater depth ratio η with and without bed friction. It can be observed in Fig. 6.5 that the bed shear stress reduces (F_{bw}/M_o) by an amount of ϵ .

6.3 Dimensional Analysis

Considering the problem illustrated in Fig. 6.1(a), any property (m) of the flow can be expressed as a function of various parameters of the flow, fluid and channel dimensions as

$$m = f(U_o, g, b_o, y_t, \rho, \mu) \quad (6.18)$$

The above relation can be represented in a dimensionless form as follows

$$M = f' \left[\frac{U_o}{\sqrt{gb_o}}, \frac{\rho U_o b_o}{\mu}, \frac{y_t}{b_o} \right] \quad (6.19)$$

The above relation shows that any property of the flow can be expressed as a function of the Froude number, the Reynolds number and the tailwater depth ratio. For large values of the Reynolds number, $R = \rho U_o b_o / \mu$, where ρ and μ are respectively the mass density and dynamic viscosity of the fluid, viscosity is known to have negligible effects. Hence, Eq. 6.21 becomes

$$M = f''[F_o, \eta] \quad (6.20)$$

Eq. 6.20 shows that the main variables affecting the different characteristics of the flow are the Froude number and the tailwater depth ratio.

6.4 Experimental Study

6.4.1 Experimental arrangement

Plane turbulent wall jets were produced in a flume, 0.446 m wide, 0.60 m deep and 7.6 m long, with aluminum bottom and Plexiglas sides (see Fig. 6.6). Two pumps were used to supply the head-tank feeding the flume. The discharge was measured by a magnetic flow-meter located in the supply line. Water entered the flume under a sluice gate with a streamlined lip thereby producing an uniform jet with a thickness of b_o (see Fig. 6.7). A tailgate was used to control the tailwater depth in the flume.

A Prandtl tube with an external diameter of 3.0 mm was used to measure the time-averaged longitudinal velocity u (see Fig. 6.8). Velocity distributions of the forward and backward flows, were measured along vertical sections at different longitudinal distances from the nozzle producing the jet. The Prandtl tube was also used as a Preston tube for measuring the bed shear stress (Preston (1954); Patel (1965)). All of the measurements were taken in the middle third of the flume.

One transducer (Validyne model DP45-16 Northridge, Calif) was used in the experiments to measure the pressure difference indicated by the Prandtl tube. The output of the transducer was connected to a Macintosh IIfx computer. When the pressure difference was outside the transducer range (± 25.4 mm), the pressure connections were switched to a manometer board (see Fig. 6.8). The computer displayed the results on a strip chart on the screen in real time. When the required number of samples (usually 5000) were recorded at each point with a sampling rate of 40 samples/s, the computer processed all the samples to obtain the mean value and the standard deviation for each variable and saved the results in an open file. The computer programs used in the experiments were written in LabView Language.

6.4.2 Experiments

Table 1 shows the primary details of the experiments of series A. The first two experiments were conducted for the present study and the results of experiments 3 to 6 (conducted in the same flume) were taken from Wu and Rajaratnam (1995). In these experiments, the tailwater depth ratio η was equal to 50, 50, 45, 35, 30 and 25 and the Froude number was equal to 8.0, 4.0, 5.5, 7.5, 7.5 and 7.5, respectively. The submergence factor (Rajaratnam, 1965) defined as $S = (y_t - y_2)/y_2 = (\eta/\eta_t - 1)$, ranged approximately between 2.00 to 9.00 where y_2 in Table 1 is the subcritical sequent depth for the hydraulic jump, obtained from the Belanger equation. The Reynolds number of

the jet was in the range of 12500 to 42900. Figs. 6.9(a-d) show the wall jets produced with the tailwater depth ratio equal to 25, 30, 40 and 50 respectively.

A further series of experiments (series B) were conducted mainly to measure the drop in the water surface elevation at the gate, from that of the tailwater, as well as the length of the surface eddy. The series B experiments were conducted for Froude numbers equal to 2, 4, 6, 8, 10 with the tailwater depth ratio η varying from η_r to 50.

6.5 Experimental Results and Analysis

6.5.1 Eddy length

As soon as the jet issues from the slot, a recirculating flow region starts to develop above the jet (see Fig. 6.1(b)). If L_e is the length of the recirculating region (or the eddy length), it could be written that

$$L_e = f[U_o, b_o, g, \rho, \mu, y_t] \quad (6.21)$$

Using the Pi theorem, it can be shown that

$$\frac{L_e}{b_o} = f_1 \left[\frac{y_t}{b_o}, \frac{U_o}{\sqrt{gb_o}}, \frac{\rho U_o b_o}{\mu} \right] \quad (6.22)$$

For large values of the Reynolds number, viscous effects may be neglected and Eq. 6.22 reduces to

$$\frac{L_e}{b_o} = f_2 \left[\frac{y_t}{b_o}, F_o \right] \quad (6.23)$$

As the sequent-depth ratio η_r is a function of mainly the Froude number (Eq. 6.8), the above equation may be rewritten as

$$\frac{L_e}{b_o} = f_3[\eta, \eta_r] \quad (6.24)$$

If Eq. 6.24 is rewritten as

$$\frac{L_e}{b_o} = 6\eta_r + k(\eta - \eta_r) \quad (6.25)$$

Wherein the length of the free jump has been assumed to be equal to approximately 6 times the subcritical sequent depth and k is an empirical coefficient. The coefficient k was evaluated using the observations made in this study and those of Rajaratnam (1965) and was found to be equal to 4.0. Hence Eq. 6.25 can be written as

$$\frac{L_e}{b_o} - 6\eta_r = 4.0(\eta - \eta_r) \quad (r^2 = 0.97) \quad (6.26)$$

where r^2 is the correlation coefficient. The experimental results are shown plotted in Fig. 6.10 with $(L_e/b_o - 6\eta_r)$ versus $(\eta - \eta_r)$.

6.5.2 Velocity profiles

Figs. 6.11(a-f) show typical velocity fields along with the water surface profiles of the wall jets for experiment 1 to experiment 6 respectively. They show the velocity profiles in the forward as well as reverse flows at several sections with x/b_o varying from 6 to 200. In these figures, y is the distance above the bed. In Figs. 6.11(a-f), it

may be noticed that the water surface in the vicinity of the gate is approximately horizontal and a rise in the water surface elevation may be observed further downstream. The depression in the tailwater elevation at the gate is also shown in Fig. 6.11(a-f). The strong shear layer that separates the forward and the backward flows is distinct in the six experiments. No velocity measurements could be taken within this layer. The section at which the jet surfaces was found using dye injection. The maximum reverse velocity, at any station, was found to occur at or very close to the water surface. The maximum reverse velocity for any experiment was found to occur at a distance of $L_e/2$ from the gate where L_e is the length of the surface eddy.

6.5.3 Wall jet

Returning to the discussion on the velocity field, velocity measurements in the forward flow clearly show the structure of the wall jet. To test for the similarity of the velocity profiles, the maximum velocity, u_m , at any station was chosen as the velocity scale. It occurs at a distance of δ above the bed where δ is the boundary layer thickness. The length scale, b , is equal to y where $u = 0.5u_m$ and $\partial u/\partial y < 0$ (see Fig. 6.1(c)). Figs. 6.12(a-b) show the velocity distributions and the similarity profiles in the developing flow region, which is the region between the slot and the end of the potential core. Fig. 6.12(b) shows the variation of u/u_m with y/b for a station located approximately in the middle of the developing region (at $x/b_o = 6$). Experiments 1, 2 and 3 showed similar distributions of the velocity profiles, at this station, in the developing flow region.

The velocity distributions and the similarity profiles in the fully-developed flow region ($x/b_o \geq 12$) are shown in Fig. 6.13(a-l) for experiment 1 to experiment 6, respectively which clearly show the wall jet features. In the similarity profiles, u_m and b were chosen as the velocity and length scales, respectively. Fig. 6.14 shows a consolidated plot of all the data for the six experiments. Although some velocity

profiles were taken for larger values of x/b_o , these profiles were excluded as they were somewhat different from those shown in Fig. 6.13. A study of these profiles established that except for the sections far away from the nozzle (in the region where the water surface elevation begins to rise (see Fig. 6.11(a-f)), the velocity distributions are similar. The similarity profile follows that of the classical plane turbulent wall jet except near the upper end of the profile where it showed a linear distribution. This deviation, between the similarity profile of the present data and that of the classical wall jet profile, is possibly due to the interaction between the forward and the backward flows.

6.5.4 Velocity and length scales

Having found that the velocity profiles in the forward flow are similar, it is necessary to study the variation of the velocity scale, u_m , and the length scale, b , with the distance x . Fig. 6.15(a) shows the decay of the maximum velocity with the longitudinal distance from the nozzle. The maximum velocity at the nozzle was varied from 1.25 to 2.86 m/s and u_m was measured for x up to about 2.00 m. At the last section, the maximum velocity was in the range of 0.25-0.60 m/s. Fig. 6.15(b) shows the decay of the maximum velocity u_m at any section in terms of the velocity of the jet at the nozzle U_o with the normalized distance from the gate x/b_o . The decay of the maximum velocity shows the existence of two stages. The first stage represents the plane wall jet with large depth of tailwater and starts at the end of the development region. The decay of the normalized velocity scale in this region can be described by the following equation

$$\frac{u_m}{U_o} = \frac{4.00}{\sqrt{x/b_o}} \quad (6.27)$$

The coefficient in Equation 6.27 is larger than the value of 3.5 suggested for plane turbulent wall jets with large submergence (Rajaratnam 1976). The second stage of the velocity decay starts at a distance x_o from the gate, where the observations begin to deviate from the curve described Eq. 6.27 and the maximum velocity decays more rapidly. This behavior can be noticed more easily in Fig. 6.15(c) which shows the variation of $(U_o/u_m)^2$ with x/b_o where Eq. 6.27 would plot as a straight line. The decay of the maximum velocity in this second stage is linear and can be described by the equation

$$\frac{u_m}{U_o} = A \left(\frac{x}{b_o} \right) + B \quad (6.28)$$

where B is a constant equal to 0.82 and A was found to be a function of the tailwater depth ratio $\eta = y_t/b_o$ and was described by the equation

$$A = 7 * 10^{-5}(\eta - 100) \quad (r^2 = 0.95) \quad (6.29)$$

The value of x_o was also found to be a function of the tailwater depth ratio (see Fig. 6.15(d)) and is described by the equation

$$\left(\frac{x_o}{b_o} \right) = 2.85(\eta - 2.00) \quad (r^2 = 0.995) \quad (6.30)$$

These considerations show that as the tailwater depth ratio decreases, the length of the first stage of decay decreases and the maximum-velocity decay will be more rapid. It

was also found that the Froude number does not have any significant effect on the velocity decay.

The growth of the length scale of the jet (or half-width) with distance is shown in Fig. 6.16. The growth rate was 0.076 for x/b_o up to about 120, which is somewhat larger than the value of 0.068 suggested by Rajaratnam (1976) for plane turbulent wall jets with large submergence. The growth rate of the jet half-width was found to change at a particular value of x/b_o . For experiments 1, 2 and 3, this breakdown occurred at $x/b_o = 140, 140$ and 120 , respectively, whereas for experiments 4, 5 and 6 this breakdown was not clear. After the breakdown, the jet half-width grew with a rate of 0.20 in experiment 1 and 2 and 0.35 in experiment 3. It is interesting to note that the breakdown in the growth of the jet half-width (for at least the three experiments) and in the decay of the maximum-velocity occurred at the same location, x_o , which is described by Eq. 6.30.

6.5.5 Wall-jet discharge

For all the experiments, at every section where velocity observations were made, the forward flow rate Q and momentum flux per unit width M were calculated as the sum of the fluxes through thin strips (whose thicknesses varied from 2.5 to 25 mm). Fig. 6.17(a) shows the variation of the relative discharge Q/Q_o in the wall jet with distance x/b_o . A study of Fig. 6.17(a) shows that the relative discharge increases with the relative distance at the same rate as that of the wall jet with large tailwater up to a certain section and then deviates from it, to eventually reach the value of one. Secondly, the maximum value of the relative discharge decreases from about 4 for $y_t/b_o = 50$ to 2.5 for $y_t/b_o = 25$. If x_{Qm} is the longitudinal distance where the relative discharge reaches the maximum value, x_{Qm}/b_o was found to decrease from about 140 for $y_t/b_o = 50$ to about 65 for $y_t/b_o = 25$. The variation of Q/Q_o with x/b_o could be represented by the cubic equation

$$\frac{Q}{Q_0} = A' \left(\frac{x}{b_0} \right)^3 + B' \left(\frac{x}{b_0} \right)^2 + C' \left(\frac{x}{b_0} \right) + 1 \quad (6.31)$$

where the coefficients A' , B' and C' were found to be functions of the tailwater depth ratio, η as described by the following equations

$$A' = -0.43168 * 10^{-10} \eta^4 + 0.68303 * 10^{-8} \eta^3 - 0.40273 * 10^{-6} \eta^2 + 0.10608 * 10^{-4} \eta - 0.10802 * 10^{-3} \quad (r^2 = 1.00) \quad (6.32)$$

$$B' = 0.26089 * 10^{-8} \eta^4 - 0.41366 * 10^{-6} \eta^3 + 0.24496 * 10^{-4} \eta^2 - 0.64942 * 10^{-3} \eta + 0.66369 * 10^{-2} \quad (r^2 = 1.00) \quad (6.33)$$

$$C' = 0.58533 * 10^{-7} \eta^4 - 0.91320 * 10^{-5} \eta^3 + 0.51054 * 10^{-3} \eta^2 - 0.11970 * 10^{-1} \eta + 0.12740 \quad (r^2 = 1.00) \quad (6.34)$$

For a wall jet with a very large value of η , the variation of Q/Q_0 with x/b_0 should be independent of the tailwater depth ratio and for such a jet, Q/Q_0 would be proportional to $(x/b_0)^{0.50}$. This equation is shown plotted in Fig. 6.17(a) with the value of the coefficient in this relation equal to 0.35.

Figs. 6.17(b-c) show linear variations of the maximum value of the relative flow Q_m/Q_0 and the distance where this occurs x_{Qm}/b_0 with the tailwater depth ratio η and these variations could be described by the equations

$$\frac{Q_m}{Q_o} = 0.058\eta + 1.00 \quad (r^2 = 0.97) \quad (6.35)$$

$$\frac{x_{Qm}}{b_o} = 2.77\eta \quad (r^2 = 0.89) \quad (6.36)$$

6.5.6 Bed shear stress

The integrated bed shear stress is one of the main forces involved in the momentum balance equation and it was essential to evaluate, experimentally, the bed shear stress and its scales. Fig. 6.18(a) shows the variation of the bed shear stress with distance. Fig. 6.18(b) shows the variation of the skin friction coefficient $C_{fo} = \tau/(\rho U_o^2/2)$ with x/b_o . At $x/b_o = 0$, C_{fo} was in the range of 0.006 to 0.007. A breakdown in the skin friction coefficient C_{fo} can be observed in Fig. 6.18(b) and this breakdown is very similar to that occurred in the maximum velocity decay (see Fig. 6.15(b-c)). The distance at which this breakdown occurred could also be described by Eq. 6.30. Fig. 6.18(c) shows a similarity profile where the maximum shear stress τ_m and b_τ , which is the distance between τ_m and $0.5\tau_m$, were chosen as the shear and length scales respectively. The distributions are quite similar up to a distance of $4b_\tau$ after which the similarity breaks down. The length scale b_τ was found to be a function of the tailwater depth, y_t and the Reynolds number, R and this relationship can be described by the equation

$$\frac{b_\tau}{y_t} = 6.10^{-6}R + 0.3 \quad (r^2 = 0.97) \quad (6.37)$$

Fig. 6.18(d) shows the variation of the shear force coefficient $\epsilon_x = F_{\tau x} / M_o$ with x/b_o where ϵ_x and $F_{\tau x}$ are respectively the shear force coefficient and the integrated bed shear stress at a longitudinal distance x measured from the slot. The values of ϵ_x and $F_{\tau x}$, where $x = L_e$, would be ϵ and F_{τ} . At $x/b_o = 160$, the shear force coefficient ranged between 0.12-0.15 with an average value of 0.135. The variation of an average value of ϵ_x with x/b_o could be represented by the following equation

$$\epsilon_x = -0.6635 * 10^{-9} \left(\frac{x}{b_o} \right)^4 + 0.2717 * 10^{-6} \left(\frac{x}{b_o} \right)^3 - 0.4125 * 10^{-4} \left(\frac{x}{b_o} \right)^2 + 0.3198 * 10^{-2} \left(\frac{x}{b_o} \right) \quad (r^2 = 0.98) \quad (6.38)$$

Fig. 6.19 shows a plot of Eq. 6.13 with θ against η for ϵ equal to 0.12 & 0.15 and for the Froude number equal to 10.0, 8.0, 6.0, 4.0 and 2.0 along with the experimental data of series B. In Fig. 6.19, the experimental observations of series B are well represented by Eq. 6.13 with ϵ in the range of 0.12-0.15.

6.5.7 Wall-jet momentum flux

It was mentioned earlier that the wall jet could lose a substantial portion of its momentum flux as it travels downstream when the depth of tailwater is relatively shallow, due to the entrainment of the recirculating flow with opposite momentum. Fig. 6.20 shows the variation of the normalized momentum flux of the wall jet with the normalized distance from the nozzle for different tailwater depth ratios. Fig. 6.20 also shows that the losses in the normalized momentum flux are 0.980, 0.978, 0.971, 0.967 and 0.960 for tailwater depth ratios equal to 50, 45, 35, 30 and 25, respectively.

The momentum flux may be considered preserved for a distance of x_{M1} , measured from the gate, after which it starts to decay. If x_{M2} is the distance at which the momentum flux approaches zero, a simple function was found to describe the decay in the momentum flux and is written as

$$\frac{M}{M_o} = \cos \left[\left(\frac{x/b_o - x_{M1}/b_o}{x_{M2}/b_o - x_{M1}/b_o} \right) \cdot \pi/2 \right] \quad (6.39)$$

It should be noted that for the range of η used in this study, the value of x_{M2}/b_o is approximately equal to the normalized eddy length L_e/b_o and hence Eq. 6.26 could be used to predict L_e/b_o for use in Eq. 6.39. Further, x_{M1}/b_o was found to increase from 50 for $\eta = 25$ to about 75 for $\eta = 50$ and the variation of x_{M1}/b_o with η can be described by the following equation

$$\frac{x_{M1}}{b_o} = -0.0181\eta^2 + 2.3855\eta \quad (r^2 = 1.00) \quad (6.40)$$

It is interesting to see that the distance at which the momentum flux starts to decay, x_{M1} , is very close to the distance at which the relative discharge, Q/Q_o , deviates from the corresponding curve of the wall jets in deep tailwater (see Fig. 6.17(a)).

6.6 Conclusions

For turbulent wall jets in shallow tailwater, it has been shown theoretically and experimentally that the momentum flux in the forward flow region of the wall jet is not preserved. In the theoretical study, the momentum loss was evaluated at a section just downstream of the line of the jet attachment to the free surface. The depression in the water surface elevation and the loss in the hydrostatic pressure force at the wall were evaluated with and without the bed shear stress. The experimental results showed that the length of the return-flow region is dependent on the tailwater depth ratio and the Froude number. The velocity profiles in the wall jet were found to be similar, in the developing as well as in the developed regions. Two stages were seen to exist in the decay of the maximum velocity in the region of fully developed flow. The rate of the velocity decay in the first stage was independent of the relative depth of the tailwater whereas the faster rate in the second stage depended on it. The length of the first stage of decay was directly proportional to the tailwater depth ratio. The length scale of the jet grew at a rate of 0.076 in the early stage and the rate of growth was much larger in the second stage. The volume flux in the wall jet with limited tailwater was affected significantly. The momentum flux was preserved for a certain distance after which it decayed rapidly. The momentum decay was correlated with the tailwater depth ratio, the eddy length and the relative longitudinal distance. On the whole, the results from this study highlight the effect of limited tailwater depth on the behavior of plane turbulent wall jets.

6.7 References

- Albertson, M. L., Dai, Y. B., Jensen, R. A. & Rouse, H. (1950). "Diffusion of submerged jets." Trans. ASCE, 115, 639-664.
- Goldschmidt, V., and Eskinazi, S. (1966). "Two phase turbulent flow in a plane jet." Trans. ASME, Series E, J. Appl. Mech., 33(4), 735-747.

- Heskestad, G. (1965). "Hot wire measurements in a plane turbulent jet." Trans. ASME, Series E, J. Appl. Mech., 32(4), 721-734.
- Kotsovinos, N. E. (1975). "A study of the entrainment and turbulence in a plane turbulent jet." W. M. Keck Lab. Hydr. Water Resources, Calif. Inst. Tech. Rept. KH R-32.
- Kotsovinos, N. E. (1978). "A note on the conservation of the axial momentum of a turbulent jet." J. Fluid Mech., 87(7), pp. 55-63.
- Miller, D. R., and Comings, E. W. (1957). "Static pressure distribution in the free turbulent jet." J. Fluid Mech., 3(10), pp. 1-16.
- Patel, V. C. (1965). "Calibration of the Preston tube and limitations on its use in pressure gradients." J. Fluid Mech., Vol. 23, pp. 185-208.
- Preston, J. H. (1954). "The determination of turbulent skin friction by means of Pitot tubes." J. Royal Aero. Soc., Vol. 54, pp. 109-121.
- Rajaratnam, N. (1965). "Flow below a submerged sluice gate as a wall jet problem." 2nd Australation Conf. on Hydraulics and Fluid Mechanics, Auckland, New Zealand.
- Rajaratnam, N. (1976). Turbulent Jets. Elsevier Publishing Co, The Netherlands, 304p.
- Rajaratnam, N., and Humphries, J. A. (1984). "Turbulent non-buoyant surface jet." J. Hydr. Res., 22(2), pp. 103-115.
- Schlichting, H. (1960). "Boundary layer theory." 4th Edn. McGraw-Hill: New York.
- Schneider, W. (1985). "Decay of momentum flux in submerged jets." J. Fluid Mech., 154(5), pp. 91-110.
- Swearn Jr, T. F., Ramberg, S. E., Plesniak, M. W. Stewart., M. B. (1989). "Turbulent surface jet in channel of limited depth." J. Hydr. Engrg., ASCE, 115(12), pp. 1587-1606.

- Vanvari, M. R., and Chu, V. H. (1974). "Two-dimensional turbulent surface jets of low Richardson number." Tech. Report No. 74-2 [FML], Fluid Mech. Lab., Dept. of Civ. Engrg. and Appl. Mech., McGill Univ., Montreal, Canada.
- Wu, S. and Rajaratnam, N. (1995). "Free jumps, submerged jumps and wall jets." J. Hydr. Res., 33(2), pp. 197-212.

Table 6.1. Primary details of experiments (series A)*

Expt.	b_o (mm)	W (mm)	U_o (m/s)	F_o	y_1 (mm)	y_2 (mm)	$\eta = y_1/b_o$	$S = \eta/\eta_f - 1$	R ($\times 10^3$)
(1)	(2)	(3)	(4)	(5)	(6)	(7)	(8)	(9)	(10)
1	10	446	2.50	8.0	500	108	50	3.63	25.00
2	10	446	1.25	4.0	500	52	50	8.68	12.50
3	10	446	1.72	5.5	440	73	45	5.04	17.20
4	15	446	2.86	7.5	530	151	35	2.51	42.90
5	15	446	2.86	7.5	460	151	30	2.05	42.90
6	15	446	2.86	7.5	390	151	25	1.59	42.90

* Experiments 3, 4, 5 and 6 were conducted by Wu and Rajaratnam (1995)

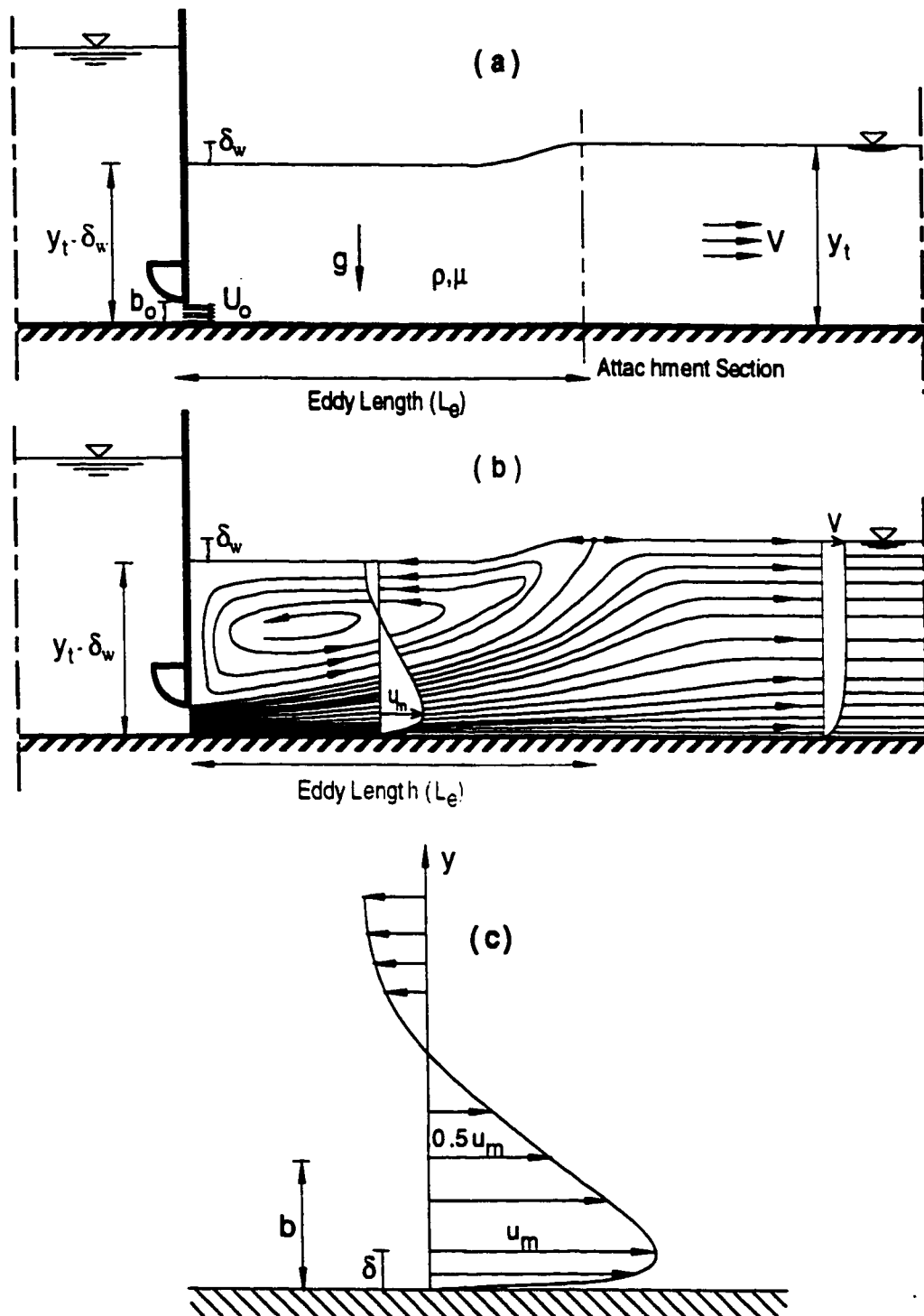


Fig. 6.1 (a) Definition sketch; (b) Flow pattern and (c) Typical velocity distribution



Fig. 6.2 Water surface elevation ($F_0 = 8$, $y/b_0 = 25$)

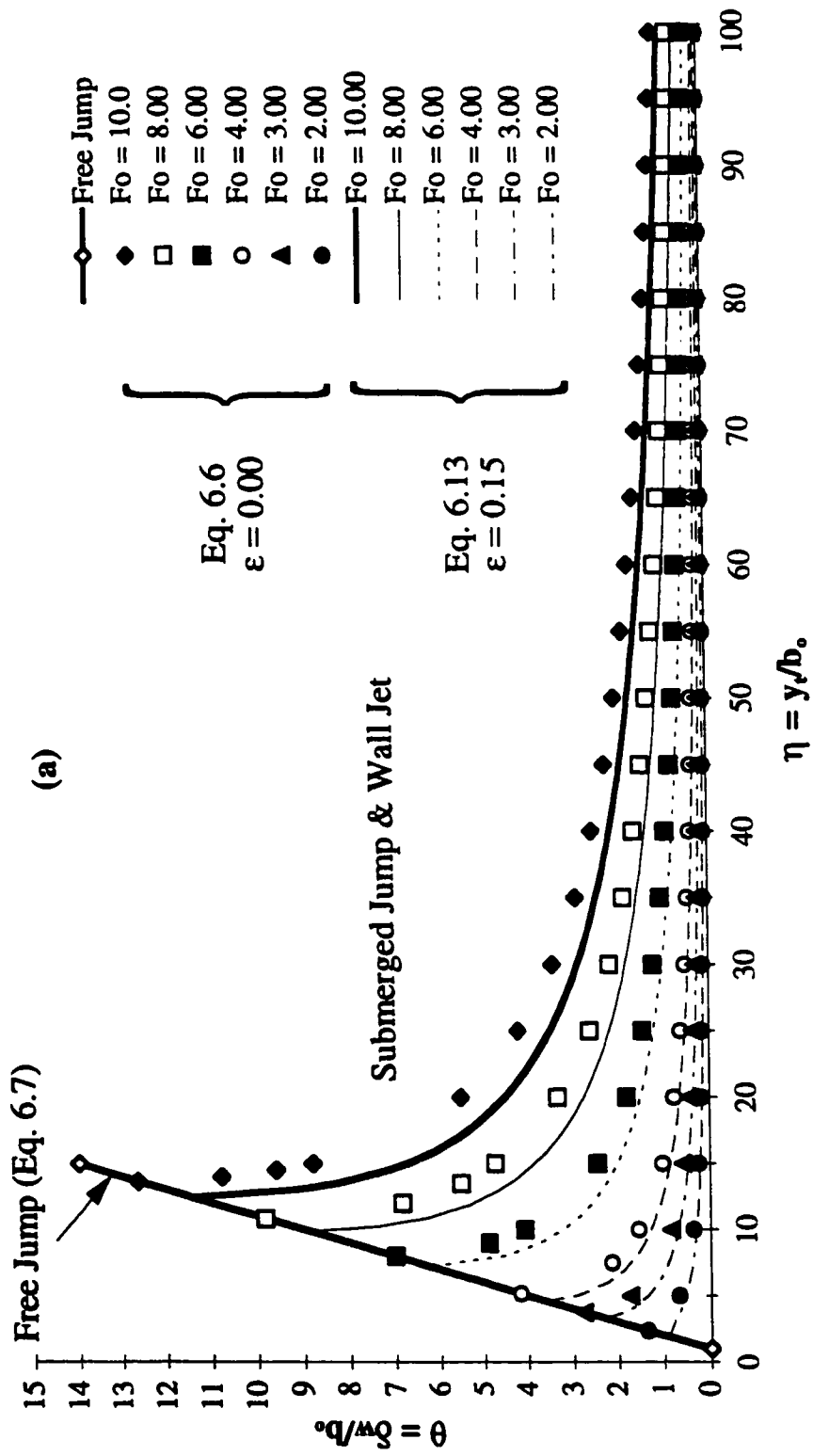


Fig. 6.3(a) Variation of θ with η for various Froude numbers F_0 , with and without shear stress

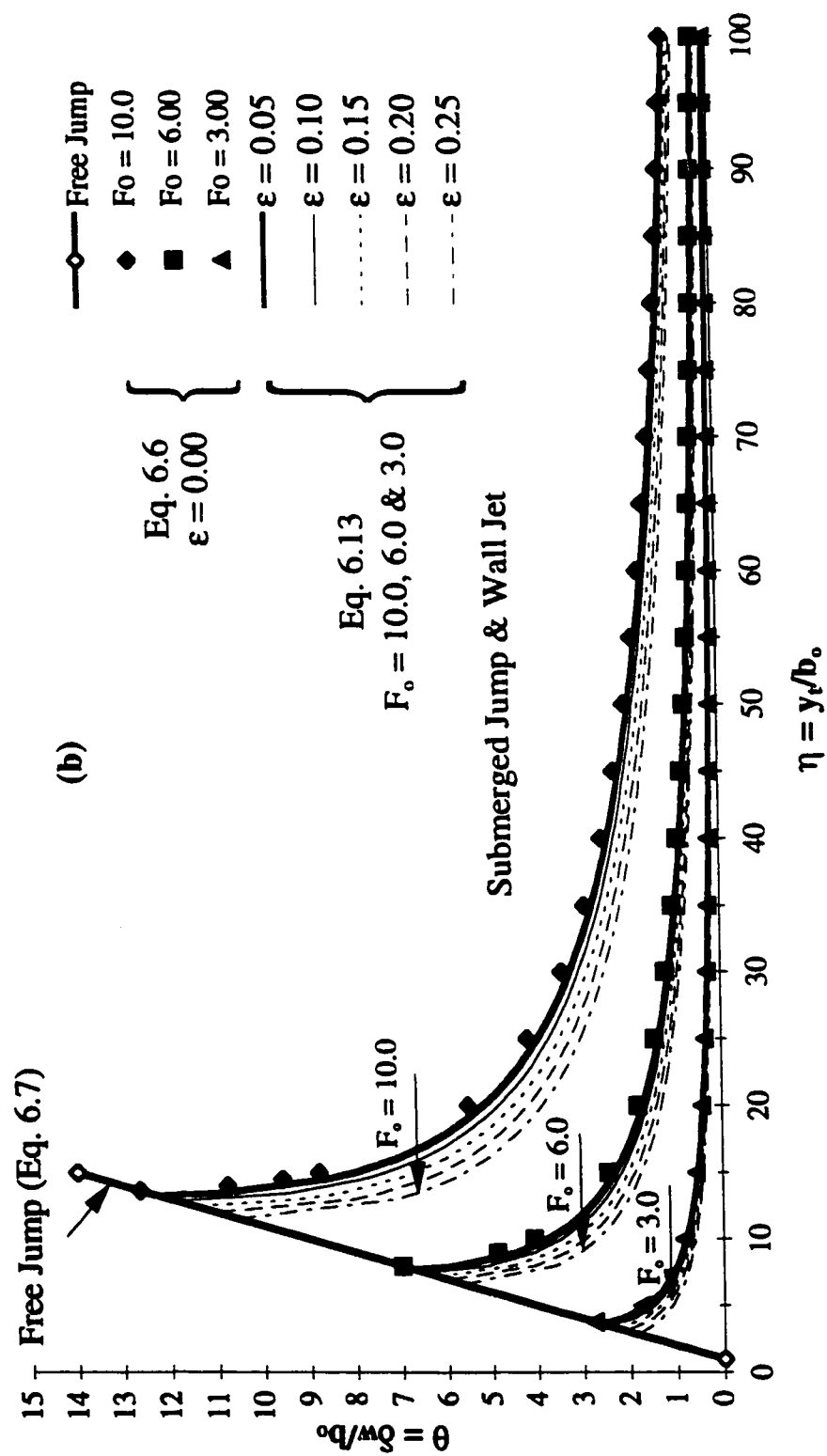


Fig. 6.3(b) Variation of θ with η for various shear coefficients ϵ

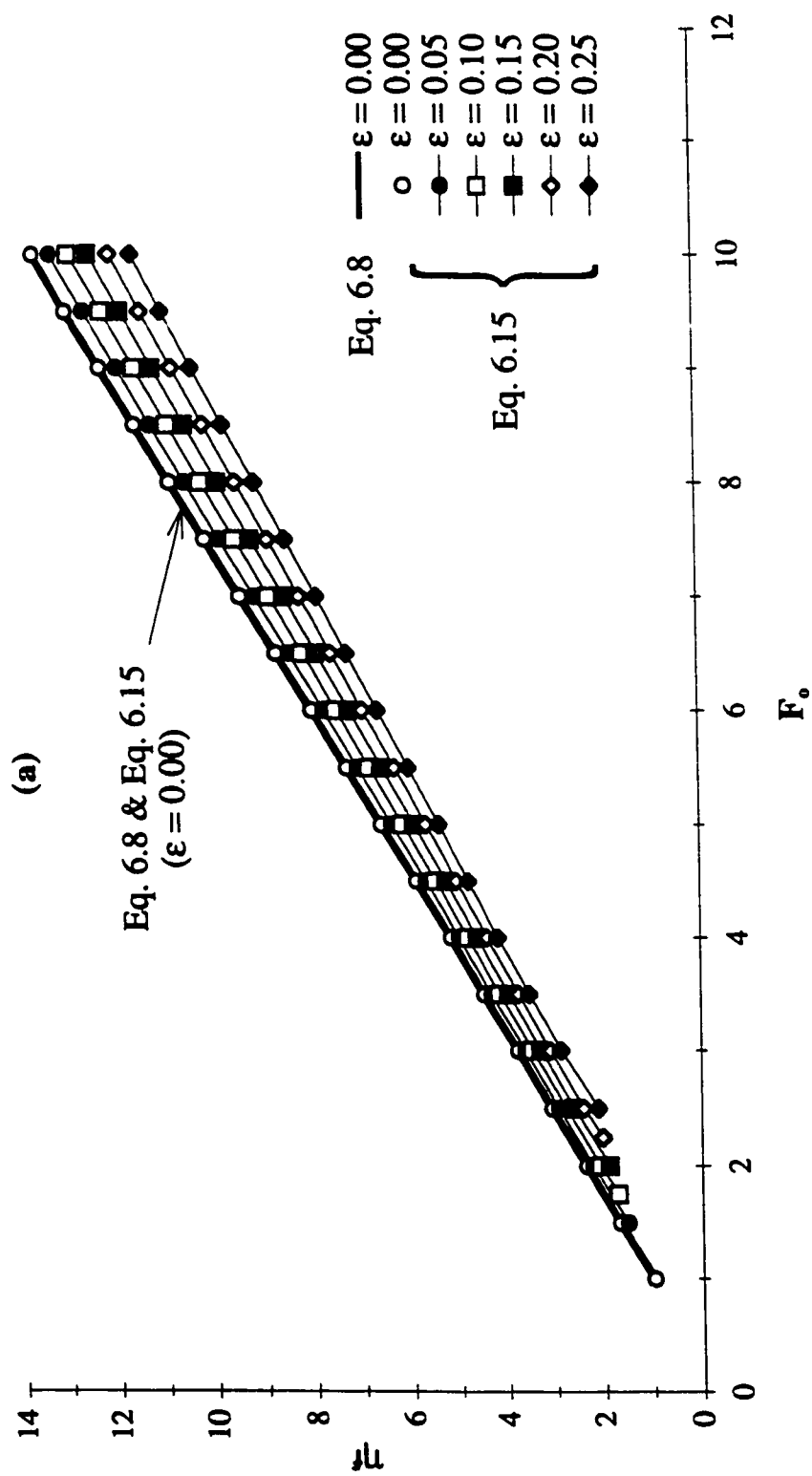


Fig. 6.4(a) Variation of η_r with F_o for various values of ϵ

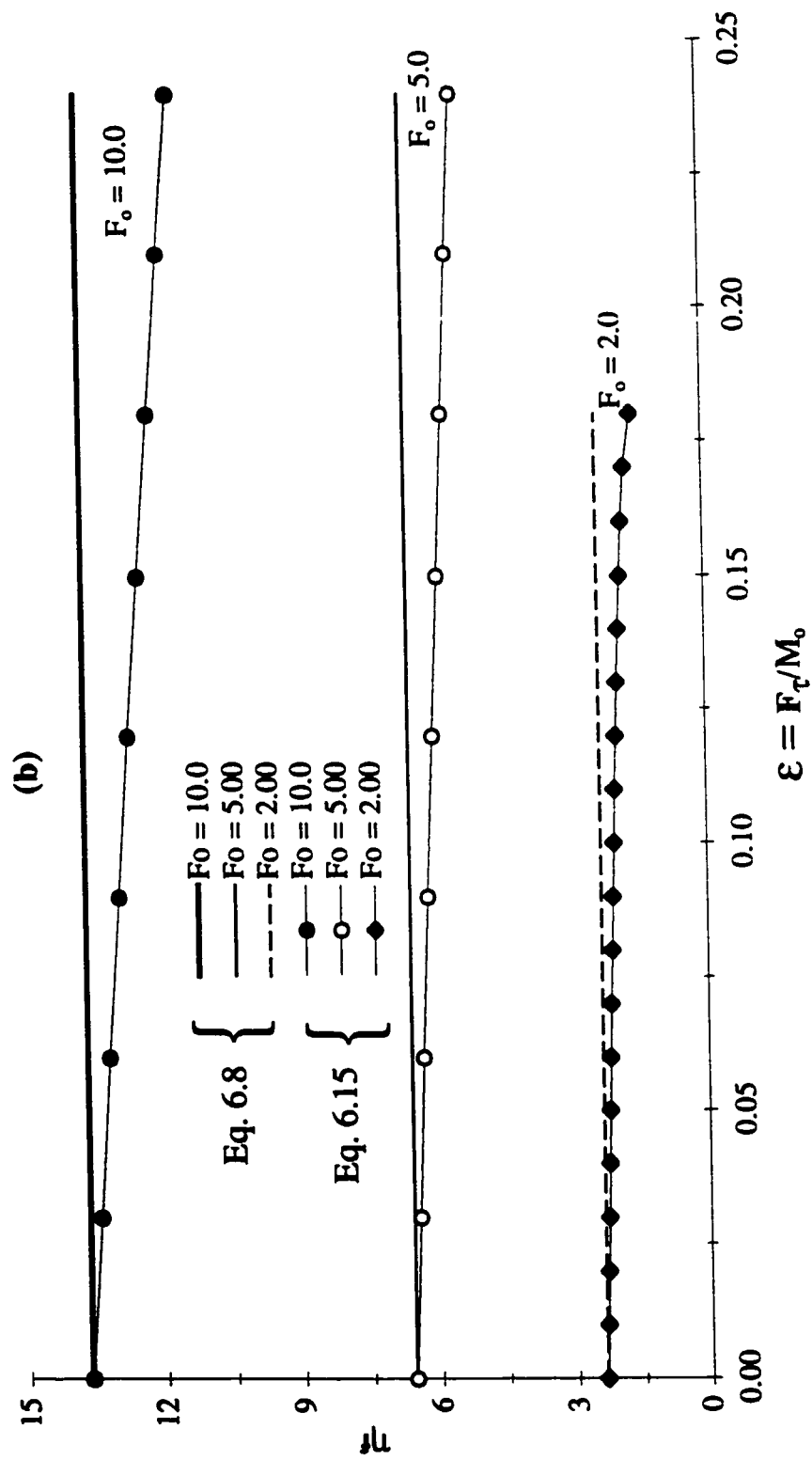


Fig. 6.4(b) Variation of η_r with ε for various values of F_0 .

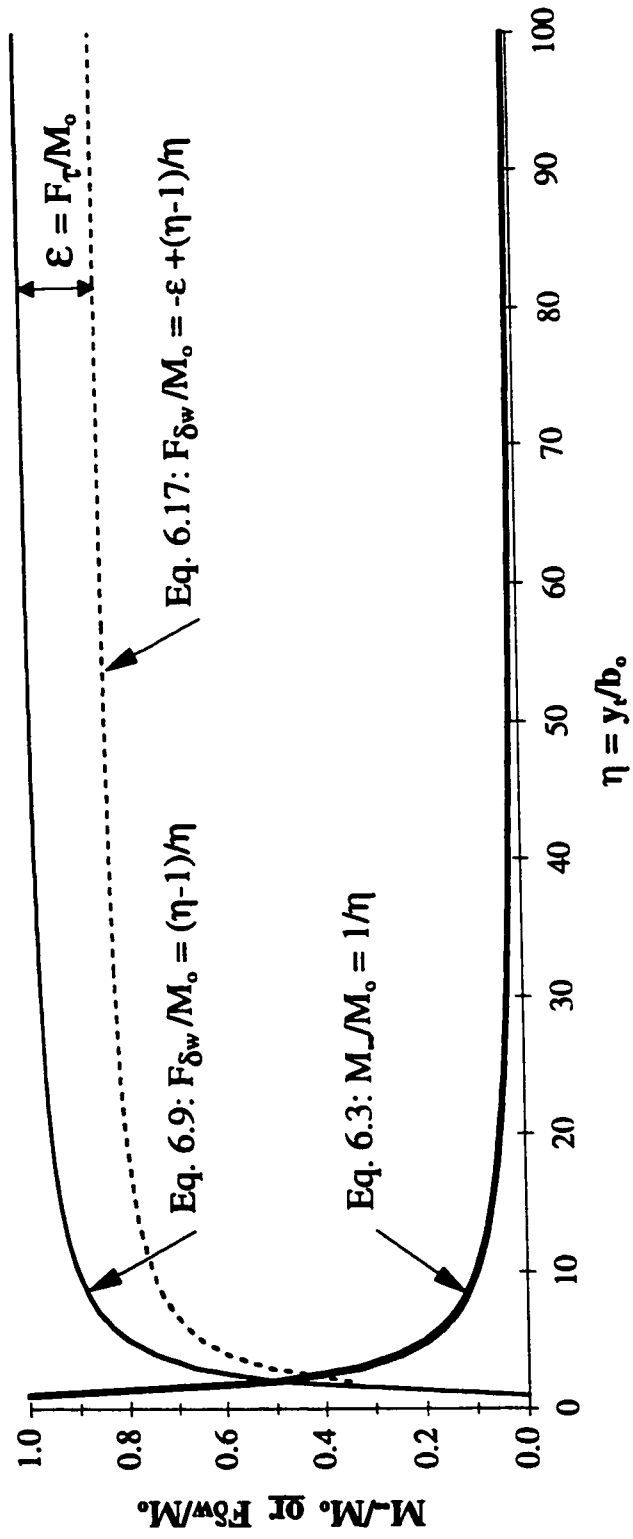


Fig. 6.5 Variation of (M_-/M_o) and $(F_{\delta w}/M_o)$ with (η)

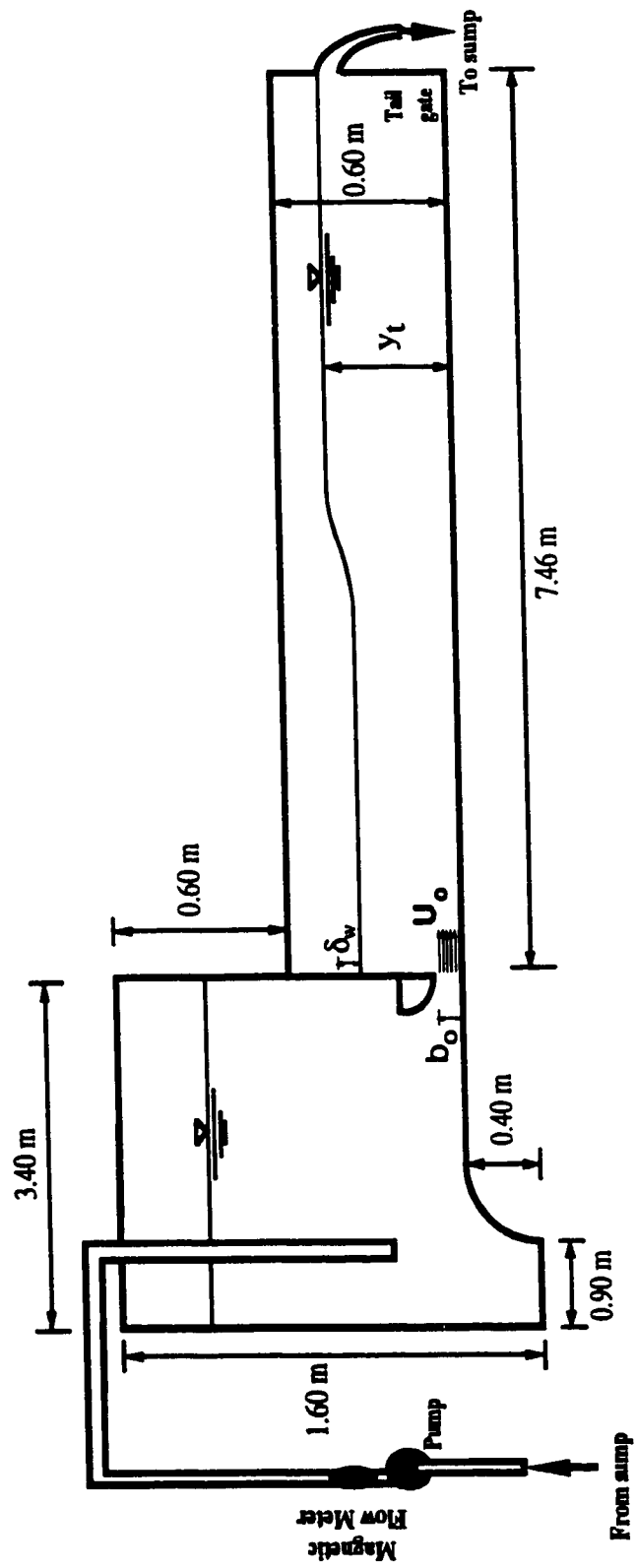


Fig. 6.6 Experimental flume

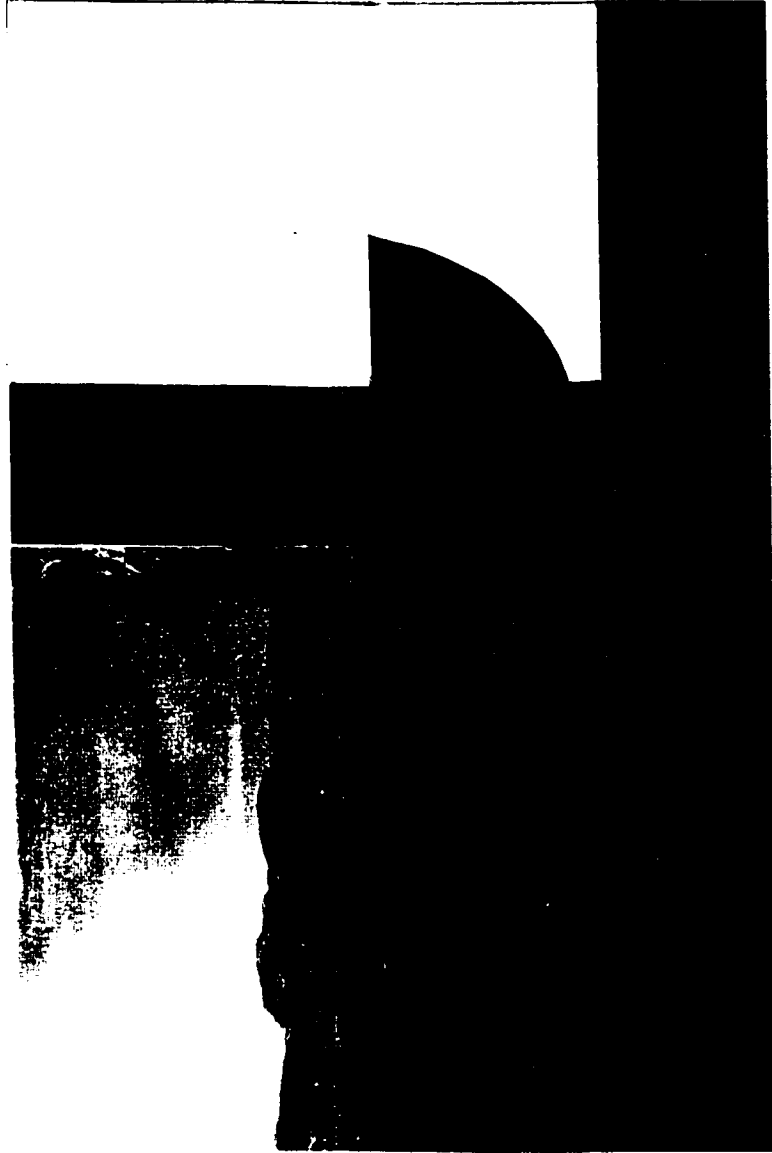


Fig. 6.7 Streamlined entrance to produce an uniform jet of thickness b .

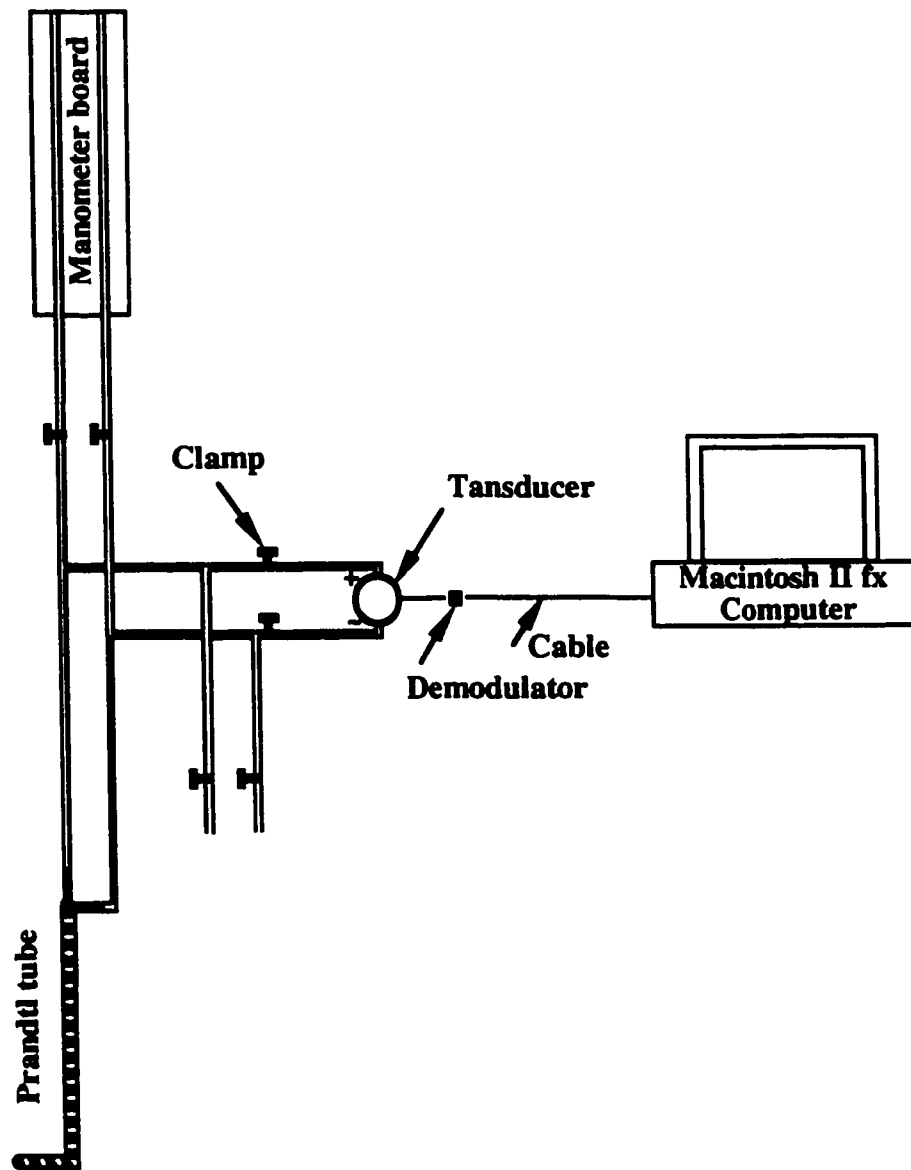


Fig. 6.8 Prandtl tube



Fig. 6.9(a) Wall jet ($F_o = 8$, $y/b_o = 25$)

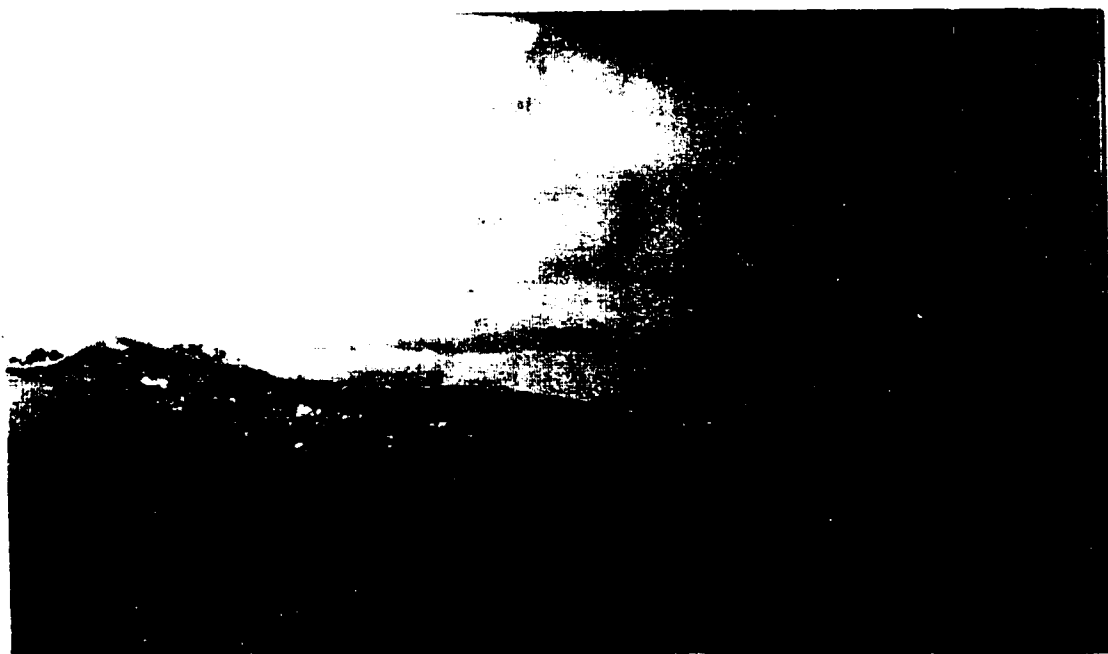


Fig. 6.9(b) Wall jet ($F_o = 8$, $y/b_o = 35$)



Fig. 6.9(c) Wall jet ($F_o = 8$, $y_t/b_o = 40$)



Fig. 6.9(d) Wall jet ($F_o = 8$, $y_t/b_o = 50$)

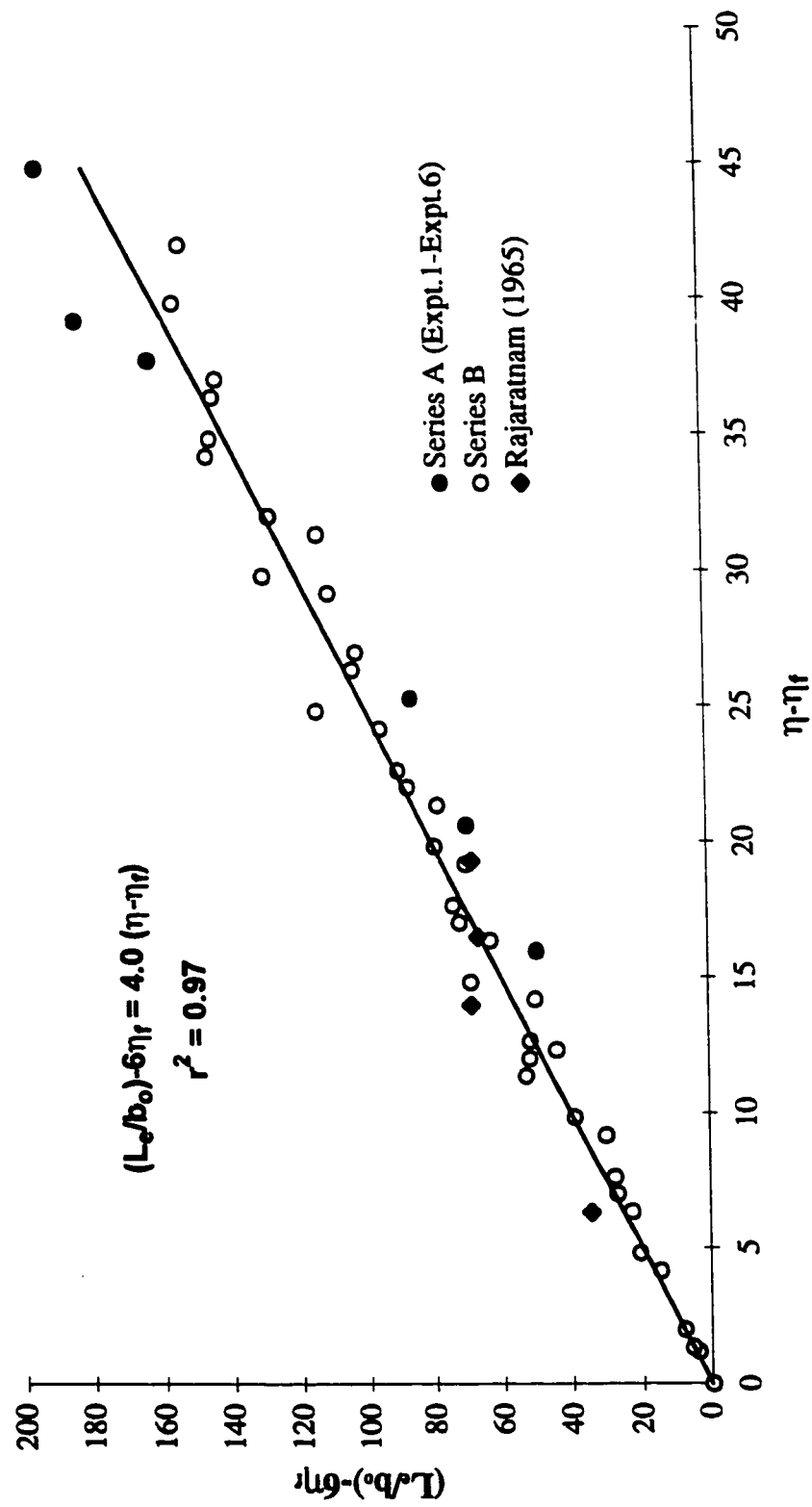


Fig. 6.10 Variation of the eddy length L_e/b_o with $(\eta - \eta_f)$

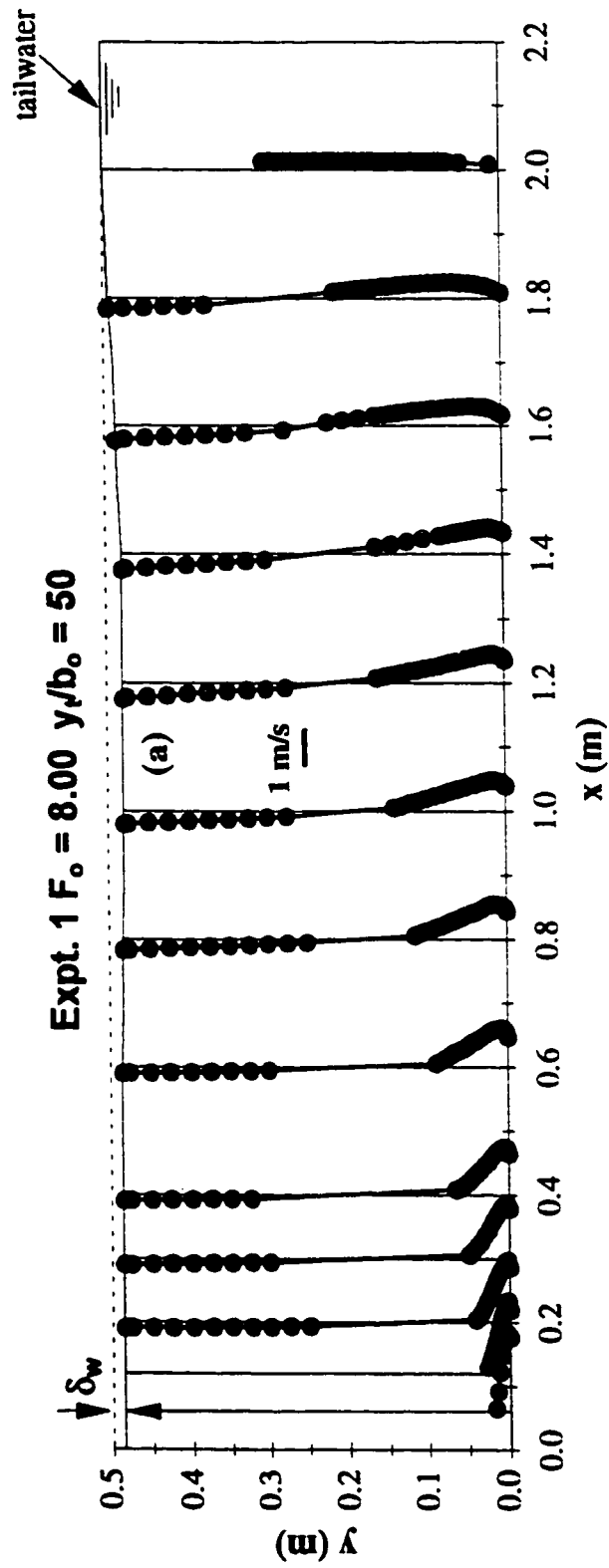


Fig. 6.11(a) Typical velocity fields of wall jets in shallow tailwaters (Expt. 1)

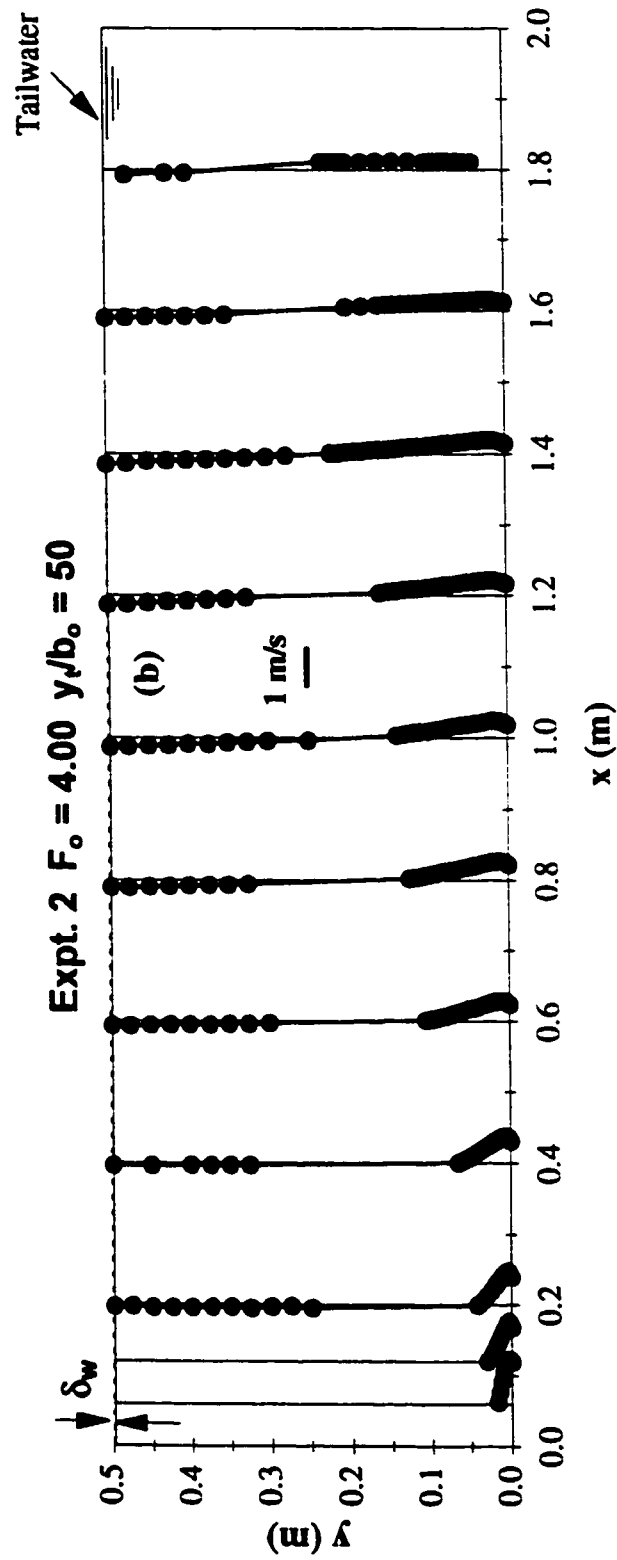


Fig. 6.11(b) Typical velocity fields of wall jets in shallow tailwaters (Expt. 2)

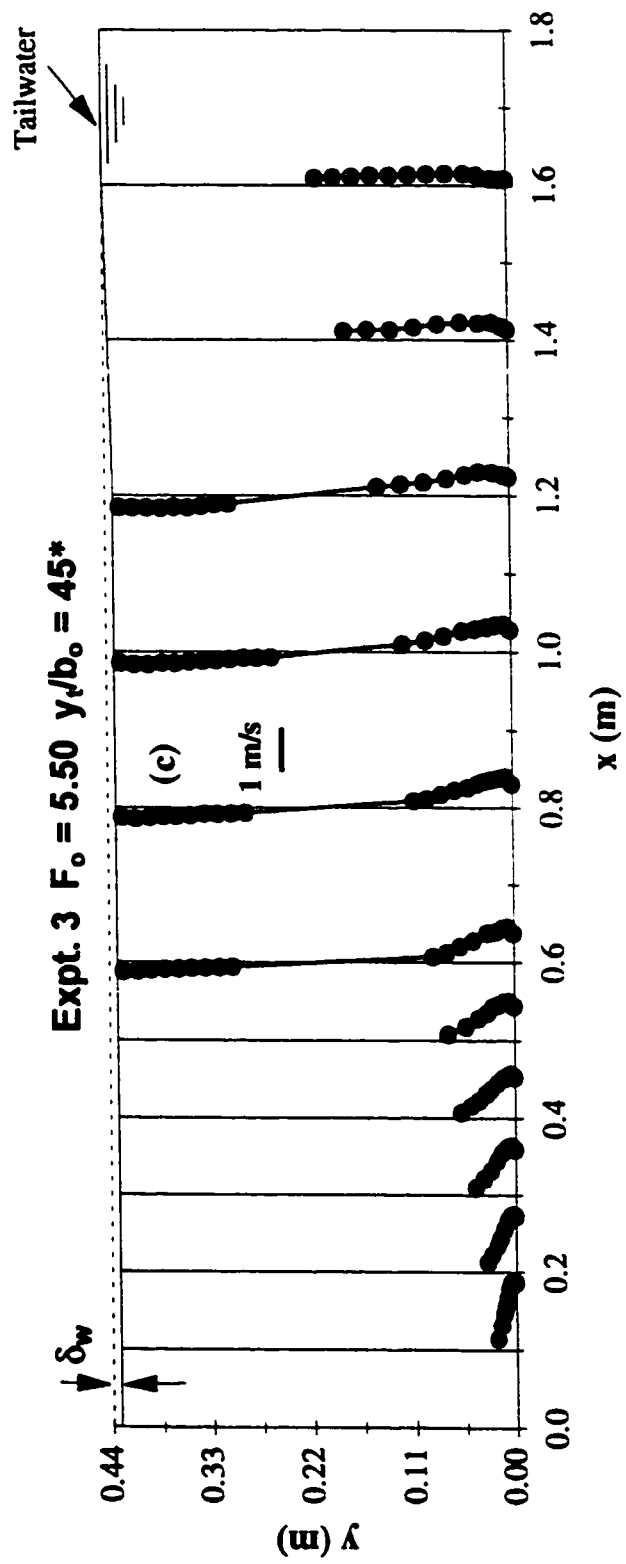


Fig. 6.11(c) Typical velocity fields of wall jets in shallow tailwaters (Expt. 3)
*** Wu and Rajaratnam (1995)**

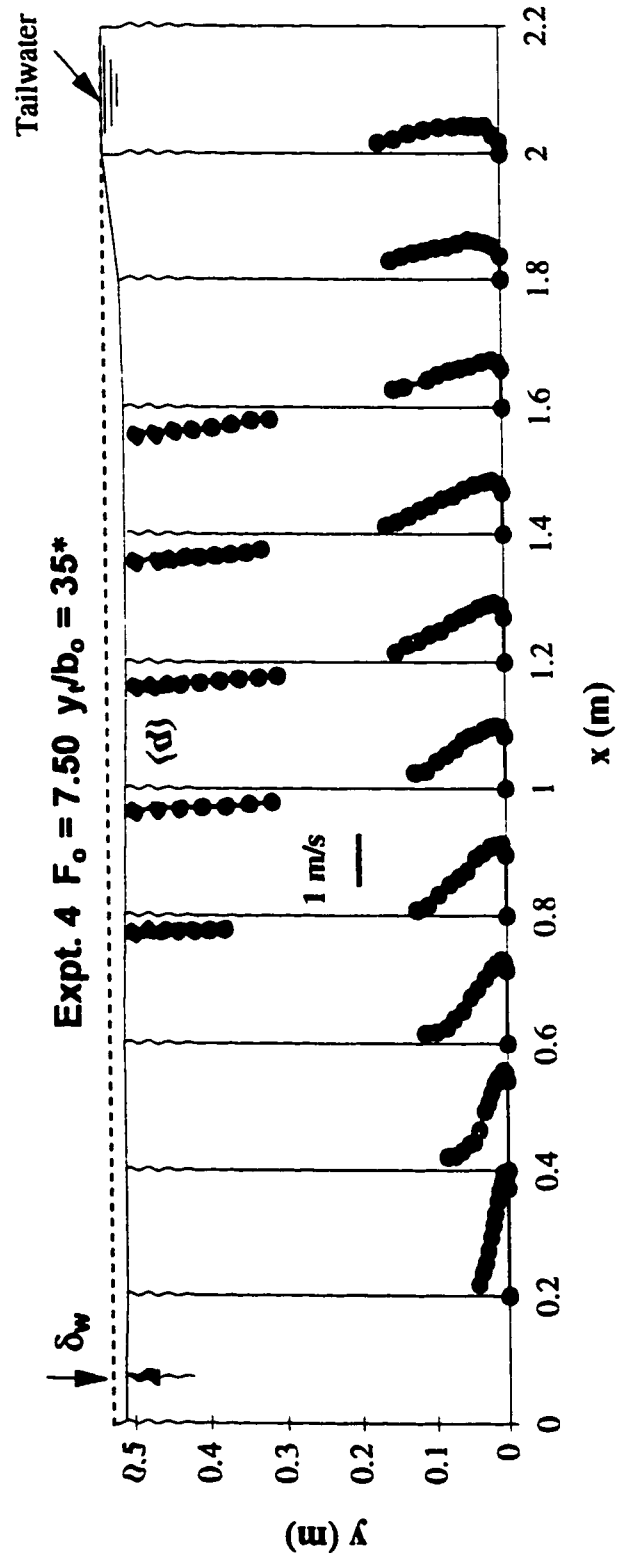


Fig. 6.11(d) Typical velocity fields of wall jets in shallow tailwaters (Expt. 4)
*** Wu and Rajaratnam (1995)**

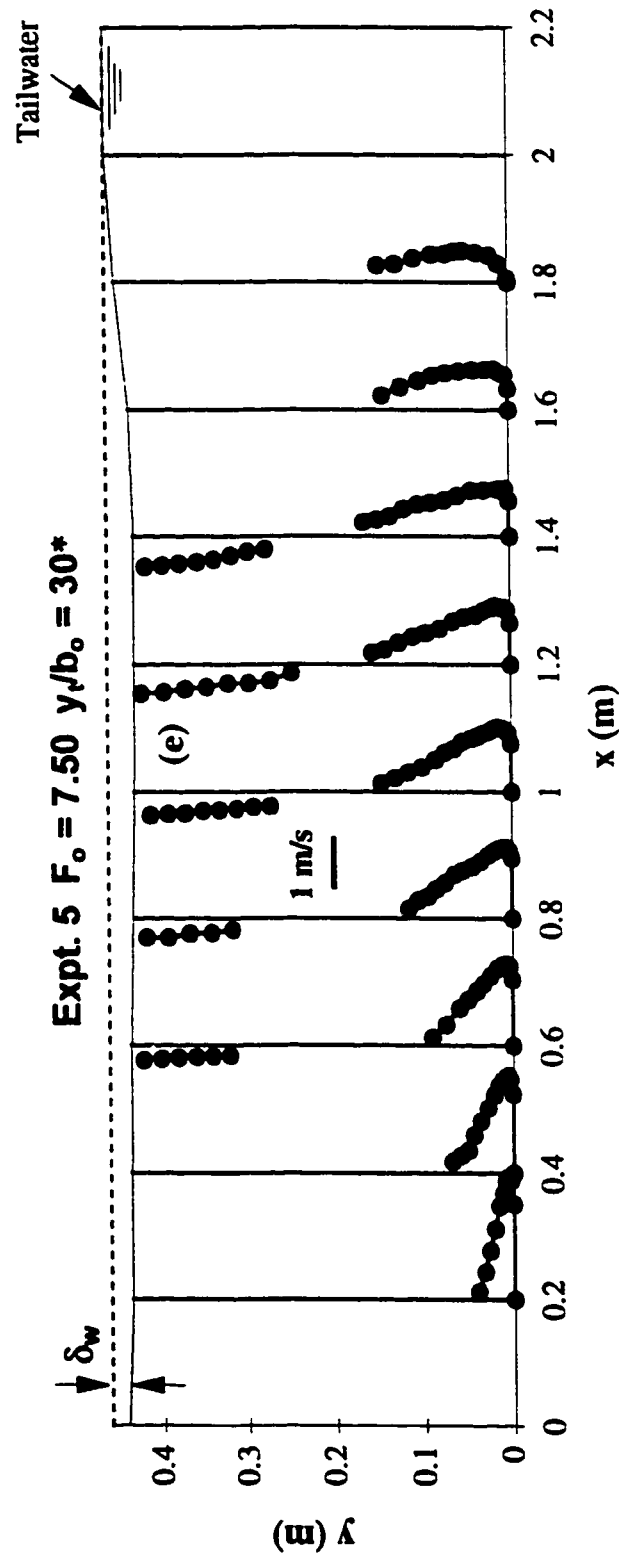


Fig. 6.11(e) Typical velocity fields of wall jets in shallow tailwaters (Expt. 5)
*** Wu and Rajaratnam (1995)**

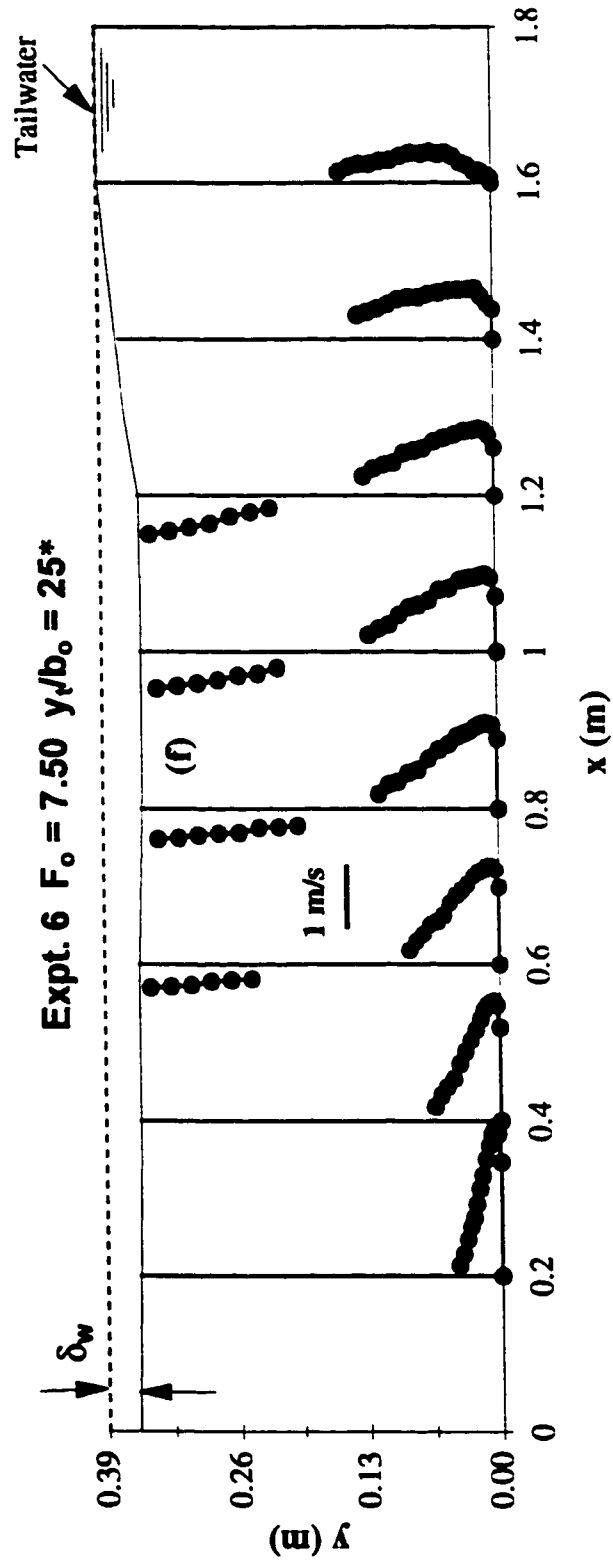


Fig. 6.11(f) Typical velocity fields of wall jets in shallow tailwaters (Expt. 6)
*** Wu and Rajaratnam (1995)**

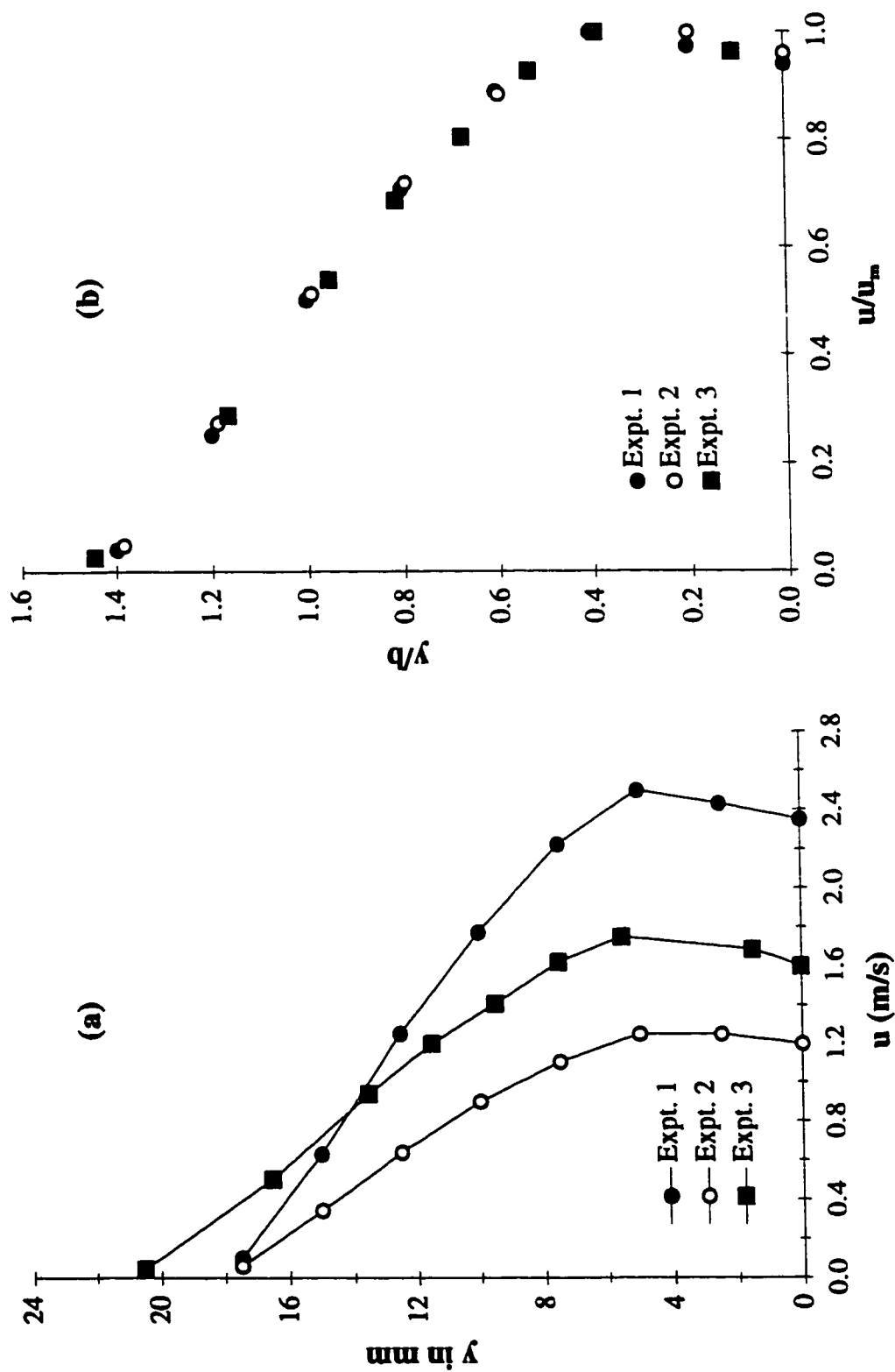
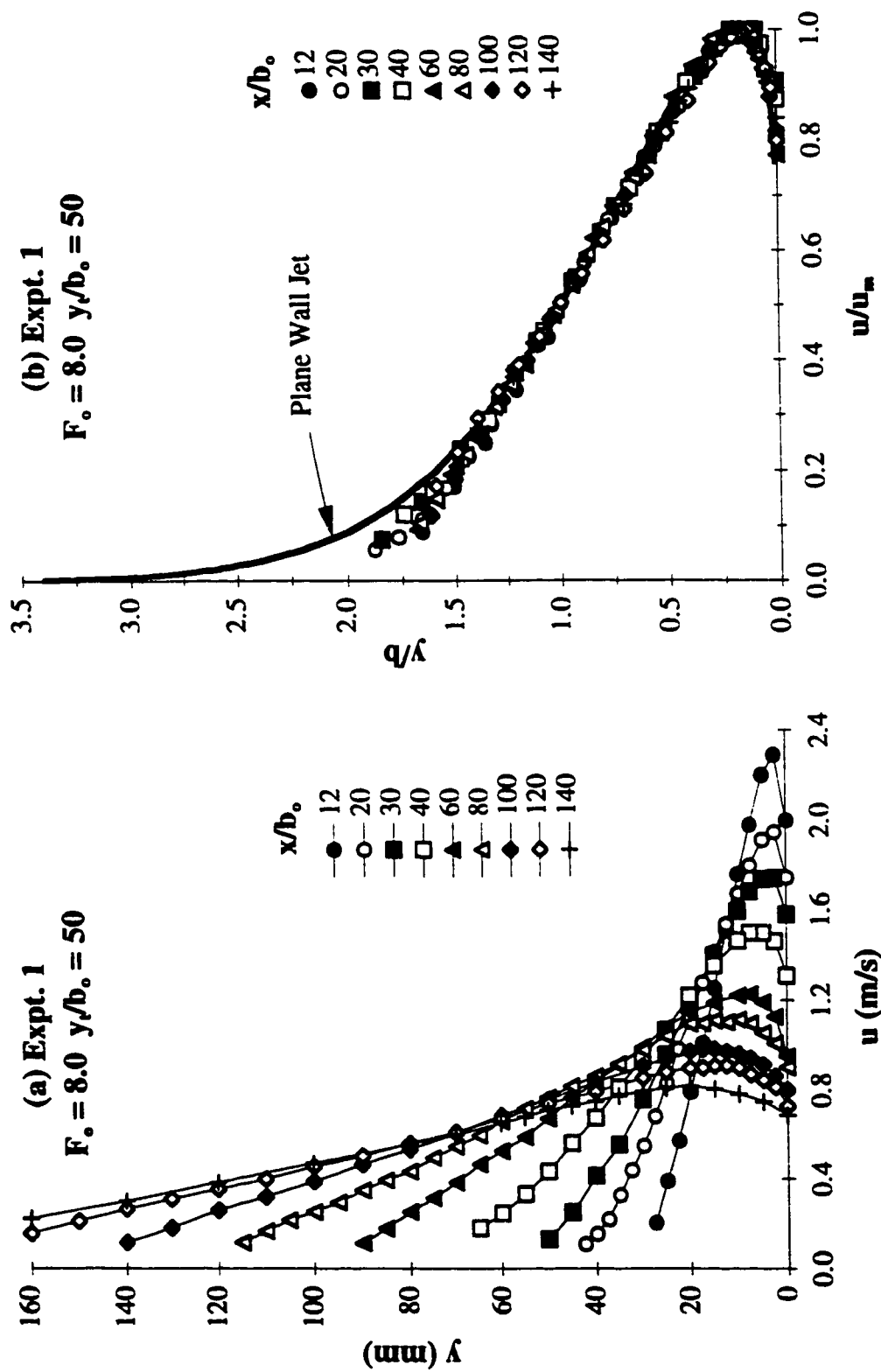


Fig. 6.12(a-b) Velocity distribution in partially-developed flow ($x/b_o = 6$)
(a) Velocity profiles; and (b) Similarity profile



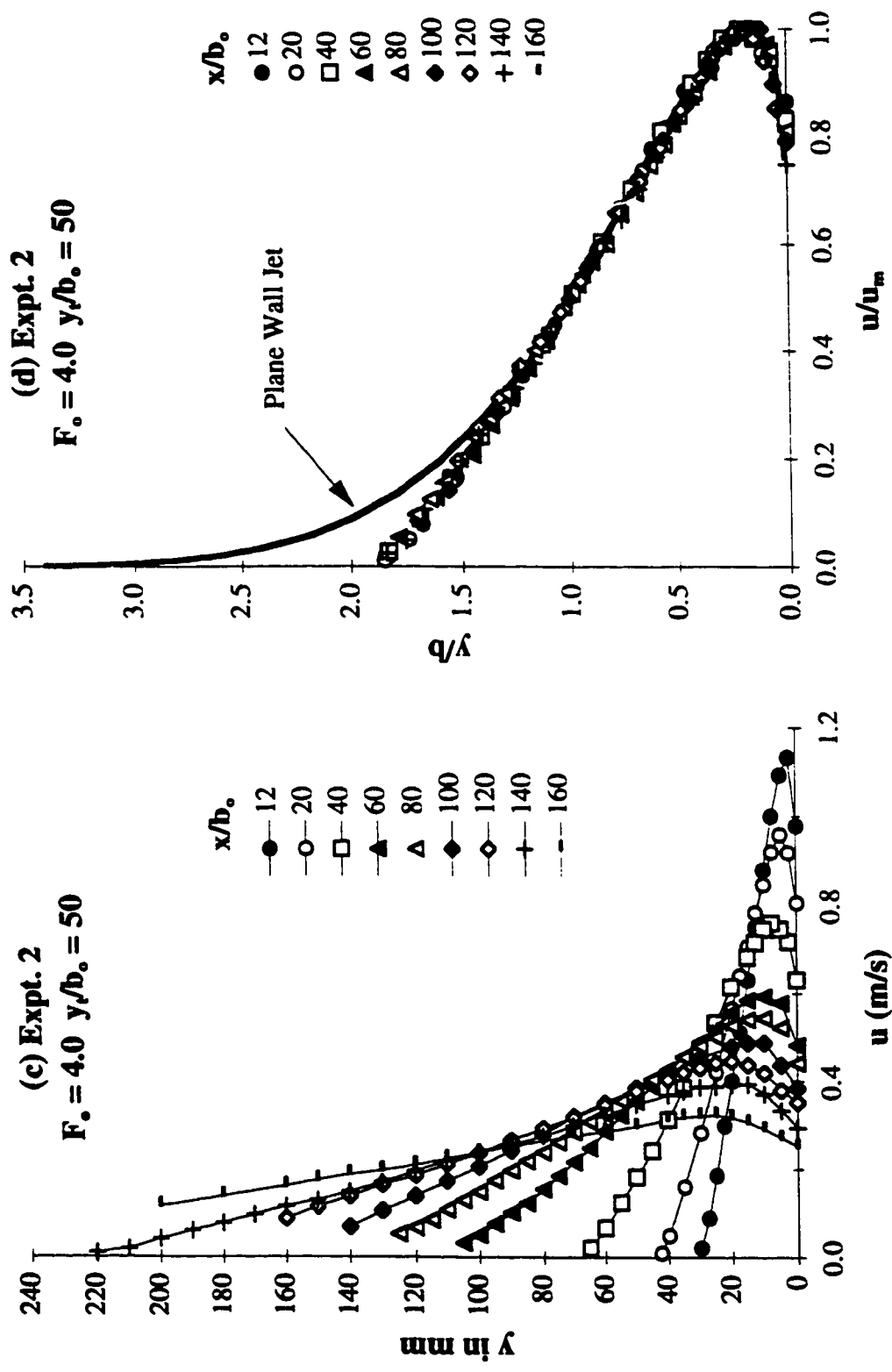


Fig. 6.13(c-d) Velocity distribution in fully-developed flow (Expt. 2)
(c) Velocity profiles; and (d) Similarity profile

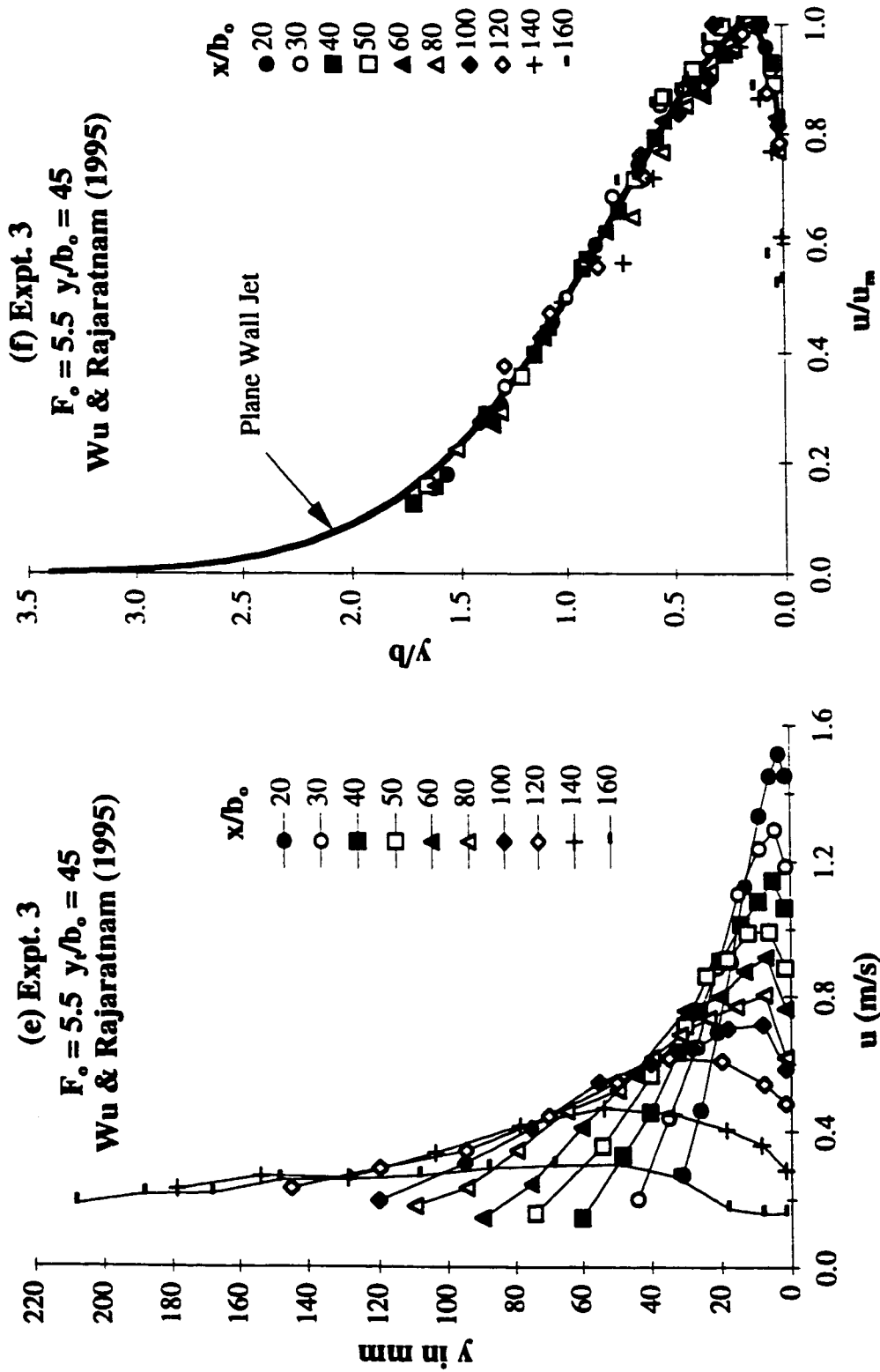


Fig. 6.13(e-f) Velocity distribution in fully-developed flow (Expt. 3)
 (e) Velocity profiles; and (f) Similarity profile

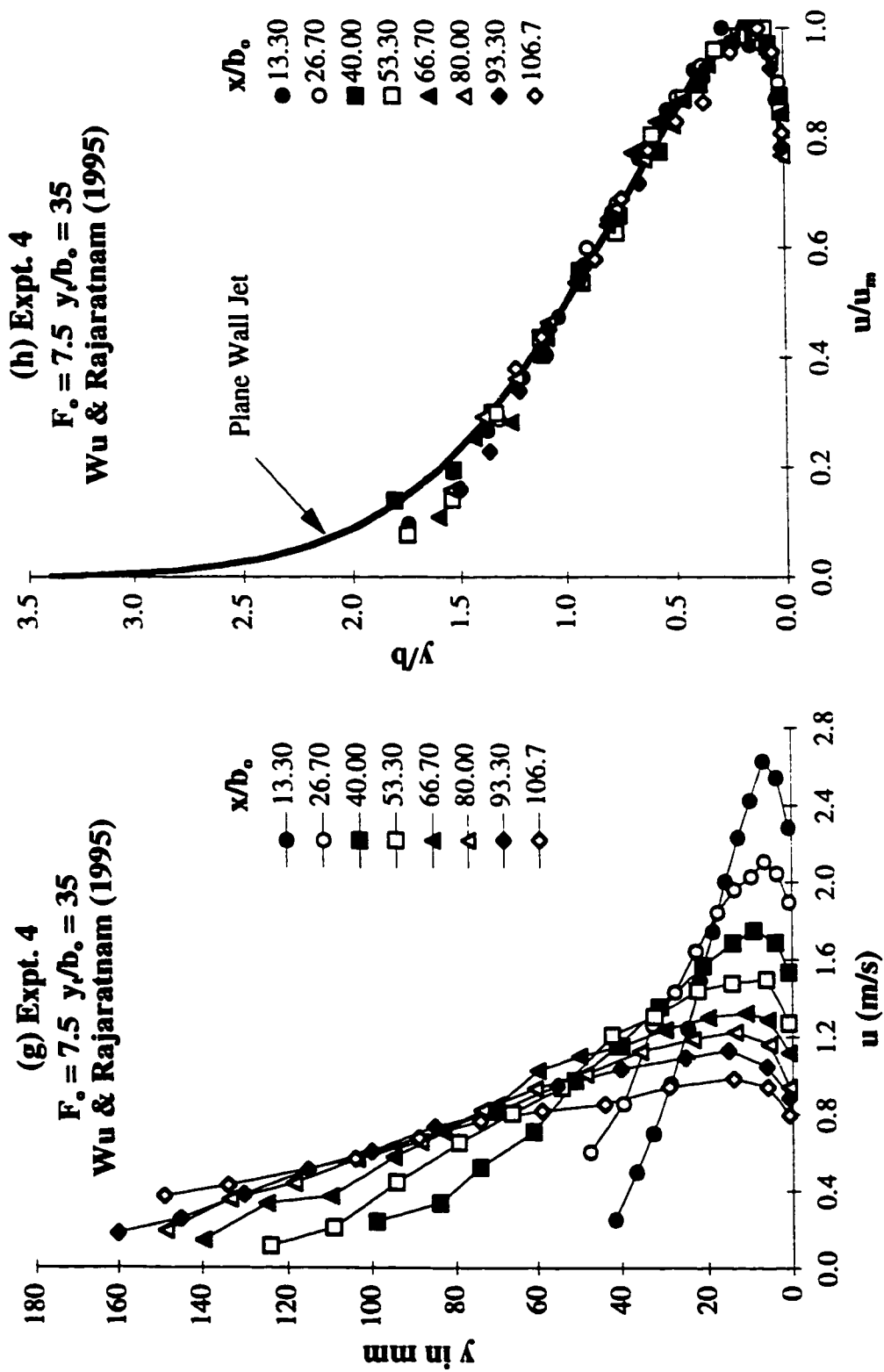


Fig. 6.13(g-h) Velocity distribution in fully-developed flow (Expt. 4)
 (g) Velocity profiles; and (h) Similarity profile

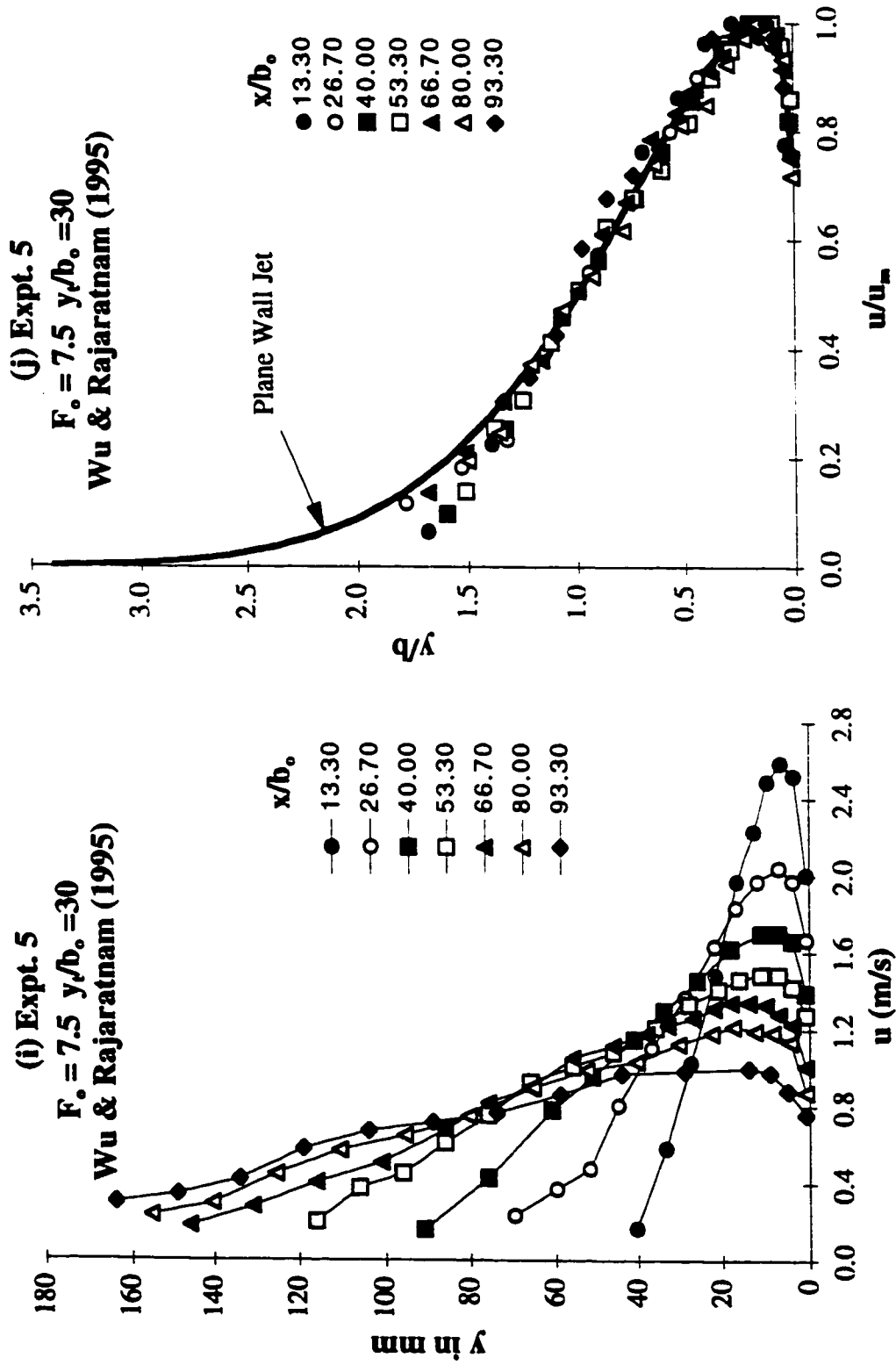


Fig. 6.13(i-j) Velocity distribution in fully-developed flow (Expt. 5)
 (i) Velocity profiles; and (j) Similarity profile

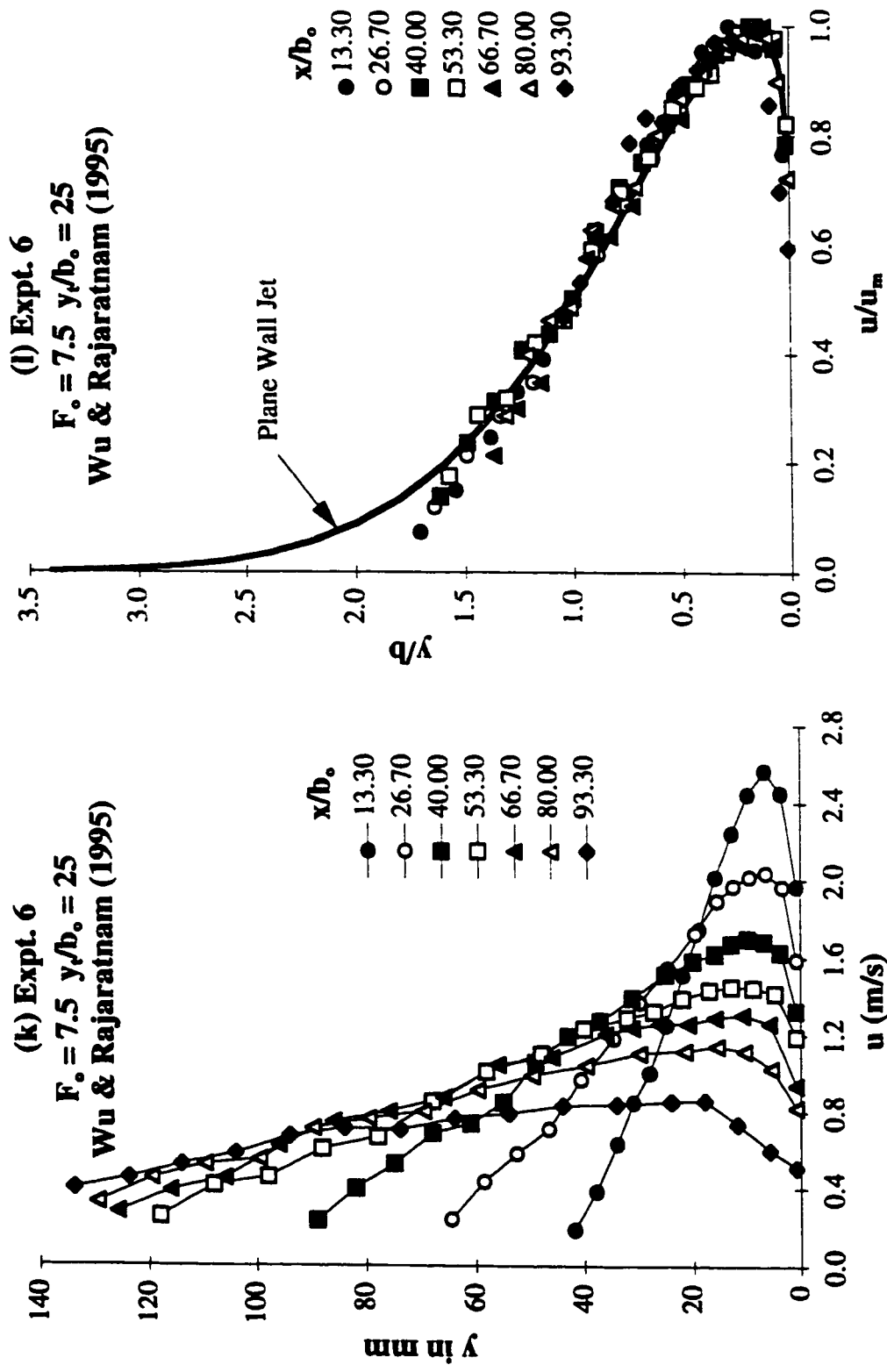


Fig. 6.13(k-l) Velocity distribution in fully-developed flow (Expt.6)
(k) Velocity profiles; and (l) Similarity profile

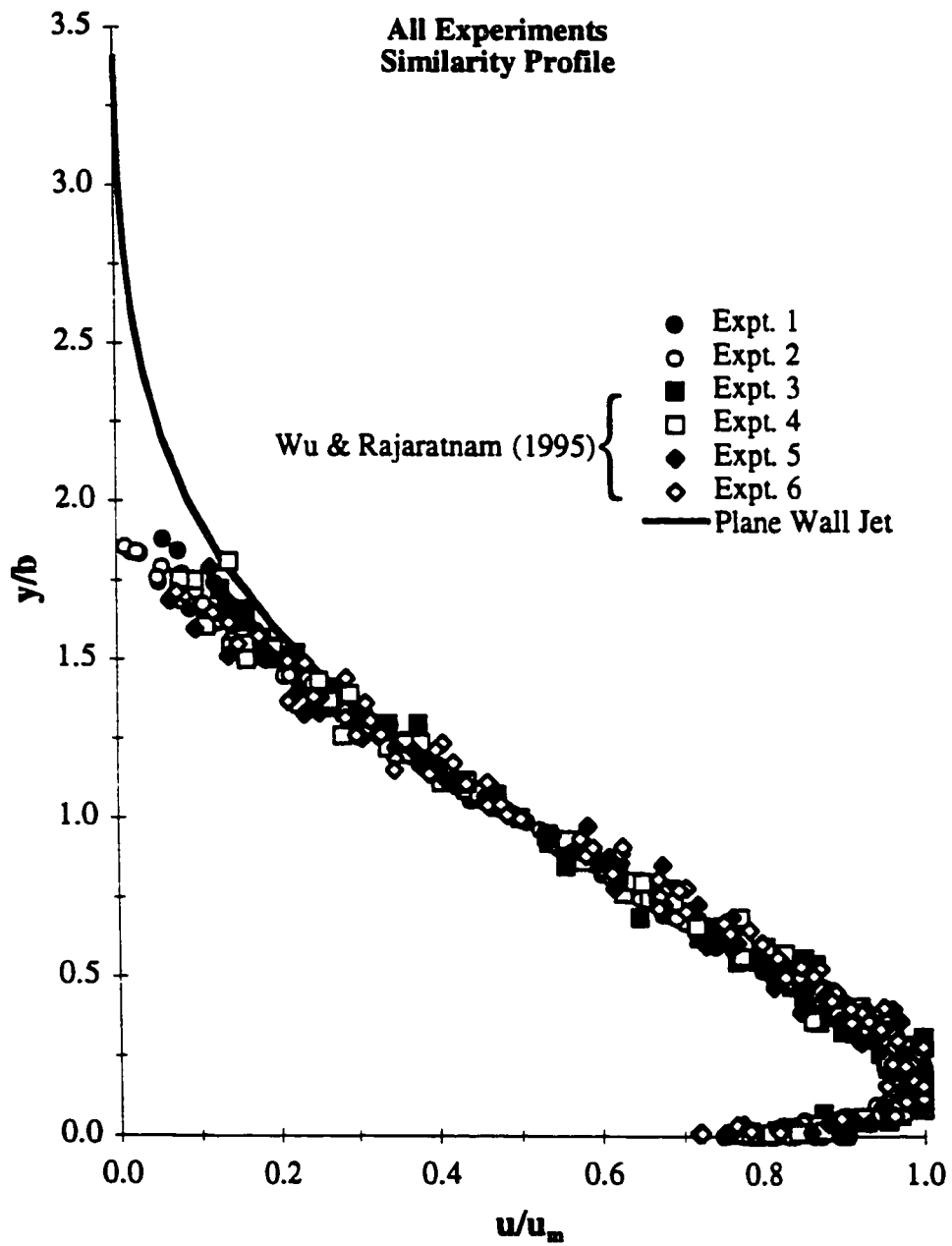


Fig. 6.14 Consolidated non-dimensional plot for the velocity distribution in the wall jet

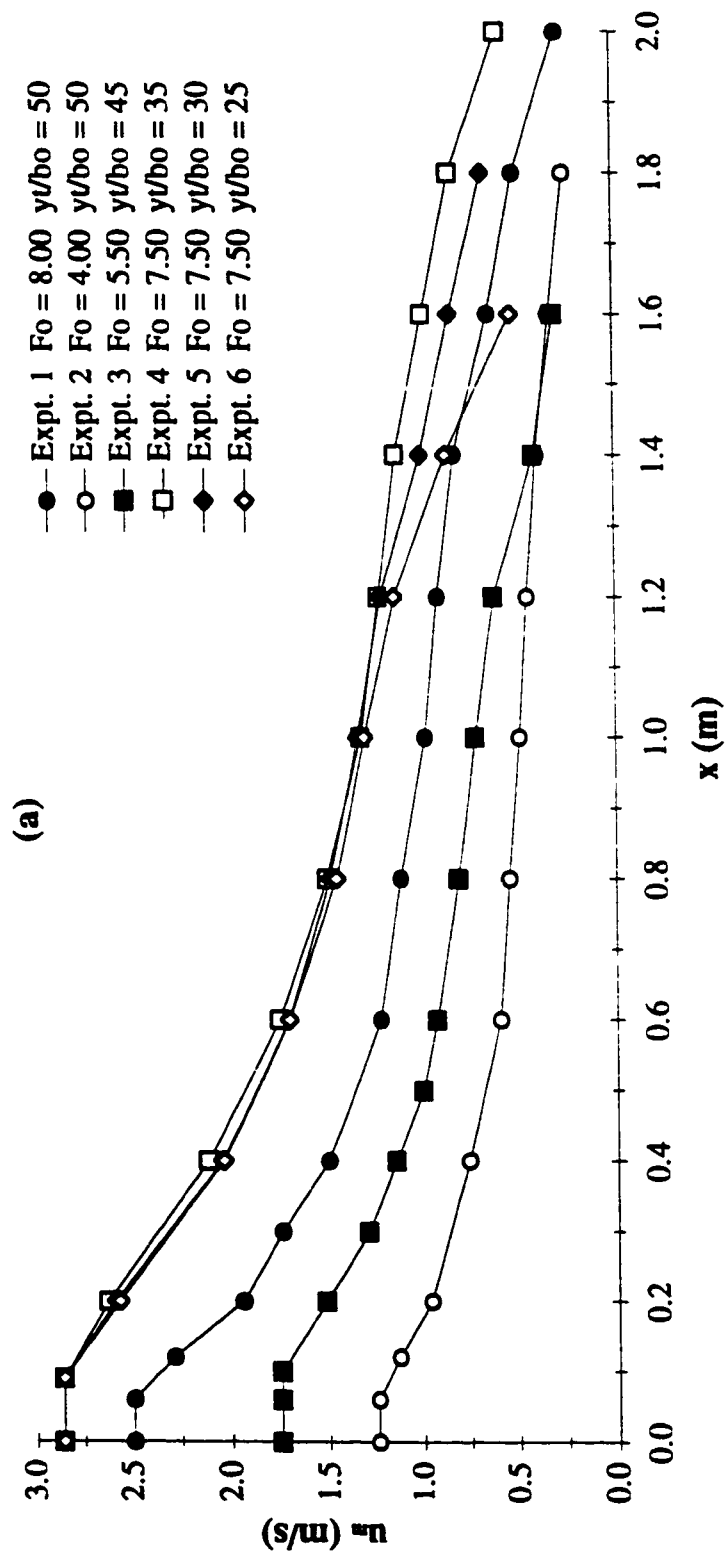


Fig. 6.15(a) Variation of the maximum jet velocity, u_m , with distance

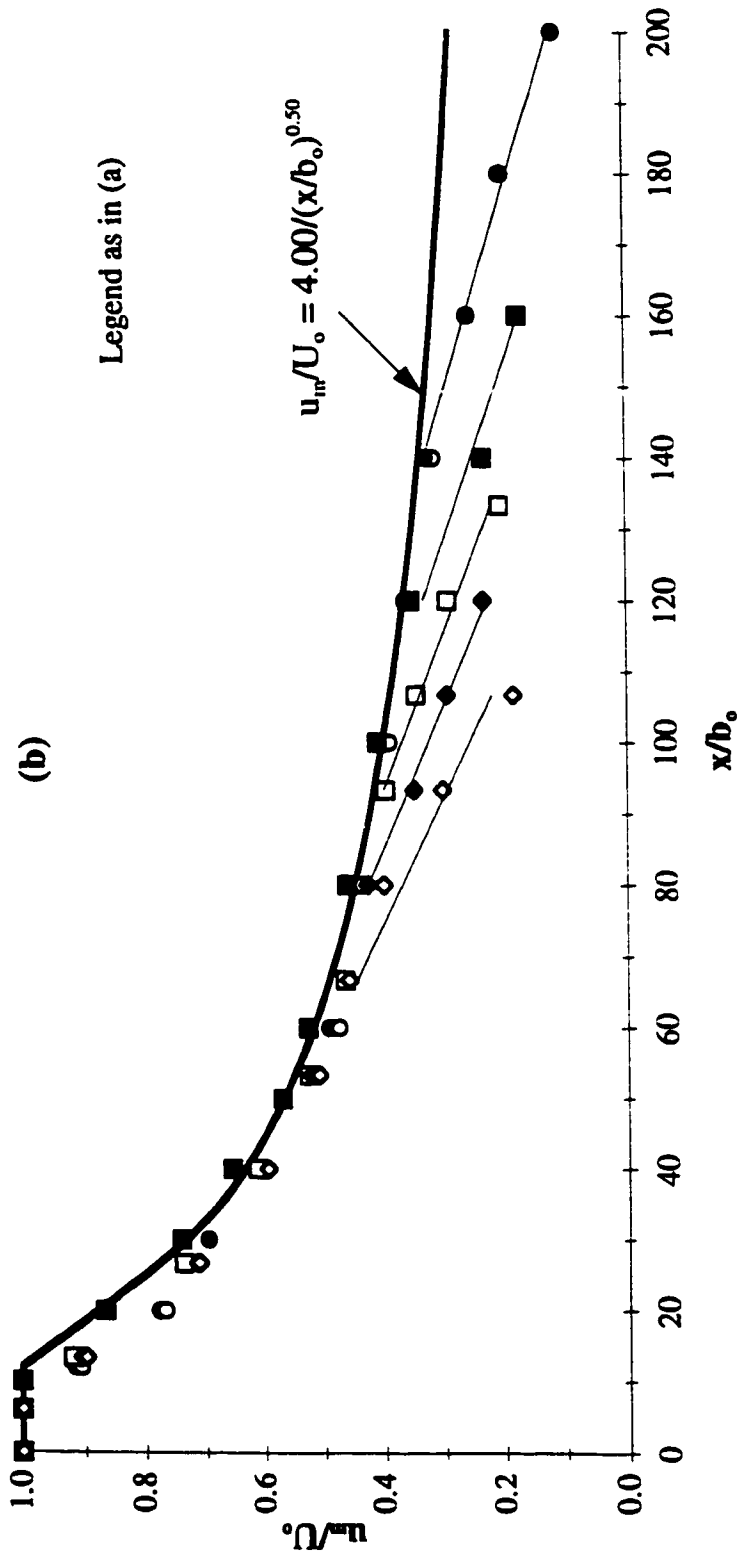


Fig. 6.15(b) Variation of u_{in}/U_o with x/b_o .

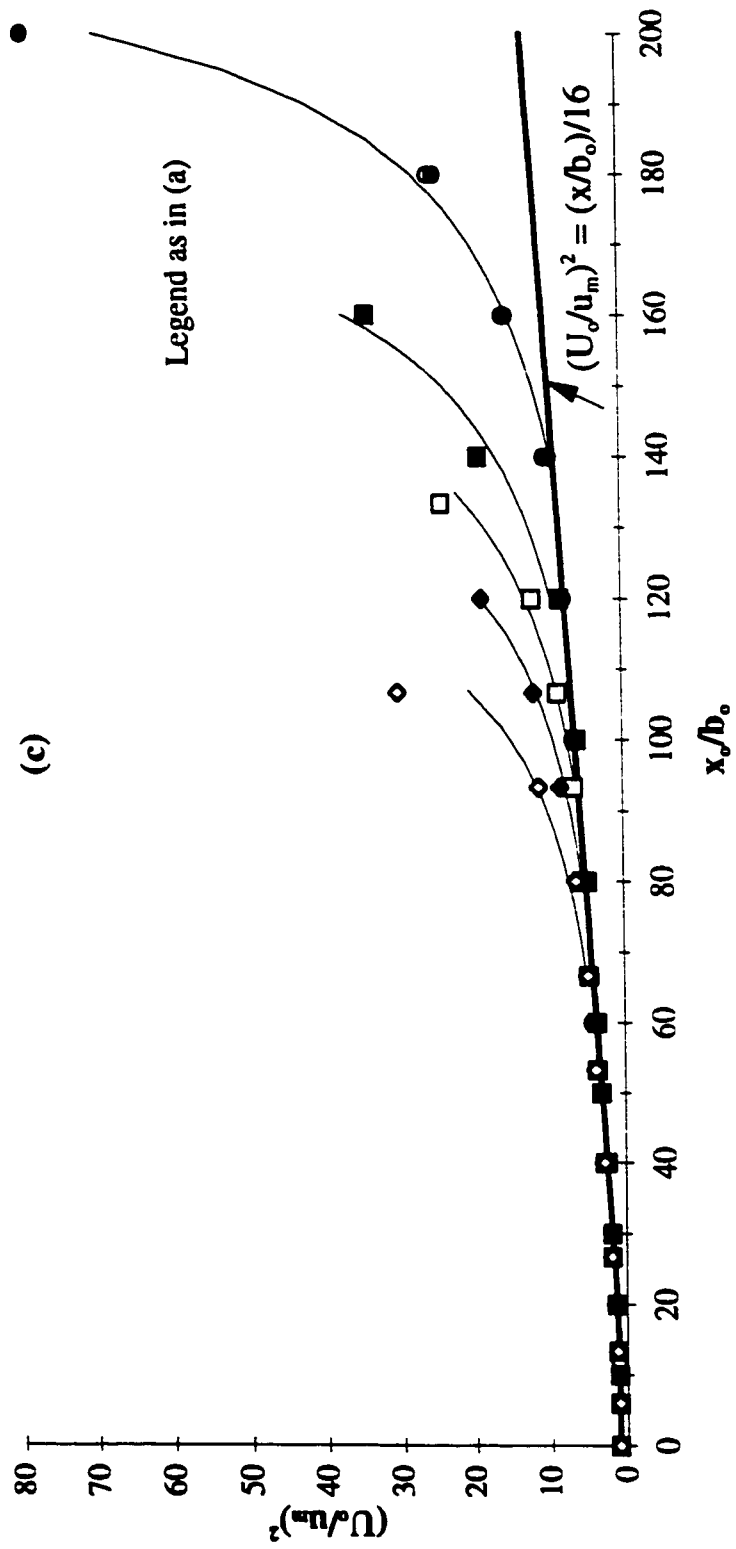


Fig. 6.15(c) Variation of $(U_o/U_m)^2$ with x/b_o .

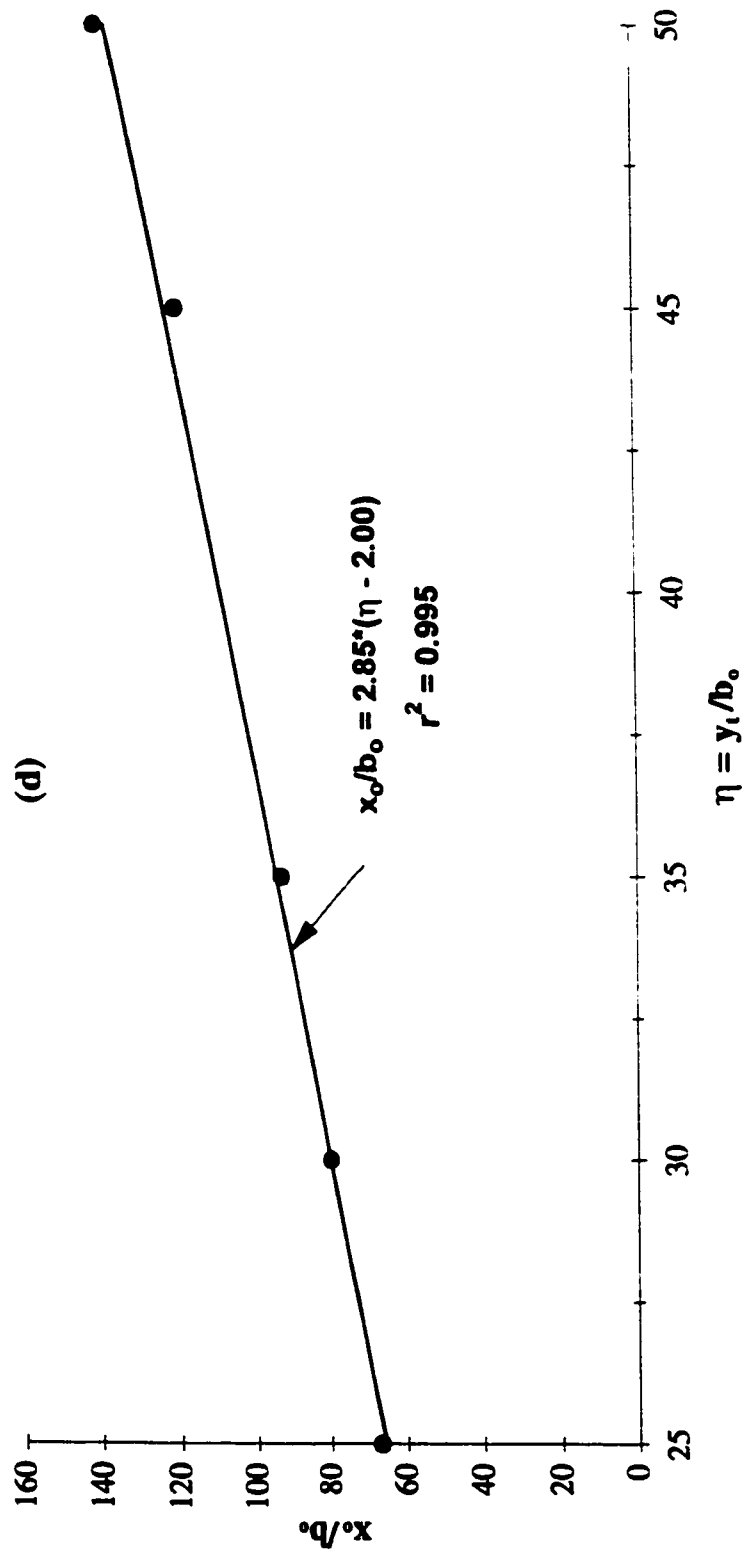


Fig. 6.15(d) Effect of the tailwater depth ratio on the breakdown distance

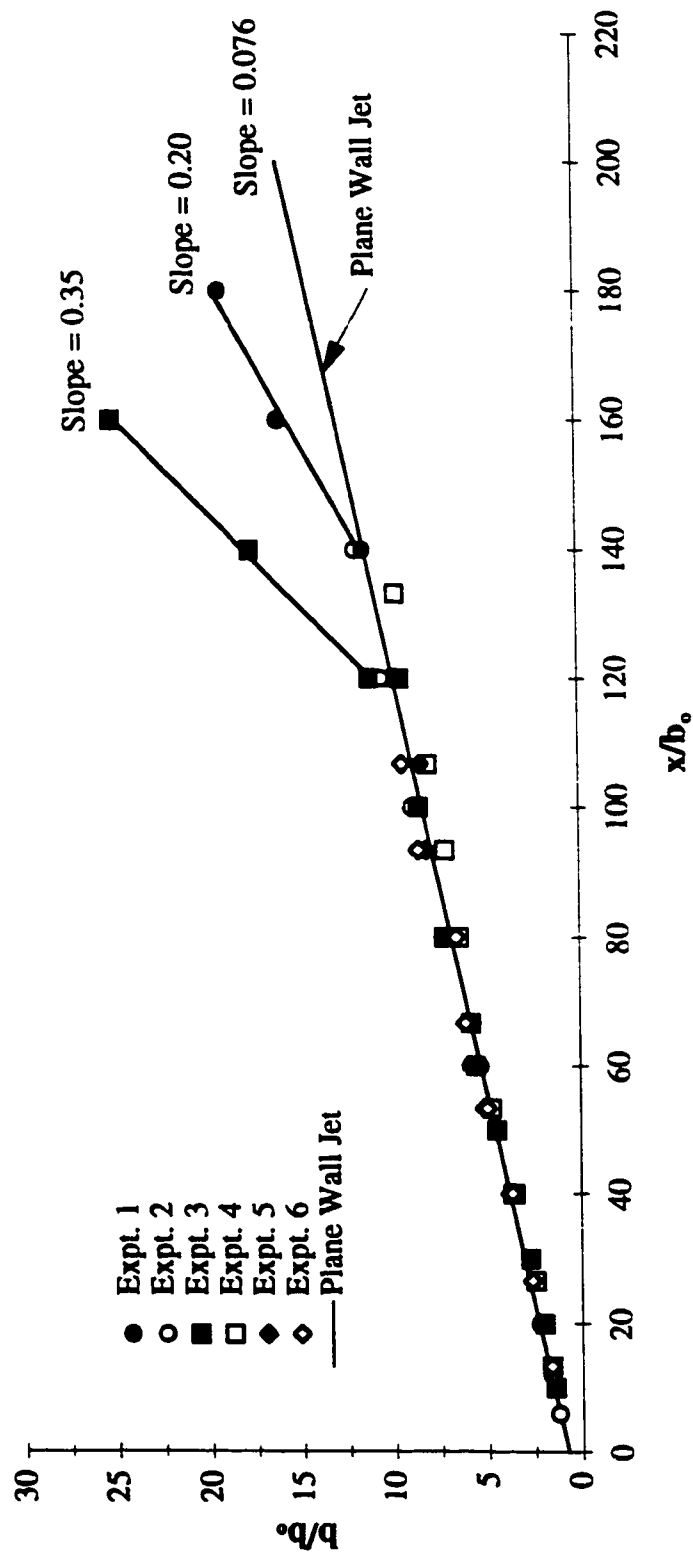


Fig.6.16 Variation of the jet half-width with distance

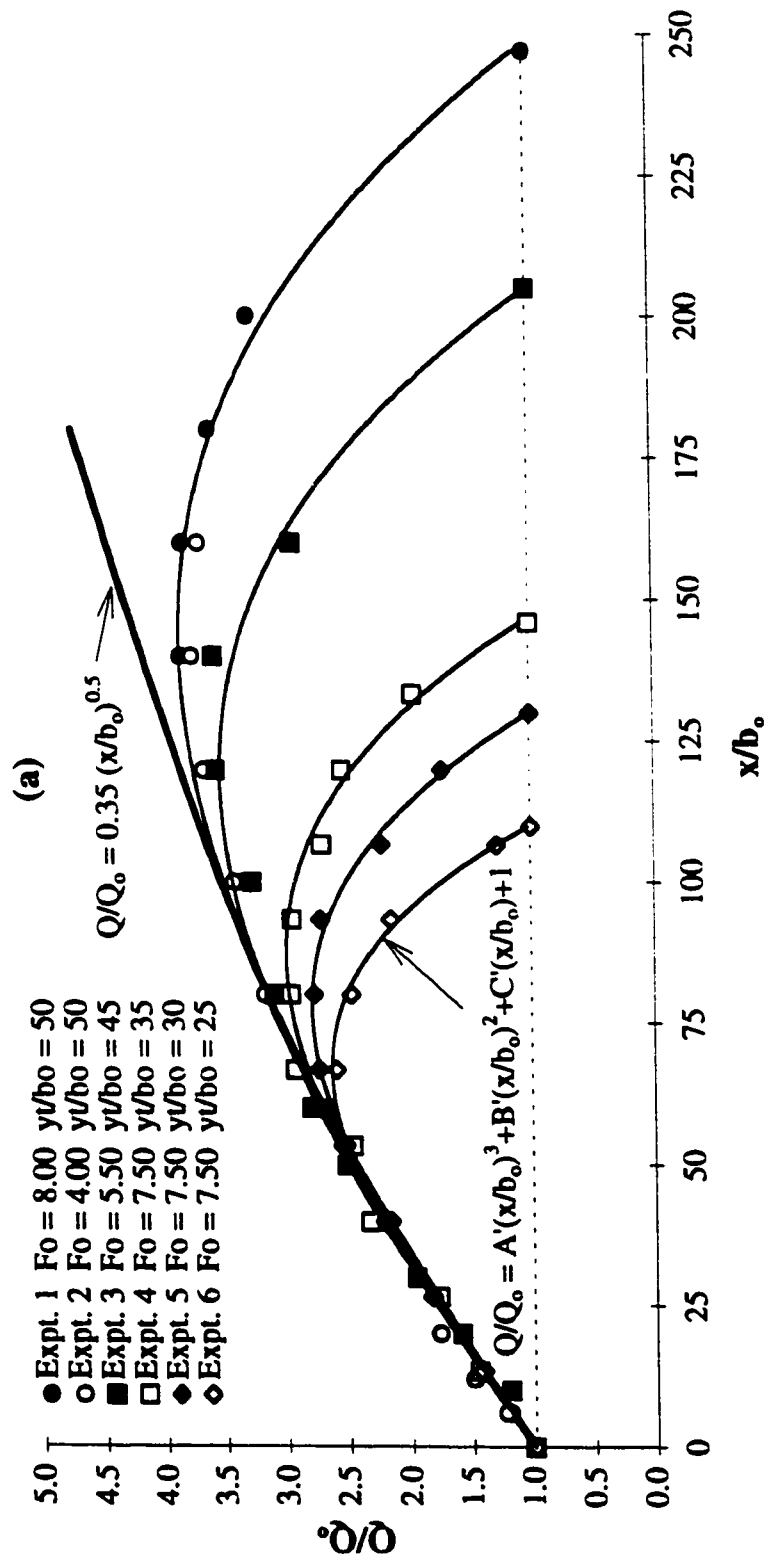


Fig. 6.17(a) Variation of the wall jet discharge with distance

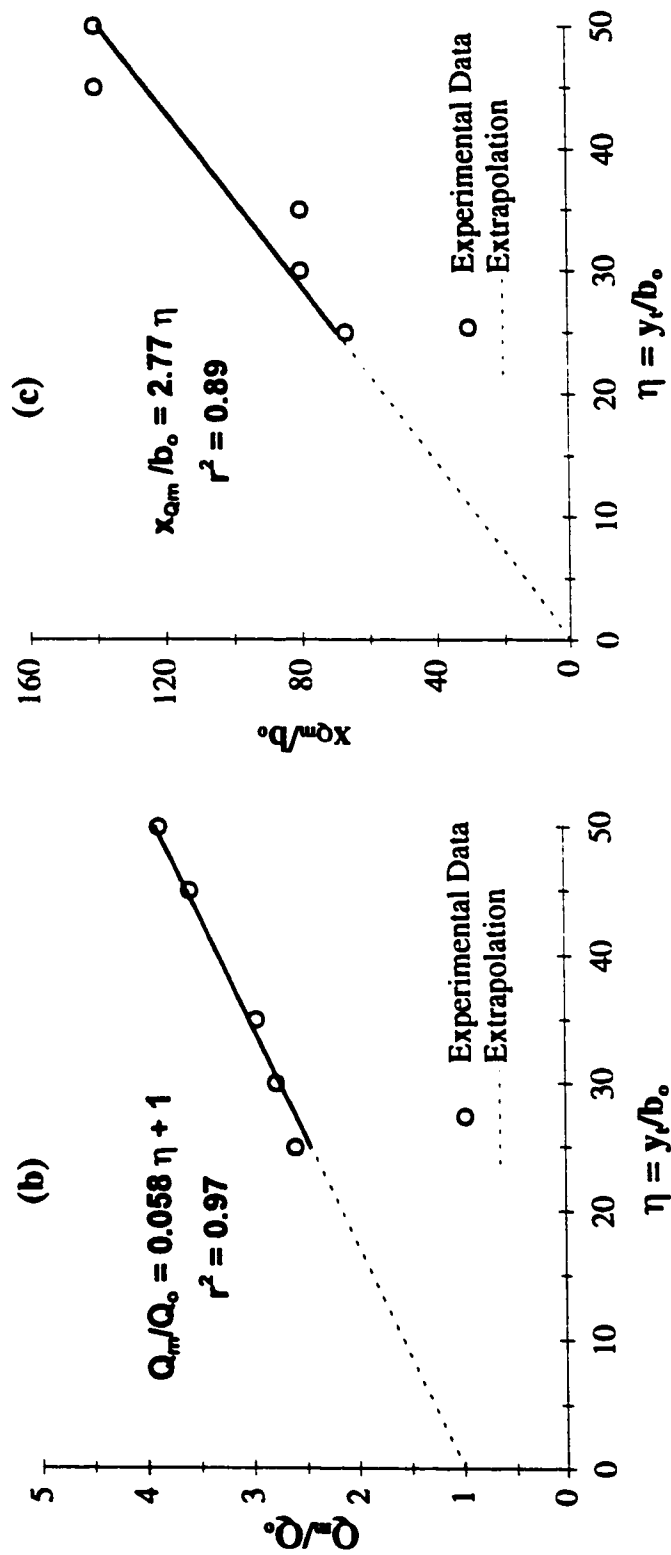


Fig. 6.17(b-c) Effect of y/b_0 on the magnitude and location of the maximum discharge

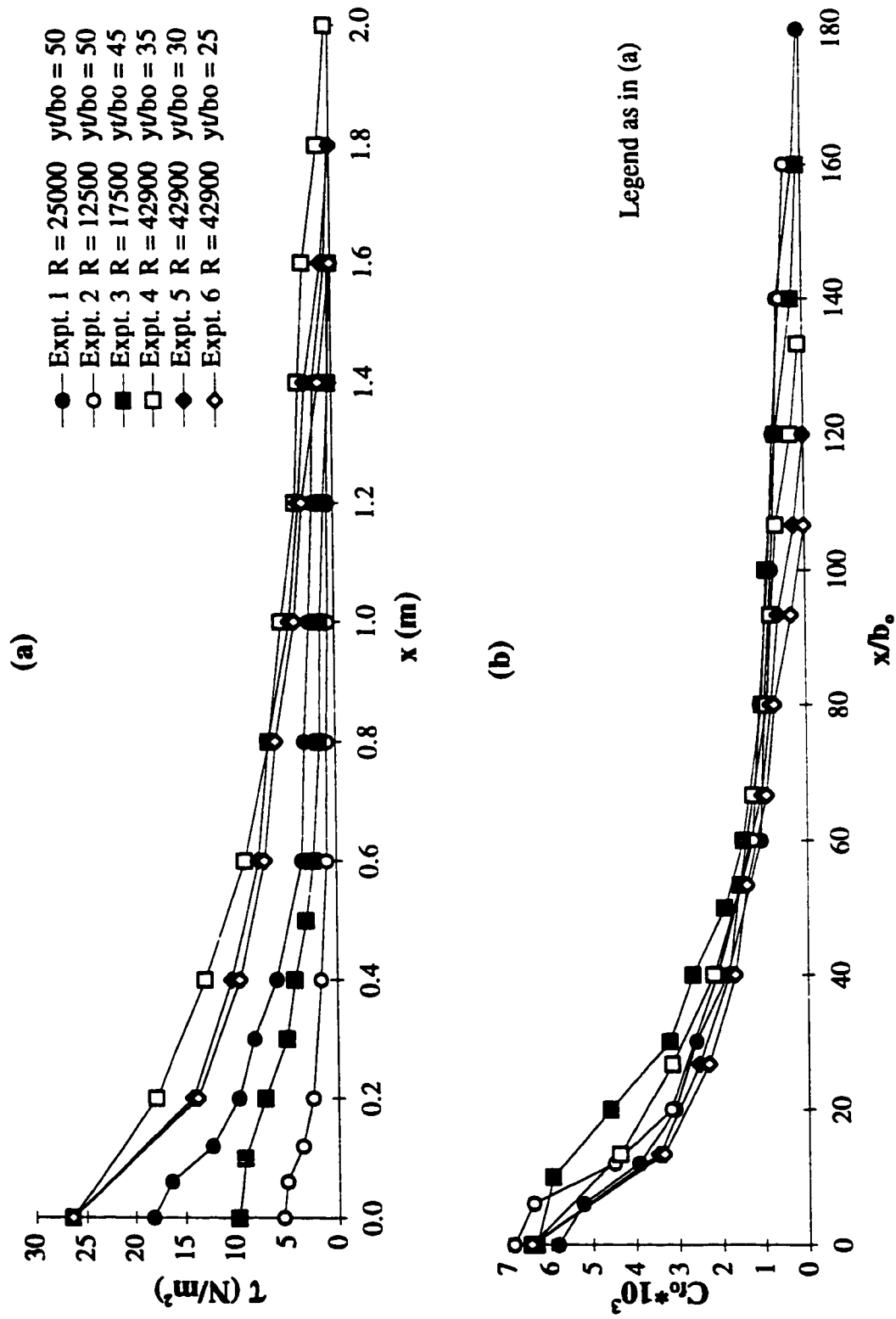


Fig. 6.18(a-b) Variation of the bed shear stress with distance

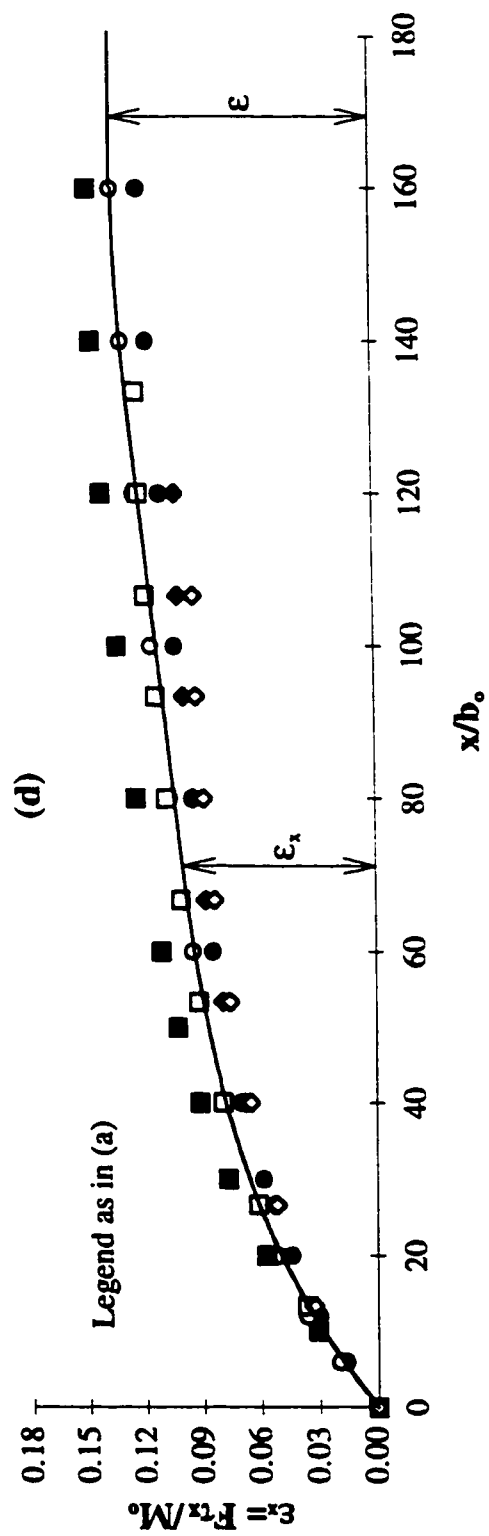
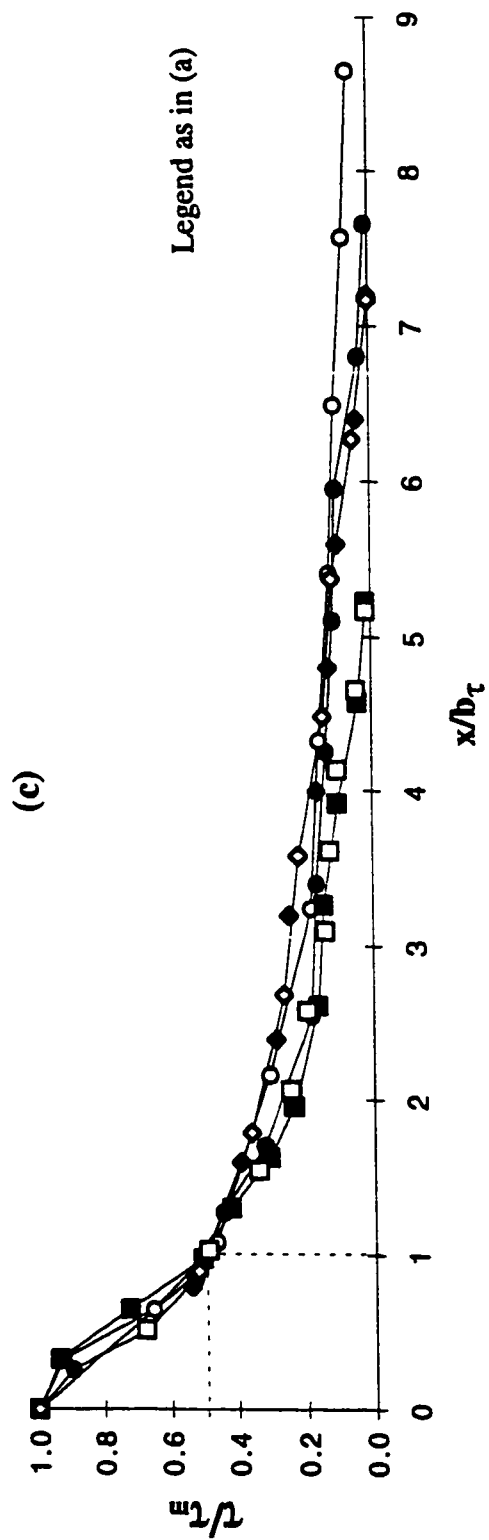


Fig. 6.18(c-d) Variation of the bed shear stress with distance

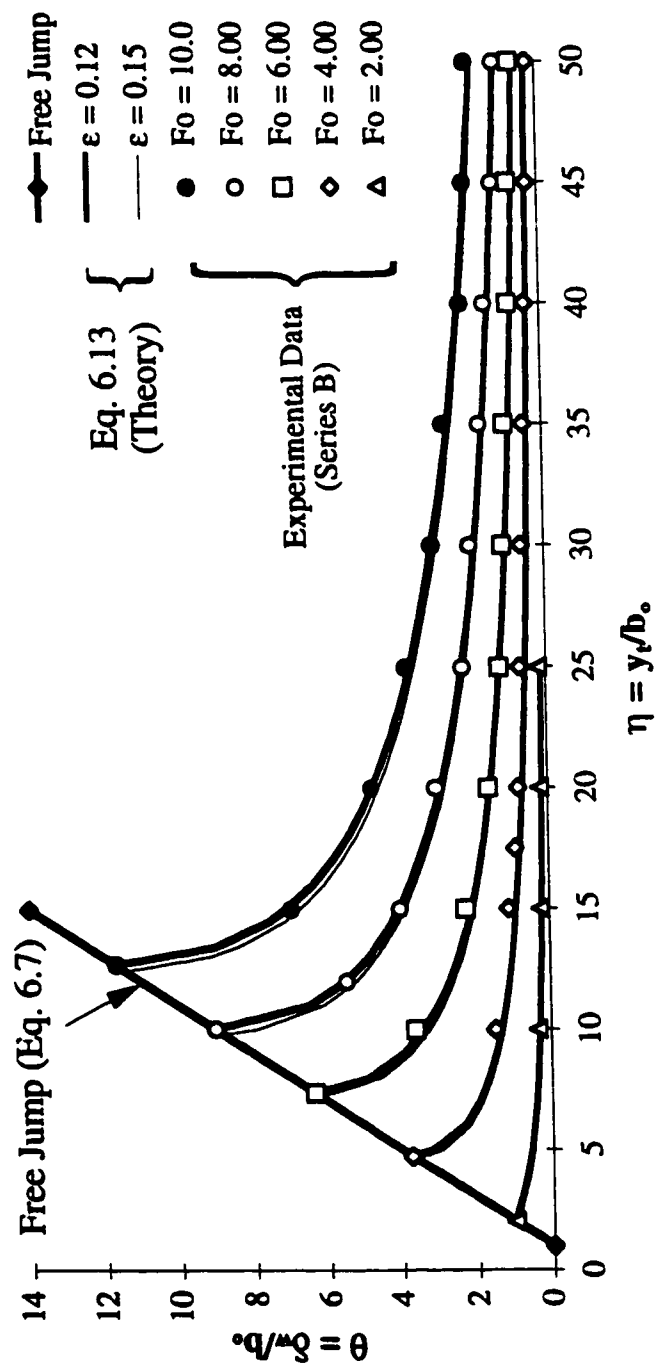


Fig. 6.19. Determination of the shear force coefficient ϵ

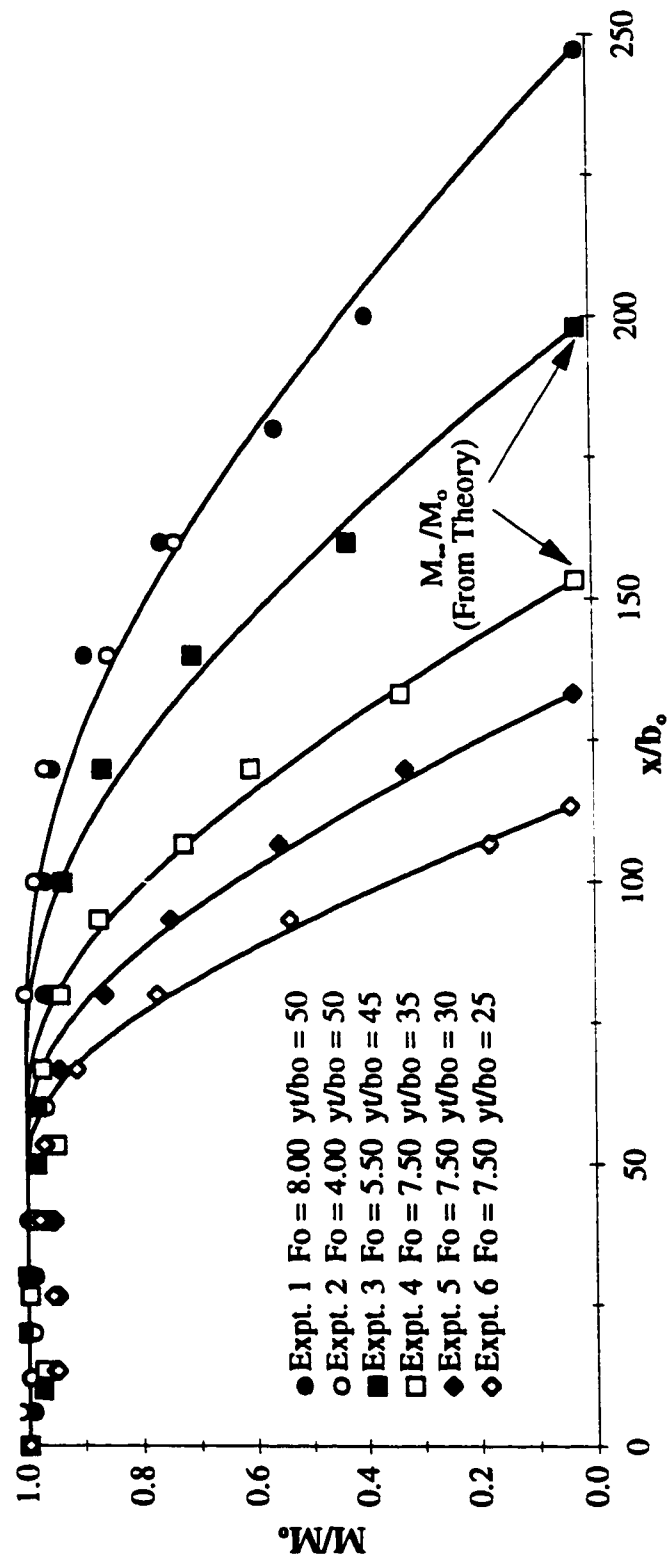


Fig. 6.20 Variation of the wall jet momentum flux with distance

Chapter 7

Conclusions and Recommendations

In the preceding three chapters, three studies have been presented on the behavior of turbulent jets in shallow tailwater. This chapter introduces a brief discussion on each of these contributions as well as recommendations for future research work.

Chapter 4 presented the results of an experimental study performed to introduce a new energy dissipator for use downstream of flow regulators. In the new design, a double-leaf gate is used where an inclined high-velocity jet issues between the two gates towards the free surface. In the double-leaf gate, the upper gate is located upstream of the lower one to create the opening which produces the inclined jet. The double-leaf gate is recommended for use in deeply submerged flow regulators where the discharge is independent of the location of the opening. Flow pattern A is recommended for design and can easily be achieved in flow regulators by keeping the opening, between the two gates, submerged and having side aeration to prevent jet oscillation.

The experimental work was performed mainly to study the decay of the maximum velocity and to compare it with that of free and submerged jumps. With a considerable submergence, the maximum velocity decays rapidly. The limited extent of the tailwater was the main reason for this enhanced decay. As soon as the jet issues from the slot, two recirculating flow regions, above and below the inclined jet, form and the return flow in these regions causes the momentum flux in the forward flow to decay significantly. The turbulent jet issues between the two gates towards the free surface and after striking the water surface proceeds as a surface jet. Shear stress on the bed is caused by the return flow which is relatively weak and hence, minor scour is

anticipated downstream of the new dissipator. However, using an apron downstream of the prototype, or using an equivalent sheet pile wall, is still essential for percolation requirements.

Most of existing flow regulators have single-leaf gates (sluice gates). For the new design to be used in these regulators, an upward sloping sill may be installed under the gate. Few experiments were performed, in the present study, to investigate the behavior of the inclined jet with zero offset ratio. However, the design with the gate opening at the bed needs more experiments, especially for the effect of the inclination angle on jet stability. Also, a future study on the scour downstream of double-leaf gate energy dissipators is recommended. The main objective of such study would be to check for the possibility of using a relatively short apron, with a sheet pile wall driven under the gate, downstream of this type of dissipators.

Chapter 5 presented a comprehensive study of plane turbulent surface jets in shallow tailwater. This study may be considered as a special case of the inclined turbulent jet used in the double-leaf gate model, with the inclination angle and the submergence ratio are equal to zero. In the first study (the double-leaf gate) it has been found from the experimental results that the momentum flux in the forward flow decays significantly. As it has been generally assumed that the momentum flux in turbulent jets discharged into large ambients would be preserved, it was interesting to perform a theoretical and an experimental study of a turbulent jet, of a simple geometry, in shallow tailwater. The main objective of such study was to investigate the reasons causing the momentum of turbulent jets in shallow tailwater to decay rapidly and to study the effect of the relative tailwater on the different characteristics of turbulent jets.

In the theoretical study, expressions for the momentum loss and the piezometric-pressure increase were formulated at a section just downstream of the line of the jet attachment to the bed. Nine experiments covering a wide range of the Froude

number and the offset ratio, were conducted. The experimental results showed that the length of the recirculating-flow region is about 6.50 times the offset distance. The velocity profiles in the surface jet were found to be similar, in the developing as well as in the developed flow regions. The maximum velocity was found to decay in two stages. In the first stage, the rate of decay was independent of the relative depth of tailwater whereas the faster rate in the second stage depended on it. The length of the first stage of decay was directly proportional to the offset ratio. The length scale of the jet grew at a rate of 0.065 in the early stage and the rate of growth was much smaller in the second stage. The variation of the volume flux in the surface jet was affected significantly by the tailwater depth ratio. The decay of the momentum flux in the surface jet, with the distance from the nozzle, was observed and correlated with the offset ratio and the relative longitudinal distance. The experimental observations of the momentum loss were found to be in agreement with theory. Empirical expressions for the above characteristics were developed.

This study has contributed to the theory of turbulent jets when the ambient fluid has a limited extent. A theoretical study of the momentum decay and the rise in the water surface elevation at any x-station, in the distance between the opening and the section at which the jet attaches to the bed, is challenging and needs further research. Surface jets in shallow tailwater could be used as the design element in what might be referred to as Surface Energy Dissipators. Experimental studies are needed, especially for the effect of relative tailwater on erosion downstream of these dissipators.

Chapter 6 presented a theoretical and a laboratory study of plane turbulent wall jets in shallow tailwater. After the completion of the first and second studies, it was interesting and useful to study the plane turbulent wall jets in a tailwater of limited extent. The combination of the three studies would make the subject, turbulent jets in shallow tailwater, more coherent and understandable.

The first thought implied that the two problems of surface and plane jets were very similar with the only difference in the location of the source discharge in both of them. But, the theoretical study revealed a subtle difference between the two problems regarding the tailwater depth in each of them. A surface jet with specific characteristics can be formed with only one value of the tailwater depth. On the other hand, a plane jet, having the same characteristics as the surface jet, can be formed with an infinite number of tailwater depths. This subtle difference made the theoretical approaches in the two problems quite different.

In the theoretical study, the momentum loss, in terms of the momentum at the nozzle, was evaluated at a section just downstream of the line of the jet attachment to the free surface. Also, the depression in the water surface elevation and the loss in the hydrostatic pressure force at the gate were evaluated with and without the inclusion of the bed shear stress. A general equation for the sequent depth ratio in free hydraulic jump with the inclusion of the bed shear stress, was also formulated. Experiments were conducted, for different Froude numbers and tailwater depth ratios, to measure the longitudinal velocity, the bed shear stress, the eddy length and the depression in the water surface elevation at the gate. The experimental results showed that the length of the return-flow region is dependent on the tailwater depth ratio and the Froude number. The velocity profiles in the wall jet were found to be similar, in the developing as well as in the developed flow regions. The maximum velocity in the fully developed flow region decayed in two stages. The rate of the velocity decay in the first stage was independent of the relative depth of tailwater while the length of this stage depended on it. In the second stage, the maximum velocity rate of decay was faster than that of the first stage and was affected by the relative tailwater. Empirical equations, in a non-dimensional form, for the effect of the relative tailwater on the discharge variation with distance, were developed. The integrated bed shear stress from the gate till the jet surfaced was estimated to be about 12%-15% of the momentum flux at the nozzle. The

measured drops in the water surface elevation at the gate were compared with the corresponding values from theory where both, measurements and theory, gave almost the same results. Momentum flux was preserved for a certain distance after which it decayed rapidly. Momentum decay was correlated with the tailwater depth ratio, the eddy length and the relative longitudinal distance.

In conclusion, the results from this study have highlighted the effect of limited tailwater depth on the behavior of plane turbulent wall jets. Again, recommended for future research is a study of the effect of the relative tailwater on downstream scour. Also, it would be interesting to perform a theoretical study for the momentum decay at any x-station between the gate and the section where the jet surfaces.

Appendix

1. A Double-Leaf Gate for Energy Dissipation Below Regulators

1.1 Velocity Measurements along Vertical Sections at x-stations

Expt. 1		7.5	0.212	22.5	0.264	20.5	0.2188	19	0.3333
x = 50 cm		8	0.178	23	0.317	21	0.2497	20	0.3472
y (cm)	u (m/s)	8.5	0.163	23.5	0.345	21.5	0.2806	21	0.4061
0	0.398	9	0.160	24	0.429	22	0.3066	22	0.4461
1	0.377	14	-0.123	24.5	0.453	22.5	0.3383	22.5	0.4425
2	0.370	16	-0.158	25	0.485	23	0.3517	23	0.4667
4	0.349	18	-0.187	25.5	0.493	23.5	0.3991	23.5	0.497
6	0.251	20	-0.200	26	0.476	24	0.4248	24	0.5266
8	0.164	22	-0.212	26.5	0.481	24.5	0.455	24.5	0.5377
11	-0.109	24	-0.226	27	0.495	25	0.4669	25	0.5493
12	-0.135	25	-0.214	27.5	0.504	25.5	0.494	25.5	0.5786
14	-0.164	25.5	-0.232	x = 40 cm		26	0.4967	26	0.5901
16	-0.189	x = 100 cm		y (cm)	u (m/s)	26.5	0.5045	26.5	0.5951
18	-0.202	y (cm)		u (m/s)		27	0.5096	27	0.5981
20	-0.211	0	0.207	0	-0.0948	27.5	0.5145	27.5	0.6072
22	-0.202	1	0.269	1	-0.1066	x = 60 cm		x = 100 cm	
24	-0.204	2	0.285	2	-0.0987	y (cm)		u (m/s)	
25	-0.201	3	0.279	3	-0.0908	17.5	0.1942	12	0.1537
25.5	-0.177	4	0.251	4	-0.0841	18	0.1843	13	0.1659
x = 60 cm		5	0.228	5	-0.0872	18.5	0.2007	14	0.1921
y (cm)		6	0.223	19	0.0893	19	0.2746	15	0.2121
0	0.517	7	0.217	19.5	0.1395	19.5	0.2717	16	0.22
1	0.552	8	0.178	20	0.1671	20	0.2776	17	0.2641
2	0.492	9	0.159	20.5	0.2053	20.5	0.3185	18	0.2841
4	0.376	10	0.146	21	0.2331	21	0.3453	19	0.2783
6	0.239	17	-0.109	21.5	0.2837	21.5	0.4025	20	0.3344
7	0.181	18	-0.107	22	0.3675	22	0.3914	21	0.3666
12	-0.157	20	-0.156	22.5	0.3758	22.5	0.4664	22	0.3886
14	-0.180	22	-0.150	23	0.4223	23	0.4651	22.5	0.4041
16	-0.214	24	-0.152	23.5	0.466	23.5	0.5118	23	0.4311
18	-0.227	25	-0.153	24	0.4996	24	0.5217	23.5	0.4374
20	-0.229	25.5	-0.147	24.5	0.5484	24.5	0.5514	24	0.4481
22	-0.229	x = 120 cm		25	0.5831	24.5	0.5514	24	0.4481
24	-0.233	y (cm)		25.5	0.5982	25	0.5847	24.5	0.4823
25	-0.230	4	0.128	26	0.6056	25.5	0.6063	25	0.4895
25.5	-0.222	5	0.128	26.5	0.6153	26	0.6344	25.5	0.4822
x = 80 cm		6	0.140	27	0.6283	26.5	0.6518	26	0.5016
y (cm)		7	0.125	27.5	0.6382	27	0.6698	26.5	0.52
0	0.367	8	0.126	x = 50 cm		27.5	0.6718	27	0.5428
1	0.441	9	0.117	y (cm)		x = 80 cm		27.5	0.55
2	0.439	10	0.112	0	-0.1097	y (cm)		x = 120 cm	
3	0.402	Expt. 2		1	-0.1273	13	0.1812	y (cm)	
4	0.356	x = 30 cm		2	-0.1003	14	0.1811	12.5	0.1515
5	0.319	y (cm)		3	-0.0904	15	0.2265	13	0.1389
6	0.303	21.5	0.164	19	0.1194	16	0.2449	14	0.1572
7	0.222	22	0.188	19.5	0.1542	17	0.268	15	0.1987
				20	0.169	18	0.3098	16	0.1848

17	0.201	21.5	0.105	41	0.222	2	-0.130	40	0.237
18	0.232	22	0.108	42	0.284	4	-0.125	41	0.239
19	0.243	22.5	0.115	43	0.388	6	-0.119	42	0.278
20	0.275	23	0.129	44	0.444	8	-0.151	43	0.300
21	0.282	23.5	0.144	45	0.495	10	-0.148	44	0.343
22	0.310	24	0.135	45.5	0.515	12	-0.157	45	0.365
23	0.349	24.5	0.152	46	0.525	14	-0.157	45.5	0.398
24	0.354	25	0.165	46.5	0.540	16	-0.152	46	0.410
25	0.363	25.5	0.178	47	0.545	18	-0.151	46.5	0.429
25.5	0.401	26	0.189	47.5	0.559	20	-0.154	47	0.449
26	0.400	26.5	0.195	48	0.570	22	-0.151	47.5	0.461
26.5	0.403	27	0.199	x = 40 cm		24	-0.156	48	0.480
27	0.412	27.5	0.202	y (cm) u (m/s)		26	-0.159	x = 100 cm	
27.5	0.422	x = 200 cm		0	-0.078	28	-0.140	y (cm) u (m/s)	
x = 140 cm		y (cm) u (m/s)		2	-0.108	30	-0.127	0	-0.115
y (cm) u (m/s)		23	0.087	4	-0.136	32	-0.100	1	-0.130
15.5	0.155	23.5	0.089	6	-0.128	39	0.165	2	-0.145
16	0.144	24	0.102	8	-0.125	40	0.213	4	-0.147
17	0.146	24.5	0.110	10	-0.123	41	0.237	6	-0.154
18	0.165	25	0.105	12	-0.137	42	0.282	8	-0.153
19	0.186	25.5	0.119	14	-0.135	43	0.308	10	-0.173
20	0.195	26	0.152	16	-0.139	44	0.357	12	-0.164
21	0.219	26.5	0.162	18	-0.143	45	0.412	14	-0.161
22	0.248	27	0.165	20	-0.144	45.5	0.422	16	-0.162
23	0.244	27.5	0.166	22	-0.154	46	0.459	18	-0.165
24	0.255	Expt. 3		24	-0.141	46.5	0.484	20	-0.140
25	0.294	x = 30 cm		26	-0.142	47	0.500	22	-0.152
25.5	0.282	y (cm) u (m/s)		28	-0.144	47.5	0.505	23	-0.134
26	0.283	0	-0.096	30	-0.131	48	0.519	24	-0.135
26.5	0.302	2	-0.113	32	-0.127	x = 80 cm		25	-0.121
27	0.324	4	-0.127	34	-0.104	y (cm) u (m/s)		26	-0.117
27.5	0.334	6	-0.130	39.5	0.152	0	-0.100	37	0.136
x = 160 cm		8	-0.124	40	0.179	1	-0.131	38	0.161
y (cm) u (m/s)		10	-0.134	41	0.240	2	-0.152	39	0.165
19	0.119	12	-0.120	42	0.293	4	-0.156	40	0.203
20	0.117	14	-0.135	43	0.387	6	-0.153	41	0.224
21	0.147	16	-0.134	44	0.436	8	-0.156	42	0.248
22	0.169	18	-0.125	45	0.502	10	-0.157	43	0.263
23	0.168	20	-0.132	45.5	0.535	12	-0.166	44	0.286
24	0.190	22	-0.125	46	0.571	14	-0.152	45	0.323
25	0.208	24	-0.130	46.5	0.591	16	-0.167	45.5	0.347
25.5	0.204	26	-0.128	47	0.603	18	-0.167	46	0.373
26	0.212	28	-0.139	47.5	0.612	20	-0.159	46.5	0.369
26.5	0.230	30	-0.133	48	0.626	22	-0.155	47	0.385
27	0.242	32	-0.127	x = 60 cm		24	-0.152	47.5	0.402
27.5	0.255	34	-0.115	y (cm) u (m/s)		26	-0.123	48	0.423
x = 180 cm		36	-0.107	0	-0.095	28	-0.115	x = 120 cm	
y (cm) u (m/s)		40	0.148	1	-0.112	39	0.183	y (cm) u (m/s)	

0	-0.094	42	0.187	16	-0.090	36	-0.115	50.5	0.421
1	-0.141	43	0.203	18	-0.078	38	-0.113	51	0.439
2	-0.130	44	0.224	41	0.108	40	-0.104	51.5	0.444
4	-0.149	45	0.244	42	0.121	43	0.189	52	0.463
6	-0.166	45.5	0.253	43	0.139	44	0.228	52.5	0.472
8	-0.149	46	0.276	44	0.147	45	0.278	53	0.498
10	-0.157	46.5	0.284	45	0.160	46	0.316	53.5	0.502
12	-0.151	47	0.296	45.5	0.164	47	0.337	54	0.494
14	-0.157	47.5	0.305	46	0.174	48	0.362	x = 60 cm	
16	-0.149	48	0.311	46.5	0.185	49	0.359	y (cm) u (m/s)	
18	-0.136	x = 160 cm		47	0.195	50	0.370	1	-0.101
20	-0.128	y (cm) u (m/s)		47.5	0.204	50.5	0.347	2	-0.119
22	-0.124	0	-0.099	48	0.213	51	0.342	4	-0.123
24	-0.103	1	-0.120	x = 200 cm		51.5	0.351	6	-0.134
38	0.128	2	-0.122	y (cm) u (m/s)		52	0.332	8	-0.128
39	0.148	4	-0.115	11	-0.127	52.5	0.316	10	-0.136
40	0.157	6	-0.123	45.5	0.136	53	0.286	12	-0.143
41	0.197	8	-0.130	46	0.142	53.5	0.269	14	-0.152
42	0.212	10	-0.124	46.5	0.152	54	0.266	16	-0.132
43	0.237	12	-0.131	47	0.144	54.5	0.253	18	-0.128
44	0.268	14	-0.133	47.5	0.152	x = 40 cm		20	-0.143
45	0.272	16	-0.116	48	0.156	y (cm) u (m/s)		22	-0.147
45.5	0.288	18	-0.102	Expt. 4		1	-0.091	24	-0.141
46	0.294	20	-0.098	x = 30 cm		2	-0.105	26	-0.139
46.5	0.317	21	-0.094	y (cm) u (m/s)		4	-0.108	28	-0.139
47	0.329	22	-0.101	2	-0.096	6	-0.100	30	-0.145
47.5	0.349	23	-0.104	4	-0.107	8	-0.100	32	-0.124
48	0.358	40	0.126	6	-0.101	10	-0.110	34	-0.119
x = 140 cm		41	0.133	8	-0.114	12	-0.106	35	-0.118
y (cm) u (m/s)		42	0.167	10	-0.107	14	-0.101	45	0.194
0	-0.114	43	0.174	12	-0.124	16	-0.111	46	0.216
1	-0.126	44	0.181	14	-0.133	18	-0.108	47	0.257
2	-0.139	45	0.203	16	-0.127	20	-0.118	48	0.299
4	-0.132	45.5	0.212	18	-0.135	22	-0.109	49	0.326
6	-0.128	46	0.229	19	-0.126	24	-0.109	50	0.376
8	-0.147	46.5	0.239	20	-0.134	26	-0.112	50.5	0.381
10	-0.148	47	0.249	21	-0.132	28	-0.111	51	0.410
12	-0.137	47.5	0.256	22	-0.131	30	-0.116	51.5	0.431
14	-0.146	48	0.269	24	-0.136	32	-0.118	52	0.455
16	-0.142	x = 180 cm		25	-0.132	34	-0.106	52.5	0.478
18	-0.129	y (cm) u (m/s)		26	-0.134	36	-0.113	53	0.496
20	-0.102	3	-0.102	27	-0.123	38	-0.106	53.5	0.515
22	-0.105	4	-0.111	28	-0.123	45	0.151	54	0.504
23	-0.105	6	-0.105	29	-0.125	46	0.187	x = 80 cm	
38	0.119	8	-0.096	30	-0.122	47	0.248	y (cm) u (m/s)	
39	0.131	10	-0.108	31	-0.121	48	0.313	0	-0.088
40	0.141	12	-0.103	32	-0.115	49	0.357	1	-0.119
41	0.177	14	-0.100	34	-0.109	50	0.396	2	-0.134

4	-0.140	28	-0.123	y (cm)	u (m/s)	46	0.120	50	0.15
6	-0.132	30	-0.106	0	-0.111	47	0.135	50.5	0.16
8	-0.148	46	0.201	1	-0.135	48	0.155	51	0.14
10	-0.150	47	0.216	2	-0.151	49	0.192	51.5	0.14
12	-0.148	48	0.238	4	-0.148	50	0.183	52	0.139
14	-0.155	49	0.252	6	-0.145	50.5	0.200	52.5	0.163
16	-0.156	50	0.295	8	-0.135	51	0.197	53	0.168
18	-0.162	50.5	0.298	10	-0.149	51.5	0.210	53.5	0.196
20	-0.163	51	0.315	12	-0.148	52	0.216	54	0.189
22	-0.161	51.5	0.334	14	-0.150	52.5	0.209	Expt. 8	
24	-0.150	52	0.357	16	-0.151	53	0.234	x = 35 cm	
26	-0.150	52.5	0.362	18	-0.140	53.5	0.224	y (cm)	u (m/s)
28	-0.133	53	0.392	20	-0.135	54	0.242	0	-0.102
30	-0.129	53.5	0.400	22	-0.119	x = 180 cm		1	-0.157
32	-0.112	54	0.392	23	-0.130	y (cm)	u (m/s)	2	-0.127
33	-0.116	x = 120 cm		24	-0.113	0	-0.099	5	-0.153
44	0.134	y (cm)	u (m/s)	25	-0.118	1	-0.103	8	-0.174
45	0.198	1	-0.141	45	0.149	2	-0.103	11	-0.172
46	0.196	2	-0.142	46	0.166	4	-0.119	14	-0.162
47	0.257	4	-0.158	47	0.157	6	-0.100	17	-0.170
48	0.262	6	-0.145	48	0.172	8	-0.106	20	-0.178
49	0.305	8	-0.147	49	0.203	10	-0.111	23	-0.164
50	0.319	10	-0.162	50	0.212	12	-0.104	25	-0.154
50.5	0.357	12	-0.160	50.5	0.234	14	-0.105	26	-0.116
51	0.349	14	-0.161	51	0.232	16	-0.103	33	0.215
51.5	0.384	16	-0.155	51.5	0.254	17	-0.109	34	0.261
52	0.394	18	-0.152	52	0.254	48	0.125	35	0.358
52.5	0.416	20	-0.149	52.5	0.270	49	0.136	36	0.437
53	0.449	22	-0.131	53	0.293	50	0.154	37	0.504
53.5	0.452	24	-0.117	53.5	0.298	50.5	0.145	38	0.562
54	0.452	26	-0.122	54	0.294	51	0.186	39	0.589
x = 100 cm		43	0.124	x = 160 cm		51.5	0.175	40	0.602
y (cm)	u (m/s)	44	0.170	y (cm)	u (m/s)	52	0.179	41	0.629
0	-0.125	45	0.147	0	-0.110	52.5	0.171	x = 45 cm	
1	-0.139	46	0.179	1	-0.132	53	0.200	y (cm)	u (m/s)
2	-0.150	47	0.184	2	-0.126	53.5	0.201	0	-0.115
4	-0.154	48	0.206	4	-0.128	54	0.203	1	-0.137
6	-0.150	49	0.230	6	-0.132	x = 200 cm		2	-0.160
8	-0.160	50	0.247	8	-0.127	y (cm)	u (m/s)	5	-0.164
10	-0.147	50.5	0.270	10	-0.127	7	-0.08	8	-0.195
12	-0.155	51	0.276	12	-0.136	8	-0.10	11	-0.199
14	-0.160	51.5	0.299	14	-0.123	10	-0.10	14	-0.200
16	-0.168	52	0.282	16	-0.128	12	-0.09	17	-0.189
18	-0.156	52.5	0.317	18	-0.131	14	-0.10	20	-0.214
20	-0.163	53	0.307	20	-0.121	15	-0.09	23	-0.196
22	-0.151	53.5	0.342	22	-0.104	16	-0.09	25	-0.146
24	-0.149	54	0.326	23	-0.102	48	0.10	26	-0.144
26	-0.129	x = 140 cm		45	0.114	49	0.11	27	-0.149

30	0.116	39	0.450	5	-0.130	2	-0.082	6	-0.146
32	0.200	40	0.476	8	-0.144	5	-0.092	7	-0.136
34	0.283	41	0.501	11	-0.137	8	-0.096	8	-0.171
36	0.403	x = 100 cm		14	-0.122	11	-0.093	10	-0.149
38	0.496	y (cm)	u (m/s)	17	-0.145	14	-0.084	12	-0.161
39	0.529	0	-0.133	20	-0.131	17	-0.084	14	-0.152
40	0.553	1	-0.174	23	-0.111	20	-0.106	16	-0.171
41	0.588	2	-0.169	24	-0.090	23	-0.069	18	-0.161
x = 60 cm		5	-0.170	25	-0.093	26	-0.068	20	-0.178
y (cm)	u (m/s)	8	-0.185	26	-0.087	29	-0.059	22	-0.179
0	-0.139	11	-0.176	27	-0.104	33	0.098	24	-0.162
1	-0.187	14	-0.188	28	-0.077	34	0.106	26	-0.146
2	-0.191	17	-0.182	29	-0.082	36	0.125	28	-0.161
5	-0.191	20	-0.170	30	-0.074	38	0.150	30	-0.159
8	-0.198	23	-0.124	33	0.094	39	0.191	32	-0.148
11	-0.213	31	0.152	34	0.130	40	0.236	34	-0.154
14	-0.208	32	0.176	36	0.182	41	0.288	36	-0.150
17	-0.216	34	0.260	38	0.205	x = 200 cm		38	-0.137
20	-0.210	36	0.297	39	0.252	y (cm)	u (m/s)	40	-0.123
23	-0.169	38	0.362	40	0.283	1	-0.078	41	-0.126
25	-0.106	39	0.392	41	0.308	2	-0.081	42	-0.117
26	-0.131	40	0.420	x = 160 cm		5	-0.078	45.5	0.160
30	0.136	41	0.454	y (cm)	u (m/s)	8	-0.083	46	0.168
32	0.191	x = 120 cm		0	-0.089	11	-0.095	46.5	0.216
34	0.294	y (cm)	u (m/s)	1	-0.103	14	-0.074	46.25	0.180
36	0.359	0	-0.120	2	-0.092	17	-0.082	47	0.247
38	0.469	1	-0.135	5	-0.112	20	-0.076	47.5	0.281
39	0.507	2	-0.132	8	-0.120	23	-0.087	48	0.328
40	0.533	5	-0.154	11	-0.106	25	-0.064	48.5	0.384
41	0.565	8	-0.151	14	-0.112	27	-0.060	49	0.391
x = 80 cm		11	-0.147	17	-0.097	28	-0.059	49.5	0.446
y (cm)	u (m/s)	14	-0.152	20	-0.101	30	0.085	50	0.506
0	-0.145	17	-0.149	23	-0.099	32	0.074	50.5	0.514
1	-0.178	20	-0.145	25	-0.100	34	0.079	51	0.541
2	-0.208	22	-0.124	27	-0.085	36	0.128	51.5	0.561
5	-0.190	23	-0.117	29	-0.060	38	0.138	52	0.590
8	-0.208	32	0.140	32	0.102	39	0.145	52.5	0.600
11	-0.208	34	0.163	33	0.104	40	0.204	53	0.603
14	-0.218	36	0.210	34	0.121	41	0.289	53.5	0.611
17	-0.218	38	0.281	36	0.158	Expt. 9		54	0.616
20	-0.189	39	0.304	38	0.176	x = 35 cm		54.5	0.609
23	-0.165	40	0.327	39	0.220	y (cm)	u (m/s)	55	0.587
24	-0.114	41	0.353	40	0.235	1	-0.115	x = 45 cm	
30	0.148	x = 140 cm		41	0.292	2	-0.111	y (cm)	u (m/s)
32	0.201	y (cm)	u (m/s)	x = 180 cm		2.5	-0.137	1.5	-0.146
34	0.269	0	-0.103	y (cm)	u (m/s)	3	-0.141	2	-0.156
36	0.360	1	-0.124	0	-0.064	4	-0.136	3	-0.149
38	0.437	2	-0.128	1	-0.085	5	-0.150	4	-0.129

5	-0.159	16	-0.171	22	-0.211	26	-0.209	44	0.249
6	-0.149	18	-0.208	24	-0.193	28	-0.196	44.5	0.275
8	-0.127	20	-0.189	26	-0.195	30	-0.188	45	0.249
10	-0.170	22	-0.181	28	-0.196	31	-0.172	45.5	0.281
12	-0.151	24	-0.186	30	-0.182	32	-0.153	46	0.264
14	-0.155	26	-0.189	32	-0.180	32.5	-0.145	46.5	0.321
16	-0.174	28	-0.171	34	-0.146	42.5	0.223	47	0.335
18	-0.157	30	-0.177	36	-0.143	43	0.199	47.5	0.345
20	-0.168	32	-0.178	43	0.185	43.5	0.224	48	0.335
22	-0.175	34	-0.150	43.5	0.196	44	0.233	48.5	0.373
24	-0.170	34.5	-0.151	44	0.221	44.5	0.266	49	0.391
26	-0.176	43.5	0.177	44.5	0.247	45	0.278	49.5	0.413
28	-0.161	44	0.175	45	0.263	45.5	0.298	50	0.432
30	-0.141	44.5	0.210	45.5	0.263	46	0.319	50.5	0.430
32	-0.164	45	0.236	46	0.297	46.5	0.318	51	0.453
34	-0.151	45.5	0.251	46.5	0.334	47	0.348	51.5	0.452
36	-0.142	46	0.287	47	0.337	47.5	0.372	52	0.481
37	-0.138	46.5	0.316	47.5	0.387	48	0.382	52.5	0.496
44.5	0.160	47	0.327	48	0.376	48.5	0.418	53	0.527
45.5	0.196	47.5	0.363	48.5	0.427	49	0.406	53.5	0.544
46	0.235	48	0.374	49	0.434	49.5	0.452	54	0.519
46.5	0.263	48.5	0.423	49.5	0.471	50	0.466	54.5	0.467
47	0.307	49	0.458	50	0.487	50.5	0.468	x = 120 cm	
47.5	0.341	49.5	0.461	50.5	0.489	51	0.502	y (cm) u (m/s)	
48	0.390	50	0.473	51	0.535	51.5	0.501	0.5	-0.182
48.5	0.422	50.5	0.530	51.5	0.563	52	0.526	1	-0.203
49	0.472	51	0.565	52	0.580	52.5	0.562	2	-0.183
49.5	0.511	51.5	0.587	52.5	0.602	53	0.585	3	-0.210
50	0.549	52	0.605	53	0.620	53.5	0.591	4	-0.199
50.5	0.588	52.5	0.633	53.5	0.636	54	0.570	6	-0.208
51	0.630	53	0.655	54	0.629	54.5	0.503	8	-0.210
51.5	0.667	53.5	0.647	54.5	0.595	x = 100 cm		10	-0.205
52	0.714	54	0.609	x = 80 cm		y (cm) u (m/s)		12	-0.202
52.5	0.714	54.5	0.687	y (cm) u (m/s)		3.5	-0.204	14	-0.203
53	0.741	x = 60 cm		1.5	-0.164	4	-0.202	16	-0.198
53.5	0.714	y (cm) u (m/s)		2	-0.157	6	-0.202	18	-0.195
54	0.682	0.5 -0.1429		2.5	-0.183	8	-0.195	20	-0.180
x = 55 cm		1 -0.155		3	-0.168	10	-0.217	21	-0.176
y (cm) u (m/s)		2.5 -0.1568		4	-0.171	12	-0.213	22	-0.182
0.5	-0.117	3 -0.1568		6	-0.182	14	-0.226	24	-0.168
1	-0.134	4 -0.1631		8	-0.215	16	-0.215	41	0.193
1.5	-0.133	6 -0.1644		10	-0.205	18	-0.226	41.5	0.204
2	-0.181	8 -0.172		12	-0.199	20	-0.206	43	0.222
4	-0.174	10 -0.176		14	-0.219	22	-0.197	43.5	0.227
6	-0.163	12 -0.1877		16	-0.230	24	-0.191	44	0.237
8	-0.155	14 -0.1905		18	-0.221	26	-0.180	44.5	0.240
10	-0.167	16 -0.1984		20	-0.224	42.5	0.211	45	0.295
12	-0.182	18 -0.1844		22	-0.223	43	0.221	45.5	0.299
14	-0.181	20 -0.1908		24	-0.211	43.5	0.227	46	0.306

46.5	0.312	51.5	0.376	6	-0.153	45.5	0.190	x = 60 cm	
47	0.311	52	0.360	8	-0.150	46	0.191	y (cm)	u (m/s)
47.5	0.321	52.5	0.394	10	-0.15	46.5	0.192	4	-0.258
48	0.309	53	0.390	12	-0.14	47	0.172	6	-0.238
48.5	0.333	53.5	0.390	13	-0.15	47.5	0.196	9	-0.286
49	0.373	54	0.431	16	-0.14	48	0.199	12	-0.276
49.5	0.365	54.5	0.401	18	-0.14	48.5	0.192	15	-0.296
50	0.376	x = 160 cm		43.5	0.18	49	0.221	18	-0.297
50.5	0.402	y (cm)	u (m/s)	44	0.20	49.5	0.219	21	-0.301
51	0.405	1	-0.177	45	0.17	50	0.242	24	-0.280
51.5	0.439	2	-0.185	45.5	0.18	50.5	0.257	27	-0.254
52	0.450	4	-0.171	46	0.18	51	0.249	29	-0.244
52.5	0.469	6	-0.187	46.5	0.23	51.5	0.274	42	0.283
53	0.465	8	-0.175	47	0.20	52	0.272	43	0.344
53.5	0.470	10	-0.173	47.5	0.18	52.5	0.289	44	0.394
54	0.464	12	-0.186	48	0.22	53	0.267	45	0.459
54.5	0.437	14	-0.173	48.5	0.24	53.5	0.305	46	0.498
x = 140 cm		16	-0.163	49	0.23	54	0.297	47	0.579
y (cm)	u (m/s)	17	-0.167	49.5	0.24	54.5	0.314	48	0.639
1	-0.172	20	-0.145	50	0.23	Expt. 12		49	0.728
2	-0.191	41	0.165	50.5	0.25	x = 40 cm		50	0.780
4	-0.203	43.5	0.189	51	0.27	y (cm)	u (m/s)	51	0.864
6	-0.196	44	0.203	51.5	0.29	0	-0.131	52	0.929
8	-0.200	44.5	0.197	52	0.29	1	-0.170	53	0.908
10	-0.189	45	0.204	52.5	0.29	2	-0.187	54	0.908
12	-0.188	45.5	0.201	53	0.28	4	-0.179	x = 80 cm	
14	-0.194	46	0.221	53.5	0.32	7	-0.196	y (cm)	u (m/s)
16	-0.179	46.5	0.226	54	0.33	10	-0.221	0	-0.242
18	-0.169	47	0.233	54.5	0.32	13	-0.253	1	-0.275
20	-0.173	47.5	0.253	x = 200 cm		16	-0.256	2	-0.310
42.5	0.223	48	0.249	y (cm)	u (m/s)	19	-0.234	5	-0.326
43	0.203	48.5	0.280	0	-0.113	22	-0.251	8	-0.337
43.5	0.231	49	0.277	2	-0.136	25	-0.224	11	-0.336
44	0.212	49.5	0.288	4	-0.149	28	-0.253	14	-0.353
44.5	0.219	50	0.282	6	-0.136	31	-0.223	17	-0.343
45	0.232	50.5	0.317	8	-0.124	34	-0.218	20	-0.329
45.5	0.220	51	0.311	10	-0.107	37	-0.153	23	-0.330
46	0.234	51.5	0.291	12	-0.120	40	-0.146	26	-0.305
46.5	0.234	52	0.342	14	-0.126	46	0.191	28	-0.258
47	0.259	52.5	0.293	16	-0.114	47	0.235	30	-0.230
47.5	0.266	53	0.346	42	0.138	48	0.363	31	-0.206
48	0.315	53.5	0.341	41	0.159	49	0.438	39	0.234
48.5	0.291	54	0.379	41.5	0.139	50	0.547	40	0.276
49	0.301	54.5	0.365	42.5	0.136	51	0.632	41	0.284
49.5	0.320	x = 180 cm		43.5	0.163	52	0.714	42	0.368
50	0.316	y (cm)	u (m/s)	44	0.172	53	0.754	43	0.371
50.5	0.332	2	-0.163	44.5	0.180	54	0.780	44	0.442
51	0.347	4	-0.151	45	0.157	55	0.780	45	0.506

46	0.530	23	-0.264	2	-0.246	2	-0.197	45	0.224
47	0.550	24	-0.251	5	-0.264	5	-0.187	47	0.300
48	0.594	25	-0.250	8	-0.258	8	-0.195	49	0.386
49	0.631	26	-0.253	11	-0.251	11	-0.185	51	0.463
50	0.670	41	0.260	14	-0.246	14	-0.174	53	0.521
51	0.754	42	0.298	17	-0.221	16	-0.140	53.5	0.545
52	0.780	43	0.380	20	-0.182	43	0.240	x = 80 cm	
53	0.792	44	0.398	43	0.280	44	0.269	y (cm) u (m/s)	
54	0.792	45	0.425	44	0.314	45	0.274	41	0.129
x = 100 cm		46	0.436	45	0.332	46	0.285	43	0.191
y (cm) u (m/s)		47	0.493	46	0.369	47	0.289	45	0.244
0	-0.230	48	0.516	47	0.360	48	0.310	47	0.310
1	-0.292	49	0.550	48	0.375	49	0.321	49	0.389
2	-0.298	50	0.586	49	0.402	50	0.329	51	0.433
5	-0.314	51	0.624	50	0.417	51	0.345	53	0.487
8	-0.320	52	0.649	51	0.452	52	0.374	53.5	0.501
11	-0.348	53	0.659	52	0.508	53	0.386	x = 120 cm	
14	-0.334	54	0.615	53	0.526	54	0.391	y (cm) u (m/s)	
17	-0.315	x = 140 cm		54	0.520	Expt. 14		39	0.095
20	-0.315	y (cm) u (m/s)		x = 180 cm		x = 40 cm		41	0.157
23	-0.284	0	-0.243	y (cm) u (m/s)		y (cm) u (m/s)		43	0.203
26	-0.245	1	-0.268	0	-0.203	43	0.182	45	0.255
27	-0.243	2	-0.283	1	-0.241	44	0.169	47	0.275
41	0.356	5	-0.289	2	-0.235	45	0.202	49	0.326
42	0.409	8	-0.295	5	-0.219	46	0.229	51	0.365
43	0.401	11	-0.281	8	-0.211	47	0.300	53	0.408
44	0.451	14	-0.273	11	-0.214	48	0.340	53.5	0.409
45	0.469	17	-0.259	14	-0.172	49	0.381	x = 160 cm	
46	0.516	20	-0.257	15	-0.178	50	0.437	y (cm) u (m/s)	
47	0.572	23	-0.242	16	-0.197	51	0.452	29	0.084
48	0.588	24	-0.231	17	-0.177	52	0.478	31	0.085
49	0.613	42	0.260	18	-0.199	53.5	0.497	33	0.095
50	0.686	43	0.291	43	0.284	x = 50 cm		35	0.106
51	0.686	44	0.350	44	0.284	y (cm) u (m/s)		37	0.118
52	0.714	45	0.351	45	0.298	43	0.116	39	0.155
53	0.728	46	0.386	46	0.288	45	0.187	41	0.171
54	0.686	47	0.394	47	0.309	47	0.287	43	0.181
x = 120 cm		48	0.443	48	0.353	48	0.331	45	0.199
y (cm) u (m/s)		49	0.472	49	0.379	49	0.382	47	0.223
0	-0.262	50	0.518	50	0.364	50	0.420	49	0.254
1	-0.273	51	0.521	51	0.411	51	0.453	51	0.298
2	-0.285	52	0.542	52	0.455	52	0.490	53	0.318
5	-0.297	53	0.579	53	0.427	53	0.531	53.5	0.346
8	-0.312	54	0.579	54	0.527	53.5	0.536	x = 200 cm	
11	-0.291	x = 160 cm		x = 200 cm		x = 60 cm		y (cm) u (m/s)	
14	-0.292	y (cm) u (m/s)		y (cm) u (m/s)		y (cm) u (m/s)		36	0.077
17	-0.296	0	-0.222	0	-0.180	41	0.100	38	0.110
20	-0.285	1	-0.258	1	-0.193	43	0.145	40	0.128

42	0.122	33	0.372	7	-0.191	31	0.139	19	0.196
44	0.147	35	0.466	10	-0.147	33	0.143	21	0.268
46	0.183	37	0.561	13	-0.153	35	0.169	23	0.404
48	0.246	39	0.591	16	-0.142	37	0.188	25	0.499
50	0.215	x = 65 cm		19	-0.127	39	0.202	25.7	0.531
52	0.258	y (cm)	u (m/s)	20	-0.133	x = 240 cm		x = 70 cm	
53	0.256	0	-0.156	25	0.090	y (cm)	u (m/s)	y (cm)	u (m/s)
53.5	0.264	1	-0.174	27	0.148	0	-0.101	0	-0.122
x = 240 cm		4	-0.211	29	0.201	1	-0.096	2	-0.125
y (cm)	u (m/s)	7	-0.201	31	0.230	4	-0.095	4	-0.121
38	0.094	10	-0.210	33	0.295	7	-0.095	16	0.152
40	0.095	13	-0.220	35	0.328	10	-0.090	18	0.215
42	0.094	16	-0.219	37	0.355	13	-0.086	20	0.268
44	0.132	19	-0.195	39	0.417	16	-0.084	22	0.360
46	0.150	22	-0.155	x = 160 cm		19	-0.083	24	0.452
48	0.171	24	-0.129	y (cm)	u (m/s)	26	0.066	25	0.471
50	0.167	27	0.151	0	-0.134	29	0.088	25.7	0.491
52	0.164	29	0.240	1	-0.132	32	0.107	x = 100 cm	
53	0.186	31	0.295	4	-0.141	35	0.126	y (cm)	u (m/s)
53.5	0.213	33	0.379	7	-0.143	37	0.147	16	0.139
x = 280 cm		35	0.445	10	-0.126	39	0.162	18	0.174
y (cm)	u (m/s)	37	0.534	13	-0.127	Expt. 16		20	0.198
38	0.074	39	0.585	16	-0.111	x = 35 cm		22	0.226
40	0.084	x = 80 cm		17	-0.102	y (cm)	u (m/s)	24	0.295
42	0.082	y (cm)	u (m/s)	18	-0.097	0	-0.157	25.7	0.351
44	0.097	0	-0.202	25	0.085	1	-0.174	x = 140 cm	
46	0.107	1	-0.213	27	0.104	2	-0.172	y (cm)	u (m/s)
48	0.118	4	-0.233	29	0.142	4	-0.169	16	0.109
50	0.157	7	-0.236	31	0.191	6	-0.172	18	0.128
52	0.133	10	-0.210	33	0.208	8	-0.170	20	0.148
53	0.158	13	-0.217	35	0.223	10	-0.158	22	0.173
53.5	0.181	16	-0.211	37	0.251	12	-0.143	24	0.203
Expt. 15		19	-0.160	39	0.308	18	0.163	25.7	0.219
x = 50 cm		22	-0.127	x = 200 cm		20	0.255	x = 180 cm	
y (cm)	u (m/s)	23	-0.096	y (cm)	u (m/s)	22	0.420	y (cm)	u (m/s)
0	-0.117	27	0.148	0	-0.109	24	0.511	18	0.080
1	-0.144	29	0.227	1	-0.117	25	0.552	20	0.099
4	-0.172	31	0.291	4	-0.110	25.7	0.602	22	0.117
7	-0.161	33	0.373	7	-0.111	x = 50 cm		24	0.127
10	-0.173	35	0.416	9	-0.097	y (cm)	u (m/s)	25.7	0.133
13	-0.167	37	0.504	11	-0.103	0	-0.1696	x = 220 cm	
16	-0.184	39	0.544	14	-0.094	2	-0.1917	y (cm)	u (m/s)
19	-0.176	x = 120 cm		17	-0.097	4	-0.2177	20	0.0747
22	-0.146	y (cm)	u (m/s)	20	-0.098	6	-0.1588	22	0.0863
27	0.071	0	-0.160	21	-0.090	8	-0.1569	24	0.0988
29	0.153	1	-0.175	27	0.114	10	-0.1197	25.7	0.1071
31	0.265	4	-0.188	29	0.122	17	0.1565		

Expt. 17	19	0.2529	16	0.1173	44	0.570	48	0.609
x = 40 cm	21	0.313	18	0.1182	46	0.660	50	0.686
y (cm) u (m/s)	23	0.369	20	0.1489	48	0.720	52	0.724
0 -0.304	25.7	0.400	22	0.1591	50	0.806	54	0.758
2 -0.311	x = 120 cm		24	0.1754	52	0.840	x = 140 cm	
4 -0.316	y (cm) u (m/s)	25.7	0.1977	54	0.882	y (cm) u (m/s)		
6 -0.258	14	0.141	Expt. 18	x = 90 cm	0	-0.229		
8 -0.218	16	0.191	x = 50 cm	y (cm) u (m/s)	4	-0.266		
9 -0.214	18	0.259	y (cm) u (m/s)	0	-0.226	8	-0.276	
10 -0.191	20	0.237	5	-0.230	1	-0.249	12	-0.277
11 -0.189	22	0.293	8	-0.267	2	-0.286	16	-0.262
16 0.201	24	0.313	11	-0.272	5	-0.308	20	-0.241
18 0.409	25.7	0.336	14	-0.269	8	-0.291	22	-0.239
20 0.635	x = 140 cm		17	-0.240	11	-0.324	23	-0.231
22 0.805	y (cm) u (m/s)	20	-0.240	14	-0.327	37	0.187	
24 0.824	13	0.130	23	-0.233	17	-0.328	38	0.224
25.7 0.835	15	0.150	26	-0.252	21	-0.329	40	0.299
x = 50 cm	17	0.166	30	-0.222	24	-0.301	42	0.368
y (cm) u (m/s)	19	0.192	33	-0.237	27	-0.272	44	0.425
0 -0.3172	21	0.204	36	-0.238	30	-0.219	46	0.515
2 -0.2981	23	0.230	42	0.197	36	0.184	48	0.545
4 -0.2579	25.7	0.246	44	0.337	38	0.242	50	0.591
6 -0.2063	x = 180 cm		46	0.521	40	0.384	52	0.639
15 0.2094	y (cm) u (m/s)	48	0.754	42	0.433	53	0.647	
16 0.2716	0	0.088	50	0.820	44	0.540	54	0.659
18 0.4815	2	0.109	52	0.886	46	0.652	x = 180 cm	
20 0.6329	4	0.122	54	0.908	48	0.728	y (cm) u (m/s)	
22 0.8167	6	0.119	x = 70 cm	50	0.817	50	0.817	0 -0.1891
24 0.832	8	0.106	y (cm) u (m/s)	52	0.845	52	0.845	4 -0.2357
25.7 0.8346	10	0.103	0	-0.230	54	0.874	8	-0.2378
x = 70 cm	12	0.091	1	-0.295	x = 110 cm		12	-0.2367
y (cm) u (m/s)	14	0.109	2	-0.255	y (cm) u (m/s)		16	-0.2054
0 -0.188	16	0.125	5	-0.261	0	-0.235	19	-0.1727
2 -0.212	18	0.147	8	-0.295	4	-0.316	37	0.176
4 -0.179	20	0.164	11	-0.255	8	-0.310	38	0.2104
14 0.182	22	0.185	14	-0.256	12	-0.325	40	0.2802
16 0.267	25.7	0.201	17	-0.264	16	-0.330	42	0.3426
18 0.326	x = 220 cm		20	-0.273	20	-0.325	44	0.3699
20 0.405	y (cm) u (m/s)	23	-0.271	24	-0.263	46	0.4107	
22 0.488	0	0.0445	26	-0.265	28	-0.233	48	0.4513
24 0.540	2	0.0804	29	-0.270	29	-0.200	50	0.4961
25.7 0.566	4	0.0996	30	-0.272	38	0.237	52	0.5315
x = 100 cm	6	0.1065	31	-0.265	37	0.175	53	0.5493
y (cm) u (m/s)	8	0.1068	32	-0.275	40	0.348	54	0.5646
13 0.1494	10	0.1107	38	0.211	42	0.431	x = 220 cm	
15 0.1865	12	0.1085	40	0.330	44	0.447	y (cm) u (m/s)	
17 0.2299	14	0.1327	42	0.433	46	0.588	0	-0.167

4	-0.1636	42	0.551	40	0.382	50	0.705	42	0.194
8	-0.1649	44	0.728	42	0.501	52	0.724	44	0.210
12	-0.1653	46	0.767	44	0.639	54	0.754	46	0.239
16	-0.1426	48	0.817	46	0.700	x = 180 cm		48	0.255
37	0.1767	50	0.817	48	0.754	y (cm) u (m/s)		50	0.278
38	0.2015	52	0.847	50	0.792	0	-0.168	52	0.296
40	0.2467	54	0.884	52	0.813	4	-0.238	54	0.323
42	0.2863	x = 70 cm		54	0.854	8	-0.245	Expt. 20	
44	0.3066	y (cm) u (m/s)		x = 110 cm		12	-0.247	x = 60 cm	
46	0.3375	0	-0.127	y (cm) u (m/s)		16	-0.215	y (cm) u (m/s)	
48	0.3657	1	-0.237	0	-0.230	20	-0.202	0	-0.134
50	0.3969	2	-0.227	4	-0.350	22	-0.166	1	-0.160
52	0.4257	5	-0.265	8	-0.344	24	-0.170	4	-0.204
53	0.4515	8	-0.297	12	-0.362	36	0.148	8	-0.216
54	0.4712	11	-0.298	16	-0.369	38	0.206	12	-0.224
x = 260 cm		14	-0.320	20	-0.349	40	0.259	16	-0.274
y (cm) u (m/s)		17	-0.330	24	-0.290	42	0.290	20	-0.259
0	-0.155	20	-0.317	28	-0.235	44	0.364	24	-0.275
4	-0.167	23	-0.313	29	-0.221	46	0.414	26	-0.265
8	-0.169	26	-0.299	36	0.246	48	0.459	28	-0.272
12	-0.169	29	-0.219	38	0.360	50	0.505	30	-0.208
16	-0.159	30	-0.244	40	0.414	52	0.524	32	-0.183
36	0.177	36	0.197	42	0.566	54	0.566	36	0.332
38	0.202	38	0.310	44	0.596	x = 220 cm		38	0.444
40	0.233	40	0.465	46	0.712	y (cm) u (m/s)		42	0.741
42	0.255	42	0.594	48	0.792	0	-0.138	46	0.780
44	0.278	44	0.780	50	0.836	4	-0.146	50	0.662
46	0.295	46	0.919	52	0.866	8	-0.147	52	0.575
48	0.310	48	0.991	54	0.883	12	-0.151	54	0.566
50	0.328	50	1.052	x = 140 cm		16	-0.156	x = 80 cm	
52	0.346	52	1.093	y (cm) u (m/s)		36	0.151	y (cm) u (m/s)	
53	0.363	54	1.100	0	-0.226	38	0.171	0	-0.184
54	0.373	x = 90 cm		4	-0.276	40	0.190	1	-0.223
Expt. 19		y (cm) u (m/s)		8	-0.274	42	0.216	4	-0.236
x = 50 cm		0	-0.254	12	-0.293	44	0.234	8	-0.304
y (cm) u (m/s)		1	-0.270	16	-0.281	46	0.293	12	-0.301
2	-0.165	2	-0.315	20	-0.302	48	0.323	16	-0.306
5	-0.192	5	-0.343	22	-0.239	50	0.363	20	-0.315
8	-0.206	8	-0.330	24	-0.218	52	0.407	24	-0.333
11	-0.218	11	-0.352	26	-0.222	54	0.448	28	-0.277
14	-0.226	14	-0.344	28	-0.170	x = 260 cm		32	-0.161
17	-0.247	17	-0.378	36	0.195	y (cm) u (m/s)		38	0.198
20	-0.259	20	-0.352	38	0.262	0	-0.103	42	0.472
23	-0.247	23	-0.337	40	0.327	4	-0.100	44	0.589
26	-0.279	26	-0.323	42	0.405	8	-0.099	46	0.655
30	-0.260	29	-0.238	44	0.458	12	-0.101	48	0.714
38	0.207	36	0.206	46	0.560	16	-0.081	50	0.767
40	0.388	38	0.337	48	0.662	40	0.174	52	0.829

54	0.829	12	-0.254	26	-0.200	40	0.366	54	0.369
x = 100 cm		16	-0.213	27	-0.160	42	0.450	x = 200 cm	
y (cm)	u (m/s)	20	-0.219	32	0.278	44	0.470	y (cm)	u (m/s)
0	-0.235	24	-0.206	36	0.605	46	0.504	0	-0.138
1	-0.268	44	0.204	40	0.829	48	0.535	1	-0.158
4	-0.309	46	0.267	44	0.727	50	0.551	4	-0.164
8	-0.321	48	0.338	46	0.598	52	0.571	8	-0.167
12	-0.313	50	0.407	48	0.480	54	0.584	12	-0.153
16	-0.339	52	0.502	50	0.411	x = 120 cm		14	-0.142
20	-0.332	54	0.548	52	0.316	y (cm) u (m/s)		16	-0.125
24	-0.294	x = 200 cm		54	0.313	0	-0.207	42	0.155
28	-0.260	y (cm)	u (m/s)	x = 80 cm		1	-0.267	44	0.183
32	-0.212	0	-0.162	y (cm)	u (m/s)	4	-0.277	46	0.207
40	0.239	1	-0.166	0	-0.255	8	-0.280	48	0.218
42	0.337	4	-0.174	1	-0.333	12	-0.266	50	0.221
44	0.417	8	-0.177	4	-0.319	16	-0.254	52	0.223
46	0.527	12	-0.169	8	-0.312	20	-0.257	54	0.224
48	0.585	14	-0.190	12	-0.356	22	-0.265	x = 220 cm	
50	0.657	46	0.204	16	-0.310	23	-0.275	y (cm) u (m/s)	
52	0.728	48	0.224	20	-0.316	24	-0.268	1	-0.121
54	0.767	50	0.254	24	-0.237	25	-0.249	4	-0.130
x = 120 cm		52	0.299	26	-0.191	34	0.132	8	-0.140
y (cm)	u (m/s)	54	0.354	32	0.168	36	0.163	12	-0.142
0	-0.241	x = 220 cm		34	0.224	38	0.171	16	-0.133
1	-0.304	y (cm)	u (m/s)	36	0.324	40	0.228	44	0.168
4	-0.286	0	-0.136	38	0.440	42	0.261	46	0.180
8	-0.321	1	-0.129	40	0.515	44	0.309	48	0.192
12	-0.303	4	-0.139	42	0.573	46	0.373	50	0.202
16	-0.315	8	-0.142	44	0.638	48	0.444	52	0.207
20	-0.336	12	-0.139	46	0.656	50	0.478	54	0.208
24	-0.309	14	-0.133	48	0.647	52	0.508		
26	-0.286	46	0.184	50	0.607	54	0.547		
28	-0.280	48	0.207	52	0.578	x = 160 cm			
30	-0.249	50	0.233	54	0.550	y (cm) u (m/s)			
32	-0.206	52	0.268	x = 100 cm		0	-0.201		
42	0.245	54	0.328	y (cm)	u (m/s)	1	-0.220		
44	0.317	Expt. 21		0	-0.231	4	-0.204		
46	0.398	x = 60 cm		1	-0.371	8	-0.200		
48	0.511	y (cm)	u (m/s)	4	-0.354	12	-0.196		
50	0.610	0	-0.226	8	-0.335	16	-0.218		
52	0.687	1	-0.288	12	-0.335	18	-0.208		
54	0.683	4	-0.286	16	-0.284	19	-0.189		
x = 160 cm		8	-0.287	20	-0.245	42	0.202		
y (cm)	u (m/s)	12	-0.311	24	-0.197	44	0.234		
0	-0.235	16	-0.312	26	-0.166	46	0.241		
1	-0.203	20	-0.293	34	0.161	48	0.278		
4	-0.239	24	-0.263	36	0.238	50	0.316		
8	-0.245	25	-0.230	38	0.284	52	0.342		

1.2 Velocity Measurements for the Inclined Jet

Expt. 3				0.1282	0.3690	30	0.713
$x/b_o = 9.12$ & $y/b_o = 32.90$				0.1239	0.3715	30	0.678
x (m)	y (m)	θ (deg.)	u (m/s)	0.1195	0.3740	30	0.645
0.1172	0.3140	30	0.325	0.1152	0.3765	30	0.603
0.1128	0.3165	30	0.562	0.1109	0.3790	30	0.560
0.1085	0.3190	30	0.611	0.1022	0.3840	30	0.492
0.1042	0.3215	30	0.822	$x/b_o = 16.62$ & $y/b_o = 37.90$			
0.0998	0.3240	30	0.936	x (m)	y (m)	θ (deg.)	u (m/s)
0.0955	0.3265	30	1.018	0.2138	0.3515	30	0.3245
0.0912	0.3290	30	1.029	0.2095	0.3540	30	0.3944
0.0868	0.3315	30	0.959	0.2051	0.3565	30	0.4776
0.0825	0.3340	30	0.912	0.2008	0.3590	30	0.5112
0.0782	0.3365	30	0.812	0.1965	0.3615	30	0.4972
0.0739	0.3390	30	0.763	0.1922	0.3640	30	0.5502
$x/b_o = 11.62$ & $y/b_o = 34.65$				0.1878	0.3665	30	0.5956
x (m)	y (m)	θ (deg.)	u (m/s)	0.1835	0.3690	30	0.6146
0.1422	0.3315	30	0.514	0.1792	0.3715	30	0.6468
0.1378	0.3340	30	0.542	0.1748	0.3740	30	0.6566
0.1335	0.3365	30	0.615	0.1705	0.3765	30	0.6664
0.1292	0.3390	30	0.775	0.1662	0.3790	30	0.6713
0.1248	0.3415	30	0.802	0.1575	0.3840	30	0.6452
0.1205	0.3440	30	0.820	0.1489	0.3890	30	0.632
0.1162	0.3465	30	0.843	0.1402	0.3940	30	0.6106
0.1118	0.3490	30	0.812	0.1315	0.3990	30	0.5805
0.1075	0.3515	30	0.794	0.1142	0.4090	30	0.4841
0.1032	0.3540	30	0.726	$x/b_o = 19.12$ & $y/b_o = 39.40$			
0.0989	0.3565	30	0.672	x (m)	y (m)	θ (deg.)	u (m/s)
0.0945	0.3590	30	0.636	0.2431	0.3640	30	0.2728
$x/b_o = 14.12$ & $y/b_o = 36.15$				0.2345	0.3690	30	0.3434
x (m)	y (m)	θ (deg.)	u (m/s)	0.2258	0.3740	30	0.376
0.1758	0.3415	30	0.417	0.2215	0.3765	30	0.3858
0.1715	0.3440	30	0.477	0.2172	0.3790	30	0.3961
0.1672	0.3465	30	0.522	0.2128	0.3815	30	0.491
0.1628	0.3490	30	0.565	0.2085	0.3840	30	0.5143
0.1585	0.3515	30	0.678	0.2042	0.3865	30	0.5143
0.1585	0.3515	30	0.666	0.1998	0.3890	30	0.5484
0.1542	0.3540	30	0.704	0.1912	0.3940	30	0.5691
0.1498	0.3565	30	0.739	0.1825	0.3990	30	0.5592
0.1455	0.3590	30	0.752	0.1739	0.4040	30	0.5581
0.1412	0.3615	30	0.770	0.1652	0.4090	30	0.5323
0.1368	0.3640	30	0.766	0.1565	0.4140	30	0.5245
0.1325	0.3665	30	0.731	0.1479	0.4190	30	0.4975

0.1392	0.4240	30	0.466	$x/b_o = 10.75$ & $y/b_o = 34.40$			
$x/b_o = 20.62$ & $y/b_o = 41.40$				x (m)	y (m)	θ (deg.)	u (m/s)
x (m)	y (m)	θ (deg.)	u (m/s)	0.1845	0.3240	30	15.5
0.2928	0.3640	30	0.241	0.1758	0.3290	30	16
0.2841	0.3690	30	0.292	0.1672	0.3340	30	16.5
0.2755	0.3740	30	0.331	0.1585	0.3390	30	17
0.2668	0.3790	30	0.365	0.1498	0.3440	30	17.5
0.2581	0.3840	30	0.422	0.1412	0.3490	30	18
0.2495	0.3890	30	0.476	0.1325	0.3540	30	18.5
0.2408	0.3940	30	0.492	0.1239	0.3590	30	19
0.2322	0.3990	30	0.490	0.1152	0.3640	30	19.5
0.2235	0.4040	30	0.515	0.1065	0.3690	30	20
0.2148	0.4090	30	0.510	0.0979	0.3740	30	20.5
0.2062	0.4140	30	0.528	0.0892	0.3790	30	21
0.1975	0.4190	30	0.523	$x/b_o = 15.75$ & $y/b_o = 37.10$			
0.1889	0.4240	30	0.492	x (m)	y (m)	θ (deg.)	u (m/s)
0.1802	0.4290	30	0.473	0.2095	0.3410	30	0.080
0.1629	0.4390	30	0.415	0.2008	0.3460	30	0.110
$x/b_o = 22.62$ & $y/b_o = 41.90$				0.1922	0.3510	30	0.192
x (m)	y (m)	θ (deg.)	u (m/s)	0.1835	0.3560	30	0.345
0.3128	0.3690	30	0.111	0.1748	0.3610	30	0.729
0.2955	0.3790	30	0.130	0.1662	0.3660	30	1.037
0.2868	0.3840	30	0.173	0.1575	0.3710	30	1.298
0.2781	0.3890	30	0.232	0.1489	0.3760	30	1.147
0.2695	0.3940	30	0.300	0.1402	0.3810	30	0.682
0.2608	0.3990	30	0.356	$x/b_o = 23.90$ & $y/b_o = 47.61$			
0.2522	0.4040	30	0.395	x (m)	y (m)	θ (deg.)	u (m/s)
0.2435	0.4090	30	0.408	0.2991	0.4161	45	0.094
0.2348	0.4140	30	0.430	0.2891	0.4261	45	0.144
0.2262	0.4190	30	0.469	0.2691	0.4461	45	0.395
0.2089	0.4290	30	0.460	0.2591	0.4561	45	0.510
0.1915	0.4390	30	0.433	0.2491	0.4661	45	0.665
0.1742	0.4490	30	0.375	0.2391	0.4761	45	0.707
Expt.9				0.2291	0.4861	45	0.597
$x/b_o = 13.25$ & $y/b_o = 35.40$				0.2191	0.4961	45	0.547
x (m)	y (m)	θ (deg.)	u (m/s)	0.2091	0.5061	45	0.478
0.0554	0.3240	30	0.129	Expt.12			
0.0803	0.3290	30	0.314	$x/b_o = 13.25$ & $y/b_o = 36.20$			
0.1248	0.3340	30	0.702	x (m)	y (m)	θ (deg.)	u (m/s)
0.1162	0.3390	30	1.236	0.1498	0.3520	30	0.760
0.1075	0.3440	30	1.413	0.1412	0.3570	30	1.585
0.0989	0.3490	30	0.948	0.133	0.3620	30	1.773
0.0902	0.3540	30	0.361	0.1239	0.3670	30	0.813

$x/b_o = 25.41$ & $y/b_o = 47.31$				0.0662	0.3090	30	0.281
x (m)	y (m)	θ (deg.)	u (m/s)	0.0662	0.3140	30	0.501
0.2741	0.4531	45	0.501	0.0662	0.3190	30	0.720
0.2691	0.4581	45	0.633	0.0662	0.3240	30	0.892
0.2641	0.4631	45	0.735	0.0662	0.3290	30	0.936
0.2591	0.4681	45	0.952	0.0662	0.3340	30	0.875
0.2541	0.4731	45	1.018	0.0662	0.3390	30	0.688
0.2491	0.4781	45	0.987	0.0662	0.3440	30	0.547
0.2441	0.4831	45	0.988	0.0662	0.3490	30	0.401
0.2391	0.4881	45	0.862	0.0662	0.3540	30	0.308
0.2341	0.4931	45	0.840	0.0662	0.3590	30	0.240
0.2291	0.4981	45	0.762	$x/b_o = 5.81$ & $y/b_o = 17.70$			
0.2241	0.5031	45	0.630	x (m)	y (m)	θ (deg.)	u (m/s)
0.2191	0.5081	45	0.599	0.1162	0.3090	30	0.1605
0.2141	0.5131	45	0.554	0.1162	0.3140	30	0.1594
$x/b_o = 29.41$ & $y/b_o = 51.06$				0.1162	0.3190	30	0.1734
x (m)	y (m)	θ (deg.)	u (m/s)	0.1162	0.3240	30	0.2526
0.3241	0.4806	45	0.658	0.1162	0.3290	30	0.354
0.3191	0.4856	45	0.640	0.1162	0.3340	30	0.4727
0.3141	0.4906	45	0.726	0.1162	0.3390	30	0.546
0.3091	0.4956	45	0.868	0.1162	0.3440	30	0.6631
0.3041	0.5006	45	0.886	0.1162	0.3490	30	0.7436
0.2991	0.5056	45	0.923	0.1162	0.3540	30	0.763
0.2941	0.5106	45	0.934	0.1162	0.3590	30	0.7602
0.2891	0.5156	45	0.854	0.1162	0.3640	30	0.6927
0.2841	0.5206	45	0.708	0.1162	0.3690	30	0.616
0.2791	0.5256	45	0.657	0.1162	0.3740	30	0.551
Expt. 14				0.1162	0.3790	30	0.472
$x/b_o = 0.81$ & $y/b_o = 14.95$				0.1162	0.3840	30	0.3835
x (m)	y (m)	θ (deg.)	u (m/s)	0.1162	0.3890	30	0.3215
0.0162	0.2790	30	0.154	0.1162	0.3940	30	0.2863
0.0162	0.2840	30	0.285	0.1162	0.3990	30	0.2783
0.0162	0.2890	30	0.447	$x/b_o = 8.31$ & $y/b_o = 19.70$			
0.0162	0.2940	30	0.728	x (m)	y (m)	θ (deg.)	u (m/s)
0.0162	0.2952	30	0.860	0.1662	0.3390	30	0.1137
0.0162	0.2970	30	0.979	0.1662	0.3440	30	0.1642
0.0162	0.2990	30	1.060	0.1662	0.3490	30	0.24
0.0162	0.3040	30	1.040	0.1662	0.3540	30	0.2971
0.0162	0.3090	30	0.920	0.1662	0.3590	30	0.36
0.0162	0.3140	30	0.597	0.1662	0.3640	30	0.4373
0.0162	0.3190	30	0.285	0.1662	0.3690	30	0.4854
$x/b_o = 3.31$ & $y/b_o = 16.45$				0.1662	0.3740	30	0.554
x (m)	y (m)	θ (deg.)	u (m/s)	0.1662	0.3790	30	0.632
0.0662	0.3040	30	0.134	0.1662	0.3840	30	0.673

0.1662	0.3890	30	0.704	0.2662	0.4990	30	0.656
0.1662	0.3940	30	0.716	0.2662	0.5090	30	0.641
0.1662	0.3990	30	0.708	0.2662	0.5190	30	0.602
0.1662	0.4035	30	0.680	0.2662	0.5290	30	0.532
0.1662	0.4090	30	0.630	0.2662	0.5390	30	0.456
0.1662	0.4140	30	0.560	0.2662	0.5490	30	0.424
0.1662	0.4190	30	0.507	0.2662	0.5590	30	0.396
0.1662	0.4240	30	0.455	0.2662	0.5690	30	0.395
0.1662	0.4290	30	0.411	Expt.16			
0.1662	0.4340	30	0.375	$x/b_o = 0.81$ & $y/b_o = 14.33$			
0.1662	0.4390	30	0.318	x (m)	y (m)	θ (deg.)	u (m/s)
0.1662	0.4440	30	0.279	0.0595	0.2615	30	0.204
0.1662	0.4490	30	0.260	0.0508	0.2665	30	0.168
$x/b_o = 10.81$ & $y/b_o = 21.45$				0.0422	0.2715	30	0.420
x (m)	y (m)	θ (deg.)	u (m/s)	0.0335	0.2765	30	0.930
0.2162	0.3690	30	0.411	0.0248	0.2815	30	1.057
0.2162	0.3790	30	0.421	0.0162	0.2865	30	1.060
0.2162	0.3890	30	0.520	0.0075	0.2915	30	1.010
0.2162	0.3990	30	0.643	$x/b_o = 3.31$ & $y/b_o = 16.58$			
0.2162	0.4090	30	0.723	x (m)	y (m)	θ (deg.)	u (m/s)
0.2162	0.4190	30	0.740	0.1181	0.3015	30	0.2666
0.2162	0.4290	30	0.743	0.1095	0.3065	30	0.2905
0.2162	0.4390	30	0.738	0.1008	0.3115	30	0.4036
0.2162	0.4490	30	0.715	0.0922	0.3165	30	0.5868
0.2162	0.4590	30	0.690	0.0835	0.3215	30	0.7298
0.2162	0.4690	30	0.643	0.0748	0.3265	30	0.8745
0.2162	0.4790	30	0.600	0.066	0.332	30	0.9590
0.2162	0.4890	30	0.568	0.0575	0.3365	30	0.9447
0.2162	0.4990	30	0.534	0.0489	0.3415	30	0.8355
0.2162	0.5090	30	0.495	0.0402	0.3465	30	0.7106
0.2162	0.5190	30	0.468	0.0315	0.3515	30	0.5987
0.2162	0.5240	30	0.463	0.0229	0.3565	30	0.4677
$x/b_o = 13.31$ & $y/b_o = 23.95$				0.0142	0.3615	30	0.4066
x (m)	y (m)	θ (deg.)	u (m/s)	0.0056	0.3665	30	0.3600
0.2662	0.3990	30	0.423	0.0000	0.3715	30	0.3457
0.2662	0.4090	30	0.425	$x/b_o = 5.81$ & $y/b_o = 18.58$			
0.2662	0.4190	30	0.458	x (m)	y (m)	θ (deg.)	u (m/s)
0.2662	0.4290	30	0.519	0.1681	0.3415	30	0.2975
0.2662	0.4390	30	0.568	0.1595	0.3465	30	0.3906
0.2662	0.4490	30	0.600	0.1508	0.3515	30	0.5899
0.2662	0.4590	30	0.655	0.1422	0.3565	30	0.7155
0.2662	0.4690	30	0.669	0.1335	0.3615	30	0.7418
0.2662	0.4790	30	0.673	0.1248	0.3665	30	0.7389
0.2662	0.4890	30	0.668	0.1162	0.3715	30	0.7569

0.1075	0.3765	30	0.7064	0.1315	0.4365	30	0.5520
0.0989	0.3815	30	0.6476	0.1229	0.4415	30	0.5061
0.0902	0.3865	30	0.6068	0.1142	0.4465	30	0.4759
0.0815	0.3915	30	0.5204	0.1056	0.4515	30	0.4552
0.0729	0.3965	30	0.4553	0.0969	0.4565	30	0.4040
0.0642	0.4015	30	0.4186	0.0882	0.4615	30	0.3843
0.0556	0.4065	30	0.3595	0.0796	0.4665	30	0.3163
0.0469	0.4115	30	0.3421	0.0709	0.4715	30	0.2800
0.0382	0.4165	30	0.2858	0.0536	0.4815	30	0.2183
0.0296	0.4215	30	0.2725	$x/b_o = 10.81$ & $y/b_o = 22.33$			
0.0123	0.4315	30	0.2458	x (m)	y (m)	θ (deg.)	u (m/s)
$x/b_o = 8.31$ & $y/b_o = 20.83$				0.2941	0.4015	30	0.2568
x (m)	y (m)	θ (deg.)	u (m/s)	0.2855	0.4065	30	0.2872
0.2788	0.3515	30	0.1929	0.2768	0.4115	30	0.3110
0.2701	0.3565	30	0.2005	0.2681	0.4165	30	0.3422
0.2614	0.3615	30	0.2174	0.2595	0.4215	30	0.3824
0.2528	0.3665	30	0.2319	0.2508	0.4265	30	0.3887
0.2441	0.3715	30	0.2520	0.2422	0.4315	30	0.4280
0.2355	0.3765	30	0.2953	0.2335	0.4365	30	0.4386
0.2268	0.3815	30	0.3295	0.2248	0.4415	30	0.4342
0.2181	0.3865	30	0.4010	0.2162	0.4465	30	0.4501
0.2095	0.3915	30	0.4357	0.2075	0.4515	30	0.4499
0.2008	0.3965	30	0.4678	0.1989	0.4565	30	0.4179
0.1922	0.4015	30	0.5270	0.1902	0.4615	30	0.4041
0.1835	0.4065	30	0.5542	0.182	0.467	30	0.3578
0.1748	0.4115	30	0.6052	0.1729	0.4715	30	0.3408
0.1662	0.4165	30	0.6106	0.1642	0.4765	30	0.3005
0.1575	0.4215	30	0.6005	0.1556	0.4815	30	0.2909
0.1489	0.4265	30	0.5958	0.1469	0.4865	30	0.2588
0.1402	0.4315	30	0.5704	0.1382	0.4915	30	0.2289

1.3 Bed Shear Stress Measurements

Expt. 1	0.94	0.310	0.70	-0.054	0.80	-0.272	1.35	-0.071
x (m) τ (N/m ²)	0.96	0.301	0.75	-0.063	0.85	-0.238	1.40	-0.071
0.13 -0.103	0.98	0.201	0.80	-0.063	0.90	-0.185	1.45	-0.078
0.14 -0.107	1.00	0.224	0.85	-0.073	0.95	-0.1441	1.50	-0.079
0.16 -0.136	1.02	0.127	0.90	-0.060	1	-0.147	1.60	-0.043
0.18 -0.193	1.04	0.177	0.95	-0.069	1.1	-0.1266	1.70	-0.049
0.20 -0.343	Expt. 2		1.00	-0.083	1.3	-0.1041	1.80	-0.039
0.22 -0.445	x (m) τ (N/m ²)		1.05	-0.083	1.4	-0.1058	1.90	-0.052
0.24 -0.521	0.40	-0.110	1.10	-0.077	1.5	-0.0963	2.00	-0.031
0.26 -0.571	0.42	-0.152	1.15	-0.075	Expt. 7		Expt. 9	
0.28 -0.626	0.44	-0.116	1.20	-0.086	x (m) τ (N/m ²)		x (m) τ (N/m ²)	
0.30 -0.799	0.46	-0.127	1.25	-0.087	0.35	-0.105	0.30	-0.063
0.32 -0.868	0.48	-0.123	1.30	-0.090	0.40	-0.128	0.40	-0.063
0.34 -0.885	0.50	-0.156	1.35	-0.090	0.45	-0.199	0.50	-0.092
0.36 -0.941	0.52	-0.151	1.40	-0.077	0.50	-0.209	0.60	-0.102
0.38 -0.745	0.54	-0.154	1.45	-0.082	0.55	-0.224	0.70	-0.100
0.40 -0.356	0.56	-0.116	1.50	-0.071	0.60	-0.228	0.80	-0.118
0.41 -0.256	0.60	-0.108	1.60	-0.082	0.65	-0.224	0.90	-0.149
0.46 0.389	Expt. 3		1.70	-0.065	0.70	-0.168	1.00	-0.157
0.48 0.666	x (m) τ (N/m ²)		1.80	-0.053	Expt. 8		1.10	-0.167
0.50 0.970	0.60	-0.030	1.90	-0.051	x (m) τ (N/m ²)		1.20	-0.156
0.52 1.186	0.70	-0.052	Expt. 5		0.30	-0.103	1.30	-0.158
0.54 1.216	0.75	-0.048	x (m) τ (N/m ²)		0.35	-0.101	1.40	-0.145
0.56 1.253	0.80	-0.054	0.10	0.043	0.40	-0.087	1.50	-0.155
0.58 1.311	0.90	-0.068	0.15	0.063	0.45	-0.091	1.60	-0.154
0.60 1.272	0.95	-0.078	0.20	0.049	0.50	-0.125	1.70	-0.137
0.62 1.119	1.00	-0.075	0.25	0.043	0.55	-0.120	1.80	-0.121
0.64 1.039	1.05	-0.079	0.60	-0.109	0.60	-0.124	1.90	-0.109
0.66 1.030	1.10	-0.082	0.65	-0.319	0.65	-0.115	2.00	-0.088
0.68 0.950	1.15	-0.081	0.70	-0.556	0.70	-0.138	Expt. 10	
0.70 0.891	1.20	-0.080	0.75	-0.427	0.75	-0.123	x (m) τ (N/m ²)	
0.72 0.863	1.25	-0.076	0.80	0.952	0.80	-0.148	0.90	-0.188
0.74 0.767	1.30	-0.066	0.85	1.082	0.85	-0.143	0.95	-0.392
0.76 0.720	1.35	-0.060	1.00	0.580	0.90	-0.120	1.00	-0.598
0.78 0.724	1.40	-0.055	1.10	0.296	0.95	-0.118	1.05	-0.770
0.80 0.628	1.45	-0.053	1.20	0.150	1.00	-0.131	1.10	-0.899
0.82 0.524	1.50	-0.051	Expt. 6		1.05	-0.110	1.15	-0.938
0.84 0.510	1.60	-0.032	x (m) τ (N/m ²)		1.10	-0.101	1.20	-1.029
0.86 0.422	1.70	-0.026	0.60	-0.179	1.15	-0.094	1.25	-0.853
0.88 0.468	Expt. 4		0.65	-0.217	1.20	-0.097	1.30	-0.631
0.90 0.393	x (m) τ (N/m ²)		0.70	-0.285	1.25	-0.087	1.35	-0.582
0.92 0.372	0.65	-0.051	0.75	-0.329	1.30	-0.072	1.40	-0.484

1.45	-0.429	1.80	-0.183	1.40	-0.087	1.35	-0.303	1.70	-0.177
1.50	-0.394	1.90	-0.173	1.45	-0.095	1.40	-0.300	1.75	-0.160
1.60	-0.303	2.00	-0.143	1.50	-0.094	1.45	-0.300	1.80	-0.149
1.70	-0.284	Expt. 13		1.60	-0.087	1.50	-0.282	1.85	-0.140
1.80	-0.231	x (m) τ (N/m ²)		1.70	-0.092	1.55	-0.281	1.90	-0.126
1.90	-0.215	0.15	-1.088	1.80	-0.081	1.65	-0.279	1.95	-0.116
2.00	-0.215	0.18	-1.233	1.90	-0.088	1.70	-0.274	2.00	-0.104
2.10	-0.168	0.20	-1.394	2.00	-0.076	1.75	-0.243	2.05	-0.099
2.20	-0.137	0.23	-1.534	2.10	-0.073	1.80	-0.228	2.10	-0.094
2.30	-0.117	0.25	-1.300	2.20	-0.058	1.85	-0.201	2.15	-0.087
Expt. 11		0.28	-0.730	2.30	-0.059	1.90	-0.191	2.20	-0.081
x (m) τ (N/m ²)		0.28	-0.578	2.40	-0.058	1.95	-0.187	2.25	-0.074
0.80	-0.189	0.29	-0.347	2.50	-0.046	2.00	-0.165	2.30	-0.073
0.85	-0.248	0.30	0.618	2.60	-0.040	2.05	-0.164	Expt. 20	
0.90	-0.271	0.33	1.579	Expt. 15		2.10	-0.145	x (m) τ (N/m ²)	
0.95	-0.257	0.35	2.021	x (m) τ (N/m ²)		2.15	-0.134	0.50	-0.140
1.00	-0.250	0.38	2.158	0.50	-0.099	2.20	-0.116	0.60	-0.148
1.05	-0.203	0.40	2.277	0.60	-0.109	2.25	-0.129	0.70	-0.172
1.10	-0.207	0.43	2.157	0.70	-0.111	2.30	-0.127	0.80	-0.250
1.15	-0.172	0.45	2.087	0.80	-0.116	2.35	-0.117	0.90	-0.248
1.20	-0.157	0.50	1.830	0.90	-0.122	Expt. 19		1.00	-0.281
1.25	-0.139	0.55	1.517	1.00	-0.121	x (m) τ (N/m ²)		1.10	-0.275
1.30	-0.138	0.60	1.251	1.10	-0.116	0.60	-0.206	1.20	-0.333
1.35	-0.131	0.65	0.970	1.20	-0.114	0.65	-0.242	1.30	-0.285
1.40	-0.127	0.70	0.759	1.30	-0.107	0.70	-0.242	1.40	-0.268
1.45	-0.141	0.80	0.336	1.40	-0.106	0.75	-0.262	1.50	-0.252
1.50	-0.128	0.90	0.181	1.50	-0.095	0.80	-0.285	1.60	-0.221
1.55	-0.125	1.00	0.154	1.60	-0.087	0.85	-0.298	1.70	-0.193
Expt. 12		1.10	0.160	1.70	-0.080	0.90	-0.286	1.80	-0.174
x (m) τ (N/m ²)		1.20	0.078	1.80	-0.075	0.95	-0.305	1.90	-0.136
0.40	-0.130	Expt. 14		1.90	-0.073	1.00	-0.316	2.00	-0.135
0.50	-0.154	x (m) τ (N/m ²)		Expt. 18		1.05	-0.322	2.10	-0.111
0.60	-0.176	0.70	-0.049	x (m) τ (N/m ²)		1.10	-0.327	Expt. 21	
0.70	-0.186	0.80	-0.054	0.75	-0.250	1.15	-0.322	x (m) τ (N/m ²)	
0.80	-0.217	0.90	-0.060	0.80	-0.246	1.20	-0.315	0.35	-0.101
0.90	-0.223	0.95	-0.066	0.85	-0.258	1.25	-0.306	0.40	-0.133
1.00	-0.226	1.00	-0.067	0.90	-0.279	1.30	-0.292	0.50	-0.163
1.10	-0.241	1.05	-0.073	0.95	-0.261	1.35	-0.280	0.60	-0.235
1.20	-0.214	1.10	-0.076	1.00	-0.277	1.40	-0.270	0.70	-0.285
1.30	-0.226	1.15	-0.084	1.05	-0.284	1.45	-0.253	0.80	-0.319
1.40	-0.200	1.20	-0.075	1.10	-0.290	1.50	-0.235	0.90	-0.352
1.50	-0.202	1.25	-0.076	1.15	-0.299	1.55	-0.220	1.00	-0.370
1.60	-0.183	1.30	-0.085	1.20	-0.302	1.60	-0.201	1.10	-0.326
1.70	-0.177	1.35	-0.084	1.25	-0.305	1.65	-0.187	1.20	-0.282

Expt. 21 (Cont.)	
x (m)	τ (N/m²)
1.30	-0.239
1.40	-0.208
1.50	-0.173
1.60	-0.148
1.70	-0.127
1.80	-0.108
1.90	-0.088
2.00	-0.082

1.4 Variation of Velocity Scale, Length Scale, Jet Discharge and Momentum Flux with Distance

Expt. 1

x (m)	u_m (m/s)	x/b_o	u_m/U_o
0.00	1.430	0.00	1.000
0.50	0.398	55.56	0.278
0.60	0.552	66.67	0.386
0.65	0.448	72.22	0.313
0.70	0.418	77.78	0.292
0.75	0.379	83.33	0.265
0.80	0.441	88.89	0.308
0.85	0.310	94.44	0.217
0.90	0.262	100.00	0.183
0.95	0.203	105.56	0.142
1.00	0.285	111.11	0.199
1.05	0.140	116.67	0.098
1.20	0.140	133.33	0.098

Expt. 2

x (m)	u_m (m/s)	b_s (cm)	x/b_o	u_m/U_o	b_s/b_o
0.00	1.430	-	0.00	1.000	-
0.07	1.430	-	7.22	0.997	-
0.10	1.284	-	11.11	0.892	-
0.19	1.379	-	21.11	0.958	-
0.29	0.524	-	32.22	0.364	-
0.30	0.504	-	33.33	0.350	-
0.40	0.638	5.75	44.44	0.443	6.39
0.50	0.515	6.50	55.56	0.357	7.22
0.60	0.672	6.75	66.67	0.467	7.50
0.80	0.607	9.50	88.89	0.422	10.56
1.00	0.550	11.00	111.11	0.382	12.22
1.20	0.422	10.50	133.33	0.293	11.67
1.40	0.334	9.50	155.56	0.232	10.56
1.60	0.255	7.00	177.78	0.177	7.78
1.80	0.202	5.50	200.00	0.140	6.11
2.00	0.166	4.50	222.22	0.115	5.00

Expt. 3

x (m)	u_m (m/s)	u_t (m/s)	b_s (cm)	x/b_o	u_m/U_o	u_t/U_o	b_s/b_o	Q/Q_o	M/M_o
0.00	1.430	-	-	0.00	1.000	-	-	1.000	1.000
0.04	1.430	-	-	4.57	1.000	-	-	-	-
0.07	1.200	-	-	7.35	0.833	-	-	-	-
0.09	1.029	-	-	10.13	0.715	-	-	-	-
0.12	0.843	-	-	12.91	0.585	-	-	-	-
0.14	0.770	-	-	15.69	0.534	-	-	-	-
0.17	0.671	-	-	18.46	0.466	-	-	-	-
0.19	0.569	-	-	21.24	0.395	-	-	-	-
0.21	0.528	-	-	22.91	0.367	-	-	-	-
0.23	0.469	-	-	25.13	0.326	-	-	-	-
0.30	0.570	-0.125	-	33.33	0.396	-0.087	-	4.492	1.186
0.40	0.626	-0.130	5.75	44.44	0.435	-0.090	6.39	4.429	1.284
0.60	0.519	-0.138	6.40	66.67	0.361	-0.096	7.11	4.431	1.065
0.80	0.480	-0.147	7.00	88.89	0.334	-0.102	7.78	4.207	0.935
1.00	0.423	-0.145	7.50	111.11	0.294	-0.101	8.33	3.930	0.770
1.20	0.358	-0.138	7.40	133.33	0.249	-0.096	8.22	3.575	0.593
1.40	0.311	-0.128	7.50	155.56	0.216	-0.089	8.33	3.295	0.474
1.60	0.269	-0.114	6.80	177.78	0.187	-0.079	7.56	3.038	0.378
1.80	0.213	-0.099	7.20	200.00	0.148	-0.069	8.00	2.385	0.236
2.00	0.156	-0.092	8.00	222.22	0.109	-0.064	8.89	-	-

Expt. 4

x (m)	u_m (m/s)	u_t (m/s)	b_s (cm)	x/b_o	u_m/U_o	u_t/U_o	b_s/b_o	Q/Q_o	M/M_o
0.00	1.430	-	-	0.00	1.000	-	-	1.000	1.000
0.04	1.430	-	-	4.57	1.000	-	-	-	-
0.07	1.189	-	-	7.35	0.825	-	-	-	-
0.09	1.047	-	-	10.13	0.727	-	-	-	-
0.12	0.922	-	-	12.91	0.641	-	-	-	-
0.14	0.844	-	-	15.69	0.586	-	-	-	-
0.17	0.743	-	-	18.46	0.516	-	-	-	-
0.23	0.519	-	-	26.01	0.360	-	-	-	-
0.24	0.431	-	-	27.12	0.299	-	-	-	-
0.25	0.361	-	-	28.23	0.251	-	-	-	-
0.30	0.370	-0.121	-	33.33	0.257	-0.084	-	3.940	1.000
0.40	0.502	-0.108	-	44.44	0.348	-0.075	-	4.181	0.971
0.60	0.515	-0.132	6.50	66.67	0.358	-0.092	7.22	4.590	1.095
0.80	0.452	-0.139	7.50	88.89	0.314	-0.097	8.33	4.570	0.956
1.00	0.400	-0.146	7.50	111.11	0.278	-0.102	8.33	4.407	0.817
1.20	0.342	-0.146	9.50	133.33	0.237	-0.101	10.56	3.942	0.624
1.40	0.298	-0.136	8.50	155.56	0.207	-0.094	9.44	3.642	0.502
1.60	0.242	-0.123	8.00	177.78	0.168	-0.086	8.89	3.203	0.359
1.80	0.222	-0.106	8.00	200.00	0.154	-0.073	8.89	2.559	0.263
2.00	0.196	-0.093	5.50	222.22	0.136	-0.065	6.11	2.157	0.196

Expt. 5

x (m)	u_m (m/s)	x/b_o	u_m/U_o
0.00	2.14	0.00	1.000
0.85	0.51	94.44	0.238
0.90	0.58	100.00	0.269
0.95	0.57	105.56	0.266
1.00	0.48	111.11	0.225
1.05	0.51	116.67	0.240
1.10	0.44	122.22	0.206
1.15	0.41	127.78	0.192
1.20	0.36	133.33	0.166
1.25	0.29	138.89	0.137
1.30	0.25	144.44	0.117
1.35	0.25	150.00	0.118
1.40	0.18	155.56	0.082
1.45	0.15	161.11	0.068

Expt. 8

x (m)	u_m (m/s)	u_t (m/s)	b_s (cm)	x/b_o	u_m/U_o	u_t/U_o	b_s/b_o	Q/Q_o
0.00	2.140	-	-	0.00	1.000	-	-	1.000
0.35	0.629	-0.153	6.50	38.89	0.294	-0.071	7.22	3.054
0.45	0.588	-0.170	7.00	50.00	0.275	-0.079	7.78	3.373
0.60	0.565	-0.180	7.00	66.67	0.264	-0.084	7.78	3.418
0.80	0.501	-0.185	7.00	88.89	0.234	-0.087	7.78	3.305
1.00	0.454	-0.167	8.00	111.11	0.212	-0.078	8.89	2.989
1.20	0.353	-0.139	7.00	133.33	0.165	-0.065	7.78	2.652
1.40	0.308	-0.111	6.00	155.56	0.144	-0.052	6.67	2.718
1.60	0.292	-0.098	5.00	177.78	0.136	-0.046	5.56	2.474
1.80	0.288	-0.082	4.00	200.00	0.135	-0.038	4.44	2.226
2.00	0.289	-0.077	2.00	222.22	0.135	-0.036	2.22	2.109

Expt. 9

x (m)	u_m (m/s)	u_t (m/s)	b_s (cm)	x/b_o	u_m/U_o	u_t/U_o	b_s/b_o	Q/Q_o	M/M_o
0.00	2.140	-	-	0.00	1.000	-	-	1.000	1.000
0.04	2.140	-	-	4.57	1.000	-	-	-	-
0.07	1.839	-	-	7.35	0.858	-	-	-	-
0.09	1.533	-	-	10.13	0.716	-	-	-	-
0.12	1.345	-	-	12.91	0.628	-	-	-	-
0.14	1.118	-	-	15.69	0.522	-	-	-	-
0.17	0.983	-	-	18.46	0.459	-	-	-	-
0.22	0.730	-	-	24.90	0.341	-	-	-	-
0.23	0.768	-	-	26.01	0.358	-	-	-	-
0.24	0.657	-	-	27.12	0.307	-	-	-	-
0.26	0.602	-	-	28.79	0.281	-	-	-	-
0.27	0.536	-	-	30.45	0.250	-	-	-	-
0.28	0.518	-	-	31.56	0.242	-	-	-	-
0.29	0.520	-	-	32.68	0.243	-	-	-	-
0.35	0.616	-0.151	-	38.89	0.287	-0.071	-	4.293	1.000
0.45	0.741	-0.155	5.00	50.00	0.346	-0.073	5.56	4.450	1.028
0.55	0.680	-0.171	6.00	61.11	0.318	-0.080	6.67	4.340	0.919
0.60	0.636	-0.175	7.00	66.67	0.297	-0.082	7.78	4.270	0.846
0.80	0.591	-0.192	8.00	88.89	0.276	-0.090	8.89	4.230	0.779
1.00	0.544	-0.206	8.00	111.11	0.254	-0.096	8.89	3.768	0.639
1.20	0.470	-0.194	9.50	133.33	0.219	-0.091	10.56	3.409	0.499
1.40	0.431	-0.187	10.00	155.56	0.201	-0.087	11.11	2.934	0.393
1.60	0.379	-0.173	10.50	177.78	0.177	-0.081	11.67	2.791	0.329
1.80	0.329	-0.148	-	200.00	0.154	-0.069	-	2.381	0.244
2.00	0.314	-0.128	11.00	222.22	0.146	-0.060	12.22	2.061	0.201

Expt. 12

x (m)	u_m (m/s)	u_t (m/s)	b_s (cm)	x/b_o	u_m/U_o	u_t/U_o	b_s/h_o	Q/Q_o	M/M_o
0.00	3.090	-	-	0.00	1.000	-	-	1.000	1.000
0.04	3.026	-	-	4.57	0.976	-	-	-	-
0.07	2.466	-	-	7.35	0.796	-	-	-	-
0.09	2.209	-	-	10.13	0.712	-	-	-	-
0.12	1.969	-	-	12.91	0.635	-	-	-	-
0.14	1.773	-	-	15.69	0.572	-	-	-	-
0.17	1.511	-	-	18.46	0.487	-	-	-	-
0.19	1.140	-	-	21.24	0.368	-	-	-	-
0.26	1.018	-	-	28.79	0.328	-	-	-	-
0.27	0.738	-	-	29.90	0.238	-	-	-	-
0.29	0.675	-	-	32.12	0.218	-	-	-	-
0.40	0.780	-0.206	-	44.44	0.252	-0.066	-	3.951	1.000
0.60	0.929	-0.273	9.00	66.67	0.300	-0.088	10.00	4.280	0.855
0.80	0.792	-0.299	10.50	88.89	0.256	-0.096	11.67	4.317	0.736
1.00	0.728	-0.295	12.75	111.11	0.235	-0.095	14.17	3.853	0.603
1.20	0.659	-0.278	12.00	133.33	0.213	-0.090	13.33	3.589	0.509
1.40	0.579	-0.265	11.00	155.56	0.187	-0.086	12.22	3.282	0.409
1.60	0.526	-0.239	11.50	177.78	0.170	-0.077	12.78	2.711	0.307
1.80	0.455	-0.204	12.00	200.00	0.147	-0.066	13.33	2.317	0.227
2.00	0.391	-0.181	12.00	222.22	0.126	-0.058	13.33	2.039	0.171

Expt. 14

x (m)	u_m (m/s)	b_s (cm)	x/b_o	u_m/U_o	b_s/b_o
0.00	1.060	-	0.00	1.000	-
0.02	1.060	-	0.81	1.000	-
0.07	0.936	-	3.31	0.883	-
0.12	0.763	-	5.81	0.720	-
0.17	0.716	-	8.31	0.676	-
0.22	0.743	-	10.81	0.701	-
0.27	0.673	-	13.31	0.635	-
0.40	0.497	-	20.00	0.469	-
0.50	0.536	-	25.00	0.506	-
0.60	0.545	6.50	30.00	0.514	3.25
0.80	0.501	8.50	40.00	0.472	4.25
1.20	0.409	10.5	60.00	0.386	5.25
1.60	0.346	12.5	80.00	0.326	6.25
2.00	0.264	13.50	100.00	0.249	6.75
2.40	0.213	11.50	120.00	0.201	5.75
2.80	0.181	11.5	140.00	0.171	5.75

Expt. 15

x (m)	u_m (m/s)	u_t (m/s)	b_s (cm)	x/b_o	u_m/U_o	u_t/U_o	b_s/b_o
0.00	1.060	-	-	0.00	1.000	-	-
0.05	1.060	-	-	2.50	1.000	-	-
0.10	0.850	-	-	5.00	0.802	-	-
0.20	0.660	-	-	10.00	0.623	-	-
0.30	0.520	-	-	15.00	0.491	-	-
0.40	0.480	-	-	20.00	0.453	-	-
0.50	0.591	-0.160	7.00	25.00	0.558	-0.151	3.50
0.65	0.585	-0.187	8.00	32.50	0.552	-0.176	4.00
0.80	0.544	-0.190	8.50	40.00	0.513	-0.180	4.25
1.20	0.417	-0.157	9.75	60.00	0.394	-0.148	4.88
1.60	0.308	-0.124	9.75	80.00	0.290	-0.117	4.88
2.00	0.202	-0.103	12.50	100.00	0.190	-0.097	6.25
2.40	0.162	-0.091	10.50	120.00	0.153	-0.086	5.25

Expt. 16

x (m)	u_m (m/s)	b_s (cm)	x/b_o	u_m/U_o	b_s/b_o	Q/Q_o	M/M_o
0.00	1.060	-	0.00	1.000	-	1.000	1.000
0.02	1.060	-	0.81	1.000	-	-	-
0.07	0.959	-	3.31	0.905	-	-	-
0.12	0.757	-	5.81	0.714	-	-	-
0.17	0.611	-	8.31	0.576	-	-	-
0.22	0.450	-	10.81	0.425	-	-	-
0.35	0.602	4.95	17.50	0.568	2.48	1.490	0.564
0.50	0.531	4.70	25.00	0.500	2.35	1.552	0.518
0.70	0.491	6.70	35.00	0.463	3.35	1.435	0.443
1.00	0.351	7.70	50.00	0.331	3.85	1.106	0.244
1.40	0.219	9.70	70.00	0.206	4.85	1.000	0.137
1.80	0.133	8.70	90.00	0.125	4.35	1.000	0.084
2.20	0.107	7.70	110.00	0.101	3.85	1.000	0.067
2.60	0.092	8.70	130.00	0.087	4.35	1.000	0.058

Expt. 17

x (m)	u_m (m/s)	b_z (cm)	x/b_o	u_m/U_o	b_z/b_o	Q/Q_o	M/M_o
0.00	1.590	-	0.00	1.000	-	1.000	1.000
0.02	1.590	-	0.81	1.000	-	-	-
0.04	1.590	-	2.06	1.000	-	-	-
0.07	1.339	-	3.31	0.837	-	-	-
0.12	1.065	-	5.81	0.666	-	-	-
0.17	0.890	-	8.31	0.556	-	-	-
0.22	0.643	-	10.81	0.402	-	-	-
0.40	0.835	7.70	20.00	0.522	3.85	1.838	0.640
0.50	0.835	7.70	25.00	0.522	3.85	1.753	0.610
0.70	0.566	9.20	35.00	0.354	4.60	1.528	0.360
1.00	0.400	9.70	50.00	0.250	4.85	1.021	0.170
1.20	0.336	10.70	60.00	0.210	5.35	1.000	0.140
1.40	0.246	12.70	70.00	0.154	6.35	1.000	0.103
1.80	0.201	13.70	90.00	0.125	6.85	1.000	0.084
2.20	0.198	13.70	110.00	0.124	6.85	1.000	0.082

Expt. 18

x (m)	u_m (m/s)	u_r (m/s)	b_s (cm)	x/b_o	u_r/U_o	u_r/U_o	b_s/b_o	Q/Q_o	M/M_o
0.00	2.130	-	-	0.00	1.000	-	-	1.000	1.000
0.04	2.126	-	-	2.06	1.000	-	-	-	-
0.07	1.744	-	-	3.31	0.820	-	-	-	-
0.12	1.595	-	-	5.81	0.750	-	-	-	-
0.17	1.526	-	-	8.31	0.718	-	-	-	-
0.26	1.319	-	-	12.95	0.620	-	-	-	-
0.50	0.908	-0.245	8.50	25.00	0.427	-0.115	4.25	3.192	0.909
0.70	0.882	-0.267	12.00	35.00	0.415	-0.125	6.00	3.509	0.971
0.90	0.874	-0.288	12.00	45.00	0.411	-0.135	6.00	3.237	0.887
1.10	0.758	-0.282	13.50	55.00	0.356	-0.132	6.75	3.187	0.757
1.40	0.659	-0.253	13.00	70.00	0.310	-0.119	6.50	2.811	0.581
1.80	0.565	-0.213	14.00	90.00	0.266	-0.100	7.00	2.402	0.425
2.20	0.471	-0.161	14.00	110.00	0.222	-0.075	7.00	1.963	0.290
2.60	0.373	-0.164	14.00	130.00	0.175	-0.077	7.00	1.982	0.232

Expt. 19

x (m)	u_m (m/s)	u_t (m/s)	b_s (cm)	x/b_o	u_m/U_o	u_t/U_o	b_s/b_o	Q/Q_o	M/M_o
0.000	2.130	-	-	0.00	1.000	-	-	1.000	1.000
0.004	2.130	-	-	0.21	1.002	-	-	-	-
0.046	1.982	-	-	2.31	0.932	-	-	-	-
0.146	1.549	-	-	7.31	0.729	-	-	-	-
0.196	1.357	-	-	9.81	0.638	-	-	-	-
0.246	1.160	-	-	12.31	0.545	-	-	-	-
0.296	0.998	-	-	14.81	0.469	-	-	-	-
0.346	0.807	-	-	17.31	0.380	-	-	-	-
0.500	0.804	-0.230	13.00	25.00	0.378	-0.108	6.50	2.838	0.715
0.600	1.000	-0.269	12.00	30.00	0.470	-0.126	6.00	3.085	0.967
0.900	0.924	-0.320	13.00	45.00	0.435	-0.150	6.50	3.405	0.987
1.100	0.883	-0.305	13.75	55.00	0.415	-0.143	6.88	3.298	0.913
1.400	0.754	-0.250	13.00	70.00	0.354	-0.117	6.50	2.881	0.681
1.800	0.566	-0.206	12.00	90.00	0.266	-0.097	6.00	2.504	0.445
2.200	0.448	-0.148	12.00	110.00	0.211	-0.069	6.00	1.902	0.267
2.600	0.323	-0.097	14.00	130.00	0.152	-0.045	7.00	1.523	0.154

Expt. 20

x (m)	u_m (m/s)	u_t (m/s)	b_s (cm)	x/b_o	u_m/U_o	u_t/U_o	b_s/h_o	Q/Q_o	M/M_o
0.000	2.130	-	-	0.00	1.000	-	-	1.000	1.000
0.004	2.130	-	-	0.21	1.000	-	-	-	-
0.034	2.120	-	-	1.71	0.996	-	-	-	-
0.084	1.871	-	-	4.21	0.879	-	-	-	-
0.134	1.587	-	-	6.71	0.745	-	-	-	-
0.184	1.393	-	-	9.21	0.654	-	-	-	-
0.239	1.209	-	-	11.96	0.568	-	-	-	-
0.289	1.087	-	-	14.46	0.510	-	-	-	-
0.339	0.981	-	-	16.96	0.461	-	-	-	-
0.389	0.889	-	-	19.46	0.417	-	-	-	-
0.439	0.768	-	-	21.96	0.361	-	-	-	-
0.489	0.660	-	-	24.46	0.310	-	-	-	-
0.539	0.611	-	-	26.96	0.287	-	-	-	-
0.559	0.592	-	-	27.96	0.278	-	-	-	-
0.600	0.780	-0.223	-	30.00	0.366	-0.105	-	3.227	0.788
0.800	0.829	-0.264	-	40.00	0.389	-0.124	-	3.638	0.943
1.000	0.767	-0.288	11.00	50.00	0.360	-0.135	25.00	4.049	0.972
1.200	0.683	-0.286	8.50	60.00	0.321	-0.134	30.00	4.113	0.880
1.600	0.548	-0.227	8.00	80.00	0.257	-0.106	40.00	3.265	0.560
2.000	0.354	-0.173	12.00	100.00	0.166	-0.081	50.00	2.474	0.274
2.200	0.328	-0.136	11.00	110.00	0.154	-0.064	55.00	2.122	0.218

Expt. 21

x (m)	u_m (m/s)	u_t (m/s)	b_s (cm)	x/b_o	u_m/U_o	u_t/U_o	b_s/b_o	Q/Q_o	M/M_o
0.000	2.130	-	-	0.00	1.000	-	-	1.000	1.000
0.004	2.130	-	-	0.21	1.000	-	-	-	-
0.034	2.055	-	-	1.71	0.966	-	-	-	-
0.084	1.736	-	-	4.21	0.817	-	-	-	-
0.134	1.464	-	-	6.71	0.689	-	-	-	-
0.184	1.275	-	-	9.21	0.600	-	-	-	-
0.234	1.044	-	-	11.71	0.491	-	-	-	-
0.284	0.939	-	-	14.21	0.442	-	-	-	-
0.334	0.921	-	-	16.71	0.433	-	-	-	-
0.384	0.800	-	-	19.21	0.376	-	-	-	-
0.434	0.761	-	-	21.71	0.358	-	-	-	-
0.484	0.707	-	-	24.21	0.332	-	-	-	-
0.534	0.664	-	-	26.71	0.312	-	-	-	-
0.600	0.709	-0.260	-	30.00	0.333	-0.122	-	4.417	0.982
0.800	0.578	-0.292	-	40.00	0.272	-0.137	-	4.984	0.903
1.000	0.584	-0.280	16.00	50.00	0.275	-0.131	8.00	4.950	0.907
1.200	0.547	-0.260	12.00	60.00	0.257	-0.122	6.00	5.164	0.886
1.600	0.369	-0.205	13.00	80.00	0.174	-0.096	6.50	3.886	0.450
2.000	0.224	-0.150	19.00	100.00	0.105	-0.070	9.50	2.828	0.199
2.200	0.208	-0.133	18.00	110.00	0.098	-0.063	9.00	2.629	0.171

2. Plane Turbulent Surface Jets in Shallow Tailwater

2.1 Velocity Measurements along Vertical Sections at x-stations

Expt. 1		48	0.442	45	0.267	46	0.292	50.5	0.328
x = 10 cm		49	0.598	46	0.309	48	0.342	x = 180 cm	
y (cm)	u (m/s)	50	0.71	47	0.372	50	0.397	y (cm)	u (m/s)
48.5	0.063	50.5	0.72	48	0.414	50.5	0.408	0	-0.126
48.75	0.084	x = 60 cm		49	0.463	x = 140 cm		1	-0.137
49	0.166	y (cm)	u (m/s)	50	0.513	y (cm)	u (m/s)	4	-0.144
49.25	0.360	0	-0.083	50.5	0.531	0	-0.127	8	-0.149
49.5	0.601	1	-0.091	x = 100 cm		1	-0.132	12	-0.150
49.75	0.834	4	-0.096	y (cm)	u (m/s)	4	-0.142	16	-0.143
50	1.085	8	-0.097	0	-0.086	8	-0.149	20	-0.139
50.25	1.315	12	-0.091	1	-0.098	12	-0.158	24	-0.120
50.5	1.439	16	-0.094	4	-0.117	16	-0.163	28	-0.117
x = 20 cm		20	-0.097	8	-0.125	20	-0.166	30	-0.104
y (cm)	u (m/s)	24	-0.094	12	-0.132	24	-0.163	32	-0.093
38	-0.042	28	-0.091	16	-0.129	28	-0.142	33	-0.068
39	-0.045	32	-0.093	20	-0.143	32	-0.100	38	0.088
40	-0.049	36	-0.097	24	-0.149	33	-0.084	40	0.118
41	-0.047	40	-0.088	28	-0.143	36	0.073	42	0.151
42	-0.049	41	-0.075	32	-0.123	38	0.106	44	0.179
43	-0.042	43	0.113	36	-0.089	40	0.146	46	0.209
44	-0.041	44	0.176	38	0.082	42	0.188	48	0.236
45	-0.041	45	0.245	40	0.128	44	0.226	50	0.266
46	-0.045	46	0.309	42	0.185	46	0.265	50.5	0.282
46.5	-0.050	47	0.380	44	0.249	48	0.309	x = 200 cm	
47.5	0.196	48	0.447	46	0.310	50	0.356	y (cm)	u (m/s)
48	0.332	49	0.525	48	0.379	50.5	0.365	0	-0.112
48.5	0.473	50	0.594	50	0.446	x = 160 cm		1	-0.127
49	0.603	50.5	0.615	50.5	0.464	y (cm)	u (m/s)	4	-0.133
49.5	0.742	x = 80 cm		x = 120 cm		0	-0.120	8	-0.153
50	0.889	y (cm)	u (m/s)	y (cm)	u (m/s)	1	-0.134	12	-0.155
50.5	1.000	0	-0.069	0	-0.094	4	-0.148	16	-0.156
x = 40 cm		1	-0.090	1	-0.113	8	-0.154	20	-0.151
y (cm)	u (m/s)	4	-0.099	4	-0.131	12	-0.156	24	-0.131
18	-0.062	8	-0.098	8	-0.145	16	-0.164	28	-0.101
20	-0.068	12	-0.102	12	-0.158	20	-0.154	30	-0.092
24	-0.068	16	-0.104	16	-0.151	24	-0.145	31	-0.090
28	-0.069	20	-0.112	20	-0.155	28	-0.110	32	-0.083
32	-0.061	24	-0.128	24	-0.153	30	-0.103	33	-0.071
36	-0.061	28	-0.114	28	-0.150	32	-0.064	34	-0.061
40	-0.065	32	-0.128	32	-0.131	38	0.084	35	-0.054
42	-0.064	36	-0.111	34	-0.096	40	0.134	38	0.079
43	-0.060	40	0.085	36	0.036	42	0.173	40	0.105
44.5	0.069	41	0.113	38	0.088	44	0.202	42	0.131
45	0.107	42	0.149	40	0.142	46	0.243	44	0.158
46	0.195	43	0.189	42	0.198	48	0.279	46	0.181
47	0.309	44	0.229	44	0.245	50	0.317	48	0.212

50	0.235	x = 260 cm		38	0.045	x = 40 cm		28	-0.052
50.5	0.242	y (cm)	u (m/s)	40	0.054	y (cm)	u (m/s)	32	-0.051
x = 220 cm		0	-0.063	42	0.066	22	-0.028	36	-0.051
y (cm)	u (m/s)	1	-0.086	44	0.077	28	-0.031	38	-0.053
0	-0.105	4	-0.086	46	0.083	30	-0.036	40	-0.051
1	-0.114	8	-0.084	48	0.093	32	-0.035	44	0.132
4	-0.118	12	-0.090	50	0.103	36	-0.041	45	0.152
8	-0.113	16	-0.083	50.5	0.108	40	-0.043	46	0.194
12	-0.118	20	-0.071	x = 320 cm		42	-0.045	47	0.239
16	-0.117	24	-0.075	y (cm)	u (m/s)	43	-0.042	48	0.274
20	-0.117	28	-0.070	0	-0.033	46	0.143	49	0.307
24	-0.115	30	-0.080	1	-0.032	47	0.208	50	0.337
28	-0.111	31	-0.064	4	-0.031	48	0.272	50.5	0.346
30	-0.106	32	-0.044	38	0.038	49	0.337	51	0.350
31	-0.095	36	0.045	40	0.048	50	0.409	x = 100 cm	
32	-0.071	38	0.058	42	0.059	50.5	0.439	y (cm)	u (m/s)
38	0.071	40	0.071	44	0.071	51	0.465	0	-0.048
40	0.094	42	0.084	46	0.076	x = 60 cm		1	-0.046
42	0.115	44	0.099	48	0.086	y (cm)	u (m/s)	4	-0.049
44	0.134	46	0.114	50	0.090	2	-0.048	8	-0.060
46	0.156	48	0.127	50.5	0.092	4	-0.047	12	-0.070
48	0.178	50	0.145	Expt. 2		10	-0.052	16	-0.071
50	0.202	50.5	0.149	x = 6 cm		12	-0.050	20	-0.069
50.5	0.208	x = 280 cm		y (cm)	u (m/s)	16	-0.054	24	-0.073
x = 240 cm		y (cm)	u (m/s)	49	0.036	20	-0.056	28	-0.066
y (cm)	u (m/s)	0	-0.059	49.5	0.211	24	-0.052	32	-0.071
0	-0.102	1	-0.069	50	0.515	28	-0.050	36	-0.058
1	-0.104	4	-0.061	50.5	0.750	32	-0.056	41	0.079
4	-0.103	8	-0.058	51	0.750	36	-0.052	42	0.108
8	-0.114	12	-0.054	x = 20 cm		40	-0.048	43	0.132
12	-0.116	16	-0.049	y (cm)	u (m/s)	41	-0.041	44	0.161
16	-0.116	20	-0.046	35	-0.023	44	0.092	45	0.184
20	-0.112	24	-0.044	36	-0.023	45	0.142	46	0.206
24	-0.112	38	0.051	38	-0.024	46	0.176	47	0.236
26	-0.104	40	0.063	40	-0.031	47	0.223	48	0.264
27	-0.107	42	0.076	42	-0.038	48	0.276	49	0.290
28	-0.102	44	0.088	44	-0.031	49	0.327	50	0.310
29	-0.106	46	0.100	45	-0.027	50	0.372	50.5	0.318
30	-0.097	48	0.112	46	-0.035	50.5	0.391	51	0.332
31	-0.072	50	0.125	47	-0.032	51	0.398	x = 120 cm	
38	0.071	50.5	0.128	47.5	-0.029	x = 80 cm		y (cm)	u (m/s)
40	0.084	x = 300 cm		48	0.098	y (cm)	u (m/s)	4	-0.080
42	0.097	y (cm)	u (m/s)	48.5	0.200	4	-0.044	8	-0.079
44	0.108	0	-0.047	49	0.287	8	-0.047	12	-0.071
46	0.126	1	-0.047	49.5	0.402	12	-0.057	16	-0.076
48	0.143	4	-0.047	50	0.514	16	-0.053	20	-0.092
50	0.178	8	-0.044	50.5	0.586	20	-0.051	24	-0.092
50.5	0.178	12	-0.048	51	0.629	24	-0.053	28	-0.087

32	-0.069	12	-0.0959	40	0.040	49	0.667	45	0.327
34	-0.056	16	-0.1092	42	0.048	50	0.808	46	0.406
40	0.090	20	-0.0979	44	0.053	50.5	0.954	47	0.476
41	0.112	24	-0.0854	46	0.060	51	0.986	48	0.545
42	0.133	28	-0.0809	48	0.068	x = 60 cm		49	0.595
43	0.152	38	0.0758	50	0.078	y (cm) u (m/s)		50	0.666
44	0.169	40	0.0971	51	0.080	0	-0.097	50.5	0.700
45	0.189	42	0.1198	Expt. 3		1	-0.095	51	0.700
46	0.208	44	0.1388	x = 6 cm		4	-0.091	x = 100 cm	
47	0.229	46	0.1577	y (cm) u (m/s)		8	-0.107	y (cm) u (m/s)	
48	0.252	48	0.1847	49	0.106	12	-0.108	0	-0.109
49	0.269	50	0.2085	50	0.953	16	-0.108	1	-0.116
50	0.289	50.5	0.2125	50.5	1.500	20	-0.102	4	-0.123
50.5	0.298	51	0.2175	51	1.500	24	-0.102	8	-0.126
51	0.305	x = 240 cm		x = 20 cm		28	-0.102	12	-0.133
x = 160 cm		y (cm) u (m/s)		y (cm) u (m/s)		32	-0.108	16	-0.154
y (cm)	u (m/s)	0	-0.096	32	-0.065	36	-0.106	20	-0.158
0	-0.0701	1	-0.086	34	-0.069	38	-0.107	24	-0.148
1	-0.0745	4	-0.077	40	-0.070	40	-0.103	28	-0.153
4	-0.0897	8	-0.094	41	-0.064	42	-0.094	32	-0.141
8	-0.0934	12	-0.094	42	-0.062	44	0.158	34	-0.113
12	-0.0923	16	-0.092	43	-0.069	45	0.252	38	0.059
16	-0.0998	20	-0.073	44	-0.061	46	0.366	39	0.096
20	-0.0901	24	-0.057	45	-0.067	47	0.453	40	0.136
24	-0.0963	28	-0.061	46	-0.068	48	0.550	41	0.178
28	-0.0829	38	0.067	47	-0.069	49	0.650	42	0.225
30	-0.0803	40	0.076	47.5	0.077	50	0.745	43	0.282
32	-0.0687	42	0.089	48	0.250	50.5	0.788	44	0.321
39	0.0985	44	0.102	48.5	0.444	51	0.805	45	0.367
40	0.1137	46	0.116	49	0.626	x = 80 cm		46	0.414
41	0.1286	48	0.133	49.5	0.840	y (cm) u (m/s)		47	0.464
42	0.1405	50	0.146	50	1.000	0	-0.096	48	0.519
43	0.1523	51	0.155	50.5	1.125	1	-0.110	49	0.556
44	0.1629	x = 280 cm		51	1.129	4	-0.114	50	0.603
45	0.1761	y (cm) u (m/s)		x = 40 cm		8	-0.119	50.5	0.643
46	0.19	1	-0.0436	y (cm) u (m/s)		12	-0.132	51	0.645
47	0.2021	4	-0.0415	18	-0.081	16	-0.140	x = 120 cm	
48	0.2146	8	-0.0482	22	-0.085	20	-0.139	y (cm) u (m/s)	
49	0.2308	12	-0.0453	26	-0.090	24	-0.144	0	-0.097
50	0.2472	16	-0.0448	30	-0.092	28	-0.127	1	-0.143
50.5	0.2589	42	0.0655	34	-0.096	32	-0.130	4	-0.148
51	0.2658	44	0.0775	38	-0.090	34	-0.113	8	-0.166
x = 200 cm		46	0.0857	40	-0.091	36	-0.106	12	-0.180
y (cm) u (m/s)		48	0.0956	42	-0.081	38	-0.097	16	-0.187
0	-0.0855	50	0.1049	44	-0.088	41	0.089	20	-0.180
1	-0.0896	51	0.1088	46	0.199	42	0.142	24	-0.187
4	-0.1002	x = 320 cm		47	0.305	43	0.204	28	-0.148
8	-0.1024	y (cm) u (m/s)		48	0.536	44	0.272	32	-0.130

34	-0.114	8	-0.2265	1	-0.124	y (cm)	u (m/s)	45	0.4235
35	-0.089	12	-0.2012	4	-0.1107	40	-0.095	46	0.5678
38	0.084	16	-0.2124	8	-0.1093	41	-0.090	47	0.7381
39	0.130	20	-0.1617	10	-0.1108	42	-0.090	48	0.9004
40	0.172	24	-0.1553	12	-0.1065	43	-0.092	49	1.0205
41	0.214	28	-0.1318	36	0.0729	44	-0.090	50	1.085
42	0.261	38	0.155	38	0.0912	45	-0.096	51	1.1018
43	0.306	39	0.1789	40	0.1078	46	-0.092	x = 80 cm	
44	0.346	40	0.201	42	0.1252	47	-0.099	y (cm)	u (m/s)
45	0.373	41	0.215	44	0.1397	47.5	-0.096	5	-0.132
46	0.422	42	0.2305	46	0.1543	48.5	0.647	8	-0.137
47	0.454	43	0.2546	48	0.1744	49	1.049	12	-0.166
48	0.494	44	0.278	50	0.2006	49.5	1.401	16	-0.150
49	0.519	45	0.2941	50.5	0.2054	50	1.633	20	-0.202
50	0.558	46	0.3189	51	0.2118	50.5	1.656	24	-0.185
50.5	0.583	47	0.3303	x = 320 cm		51	1.657	28	-0.169
51	0.601	48	0.3589	y (cm)	u (m/s)	x = 40 cm		32	-0.171
x = 160 cm		49	0.3715	0	-0.0515	y (cm)	u (m/s)	36	-0.169
y (cm)	u (m/s)	50	0.3994	1	-0.0737	18	-0.0862	38	-0.127
0	-0.138	50.5	0.4057	4	-0.0785	22	-0.0864	41	0.226
1	-0.185	51	0.4134	6	-0.0711	26	-0.1269	42	0.307
4	-0.213	x = 240 cm		7	-0.0735	30	-0.1484	43	0.372
8	-0.217	y (cm)	u (m/s)	8	-0.0705	34	-0.1265	44	0.442
12	-0.209	0	-0.119	9	-0.0738	36	-0.0981	45	0.517
16	-0.218	1	-0.150	10	-0.0712	38	-0.1231	46	0.594
20	-0.202	4	-0.156	12	-0.0666	40	-0.0984	47	0.674
24	-0.191	8	-0.152	14	-0.0619	42	-0.134	48	0.767
28	-0.159	12	-0.150	40	0.0796	43	-0.1111	49	0.849
38	0.195	16	-0.151	42	0.0921	45	0.1724	50	0.930
39	0.214	20	-0.134	44	0.1047	46	0.3993	51	1.010
40	0.234	24	-0.113	46	0.1158	47	0.6265	x = 100 cm	
41	0.258	39	0.127	48	0.1289	48	0.8772	y (cm)	u (m/s)
42	0.283	40	0.153	50	0.1446	49	1.0868	0	-0.103
43	0.311	41	0.174	50.5	0.1486	50	1.2528	1	-0.123
44	0.336	42	0.201	51	0.1532	51	1.2828	4	-0.172
45	0.356	43	0.219	Expt. 4		x = 60 cm		8	-0.200
46	0.377	44	0.224	x = 6 cm		y (cm)	u (m/s)	12	-0.202
47	0.399	45	0.238	y (cm)	u (m/s)	12	-0.1201	16	-0.219
48	0.425	46	0.258	49	0.067	16	-0.1436	20	-0.211
49	0.447	47	0.268	49.25	0.339	20	-0.1402	24	-0.220
50	0.471	48	0.275	49.5	0.717	24	-0.1335	28	-0.238
50.5	0.483	49	0.282	49.75	1.091	28	-0.1418	32	-0.170
51	0.492	50	0.290	50	1.505	32	-0.1576	34	-0.153
x = 200 cm		50.5	0.296	50.25	1.906	36	-0.1414	40	0.162
y (cm)	u (m/s)	51	0.299	50.5	2.190	40	-0.117	42	0.304
0	-0.1774	x = 280 cm		50.75	2.250	41	-0.1008	44	0.483
1	-0.2033	y (cm)	u (m/s)	51	2.250	43	0.1807	46	0.635
4	-0.2123	-0.08	0	x = 20 cm		44	0.2949	48	0.777

50	0.920	4	-0.329	46	0.236	24	-0.122	31	0.908
51	0.950	8	-0.317	48	0.266	25	-0.107	x = 80 cm	
x = 120 cm		12	-0.312	50	0.299	28	0.324	y (cm) u (m/s)	
y (cm)	u (m/s)	16	-0.289	51	0.313	28.5	0.578	0	-0.271
0	-0.12	20	-0.222	x = 320 cm		29	0.808	2	-0.300
1	-0.1698	24	-0.200	y (cm)	u (m/s)	29.5	1.028	4	-0.295
4	-0.2186	28	-0.176	36	0.082	30	1.229	6	-0.307
8	-0.2496	38	0.207	38	0.099	30.5	1.415	8	-0.303
12	-0.275	40	0.264	40	0.118	31	1.535	10	-0.281
16	-0.2392	42	0.338	42	0.139	x = 40 cm		12	-0.298
20	-0.2635	44	0.393	44	0.159	y (cm)	u (m/s)	14	-0.220
24	-0.2539	46	0.473	46	0.179	0	-0.125	16	-0.175
28	-0.2267	48	0.529	48	0.202	2	-0.158	20	0.099
30	-0.2183	50	0.587	50	0.226	4	-0.208	21	0.176
32	-0.1812	51	0.591	51	0.235	8	-0.210	22	0.244
34	-0.15	x = 240 cm		Expt. 5		12	-0.218	23	0.312
38	0.1632	y (cm)	u (m/s)	x = 6 cm		16	-0.188	24	0.382
40	0.2641	0	-0.2048	y (cm)	u (m/s)	20	-0.155	25	0.438
42	0.3805	1	-0.224	29.5	0.432	21	-0.157	26	0.509
44	0.5294	4	-0.2445	29.75	0.880	25	0.256	27	0.580
46	0.6113	8	-0.2483	30	1.296	26	0.397	28	0.644
48	0.7412	12	-0.2104	30.5	1.880	27	0.524	29	0.707
50	0.8404	16	-0.2089	31	1.880	28	0.676	30	0.769
51	0.8859	20	-0.1897	x = 12 cm		29	0.846	31	0.829
x = 160 cm		24	-0.1582	y (cm)	u (m/s)	30	1.013	x = 100 cm	
y (cm)	u (m/s)	26	-0.1536	1	-0.073	31	1.170	y (cm)	u (m/s)
0	-0.259	28	-0.1555	4	-0.086	x = 60 cm		0	-0.2555
1	-0.289	38	0.1656	8	-0.094	y (cm)	u (m/s)	2	-0.2994
4	-0.293	40	0.2038	12	-0.094	0	-0.158	4	-0.2985
8	-0.301	42	0.2425	16	-0.094	2	-0.253	6	-0.2955
12	-0.326	44	0.289	20	-0.096	4	-0.253	8	-0.2969
16	-0.312	46	0.3393	24	-0.091	6	-0.252	10	-0.2956
20	-0.309	48	0.3804	26	-0.095	8	-0.258	12	-0.2959
24	-0.287	50	0.4198	29	0.395	10	-0.252	14	-0.1951
28	-0.193	51	0.4329	29.25	0.626	12	-0.258	21	0.2298
30	-0.162	x = 280 cm		29.5	0.853	14	-0.252	22	0.2981
38	0.232	y (cm)	u (m/s)	29.75	1.081	16	-0.225	23	0.3525
40	0.313	0	-0.1453	30	1.282	18	-0.197	24	0.3976
42	0.401	1	-0.1489	30.5	1.655	19	-0.162	25	0.4533
44	0.484	4	-0.1449	31	1.880	22	0.165	26	0.5049
46	0.581	8	-0.1448	x = 20 cm		23	0.246	27	0.5532
48	0.639	12	-0.1397	y (cm)	u (m/s)	24	0.326	28	0.6118
50	0.700	14	-0.1277	1	-0.125	25	0.403	29	0.6678
51	0.720	36	0.1118	4	-0.124	26	0.483	30	0.7172
x = 200 cm		38	0.1317	8	-0.128	27	0.591	31	0.7672
y (cm)	u (m/s)	40	0.1512	12	-0.121	28	0.685	x = 120 cm	
0	-0.270	42	0.1782	16	-0.129	29	0.769	y (cm)	u (m/s)
1	-0.315	44	0.2061	20	-0.124	30	0.858	0	-0.244

2	-0.253	x = 240 cm		49	0.618	y (cm) u (m/s)		38	0.275
4	-0.270	y (cm) u (m/s)		49.5	0.998	4	-0.169	40	0.401
6	-0.299	22	0.088	50	1.417	8	-0.237	42	0.536
8	-0.274	23	0.099	50.5	1.826	12	-0.240	44	0.655
10	-0.203	24	0.109	51	2.130	16	-0.239	46	0.807
12	-0.182	25	0.119	51.5	2.130	20	-0.237	48	0.920
20	0.186	26	0.132	52	2.130	24	-0.239	50	0.989
21	0.226	27	0.142	x = 12 cm		28	-0.239	52	1.012
22	0.261	28	0.152	y (cm) u (m/s)		32	-0.240	x = 200 cm	
23	0.301	29	0.167	48.5	0.368	36	-0.189	y (cm) u (m/s)	
24	0.353	30	0.178	49	0.725	40	0.187	0	-0.381
25	0.401	31	0.191	49.5	1.084	42	0.366	1	-0.419
26	0.464	32	0.202	50	1.409	44	0.568	4	-0.412
27	0.519	x = 280 cm		50.5	1.757	46	0.773	8	-0.412
28	0.548	y (cm) u (m/s)		51	2.010	48	0.971	12	-0.365
29	0.576	0	0.030	51.5	2.130	50	1.159	16	-0.349
30	0.599	4	0.030	52	2.130	52	1.309	20	-0.343
31	0.619	8	0.030	x = 24 cm		x = 120 cm		24	-0.265
x = 160 cm		20	0.057	y (cm) u (m/s)		y (cm) u (m/s)		28	-0.203
y (cm) u (m/s)		21	0.066	47	0.202	0	-0.160	36	0.200
0	-0.113	22	0.073	47.5	0.413	1	-0.307	38	0.332
2	-0.148	23	0.080	48	0.593	4	-0.320	40	0.424
4	-0.134	24	0.089	48.5	0.798	8	-0.365	42	0.506
6	-0.189	25	0.098	49	0.980	12	-0.323	44	0.577
8	-0.150	26	0.106	49.5	1.169	16	-0.322	46	0.686
10	-0.155	27	0.115	50	1.391	20	-0.338	48	0.754
11	-0.117	28	0.124	50.5	1.617	24	-0.307	50	0.835
12	-0.128	29	0.132	51	1.846	28	-0.282	52	0.886
19	0.127	30	0.142	51.5	2.030	32	-0.246	x = 240 cm	
21	0.175	31	0.149	52	2.030	38	0.250	y (cm) u (m/s)	
23	0.230	32	0.159	x = 40 cm		40	0.410	0	-0.3384
25	0.287	x = 320 cm		y (cm) u (m/s)		42	0.537	1	-0.3158
27	0.342	y (cm) u (m/s)		16	-0.116	44	0.680	4	-0.3439
29	0.402	0	0.045	24	-0.158	46	0.816	8	-0.3247
31	0.452	4	0.045	28	-0.143	48	0.930	12	-0.3302
x = 200 cm		8	0.045	32	-0.142	50	1.028	16	-0.2888
y (cm) u (m/s)		12	0.045	36	-0.162	52	1.088	18	-0.2876
0	-0.077	16	0.045	40	-0.165	x = 160 cm		20	-0.2574
22	0.135	20	0.046	42	-0.139	y (cm) u (m/s)		36	0.271
23	0.148	22	0.056	45	0.183	0	-0.342	38	0.3191
25	0.171	24	0.069	46	0.355	1	-0.387	40	0.3785
26	0.186	26	0.081	47	0.578	4	-0.392	42	0.4327
27	0.199	28	0.095	48	0.864	8	-0.381	44	0.4864
28	0.220	30	0.113	49	1.180	12	-0.392	46	0.5507
29	0.237	32	0.127	50	1.416	16	-0.401	48	0.6064
30	0.259	Expt. 6		51	1.577	20	-0.376	50	0.6718
31	0.273	x = 6 cm		52	1.701	24	-0.314	52	0.7278
31.5	0.296	y (cm) u (m/s)		x = 80 cm		28	-0.216	x = 280 cm	

y (cm) u (m/s)	6 -0.070	y (cm) u (m/s)	16 0.113	2 0.032
0 -0.190	8 -0.081	0 -0.174	17 0.131	4 0.033
1 -0.209	10 -0.098	2 -0.214	18 0.149	6 0.032
4 -0.218	12 -0.087	4 -0.203	19 0.167	8 0.032
8 -0.222	14 -0.096	6 -0.194	20 0.188	10 0.032
10 -0.212	16 -0.094	8 -0.162	21 0.204	12 0.033
12 -0.189	18 0.150	10 -0.118	x = 140 cm	14 0.033
36 0.196	18.5 0.264	11 -0.119	y (cm) u (m/s)	16 0.040
38 0.231	19 0.365	12 -0.096	0 0.000	18 0.051
40 0.278	19.5 0.473	14 0.125	2 0.011	20 0.066
42 0.313	20 0.576	15 0.169	4 0.011	21 0.075
44 0.353	20.5 0.687	16 0.215	6 0.011	21.75 0.082
46 0.395	21 0.780	17 0.255	8 0.010	x = 240 cm
48 0.428	x = 40 cm	18 0.292	10 0.018	y (cm) u (m/s)
50 0.465	y (cm) u (m/s)	19 0.336	11 0.025	0 0.036
52 0.496	0 -0.098	20 0.378	12 0.033	2 0.037
x = 320 cm	2 -0.135	21 0.416	13 0.044	4 0.036
y (cm) u (m/s)	4 -0.135	x = 100 cm	14 0.053	6 0.036
36 0.142	6 -0.140	y (cm) u (m/s)	15 0.062	8 0.037
38 0.173	8 -0.128	0 -0.146	16 0.071	10 0.037
40 0.208	10 -0.151	2 -0.162	17 0.087	12 0.036
42 0.232	12 -0.120	4 -0.157	18 0.099	14 0.037
44 0.260	14 -0.101	6 -0.157	19 0.110	16 0.038
46 0.289	16 0.148	8 -0.160	20 0.120	18 0.045
48 0.315	17 0.238	10 -0.162	21 0.133	20 0.054
50 0.334	18 0.323	11 -0.152	21.75 0.144	21 0.059
52 0.358	19 0.413	13 0.053	x = 160 cm	21.75 0.063
Expt. 7	20 0.498	14 0.084	y (cm) u (m/s)	x = 280 cm
x = 6 cm	21 0.591	15 0.121	0 0.000	y (cm) u (m/s)
y (cm) u (m/s)	x = 60 cm	16 0.163	2 0.029	0 0.038
19.5 0.253	y (cm) u (m/s)	17 0.215	4 0.031	2 0.038
19.75 0.438	0 -0.154	18 0.253	6 0.033	4 0.039
20 0.615	2 -0.186	19 0.283	8 0.034	6 0.039
20.5 0.000	4 -0.189	20 0.293	10 0.034	8 0.039
21 0.000	6 -0.180	21 0.297	12 0.034	10 0.038
x = 12 cm	8 -0.150	x = 120 cm	13 0.034	12 0.038
y (cm) u (m/s)	10 -0.109	y (cm) u (m/s)	14 0.038	14 0.038
19 0.3172	12 -0.089	0 -0.133	15 0.046	16 0.038
19.25 0.3831	13 -0.091	2 -0.103	16 0.057	18 0.039
19.5 0.4469	14 0.042	4 -0.066	17 0.067	20 0.041
20 0.601	15 0.116	6 0.057	18 0.077	21 0.047
20.5 0.7612	16 0.185	8 0.039	19 0.086	21.75 0.053
21 0.8859	17 0.253	10 0.031	20 0.097	x = 320 cm
x = 20 cm	18 0.318	11 0.045	21 0.108	y (cm) u (m/s)
y (cm) u (m/s)	19 0.389	12 0.048	21.75 0.113	0 0.040
0 -0.053	20 0.459	13 0.063	x = 200 cm	2 0.040
2 -0.085	21 0.496	14 0.077	y (cm) u (m/s)	4 0.040
4 -0.075	x = 80 cm	15 0.096	0 0.032	6 0.040

8	0.040	9.0	0.4862	11.0	0.268	y (cm)	u (m/s)	0.5	-0.098
10	0.040	9.5	0.6499	12.0	0.308	0.00	0.098	1	-0.104
12	0.041	10.0	0.8635	x = 100 cm		1.00	0.098	1.5	-0.088
14	0.040	10.5	0.9805	y (cm) u (m/s)		2.00	0.098	2	-0.079
16	0.040	11.0	0.9905	0.0		3.00	0.099	2.5	0.122
18	0.040	x = 40 cm		1.0		4.00	0.098	3	0.173
20	0.040	y (cm) u (m/s)		2.0		5.00	0.099	3.5	0.228
21	0.042	0.0		3.0		6.00	0.099	4	0.268
21.75	0.044	1.0		4.0		7.00	0.099	4.5	0.302
Expt. 8		2.0		5.0		8.00	0.099	5	0.327
x = 6 cm		3.0		6.0		9.00	0.098	5.3	0.338
y (cm) u (m/s)		4.0		7.0		10.00	0.098	x = 40 cm	
8.5	0.013	5.0		8.0		11.00	0.098	y (cm) u (m/s)	
9.0	0.083	6.0		9.0		12.00	0.099	0	-0.072
9.5	0.400	7.0		10.0		12.25	0.091	0.5	-0.071
10.0	0.841	7.5		11.0		Expt. 9		1	-0.044
10.3	1.029	8.0		12.0		x = 6 cm		1.5	0.041
10.5	1.205	8.5		x = 120 cm		y (cm) u (m/s)		2	0.097
10.8	1.250	9.0		y (cm) u (m/s)		3	0.043	2.5	0.120
11.0	1.250	9.5		0.0		3.5	0.156	3	0.171
x = 12 cm		10.0		1.0		4	0.345	3.5	0.195
y (cm) u (m/s)		10.5		2.0		4.5	0.487	4	0.215
0.0	-0.063	11.0		3.0		5	0.500	4.5	0.232
1.0	-0.086	x = 60 cm		4.0		x = 12 cm		5	0.243
2.0	-0.114	y (cm) u (m/s)		5.0		y (cm) u (m/s)		5.5	0.261
3.0	-0.133	0.00		6.0		2	0.025	x = 50 cm	
4.0	-0.155	1.00		7.0		2.5	0.054	y (cm) u (m/s)	
5.0	-0.136	2.00		8.0		3	0.123	0	0.012
6.0	-0.121	3.00		9.0		3.5	0.239	1	0.039
7.0	-0.132	6.50		10.0		4	0.349	2	0.070
8.5	0.151	7.00		11.0		4.5	0.432	3	0.102
9.0	0.367	7.50		12.0		5	0.469	4	0.130
9.5	0.615	8.00		x = 160 cm		x = 20 cm		5	0.163
10.0	0.847	8.50		y (cm) u (m/s)		y (cm) u (m/s)		5.5	0.181
10.5	1.062	9.00		0.0		0	-0.120	x = 60 cm	
11.0	1.202	9.50		1.0		0.5	-0.124	y (cm) u (m/s)	
x = 20 cm		10.00		2.0		1	-0.137	0	0.029
y (cm) u (m/s)		10.50		3.0		1.5	-0.086	1	0.049
0.0	-0.165	11.00		4.0		2	-0.061	2	0.071
1.0	-0.1922	11.50		5.0		2.5	0.114	3	0.094
2.0	-0.1912	x = 80 cm		6.0		3	0.187	4	0.117
3.0	-0.1921	y (cm) u (m/s)		7.0		3.5	0.256	5	0.142
4.0	-0.1794	5.0		8.0		4	0.322	5.6	0.159
5.0	-0.1639	6.0		9.0		4.5	0.390	x = 80 cm	
6.0	-0.1334	7.0		10.0		5	0.432	y (cm) u (m/s)	
7.0	-0.0932	8.0		11.0		x = 30 cm		0	0.070
8.0	0.1981	9.0		12.0		y (cm) u (m/s)		1	0.076
8.5	0.3042	10.0		x = 200 cm		0	-0.119	2	0.085

3	0.092	2	0.083	1	0.080	0	0.080	y (cm)	u (m/s)
4	0.099	3	0.090	2	0.086	1	0.084	0	0.084
5	0.106	4	0.096	3	0.091	2	0.088	1	0.086
5.6	0.111	5	0.104	4	0.095	3	0.089	2	0.089
x = 100 cm		5.6	0.108	5	0.101	4	0.093	3	0.091
y (cm)	u (m/s)	x = 120 cm		5.6	0.104	5	0.097	4	0.093
0	0.073	y (cm)	u (m/s)	x = 140 cm		5.6	0.100	5	0.095
1	0.079	0	0.076	y (cm)	u (m/s)	x = 160 cm		5.6	0.096

2.2 Variation of Velocity Scale, Length Scale, Jet Discharge and Momentum Flux with Distance
Expt. 1

x (m)	u_m (m/s)	u_t (m/s)	b (m)	x/b ₀	u_m/U_0	u_t/U_0	b/b ₀	Q/Q ₀	M/M ₀
0.00	0.000	-	-	0	1.000	-	-	1.000	1.000
0.06	1.600	-	0.007	12	1.000	-	1.382	1.472	0.999
0.10	1.439	-	0.009	20	0.899	-	1.746	1.624	0.999
0.20	1.000	-0.045	0.019	40	0.625	-0.028	3.741	2.273	0.992
0.30	0.805	-	0.028	60	0.503	-	5.611	2.784	0.978
0.40	0.724	-0.064	0.031	80	0.453	-0.040	6.204	2.948	0.935
0.50	0.678	-	0.038	100	0.424	-	7.571	3.236	0.916
0.60	0.615	-0.091	0.045	120	0.385	-0.057	9.030	3.492	0.911
0.70	0.572	-	0.049	140	0.358	-	9.857	3.702	0.883
0.80	0.531	-0.105	0.055	160	0.332	-0.065	11.074	3.829	0.845
0.90	0.486	-	0.063	180	0.304	-	12.597	3.950	0.823
1.00	0.464	-0.121	0.070	200	0.290	-0.076	14.056	4.071	0.786
1.20	0.408	-0.134	0.082	240	0.255	-0.084	16.478	4.057	0.696
1.40	0.365	-0.138	0.087	280	0.228	-0.087	17.498	3.860	0.562
1.60	0.328	-0.132	0.090	320	0.205	-0.083	17.926	3.280	0.475
1.80	0.282	-0.124	0.091	360	0.176	-0.078	18.168	2.845	0.352
2.00	0.242	-0.111	0.092	400	0.151	-0.070	18.438	2.509	0.274
2.20	0.208	-0.108	0.095	440	0.130	-0.068	19.085	2.159	0.201
2.40	0.178	-0.105	0.097	480	0.111	-0.065	19.378	1.816	0.141
2.60	0.149	-0.075	0.099	520	0.093	-0.047	19.884	1.711	0.111
2.80	0.128	-0.055	0.102	560	0.080	-0.034	20.492	1.393	0.083
3.00	0.108	-0.046	0.104	600	0.068	-0.029	20.827	1.182	0.059
3.20	0.092	-0.032	0.110	640	0.058	-0.020	21.922	1.066	0.048

Expt. 2

x (m)	u_m (m/s)	u_t (m/s)	b (m)	x/b_o	u_m/U_o	u_t/U_o	b/b_o	Q/Q_o	M/M_o
0.00	0.750	-	-	0	1.000	-	-	1.000	1.000
0.06	0.750	-	0.012	6	1.000	-	1.230	1.246	1.000
0.20	0.629	-0.029	0.019	20	0.839	-0.039	1.879	1.569	0.965
0.40	0.465	-0.038	0.036	40	0.620	-0.050	3.616	2.041	0.914
0.60	0.398	-0.050	0.045	60	0.531	-0.067	4.512	2.441	0.900
0.80	0.350	-0.051	0.055	80	0.467	-0.068	5.451	2.500	0.856
1.00	0.332	-0.062	0.068	100	0.442	-0.082	6.788	2.928	0.877
1.20	0.305	-0.078	0.080	120	0.407	-0.104	7.988	3.112	0.858
1.60	0.266	-0.085	0.096	160	0.354	-0.114	9.639	2.855	0.725
2.00	0.218	-0.094	0.100	200	0.290	-0.125	9.974	2.524	0.529
2.40	0.155	-0.081	0.108	240	0.207	-0.108	10.827	1.863	0.282
2.80	0.109	-0.045	0.109	280	0.145	-0.060	10.850	1.627	0.127
3.20	0.080	-	0.110	320	0.107	-	11.014	1.019	0.064

Expt. 3

x (m)	u_m (m/s)	u_t (m/s)	b (m)	x/b_o	u_m/U_o	u_t/U_o	b/b_o	Q/Q_o	M/M_o
0.00	1.500	-	-	0	1.000	-	-	1.000	1.000
0.05	1.500	-	0.012	5	1.000	-	1.239	1.262	0.991
0.20	1.129	-0.066	0.022	20	0.753	-0.044	2.170	1.630	0.941
0.40	0.986	-0.088	0.032	40	0.658	-0.059	3.184	1.958	0.895
0.60	0.805	-0.102	0.046	60	0.536	-0.068	4.583	2.336	0.897
0.80	0.700	-0.120	0.057	80	0.467	-0.080	5.707	2.690	0.881
1.00	0.645	-0.134	0.070	100	0.430	-0.089	6.967	3.015	0.877
1.20	0.601	-0.147	0.081	120	0.401	-0.098	8.122	3.062	0.847
1.60	0.492	-0.192	0.105	160	0.328	-0.128	10.489	2.970	0.723
2.00	0.413	-0.187	0.106	200	0.276	-0.125	10.593	2.477	0.504
2.40	0.299	-0.141	0.111	240	0.199	-0.094	11.128	1.863	0.302
2.80	0.212	-0.107	0.112	280	0.141	-0.071	11.229	1.376	0.136
3.20	0.153	-0.069	0.115	320	0.102	-0.046	11.480	1.050	0.066

Expt. 4

x (m)	u_m (m/s)	u_r (m/s)	b (m)	x/b_o	u_m/U_o	u_r/U_o	b/b_o	Q/Q_o	M/M_o
0.00	2.250	-	-	0	1.000	-	-	1.000	1.000
0.06	2.250	-	0.012	6	1.000	-	1.230	1.240	0.987
0.20	1.657	-0.093	0.023	20	0.736	-0.041	2.274	1.603	0.987
0.40	1.283	-0.114	0.039	40	0.570	-0.051	3.941	2.209	0.962
0.60	1.102	-0.133	0.051	60	0.490	-0.059	5.099	2.521	0.941
0.80	1.010	-0.161	0.062	80	0.449	-0.071	6.155	2.799	0.837
1.00	0.950	-0.183	0.071	100	0.422	-0.081	7.084	2.850	0.864
1.20	0.886	-0.214	0.082	120	0.394	-0.095	8.161	3.075	0.847
1.60	0.720	-0.273	0.099	160	0.320	-0.121	9.926	2.878	0.693
2.00	0.591	-0.270	0.102	200	0.262	-0.120	10.156	2.389	0.476
2.40	0.433	-0.200	0.103	240	0.192	-0.089	10.346	1.927	0.260
2.80	0.313	-0.142	0.106	280	0.139	-0.063	10.615	1.457	0.142
3.20	0.235	-	0.111	320	0.104	-	11.104	1.036	0.063

Expt. 5

x (m)	u_m (m/s)	u_t (m/s)	b (m)	x/b_o	u_m/U_o	u_t/U_o	b/b_o	Q/Q_o	M/M_o
0.00	1.880	-	-	0	1.000	-	-	1.000	1.000
0.06	1.880	-	0.012	6	1.000	-	1.214	1.154	0.977
0.12	1.880	-0.090	0.014	12	1.000	-0.048	1.404	1.312	0.972
0.20	1.535	-0.122	0.021	20	0.816	-0.065	2.089	1.592	0.954
0.40	1.170	-0.177	0.036	40	0.623	-0.094	3.597	2.217	0.941
0.60	0.908	-0.229	0.054	60	0.483	-0.122	5.363	2.604	0.883
0.80	0.829	-0.272	0.064	80	0.441	-0.145	6.426	2.779	0.839
1.00	0.767	-0.279	0.073	100	0.408	-0.148	7.310	2.689	0.789
1.20	0.619	-0.246	0.078	120	0.329	-0.131	7.829	2.473	0.638
1.60	0.452	-0.142	0.081	160	0.241	-0.075	8.134	1.837	0.318
2.00	0.296	-	0.085	200	0.157	-	8.523	1.024	0.116
2.40	0.202	-	0.087	240	0.108	-	8.730	1.042	0.070
2.80	0.159	-	0.091	280	0.084	-	9.075	1.001	0.047
3.20	0.127	-	0.089	320	0.067	-	8.892	1.013	0.033

Expt. 6

x (m)	u_m (m/s)	u_r (m/s)	b (m)	x/b_o	u_m/U_o	u_r/U_o	b/b_o	Q/Q_o	M/M_o
0.00	2.130	-	-	0	1.000	-	-	1.000	1.000
0.06	2.130	-	0.024	3	1.000	-	1.210	1.159	0.979
0.12	2.130	-	0.025	6	1.000	-	1.265	1.217	0.970
0.24	2.030	-	0.029	12	0.953	-	1.454	1.403	0.969
0.40	1.701	-0.146	0.040	20	0.799	-0.069	2.022	1.622	0.936
0.80	1.309	-0.225	0.072	40	0.614	-0.106	3.580	2.152	0.923
1.20	1.088	-0.297	0.099	60	0.511	-0.139	4.949	2.412	0.906
1.60	1.012	-0.356	0.104	80	0.475	-0.167	5.222	2.325	0.857
2.00	0.886	-0.350	0.115	100	0.416	-0.164	5.771	2.187	0.665
2.40	0.728	-0.311	0.125	120	0.342	-0.146	6.246	1.852	0.460
2.80	0.496	-0.206	0.133	140	0.233	-0.097	6.638	1.480	0.241
3.20	0.358	-	0.136	160	0.168	-	6.817	0.967	0.128

Expt.7

x (m)	u_m (m/s)	u_t (m/s)	b (m)	x/b_o	u_m/U_o	u_t/U_o	b/b_o	Q/Q_o	M/M_o
0.00	2.130	-	-	0	1.000	-	-	1.000	1.000
0.06	2.130	-	0.024	3	1.000	-	1.210	1.159	0.979
0.12	2.130	-	0.025	6	1.000	-	1.265	1.217	0.970
0.24	2.030	-	0.029	12	0.953	-	1.454	1.403	0.969
0.40	1.701	-0.146	0.040	20	0.799	-0.069	2.022	1.622	0.936
0.80	1.309	-0.225	0.072	40	0.614	-0.106	3.580	2.152	0.923
1.20	1.088	-0.297	0.099	60	0.511	-0.139	4.949	2.412	0.906
1.60	1.012	-0.356	0.104	80	0.475	-0.167	5.222	2.325	0.857
2.00	0.886	-0.350	0.115	100	0.416	-0.164	5.771	2.187	0.665
2.40	0.728	-0.311	0.125	120	0.342	-0.146	6.246	1.852	0.460
2.80	0.496	-0.206	0.133	140	0.233	-0.097	6.638	1.480	0.241
3.20	0.358	-	0.136	160	0.168	-	6.817	0.967	0.128

Expt. 8

x (m)	u_m (m/s)	u_t (m/s)	b (m)	x/b_o	u_m/U_o	u_t/U_o	b/b _o	Q/Q _o	M/M _o
0.00	1.250	-	-	0	1.000	-	-	1.000	1.000
0.06	1.250	-	0.012	6	1.000	-	1.245	1.270	0.982
0.12	1.202	-0.117	0.015	12	0.961	-0.094	1.528	1.427	0.977
0.20	0.991	-0.164	0.020	20	0.792	-0.131	1.972	1.551	0.943
0.40	0.767	-0.234	0.032	40	0.614	-0.187	3.228	1.767	0.844
0.60	0.468	-0.166	0.039	60	0.374	-0.133	3.884	1.395	0.412
0.80	0.308	-	0.043	80	0.247	-	4.258	1.042	0.174
1.00	0.221	-	0.050	100	0.177	-	4.982	0.989	0.111
1.20	0.180	-	0.078	120	0.144	-	7.793	1.044	0.100
1.60	0.118	-	-	160	0.094	-	-	1.000	0.084
2.00	0.091	-	-	200	0.072	-	-	0.964	0.076

Expt. 9

x (m)	u_m (m/s)	u_r (m/s)	b (m)	x/b_o	u_m/U_o	u_r/U_o	b/ h_o	Q/ Q_o	M/ M_o
0.000	0.9012	-	-	0	1.000	-	-	1.000	1.000
0.054	0.9012	-	0.013	5	1.000	-	1.286	1.162	0.982
0.108	0.8859	-	0.015	11	0.983	-	1.513	1.338	0.966
0.200	0.7799	-0.082	0.019	20	0.865	-0.091	1.883	1.569	0.944
0.400	0.5914	-0.126	0.033	40	0.656	-0.140	3.300	2.044	0.935
0.600	0.4962	-0.144	0.041	60	0.551	-0.159	4.069	2.207	0.854
0.800	0.4155	-0.160	0.052	80	0.461	-0.177	5.167	2.124	0.711
1.000	0.2969	-0.157	0.053	100	0.329	-0.174	5.346	1.760	0.453
1.200	0.2044	-0.101	0.056	120	0.227	-0.112	5.612	1.231	0.192
1.400	0.1442	-	0.057	140	0.160	-	5.660	0.958	0.102
1.600	0.1125	-	0.058	160	0.125	-	5.775	0.951	0.071
2.000	0.0824	-	-	200	0.091	-	-	0.958	0.047
2.400	0.0629	-	-	240	0.070	-	-	0.965	0.044
2.800	0.0529	-	-	280	0.059	-	-	0.942	0.041
3.200	0.0444	-	-	320	0.049	-	-	0.964	0.044

NOTE TO USERS

Page(s) not included in the original manuscript are unavailable from the author or university. The manuscript was microfilmed as received.

352

This reproduction is the best copy available.

UMI

3. Plane Turbulent Wall Jets in Shallow Tailwater

3.1 Velocity Measurements along Vertical Sections at x-stations

Expt. 1		27.5	-0.124	4	0.677	x = 80 cm		0.75	0.941
x = 6 cm		30	-0.128	4.5	0.563	y (cm) u (m/s)		1	0.961
y (cm)	u (m/s)	32.5	-0.133	5	0.435	0	0.900	1.25	0.971
0	2.352	35	-0.139	5.5	0.333	0.25	1.008	1.5	0.980
0.25	2.434	37.5	-0.143	6	0.246	0.5	1.055	1.75	0.980
0.5	2.500	40	-0.148	6.5	0.181	0.75	1.098	2	0.970
0.75	2.226	42.5	-0.153	32.5	-0.108	1	1.115	2.5	0.939
1	1.773	45	-0.158	35	-0.119	1.25	1.102	3	0.906
1.25	1.253	47.5	-0.161	37.5	-0.122	1.5	1.110	4	0.835
1.5	0.632	48.5	-0.170	40	-0.138	1.75	1.099	5	0.757
1.75	0.101	x = 30 cm		42.5	-0.142	2	1.096	6	0.686
x = 12 cm		y (cm)	u (m/s)	45	-0.153	2.5	1.041	7	0.608
y (cm)	u (m/s)	0	1.581	47.5	-0.162	3	0.979	8	0.536
0	2.00	0.25	1.744	48.5	-0.179	3.5	0.917	9	0.468
0.25	2.29	0.5	1.738	x = 60 cm		4	0.860	10	0.392
0.5	2.20	0.75	1.683	y (cm) u (m/s)		4.5	0.817	11	0.321
0.75	1.98	1	1.595	0	0.951	5	0.767	12	0.261
1	1.76	1.5	1.399	0.25	1.128	5.5	0.718	13	0.181
1.25	1.51	2	1.187	0.5	1.193	6	0.661	14	0.116
1.5	1.25	2.5	0.958	0.75	1.228	6.5	0.597	27.5	-0.157
1.75	1.01	3	0.756	1	1.222	7	0.548	30	-0.191
2	0.79	3.5	0.557	1.5	1.189	7.5	0.499	32.5	-0.215
2.25	0.57	4	0.416	2	1.146	8	0.435	35	-0.239
2.5	0.39	4.5	0.250	2.5	1.078	8.5	0.396	37.5	-0.269
2.75	0.20	5	0.132	3	0.990	9	0.351	40	-0.298
x = 20 cm		30	-0.108	3.5	0.911	9.5	0.297	42.5	-0.315
y (cm)	u (m/s)	32.5	-0.112	4	0.835	10	0.255	45	-0.343
0	1.745	35	-0.124	4.5	0.764	10.5	0.216	47.5	-0.373
0.25	1.946	37.5	-0.131	5	0.672	11	0.167	48	-0.391
0.5	1.911	40	-0.146	5.5	0.590	11.5	0.117	x = 120 cm	
0.75	1.798	42.5	-0.153	6	0.529	25	-0.107	y (cm) u (m/s)	
1	1.673	45	-0.162	6.5	0.469	27.5	-0.131	0	0.7264
1.25	1.537	47.5	-0.179	7	0.385	30	-0.154	0.25	0.8121
1.5	1.412	48.5	-0.186	7.5	0.317	32.5	-0.179	0.5	0.8448
1.75	1.276	x = 40 cm		8	0.255	35	-0.202	0.75	0.8682
2	1.124	y (cm) u (m/s)		8.5	0.180	37.5	-0.227	1	0.8994
2.25	0.981	0	1.309	9	0.115	40	-0.242	1.25	0.9084
2.5	0.829	0.25	1.461	30	-0.110	42.5	-0.267	1.5	0.9054
2.75	0.683	0.5	1.498	32.5	-0.123	45	-0.298	1.75	0.8976
3	0.550	0.75	1.498	35	-0.135	47.5	-0.323	2	0.8956
3.25	0.441	1	1.464	37.5	-0.148	48.25	-0.350	2.5	0.8798
3.5	0.330	1.5	1.355	40	-0.160	x = 100 cm		3	0.8530
3.75	0.219	2	1.221	42.5	-0.173	y (cm) u (m/s)		4	0.7906
4	0.155	2.5	1.069	45	-0.186	0	0.800	5	0.7392
4.25	0.110	3	0.948	47.5	-0.197	0.25	0.861	6	0.6725
25	-0.119	3.5	0.813	48.5	-0.209	0.5	0.911	7	0.6134

8	0.5618	48	-0.4859	7	0.504	27	0.2799	0	0.806
9	0.5061	x = 160 cm		8	0.497	28	0.2781	0.25	0.919
10	0.4578	y (cm)	u (m/s)	9	0.482	29	0.2722	0.5	0.960
11	0.4016	0	0.376	10	0.463	30	0.2705	0.75	0.920
12	0.3551	0.25	0.412	11	0.449	x = 240 cm		1	0.847
13	0.3111	0.5	0.437	12	0.434	y (cm)	u (m/s)	1.25	0.784
14	0.2675	0.75	0.477	13	0.405	0	-0.1085	1.5	0.707
15	0.2116	1	0.505	14	0.379	1	-0.1072	1.75	0.640
16	0.1565	1.25	0.546	15	0.363	2	-0.1017	2	0.564
27.5	-0.1348	1.5	0.553	16	0.340	3	-0.1116	2.5	0.420
30	-0.1769	1.75	0.573	17	0.310	4	-0.1211	3	0.284
32.5	-0.214	2	0.604	18	0.289	5	-0.1041	3.5	0.160
35	-0.2459	2.5	0.612	19	0.260	6	-0.1352	4	0.050
37.5	-0.2833	3	0.636	20	0.229	35	0.1321	4.25	0.011
40	-0.3222	4	0.638	21	0.199	37.5	0.1289	25	-0.031
42.5	-0.3672	5	0.631	37.5	-0.209	40	0.1399	27.5	-0.036
45	-0.4097	6	0.616	40	-0.233	42.5	0.2045	30	-0.040
47.5	-0.4462	7	0.588	42.5	-0.255	45	0.2017	32.5	-0.046
48	-0.4862	8	0.565	45	-0.277	47.5	0.1882	35	-0.052
x = 140 cm		9	0.537	47.5	-0.298	0.5	0.2307	37.5	-0.055
y (cm)	u (m/s)	10	0.517	49.5	-0.328	Expt. 2		40	-0.062
0	0.6859	11	0.483	x = 200 cm		x = 6 cm		42.5	-0.066
0.5	0.7472	12	0.452	y (cm)	u (m/s)	y (cm)	u (m/s)	45	-0.071
1	0.7824	13	0.424	1.25	0.1822	0	1.2	47.5	-0.075
1.5	0.8046	14	0.387	5	0.2393	0.25	1.25	49.75	-0.087
2	0.8167	15	0.351	6.5	0.2642	0.5	1.25	x = 40 cm	
2.5	0.8099	16	0.321	7	0.2625	0.75	1.1068	y (cm)	u (m/s)
3	0.7943	18	0.252	7.5	0.2728	i	0.9004	0	0.632
3.5	0.7743	20	0.181	8	0.2767	1.25	0.6412	0.25	0.718
4	0.7498	22	0.117	8.5	0.2776	1.5	0.3441	0.5	0.746
4.5	0.7292	27.5	-0.131	9.5	0.2745	1.75	0.0609	0.75	0.760
5	0.7104	32.5	-0.219	10	0.2792	x = 12 cm		1	0.746
5.5	0.6789	35	-0.241	11	0.2786	y (cm)	u (m/s)	1.25	0.716
6	0.6531	37.5	-0.277	12	0.2787	0	0.9805	1.5	0.683
7	0.6012	40	-0.313	13	0.2797	0.25	1.1339	2	0.616
8	0.5577	42.5	-0.335	14	0.2775	0.5	1.0951	2.5	0.532
10	0.4737	45	-0.377	15	0.2795	0.75	1.0018	3	0.459
12	0.3868	47.5	-0.416	16	0.2801	1	0.8800	3.5	0.386
14	0.3014	48.75	-0.462	17	0.2799	1.25	0.7504	4	0.314
16	0.2252	x = 180 cm		18	0.2768	1.5	0.6304	4.5	0.242
30	-0.1692	y (cm)	u (m/s)	19	0.2783	1.75	0.5105	5	0.183
32.5	-0.2077	0	0.190	20	0.2777	2	0.4019	5.5	0.125
35	-0.2407	1	0.309	21	0.2803	2.25	0.3005	6	0.067
37.5	-0.2863	2	0.385	22	0.2813	2.5	0.1862	6.5	0.022
40	-0.3236	3	0.441	23	0.2808	2.75	0.0896	32.5	-0.051
42.5	-0.3612	4	0.469	24	0.28	3	0.0211	35	-0.057
45	-0.404	5	0.495	25	0.2796	x = 20 cm		37.5	-0.059
47.5	-0.4445	6	0.503	26	0.279	y (cm)	u (m/s)	40	-0.064

45	-0.070	5.5	0.357	42.5	-0.194	7	0.300	16	0.162
49.75	-0.075	6	0.327	45	-0.213	8	0.276	18	0.138
x = 60 cm		6.5	0.308	47.5	-0.233	9	0.254	20	0.116
y (cm)	u (m/s)	7	0.286	49.75	-0.255	10	0.237	35	-0.110
0	0.483	7.5	0.262	x = 120 cm		11	0.219	37.5	-0.123
0.5	0.578	8	0.239	y (cm)	u (m/s)	12	0.196	40	-0.136
1	0.594	8.5	0.219	0	0.354	13	0.171	42.5	-0.149
1.5	0.585	9	0.197	0.5	0.380	14	0.149	45	-0.160
2	0.556	9.5	0.174	1	0.419	15	0.130	47.5	-0.172
2.5	0.519	10	0.149	1.5	0.438	16	0.116	50	-0.190
3	0.489	10.5	0.130	2	0.446	17	0.096	x = 160 cm	
3.5	0.456	11	0.109	2.5	0.443	18	0.077	y (cm)	u (m/s)
4	0.426	11.5	0.086	3	0.430	19	0.061	4	0.224
4.5	0.391	12	0.068	3.5	0.421	20	0.042	5	0.221
5	0.356	12.5	0.053	4	0.404	21	0.019	6	0.238
5.5	0.323	32.5	-0.115	5	0.378	22	0.010	7	0.240
6	0.288	35	-0.127	6	0.347	27.5	-0.0658	8	0.240
6.5	0.249	37.5	-0.141	7	0.319	30	-0.0894	9	0.240
7	0.218	40	-0.153	8	0.294	32.5	-0.1063	10	0.235
7.5	0.185	42.5	-0.170	9	0.265	35	-0.121	12	0.248
8	0.155	45	-0.184	10	0.237	37.5	-0.1499	14	0.240
8.5	0.123	47.5	-0.201	11	0.211	40	-0.1613	16	0.247
9	0.102	49.75	-0.214	12	0.186	42.5	-0.1897	18	0.234
9.5	0.076	x = 100 cm		13	0.166	45	-0.211	20	0.236
10	0.050	y (cm)	u (m/s)	14	0.139	47.5	-0.2541	21	0.235
10.5	0.033	0	0.385	15	0.115	50	-0.2992	22	0.227
30	-0.059	0.5	0.438	16	0.087	x = 160 cm		23	0.226
32.5	-0.061	1	0.488	32.5	-0.049	y (cm)	u (m/s)	40	-0.074
35	-0.071	1.5	0.486	35	-0.078	0	0.252	42.5	-0.086
37.5	-0.078	2	0.479	37.5	-0.101	0.5	0.271	47.5	-0.133
40	-0.084	3	0.452	40	-0.136	1	0.292	Expt. 3*	
42.5	-0.094	4	0.419	42.5	-0.162	1.5	0.307	x = 10 cm	
45	-0.110	5	0.387	45	-0.193	2	0.318	y (m)	u (m/s)
47.5	-0.119	6	0.353	47.5	-0.223	2.5	0.322	0.002	1.687
49.75	-0.128	7	0.321	49.9	-0.254	3	0.322	0.006	1.750
x = 80 cm		8	0.279	x = 140 cm		3.5	0.319	0.008	1.624
y (cm)	u (m/s)	9	0.243	y (cm)	u (m/s)	4	0.314	0.010	1.410
0	0.442	10	0.206	0	0.295	5	0.298	0.012	1.203
0.5	0.522	11	0.174	0.5	0.334	6	0.287	0.014	0.943
1	0.544	12	0.139	1	0.373	7	0.277	0.017	0.507
1.5	0.541	13	0.105	1.5	0.394	8	0.264	0.021	0.047
2	0.527	14	0.069	2	0.394	9	0.253	x = 20 cm	
2.5	0.501	25	-0.079	2.5	0.389	10	0.238	y (m)	u (m/s)
3	0.480	30	-0.097	3	0.387	11	0.223	0.002	1.454
3.5	0.456	32.5	-0.114	3.5	0.379	12	0.209	0.004	1.516
4	0.427	35	-0.131	4	0.370	13	0.197	0.006	1.452
4.5	0.406	37.5	-0.159	5	0.348	14	0.188	0.009	1.335
5	0.378	40	-0.171	6	0.325	15	0.175	0.013	1.128

0.017	0.904	x = 80 cm		y (m)	u (m/s)	y (m)	u (m/s)	0.013	1.226
0.021	0.694	y (m) u (m/s)		0.002	0.160	9E-04	1.535	0.023	1.189
0.026	0.463	0.002 0.619		0.008	0.157	0.004	1.691	0.035	1.123
0.031	0.272	0.008 0.805		0.018	0.173	0.009	1.751	0.048	1.007
x = 30 cm		0.016 0.770		0.033	0.266	0.014	1.686	0.06	0.931
y (m) u (m/s)		0.024 0.737		0.048	0.301	0.021	1.569	0.073	0.822
0.002	1.187	0.032 0.686		0.068	0.300	0.031	1.356	0.088	0.657
0.005	1.295	0.040 0.617		0.088	0.292	0.041	1.153	0.103	0.569
0.009	1.239	0.050 0.521		0.108	0.270	0.051	0.977	0.118	0.443
0.015	1.105	0.065 0.460		0.128	0.258	0.061	0.710	0.133	0.358
0.021	0.887	0.080 0.345		0.148	0.256	0.074	0.525	0.148	0.195
0.027	0.649	0.095 0.235		0.168	0.216	0.084	0.341	x = 140 cm	
0.035	0.439	0.110 0.181		0.188	0.213	0.099	0.243	y (m) u (m/s)	
0.044	0.201	x = 100 cm		0.208	0.185	0.114	0.216	9E-04	0.885
x = 40 cm		y (m) u (m/s)		Expt. 4*		x = 80 cm		0.006	1.046
y (m) u (m/s)		0.002 0.584		x = 20 cm		y (m) u (m/s)		0.015	1.130
0.002	1.066	0.008 0.716		y (m) u (m/s)		9E-04	1.273	0.025	1.094
0.005	1.145	0.018 0.704		9E-04 2.285		0.006	1.499	0.04	1.033
0.009	1.084	0.028 0.644		0.004 2.546		0.014	1.478	0.055	0.946
0.014	1.015	0.040 0.599		0.007 2.628		0.022	1.440	0.07	0.811
0.020	0.908	0.055 0.545		0.010 2.425		0.032	1.308	0.085	0.736
0.026	0.755	0.075 0.410		0.013 2.235		0.042	1.207	0.1	0.607
0.032	0.635	0.095 0.306		0.016 2.005		0.054	0.940	0.115	0.511
0.040	0.457	0.120 0.196		0.019 1.745		0.066	0.804	0.13	0.383
0.048	0.329	x = 120 cm		0.022 1.492		0.079	0.654	0.145	0.258
0.060	0.146	y (m) u (m/s)		0.025 1.244		0.094	0.446	0.16	0.180
x = 50 cm		0.002 0.484		0.029 0.956		0.109	0.211	x = 160 cm	
y (m) u (m/s)		0.008 0.540		0.033 0.699		0.124	0.117	y (m) u (m/s)	
0.002	0.887	0.020 0.607		0.037 0.500		x = 100 cm		9E-04	0.795
0.006	0.994	0.035 0.617		0.042 0.252		y (m) u (m/s)		0.006	0.941
0.012	0.990	0.050 0.545		x = 40 cm		9E-04	1.119	0.014	0.983
0.018	0.912	0.070 0.444		y (m) u (m/s)		0.006	1.289	0.029	0.940
0.024	0.863	0.095 0.343		9E-04 1.900		0.011	1.325	0.044	0.850
0.030	0.713	0.120 0.292		0.004 2.048		0.02	1.302	0.059	0.815
0.040	0.566	0.145 0.233		0.007 2.108		0.03	1.236	0.074	0.764
0.054	0.357	x = 140 cm		0.01 2.031		0.04	1.151	0.089	0.678
0.074	0.159	y (m) u (m/s)		0.014 1.964		0.05	1.100	0.104	0.568
x = 60 cm		0.002 0.286		0.018 1.844		0.06	1.024	0.134	0.430
y (m) u (m/s)		0.009 0.359		0.023 1.644		0.07	0.849	0.149	0.373
0.002	0.763	0.019 0.405		0.028 1.433		0.083	0.709	x = 180 cm	
0.007	0.919	0.034 0.449		0.033 1.262		0.095	0.577	y (m) u (m/s)	
0.013	0.877	0.054 0.468		0.04 0.855		0.11	0.373	9E-04	0.502
0.020	0.801	0.079 0.417		0.048 0.604		0.125	0.336	0.011	0.701
0.030	0.758	0.104 0.336		0.055 0.559		0.14	0.146	0.021	0.764
0.045	0.570	0.129 0.264		0.065 0.421		x = 120 cm		0.033	0.813
0.060	0.411	0.154 0.268		0.075 0.304		y (m) u (m/s)		0.046	0.835
0.075	0.247	0.179 0.230		0.085 0.300		9E-04	0.942	0.061	0.748
0.090	0.146	x = 160 cm		x = 60 cm		0.005	1.162	0.076	0.691

0.091	0.661	x = 60 cm		0.086	0.678	0.071	0.766	0.047	0.710
0.106	0.610	y (m)	u (m/s)	0.101	0.509	0.086	0.710	0.053	0.583
0.121	0.549	9E-04	1.393	0.116	0.408	0.101	0.594	0.059	0.434
0.136	0.486	0.004	1.663	0.131	0.282	0.121	0.464	0.065	0.242
0.151	0.385	0.007	1.699	0.146	0.182	0.141	0.288	x = 60 cm	
x = 200 cm		0.011	1.700	x = 120 cm		x = 180 cm		y (m)	u (m/s)
y (m)	u (m/s)	0.018	1.621	y (m)	u (m/s)	y (m)	u (m/s)	9E-04	1.330
0.000	0.000	0.026	1.455	9E-04	0.874	9E-04	0.076	0.004	1.629
0.001	0.251	0.034	1.297	0.004	1.137	0.011	0.396	0.007	1.682
0.010	0.383	0.041	1.150	0.008	1.185	0.021	0.563	0.01	1.696
0.020	0.571	0.051	0.957	0.012	1.193	0.036	0.618	0.013	1.670
0.030	0.564	0.061	0.781	0.017	1.218	0.051	0.664	0.016	1.618
0.040	0.576	0.076	0.431	0.022	1.182	0.061	0.646	0.02	1.583
0.045	0.576	0.091	0.164	0.03	1.125	0.071	0.599	0.025	1.515
0.050	0.584	x = 80 cm		0.04	1.034	0.086	0.584	0.031	1.393
0.065	0.558	y (m)	u (m/s)	0.052	0.987	0.106	0.492	0.037	1.274
0.085	0.545	9E-04	1.279	0.065	0.898	0.126	0.374	0.043	1.195
0.105	0.490	0.004	1.424	0.08	0.751	0.146	0.355	0.049	1.059
0.125	0.404	0.007	1.485	0.095	0.649	Expt. 6*		0.055	0.850
0.145	0.292	0.011	1.485	0.11	0.574	x = 20 cm		0.061	0.741
0.165	0.226	0.016	1.461	0.125	0.453	y (m)	u (m/s)	0.068	0.691
Expt. 5*		0.021	1.409	0.14	0.300	9E-04	1.968	0.075	0.530
x = 20 cm		0.028	1.333	0.155	0.238	0.004	2.453	0.082	0.401
y (m)	u (m/s)	0.036	1.211	x = 140 cm		0.007	2.567	0.089	0.235
9E-04	2.007	0.046	1.083	y (m)	u (m/s)	0.01	2.446	x = 80 cm	
0.004	2.522	0.056	1.006	9E-04	0.757	0.013	2.243	y (m)	u (m/s)
0.007	2.586	0.066	0.926	0.005	0.880	0.016	2.014	9E-04	1.192
0.010	2.491	0.076	0.754	0.009	0.974	0.019	1.743	0.005	1.420
0.013	2.230	0.086	0.612	0.014	0.997	0.022	1.512	0.009	1.444
0.017	1.972	0.096	0.456	0.029	0.983	0.025	1.249	0.013	1.452
0.022	1.482	0.106	0.379	0.044	0.969	0.028	1.003	0.017	1.432
0.028	1.028	0.116	0.205	0.059	0.860	0.031	0.850	0.022	1.389
0.034	0.583	x = 100 cm		0.074	0.767	0.034	0.634	0.027	1.324
0.041	0.169	y (m)	u (m/s)	0.089	0.717	0.038	0.385	0.032	1.289
x = 40 cm		9E-04	1.008	0.104	0.674	0.042	0.189	0.04	1.234
y (m)	u (m/s)	0.004	1.228	0.119	0.583	x = 40 cm		0.048	1.102
9E-04	1.669	0.007	1.281	0.134	0.425	y (m)	u (m/s)	0.058	1.011
0.004	1.975	0.01	1.329	0.149	0.348	9E-04	1.589	0.068	0.857
0.007	2.041	0.014	1.341	0.164	0.304	0.004	1.965	0.078	0.671
0.012	1.972	0.018	1.340	x = 160 cm		0.007	2.035	0.088	0.610
0.017	1.835	0.022	1.311	y (m)	u (m/s)	0.01	2.016	0.098	0.462
0.022	1.633	0.027	1.259	9E-04	0.441	0.013	1.966	0.108	0.417
0.029	1.367	0.033	1.223	0.004	0.718	0.016	1.892	0.118	0.255
0.037	1.102	0.038	1.178	0.009	0.767	0.02	1.725	x = 100 cm	
0.045	0.805	0.046	1.117	0.016	0.837	0.025	1.544	y (m)	u (m/s)
0.052	0.479	0.056	1.053	0.026	0.838	0.03	1.370	9E-04	0.941
0.06	0.373	0.066	0.897	0.041	0.829	0.035	1.184	0.006	1.261
0.07	0.237	0.076	0.819	0.056	0.806	0.041	0.969	0.011	1.307

0.016	1.293	y (m)	u (m/s)	0.12	0.455	0.094	0.676	0.053	0.482
0.021	1.258	9E-04	0.825	0.13	0.327	0.104	0.585	0.061	0.521
0.026	1.260	0.006	1.026	x = 140 cm		0.114	0.527	0.069	0.492
0.031	1.239	0.011	1.118	y (m)	u (m/s)	0.124	0.456	0.08	0.498
0.036	1.208	0.016	1.142	9E-04	0.511	0.134	0.401	0.09	0.448
0.046	1.085	0.022	1.117	0.006	0.600	x = 160 cm		0.1	0.387
0.056	1.047	0.03	1.106	0.012	0.736	y (m)	u (m/s)	0.11	0.371
0.066	0.877	0.04	1.040	0.018	0.860	9E-04	0.083	0.12	0.315
0.076	0.803	0.05	0.989	0.024	0.854	0.005	0.116	0.13	0.312
0.086	0.751	0.06	0.914	0.034	0.840	0.011	0.196	0.14	0.273
0.096	0.625	0.07	0.805	0.044	0.834	0.017	0.200	0.15	0.183
0.106	0.454	0.08	0.766	0.054	0.791	0.023	0.298		
0.116	0.392	0.09	0.716	0.064	0.767	0.03	0.337		
0.126	0.279	0.1	0.554	0.074	0.708	0.038	0.451		
x = 120 cm		0.11	0.527	0.084	0.716	0.045	0.511		

* Wu and Rajaratnam (1995)

3.2 Bed Shear Stress Measurements

Expt. 1		x (m)	τ (N/m ²)	0.20	7.005	0.80	6.404	1.40	2.608
x (m)	τ (N/m ²)	0.00	5.371	0.30	4.902	1.00	5.117	1.60	1.034
0.00	18.223	0.06	5.000	0.40	4.063	1.20	3.669	1.80	0.055
0.06	16.353	0.12	3.511	0.50	2.946	1.40	3.275	Expt. 6	
0.12	12.282	0.20	2.494	0.60	2.270	1.60	2.711	x (m)	τ (N/m ²)
0.20	9.652	0.40	1.634	0.80	1.577	1.80	1.221	0.00	26.398
0.30	8.112	0.60	0.982	1.00	1.386	2.00	0.398	0.20	13.695
0.40	5.827	0.80	0.841	1.20	0.987	Expt. 5		0.40	9.419
0.60	3.326	1.00	0.660	1.40	0.397	x (m)	τ (N/m ²)	0.60	6.910
0.80	3.023	1.20	0.569	1.60	0.154	0.00	26.398	0.80	5.717
1.00	2.464	1.40	0.416	Expt. 4		0.20	14.176	1.00	3.796
1.20	2.082	1.60	0.321	x (m)	τ (N/m ²)	0.40	10.272	1.20	3.019
1.40	1.884	Expt. 3		0.00	26.398	0.60	7.488	1.40	1.328
1.60	0.634	x (m)	τ (N/m ²)	0.20	17.798	0.80	6.454	1.60	0.063
1.80	0.201	0.00	9.704	0.40	12.874	1.00	4.272		
Expt. 2		0.10	9.093	0.60	8.875	1.20	3.338		

3.3 Variation of Velocity Scale, Length Scale, Jet Discharge and Momentum Flux with Distance

Expt. 1

x (m)	u_m (m/s)	b (m)	x/b_o	u_m/U_o	b/ b_o	Q/ Q_o	M/ M_o
0.00	2.50	-	0	1.000	-	1.000	1.000
0.06	2.50	1.25	6	1.000	1.250	1.204	0.992
0.12	2.29	1.66	12	0.916	1.657	1.486	1.000
0.20	1.95	2.26	20	0.778	2.262	1.779	1.000
0.30	1.74	2.71	30	0.697	2.714	1.955	0.987
0.40	1.50	3.73	40	0.599	3.735	2.281	1.000
0.60	1.23	5.35	60	0.491	5.354	2.659	0.965
0.80	1.12	6.90	80	0.446	6.901	3.084	0.968
1.00	0.98	8.67	100	0.392	8.671	3.347	0.964
1.20	0.91	10.06	120	0.363	10.064	3.603	0.949
1.40	0.82	11.50	140	0.327	11.504	3.854	0.891
1.60	0.64	16.07	160	0.255	16.069	3.834	0.758
1.80	0.50	19.27	180	0.201	19.266	3.599	0.558
2.00	0.28	-	200	0.113	-	3.268	0.392

Expt. 2

x (m)	u_m (m/s)	b (m)	x/b_o	u_m/U_o	b/b_o	Q/Q_o	M/M_o
0.00	1.25	-	0	1.000	-	1.000	1.000
0.06	1.25	1.26	6	1.000	1.264	1.231	1.017
0.12	1.13	1.63	12	0.907	1.632	1.496	0.998
0.20	0.96	2.29	20	0.768	2.292	1.767	0.991
0.40	0.76	3.54	40	0.608	3.543	2.179	0.971
0.60	0.59	5.86	60	0.475	5.863	2.790	0.965
0.80	0.54	7.28	80	0.436	7.284	3.176	1.002
1.00	0.49	8.97	100	0.390	8.966	3.418	0.985
1.20	0.45	10.53	120	0.356	10.531	3.663	0.964
1.40	0.39	11.95	140	0.315	11.953	3.758	0.851
1.60	0.32	16.05	160	0.258	16.048	3.693	0.734
2.50	0.25	-	224	0.198	-	1.000	-

Expt. 3

x (m)	u_m (m/s)	b (m)	x/b_o	u_m/U_o	b/b _o	Q/Q _o	M/M _o
0.00	1.750	-	0	1.000	-	1.000	1.000
0.10	1.750	0.014	10	1.000	1.418	1.191	0.974
0.20	1.516	0.020	20	0.866	1.978	1.587	1.010
0.30	1.295	0.027	30	0.740	2.700	1.958	1.002
0.40	1.145	0.035	40	0.654	3.490	2.221	0.964
0.50	0.994	0.045	50	0.568	4.462	2.512	0.982
0.60	0.919	0.056	60	0.525	5.558	2.793	0.980
0.80	0.805	0.072	80	0.460	7.199	3.089	0.949
1.00	0.716	0.085	100	0.409	8.506	3.263	0.931
1.20	0.617	0.112	120	0.352	11.160	3.552	0.861
1.40	0.405	0.176	140	0.231	17.624	3.571	0.703
1.60	0.301	0.250	160	0.172	25.000	2.927	0.427

Expt. 4

x (m)	u_m (m/s)	b (m)	x/b_o	u_m/U_o	b/b_o	Q/Q_o	M/M_o
0.00	2.860	-	0	1.000	-	1.000	1.000
0.20	2.860	0.024	13	1.000	1.587	1.446	0.972
0.40	2.628	0.036	27	0.919	2.408	1.771	0.996
0.60	2.108	0.055	40	0.737	3.643	2.328	0.984
0.80	1.751	0.071	53	0.612	4.719	2.461	0.947
1.00	1.499	0.087	67	0.524	5.804	2.924	0.971
1.20	1.325	0.096	80	0.463	6.396	2.955	0.937
1.40	1.226	0.107	93	0.429	7.109	2.942	0.869
1.60	1.130	0.120	107	0.395	8.031	2.702	0.721
1.80	0.983	0.142	120	0.344	9.467	2.534	0.603
2.00	0.835	0.145	133	0.292	9.697	1.951	0.334

Expt. 5

x (m)	u_m (m/s)	b (m)	x/b _o	u_m/U_o	b/b _o	Q/Q _o	M/M _o
0.00	0.000	-	0	0.000	-	1.000	1.000
0.20	2.586	0.024	13	0.904	1.603	1.411	0.953
0.40	2.041	0.039	27	0.714	2.604	1.834	0.946
0.60	1.700	0.057	40	0.594	3.796	2.161	0.952
0.80	1.485	0.077	53	0.519	5.112	2.516	0.967
1.00	1.341	0.087	67	0.469	5.770	2.732	0.942
1.20	1.218	0.103	80	0.426	6.895	2.769	0.861
1.40	0.997	0.122	93	0.349	8.133	2.717	0.747
1.60	0.838	0.126	107	0.293	8.418	2.217	0.556
1.80	0.664	0.142	120	0.232	9.467	1.724	0.326

Expt. 6

x (m)	u_m (m/s)	b (m)	x/b_o	u_m/U_o	b/b_o	Q/Q_o	M/M_o
0.00	2.86	-	0	1.000	-	1.000	1.000
0.20	2.567	0.024	13	0.898	1.631	1.430	0.948
0.40	2.035	0.039	27	0.712	2.613	1.822	0.955
0.60	1.696	0.055	40	0.593	3.665	2.209	0.979
0.80	1.452	0.075	53	0.508	4.993	2.550	0.970
1.00	1.307	0.092	67	0.457	6.133	2.593	0.910
1.20	1.142	0.099	80	0.399	6.568	2.468	0.771
1.40	0.860	0.129	93	0.301	8.571	2.144	0.538
1.60	0.521	0.141	107	0.182	9.426	1.275	0.180